2002

Precision Control of a Sensorless Brushless Direct Current Motor System

Knight, Matthew John

Precision Control of a Sensorless Brushless Direct Current Motor System

by

Matthew John Knight

A thesis submitted to the University of Plymouth in partial fulfilment for the degree of

Doctor of Philosophy

Marine and Industrial Dynamic Analysis Group

Department of Mechanical and Marine Engineering
Faculty of Technology

In collaboration with Research Instruments Ltd.

April 2002

Author's Declaration

At no time during the registration for the degree of Doctor of Philosophy has the author been registered for any other University degree.

This study was financed with the aid of the Engineering and Physical Sciences Research Council and was carried out under the sponsorship of Research Instruments Ltd, Penryn.

Relevant scientific seminars, conferences and exhibitions were regularly attended.

A series of papers have been published as a result of this work.

Signed: ..... M.J.Knight

Date: 12/7/02

Precision Control of a Sensorless Brushless Direct Current Motor System

Matthew John Knight

Abstract

Sensorless control strategies were first suggested well over a decade ago with the aim of reducing the size, weight and unit cost of electrically actuated servo systems. The resulting algorithms have been successfully applied to the induction and synchronous motor families in applications where control of armature speeds above approximately one hundred revolutions per minute is desired. However, sensorless position control remains problematic.

This thesis provides an in depth investigation into sensorless motor control strategies for high precision motion control applications. Specifically, methods of achieving control of position and very low speed thresholds are investigated. The developed grey box identification techniques are shown to perform better than their traditional white or black box counterparts. Further, fuzzy model based sliding mode control is implemented and results demonstrate its improved robustness to certain classes of disturbance. Attempts to reject uncertainty within the developed models using the sliding mode are discussed. Novel controllers, which enhance the performance of the sliding mode are presented.

Finally, algorithms that achieve control without a primary feedback sensor are successfully demonstrated. Sensorless position control is achieved with resolutions equivalent to those of existing stepper motor technology. The successful control of armature speeds below sixty revolutions per minute is achieved and problems typically associated with motor starting are circumvented.

Acknowledgements

The previous three years have truly personified the peaks and troughs of research as initially described by my director of studies at the beginning of this work. Despite the fact that the work has often been as commensurately rewarding as difficult, there is little doubt that if it were not for the support of my friends and colleagues, this thesis would never have come into existence. I therefore record my debt of gratitude to those many special people.

There are the few who's contribution to this work has been of exceptional significance and should be acknowledged personally; first and foremost among these people is Professor Robert Sutton, my director of studies. The many hours spent in his tutelage, and under the guidance of a red pen, has provided me with the confirmation that whilst thunder takes the credit, it is lightning that does the work. My remaining supervisors, Professor Roland Burns and Dr David Jenkins and their contribution to this work is also recognised here and my thanks extended.

I acknowledge the help received by the technical staff within and outside the department; Mr Michael Sloman, Mr Brian Lord and Mr Colin Stansbury have served to provide a perspective on work and life that has allowed me to maintain balance even in the deepest of troughs. I would also like to acknowledge Mr Bob Bray, Mr John Eastment, Ms Sheila Storm and Mr Mike Frise who have taken so much on trust that their equipment will be returned unmolested.

I would like to thank the administrative staff within the department, specifically Ms Sue Locke and Ms Barbara Fuller whose kind words over the last three years have been greatly appreciated.

Perhaps the greatest level of support has come from my wife and children who have managed to muster seemingly saintly patience under the most extreme circumstances. It is natural that this work is dedicated to them.

Finally, I would like to acknowledge the financial support of my CASE award sponsors.

~MJK, Plymouth 2002

Contents

Table of Figures

Nomenclature

Operators

$\text{rank}(m)$	Dimension of largest square matrix in m with nonzero determinant
m^{-1}	Inverse of square matrix m
m^T	Transpose of matrix m
$m^\dagger$	Matrix m pseudo-inverse
[t,T]	Closed interval $t \leq \tau \leq T$
$E\{x\}$	Expected value of random variable x
$\text{diag}(d_1,\ldots,d_n)$	Diagonal matrix with elements $d_1,\ldots,d_n$ along the diagonal
$\det(m)$	Determinant of square matrix m
$\text{tr}(m)$	Trace of matrix m
$\cdot$	Vector inner product
$\dot{x}$	Derivative of x
$\ddot{x}$	Second derivative of x
$\|\cdot\|$	Euclidean or Spectral norm
$\|\cdot\|_\infty$	Infinity norm
$\|\cdot\|_{rms}$	Root mean squared semi norm
$\text{sgn}(x)$	Signum of function x
$\varnothing$	Null
$\cap$	Intersection
$\cup$	Union
$\subset$	Subset
$\in$	Element
$\|\cdot\|$	Induced Euclidean norm
$\det(\cdot)$	Determinant

$\max(\cdot)$	Supremum of value
$\text{sgn}(\cdot)$	Signum function
$\lim(\cdot)$	Limit of function
$\hat{\cdot}$	Estimate of value
$\Re$	Range Space
$\aleph$	Null Space
$\kappa(\cdot)$	Condition Number
$\mathbb{R}$	Real number
$\mathbb{C}_-$	Complex left hand plane

Symbols common to all Chapters

$x \in \mathbb{R}^{n\times 1}$	:	Vector of states
$u \in \mathbb{R}^{m\times 1}$	:	Vector of controls
$y(t)$	:	Output vector
$A \in \mathbb{R}^{n\times n}$	:	Transition matrix
$B \in \mathbb{R}^{n\times m}$	:	Driving Matrix
$C \in \mathbb{R}^{p\times n}$	:	Output Matrix
$D \in \mathbb{R}^{n\times q}$	:	Transmission Matrix
θ	:	Angular position
ω	:	Angular velocity
d	:	Direct axis
q	:	Quadrature axis
ζ	:	Damping ratio
ω_n	:	Natural frequency
β	:	Degree of fulfillment
μ	:	Set membership

Symbols for Chapters 2 and 3

V	:	Phase voltage
R	:	Phase Resistance
i	:	Phase current
L	:	Phase Inductance
λ	:	Flux linkage
ω	:	Armature velocity
T_e	:	Electrically generated torque
T_l	:	Load torque
T_x	:	Exogenous load torque
τ_{em}	:	Electromechanical time constant
K_C	:	Power converter gain
K_T	:	Torque constant
K_I	:	Current sensor gain
K_{SI}	:	Torque controller gain
τ_{si}	:	Torque controller time constant
W_{co}	:	Magnetic coenergy
$\Delta\theta$	:	Torque angle increment
α_a	:	Advance angle
E	:	Back electromotive force
G	:	Observer gain sequence
S	:	Sliding manifold
γ	:	Bandwidth
P_i	:	Applied electrical power
P_o	:	Mechanical output power
P_l	:	Power loss
T_c	:	Total encoder count

k	:	Current sample
n	:	Speed
ω_i	:	Ideal no load angular velocity
s	:	Laplace operator

Symbols for Chapter 4

φ	:	Regression vector
θ	:	Regressions
Z	:	Data set
$\varepsilon(t,\theta)$	:	Prediction error
V_N	:	Performance measure
G	:	Gradient
H	:	Hessian
c	:	Number of clusters
v	:	Cluster prototype
μ	:	Step size
η	:	Search direction
W	:	Network weights
N	:	Number of data in the training sets
F	:	Activation function
r	:	Number of regressors
λ	:	Eigenvalue
ϕ	:	Eigenvector
Φ	:	Shortest eigenvector
s_{ij}	:	Cluster compatibility criteria
X	:	Matrix of regression vectors
Y	:	Vector of regressands
U	:	Partition matrix
γ	:	Normalised degree of fulfilment

D	:	Distance
F	:	Cluster Covariance Matrices
ϕ	:	Number of searches across minimum
τ_{crit}	:	Termination criterion
δ	:	Maximum number of training epochs

Symbols for Chapters 5 and 6

S	:	Sliding manifold
M	:	Constant design parameter
a_1	:	Constant design parameter
a_2	:	Constant design parameter
c	:	Constant design parameter
ΔA	:	Uncertainty and variation within the plant parameters
ΔB	:	Uncertainty and variation within the control interface
$S \in \mathbb{R}^{m \times n}$	:	Switching function
$T_r \in \mathbb{R}^{n \times n}$	:	Orthogonal Transform Matrix
$B_2 \in \mathbb{R}^{m \times n}$	:	Submatrix resulting from partitioning B into the regular form
$A_{11}, A_{12}, A_{21}, A_{22}$		Submatrices of A resulting from partitioning into the regular form
$\Lambda \in \mathbb{R}^{m \times m}$	:	Diagonal, Stable Design Matrix
$\Phi \in \mathbb{R}^{m \times m}$	:	Stable design matrix
$\xi(t, y, u)$	:	Bounded matched uncertainty
ε	:	Error
ε_l	:	Regression vector
t_s	:	Time taken to reach sliding manifold
T_r	:	Rise time
T_s	:	Settling time
SSE	:	Sum of Squares Error
κ	:	Condition number

B	:	Viscous friction
J	:	Inertia
F	:	Covariance matrix
D	:	Distance Matrix
λ	:	Eigen value
ϕ	:	Eigen vector
θ_r	:	Electrical angular position
θ_{rm}	:	Mechanical angular position
f	:	uncertain, time-varying, unknown bounded term
ε	:	Radius of boundary layer
T_{ms}	:	Motor stall torque
ζ	:	Vector of Polynomials
η	:	Vector of Polynomials
θ	:	Offset

Symbols for Chapter 7

ΔT_p	:	Plant sample frequency
ΔT_m	:	Model sample frequency
ΔT_{sw}	:	Time taken to reach next Hall effect device status change
ΔT_{HED}	:	Least squares estimate of ΔT_{sw}
θ	:	Position
θ_{MOD}	:	Model predicted position
ω	:	Velocity
H	:	Position indicated by Hall effect devices
ΔH	:	Magnitude of angle associated with Hall effect device status change
G	:	Discrete time state transition matrix
H	:	Discrete time driving matrix
J	:	Measurement jacobian
k	:	Sample number

ε	:	Measurement residual
h_1	:	Single winding holding torque
h_2	:	Double winding holding torque
W	:	Angle between motor phases
K	:	Kalman gain
P	:	Covariance matrix

Abbreviations and Acronyms

ARMA :	Autoregressive Moving Average
ARMAX :	Autoregressive Moving Average with exogenous input
ARX :	Autoregressive Moving Average with exogenous input
BJ :	Box Jenkins model structure
BL :	Boundary Layer
BLAC :	Brushless A.C.
BLDC :	Brushless DC
DC :	Direct Current
DIRAPP:	Direct Approach Algorithm
DISO:	Dual input single output
DSCAPP:	Discrete Approximations Approach
EKF :	Extended Kalman Filter
EMF:	Electro Motive Force
ep:	Encoder Pulses
FCM :	Fuzzy C-Means
FCARX:	Fuzzy Clustered ARX
FIR :	Finite Impulse Response
FSMC :	Fuzzy SMC
FMBSSMC:	Fuzzy Model Based Sensorless SMC
FRESPBE:	Fuzzy model trained on PBEQU residuals
GBM :	Grey Box Model
GK :	Gustafson Kessel
HED :	Hall Effect Device
ISMC :	Integral SMC
KF :	Kalman Filter
KFSIDA:	Kalman Filter with Sterling Interpolation using Direct Approach Algorithm and the Fuzzy model for Observation Streams
KFSIFM:	Kalman Filter with Sterling Interpolation using the Fuzzy model and Hall effect data for Observation Streams
LS :	Least Squares
mmf :	Magneto motive force
MSE :	Minimum Squared Error
NARX :	Nonlinear ARX

NNARX :	Neural Network ARX
N.m :	Newton Meter
OE :	Output Error
P :	Proportional
PBEQU:	Power Balance Equations
PBEGD:	PBEQU trained on gradient descent
PBEREG:	PBE used as a regressor in a fuzzy model
PC:	Phase Coordinate
PD :	Proportional plus Derivative
PEC :	Power Electronic Converter
PEM :	Prediction Error Method
PID :	Proportional plus Integral plus Derivative
PMSM :	Permanent Magnet Synchronous Motor
PWM :	Pulse Width Modulation
RLS :	Recursive Least Squares
RMS :	Root Mean Squared
RMSE :	Root Means Squared Error
RPEM :	Recursive PEM
RPLR :	Recursive PLR
RPM :	Revolutions per Minute
SISO :	Single Input Single Output
SMC :	Sliding Mode Control
VAF :	Variance Accounted For
w.p.:	with probability
w.p. 1 :	with probability 1
w.r.t. :	with respect to

Chapter 1

Introduction

Micro-actuation has relevance in many highly technological areas. Such areas include medical procedures, computer sciences, fibre-optics and the related photonics field. As each of these areas is drawn inexorably toward the miniature, so the requirement for improved accuracy, repeatability and resolution in manipulation increases. At the same time, greater impetus has been placed on the reduction of size, weight and cost of the manipulation.

Precision motion control is defined within this work to be the control of the position of a device to within microns, over a minimum range of tens of millimetres. This has been traditionally achieved through the use of a controller, a motor, a threaded shaft and a feedback device. There are naturally variations around this theme, for instance linear motors are beginning to enjoy significant application because they circumvent the requirement for a threaded shaft (Coelingh *et al*, 1998).

In recent times permanent magnet motors have come to the fore as attractive devices for actuation. The maturation of these permanent magnet motors has been driven mainly by their enhanced performance characteristics over the brushed or stepping alternatives (Rahman and Zhou (1996), Ellis (1996), Mighdoll (1996), Sen (1990)), the ever improving performance of magnetic materials available and the decreasing cost of high speed electronic components (Rahman and Zhou, 1996). One of the major drawbacks associated with the permanent magnet machine, as viewed in many areas of technology, is the need for sensors in rotor position feedback. These sensors are required for efficient

commutation of the motor; however they effect the system in the same manner as the addition of a position feedback device (Ogasawara and Akagi (1991), Iizuka *et al* (1985), Matsui (1996)). "Sensorless" control of the motor has therefore been the subject of much research over recent years. The term "Sensorless" in this case is a misnomer; parametric variations within the motor itself have been shown to yield armature position (Matsui and Shigyo (1992), Wu and Slemon (1991), Corley and Lorenz (1998)); in this sense the motor becomes not only the actuator but also the sensor.

The typical precision motion control system, as described above may be improved in one of two ways.

1) Performance – In terms of repeatability, accuracy and resolution.

2) Cost – In terms of size, assembly, weight and financial.

There is significant research effort dedicated to the first of these approaches, and nanometer resolution has been achieved, e.g. Awabdy *et al* (1998). In addition devices may be found commercially from companies such as Newport Motion Controls, Melles Griot and SDS Queensgate to achieve similar performance.

The second of these approaches may in the limit be considered to fall into the area of the so called 'nano-technologies', if size alone is considered. There are distinct advantages to be gained from also minimising the cost to the system in terms of the remaining categories. In 1983, in the sequel to his famous speech from 1960, '*There's plenty of room at the bottom*' (Feynman, 1992), Feynman asks how to make '*precise things from imprecise tools*' (Feynman, 1993). Taken within context, he was of course discussing the possibility of producing miniscule devices from the technology available at the time. However, the question may be paraphrased '*How do you make precise devices from*

imprecise measurements?', and in so doing an area of significance to all precision motion control applications is revealed.

It will be shown within Chapter 2 that research to date within the field of sensorless drive control has focused on the accurate speed control of the motor armature. Since, when the rotor position is known, efficient commutation of the motor may be achieved without the presence of sensors. This rotor position is more easily estimated at higher speeds. Approaches such as observers and Kalman filters have been prevalent within the literature (Tomita *et al* (1998), Dhaouadi *et al* (1991), Bierke *et al* (1997), Kettle *et al* (1998), Navrapescu and Craciunescu (1997)), since often direct measurement of motor parameters is not achievable (Matsui and Shigyo, 1992). The fundamental problem with both has been the dependence upon accurate *a priori* knowledge of motor parameters (Stronach and Vas, (1998)). Sliding mode has been also applied to sensorless control (Utkin (1993), Furuhashi *et al* (1992)), the inherent problems associated with sliding mode, i.e. chattering and high gain have posed problems in application (Ishigame *et al* (1993), Suyitno *et al* (1993)).

The objective of this work is therefore to define an algorithm that will reliably provide an indication of armature position at very low or zero speed. The algorithm should not rely on an explicit actuator model. In addition, the algorithm must be capable of producing rotational measurement accuracies equal to that of equivalent technology without introducing sensors which do not already exist within the system.

The objective of this work will be achieved by fulfilling the following aims

- A thorough literature review of existing methods for sensorless control will be undertaken, in order to assess the applicability of existing methods to low and zero speed sensorless control.
- An experimental test system will be developed to provide analogy to systems commonly encountered in industry. This system will be capable of data capture for subsequent analysis.
- Modelling and identification of the system will be undertaken, the performance of the techniques assessed according to a defined set of measures.
- Sliding mode control will be investigated because of its invariance property; methods of incorporating the most accurate models will be developed.
- A variety of methods for estimating or controlling motor kinematic parameters will be developed.

1.1 Thesis Organisation

Chapter 2: ***Motion Control Systems*** begins with an introduction to permanent magnet motors, and their application to small drive systems. Several members of the permanent magnet motor family, and their performances are discussed.

Sensorless control methods for the synchronous motor, invented a little under two decades ago were made possible by the advent of high speed, low cost electronics. The Chapter continues with an exposition of the techniques which have been successfully applied within the technology over that time. It is shown that in general, sensorless control methodologies fit into one of three categories, and that with the exception of a

few algorithms have dealt with accurate speed control, but not position control at low speed or standstill.

Chapter 3: ***Experimental Test Rig Modelling and Control*** then moves on to discuss the development of a test rig capable of precision motion control. Aspects of it's mechanical, electrical and software design are considered where departures from the industry standards are made. These departures are made in order to ensure full state feedback from the system.

The system is then modelled from first principles and the models, once developed, are compared to assess their accuracy and viability within a controller operating in real time. Controllers based on the selected model are then developed and implemented on the experimental system.

Chapter 4: ***System Identification*** considers the use of techniques other than those in Chapter 3, to describe system dynamics. The approaches of Chapter 3 are classically defined as being modelling techniques, whereas the approaches described in Chapter 4 move into the science of system identification. Within this Chapter, models are first developed based on the linear difference equation. Following on, advanced nonlinear identification techniques, specifically those based on artificial neural networks and fuzzy clustering, are used to obtain high fidelity models of the system. Finally within this Chapter, methods to incorporate known information about the system are discussed and implemented. The approach, which is a hybrid of the modelling strategy (white-box) and the nonlinear identification strategies (black-box), is referred to as the grey-box approach and is demonstrably better than either of the alternative approaches.

Chapter 5: ***Sliding Mode Control ~ Classical Approaches*** serves to introduce the robust control strategy referred to within the literature as the sliding mode. It is discussed within the text that this controller is able to force a system state to converge to a manifold within the state space, and from thereafter to remain on it. This is an extremely attractive prospect, since it results in a controller that demonstrates reduced order performance and complete invariance to parametric error within the plant model and to a certain class of disturbance. This Chapter provides the theory and implementations of sliding mode controllers for use with the experimental test rig.

Chapter 6: ***Sliding Mode Control ~ Advanced Approaches*** continues with the theme of robust control. It was shown in Chapter 5 that whilst the sliding mode maintains many attractive properties, there are also some decidedly unattractive characteristics. The primary drawback in the implementation is a phenomenon referred to as control chatter. A second drawback is that the controllers implemented in Chapter 5 are only invariant to a certain class of disturbance. The work presented in this Chapter has two main threads. The first is the use of an integral action to enhance the robustness of the controller. Two novel controllers are suggested. The second part of the Chapter considers the use of a discontinuous control action within observers and model following controllers to incorporate robustness and convergence properties.

Chapter 7: ***Precision Sensorless Motion Control*** combines all of the previous work to produce sensorless control algorithms which meet the specification of the objective described earlier within this Chapter. The problem is initially defined and the performance of equivalent technology is also described. Algorithms based on optimal estimates of position are then developed. A fundamentally different approach is

subsequently adopted using the sliding mode controllers of Chapter 6. Results are presented.

Finally this work is concluded in Chapter 8 with a discussion and recommendations for future work.

1.2 Motivations and Contributions of this Work

The rapid evolution of motor technology, and the subsequent research activity has led to a proliferation of motor models and approaches to the estimation of model performance. Upon inspection of the literature, however, there is very little dedicated to the identification of a synchronous motor with a time variant load. Further, the emergent grey-box modelling techniques have yet to become established as methods for achieving high performance system models. The first motivation of this work was therefore to provide a study of the methods applicable to the identification of a brushless D.C. motor servomechanism. In addition, because the system is understood to an extent, methods were sought to incorporate this knowledge into the identified models, and thus adhere to the fundamental tenet within the field of system identification that only the phenomena which are not understood should be modelled. The resulting study, embodied in Chapter 4 is believed to be an original contribution to the study of nonlinear systems identification.

Having learned from the experience of modelling and identification that no model is perfect, but some are useful, it was a natural progression to consider the invariance property of the sliding mode. Despite tremendous research effort in this field, some difficulties still exist. Unknown nonlinear functions as disturbance have not been

considered and the existence of the chatter phenomenon frequently leads to a controller that can only guarantee tracking accuracy to within a certain vicinity of the set point, and certain classes of disturbance are not formally considered within the theory. It is an appealing prospect to use the stochastically optimal models of the system from chapter 4 in the adaptation of the deterministic controller parameters, such that the performance of the controller is enhanced. This is precisely what is achieved with the fuzzy model based sliding mode controllers discussed in Chapters 6 and 7. There is no doubt that these enhanced controllers perform better than the classical sliding mode controllers, yet maintain their advantages in implementation. These controllers therefore constitute a contribution to the field of adaptive robust control.

The original motivation of this work was to produce a sensorless precision motion control algorithm capable of operation at low speed and standstill of the armature. The majority of sensorless control methods within the literature to date have considered the accurate control of the armature at high to medium speed. The application of the fuzzy model based controllers to this problem, and the successful control of kinematic parameters associated with the armature, at low and zero speed, is therefore the last of the significant contributions made by this work.

1.3 References

Awabdy B.A., Shih W.-C. and Auslander D.M., 1998, 'Nanometer Positioning of a Linear Motion Stage under Static Load', IEEE/ASME Transactions on Mechatronics, 3(2), 113-120

Beierke S., Vas P., Simor B. and Stronach A.F., 1997, 'DSP Controlled Sensorless AC Vector Drives using the Extended Kalman Filter', Proc PCIM 97, Nuremburg, 31-41

Coelingh E., De Vries T.J.A., Holtermann J. and Van Amorongen J., 1998, 'Mechatronic systems with uncertain physical parameters', Mechatronics '98, Adolfsson and Karlsen (eds), 187-192

Corley M. and Lorenz R., 1998, 'Rotor Position and Velocity Estimation for a Salient Pole Permanent Magnet Synchronous Machine at Standstill and High Speeds', IEEE Trans. Industry Applications, 34(**4**), 752-757

Dhaouadi R., Mohan N. and Norum L., 1991, 'Design and Implementation of an Extended Kalman Filter for the State Estimation of a Permanent Magnet Synchronous Motor', IEEE Trans. Power Electronics, 6(**3**), 491-497

Ellis G., 1996, 'Driven by Technology Advancements, Brushless DC Motors are Displacing Brush Types', PCIM magazine, 42-48

Feynman R.P., 1992, 'There's Plenty of Room at the Bottom', IEEE Journal of Microelectromechanical Systems, 1(**1**), 60-66

Feynman R.P., 1993, 'Infinitesimal Machinery', IEEE Journal of Microelectro-mechanical Systems, 2(**1**), 4-14

Furuhashi T., Sangwongwanich S. and Okuma S., 1992. 'A Position and Velocity Sensorless Control for Brushless DC Motors Using an Adaptive Sliding Mode Observer', IEEE Trans. Industrial Electronics. 39(**2**), 89-95

Iizuka K., Uzuhashi H., Kano M., Endo T. and Mohri K., 1985. 'Microcomputer Control for Sensorless Brushless Motor', IEEE Trans. Industry Applications, IA-21(**3**), 595-601.

Ishigame A., Furukawa T., Kawamoto S. and Taniguchi T., 1993, 'Sliding Mode Controller Design Based On Fuzzy Inference For Non-Linear Systems', IEEE Trans on Industrial Electronics, 40(**1**), 64-70

Kettle P., Murray A. and Moynihan F., 1998, 'Sensorless Control Of A Brushless DC Motor Using An Extended Kalman Estimator', Proc PCIM 98, Nuremburg, 385-392

Matsui N., 1996, 'Sensorless PM Brushless DC Motor Drives', IEEE Trans. Industrial Electronics, 43(**2**), 300-308

Matsui N. and Shigyo M., 1992, 'Brushless DC Motor Control Without Position and Speed Sensors', IEEE Trans. Industry Applications, 28(**1**), 120-127

Mighdoll D., 1996, 'Brushless DC Motor Basics', PCIM magazine, 18-31

Navrapescu V. and Craciunescu A., 1997, 'A New Discrete Speed Estimator Based On Kalman Theory', Proc PCIM 97, Nuremburg, 43-48

Ogasawara S. and Akagi H., 1991, 'An Approach to Position Sensorless Drive for Brushless DC Motors', IEEE Trans. Industry Applications, 27(**5**), 928-933

Rahman M. and Zhou P., 1996, 'Analysis of Brushless Permanent Magnet Synchronous' Motors', IEEE Trans. Industrial Electronics. 43(**2**), 256-267

Sen P., 1990, 'Electric Motor Drives and Control – Past, Present, and Future', IEEE Trans. on Industrial Electronics, 37(**6**), 562-575

Stronach A.F. and Vas P., 1998, 'Design, DSP Implementation, And Performance Of Artificial-Intelligence-Based Speed Estimators For Electromechanical Drives', IEE Proc D, 145(**2**)

Suyitno A., Fujikawa J., Kobayashi H. and Dote Y., 1993, "Variable Structure Robust Controller by Fuzzy Logic for Servomotors", IEEE Trans. on Industrial Electronics, 40(**1**), 80-88

Tomita M., Senjyu T., Doki S. and Okuma S., 1998, 'New Sensorless Control for Brushless DC Motors Using Disturbance Observers and Adaptive Velocity Estimations', IEEE Trans. Industrial Electronics, 45(**2**), 274-282,

Utkin V., 1993, 'Sliding Mode Control Design Principles and Applications to Electric Drives', IEEE Trans. Industrial Electronics, 40(**1**), 23-36

Wu R. and Slemon G., 1991, 'A Permanent Magnet Motor Drive Without a Shaft Sensor', IEEE Trans. Industry Applications, 27(**5**), 1005-1011

Chapter 2

Motion Control Systems

2.1 Introduction

Motion Control refers to the control of kinematic parameters such as torque, velocity or position. This Chapter is dedicated to reviewing those technologies which serve to provide the vital interface between electrical and mechanical engineering. This interface is found wherever mechanical motion is controlled by electronics and pervades a vast range of products. Consideration of this interface reveals a large and important area of technology, to which motor drives are fundamental. In Japan the term '*Mechatronics*' has been coined to describe these technologies, and usually carries the connotation of small drives. This term is now well established in the West, but the term 'motion control system' is often used in its stead to describe small controlled drives such as position or velocity servomechanisms. Motion control systems are in general characterised by precision, low transient response times, immunity to parameter variations, torque and inertia perturbations.

Two important reasons for the research activity within this area, and for the increasing technical variety of the drive systems to be found are:

1) Increasing use of computers and electronics to control mechanical motion. The trend towards automation demands new devices with a wide variety of physical and control characteristics.

2) New 'enabling technology' in power semiconductors and integrated circuits, leading to the development of nonclassical motors such as the brushless D.C. (BLDC) motors and steppers in a wide variety of designs.

The scope of the technologies encompassed in the 'motion control system' is far too broad to be comprehensively discussed within this work. Instead, the reader is referred to the many excellent introductory texts on the subject (e.g. Bolton, 1999), and this Chapter concentrates specifically on the technology which will be subsequently applied in later Chapters. It begins with a discussion of drives in general and describes the primary reasons for the selection of one drive over another. The salient features of the selected drive are then discussed. Finally within this Chapter, sensorless control methodologies are discussed with specific reference to the brushless motor.

2.2 Adjustable Speed Drives

Three common reasons for preferring an adjustable speed drive over a fixed speed motor in general are:

1) Energy saving.

2) Velocity or position control.

3) Amelioration of transient performance.

Whilst for the smaller drives the singular most important of these is the velocity or position control, the other two factors have been significant in forcing the development of the technologies. Here, only velocity/position control is considered for motion control systems. Obvious examples of velocity control are the electric train, portable hand tools, and domestic washing machine drives. In buildings, elevators are interesting examples in which not only position and velocity are controlled, but also acceleration and its

derivative, jitter. Countless processes in the manufacturing industry require position and velocity control to varying degrees of precision. Particularly with the trend towards automation, the technical and commercial growth in drives below about 20 kW is very vigorous. Many system level products incorporate an adjustable speed drive as a component. A robot, for example, may contain between three and six independent drives, one for each axis of movement. Other familiar examples are found in office machinery: positioning mechanisms for paper, printheads, magnetic tape, and read/write heads in floppy, hard disk and CD rom drives.

2.3 Motor Selection

The proliferation of new ideas, materials and components obviously generates many opportunities but also complicates the selection of the optimum drive for a particular application. Attempting to trace the evolution of the different motor types in such a way as to bring out their prominent features, provides a clear framework to reduce the ambiguity frequently faced in the selection of the optimum drive. The motor plays a significant part in determining the characteristics of the system and also serves to determine the requirements on the power semiconductors, the converter circuit and the controller. Within this work, the a.c. induction motor will not be considered since it is not an efficient drive to apply to small motion control systems. This is because the efficiency and power factor of the induction motor drops in small motor sizes due to the natural laws of scaling. If a motor of given geometry was scaled down at the same rate, the magneto motive force (m.m.f.) required to produce a given flux density decreases in proportion to the linear dimensions. However the cross-section available for conductors decreases with the square of the linear dimension, as does the area available for heat

transfer. This continues down to the size at which the mechanical air-gap reaches a lower limit determined by manufacturing tolerances. Further scaling down results in an approximately constant m.m.f. requirement, whilst the areas continue to decrease with the square of the linear dimension. There is an 'excitation penalty' which becomes more severe as the scale is reduced. It is for this reason that permanent magnets are so necessary in small motors.

2.3.1 Small Motors For Drives

The evolution of brushless motors is based around three generations. The classical motors: D.C. commutator (wound field) and a.c. synchronous constitute the first of these generations. The term classical emphasises the fact that these motors satisfy three important criteria

1) They all produce essentially constant instantaneous torque
2) They operate from pure D.C. or a.c. sinewave supplies
3) They can start and run without electronic controllers

The classical motors of the first generation are readily coupled to electronic controllers to provide adjustable speed; indeed it is with them that most of the technical and commercial development of power electronic control has taken place.

The second generation motors are derived from those of the first generation by replacing the field windings with permanent magnets. The synchronous motor immediately becomes brushless, but the D.C. motor must go through an additional transformation, from second to third generation with the inversion of the stator and rotor, before the brushless version is achieved. Each of the motors will be treated below in turn

The D.C. Commutator Motor

The traditional D.C. commutator motor with electronically adjustable voltage has always been prominent in motion control. It is easy to control, stable, and requires relatively few semiconductor devices. Developments in electronics have helped to keep it competitive in spite of efforts to displace it with a.c. drives.

Many objections to the commutator motor arise from operational problems associated with the brush gear. It is not that brush gear is unreliable, on the contrary, it is reliable, well proven and forgiving of abuse. However commutator speed is a limitation, additionally noise, wear, commutator and brush gear is considerable. Cooling of the rotor, which carries the torque producing winding is not always easy, and is a further limiting factor.

The PM D.C. Commutator Motor

In small D.C. commutator motors, replacing the field winding and pole structure with permanent magnets usually permits a considerable reduction in stator diameter, because of the efficient use of radial space by the magnet and the elimination of field losses. Armature reaction is usually reduced and commutation is improved, owing to the low permeability of the magnet. The loss of field control is not as important as it would be in a larger drive, because it can be overcome by the controller and in small drives, the need for field weakening is less common anyway. The PM D.C. motor is usually fed from an adjustable voltage supply, either linear or pulse width modulated.

The Brushless D.C. PM Motor

The smaller the motor, the more sense it makes to use permanent magnets for excitation. There is no single breakpoint below which PM brushless D.C. (BLDC) motors

outperform induction motors, but it is in the 1-10kW range. Above this size the induction motor improves rapidly, whilst the cost of magnets works against the PM motor. Below it, the PM motor has better efficiency, torque per ampere, and effective power factor. Moreover, the power winding is on the stator where its heat can be removed more easily, while the rotor losses are extremely small. These factors combine to keep the torque/inertia ratio high in small motors.

The brushless D.C. motor is also easier to control, especially in its squarewave configuration. Although the inverter is similar to that required for induction motors, usually with six transistors for a three phase system, the control algorithms are simpler and readily implemented in a microprocessor.

The Brushless PM a.c. Motor

The permanent magnet synchronous machine (PMSM) has permanent magnets instead of a field winding. Field control is once again sacrificed for the elimination of brushes, sliprings and field copper losses. This motor is a 'classical' salient pole synchronous a.c. motor with approximately sine distributed windings, and it can therefore run from a sinewave supply without electronic commutation.

The magnets can be mounted on the rotor surface or they can be internal to the rotor. The interior construction simplifies the assembly and relieves the problem of retaining the magnets against centrifugal force. It also permits the use of rectangular instead of arc shaped magnets, and usually there is an appreciable reluctance torque which leads to a wide speed range at constant power.

It should be noted that the three motors discussed provide smooth torque with low ripple. An important class of brushless motor which has not been discussed is the stepper motor. This type of motor is always brushless and unlike the BLDC or PMSM motors, are used almost exclusively without any form of shaft position sensing. By definition, the stepper motor is a pulsed torque machine, and is therefore incapable of achieving ripple free torque by conventional means. Variable reluctance and hybrid stepper motors can achieve an internal torque multiplication through the use of multiple teeth per stator pole and through the 'Vernier' effect of having different numbers of teeth on the rotor and stator. Both of these effects work by increasing the number of torque impulses per revolution, and the price paid is an increase in the commutation frequency and iron losses. Stepper motors therefore have high torque to weight and high torque to inertia ratios but are limited in top speed and power to weight ratio. The fine tooth structure requires a small airgap, which adds to the manufacturing cost. Beyond a certain number of teeth per pole the torque gain is 'washed out' be scale effects that diminish the variation of inductance on which the torque depends. Because of the high magnetic frequency and the effect of m.m.f. drop in the iron, such motors require expensive lamination steels to get the best out of them. Further details on the stepper motor may be found in Kenjo, (1985).

2.3.2 Cascaded Motion Control

The singular most typical method for motor control is the so called 'cascaded motion control', which consists of three control loops (see for example Subrahmanyam, 1996). One for the control of torque, one for speed and one for position. It is assumed that each of these loops will be equipped with appropriate sensing devices. Whilst the outer two

loops, and their realisation, are considered in some detail in later chapters, the torque control loop is not. This is primarily because this control loop is already realised within the commercially available power electronic converter, providing a simple potentiometer for its gain adjustment. The torque control loop is therefore considered here for completeness. The Permanent Magnet D.C. commutator machine dynamics, which maintain a notable generality to all motors, are given by the equations

$$V = Ri + L\frac{di}{dt} + \lambda\omega_r \tag{2.1}$$

$$J\frac{d\omega_r}{dt} = T_e - T_l \tag{2.2}$$

$$\frac{d\theta}{dt} = \omega_r \tag{2.3}$$

$$T_e = \lambda I \tag{2.4}$$

The torque (2.1) control loop for the constant flux linkage (λ) machine implies armature current control for the permanent magnet D.C. brush (DC) motor. In the case of the brushless D.C. motor, with constant flux linkage, this implies current control within the stator phases. The design of the torque loop requires knowledge of the load torque. In practice, this is not known precisely (see Chapter 3 for a discussion of this), and the load torque is assumed to be constant. Once the design is complete, the effect of load variations are observed and suitable corrections are made to the controller gains if required. For a constant load torque, the DC motor current/voltage relationship can be written from (2.1)-(2.4)

$$G(s) = \frac{I(s)}{V(s)} = \frac{s\tau_{em}}{\left(s^2\tau_{em}\tau_e + s\tau_{em} + 1\right)R} \tag{2.5}$$

where τ_{em} is the electromechanical time constant of the motor given by the equation

$$\tau_{em} = \frac{JR}{\lambda^2} \tag{2.6}$$

The typical torque controller is based on a proportional integral (PI) structure, with the gain K_{SI} and time constant τ_{si}. The open loop transfer function of the system using a PI controller is given

$$A(s) = \frac{K_{si}(1+s\tau_{si})}{s\tau_{si}R} \frac{K_C K_T K_I s\tau_{em}}{s^2\tau_{em}\tau_e + s\tau_{em} + 1} \tag{2.7}$$

where K_C is the gain of the power converter between controller and motor, $K_T = T_e/I$ is the torque constant and K_I is the current sensor gain.

2.4 Synchronous Motors for Drives

The Brushless D.C. and the Permanent Magnet a.c. machines were discussed briefly above. This section serves to provide further detail on their characteristics, greater detail may be found in Miller (1993). Synchronous motors (SMs) are in general three phase a.c. fed in the stator and D.C. (or PM) excited in the rotor. As the stator currents produce an m.m.f. traveling at the angular velocity ω_1:

$$\omega_1 = 2\pi f_1 \tag{2.8}$$

the rotor m.m.f. (or PM) is fixed to the rotor. The rotor angular velocity ω_r is:

$$\omega_r = \omega_l = 2\pi np \tag{2.9}$$

in order to obtain two standing m.m.f. waves. It is a known fact that only in this situation a non zero average torque per revolution is obtained. Yet, in an alternative interpretation, non zero average torque is produced when the magnetic co-energy in the machine W_{co} varies with rotor position:

$$T_e = \left(\frac{\partial W_{co}}{\partial \theta_r}\right)_{i_i=ct}; \frac{d\theta_r}{dt} = \frac{\omega_r}{p} \tag{2.10}$$

θ_r is the geometrical rotor position angle. Thus a magnetically anisotropic (reluctance) exciterless rotor may also be used. In all cases the number of pole pairs is the same on the stator and on the rotor.

As the synchronous motor speed is rigidly related to the stator frequency only the development of power electronic converters (PEC), variable voltage and frequency sources, has made the synchronous motor suitable for variable speed drives.

The higher efficiency, power density and, power levels per unit have thus become the main assets of variable speed synchronous motor drives.

2.4.1 Drive Classification

Permanent magnet synchronous motor drives exist in several distinct forms. These forms may be differentiated with respect to the generated current waveform, voltage/frequency correlation and motion sensor presence (Moczala *et al*, 1998).

Classification based on the applied current waveform reveals two distinct types, those with a rectangular current waveform and those with sinusoidal. This leads to the common names that differentiate the two, the BLDC and the PMSM drive. Secondly consideration can be paid to the presence of motion sensors, predictably BLDC or PMSM drives without motion sensors are prefixed with the term "sensorless". Finally PMSM drives may controlled through one of the following means

- Scalar (V / f) control - a damper cage on the rotor is required;
- Vector control (current or current and voltage);
- Direct torque and flux control (DTFC).

Regardless of the method of control, the stator current waveforms must be synchronised with the rotor position in order to guarantee efficient commutation of the motor. This is where sensorless control has grown from. In essence an attempt is made to synchronise the rotor position with the excited stator coil without the use of sensors. Clearly there are distinct advantages in terms of unit cost, robustness and to some extent size. Sensorless control is quite naturally a subject of significance as far as this work is concerned. Further discussion is deferred until the next section. It is sufficient to state that sensors on the rotor provide gating signals with respect to the rotor position θ_{er}, for the inverter drive.

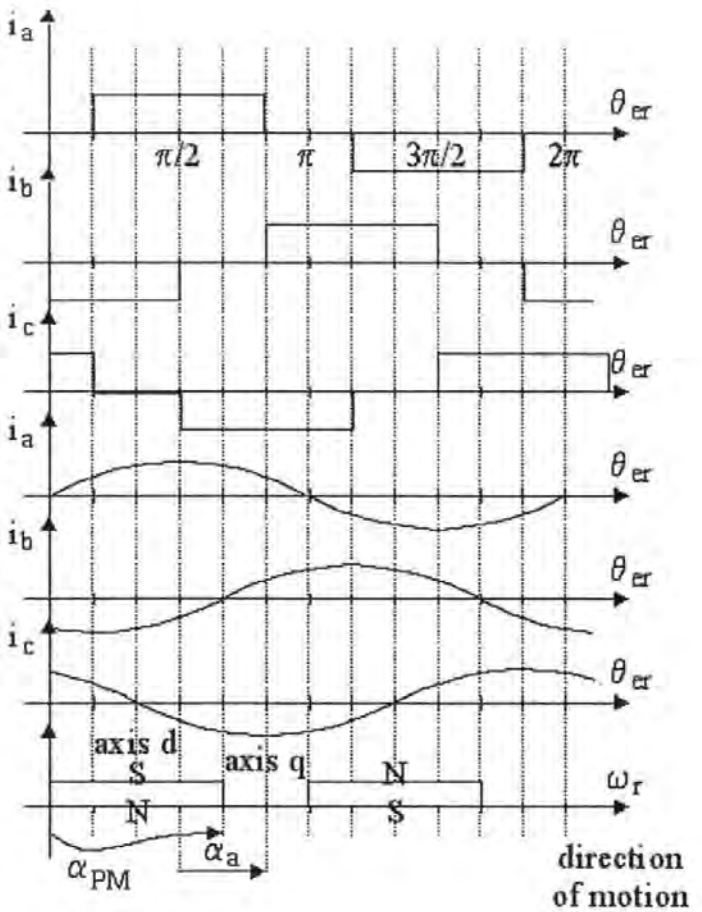

Figure 2.1: *Rectangular or sinusoidal current control; α_a - advance angle*

Rectangular current control is preferred when the PM e.m.f. is nonsinusoidal (trapezoidal) - q = 1, concentrated coil stator windings - to reduce torque pulsations and take advantage of a simpler position (proximity) sensor or estimator.

Scalar control (V / f) is related to sinusoidal current control without motion sensors (sensorless) (Figure 2.2).

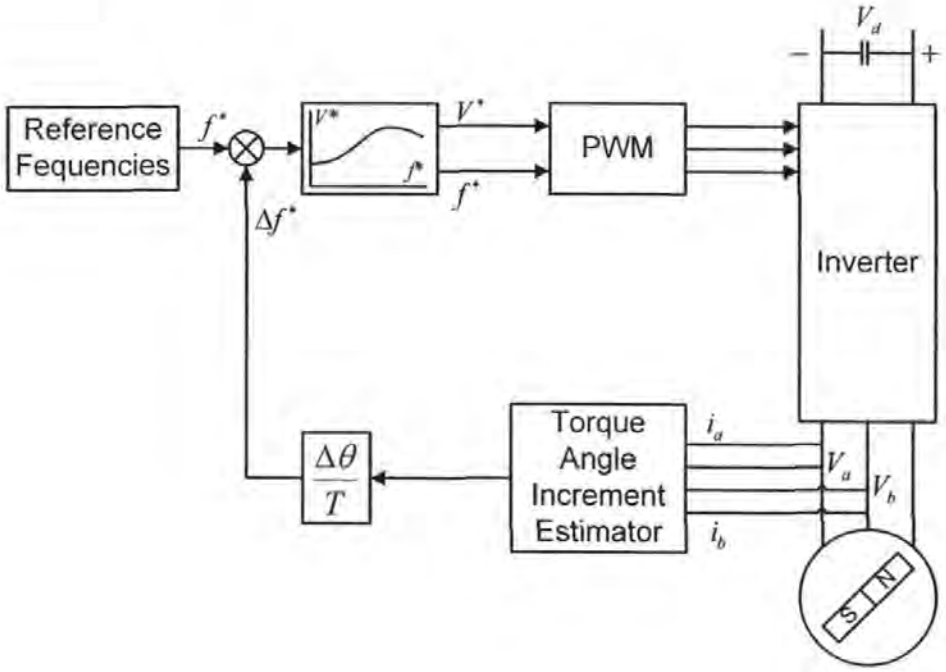

Figure 2.2: V / f (scalar) control for PM - SM (and for RSM) with torque angle increment compensation

The torque angle increment $\Delta\theta$ is estimated and the reference frequency is increased by Δf^* to compensate for the torque variation and keep the motor currents in synchronism with the rotor during transients. A rotor cage is useful to damp the oscillations, as ramping the frequency is limited.

Low dynamics applications may take advantage of such simplified solutions. For faster dynamics applications vector control is used (Figure 2.3).

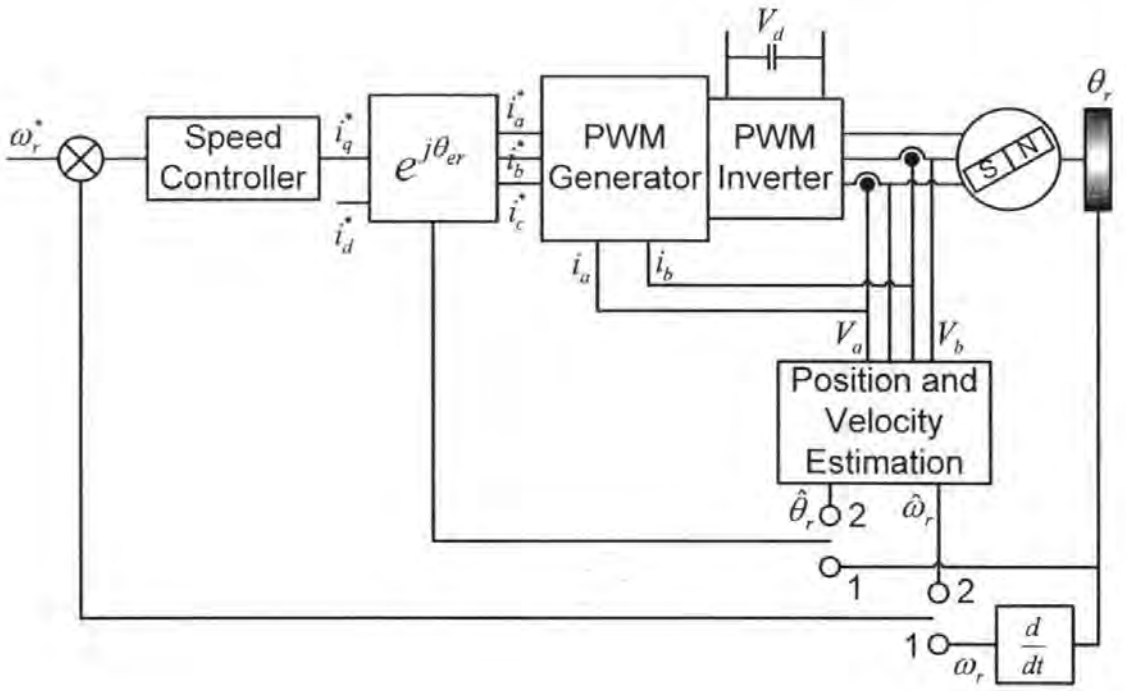

Figure 2.3: *Basic vector control of PM - SM (1) with motion sensor (2) Sensorless*

The rotor position and speed are either measured or estimated (for sensorless drives) and used as velocity feedback (ω_r) and vector rotator (θ_{er}) to generate reference phase currents. Closed loop or open loop PWM is used to "construct" the current (or voltage) waveforms locked into synchronism with the rotor. The PMSM is controlled along the d - q model in rotor co-ordinates which corresponds to D.C. for steady state.

Correlating i_d^* with i_q^* is a matter of optimisation according to some criterion. Vector control is considerably more complicated in comparison with V / f control but superior dynamic performance is obtained (faster torque control, in essence).

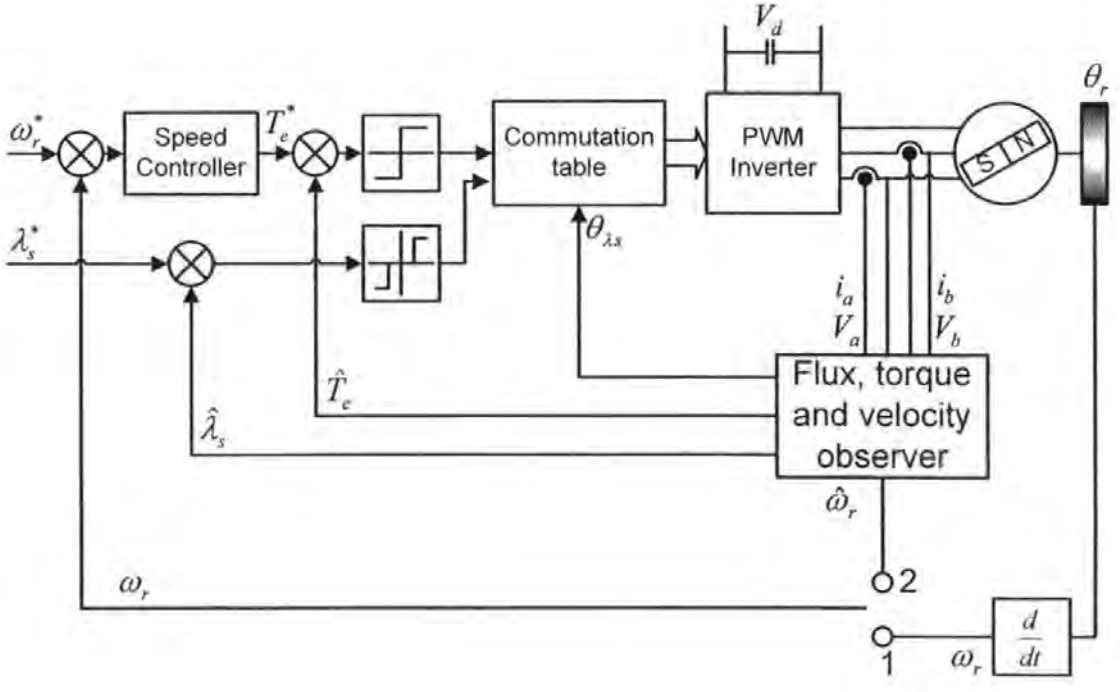

Figure 2.4: *Direct torque and flux control (DTFC) of PM - SMs*

To simplify the motor control, the direct torque and flux control (DTFC for IMs) has been extended to PM - SM (and to RSMs) as torque vector control (TVC) in Sousa and Bose (1994).

The stator flux and torque direct control leads to a table of voltage switchings (voltage vector sequence). Vector rotation has been dropped but flux and torque observers are required. While speed is to be observed, rotor position estimation is not required in sensorless driving.

Again, fast flux and torque control may be obtained even in sensorless driving.

Rectangular current control and sinusoidal current control (through vector control or DTFC) are going to be detailed in what follows for motion sensor and sensorless driving.

2.4.2 The Rectangular Current Control System

In general a rectangular current control system contains the BLDC motor, the PWM inverter and the cascaded motion control loop (Figure 2.5).

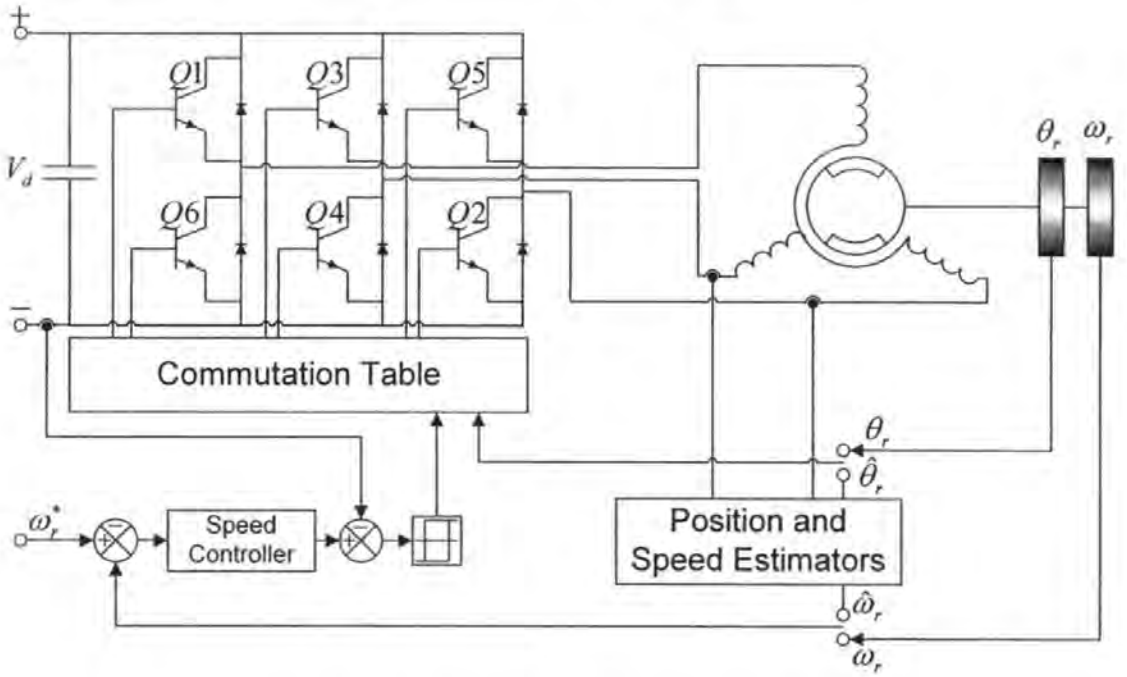

Figure 2.5. *Rectangular current control of BLDC*

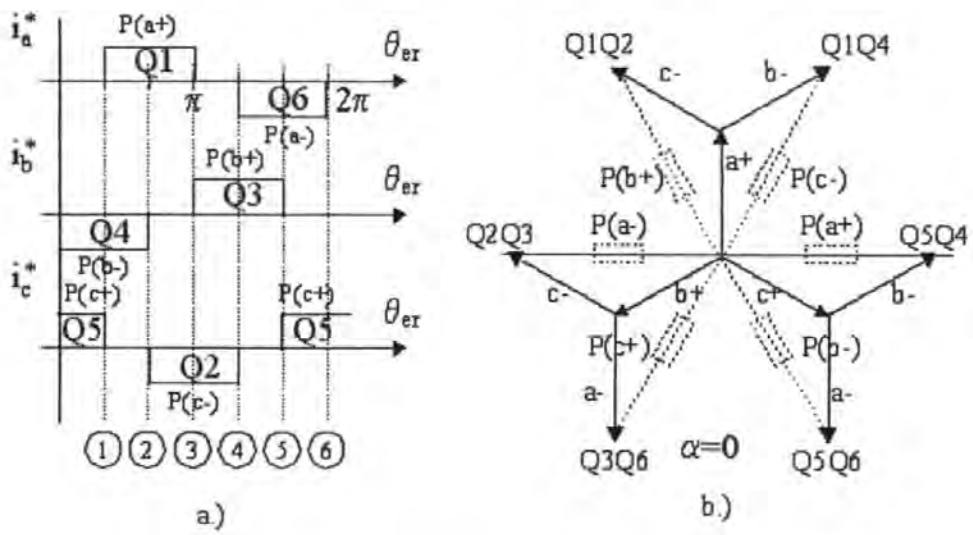

Figure 2.6: *a.) Current sequencing b.) Phase connection*

The current sequence, produced through the inverter provides adequate control, with 120^0 current waveforms. In Figure 2.6 shows also the position of the 6 elements of the proximity sensors with respect to the axis of the phase a for a zero advance angle $\alpha_a = 0$. The location of proximity sensors P(a+, a-, b+, b-, c+, c-) is situated 90^0 (electrical) behind the pertinent phase with respect to the direction of motion.

With two phases conducting the stator active m.m.f. is on from 60^0 to 120^0 with respect to the rotor position. The ideal voltage vector (Figure 2.6) also jumps 60^0 for any phase commutation in the inverter. Each phase is on 120^0 out of 180^0 for the 120^0 conducting strategy.

To reverse the speed the addresses (Power Switches) of the proximity sensor elements action are shifted by 180^0 (P(a+) → P(a-); P(b+) → P(b-); P(c+) → P(c-)). The proximity sensor has been located for zero advance angle to provide similar performance for direct and reverse motion. However, through electronic means, the advance angle may be increased as speed increases to reduce the peak PM flux in the stator phase and thus produce more torque, for limited voltage, at high speeds.

Using the same hardware, 180^0 conduction conditions may also be provided for at high speeds, when all three phases conduct at any time.

2.4.3 Practical Performance

So far the phase commutation transients have been neglected. They however introduce notable torque pulsations at a frequency of $6\omega_r$ (Figure 2.7), which is much lower than those due to current chopping. To account for them complete simulation or testing is required (Vanlandingham, 1985).

There are also some spikes in the conducting phase when the other two phases commute (points A and B on Figure 2.7).

Not shown in Figures 2.6 and 2.7 is the cogging torque produced at zero current by the slot - openings in presence of rotor PMs. Special measures are required to reduce the cogging torque to less than 2 - 5% of rated torque for high performance drives.

Torque Ripple

It is a known fact that an ideal SM - with sinusoidal m.m.f. and constant airgap, when fed with sinusoidal symmetric currents in the stator at frequency $\omega_1 = \omega_r$, produces a constant torque (Nasar et al, 2000).

In reality torque ripple[1] may occur due to:

a. stator (and rotor) slot openings;
b. magnetic saturation caused flux harmonics;
c. current waveforms;
d. PM field pulsations due to stator slot openings (cogging torque).

Items a to c cause the so called electromagnetic pulsating torques while d causes the zero stator current or cogging torque.

Rotor pole (or PM) span correlation with stator slot openings, stator slot inclination or PM pole inclination, fractional q (slots per pole and phase) and, finally, special current waveform shaping through PEC control are all methods to reduce these, basically reluctance, parasitic torques (Lorenz et al, 1994) to less than 1% of rated torques. High

---

[1] Torque ripple investigation requires, in most cases, FEM analysis - two, quasi - two or three dimensional (Lorenz *et al*, 1994)

performance smooth torque drives capable to operate below 20rpm in sensorless control or under 1rpm with position sensor control are thus obtained.

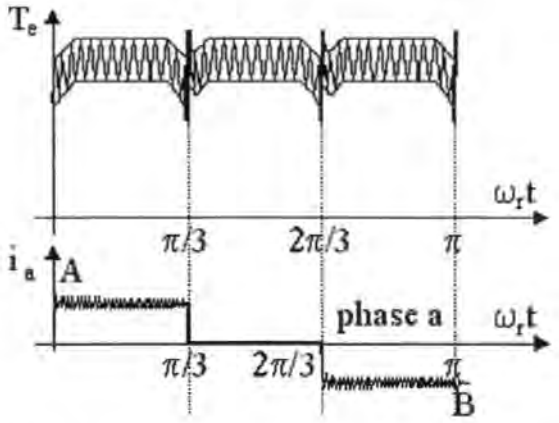

Figure 2.7: *Torque pulsations due to phase commutation*

While at low speeds current chopping is feasible at high speeds, one current pulse remains (Figure 2.8). The current controller gets saturated and the required current is not reached.

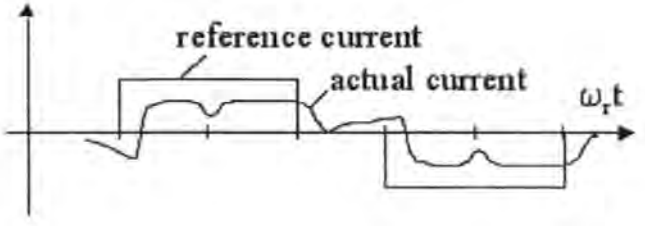

Figure 2.8. Current waveform at high speeds

As the advance angle is zero ($\alpha_a = 0$) there is a delay in "installing" the current and thus, as the e.m.f. is "in phase" with the reference current, a further reduction in torque occurs.

2.5 Sensorless Control

Sensorless control within the literature is intended for speed controlled drives. The alleviation of the sensor requirement reduces hardware costs and improves mechanical reliability. It will be shown here that high performance drives that are designed for either low speed or accurate positioning are not considered within the literature and position sensors are still required (Boldea and Nasar, 1999). It is the aim of this work to relieve the need for position sensors in precision control of the motor armature position. This section serves as a thorough exposition of the technology and methods associated with sensorless control. Since the induction motor has been identified in previous sections of this chapter as inappropriate for small motion control drives, it is not considered within the following text. It is acknowledged that sensorless control of this type of motor has been and continues to be a fruitful area of research. The reader is referred to one of the many research papers available, e.g. Joetten and Maeder (1983), Ferrah *et al* (1992), Xu and Novotny (1991) and Simones and Bose (1995).

2.5.1 Sensorless Control Based on Back EMF Measurement

Sensorless control based on the back EMF is perhaps the best known of the approaches. It is important to draw attention to the fundamental differences between the PMSM and the BLDC motor. These are given in detail in Pillay and Krishnan, (1991). Of concern here is that the back EMF waveforms of the PMSM and the BLDC motor are sinusoidal and trapezoidal respectively. In addition, one phase of the BLDC motor is left non-excited at any given instant, leaving the winding free for use as an interface between the motor and relevant instrumentation for parametric variation measurement. Conversely,

the PMSM has all three windings excited at any one time, exacerbating the problem of direct measurement.

Neutral Point Voltage Computation

It may be demonstrated (Voultoury, 1998) that the phases of the BLDC motor are commutated every 60 electrical degrees. This implies that only six signals are required to drive the BLDC motor. The importance of synchronisation between phase excitation and zero crossing of the back EMF, should at this point be noted; since for efficient commutation of the motor this is a major design goal.

It transpires that the zero crossing point of the trapezoidal back EMF waveform occurs at specific rotor positions. At any given time, two phase currents are opposite, the third is equal to zero.

The stator terminal voltages may be modelled, point x in the diagram has been chosen here, according to the following equations:

$$V_A = E_A + V_N \tag{2.11}$$

$$V_B = Ri_B + L_B \frac{di_B}{dt} + E_B + V_N \tag{2.12}$$

$$V_C = -Ri_C - L_C \frac{di_C}{dt} + E_C + V_N \tag{2.13}$$

where R and L represent the phase resistance and inductance respectively; E represents the phase back EMF; V is the phase voltage referenced to ground and V_N is the stator connection voltage referenced to ground, the suffixes A,B and C represent the motor phases.

It may be seen by inspection of the equations (2.11), (2.12)and (2.13) that at the point where the back EMF of phase A is equal to zero, the following is true

$$V_A = \frac{V_B + V_C}{2} \tag{2.14}$$

or, expressed in another way,

$$V_A = V_N = \frac{V_O}{2} \tag{2.15}$$

In this case, V_A is the terminal voltage of winding A; V_N is the neutral voltage and V_0 is the inverter source D.C. voltage.

A simple comparator circuit may be used to turn the zero crossing points into digital signals for commutation, as demonstrated by Iizuka *et al* (1985). Here it was shown that by delaying these points by 90 electrical degrees, the inverter could be driven directly from the comparator signal. Variable speed control was achieved by chopping the motor with a PWM signal generator with variable duty cycle.

It is perhaps noteworthy to mention that this approach led to the effective solution of sensorless control for air conditioner compressor motors, and in so doing was the first to demonstrate the practical implementation of sensorless control. Since this time, neutral point voltage commutation (or zero crossing commutation) has become the subject of much research and practical implementation. It is probably the most widely used approach to sensorless control of the BLDC motor (Kenjo and Nagomori, (1985), Voultoury, (1998), Gee and Thorn, (1988), Jeong *et al*, (1999)).

Third Harmonic Commutation

An alternative approach to the neutral point voltage computation cited above is that of third harmonic commutation. This approach was originally suggested and patented by Vukosavic, (1990). The approach relies on the fact that the phase angle of the third harmonic of the back EMF is a function of the rotor position. As per the approach above, the back EMF of the non-excited phase winding (equation (2.15)) may be derived.

Examination of the back EMF waveform reveals that it is according to Fourier, an odd function. This observation is extremely important, since it is possible to represent an odd function by its fundamental component and harmonics. Specifically, the trapezoidal waveform may be represented as

$$f(\theta) = \sum_{0}^{\infty} b_{2n-1} \sin((2n-1)\theta) \tag{2.16}$$

where $b_{2n-1} = \dfrac{4E \cdot \sin((2n-1)\alpha)}{\pi(2n-1)^2 \alpha}$

In this equation E is constant, representing the magnitude of the back EMF waveform excursions; n is an integer and α is the angle of the waveform as it traverses from its positive to negative (typically 30° for a 120° commutated motor). From examination of the equations above it may be seen that $f(2)$ contains not only the fundamental component, but also the odd harmonics. Further consideration shows that the amplitudes of the higher harmonics decrease rapidly. By substituting values for n and assuming that α is 30°, $f(2)$ may be shown to be 22% of the fundamental. Since the third harmonic amplitude is far greater than any other, the terminal voltages of the motor may be satisfactorily expressed as

$$\begin{aligned} V_A &= V_1 \sin(\theta) + 0.22\ V_1 \sin\ (3\theta) \\ V_B &= V_1 \sin\left(\theta + \frac{2\pi}{3}\right) + 0.22\ V_1 \sin\ 3\left(\theta + \frac{2\pi}{3}\right) \\ V_C &= V_1 \sin\left(\theta - \frac{2\pi}{3}\right) + 0.22\ V_1 \sin\ 3\left(\theta - \frac{2\pi}{3}\right) \end{aligned} \tag{2.17}$$

where V_1 is the magnitude of the applied voltage.

Summation of these equations will remove the fundamental component, leaving only the harmonics, in fact, the fifth, seventh, eleventh and the thirteenth harmonics are also

cancelled out. It is the third harmonic that constitutes the majority of the remaining waveform. Therefore summation of the terminal voltages actually serves as an efficient extraction of the third harmonic from the terminal voltages. Analysis of the voltage applied by the motor driver, in the same manner as above, will not yield a third harmonic component. This demonstrates that the third harmonic is therefore a product of the back EMF, which is in turn a product of the rotation of the rotor. It follows from this observation that the third harmonic of the back EMF contains information about the rotor position.

This method relies on the premise that the sum of the terminal voltages will contain no fundamental component, in practice however, asymmetry of the motor may be given to introduce some of the fundamental component. A more robust method of extracting the third harmonic of the back EMF is then required. Commonly, the sensed voltages are integrated as an approach to solve this problem, however it is not applicable in this case, since integration results in severe distortion of the position information as the noise is emphasised with respect to the third harmonic. In addition, the use of resistors with wide tolerances and large offset operational amplifiers in the practical system serves to exacerbate the motor asymmetry.

Problems Associated with Back EMF Measurement

There are fundamental problems associated with using the back EMF in sensorless control:

- Since the induced back EMF at zero speed is zero, there can be no means of knowing the rotor position. It is clearly important to have knowledge of the rotor position for stable starting of the motor.

- Below a certain speed, the stator resistance drop and the switching noise of the inverter dominates the stator voltage, the back EMF is very difficult to measure and once again efficient commutation becomes difficult.

Low Speed Operation

There have been approaches adopted to overcome these problems. The problems associated with low speed operation have been dealt with by Ogasawara and Akagi, (1991). This approach was based on the detection of the on/off state of the free wheeling diodes connected in anti-parallel with the power transistors of the inverter, in order to determine the commutation instant.

Starting

Starting the motor represents a serious problem when considering the application of the sensorless control of a permanent magnet motor. Of the proposed methods for starting, some that have been suggested are as follows (Matsui, 1996):

- Use of an auxiliary sensor
- Open loop control
- Specific gate pattern
- Arbitrary starting
- Salient pole motor

A low cost auxiliary sensor, such as a Hall effect device, may be used to detect rotor position at standstill. Within the context of this paper, adding a sensor to the system is clearly undesirable, since the problems discussed earlier, specifically robustness and size once again become a consideration.

Open loop control involves the use of a rotating magnetic field. If the rotor position is predefined then control of the motor from standstill to a point where rotor position may be reliably calculated has been achieved. If the rotor position is not known then the use

of open loop control may result in a temporary reverse of the motor or worse still may lead to starting failure.

Firing of a specific gate pattern of the inverter has been reported in Matsui and Shigyo (1992) and the method involves the high frequency chopping of a given gate pattern. This will align the rotor to the excited phase. Once alignment has been achieved then the open loop starting method may be employed.

Firing of an arbitrary gate pattern is achieved as above but with an arbitrary gate pattern. In some cases, however, this approach may lead to a temporary reverse of the motor. In extreme cases, stable starting cannot be achieved.

Use of the salient pole motor for starting has been described by Wu and Slemon, (1991). This approach not only forms the basis for a robust starting procedure but is the basis of position and speed control based on magnetic saliency discussed below.

2.5.2 Sensorless Control Based on Magnetic Saliency

Control based on back EMF, in most cases, is only practically applicable at mid to high speeds, where inverter losses are negligible in comparison to the magnitude of the induced back EMF. At zero and low speed the EMF is too small and accurate position estimation is not possible. The approach based on magnetic saliency, however, could potentially be applied at any speed, including zero speed (Acarnley *et al* 1985, Ertugrul and Acarnley 1994, Kulkarni and Ehsani 1992). This method is based on the detection of the current gradient, since this is dictated by the incremental inductance of the motor windings, which is in turn dependent upon the rotor position. When the rotor and winding are aligned, the flux linkage is maximised; when rotor and winding are completely misaligned, the magnetic circuit is dominated by the large air gap. If it is

assumed that the mutual inductance between phases is small, then the voltage equation for one phase may be written in terms of the current and flux linkage

$$V = Ri + \frac{d\psi}{dt} \tag{2.18}$$

since the flux linkage may be expressed in terms

$$V = Ri + \frac{d\psi}{di}\cdot\frac{di}{dt} + \frac{d\psi}{d\theta}\cdot\frac{d\theta}{dt} \tag{2.19}$$

then

$$V = Ri + l\frac{di}{dt} + \frac{d\psi}{d\theta}\cdot\frac{d\theta}{dt} \tag{2.20}$$

Rearranging to give an expression for the rate of change of current with respect to time

$$\frac{di}{dt} = \frac{V - Ri - \frac{d\psi}{d\theta}\cdot\frac{d\theta}{dt}}{l} \tag{2.21}$$

the incremental inductance shown in the denominator is rotor position dependent. Hence the rate of change of current is also related to rotor position. It may be seen that this relationship is confounded by the dependence on current and on the back EMF term.

2.5.3 Observer Approaches to Sensorless Control

In the preceding sections the permanent magnet motor and direct sensorless control has been considered. As explained, there are cases whereby the direct approach to sensorless control is impractical, either in the face of unacceptable noise, or in the case of the PMSM no direct method of measurement of machine parameters. It is at this point that alternative methods of deriving motor state are employed. Within this section special consideration to the use of such approaches as the Kalman filter, Luenberger observer and sliding mode is paid, with specific reference to the control of the permanent magnet motor.

Observers

The observer is by definition, a system that recursively estimates the state of another system. The Luenberger observer (Luenberger, 1971), such as the type under discussion here may be used in the state estimation of a deterministic, time varying system. In practical application, there is no direct method of parameter measurement using the PMSM and the measurement of the BLDC parameters can be adversely effected by phenomena such as switching noise. Whilst the Luenberger will not directly compensate noise, it does allow the controller access to such parameters as back EMF or incremental inductance within the motor windings.

Observers, such as those cited in the literature (Consoli *et al* 1994; Matsui 1996; Matsui and Shigyo 1992; Jones and Lang, 1989) have generally either made use of the voltage or the current equations of the motor. The approach developed below is based on the arguments found in Matsui (1996), before the development of the observer may begin a new orthogonal axis, γ-δ must be introduced (Figure 2.9). This hypothetical axis will represent the assumed position of the rotor. The *d-q* axis, as ever, represents the actual rotor position. Introduction of this second frame (i.e. γ-δ) is imperative, since as will be apparent, it must be possible to estimate the error between the estimated and the actual rotor position. It is important to note, therefore, that the state of the electrical machine is independent of the frame of reference from which it is observed.

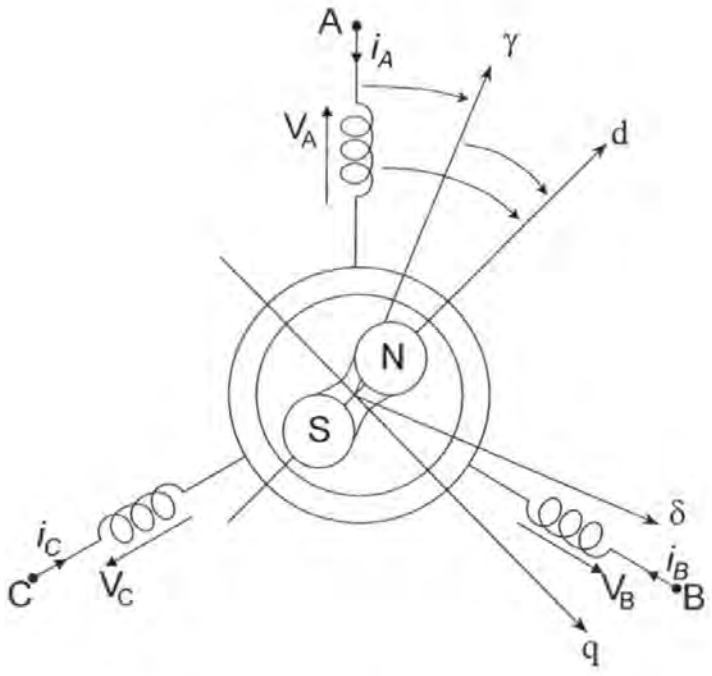

Figure 2.9: *Adding the γ-δ axis*

The aim of the observer is to minimise the angular error, ΔE, between the γ-δ and the *d-q* axis. The angular error may be formally expressed as

$$\Delta E = \theta - \hat{\theta} \tag{2.22}$$

where θ is the actual rotor position (*d-q)* and $\hat{\theta}$ is the estimated rotor position (γ-δ). With slight modification to the voltage equations derived above, the voltage equation of the PMSM may be obtained. In this case R_a and L_a represent the armature resistance and inductance. K represents the EMF constant.

$$\begin{bmatrix} V_A \\ V_B \\ V_C \end{bmatrix} = \begin{bmatrix} R_a + \frac{dL_a}{dt} & L_a Cos\left(\frac{2\pi}{3}\right) & \frac{dL_a}{dt} Cos\left(\frac{4\pi}{3}\right) \\ \frac{dL_a}{dt} Cos\left(\frac{4\pi}{3}\right) & R_a + \frac{dL_a}{dt} & \frac{dL_a}{dt} Cos\left(\frac{2\pi}{3}\right) \\ \frac{dL_a}{dt} Cos\left(\frac{2\pi}{3}\right) & \frac{dL_a}{dt} Cos\left(\frac{4\pi}{3}\right) & R_a + \frac{dL_a}{dt} \end{bmatrix} \times \begin{bmatrix} i_A \\ i_B \\ i_C \end{bmatrix} + K \frac{d}{dt} \begin{bmatrix} Cos\theta \\ Cos\left(\theta - \frac{2\pi}{3}\right) \\ Cos\left(\theta + \frac{2\pi}{3}\right) \end{bmatrix} \tag{2.23}$$

In order to obtain the γ-δ equivalent two-axis model; the transformation matrix, which is based on the assumed rotor position must be used

$$\begin{bmatrix} \gamma \\ \delta \end{bmatrix} = \sqrt{\frac{2}{3}} \begin{bmatrix} Cos\theta & Cos\left(\theta - \frac{2\pi}{3}\right) & Cos\left(\theta + \frac{2\pi}{3}\right) \\ -Sin\theta & -Sin\left(\theta - \frac{2\pi}{3}\right) & -Sin\left(\theta + \frac{2\pi}{3}\right) \end{bmatrix} \times \begin{bmatrix} A \\ B \\ C \end{bmatrix} \tag{2.24}$$

By following conventional control, the γ axis current is controlled to be zero and the generated torque may be expressed

$$\begin{bmatrix} V_\gamma \\ V_\delta \end{bmatrix} = \begin{bmatrix} R + \frac{dL}{dt} & -L\dot{\theta}_C \\ L\dot{\theta}_C & R + \frac{dL}{dt} \end{bmatrix} \begin{bmatrix} i_\gamma \\ i_\delta \end{bmatrix} + K_E \theta \begin{bmatrix} -Sin\Delta\theta \\ Cos\Delta\theta \end{bmatrix} \tag{2.25}$$

$$\tau = K_T i_\delta \cos\Delta\theta \tag{2.26}$$

Where

$$K_E = \sqrt{\frac{3}{2}} K \ , \dot{\theta} = \frac{d\theta}{dt} \ , \dot{\theta}_C = \frac{d\theta_C}{dt} \ , R = R_a \ , L = \frac{3}{2} L_a$$

If the ideal condition is assumed, then ΔE=0 and $\dot{\theta}_e = \dot{\theta}$, from here an estimation for the rotor speed and position may be developed by rearranging (2.24).

$$\begin{bmatrix} V_{\gamma M} \\ V_{\delta M} \end{bmatrix} = \begin{bmatrix} R + \frac{dL}{dt} & -L\dot{\theta}_C \\ L\dot{\theta}_C & R + \frac{dL}{dt} \end{bmatrix} \begin{bmatrix} i_\gamma \\ i_\delta \end{bmatrix} + K_E \theta \begin{bmatrix} 0 \\ 1 \end{bmatrix} \tag{2.27}$$

From this equation the hypothetical speed, θ_e may be obtained by the following

$$\dot{\theta}_e = \frac{v_{\delta M} - \left(R + \frac{dL}{dt}\right) i_\delta}{K_E + L i_\gamma} \tag{2.28}$$

From the assumption that $\Delta E = 0$ it may be stated that $v_{\delta M} = v_\delta$. From (2.27)

$$\dot{\theta}_e = \frac{v_\delta - \left(R + \frac{dL}{dt}\right) i_\delta}{K_E + L i_\gamma} \tag{2.29}$$

In reality, the ideal operating condition is not constant; corresponding correction of the hypothetical speed is required. Consider the voltage applied to the γ axis, under ideal conditions it may be expressed from (2.26) as

$$v_{\gamma M} = \left(R + \frac{dL}{dt}\right) i_\gamma - L \dot{\theta}_e i_\delta \tag{2.30}$$

This voltage is hypothetical, but may be calculated by transforming the actual current by equation (2.23). In a similar manner, the actual applied voltage may also be obtained from equation (2.24). The γ axis voltage difference may be obtained as

$$\Delta v_\gamma = v_\gamma - v_{\gamma M} = -\dot{\theta} K_E \sin \Delta\theta \tag{2.31}$$

assuming that the rotor is not stationary, and that the angular error $\Delta\theta$ is approximately zero, then (2.30) may be approximated as

$$\Delta v_\gamma = -\dot{\theta} K_E \Delta\theta \tag{2.32}$$

This equation is critical in that it demonstrates the direct relationship between the angular error and the voltage difference. In order to control the position of the rotor, a simple algorithm may be applied to increase or decrease the applied voltage according to the position error. As stated this approach has been documented in (Matsui, 1996). Control with the voltage observer was achieved above a threshold of approximately 100 rpm. Below this speed, the voltage observer was found to be incapable of satisfactory control.

This was attributed to the fact that current ripple increases with reduced speed, and by virtue of this, the variation in estimated speed increased. Secondly, it was shown that in the lower speed range, the applied voltage was correspondingly lower and the effect of dead time, voltage drop across the switching devices and power feeder was more significant. Whilst in the literature the effect of dead time was compensated for, the voltage drop was not.

A second observer based instead on the current model was subsequently suggested within the same work. Within this model the current input to the motor was measured using a current sensor and fed into the observer. Since the current based observer did not use the voltage information, the controller was free of the errors introduced by inverter inaccuracy. It was shown that the current model based control was more stable than the voltage based alternative.

There have been other forms of observer employed in sensorless control of rotor position and velocity. One method proposed (Wu and Slemon, 1991) uses motor current harmonics to calculate the inductance matrix, which contains the rotor position information. This method capitalises on the fact that the harmonic voltage vector is equal to the difference between the inverter output voltage vector and the average output voltage vector. Another rather sophisticated approach has been proposed by Cardoletti and Cassat (1992) and later, a modified approach by Corley and Lorenz, (1998), this approach estimates flux, position and speed from zero through to high speed. This method is based on tracking the magnetic saliency via an inverter generated high frequency voltage, which serves to produce high frequency currents that vary with rotor position. The sensed currents are then demodulated using a heterodyning technique to

produce a signal that is roughly proportional to the difference between the actual rotor position and estimated rotor position.

It is interesting to note that a disturbance observer based disturbance cancellation has been used as a method to achieve robust control (Tomita *et al,* 1998). In this method a disturbance is added to the open loop system, and is estimated by the observer. The estimated disturbance is then fed back to cancel the actual disturbance. It has been shown in Mita *et al*, (1998) that this method actually only amounts to an alternative integral controller and thereby robust stability is not assured. In order to achieve true robust stability, the observer must include a filter based on robust control theory. Such an approach would be to include the use of deterministic robust control or artificial intelligence based control.

Kalman Filters

An alternative approach to the Luenberger observer in the estimation of system states is to employ the Kalman filter. In the case of sensorless motor control, however, the Kalman filter is not sufficient since the equations of the motor are non-linear. Where the Kalman filter is an optimum estimator, the Extended Kalman filter (EKF) is not; since the nonlinear equations of the system are linearised about the current estimated state trajectory. In this case, optimality is defined as the minimisation of a mean square error cost function. Despite this, the EKF has been used to solve the problems associated with sensorless control (Dhaouadi *et al*, (1991), Beierke S. *et al*,(1997) Kettle *et al*, (1998) Navrapescu and Craciunescu, (1997)). Within this context, the EKF is able to estimate motor states despite the fact that the measured input signals may be corrupted by random noise and may be subject to measurement error.

The process and measurement noise is assumed to be uncorrelated, having zero mean and normal gaussian distribution Kettle *et al*, (1998).

It will be shown later in Chapter 3 that the motor may be described by the following

$$x=\begin{bmatrix}\theta\\ \omega\\ i\end{bmatrix},\quad \Phi=\begin{bmatrix}0 & 1 & 0\\ 0 & -\frac{B}{J} & \frac{K_m}{J}\\ 0 & -\frac{K_e}{L} & -\frac{R_a}{L}\end{bmatrix},\quad \Gamma=\begin{bmatrix}0\\ -\frac{1}{J}\\ \frac{1}{L}\end{bmatrix} \tag{2.33}$$

The feedback measurement is to be the back EMF of the motor. Whilst the motor model assumes that the back EMF will be a linear function of speed, it may be sensibly expected that the back EMF when the motor is in steady state will take the form as discussed earlier in this chapter, therefore the measurement matrix $H\left(\hat{x}_{k|k-1}\right)$ will be of the form

$$H\left(\hat{x}_{k|k-1}\right)=\begin{bmatrix}1 & 0 & 0\\ 0 & \lambda cos\left(\hat{\theta}_{k|k-1}\right) & 0\\ 0 & 0 & 1\end{bmatrix} \tag{2.34}$$

Note that in the above equations, V is presented as an input and *i* as a state variable. This has been adopted primarily because the applied control signal is likely to be a voltage under a pulse width modulation regime.

The state equations and Kalman filter may be used to estimate the motor states; in this case rotor position and velocity. If using the EKF for state estimation then it may be used as an observer. The estimation of rotor position may be used for commutation and estimated velocity used for regulation of speed. Approaches to sensorless control cited in the references above have all employed and confirmed the validity of this approach.

Extended Kalman Filter for State Estimation

The motor model describes a deterministic system with additional stochastic disturbances (i.e. the external load torque). The EKF produces a generalised weighted least squares solution for the state estimate with a minimum expected square error. When system states are inaccessible, the estimates of state generated by the EKF may be used instead. In such a case, use of the EKF estimates will yield the optimal feedback system in the expected mean square sense.

Used as an observer, the filter inputs will be the plant outputs (z) and the deterministic inputs (u); as per the definition of the Luenberger observer. The filter outputs will be the optimal plant state estimate $\hat{x}_{(k|k)}$. It may be shown, (Furuhashi *et al*, 1992), that if an observer's gain sequence is chosen to be $G = \Phi K$, then the observer is a Kalman filter.

Of importance to note is that the EKF is sub-optimal. Therefore, the established relationship between the Kalman filter gain and the observer gain sequence, should not infer that using the Kalman filter approach to determining observer gains for state estimation is necessarily better than design by stipulation of desired convergence properties through use of a eigenvalue placement method.

Sliding Mode

The use of sliding mode for motor control has been well documented e.g. Furuhashi et al (1992), Lin and Chiu (1998), Utkin (1993). It has been shown that variable structure control demonstrates the following advantages; order reduction, decoupling design procedure, disturbance rejection, insensitivity to parameter variation and simple implementation (Utkin, 1993), for these reasons, sliding mode will feature heavily within this work and supporting theory is treated rigorously in Chapter 5. At this point, however,

sliding mode is introduced as a means to achieve sensorless control of the synchronous motor. This section is begun by the introduction of principles associated with sliding mode control of the synchronous motor, before describing how it may be employed in state estimation. Pre-empting the discussion in Chapter 5, sliding mode may best be described by a diagram (Figure 2.10), Figure 2.10.a is the phase plane trajectory of a system. Figure 2.10.b represents the same system with negative feedback sign. It can be seen that Figure 2.10.c is a combination of these two systems. Figure 2.10.c illustrates how the combination of these two systems results in stability. The straight line intersecting the axis is known as the sliding plane. Figure 2.10.d illustrates the "chattering" phenomenon that is caused by finite switching times between the two systems.

The motor may be expressed in the *d-q* axis with the following differential equations:

$$V_d = ri_d + L_d \frac{di_d}{dt} + L_d i_q \omega \tag{2.35}$$

$$V_q = ri_q + L_q \frac{di_q}{dt} + \left(L_q i_d + \theta\right)\omega \tag{2.36}$$

$$T = J\frac{d\omega}{dt} + B\omega \ , \quad T = i_q\left(\left(L_d - L_q\right)i_d + \phi\right) \tag{2.37}$$

$$\frac{d\alpha}{dt} = \omega \tag{2.38}$$

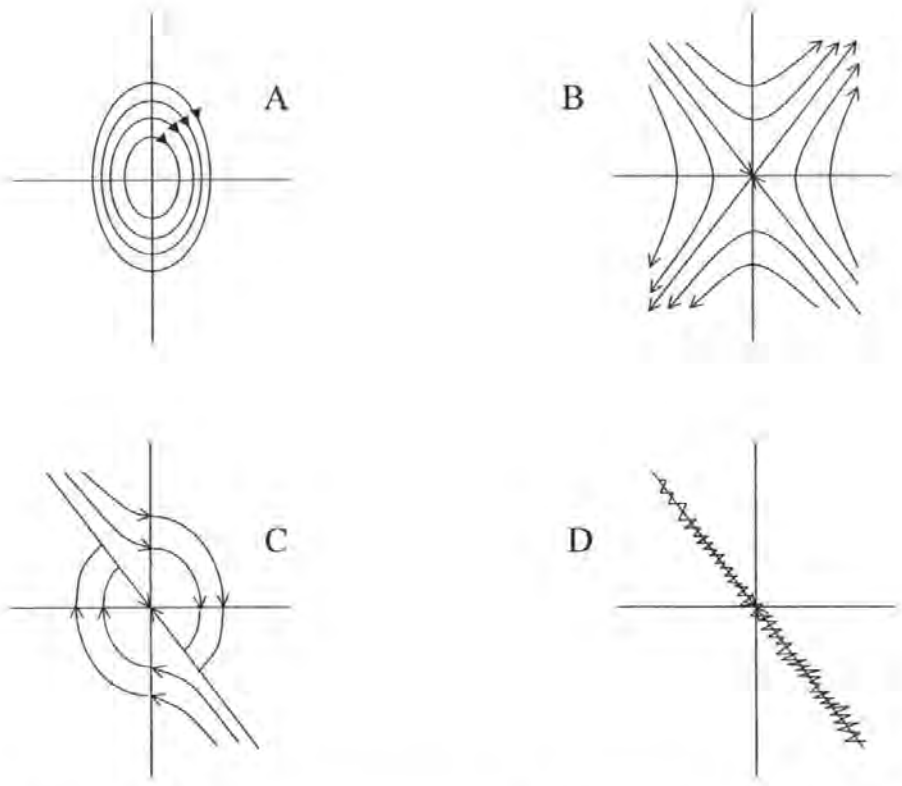

Figure 2.10: *The principle of sliding mode a)Phase portrait of system displaying limit cycles b) Phase portrait of unstable system c)Phase portrait of combined system d)Chattering*

From previous work, it may be written

$$\begin{bmatrix} V_d \\ V_q \end{bmatrix} = k \cdot \begin{bmatrix} V_A \\ V_B \\ V_C \end{bmatrix} \quad \text{and} \quad \begin{bmatrix} i_d \\ i_q \end{bmatrix} = k \cdot \begin{bmatrix} i_A \\ i_B \\ i_C \end{bmatrix} \tag{2.39}$$

where k is the Park transformation matrix (Krause *et al*, 1995). The suffixes A, B and C represent the stator phase windings. The goal of the sliding mode controller will be to make the error between the angular speed and a reference speed equal to zero. The deviation from the desired motion may be described by

$$S_1 = c[\omega_0 - \omega(t)] + \frac{d}{dt}[\omega_0 - \omega(t)] \tag{2.40}$$

where c is a positive real value; ω_0 is a reference input and $\omega(t)$ is the rotor velocity. The next objective for the controller will be to make the component i_d equal to some reference input i_0.

$$S_2 = i_0 - i_d \tag{2.41}$$

Let the voltages of the inverter, V_A,V_B and V_C constitute a three phased balanced system such that

$$S_3 = \int_0^T (V_A + V_B + V_C)dt \tag{2.42}$$

S_3 should equal zero for all T.

The control $V^T = (V_A \quad V_B \quad V_C)$ should enforce the sliding mode along the manifold $S^T = (S_1 \quad S_2 \quad S_3)$. The equations of motion of the system (2.35) and (2.36) projected onto s sub-space are derived by the differentiating vector s.

$$\frac{ds}{dt} = F + DV \tag{2.43}$$

where $F^T=(f_1 , f_2 , f_3)$. $f_3=0$ and the scalars f_1 and f_2 depend on the motor state and reference inputs, load torque and their time derivatives. D will depend upon the task at hand, the approach documented by Lin and Chiu (1998), is examined in order to continue development from here.

The problem associated with sliding mode is that of 'chattering'. Sliding mode relies on the infinite switching speed of the controller. In a practical system, this is not realisable and the result is that the manipulated variable will be discontinuous and overshoot around the sliding manifold will occur. One approach to alleviate the 'chattering phenomenon' was discussed by Utkin, (1993). In this method a low pass filter is added to the controller, thus introducing a boundary layer around the manifold (Figure 2.11).

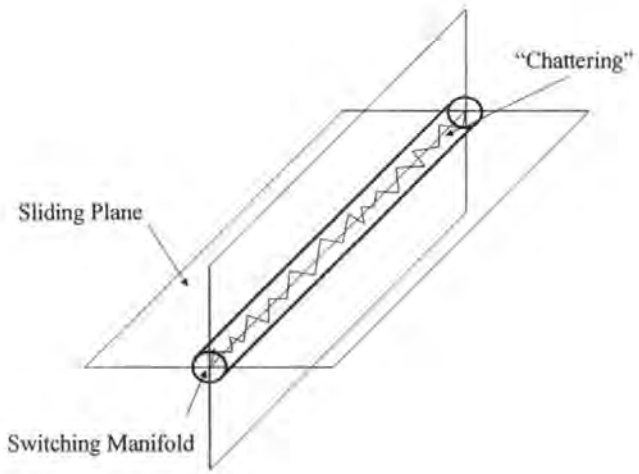

Figure 2.11: *Boundary layer normalisation*

The Sliding Mode Observer

The alternative method of avoiding chattering is to avoid introducing the control effort from the sliding mode directly to the motor. If, instead an observer is introduced and the sliding mode is allowed to occur within that, then no stress will be applied to the motor. The sliding mode observer maintains the salient feature of the sliding mode, which is being robust to disturbance.

Since the switching signals of the sliding mode observer contain the induced voltages of the motor, rotor position and velocity estimation may be achieved directly from the switching signals. The estimated position may be used directly for locating the position of the rotor, however estimated velocity is heavily contaminated by switching signal noise.

Therefore the adaptive sliding mode observer is introduced. The switching ripples of the sliding mode observer have no effect on this method. It may be seen that the equation of the motor might be rewritten as:

$$\frac{d}{dt}\begin{bmatrix} i_{qs} \\ i_{ds} \end{bmatrix} = \begin{bmatrix} -\frac{R_s}{L_{ss}} & 0 \\ 0 & -\frac{R_s}{L_{ss}} \end{bmatrix} \times \begin{bmatrix} i_{qs} \\ i_{ds} \end{bmatrix} + \begin{bmatrix} -\frac{1}{L_{ss}} & 0 \\ 0 & -\frac{1}{L_{ss}} \end{bmatrix} \times \begin{bmatrix} V_{qs} \\ V_{ds} \end{bmatrix} - \frac{3k_e}{2I}\begin{bmatrix} -\omega \sin\theta \\ \omega \cos\theta \end{bmatrix} + \begin{bmatrix} W_q \\ W_d \end{bmatrix} \tag{2.44}$$

where W represents the disturbance due to parameter variations and V_i represents the induced back EMF. From this equation, the observer may be constructed as follows

$$\frac{d}{dt}\hat{i}_s = H\hat{i}_s + IV_S + J\hat{V}_i + K1\left(\hat{i}_s - i_s\right) \tag{2.45}$$

where ^ denotes an estimated value, K the switching gain and

$$1\left(\hat{i}_S - i_S\right) = \left(\text{sgn}\left(\hat{i}_d - i_d\right), \text{sgn}\left(\hat{i}_q - i_q\right)\right)^T \tag{2.46}$$

The sliding manifold is realised by the switching function as

$$S = \hat{i}_s - i_s = 0 \equiv e_s \tag{2.47}$$

Once this has been established then the error equation may be obtained by subtracting (2.45) from (2.46) to give

$$\dot{e}_s = H e_s + J(\hat{V}_i - V_i) + K1(e_s) \tag{2.48}$$

Once the switching gain is chosen correctly the following will hold true

$$\dot{e}_s = e_s = 0 \tag{2.49}$$

and may be rewritten as

$$z = -K1(e_s) \tag{2.50}$$

The signal z will contain information of the induced voltages of the motor. As seen previously, position and velocity may be estimated from this signal.

It is shown in Furuhashi *et al* (1992) that the observer may be made adaptive by replacing the error function by an estimation of the induced voltage and applying an adaptive scheme.

The sliding mode observer can be shown to differentiate the output error, however it incorporates a low pass filter with a cutoff frequency which varies with the measurement noise. This will alleviate the problem associated with finding the speed by differentiating a position signal that is contaminated by the switching ripples, and speed measurement may take place.

2.5.4 Artificial Intelligence in Sensorless Control of Drives

Until this point, observers for sensorless control have been considered. It has been demonstrated how at reasonable speeds, accurate control of rotor speed and position has been achieved. The application of artificial intelligence (AI) techniques has, until recently, seldom been considered in control of drive systems (Stronach and Vas , 1998), fewer still in the control of the sensorless permanent magnet machine. Impetus at this point is therefore shifted from the practical implementation and results achieved with the methods discussed so far, to the perceived benefits that AI techniques are likely to yield.

The control systems considered so far have required knowledge of the motor. This knowledge is represented as a set of differential equations that rapidly become complex and they are based around many assumptions about the system. In addition, these models may depend upon knowledge of motor parameters that are either difficult to measure, or change significantly when the system is in use. In Vas (1999) various AI techniques including associative memory networks, artificial neural networks and neuro-fuzzy networks were implemented in a sensorless drive control system in order to demonstrate their ability to cope with sensorless control without explicit *a priori* knowledge of the motor. Torque ripple of the motor can be minimised by the application of optimum current waveforms (Carlson R. *et al,* 1992), however the optimum waveform changes

with load (Kocybik and White, 1997). The optimum waveform therefore must be calculated with knowledge of the load, alternatively, the waveform generator must be made adaptive. Work in Kocybik and White, (1997) demonstrated the effective removal of torque ripple from the system through calculation of the optimum waveform. It may noteworthy to point out that one of the principle limiting factors of the observers application (discussed above) was the occurrence of greater torque ripple at low speed. It is clear that minimisation of torque ripple is therefore attractive.

In Tzes *et al* (1995), the back propagation neural network in the specialised learning mode was employed in order to compensate the effects of friction in a micro-maneuvering system. Whilst this drive was not specifically sensorless, the principle of employing AI techniques was demonstrated, since an explicit model of the system was not available and a sufficient model would have been very difficult to derive.

In Denai and Hazzab (1997), Ishigame *et al* (1993), Suyitno *et al* (1993), fuzzy logic is employed in the controller as per the AI improved observers from the list above. Of special relevance to this paper is the use of fuzzy logic in order to improve the behavior of a sliding mode controller. As pointed out in Tzes *et al* (1995), there have been many attempts to eliminate chattering; but of these attempts, none have simultaneously considered robustness. In addition the observation noise caused by high gain of the controller has not been compensated for. The papers Ishigame *et al* (1993) and Suyitno *et al* (1993) introduce a non-linear system which is composed of the weighted average of linear systems with fuzzy inference. The chattering phenomenon is shown to be reduced by combining the sliding mode control input and the equivalent control input through use

of fuzzy inference. This approach is shown to improve the performance of a sliding mode controller.

2.6 Discussion

This chapter has served to introduce the permanent magnet synchronous motor and the brushless D.C. motor and explain why these motors are most attractive to drive applications. Further, their differences have been explained and common methods available for their control have also been discussed. It has been seen that position sensing devices are required not only for speed control, but more fundamentally for efficient commutation of the motor. Sensorless methodologies for control of the brushless D.C. motor specifically have been discussed. The direct measurement methods have been based on the premise that the motor will be symmetrical, unfortunately they tend not to be, and in high accuracy applications some form of compensation is required. The PMSM is known to produce a reduced torque ripple, and has therefore it too has been the subject of much interest. The unfortunate aspect of the PMSM is that all three windings of the motor are energised at any given instant. Direct measurement of motor parameters, therefore, becomes difficult and some form of estimation is required. Estimation, within this context, is described as the process of extracting information unavailable for measurement, for any reason, from the available data. This data may contain measurement error and may also be influenced by external random disturbances.

The observer approach has been shown to provide reasonable performance when estimating speed. The accuracy of the full state Luenberger Observer is as before contingent by the accuracy of the plant model and knowledge of the plant parameters, the motor when coupled to a nonlinear load is likely to demonstrate very different dynamics

to the idealised model. The Kalman filter approaches alleviate the need for a highly accurate model, however, acquisition of the initial covariance matrices are often difficult since statistical descriptions of the sensor errors are required (Dhaouadi *et al.*,1991). The sliding mode observer has been seen to perform very much better than the Luenberger observer, this is due to the invariance property of the sliding mode. The chatter phenomenon does not cause any problems within the implementation of an observer, since no physical properties need consideration. Sliding mode is invariant only to a class of uncertainty, and therefore the observer error dynamics may be effected by certain types of exogenous disturbance. The sliding mode has the advantage over the Kalman filter that no initial covariance matrix is required, but very similar performance can be obtained. (In fact it will be described in Chapter 6 that the Kalman filter and sliding mode observer have the same convergence properties).

The remainder of this work therefore concentrates on the use of the sliding mode and the modelling and identification of the test system in order to arrive at a low speed position sensorless control drive.

2.7 References

Acarnley P., Hill R. and Hooper C., 1985, 'Detection of Rotor Position in Stepping and Switched Motors by Monitoring of Current Waveforms', IEEE Trans. Industrial Electronics, 32(3), 215-221

Beierke S., Vas P., Simor B. and Stronach A.F., 1997, 'DSP Controlled Sensorless AC Vector Drives using the Extended Kalman Filter', Proc PCIM 97, Nuremburg, 31-41

Boldea I. and Nasar S.A. 1999, 'Electric Drives', CRC press

Bolton W., 1999, 'Mechatronics', Addison Wesley Longman

Cardoletti L. and Cassat A., 1992, 'Sensorless Position and Speed Control of a Brushless DC Motor from Start-up to Nominal Speed', EPE Journal, 2(**1**), 25-34

Carlson R. Lajoie-Mazenc M. and Fagundes J. C. dos S., 1992, 'Analysis of Torque Ripple due to Phase Commutation in Brushless DC Machines', IEEE Trans. on Industry Applications, 28(**3**), 632-638

Consoli A., Musumeci S., Raciti A. and Testa A., 1994, 'Sensorless Vector and Speed Control of Brushless Motor Drives', IEEE Trans. Industrial Electronics. 41(**1**), 91-96.

Corley M. and Lorenz R., 1998, 'Rotor Position and Velocity Estimation for a Salient Pole Permanent Magnet Synchronous Machine at Standstill and High Speed', IEEE Trans. Industry Applications, 34(**4**), 752-757

Denai M. and Hazzab A., 1997, 'Real Time Fuzzy PID Control of a Separately Excited DC Motor', 4th Int. Symp. On Methods and Models in Automation, 819-824

Dhaouadi R., Mohan N. and Norum L.,1991 'Design and Implementation of an Extended Kalman Filter for the State Estimation of a Permanent Magnet Synchronous Motor', IEEE Trans. Power Electronics, 6(**3**), 491-497

Ertugrul N. and Acarnley P., 1994, 'A New Algorithm for Sensorless Operation of Permanent Magnet Motors', IEEE Trans. Industry Applications, 30(**1**), 126-133

Ferrah A., Bradley K.J. and Asher G.M., 1992, 'An FFT Based Novel Approach to Noninvasive Speed Measurement in Induction Motor Drives', IEEE Trans. on Instrumentation and Measurement, 41(**6**), 797-802

Furuhashi T, Sangwongwanich S. and Okuma S., 1992, 'A Position and Velocity Sensorless Control for Brushless DC Motors Using an Adaptive Sliding Mode Observer', IEEE Trans. Industrial Electronics, 39(**2**), 89-95

Gee D. and Thorn J., 1988, 'Brushless Permanent Magnet Motor System', Emerson Electric Co., United States Patent No. 4743815

Iizuka K. Uzuhashi H. Kano M. Endo T. and Mohri K., 1985, 'Microcomputer Control for Sensorless Brushless Motor', IEEE Trans. Industry Applications, IA-21(3), 595-601

Ishigame A. Furukawa T. Kawamoto S and Taniguchi T., 1993, 'Sliding Mode Controller Design Based on Fuzzy Inference for Non-Linear Systems', IEEE Trans on Industrial Electronics, 40(1), 64-70

Jeong S. In-joong H. and Doo-hee J., 1999, 'Sensorless Brushless DC Motor', Samsung Electronics Ltd, United States Patent 5886486

Joetten R. and Maeder G., 1983, 'Control Methods for Good Dynamic Performance Induction Motor Drives Based on Current and Voltage as Measured Quantities', IEEE Trans. on Industry Applications. **IA-19**. 356-363.

Jones L.A. and Lang J.H., 1989, 'A State Observer for the Permanent Magnet Synchronous Motor', IEEE Trans. on Industrial Electronics, 36(3), 374-382

Kenjo T. 1985. 'Stepping Motors and their Microprocessor Controls', Clarendon Press

Kenjo T. and Nagomori S., 1985, 'Permanent-Magnet and Brushless DC Motors', Clarendon Press

Kettle P., Murray A. and Moynihan F, 1998. 'Sensorless Control of a Brushless DC motor using an Extended Kalman Estimator', Proc PCIM 98, Nuremburg, 385-392

Kocybik P. and White P., 1997, 'Influence of Armature Reaction on Torque Ripple in Permanent Magnet Machines', Proc PCIM 97, Nuremburg, 149-156

Krause P.C., Wasynczuk O., Sudhoff S.D., 1995, 'Analysis of Electric Machinery', IEEE Press

Kulkarni A.B. and Ehsani M., 1992, 'A Novel Position Sensor Elimination Technique for the Interior Permanent Magnet Synchronous Motor Drive', IEEE Trans. on Industry Applications. 28(1), 144-150.

Lin F.-J and Chiu S.-L, 1998, 'Adaptive Fuzzy Sliding Mode Control for PM Synchronous Servo Motor Drives', IEE Proceedings Part D: Control Theory and Applications, 145(**1**), 63-72

Luenberger D.G., 1971, 'An introduction to observers', IEEE Trans. on Automatic Control, **16**, 596-602

Lorenz R., Lipo T.A. and Novotny D.W., 1994, 'Motion Control with Induction Motors', IEEE Proceedings, 82(**8**), 1215-1240

Matsui N., 1996, Sensorless PM Brushless DC Motor Drives, IEEE Trans. Industrial Electronics, 43(**2**), 300-308

Matsui N. and Shigyo M., 1992, 'Brushless DC Motor Control without Position and Speed Sensors', IEEE Trans. Industry Applications, 28(**1**), 120-127

Miller T.J.E., 1993. 'Brushless Permanent Magnet Machines', Oxford University Press. Monographs in Electrical and Electronic Engineering No. 21

Moczala H., Draeger J., Krauss H., Schock H and Tillner S., 1998, 'Small Electric Motors', IEE. Power and Energy Series. 26

Mita T. Hirata M, Murata K. and Zhang H., 1998, 'H_∞ Control Versus Disturbance Observer Based Control', IEEE Trans. Industrial Electronics, 45(**3**), 448-495

Nasar S.A., Boldea I. and Unnewehr L.E. 2000. 'Permanent Magnet, Reluctance and Self Synchronous Motors', CRC Press

Navrapescu V. and Craciunescu A., 1997, 'A New Discrete Speed Estimator Based on Kalman Theory', Proc PCIM 97, Nuremburg, 43-48

Ogasawara S. and Akagi H., 1991, 'An Approach to Position Sensorless Drive for Brushless DC Motors', IEEE Trans. Power Electronics, 27(**5**), 928-933

Pillay P. and Krishnan R., 1991, 'Application Characteristics of Permanent Magnet Synchronous and Brushless D.C. Motors for Servo Drives', IEEE Trans. Industry

Applications, 27(5), 986-996

Simones G. and Bose B.K, 1995, 'Neural Network Based Estimation of Feedback Signals for a Vector Controlled Induction Motor Drive', IEEE Trans. on Industry Applications, 31(3), 620-629

Sousa G.D. and Bose B.K., 1994, 'A Fuzzy Set Theory Based Control of Phase-Controlled Converter DC Machine Drive', IEEE Trans. IA-30(1), 1994, 34-44

Stronach A.F. and Vas P., 1998, 'Design, DSP Implementation, and Performance of Artificial-Intelligence Based Speed Estimators for Electromechanical Drives', IEE Proceedings Part D: Control Theory and Applications, 145(2).

Subrahmanyam V.1996. 'Electric Drives – Concepts and Applications', McGraw-Hill

Suyitno A., Fujikawa J., Kobayashi H. and Dote Y. 1993, 'Variable Structure Robust Controller by Fuzzy Logic for Servomotors', IEEE Trans. on Industrial Electronics, 40(1), 80-88

Tomita M. Senjyu T. Doki S. and Okuma S., 1998, 'New Sensorless Control for Brushless DC Motors Using Disturbance Observers and Adaptive Velocity Estimations', IEEE Trans. Industrial Electronics, 45(2), 274-282

Tzes A. Peng P.-Y and Houng C.-C., 1995, 'Neural Network Control for DC Motor Micro-manoeuvring', IEEE Trans. Industrial Electronics, 42(5), 516-523

Utkin V.I., 1993, 'Sliding Mode Design Principles and Applications to Electric Drives', IEEE Trans. on Industrial Electronics, 40(1), 23-36

Vanlandingham H.F., 1985, 'Introduction to Digital Control Systems', McMillan

Vas P., 1999, 'Artificial Intelligence Based Electrical Machines and Drives - Application of Fuzzy, Neural, Fuzzy-Neural and Genetic Algorithm Based Techniques", Oxford University Press

Voultoury P., 1998, 'Sensorless Speed Controlled Brushless DC Drive using the

TMS320C242 DSP Controller', Texas Instruments inc, Part SPRA498

Vukosavic S., 1990, 'Third Harmonic Commutation Control System and Method', Emerson Electric Co, United States Patent 4912378

Wu R. and Slemon G., 1991, 'A Permanent Magnet Motor Drive Without a Shaft Sensor', IEEE Trans. Industry Applications, 27(**5**), 1005-1011

Xu X. and Novotny D.W., 1991, 'Implementation of Direct Stator Flux Orientation Control on a Versatile DSP Based System'. IEEE Trans. on Industry Applications. 27(**4**), 694-700.

Chapter 3

Experimental Test Rig Modelling and Control

3.1 Introduction

The development of an experimental test system, which will form the basis for all subsequent experimentation, is of fundamental importance to this work. It follows that development of accurate system models based on knowledge acquired *a priori* also and of extreme interest; since these models will be used to develop controllers later within this work. This Chapter is divided into major sections; first the test rig is introduced and its mechanical and electronic properties are discussed. A novel approach to sensor bandwidth reduction is developed, other measurement devices are also discussed in order to achieve full state measurement within the system. Secondly, models are developed from knowledge of the motor, and assumptions about the load torque. These models vary in complexity, from simple third order transfer function models to models based on the magnetic circuit of the motor. The performance of the respective models are subject to comparison before two controllers are developed in the final section of this Chapter. These controllers are applied to the system. The first is a proportional, integral, derivative (PID) controller, designed using the Zeigler-Nichols approach. The second is an integral action state feedback controller, which will serve to form a convenient basis for work within later Chapters.

3.2 Test Rig Properties

The diagram shown in Figure 3.1 provides a schematic overview of the system and also serves to illustrate signal inputs and outputs from which data may be acquired. Within this section, the salient mechanical features of the system are first discussed. Discussion then turns to the systems through which data may be sensed and subsequently acquired.

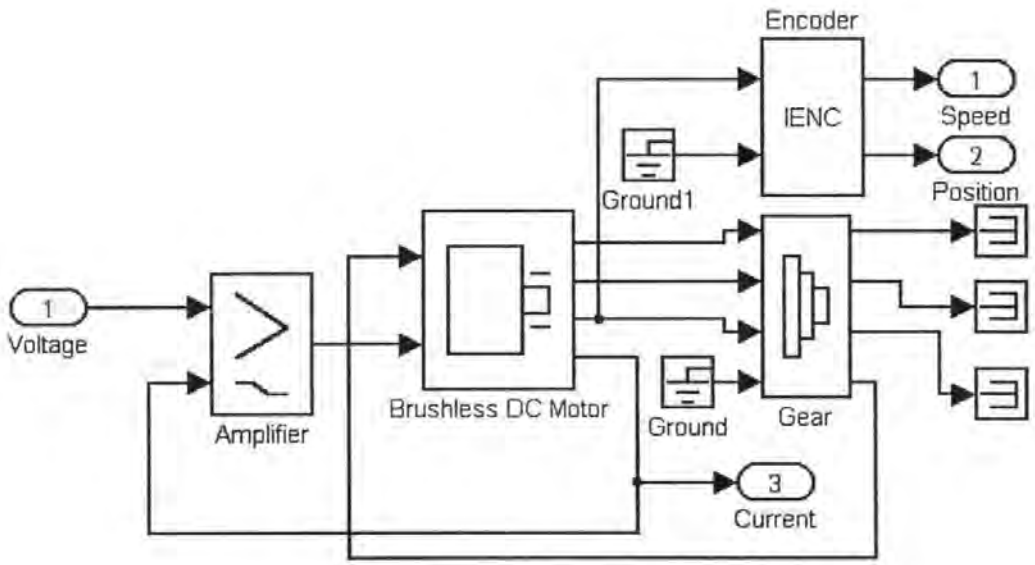

Figure 3.1: *Top Level Simulink Model of the Linear Stage and Motor*

3.2.1 Mechanical Description of the Stage

The motion control system for this work has been chosen to provide a good analogy with the type of system in common use within industry. Since the system is meant to provide proof of concept, nonlinearities which are normally associated with poor performance of a linear stage must be incorporated into the system. The commercially available brushless D.C. motor has been specifically chosen since its dynamic performance will be strongly affected by variations within the load. The motor is supplied with a 500 pulse

per revolution optical quadrature encoder. The technical specifications for both the motor and encoder may be found in Appendix B, Part A. In essence the stage consists of a lead screw, carriage and slide rails. The carriage is constrained to move in a single dimension by the slide rails and is coupled via a nut to the screw. The motor is rigidly coupled to the screw, so that when it rotates, the screw also rotates. Since the screw and carriage are linked, but since the carriage can only move linearly, a displacement of the carriage takes place. The position of the carriage is then implied from the screw pitch and knowledge of the number of rotations performed by the motor. Figure 3.2 illustrates the physical construction of the test rig.

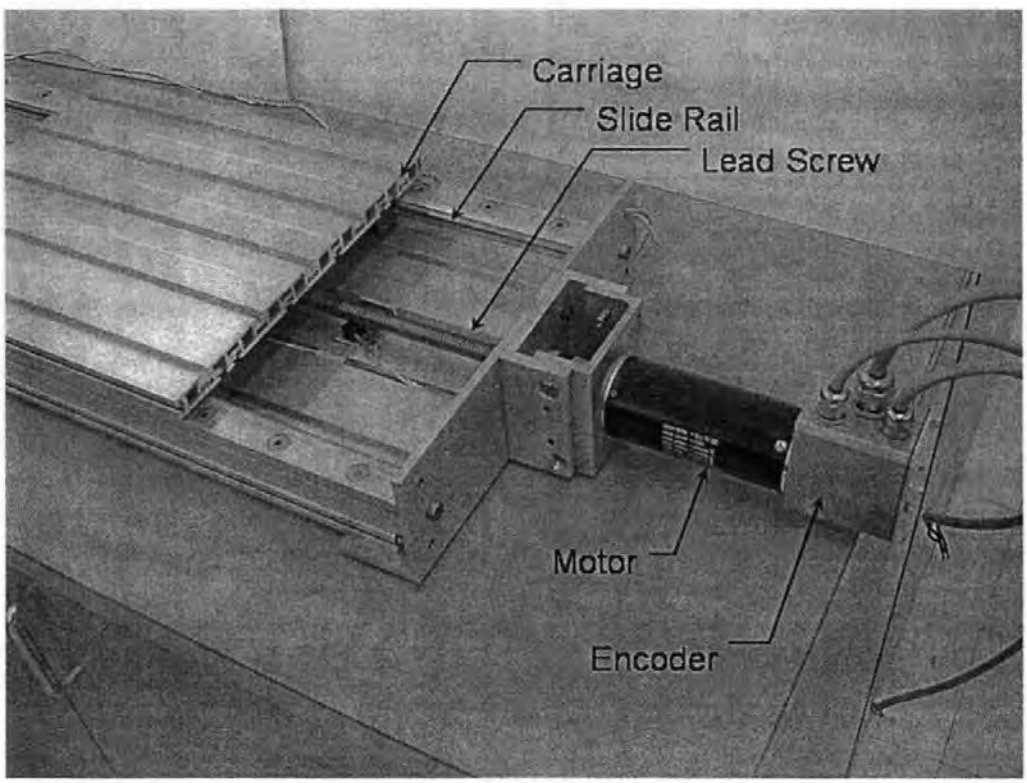

Figure 3.2: *Physical Construction of the Test Rig*

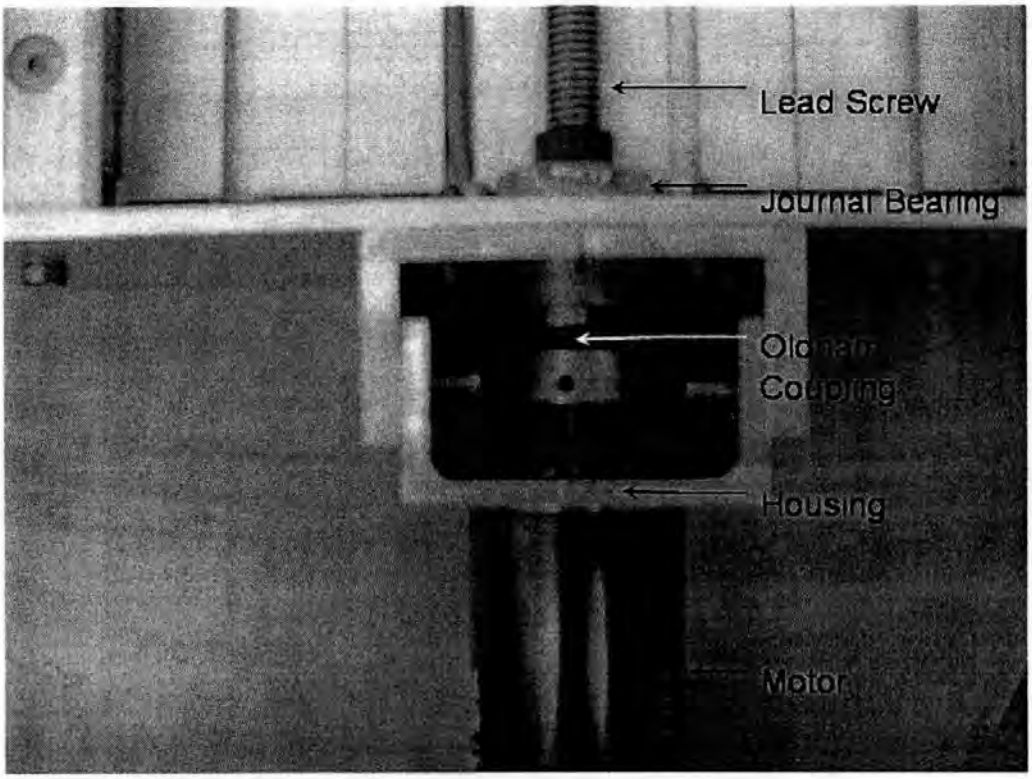

Figure 3.3: *Rigid Coupling Between Motor and Lead Screw*

The slide rails come in many guises within the typical linear motion stage, the task is to support the central carriage and constrain its movement to a single axis. It is also imperative that the movement within the selected axis is as free as possible, i.e. friction should be minimised. Typically in low load applications ball bearings in a configuration such as that shown in Figure 3.4(a) are used. If the stage is designed for higher load ratings, or if the stage is designed for greater linear displacement accuracy, then the cross roller bearing design Figure 3.4(b) is preferred (Newport, 1999). The system in use within this project uses the former (Figure 3.5).

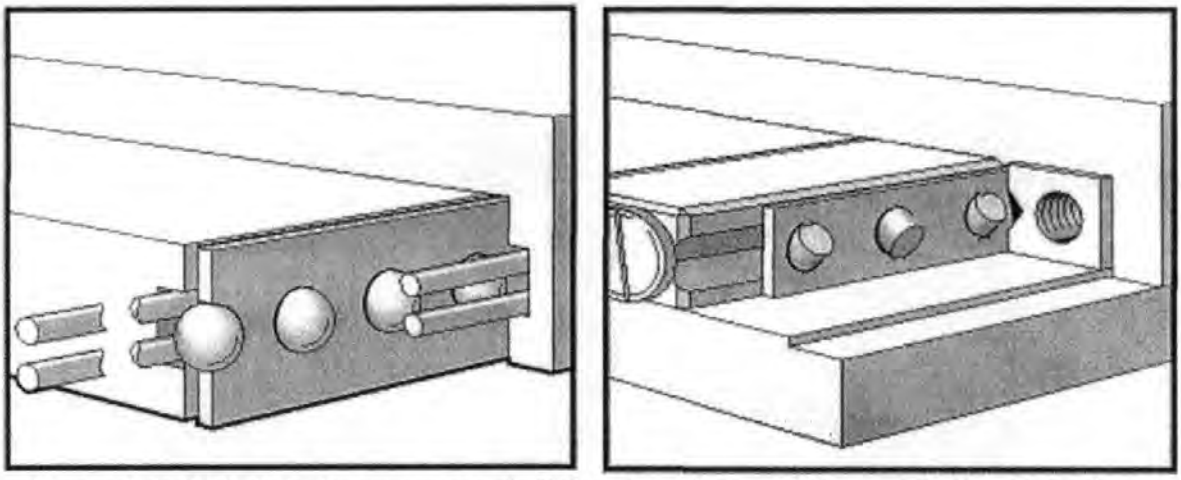

Figure 3.4: *Slide Rail Arrangements, Ball Bearings (left) and Crossed Roller (right)*[4]

The mechanism in the test rig (Figure 3.5) does not provide the bearings with their own housing, like that shown in Figure 3.4(a). Therefore the balls tend to rub against one another as well as the supporting rail. This produces high levels of point friction, which in turn leads to increased mechanical wear and acoustic noise. The bearing system in the test rig uses a recirculating ball system, the principle of which may be seen in Figure 3.5(b).

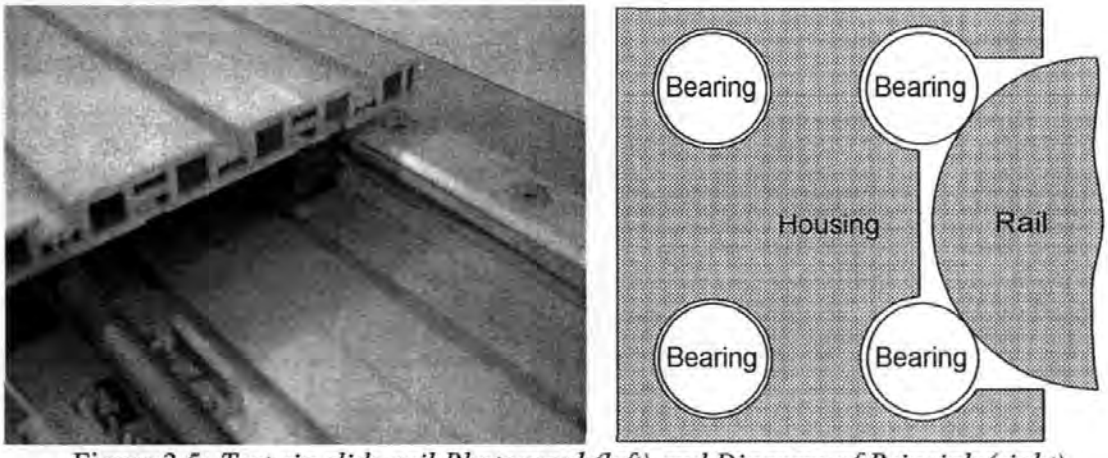

Figure 3.5: *Test rig slide rail Photograph(left) and Diagram of Principle(right)*

[4] Pictures reproduced courtesy of Newport Motion Contols Ltd

Recirculation allows the carriage to travel large distances without the need for a large bearing housing. In the re-circulating system, the balls travel along the housing in the opposite direction to the carriage. When they reach the end of the housing they are channelled back to the front of the housing. The major drawback associated with this system is that it is highly sensitive to contaminants, which can lodge between bearings and prevent proper operation. Figure 3.6 provides a cut away illustration of the recirculating system in use within the system (not to scale).

Figure 3.6: *Cut-away of the Recirculating Ball and Rail System*

The two most common types of screw are the lead screw Figure 3.7(a) and the ball screw Figure 3.7(b). The ball screw uses recirculation in the same manner as the slide rail. This approach greatly reduces the rubbing friction in comparison to the lead screw. The ball screw also allows higher load ratings. The lead screw is, however, far cheaper and is used within the test rig. Once again, contaminants can play a significant role in the overall performance of the system.

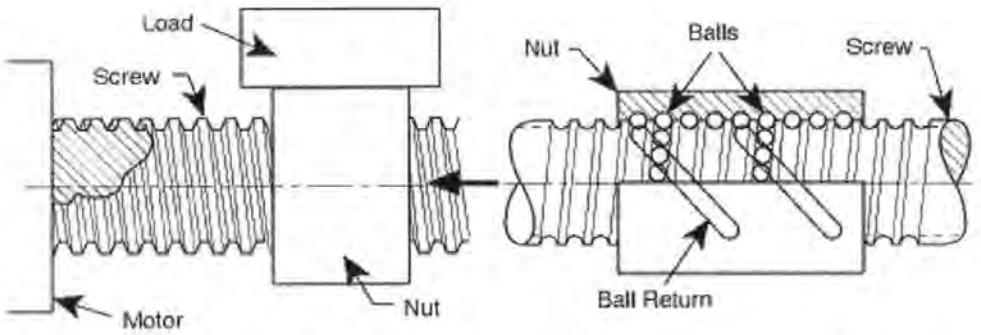

Figure 3.7: *Screw types, Leadscrew (left) and Ball Screw (right)*[+]

Use of an Oldham coupling to provide linkage between the motor and leadscrew allows positive drive whilst maintaining robustness to manufacturing error. The lead screw is supported at either end of the stage with journal bearings, their frictional contribution is insignificant at low speeds when compared to the rubbing friction associated with the screw and nut (Shing, 1994).

Throughout this work, the following will be assumed about the system

- The leadscrew is rigid
- The coupling between motor and screw is rigid.

Additionally, within this Chapter it will be assumed that the load friction apparent at the motor is constant. It will be shown in §3.3, that there is a direct correlation between motor load torque and current drawn by the motor; and models which incorporate the load current are a good deal more accurate. The next section will move on to discuss the mechanical test rig performance in terms of its open loop dynamics.

[+] Pictures reproduced courtesy of Newport Motion Contols Ltd

3.2.2 Test System Performance

Coarse measurements suggest that the frictional torque required to rotate the lead screw is 1.2N/m. As discussed, it is important to acquire accurate knowledge of system parameters. Therefore, a relationship between speed and load torque is developed. The encoder position data may then be directly applied to the calculation of the load torque across the full travel of the stage.

Based on the relationship

$$T_m = I.K_M \tag{3.1}$$

and introducing the relationship

$$K = \frac{K_M}{R} \tag{3.2}$$

and the power balance equations:

Applied electrical power: $P_i = V \cdot I$ (3.3)

Mechanical output power: $P_o = T_m \cdot \omega$ (3.4)

Power loss: $P_l = I^2 \cdot R$ (3.5)

Power balance: $P_i = P_o + P_l$ (3.6)

The motor speed may be expressed as (from (3.4))

$$\omega = \frac{P_o}{T_m} \tag{3.7}$$

from (3.3), (3.5) and (3.6), (3.7) may be re-expressed as

$$\omega = \frac{V \cdot I - I^2 R}{T_m} \tag{3.8}$$

Substitution of the equations (3.1) and (3.2) lead to the simplification

$$\omega = \frac{V}{KR} - \frac{I}{K} \tag{3.9}$$

further manipulation leads to

$$\omega = \frac{V}{KR} - \frac{T_m}{K^2 R} \tag{3.10}$$

The relationship between speed and load torque has therefore been established for constant voltage application. Manipulation of (3.10) yields the ideal angular speed, ω_i (T_m=0), (3.11) and the stall torque of the motor, T_{ms} (ω=0), (3.12)

$$\omega_i = \frac{V}{KR} = \frac{V}{K_M} \tag{3.11}$$

$$T_{ms} = \frac{VK_M}{R} \tag{3.12}$$

It is clear that a speed between zero and ideal is indicative of a load. The actual torque, assuming a linear relationship between ω and T_L is given as a fraction of the stall torque

$$T_m = T_{ms} \cdot \left(1 - \frac{n}{n_i}\right) - T_F \tag{3.13}$$

Where n denotes speed (rpm) and n_i denotes ideal no load speed. This equation will be used later within the Chapter 4. The carriage was driven across the total length of travel, in both directions, and position data was acquired. Figure 3.8 illustrates the results. The convention that forward travel is away from the motor has been adopted throughout this work. It can be readily seen that the frictional perturbation has significant effect on the stage performance. It can also be seen that the effect is not symmetrical, i.e. the frictional effect is completely different when traveling in one direction, compared with the reverse. The spikes on the graphs are due to numerical differentiation of the data.

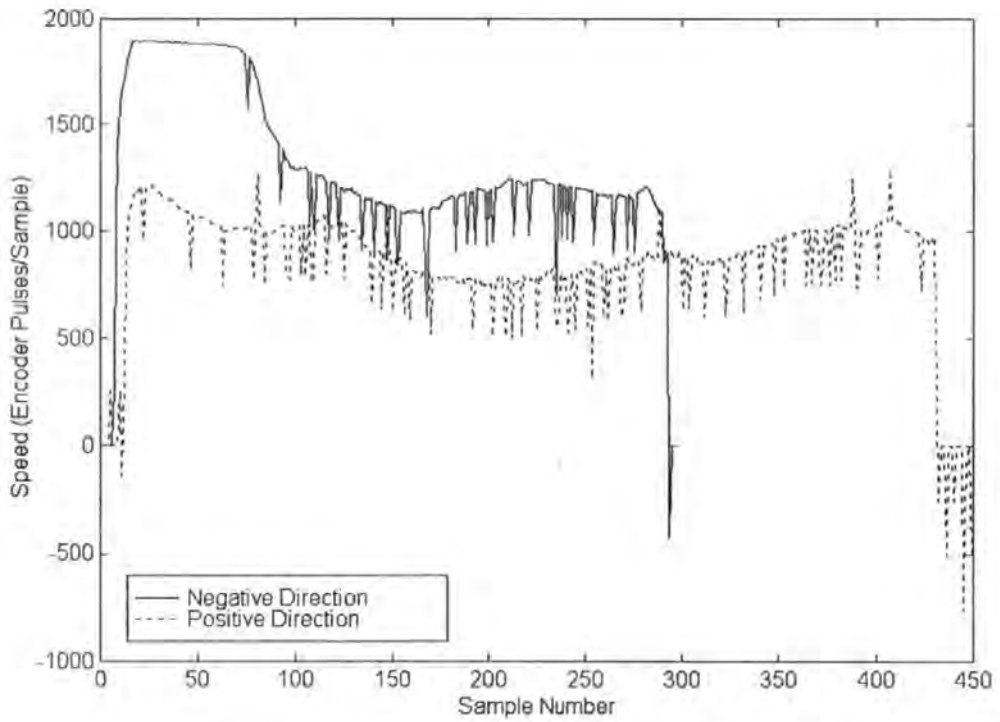

Figure 3.8: *Comparison of Carriage Speed in Forward and Reverse Direction*

3.2.3 Electrical Characteristics of the Test System

The control of motor voltage is achieved through a commercially available amplifier. From the perspective of this work, the only issue associated with the electronics is the measurement of physically relevant state variables. In principle, there are three circuits within the electronic subsystem. In order of discussion they are

- Speed control unit/controller interface
- Position measurement unit
- Current measurement unit

The following sections move on to discuss their operation. The circuit diagrams are provided in Appendix B, Part B.

Controller Interface

Control of the system was initially performed with a Motorola 68000 microprocessor system. The interface consisted of eight usable digital inputs and eight outputs. The development of the control electronics was therefore constrained to meet these specifications. Speed control is achieved by providing the amplifier with an analogue voltage, the circuit shown (Figure B.1), therefore uses a seven bit digital signal to provide a series of 128 unique speeds. The eighth output was then used to provide directional information. An amplification unit was also used to achieve proper scaling of the speed signal for the amplifier. Figure B.2 illustrates the direction circuit and the amplifier unit. Because of the relatively slow interface between the 68000 and the computer for data analysis, and because of the heavy constraint on memory within the 68000 system, development was transferred to a PCL 718 data acquisition card which interfaced to the ISA computer bus. The circuit used to provide directional information has a very low overhead in terms of output requirement and therefore remains. The amplifier circuit also remains, if only to provide a buffer between the power electronics and the computer. This section of the electronics is used to provide information about the applied excitation voltage. Rather than increasing computational overhead by measuring this voltage, its value can be determined implicitly if the electronics are calibrated correctly. The circuit in Figure B.3 is used to achieve this calibration. Of principle concern is that full speed is achieved when the speed output is at a maximum and zero speed is achieved when the output is zero. The series of amplifier circuits are used to provide a full range of

operations on the control voltage. In order to minimise the effect of controller dead-band due to friction the summing amplifier is used to add an additional regulated voltage to the control voltage, thus providing a threshold which is adjusted so that the motor is just stopped with zero control voltage. The final amplifier in the circuit is used to amplify the entire signal, judicious selection of the amplifier gains allows the system to achieve the desired zero and maximum speeds with the controller.

Position Measurement

The device used for rotary position feedback is the quadrature optical encoder which provides three output channels, A, B and I (Appendix B, Part A). Channels A and B are placed 90° out of phase with one another and provide position and direction feedback information. The index (I) channel provides an index pulse once every rotation of the encoder to enable precise 'homing' of the device; this additional channel is not important to this work, since the limit switches are used to provide a home position. The encoder provides 500 pulses per revolution. When used in quadrature (channels A and B together) the effective number of pulses per revolution increases to 2000. In order to achieve accurate position measurement, all pulses must be registered and counted by the measurement (host) software. The host bandwidth, assuming no additional computational effort is therefore automatically set to a minimum of

$$\gamma = \frac{2000 \cdot n}{60} Hz \qquad (3.14)$$

Where γ is the system bandwidth and n the speed (revolutions per minute) of the motor.

In applications such as data acquisition it would be attractive to stream data from the system to a host computer. Even in low speed applications it is clear that the bandwidth requirement acts as a constraint on minimum hardware performance.

Sensor Bandwidth Reduction

A solution to this problem has been developed using a power integrated circuit (PIC) microprocessor. The microprocessor accepts the two channel signals from the encoder line driver and acts as a state machine to provide an eight bit position signal output. In addition, an available ninth output pin is used to provide the host system with information pertaining to the rotational direction of the motor. With the addition of this output, and correct integration with the controller software the bandwidth requirement is effectively reduced from (3.14) to

$$\gamma = \frac{2000 \cdot n}{15300} Hz \tag{3.15}$$

Using this system it is possible to achieve accurate position feedback using a 68000 microprocessor and a 2000 pulse per revolution encoder at motor speeds of up to 1000 revolutions per minute, which far exceeds the mechanical capabilities of the system.

System Design

The bandwidth reduction circuit is shown in Figure B.4. The line driver (U1) is required to provide the microchip with coherent channel signals. The microprocessor interface consists simply of an oscillator circuit (U3) and the microprocessor (U2). The microprocessor provides TTL compatible signals that may then be fed to an appropriate

data acquisition unit. In the example of this work, the data acquisition unit had an effective bandwidth of 8kHz.

The host c-code and microprocessor embedded code flow diagrams are shown in Figure 3.9 and Figure 3.10 respectively. Figure 3.9 represents the logical flow through a routine that will be resident within the host process. Its function is to provide a solution to the equation

$$T_C = \sum_{i=0}^{i=k} E_i \tag{3.16}$$

where T_C represents the total encoder count from initialisation to the current sample *K*. Of significance are the facts that the motor may travel in both a forward and reverse sense, and that once having reached 255 pulses in a monotone increasing cycle, or 0 in a monotone decreasing cycle, the firmware will 'wrap' to 0 or 255 respectively. Therefore, knowledge of the previous encoder output, direction and current encoder value are all required in order to calculate the true encoder value and minimise the bandwidth requirement.

Within the diagrams, *K* and *K*-1 are used to represent the current and previous sample respectively. E represents the encoder value, S represents the encoder states. TC indicates the total encoder count and Dir or Direction are used interchangeably to indicate the direction of motor travel.

Figure 3.10 illustrates the logical flow through the firmware code. There are four possible states (S) in which the output signals might reside. Converting signals A and B to binary representation yields the states

0. Neither A nor B are logical 1
1. A but not B is logical 1
2. B but not A is logical 1

3. A and B are logical 1

In terms of flow through the states, when traveling in the forward direction the encoder sequence is given by

0→2→3→1→0→2→3→1...

The microprocessor executes, in general, 1 instruction per cycle and operates at 10MHz. Once within the software loop, state transition may be checked at up to 1.666MHz. in the event of a transition, 700ns are required for processing. The worst case operating scenario is a state change every sample, i.e. once approximately every 0.13μs, this corresponds to a motor speed of 231769 revolutions per minute, therefore effectively guaranteeing that every state generated by the encoder will be registered.

Current Measurement

The final circuit of concern is the one which is used to achieve current measurement. Since direct current was anticipated, hall effect current measurement was not viable. Instead, a shunt resistor is placed in the motor supply line. A precision amplifier is then used to measure the voltage drop across the resistor and to provide a voltage proportional to it. This method of measurement is not ideal since it is very noisy. A resistor-capacitor low pass filter is used in the output stage of the amplifier in order to try and smooth this signal. The circuit is shown in Figure B.5.

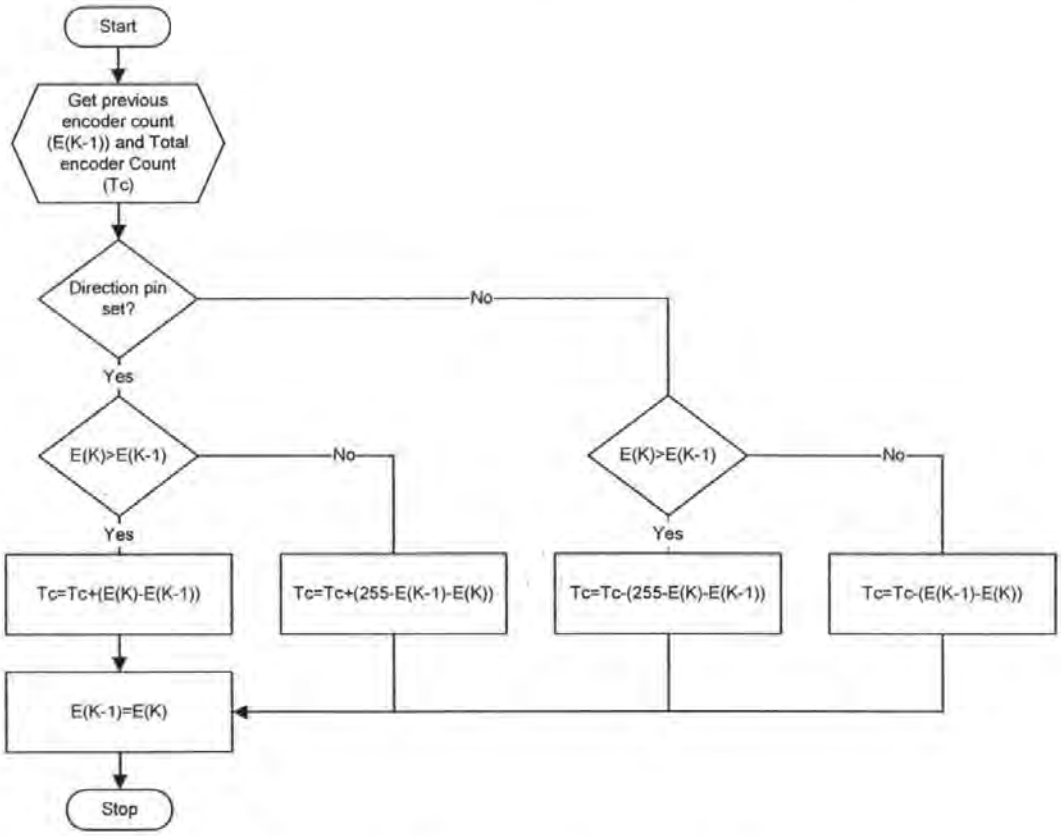

Figure 3.9: *Higher Level Programme Flow*

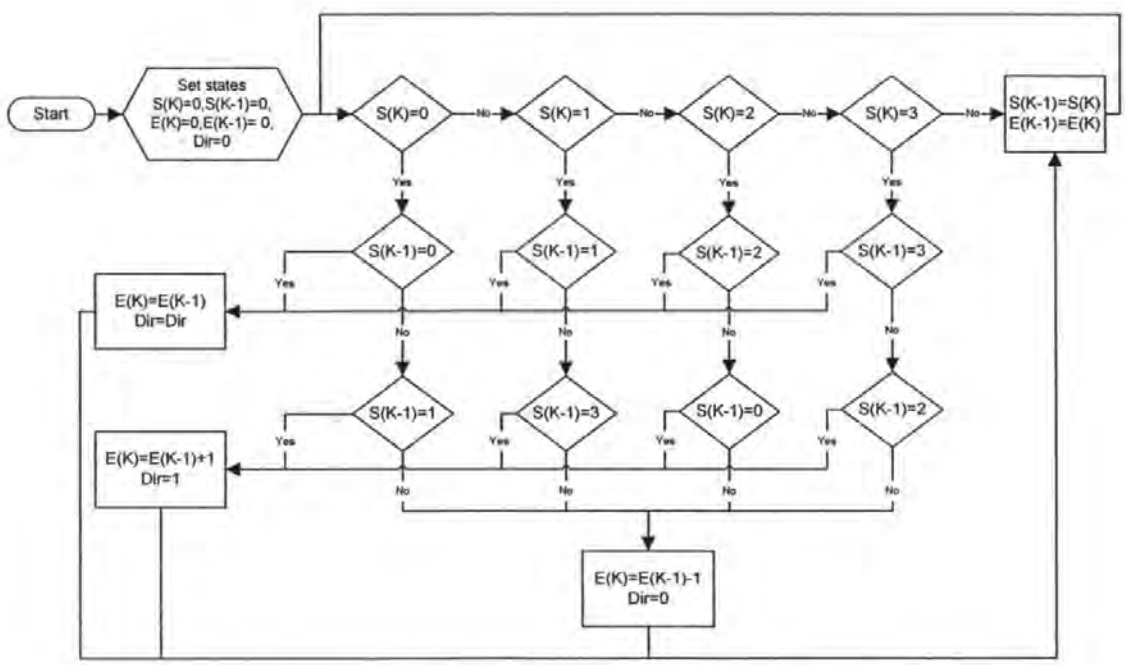

Figure 3.10: *Low Level Programme State Machine*

3.3 Model Development

Of fundamental importance to the development of efficient control algorithms for the system is the development of sufficiently accurate motor models. Since motors of all shapes and sizes have been used in innumerable applications from power generation to robot control, there exists a vast quantity of literature based on the modelling of these machines e.g. Rahman and Zhou (1996), Hemati and Leu (1992), Pillay and Krishnan (1991) and Low *et al* (1996). Extremely elaborate models have been developed based on the magnetic circuit of the motor, e.g. Shi and Li, (1996) however these models are computationally expensive, subsequently less complex models are considered within this work.

There are two motor types under consideration here. The brushed commutator D.C. (DC) motor and the brushless D.C. (BLDC) motor; although the BLDC motor will be more generally treated as the synchronous motor. Clearly, the BLDC is of direct relevance to the work, since this is the type of motor used for actuation of the stage. The selection of the DC motor has been largely dictated by the requirement for a simple motor model in order to validate control schemes later on within this work, since the BLDC motor is multi input by nature, where as the DC only requires a single control input.

This Chapter begins with the treatment of the DC motor, mathematical models are built into transfer function form and then state space form, simplifications and assumptions are highlighted where necessary.

3.3.1 Modelling with a Transfer Function

The D.C. motor is among the most simple to model. This work therefore begins with the comparatively simple task of expressing the DC motor model in terms of its transfer function and equivalent state space model. As explained in the previous section the principle reason for consideration of the DC motor lies in the ability to subsequently apply the model to control structures, complex derivation of torque ripple induced by brush commutation (e.g. Kocybik, 2000), for instance is not of primary concern here.

Consider the equivalent circuit of the DC motor:

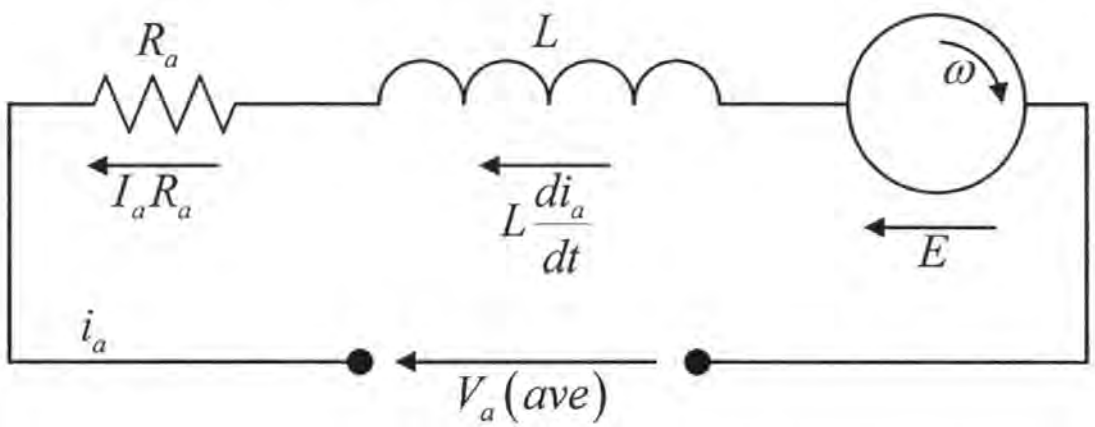

Figure 3.11: *Equivalent Circuit of the DC Motor*

From Figure 3.11 it may be written

$$V_a = E + I_a R_a + L\frac{di_a}{dt} \tag{3.17}$$

This is commonly referred to as the voltage balance equation. The generated back EMF (E) is proportional to speed and flux density of the rotor (armature) field. It may be written,

$$E = \omega K\Phi \tag{3.18}$$

In a similar manner the torque generated by the motor may be expressed as

$$T_m = i_a K\Phi \tag{3.19}$$

Finally, the motor will drive a load (even if that load is only the rotor armature), the load may be generalised as the sum of frictional and inertial components.

$$T_L = J\frac{d\omega}{dt} + B\omega \tag{3.20}$$

The torque balance equation may be expressed as

$$J\frac{d\omega}{dt} + B\omega = i_a K\Phi \tag{3.21}$$

$K\Phi$ can be seen to be constant in both equations (3.18) and (3.19). Therefore, for ease of identification, K_e will be used to indicate the electrical gain constant and k_m the mechanical constant.

Applying Laplace transforms to equations (3.17)-(3.20)

$$V(s) = (Ls + R)I(s) + E(s) \tag{3.22}$$

$$T_L(s) = (Js + B)\omega(s) \tag{3.23}$$

$$T_m(s) = K_m I(s) \tag{3.24}$$

$$E(s) = K_e \omega(s) \tag{3.25}$$

Figure 3.12 illustrates the block diagram of the motor. From this diagram the transfer function of the motor may be expressed as

$$\frac{\omega}{V}(s) = \frac{K_m}{(Ls + R)(Js + B) + K_m K_e} \tag{3.26}$$

Alternatively, (3.26) may be written

$$\frac{\theta}{V}(s) = \frac{K_m}{s(Ls+R)(Js+B) + K_m K_e s} \tag{3.27}$$

since $\theta(s) = \mathcal{L}\theta(t)$; $\theta(t) = \int \omega(t)\, dt$

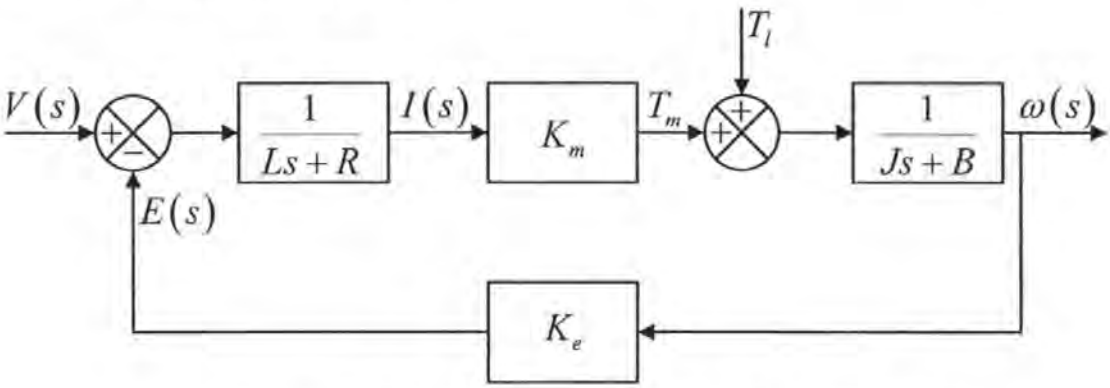

Figure 3.12: *Block Diagram Representation of the D.C. Motor*

it is desirable to further simplify the motor model. Since the motor inductance is typically negligible, its effects may be ignored. Hence (3.27) reduces to:

$$\frac{\theta}{V}(s) = \frac{K_m}{s\{R(Js+B) + K_m K_e\}} \tag{3.28}$$

and after further manipulation to:

$$\frac{\theta}{V}(s) = \frac{K_m/R}{Js^2 + \left\{B + K_m K_e/R\right\}s} \tag{3.29}$$

On inspection of equations (3.18) and (3.19), it can be seen that the effect of the constants K_e and K_m increase with speed, their effect could therefore be lumped together with the effects of viscous friction. At this point, definitions of new motor parameters will serve to tidy the equation.

Let

$$F = B + \frac{K_M K_E}{R} \tag{3.30}$$

$$K = \frac{K_M}{R} \tag{3.31}$$

combining (3.29),(3.30) and (3.31) yields

$$G(s) = \frac{K}{Js^2 + Fs} \tag{3.32}$$

alternatively

$$G(s) = \frac{K_s}{s(s+\alpha)} \tag{3.33}$$

where $K_s = \frac{K_m}{RJ}, \alpha = \frac{F}{J}$ and $\tau_m = \frac{1}{\alpha} = \frac{RJ}{RB + K_m K_e}$

K_s in this equation is the open loop gain constant, τ_m is the motor time constant.

3.3.2 State Space Modelling

The transfer function for the D.C motor has been successfully derived in the previous section. Unfortunately, transfer functions are limited to single input, single output systems. A lesser problem is that zero initial conditions are assumed. The models functionality would be significantly enhanced if position, speed and acceleration could all be expressed without the need for differentiation of the model output. Attention is therefore diverted to the state space modelling of the motor. Modelling may be achieved through either direct conversion from the transfer function previously derived, or from the differential equations given (3.17) and (3.20). Rearranging (3.27) gives

$$\frac{\theta}{V}(s) = \frac{K_m}{JLs^3 + (BL + RJ)s^2 + (BR + K_m K_e)s} \tag{3.34}$$

Alternatively, in matrix form

$$\begin{bmatrix} \dot{X}_1 \\ \dot{X}_2 \\ \dot{X}_3 \end{bmatrix} = \begin{bmatrix} 0 & 1 & 0 \\ 0 & 0 & 1 \\ 0 & -\frac{(BR + K_m K_e)}{JL} & -\frac{(BL + RJ)}{JL} \end{bmatrix} \begin{bmatrix} X_1 \\ X_2 \\ X_3 \end{bmatrix} + \begin{bmatrix} 0 \\ 0 \\ \frac{K_m}{JL} \end{bmatrix} U \qquad Y = \begin{bmatrix} 1 & 0 & 0 \end{bmatrix} \begin{bmatrix} X_1 \\ X_2 \\ X_3 \end{bmatrix}$$

(3.35)

The matrix form above is known as the companion form and will be useful later in the development of certain control schemes. As stated, the alternative method for deriving the state space model is to use the differential equations directly, reiterating,

$$V_a = E + I_a R_a + L\frac{dI_a}{dt} \tag{3.36}$$

$$E = \omega K \Phi \tag{3.37}$$

$$T_m = I_a . K \Phi \tag{3.38}$$

$$T_L = J\frac{d\omega}{dt} + B\omega \tag{3.39}$$

It will be of some benefit to split the load into internal and external components. The torque balance equation can be rewritten as

$$J\frac{d\omega}{dt} + B\omega + T_X = I_a . K \Phi \tag{3.40}$$

Where T_X is the external load torque. Rewriting equations (3.36) and (3.40)

$$L\frac{dI_a}{dt} = -I_a R_a - K_e \omega + V_a \tag{3.41}$$

$$J\frac{d\omega}{dt} = -B\omega - T_X + I_a . K \Phi \tag{3.42}$$

Now, let $X_1 = \theta, X_2 = \frac{d\theta}{dt} = \omega, and\ X_3 = i\ let\ T_X = U_1\ and\ V_a = U_2$

such that

$$\begin{aligned}
\dot{X}_1 &= X_2 \\
\dot{X}_2 &= -\frac{U_1}{J} - \frac{B}{J}X_2 + \frac{K_M}{J}X_3 \\
\dot{X}_3 &= -\frac{K_e}{L}X_2 - \frac{R}{L}X_3 + \frac{U_2}{L}
\end{aligned} \tag{3.43}$$

(3.43) may be more concisely expressed in matrix form as per equation (3.44)

$$\begin{bmatrix} \dot{X}_1 \\ \dot{X}_2 \\ \dot{X}_3 \end{bmatrix} = \begin{bmatrix} 0 & 1 & 0 \\ 0 & -\frac{B}{J} & \frac{K_m}{J} \\ 0 & -\frac{K_e}{L} & -\frac{R_a}{L} \end{bmatrix} \begin{bmatrix} X_1 \\ X_2 \\ X_3 \end{bmatrix} + \begin{bmatrix} 0 \\ -\frac{U_1}{J} \\ \frac{U_2}{L} \end{bmatrix} \qquad \begin{bmatrix} Y_1 \\ Y_2 \end{bmatrix} = \begin{bmatrix} 1 & 0 & 0 \\ 0 & 1 & 0 \end{bmatrix} \begin{bmatrix} X_1 \\ X_2 \\ X_3 \end{bmatrix} \tag{3.44}$$

At this point treatment of the DC motor model is abandoned since sufficient models for simulation have been derived and instead the BLDC is now considered.

3.3.3 The Lumped Parameter Model

Given the phase windings A, B and C, the transformation from the three-phase model to an equivalent two-phase description is desired. The Park transformation (3.45) is commonly used in obtaining this conversion, since it possesses the unique property of eliminating all time varying inductances from the machine voltage equation (Krause *et al*, 1995).

$$k = \frac{2}{3}\begin{bmatrix} Cos\theta & Cos\left(\theta - \frac{2\pi}{3}\right) & Cos\left(\theta + \frac{2\pi}{3}\right) \\ Sin\theta & Sin\left(\theta - \frac{2\pi}{3}\right) & Sin\left(\theta + \frac{2\pi}{3}\right) \\ \frac{1}{2} & \frac{1}{2} & \frac{1}{2} \end{bmatrix} \tag{3.45}$$

Another advantage of this transform is that it may be equally well applied to voltage, current, flux linkage or electrical charge. It may be written

$$f_{qd0s} = k \cdot f_{abcs} \tag{3.46}$$

Where

$$(f_{qd0s})^T = [f_{qs} \quad f_{ds} \quad f_{0s}] \tag{3.47}$$

$$(f_{abcs})^T = [f_{as} \quad f_{bs} \quad f_{cs}] \tag{3.48}$$

where f represents any of the afore mentioned sets of variables. Assuming that the three phase voltages are given

$$V_{as} = r_s i_{as} + L_{ss}\frac{di_{as}}{dt} + \lambda_m \omega_r \cos(\theta) \tag{3.49}$$

$$V_{bs} = r_s i_{bs} + L_{ss}\frac{di_{bs}}{dt} + \lambda_m \omega_r \cos\left(\theta - \frac{2\pi}{3}\right) \tag{3.50}$$

$$V_{cs} = r_s i_{cs} + L_{ss}\frac{di_{cs}}{dt} + \lambda_m \omega_r \cos\left(\theta + \frac{2\pi}{3}\right) \tag{3.51}$$

where r_s, L_{ss} and λ_m represent the stator resistance, stator self inductance and flux linkage due to the permanent magnet respectively. θ and ω represent the position and velocity respectively, suffix rm represents the mechanical rotor position and suffix r represents the electrical equivalent. The corresponding voltages in the $dq0$ axis will be

$$V_{qs} = r_s i_{qs} + L_{ss}\frac{di_{qs}}{dt} + \omega_r \lambda_m (sin(\theta_r)) \tag{3.52}$$

$$V_{ds} = r_s i_{ds} + L_{ss}\frac{di_{ds}}{dt} + \omega_r \lambda_m (cos(\theta_r)) \tag{3.53}$$

The electromagnetic torque generated by the motor may be expressed in terms of the rotor reference frame according to the following equation (Krause *et al*, 1995).

$$T_e = \left(\frac{3}{2}\right)\left(\frac{N}{2}\right)\left(\lambda_{ds} i_{qs} - \lambda_{qs} i_{ds}\right) \tag{3.54}$$

Where $\lambda_{ds} = \lambda_m cos(\theta_r)$ and $\lambda_{qs} = \lambda_m cos(\theta_r)$. In addition to this, the mechanical load placed on the motor is given

$$T_L = J\frac{d\omega}{dt} + B\omega + T_X \tag{3.55}$$

In this case, the mechanical load is given in two parts, first the viscous friction (B) and second the inertia (J) of the motor, T_X in this case represents the external load placed on the motor. This external load is extremely important to the validity the model from a practical perspective. It is this load that serves to represent the external system, in the case of this work, the load is time variant and non-linear, (Armstrong-Helouvry *et al*, 1994). The addition of T_x potentially provides a useful interface for an external torque observer. The torque balance equation may be derived by equating (3.54) and (3.55):

$$J\frac{d\omega}{dt} + B\omega + T_X = \left(\frac{3}{2}\right)\left(\lambda_m cos(\theta_r) i_{qs} - \lambda_m sin(\theta_r) i_{ds}\right) \tag{3.56}$$

The voltage and torque equations above may be used in order to model the motor to a reasonable degree of accuracy. In order to make use of these equations in a control system, they must first be converted into a usable format. Rewriting equations (3.52), (3.53) and (3.56) leads to

$$\frac{di_{qs}}{dt} = -\frac{r_s i_{qs}}{L_{ss}} - \frac{\omega_r \lambda_m}{L_{ss}}(sin(\theta_r)) + \frac{V_{qs}}{L_{ss}} \tag{3.57}$$

$$\frac{di_{ds}}{dt} = -\frac{r_s i_{ds}}{L_{ss}} - \frac{\omega_r \lambda_m}{L_{ss}}(cos(\theta_r)) + \frac{V_{ds}}{L_{ss}} \tag{3.58}$$

$$\frac{d\omega}{dt} = \frac{3}{2}\frac{\lambda_m}{J} cos(\theta_r) i_{qs} - \frac{3}{2}\frac{\lambda_m}{J} sin(\theta_r) i_{ds} - \frac{B}{J}\omega - \frac{T_X}{J} \tag{3.59}$$

$$\theta_r = \int_0^t \omega(\xi) d\xi + \theta(0) \tag{3.60}$$

Equation (3.60) gives the mathematical description of the rotor position. ξ is a dummy variable of integration, and $\theta(0)$ is the zero time position of the rotor.

Let $x_1 = \theta, x_2 = \omega, x_3 = i_{ds}$ *and* $x_4 = i_{qs}$ and let $u_1 = T_X, u_2 = V_{ds}$ *and* $u_3 = V_{qs}$,

equations (3.57) to (3.60) may now be expressed in state space format,

$$\begin{bmatrix} \dot{x}_1 \\ \dot{x}_2 \\ \dot{x}_3 \\ \dot{x}_4 \end{bmatrix} = \begin{bmatrix} 0 & 1 & 0 & 0 \\ 0 & -\frac{B}{J} & -\frac{3}{2}\frac{\lambda_m}{J} sin(x_1) & \frac{3}{2}\frac{\lambda_m}{J} cos(x_1) \\ 0 & -\frac{\lambda_m}{L_{ss}} cos(x_1) & -\frac{r_s}{L_{ss}} & 0 \\ 0 & -\frac{\lambda_m}{L_{ss}} sin(x_1) & 0 & -\frac{r_s}{L_{ss}} \end{bmatrix} \begin{bmatrix} x_1 \\ x_2 \\ x_3 \\ x_4 \end{bmatrix} + \begin{bmatrix} 0 \\ \frac{u_1}{J} \\ \frac{u_2}{L_{ss}} \\ \frac{u_3}{L_{ss}} \end{bmatrix} \tag{3.61}$$

$$\begin{bmatrix} Y_1 \\ Y_2 \end{bmatrix} = \begin{bmatrix} 1 & 0 & 0 & 0 \\ 0 & 1 & 0 & 0 \end{bmatrix} \begin{bmatrix} x_1 \\ x_2 \\ x_3 \\ x_4 \end{bmatrix} \tag{3.62}$$

3.3.4 The Phase Co-ordinate Model

The phase co-ordinate model (Kenjo and Nagamori, 1985) is based on phase equations using stator and rotor circuits. In the case where there are more than 2 slots per pole per phase the inductance matrix contains sinusoidal terms. Development of this model will focus on the salient pole rotor, since the cylindrical rotor may be viewed as a special case of the former.

The phase inductance matrix [L] is:

$$[L]=\begin{bmatrix} L_{aa} & L_{ab} & L_{ac} & L_{af} & L_{ad_r} & L_{q_r} \\ L_{ab} & L_{bb} & L_{bc} & L_{bf} & L_{bd_r} & L_{q_r} \\ L_{ac} & L_{bc} & L_{cc} & L_{cf} & L_{cd_r} & L_{q_r} \\ L_{af} & L_{bf} & L_{cf} & L_{ff} & L_{fd_r} & 0 \\ L_{ad_r} & L_{bd_r} & L_{cd_r} & L_{fd_r} & L_{d_rd_r} & 0 \\ L_{q_r} & L_{q_r} & L_{q_r} & 0 & 0 & L_{q_rq_r} \end{bmatrix} \tag{3.63}$$

For distributed windings (more than 2 slots per pole per phase) all inductance's linked to the stator (self, mutual and stator/rotor inductance's) are rotor position, θ_r, dependent:

$$L_{aa} = L_{sl} + L_0 + L_2\cos(2\theta_r) \tag{3.64}$$

$$L_{bb} = L_{sl} + L_0 + L_2\cos\left(2\theta_r + \frac{2\pi}{3}\right) \tag{3.65}$$

$$L_{cc} = L_{sl} + L_0 + L_2\cos\left(2\theta_r - \frac{2\pi}{3}\right) \tag{3.66}$$

$$L_{bc} = -\frac{L_0}{2 + L_2\cos(2\theta_r)} \tag{3.67}$$

$$L_{ac} = -\frac{L_0}{2 + L_2\cos\left(2\theta_r + \frac{2\pi}{3}\right)} \tag{3.68}$$

$$L_{ab} = -\frac{L_0}{2 + L_2\cos\left(2\theta_r - \frac{2\pi}{3}\right)} \tag{3.69}$$

$$L_{ad_r} = L_{sd_r}\cos\theta_r \tag{3.70}$$

$$L_{bd_r} = L_{sd_r}\cos\left(\theta_r - \frac{2\pi}{3}\right) \tag{3.71}$$

$$L_{cd_r} = L_{sd_r}\cos\left(\theta_r + \frac{2\pi}{3}\right) \tag{3.72}$$

$$L_{af} = L_{sf}\cos\theta_r \tag{3.73}$$

$$L_{bf} = L_{sf}\cos\left(\theta_r - \frac{2\pi}{3}\right) \tag{3.74}$$

$$L_{cf} = L_{sf}\cos\left(\theta_r + \frac{2\pi}{3}\right) \tag{3.75}$$

$$L_{aq_r} = -L_{sq_r}\sin\theta_r \tag{3.76}$$

$$L_{bq_r} = -L_{sq_r}\sin\left(\theta_r - \frac{2\pi}{3}\right) \tag{3.77}$$

$$L_{cq_r} = L_{sq_r}\sin\left(\theta_r + \frac{2\pi}{3}\right) \tag{3.78}$$

Rotor inductances are evidently independent of rotor position as the saliency is based on the rotor itself

$$L_{ff} = L_{fl} + L_{fm} \tag{3.79}$$

$$L_{d_rd_r} = L_{d_rl} + L_{d_rm} \tag{3.80}$$

$$L_{q_rq_r} = L_{q_rl} + L_{q_rm} \tag{3.81}$$

where L_{fl}, L_{d_rl} and L_{d_rl} are leakage inductances while the others are related to main flux path. On the other hand, for *concentrated* windings (1 slot per pole per phase), when cylindrical pole permanent magnet rotors are used, all stator inductances are independent of rotor position. Only the motion related inductances between the constant field current permanent magnet equivalent circuit and the stator windings depend on rotor position.

$$[L]_{PM} = \begin{bmatrix} L_s & L_{ab} & L_{ab} & L_{af}(\theta_{er}) \\ L_{ab} & L_s & L_{ab} & L_{af}(\theta_{er}) \\ L_{ab} & L_{ab} & L_s & L_{af}(\theta_{er}) \\ L_{af}(\theta_{er}) & L_{af}(\theta_{er}) & L_{af}(\theta_{er}) & 0 \end{bmatrix} \tag{3.82}$$

The stator self inductance L_s and the stator/stator mutual inductances L_{ab} are all equal to each other. To a first approximation

$$L_{ab} = -\frac{L_0}{3} \tag{3.83}$$

The voltage/current equation in phase co-ordinates is:

$$\begin{bmatrix} V_s \\ V_r \end{bmatrix} = \begin{bmatrix} r_s & 0 \\ 0 & r_r \end{bmatrix} \cdot \begin{bmatrix} i_s \\ i_r \end{bmatrix} + \frac{d}{dt} \begin{bmatrix} \lambda_s \\ \lambda_r \end{bmatrix} \tag{3.84}$$

with

$$[\lambda] = [L(\theta_{er})] \cdot [i] \tag{3.85}$$

$$[i] = [i_a, i_b, i_c, i_{f_0}] \tag{3.86}$$

$$[r] = diag[r_s, r_s, r_s, 0] \tag{3.87}$$

$$[\lambda] = [\lambda_a, \lambda_b, \lambda_c, 0] \tag{3.88}$$

Finally the electromagnetic torque T_e may be calculated from the co-energy derivative with respect to rotor position:

$$T_e = \frac{dW_{co}}{d(\theta_{er})} = \frac{d}{d(\theta_{er})} \int_0^{[i]} [\lambda] d[i]^T \tag{3.89}$$

After neglecting magnetic saturation, (3.84) is multiplied by $[i]^T$:

$$[i]^T [V] = [r] \cdot [i] \cdot [i]^T + \frac{d}{dt}\left(\frac{1}{2}[L] \cdot [i] \cdot [i]^T\right) + \frac{1}{2} \cdot [i]^T \cdot \frac{\partial}{\partial \theta_{er}} [L(\theta_{er})] \cdot [i] \tag{3.90}$$

The last term is the electromagnetic power P_{elm}

$$T_e = \frac{P_{elm} \cdot p}{\omega_r} = \frac{p}{2} \cdot [i]^T \cdot \frac{\partial}{\partial \theta_{er}} [L(\theta_{er})] \cdot [i] \tag{3.91}$$

The motion equations are

$$\frac{J}{p} \frac{d\omega_r}{dt} = T_e - T_{Load} \tag{3.92}$$

$$\frac{d(\theta_{er})}{dt} = \frac{\omega_r}{\dot{p}} \tag{3.93}$$

The result is a set of eight non-linear differential equations with time varying coefficients. These equations are used for special cases for machines with some asymmetry or for unbalanced supply voltage operation.

Also, for the concentrated stator winding and permanent magnet cylindrical rotor, the phase variable model is the model of choice as $L_{af}(\theta_{er})$, $L_{bf}(\theta_{er})$ and $L_{cf}(\theta_{er})$ are contain a high harmonic content. In order to avoid the inductance dependence on rotor position, for distributed windings, the space phasor (d-q) model is used (See Vas (1993) and Appendix B, Part C).

3.3.5 Performance Measures

Performance measures are extremely important for the validation of derived models. The selection of performance measures is heavily application dependent. Three measures of performance based on common modelling objectives will be used to quantify modelling error $\left(\varepsilon(t)\right)$. Model error is first described based on the following relationship

$$\varepsilon(t) = y(t) - \hat{y}(t) \tag{3.94}$$

where $y(t)$ is the system output and $\hat{y}(t)$ is the models estimate of the system output. The first of the three measures to be used is the infinity norm given by

$$\|\varepsilon\|_\infty \triangleq \sup_{t\geq 0} |\varepsilon(t)| \tag{3.95}$$

The infinity norm of a signal depends on the extreme values of error. Since extreme values will be sporadic, the infinity norm represents the worst-case model estimate.

The root mean square error semi-norm is also used to quantify the performance of the model. As opposed to the infinity norm, where the peak values of error were of concern, here it is the average value of error, the root mean square (RMS) of the error is given by

$$\|\varepsilon\|_{rms} \triangleq \left(\lim_{T\to\infty} \int_0^T \varepsilon(t)^2 \, dt \right)^{1/2} \tag{3.96}$$

The concept of the RMS error is used commonly within many engineering fields to describe the concept of average value, a low value for this performance measure does not imply that no large peaks in error occur, simply that they are not common and do not contain large values of energy.

The final performance measure is based on the ability of the model output to track the system output. Here, absolute error is only implicitly considered and the impetus is placed on how the signals vary with time. The percentile variance accounted for (VAF) is given as

$$VAF = 100\% \cdot \left[1 - \frac{\text{var}(\varepsilon(t))}{\text{var}(y(t))} \right] \tag{3.97}$$

When the model output ($\hat{y}$) and the system output (y) are identical, the VAF is given as 100%, if the model is in error then the measure is lower. It is interesting to note that from the perspective of developing control algorithms based on the identified model, the VAF is of more significance to the designer, since this describes how well the model has captured the system dynamics.

3.3.6 Data Selection

The selection of data upon which to validate models is a topic of some discussion within the research community. For now, a specification for the data will be presented, with the justification to come in Chapter 4.

- The data should excite both low and high order dynamics
- The variance of the data should be as broad as possible.
- The bias of the data should be zero.

In real terms, the data acquired must incorporate the dynamics from as much of the system as possible. Ideally, the excitation signal will be of variable amplitude and frequency in order to capture a wide range of system dynamics. The excitation signal should be of zero mean in order to avoid introducing unnecessary bias. To this end, a random stepwise signal with zero mean was used as a basis for the excitation signal. Random white noise was added to this signal. The system was subjected to this signal and current and position recorded as shown in Figure 3.13. The speed of the system is simply taken as the derivative of the position signal after data acquisition.

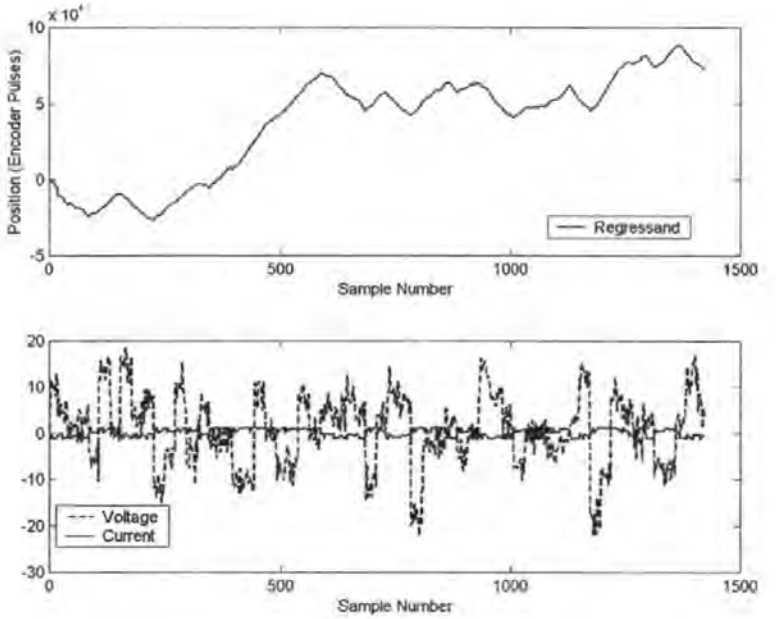

Figure 3.13: *Model Validation Data Set*

Figure 3.14 shows a comparison of the various models based on this validation data set. The transfer function model, which is the only model to use only the voltage as an input, clearly establishes that this system is multi-input in nature. The state space model performs surprisingly well in comparison to the remaining two. The lumped parameter model, on the other hand is disappointing. This poor performance may be due to inaccurate estimates of self inductance and flux linkage, which are not specified by the manufacturer. The phase coordinate model performs well, however it is extremely costly when computational overhead is considered.

provides a tabulation of the two meaningful models according to the performance measures discussed in §3.3.6. The next section within this work moves on to develop controllers based on these models. Since the state space model performs comparably to the others, but does not impose massive computational burden this will be the model used in the controller design. It is clear that the models may be improved. This could only be

achieved if the load were better understood. Since it is time variant, a method must be sought to identify the load subjected to the motor online. This will be the topic of consideration in Chapter 4.

Table 3.1: *Performance measures of the two meaningful models*

Model	$\|\varepsilon\|_{\infty}$ (ep)	$\|\varepsilon\|_{rms}$ (ep)	VAF
Phase-coordinate model	9961	5574	98.4%
Third order state space model	10943	5314	97.23%

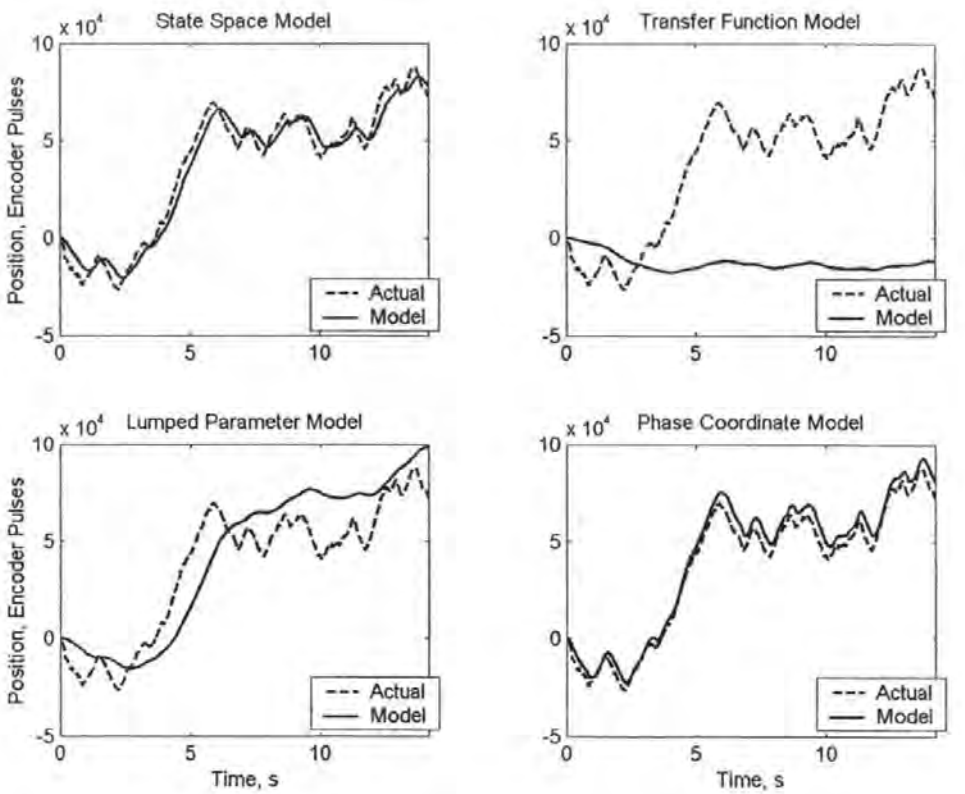

Figure 3.14: *Comparison of Models and the Actual System Performance*

3.4 Controller development

It is common that a proportional plus derivative (PD) or a PID controller is used for motor control (Seraji, 1983). It was seen in the last section that the single input single output model fails to consider the effect of load torque and therefore these models tend to be significantly less accurate than their state space counterpart. Furthermore, the state space model has been shown to perform nearly as well as the more complex phase coordinate model. Therefore, within this section two controllers will be developed. First a PID controller based on empirical observations gained from the stage is developed. The well known Zeigler-Nichols approach to this design is adopted (Unar *et al*, 1996). Following on, an integral action controller is then be developed based on the state space model. This controller will be used in later Chapters as a basis for an advanced sliding mode controller. The motor model

$$\frac{\theta}{V}(s) = \frac{K_m}{s(Ls+R)(Js+B)+K_m K_e s} \tag{3.98}$$

is thought to be acceptable for the development of these controllers.

Table 3.2: *Nominal Motor Parameters*

Parameter	Nominal Value	Units
K_m	54e-3	NmA^{-1}
K_e	54e-3	Vs/rad
L	0.0026	H
R	0.64	Ω
J	9e-3	Nms^2
B	7e-3	Nm/rad/s

Using the motor parameters given in

Table 3.2, the equation (3.98) becomes

$$\frac{\theta}{V}(s) = \frac{54\times10^{-3}}{31.2\times10^{-6}s^3 + 7.698\times10^{-3}s^2 + 4.48\times10^{-3}s} \tag{3.99}$$

Within this work, the Zeigler-Nichols reaction curve method was chosen as the design approach. This has choice has been motivated primarily by the simplicity in deriving the controller coefficients. In addition, and perhaps more importantly, the system is stable. This makes the continuous cycling method inutile as a design approach for this system (Golten and Verwer, 1991). The reaction curve method is dependent upon excitation of the open loop system with a step input; Figure 3.15 illustrates the reaction curve derived from the simulated system.

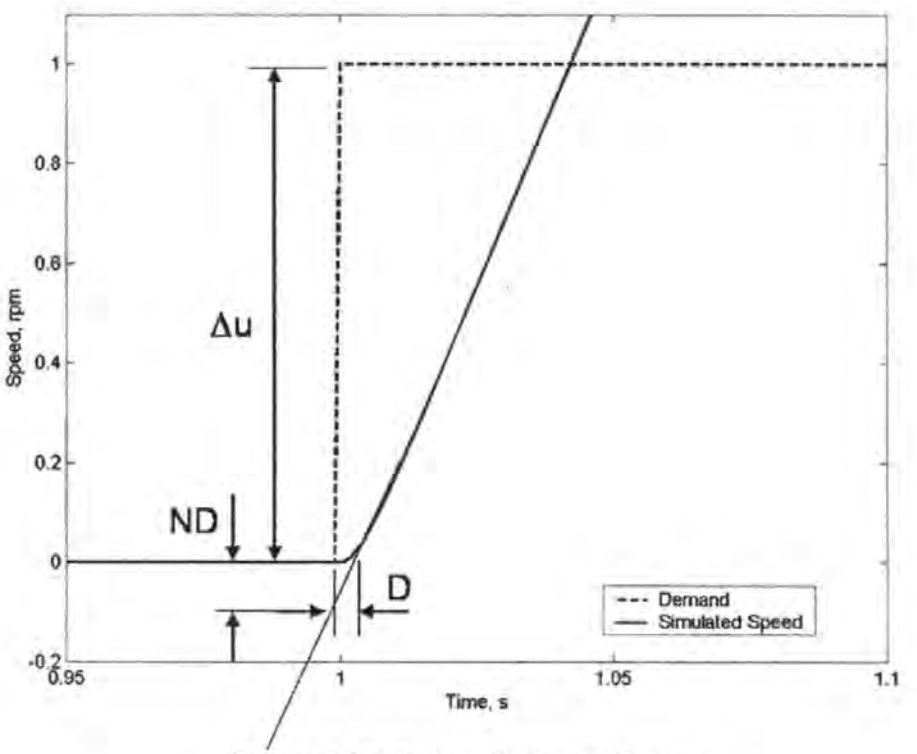

Figure 3.15: *System Reaction Curve*

The PID transfer function is given as

$$\frac{U(s)}{E(s)} = K_c\left(1 + sT_d + \frac{T_i}{s}\right) \tag{3.100}$$

where E is the system error and U is the control effort. K_c, T_d and T_i are the controller gain, derivative and integral time constant respectively. It is the Zeigler-Nichols method which is used to find these parameters, using the values from the reaction curve the parameters are given by

$$K_c = 1.2\frac{\Delta u}{ND} \tag{3.101}$$

$$T_i = \frac{D}{0.5} \tag{3.102}$$

$$T_d = \frac{D}{2} \tag{3.103}$$

Insertion of the numerical values from Figure 3.15 yields the parameters $K_c = 12, T_d = 0.025$ and $T_i = 0.1$. Figure 3.16 illustrates the result of applying this controller to the simulated system. It is feature of the Zeigler-Nichols approach that the response typically decays with a ratio of 4:1, the response is fast and these oscillations are not thought to be significant.

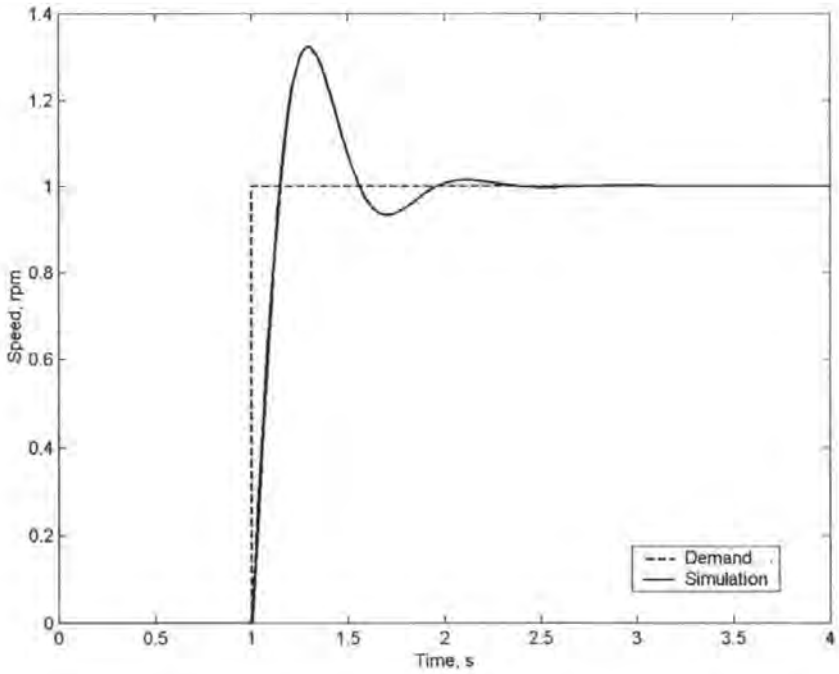

Figure 3.16: *Simulated Plant Response Under PID Control*

The PID controller was implemented in real time on the test system; Figure 3.17 illustrates the result. Clearly the response is oscillatory and is not acceptable. In addition the effect of changes within the load can clearly be observed within the plant response. The poor performance of the controller is attributed to the fact that the controller was developed on a model of the system that was known to be inaccurate. It is starkly illustrated here that a controller which is invariant to these load changes is also required, since mathematical tractability within future controller design is desired. In order to improve control performance, the system was tuned heuristically.

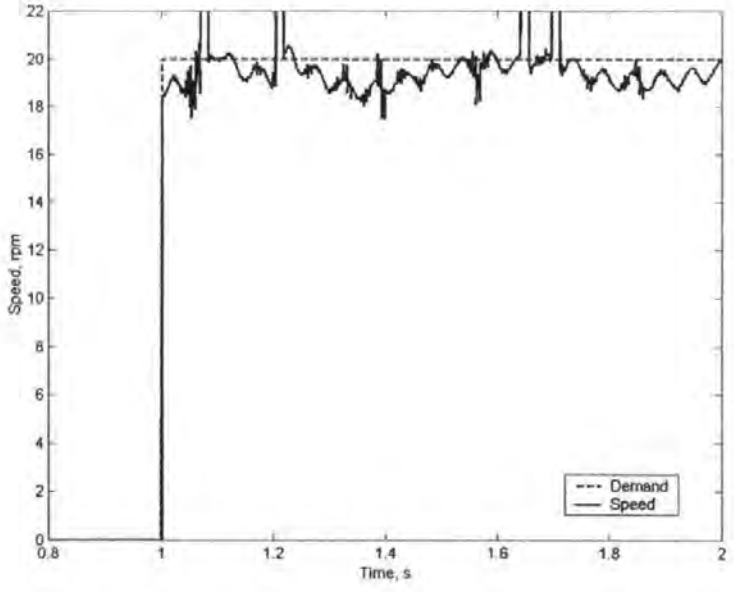

Figure 3.17: *System Response Under Zeigler-Nichols PID*

Figure 3.18 illustrates the unsmoothed results. Clearly, there is a good deal of measurement noise present, however the tuned controller performs with near zero error.

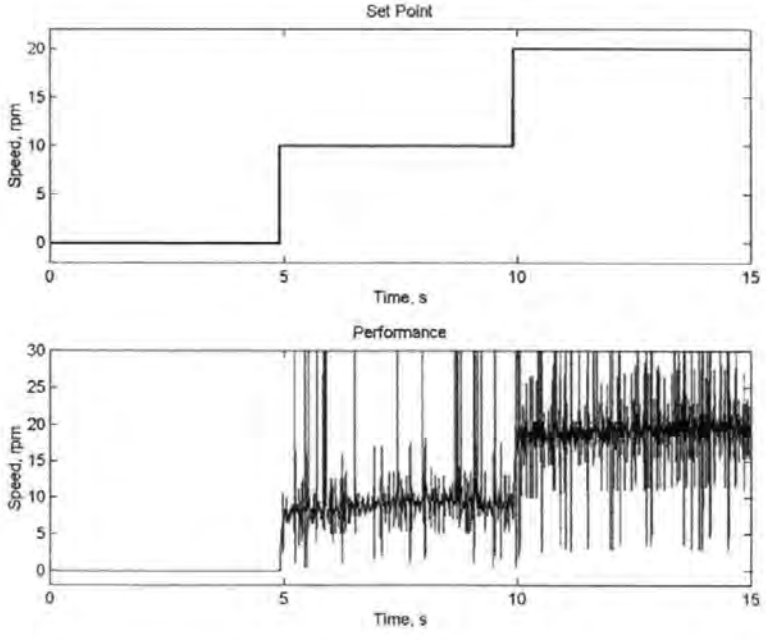

Figure 3.18: *Tuned Controller Response*

The previous controller was based entirely on the assumption that the load torque could be ignored. It was seen that the controller required significant tuning before its performance was deemed acceptable. A controller will now be developed using modern control techniques in order to take advantage of the additional understanding of the system dynamics afforded by the incorporation of the current state. Later within Chapter 6, a similar approach to incorporating an integral action into the control channel is developed. The derivation there relies on the use of a special canonical form, known as the regular form. For this section, however, concern is simply for the introduction of an integral action and the subsequent development of a controller based on pole placement techniques.

The state space model has been seen to perform reasonably in comparison to the system. It is therefore not unreasonable to use this model in developing the controller. Since concern is only with the control of motor speed, the position state is ignored to give

$$\begin{bmatrix} \dot{x}_1(t) \\ \dot{x}_2(t) \end{bmatrix} = \begin{bmatrix} -\frac{B}{J} & \frac{K_m}{J} \\ -\frac{K_e}{L} & -\frac{R}{L} \end{bmatrix} \begin{bmatrix} x_1(t) \\ x_2(t) \end{bmatrix} + \begin{bmatrix} 0 \\ \frac{1}{L} \end{bmatrix} U_1(t) \tag{3.104}$$

$$y(t) = Cx(t) \tag{3.105}$$

where $x_1(t) = \omega(t)$, $x_2(t) = i(t)$ and $U_1(t) = V(t)$. For the time being load torque will be ignored and treated as an exogenous disturbance which will need correction by the integral action. Now consider the introduction of a signal which satisfies

$$\dot{\varepsilon}(t) = r(t) - y(t) \tag{3.106}$$

where the differentiable signal r satisfies

$$\dot{r}(t) = \Gamma\left(r(t) - R\right) \tag{3.107}$$

where Γ is a stable design matrix and R a constant demand vector. Now consider the control law given by

$$u(t) = -K_1 x(t) - K_2 \int \dot{\varepsilon}(t)\, dt \tag{3.108}$$

The control effort is derived by through a summation of the system states and the integral action, after multiplication by the feedback gains. The system equations may be written

$$\begin{bmatrix} \dot{x}(t) \\ \dot{\varepsilon}(t) \end{bmatrix} = \begin{bmatrix} A & 0 \\ C & 0 \end{bmatrix} \begin{bmatrix} x(t) \\ \varepsilon(t) \end{bmatrix} - \begin{bmatrix} B \\ 0 \end{bmatrix} \begin{bmatrix} K_1 & K_2 \end{bmatrix} \begin{bmatrix} x(t) \\ \varepsilon(t) \end{bmatrix} + \begin{bmatrix} 0 \\ \Gamma \end{bmatrix} r \tag{3.109}$$

subject to compatible dimensioning of the matrices. This equation may also be written as

$$\dot{\tilde{x}}(t) = \left(\tilde{A} - \tilde{B}K\right)\tilde{x}(t) + \tilde{\Gamma} r(t) \tag{3.110}$$

with

$$\tilde{A} = \begin{bmatrix} A & 0 \\ C & 0 \end{bmatrix},\ \tilde{x}(t) = \begin{bmatrix} x(t) \\ \varepsilon(t) \end{bmatrix},\ \tilde{B} = \begin{bmatrix} B \\ 0 \end{bmatrix},\ K = \begin{bmatrix} K_1 & K_2 \end{bmatrix} \text{ and } \tilde{\Gamma} = \begin{bmatrix} 0 \\ \Gamma \end{bmatrix}.$$

This final equation is easy to recognise as the state feedback problem. A controller for the system will now be developed based on this derivation. Inserting the nominal values for the motor into the equations and selecting

$$C = \begin{bmatrix} -1 & 0 \end{bmatrix} \tag{3.111}$$

yields

$$\tilde{A} = \begin{bmatrix} -2.692 & 6 & 0 \\ -20.77 & -246.15 & 0 \\ -1 & 0 & 0 \end{bmatrix} \tag{3.112}$$

$$\tilde{B} = \begin{bmatrix} 0 \\ 384.62 \\ 0 \end{bmatrix} \tag{3.113}$$

$$\tilde{\Gamma} = \begin{bmatrix} 0 \\ 0 \\ 1 \end{bmatrix} \tag{3.114}$$

Since the matrix pair $\left(\tilde{A}, \tilde{B}\right)$ is controllable, the control law is given by

$$u(t) = k_1 x_1(t) + k_2 x_2(t) + k_3 \int \dot{\varepsilon}\, dt \tag{3.115}$$

The closed loop characteristic equation is given by

$$|\lambda I - A + BK| = \lambda^3 + (248.842 + 384.62k_2)\lambda^2 + (1035.4k_2 + 2307.72k_1 + 78.725)\lambda + 2307.72k_3 \tag{3.116}$$

The closed loop poles of the system are desired in the locations

$$\begin{bmatrix} -300 & -10 + j5 & -10 - j5 \end{bmatrix} \tag{3.117}$$

The selection of the conjugate pair as the dominant poles will provide a slightly under-damped response, as in the case of the PID controller. In order to achieve this eigenvalue spectrum, the feedback gain matrix must be

$$K = \begin{bmatrix} 2.537 & 0.185 & 16.25 \end{bmatrix} \tag{3.118}$$

Implementation of this controller yields the step response with no load as in Figure 3.19.

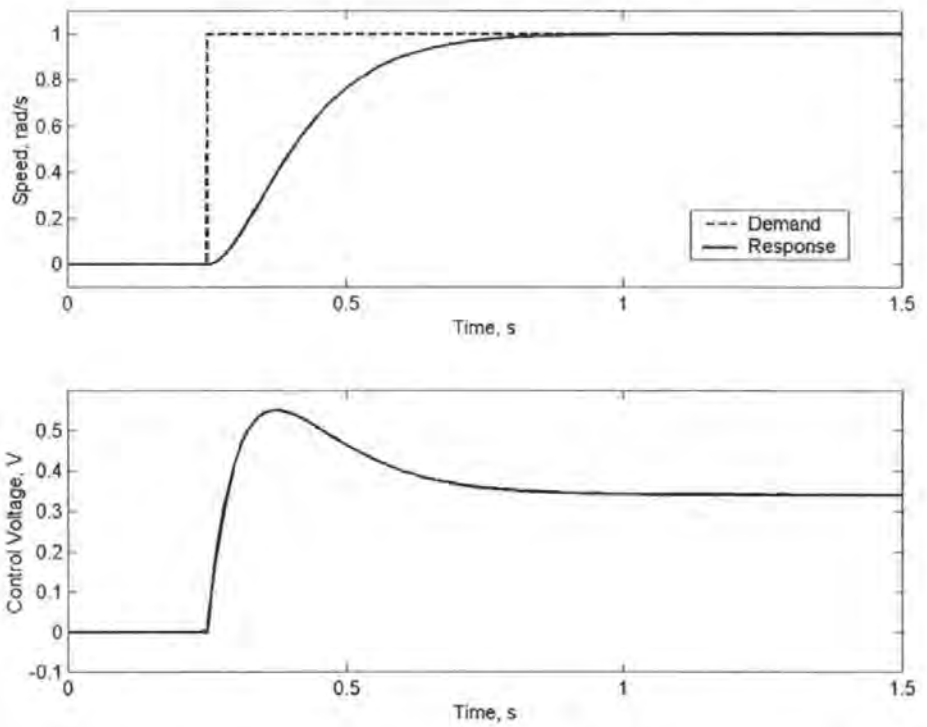

Figure 3.19: *Integral Action Controller Step Response, Time Response (top), Control Effort (bottom)*

The controller step response does not give overshoot and has a 2% settling time of 0.53 seconds. Of interest is the effect that the load torque will have on the controller. A negative load of 0.2 Nm was applied in the simulation (Figure 3.20). The system in this case has a 2% settling time of 0.54 seconds, nearly identical to that of the system under no load conditions. The clear divergence from the demand over the initial period is due to the lack of a clear error to integrate. This fact is clearly illustrated in Figure 3.21, where once the error has become significantly large, the controller then reduces the error to zero.

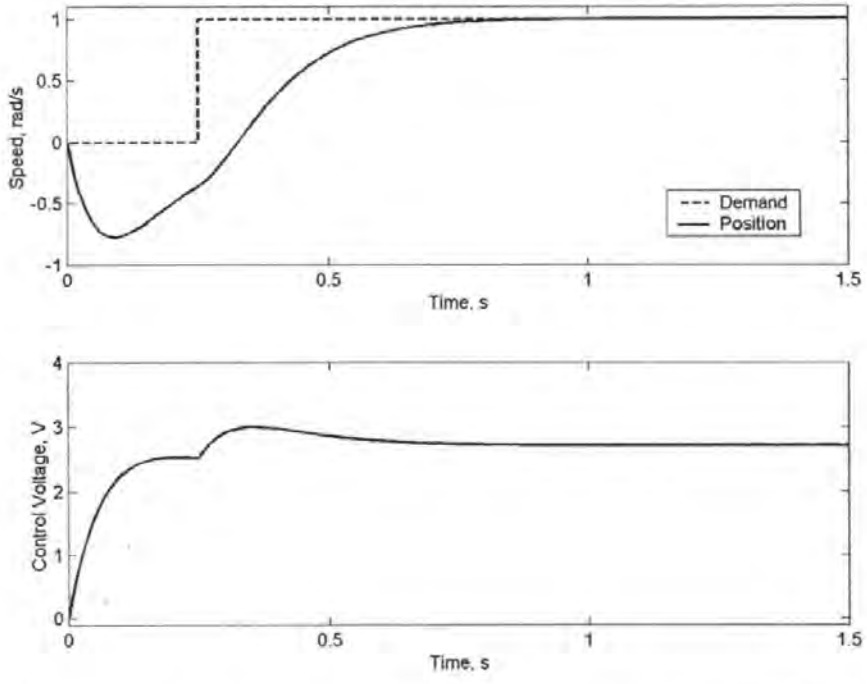

Figure 3.20: *System with -0.2Nm Load, Step Response (top), Control Effort (bottom)*

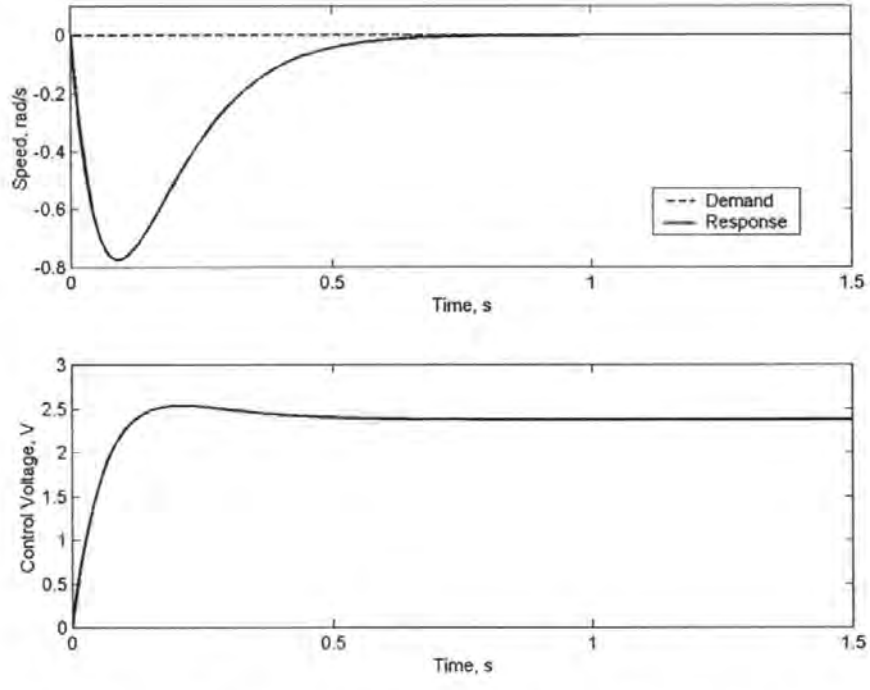

Figure 3.21: *Unforced System Response to -0.2Nm Load, Time Response (top), Control Effort (bottom)*

This controller was implemented on the test system, the response of the system can be seen in Figure 3.22. There is clearly close agreement between the simulated response and the actual response to a step input. There is slight overshoot evident on the actual system and there remains some disparity between the simulation and the actual system. This is attributed as much to measurement error as variation within the load.

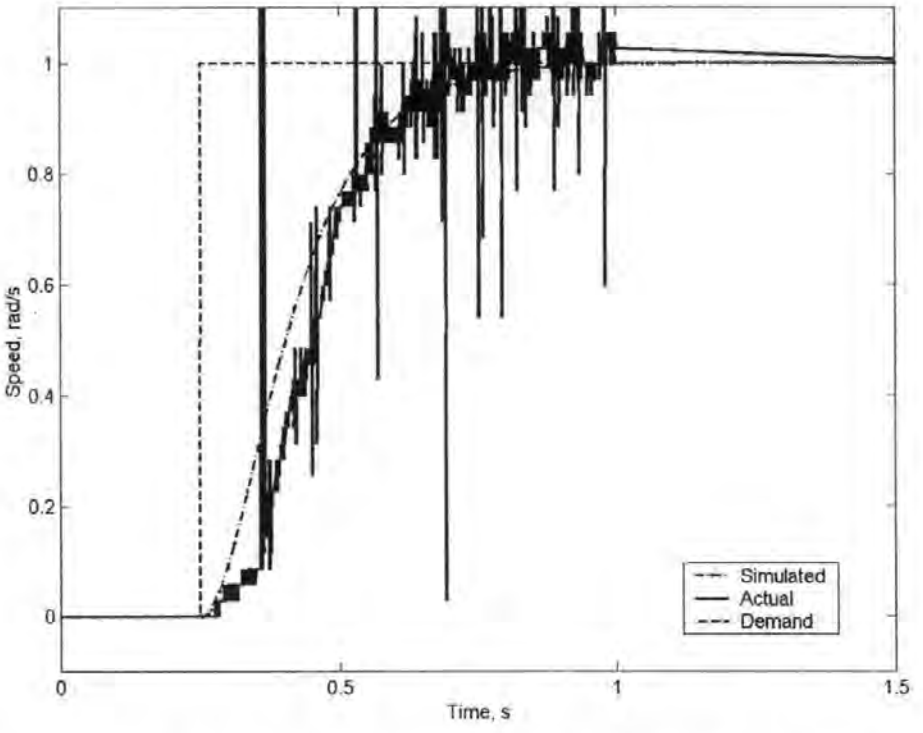

Figure 3.22: *Step Response of Actual System Compared to Simulated Response*

It is clear however that a suitable controller can be derived based on mathematically tractable results if the model is of sufficient quality. There is still a requirement, however for a controller which will be invariant to the variations within the load.

3.5 Discussion

This Chapter has served to introduce the experimental test rig. Its mechanical and electrical interfaces have been discussed. A novel approach to reducing system bandwidth requirements in the face of high frequency sensor signals has been developed. Several models of the system, based on a priori knowledge of the motor performance have been discussed, and their respective performances compared. The third order state space model has been shown to be sufficiently accurate to use as a basis from which to develop state feedback controllers. The higher order models may provide slight performance advantages, but it is clear that the load, for which only diminutive information is available, is the predominant cause of error within the models. Two controllers were developed based on the models discussed. The first was a PID controller, using the Zeigler-Nichols reaction curve method to find the initial controller parameters. These proved to provide an unacceptable controller performance. Subsequent tuning led to an acceptable controller, however it is clear that for the duration of this work, heuristic tuning of controllers is not an acceptable design approach. The second controller made use of the enhanced knowledge of system dynamics afforded by measurement of the load current. The controller was shown to perform much more predictably in practice. The integral action of the controller has been shown to reduce the steady state error of the system to zero, despite load uncertainties. This integral action may therefore be said to introduce a robustness to these disturbances. This type of controller will be used heavily later within this work.

3.6 References

Armstrong-Helouvry B., Dupont P. and Canudas De Wit C. 1994. 'A Survey of Models, Analysis Tools and Compensation Methods for the Control of Machines with Friction', Automatica, **30**(7), pp 1083-1138

Coelingh E., De Vries T.J.A, Holtermann J and Van Amorongen J. 1998, 'Mechatronic Systems with Uncertain Physical Parameters', Mechatronics '98

Golten J. and Verwer A., 1991, 'Control System Design and Simulation', McGraw-Hill

Hemati N. and Leu M. 1992. 'A Complete Model Characterisation of Brushless DC Motors', IEEE Trans. Industry Applications, **28**(1), pp 172-180

Kenjo T. and Nagamori S., 1985, 'Permanent Magnet and Brushless D.C. Motors', Clarendon Press.

Kocybik P. 2000. 'Electronic Control of Torque Ripple in Brushless D.C. Motors', PhD Thesis, University of Plymouth

Krause P., Wasynczuk O. and Sudhoff S. 1995. 'Analysis of Electric Machinery', IEEE Press

Low.T-S., Bi C. and Chang K-T. 1996. 'Motor 'Identity' – A Motor Model for Torque Analysis and Control', IEEE Trans. on Industrial Electronics, **43**(2), pp 285-291

Newport, 1999, 'Motion Control Tutorial', www.newport.com

Pillay P. and Krishnan.R. 1991. 'Application Characteristics of Permanent Magnet Synchronous and Brushless D.C. Motors for Servo Drives', IEEE Trans. Industry Applications, **27**(5). pp 986-996

Rahman M. and Zhou P. 1996, 'Analysis of Brushless Permanent Magnet Synchronous Motors', IEEE Trans. Industrial Electronics. **43**(2). pp 256-267

Seraji H. 1983, 'Design of Two and Three Term Controllers for Discrete Time Multivariable Systems', International Journal of Control, 38(4), pp 843-865

Shi C. and Li M. 1996. 'A General Model of Synchronous Machine for its Steady State Performance Analysis', IEEE Trans. on Energy Conversion, 5(3), pp 531-537

Shing T.K. 1994, 'Dynamics and Control of Geared Servomechanisms with Backlash and Friction Consideration', PhD thesis, University of Maryland

Unar M.A., Murray-Smith D.J. and Ali-Shah S.F. 1996. 'Design and Tuning of Fixed Structure PID Controllers', University of Glasgow

Vas P.,1993, 'Space Vector Analysis of Electrical Machines', Oxford University Press

Chapter 4

System Identification

4.1 Introduction

The development of models to describe system behaviour is of interest within many areas of science and engineering. The models, once developed provide the user with a method for describing the behaviour of a system, and the means to develop prediction and control algorithms. In the previous Chapter, comprehensive models of the brushless direct current motor and its accompanying system have been derived based on prior engineering knowledge of the motor's physical construction. This approach to modelling is commonly referred to as the 'white-box' method. Implicit in this approach is that nonlinearities within the motor have negligible effect on system performance, and may be ignored. Within the literature there exist many motor models for which any number of superlatives are probably quite applicable, however within this work the motor is rigidly coupled to a load for which only diminutive information about its dynamics exist. The load is known to be time variant and it was shown to vary with relative position along the length of the stage in Chapter 3. When dealing with the system at the holistic level, it becomes necessary to investigate alternative approaches to the estimation of system performance.

A common alternative to the white-box modelling methods described above is the black-box approach. This is approach represents the antithesis of the white-box method; thence its name is derived. The black-box approach relies on the collection of input excitation

and resultant output data. From a given data set, it becomes possible to search for correlation in the data and to define input-output relationships. In such a manner, the user is not strictly required to understand the latent system. The flexibility of such an approach has led to its application in fields as diverse as chemical process modelling (Hellendoorn and Driankov, 1997) to banana ripeness testing (Llobet *et al.*, 1999). Clearly, definition of such systems through the white-box approach would soon become intractable. Figure 4.1 illustrates the output of a white-box phase coordinate model and its comparison with the motor coupled with the load (from Chapter 3). There is clearly a case here for using the black-box approach in order to improve modelling accuracy.

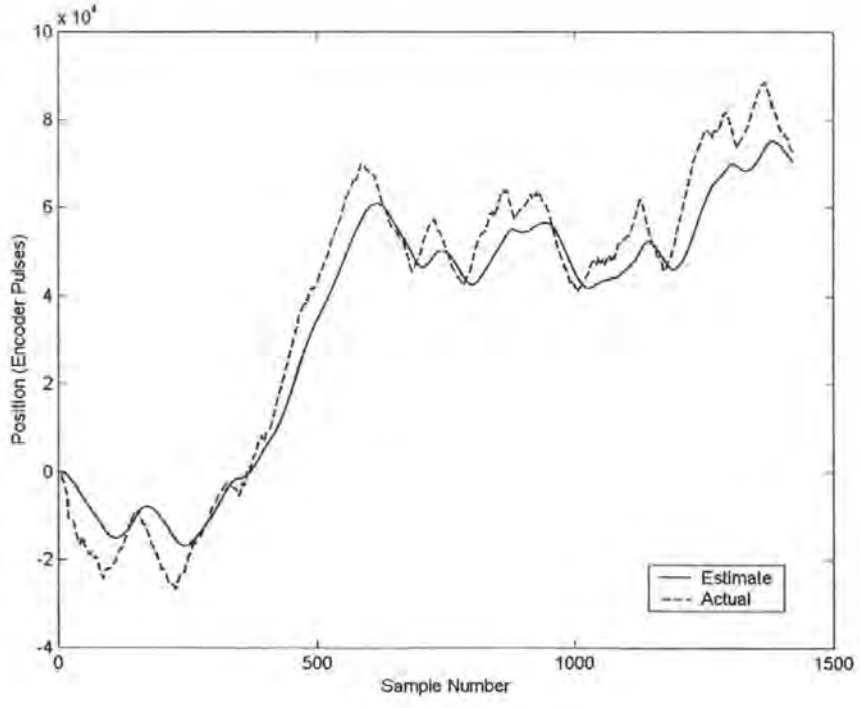

Figure 4.1: *Phase Coordinate Model Results*

It has become the case that the black-box approach is used synonymously with the field of system identification. Throughout this work, however, the definition of system identification will be that of Ljung(1998):

> [system identification is ~] "*the theory of designing mathematical models of dynamical systems from observed data*"

It will be demonstrated that black-box modelling, according to this definition comprises only one part of this research area. Neither of the two approaches discussed thus far are without merit. The white-box model is guaranteed to maintain physical relevance and thus provide an authentic characterisation of the modelled system, as opposed to a simple data description. Conversely, the black-box models are easier to construct than the white-box models and often leads to significant reduction in simulation times since the use of partial, differential and algebraic equations can be avoided.

One final area of consideration within this Chapter will be to achieve synergy between the black-box and white-box approach, such that the advantages of both are retained. This comparatively new approach has been dubbed the 'grey-box' approach within the literature (Linskog, 1996).

This Chapter now continues with the consideration of necessary mathematical foundations, upon which the black-box models are to be built. The concepts associated with fuzzy clustering are also introduced. System models are then identified using artificial neural networks and fuzzy clustering, using data acquired from the test rig. In addition, comparative measures for the assessment of model quality are made. Finally,

methods are sought whereby the system models may be improved through the application of *a-priori* knowledge.

4.2 Mathematical Foundations

In the previous section system identification is described as being concerned with the development of a system model from observed data. Essentially this is the theory of inferring system outputs from system inputs at finite time t. The process of identification is to choose a model of sufficient flexibility, and one that is known to have performed well in the past. One specific family often employed because of this is based around the linear difference equation (Leonartis and Billings, 1985a) given by:

$$y(t)+a_1y(t-1)+\ldots+a_ny(t-n)=b_1u(t-1)+\ldots+b_m(t-m) \tag{4.1}$$

the system is represented in discrete time; this is principally because the data within this work is collected through sampling. The sample interval is assumed constant. Simple transposition of (4.1) allows the determination of the next system output given previous observations

$$y(t)=-a_1y(t-1)-\ldots-a_ny(t-n)+b_1u(t-1)+\ldots+b_mu(t-m) \tag{4.2}$$

Simply for the purposes of tidiness, and more compact notation two vectors are introduced

$$\theta=\left[a_1\ldots a_n \quad b_1\ldots b_m\right] \tag{4.3}$$

$$\varphi(t)=\left[-y(t-1)\ldots-y(t-n) \quad u(t-1)\ldots u(t-m)\right] \tag{4.4}$$

Having defined (4.3) and (4.4) equation (4.2) may be rewritten as

$$y(t)=\varphi^T(t)\theta \tag{4.5}$$

$y(t)$ is an estimated value and depends heavily on the parameters within the vector θ, the equation (4.5) is therefore rewritten in order to reflect this:

$$\hat{y}(t|\theta) = \varphi^T(t)\theta \tag{4.6}$$

Model structures such as the one in (4.6), which are linear in θ are referred to as *linear regressions*, $\varphi(t)$ an *auto-regression* if it contains previous values of y(t). The vector $\varphi(t)$ is known in general as the *regression vector*, its parameters the *regressors*. The model in (4.5) contains previous values of the variable to be calculated. Based on these definitions, the model structure of equation (4.1) is given the general name Auto-Regression with eXogenous variables (or eXtra inputs), or ARX as a convenient acronym.

Ljung (1998), and others within the field generally agree that there three processes or entities within the system identification prototype. Given in logical order they are

1. The data set
2. The set of chosen candidate model structures, e.g. the ARX model above
3. The selection criteria

The data set comes from the assumption that precise parameters in θ are unknown. These are therefore recorded inputs and outputs given over time interval $1 \leq t \leq N$:

$$Z^N = \{u(1), y(1), \ldots, u(N), y(N)\} \tag{4.7}$$

It is important to note that the input – output data need not be raw data collected from the system. If it is known, as in the case here, that torque is a principal component of disturbance then a model of torque based on output data might be used instead. Typically, input – output data is collected through designed experiments subject to design

constraints. The schematic diagram of the test rig is illustrated in Figure 3.1. The diagram illustrates a series of input and output nodes. These nodes represent points within the real system from which data may be collected. The aim is to collect data that will be maximally informative during training. The selection of the model structure is generally regarded as the most difficult part within the identification process. It has already been seen that a general multi-input single output (MISO) model structure such as (4.6) can be used, where the function $f\left(\varphi(t),\theta\right)$ is a mapping which is parameterised in θ. The task of finding a suitable model structure is naturally divided into two disparate tasks

1. Choosing the regression vector $\varphi(t)$
2. Choosing the static mapping $f\left(\cdot|\cdot\right)$

These are the topics of greatest consideration within this work and it will naturally be revisited in the following sections. Figure 4.2 illustrates the standard data set which was acquired from the test rig. This data set will be used throughout the identification process, except where stated. The reasons for selecting this data set will become clear later within the text.

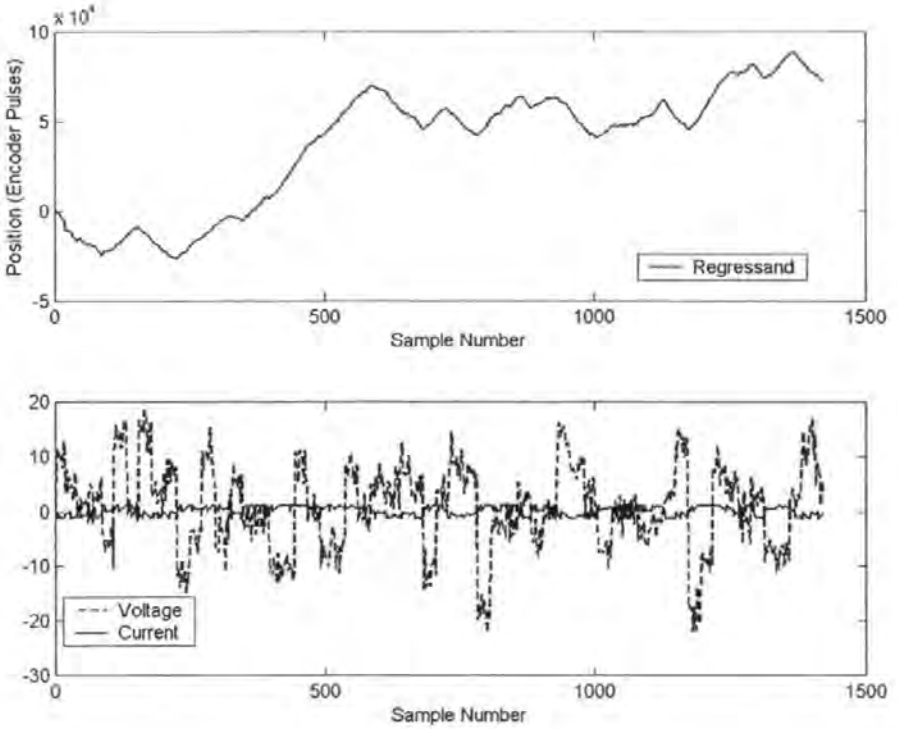

Figure 4.2: *Identification set 1*

At this point, a general transfer function of a linear system with additive disturbance is defined for future reference

$$y(t)=G(q^{-1})u(t)+H(q^{-1})e(t) \tag{4.8}$$

where q^{-1} denotes the *backward shift operator*, i.e.

$$q^{-1}u(t)=u(t-1) \tag{4.9}$$

$e(t)$ is assumed to be a sequence of independent variables with zero mean and variance λ. Choice of the selection criteria is really the choice of measure for assessment of model performance. Since model and measured outputs are never precisely matched perfectly, an error term is introduced to reflect this

$$\varepsilon(t|\theta) = y(t) - \hat{y}(t|\theta) \tag{4.10}$$

this term naturally represents both unmodelled dynamics of the system, measurement noise within the data set and the effect of disturbances on the system. A typical choice for the minimisation of this error function is the quadratic cost function. It follows that the function that minimises the error $\varepsilon(t|\theta)$ will be the function that selects θ in such a manner as to fit $\hat{y}(t|\theta)$ as closely to the measured outputs as possible.

$$\min_{\theta} V_N(\theta, Z_N) \tag{4.11}$$

where V_N in the case of the least squares method is given

$$V_N(\theta, Z^N) = \frac{1}{N}\sum_{t=1}^{N}\left(y(t) - \hat{y}(t|\theta)\right)^2 = \frac{1}{N}\sum_{t=1}^{N}\left(y(t) - \varphi^T(t)\theta\right)^2 \tag{4.12}$$

The value of θ which minimises (4.11) will be denoted $\hat{\theta}_N$

$$\hat{\theta}_N = arg \quad \min_{\theta} V_N(\theta, Z_N) \tag{4.13}$$

It then becomes a matter of finding the solution to (4.13); in this case, since V_N is quadratic in θ, the minimum is given by setting the derivative to zero

$$0 = \frac{d}{d\theta} V_N(\theta, Z^N) = \frac{2}{N}\sum_{t=1}^{N}\varphi(t)\left(y(t) - \varphi^T(t)\theta\right) \tag{4.14}$$

giving

$$\sum_{t=1}^{N}\varphi(t)y(t) = \sum_{t=1}^{N}\varphi(t)\varphi^T(t)\theta \tag{4.15}$$

this leads to

$$\hat{\theta}_N = \left[\sum_{t=1}^{N}\varphi(t)\varphi^T(t)\right]^{-1}\sum_{t=1}^{N}\varphi(t)y(t) \tag{4.16}$$

The chosen norm and method of finding θ may differ from application to application; however, in general, the principle remains the same.

The ARX model has been discussed above; there are several alternatives to this model such as *Output Error* (OE), *Auto Regression Moving Average with eXogenous variables* (ARMAX), *Box Jenkins* (BJ) and *Finite Impulse Response* (FIR). It was shown in Sjoberg *et al.* (1995), that all of the models might be summarised by the general form

$$A\left(q^{-1}\right)y(t)=\frac{B\left(q^{-1}\right)}{F\left(q^{-1}\right)}u(t)+\frac{C\left(q^{-1}\right)}{D\left(q^{-1}\right)}e(t) \tag{4.17}$$

where

$$A\left(q^{-1}\right)=1+a_1q^{-1}+\ldots+a_nq^{-n} \tag{4.18}$$

$$B\left(q^{-1}\right)=b_0+b_1q^{-1}+\ldots+b_mq^{-m} \tag{4.19}$$

$$C\left(q^{-1}\right)=1+c_1q^{-1}+\ldots+c_kq^{-k} \tag{4.20}$$

$$D\left(q^{-1}\right)=1+d_1q^{-1}+\ldots+d_lq^{-l} \tag{4.21}$$

$$F\left(q^{-1}\right)=1+f_1q^{-1}+\ldots+f_rq^{-r} \tag{4.22}$$

Each model structure can be considered to fit within this prototype, and all except the ARX structure are discussed individually in Appendix C, part 2. The ARX structure is discussed below because of its direct relevance to the remainder of this work.

4.2.1 AutoRegression with eXternal inputs (ARX)

The structure of the ARX model has already been discussed. The structure has poles within G of the transfer function description (4.8), and potential modelling accuracy is therefore improved in comparison to the FIR model (Appendix C, part 2). However, there remains only an algebraic relationship between past inputs and outputs. Therefore, the

ARX model will always be stable, irrespective of the modelled system. Figure 4.3 illustrates the results of applying the ARX model to the identification data set shown in Figure 4.2, a prediction error method was used for training, which will be discussed in greater detail in §4.4.1. A discussion of the performance of this model is deferred until comparisons can be made with other models in §4.8. The model structure used was [4 4 1], i.e. 4 previous regressors, 4 previous regressands and a time delay of 1 sample. This structure will be used throughout the nonlinear identification work since it has proved to be successful.

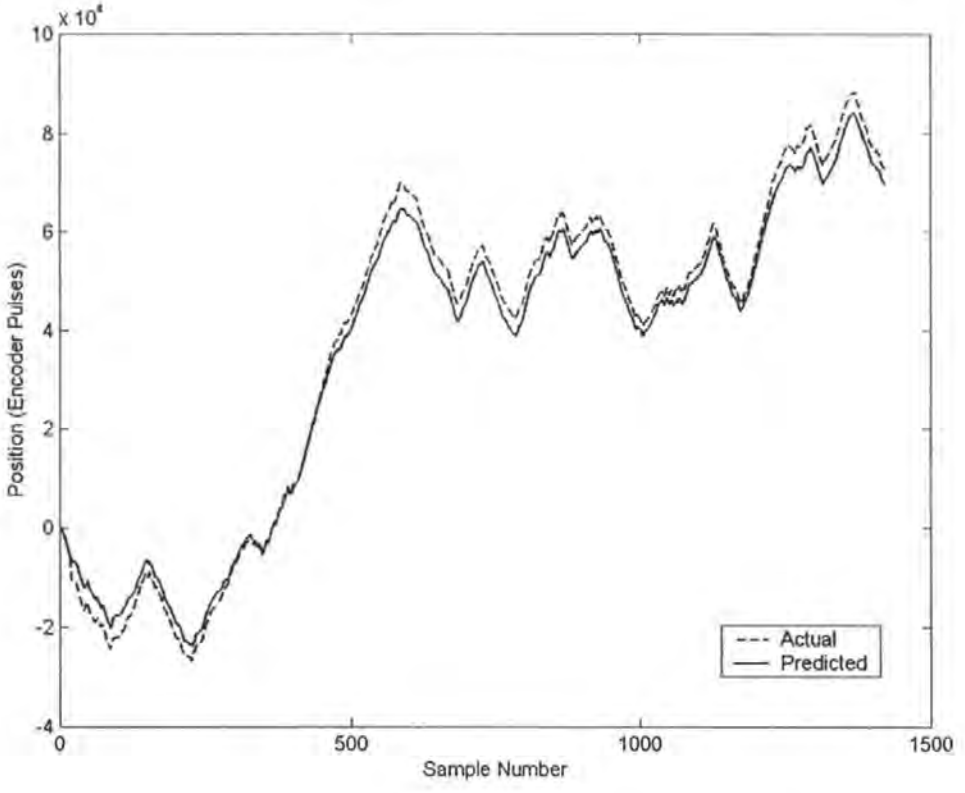

Figure 4.3: *Identification results for linear ARX model*

In application of linear black-box models, the user is attempting to describe the system's frequency response (or impulse response) which is a mapping $\mathbb{R} \to \mathbb{R}^{p \times m}$ (where p is the number of outputs and m is the number of inputs). Depending on the application, this type of model might be entirely acceptable, if however, greater model fidelity and more detailed information about the system is required then non-linear modelling is required and the problem becomes more complicated. The principle reason for this increased complexity is that in the ideal, all system information will be included within the model; this implies a very broad spectrum of possible model descriptions to be considered. There has been significant research interest in this area and the application of structures based on neural networks, radial basis networks, wavelet networks, hinging hyperplanes and models based on fuzzy logic may all be readily found within the literature, for a review see for example Juditsky *et al.*, (1995). The next section of this report moves on to consider some of the more general aspects of non-linear black-box modelling.

4.3 Non-linear Black-box Models

The regressors given within the last section provide the necessary degrees of freedom for the linear black-box case. It is therefore natural to extend their use to the non-linear case. Structures of the form

$$\hat{y}(t|\theta) = f(\varphi(t), \theta) \tag{4.23}$$

are used in non-linear black-box modelling, where f is a non-linear function parameterised by θ and the components of $\varphi(t)$ are similar to the regressors described in the linear case. With respect to the model structures described in the previous section, both the ARX and FIR models use one or both of the regressors, $u(t-k)$ and $y(t-k)$.

These data are measured variables and therefore offer no difficulty in application. The remaining models are based on previous outputs from the black-box model $y(t-k|\theta)$, so instead of $\varphi(t)$ in (4.23), the regression vector should be written $\varphi(t|\theta)$. An obvious question is how the simulated output $\hat{y}_u(t-k|\theta)$ might be computed if the network output is given as for the NFIR and NARX models as the prediction $\hat{y}(t-k|\theta)$. The solution is based on the fact that the output of the model is equal to $\hat{y}_u(t|\theta)$ if all of the measured inputs $y(t-k)$ are replaced by the previous output $\hat{y}_u(t-k|\theta)$. According to the adopted nomenclature, all of the linear models discussed above in the non-linear form are prefixed with N (Non-linear).

The linear models that employ a regression vector with past model outputs as a component (e.g. ARMA, ARMAX, NBJ, and NOE) correspond to recurrent structures (Leonartis and Billings, 1985b). In general, there is greater difficulty attributed to working with recurrent structures, since among other things, it becomes difficult to check under what conditions the obtained model is stable, and it takes an extra effort to calculate gradients for model parameter estimation (Norgaard *et al.*, 2000).

4.3.1 Other Choices of Regressors

As alluded to within section 4.2, there is no reason to restrict the choice of regressor to those that that are just linear functions of measured inputs, measured outputs, and model outputs. Should physical insight be available then it may feasibly be used to transform raw data into more pertinent regressors. From an applied perspective, it is sufficient to regard the input (u) and output (y) as transformations of the raw measurements, formed

in view of what is known about the system. For example, a so-called "Semi-physical Regressor" (Sjoberg, 1995) could be a load torque signal formed through current and angular velocity measurements, if it is believed that the torque signal is a principal stimulus of system performance. Despite the fact that the non-linear model can more readily characterise these relationships, there is no reason to waste computational effort in estimating phenomena that are already understood.

Another type of pre-processing of raw data in the light of prior knowledge is to use filtered inputs as regressors e.g.

$$L_k(q)u(t) \qquad k = 1, \ldots, d \tag{4.24}$$

rather than $u(t-k)$, where the filters L_k are tailored to the application.

4.3.2 Other Structural Issues

The combination of regressors clearly reflects structural assumptions about the system; there is obviously enhanced flexibility in using a non-linear model with a learning structure such as a neural network (Hunt *et al.*, 1992). For instance, the parameterised function f within a non-linear black-box model structure is defined either as linear or non-linear during training. A further motivation for this model is that it becomes easier to develop controllers than from the models discussed earlier, see for example Norgaard *et al.*, (2000). In Ljung and Glad (1994), it is suggested first to build a linear model for the system. The residuals from this model will then contain all unmodelled non-linear effects. The neural network based model would then be modelled on these residuals, to pick up the system non-linearity. The outputs of the two models may be recombined to provide a gross system output prediction. This approach is attractive, since as has been seen in

Chapter 3, the steps in obtaining a linear model are well founded on prior knowledge and lead to reasonable models. Subsequent application of the nonlinear model based on white-box model residuals at least guarantees a model whose performance matches the linear white-box model. Inevitably within any model there must be some error expected in the estimation. This error is due to a bias inherent within the model due to an insufficient model structure. Unfortunately, the model size cannot be increased *ad infinitum* because as the model grows, so the variance of the model coefficients must grow for a given training set. This is referred to as the bias-variance dilemma and discussed in more detail in Appendix C, part 3. The selection of the most suitable model structure within this work will be dealt with on an individual basis.

4.4 Training Algorithms

In the course of system identification, the choice of training algorithm is of critical importance, since it affects the convergence of the selected model. This section of the report is dedicated to the consideration of some of the training algorithms available. It was shown in the first section of this Chapter how quadratic minimisation based on the least squares approach may be used to minimise $V_N(\theta)$. In general, however, an analytical computation of the minimum of $V_N(\theta)$ is not possible. The minimum must be sought through a numerical search procedure. Such a procedure is commonly known as *non-linear optimisation.*

It is assumed at this point that the model structure has been selected, and that a data set has been acquired. Clearly, the task of the optimisation, or training is to obtain a mapping from the dataset to the set of candidate models.

$$Z^N \rightarrow \hat{\theta} \tag{4.25}$$

The mean square error criterion from (4.12) is a common performance measure. Training schemes based on this criteria are known as *Prediction Error Methods* (PEM), since the training objective is to minimise a given norm of the prediction error. With the criterion given in (4.12) the PE method will correspond directly to maximum likelihood estimation if the noise signal distribution is Gaussian.

4.4.1 The Prediction Error Method

It has been seen that the objective using the mean square error criterion is given by

$$\hat{\theta} = \arg \min_{\theta} V_N(\theta, Z^N) \tag{4.26}$$

Searching for the minimum is achieved by consideration of the second order Taylor series expansion of the criterion in θ_*

$$V_N(\theta, Z^N) = V_N(\theta_*, Z^N) + (\theta - \theta_*)^T V_N'(\theta_*, Z^N) + \frac{1}{2}(\theta - \theta_*)^T V_N''(\theta_*, Z^N)(\theta - \theta_*) \tag{4.27}$$

where the gradient is given by

$$G(\theta_*) = V_N'(\theta_*, Z^N) = \left. \frac{dV_N(\theta, Z^N)}{d\theta} \right|_{\theta=\theta_*} \tag{4.28}$$

and the Hessian is defined by

$$H(\theta_*) = V_N''(\theta_*, Z^N) = \left. \frac{d^2 V_N(\theta, Z^N)}{d\theta^2} \right|_{\theta=\theta_*} \tag{4.29}$$

A sufficient condition for $\theta=\theta_*$ to be at a minimum is that the gradient is zero. In addition, that the Hessian is greater than zero, for all nonzero data vectors (v) i.e.

$$G(\theta_*) = 0 \tag{4.30}$$

$$v^T H(\theta_*) v > 0 \tag{4.31}$$

The search begins with an initial guess at the parameters in θ, $\theta_{(0)}$. The selected training method then comes into its own and adjusts the weights according to some search criterion. This is usually achieved iteratively and generally takes the form

$$\theta_{(i+1)} = \theta_i + \mu_{(i)}\eta_{(i)} \tag{4.32}$$

where $\theta_{(i)}$ specifies the current iteration, $\eta_{(i)}$, the search direction and $\mu_{(i)}$ the step size. Iteration continues until the minimisation criteria are satisfied. Unfortunately, the criteria described above will generally have more than one minimum. The method as described above will not guarantee convergence to the global minimum, but instead the minimum that is actually obtained will depend entirely on the choice of $\theta_{(0)}$.

Gradient Descent

Gradient descent is a prediction error method. The task of training is to obtain the mapping from the dataset to a set of candidate models,

$$Z^N \rightarrow \hat{\theta} \tag{4.33}$$

In this case, the objective is to minimise the mean square error according to

$$\hat{\theta} = \arg\min_{\theta} V_N\left(\theta, Z^N\right) \tag{4.34}$$

The prediction error method is iterative and generally takes the form

$$\theta_{(i+1)} = \theta_i + \mu_i \eta_i \tag{4.35}$$

where $\theta_{(i)}$ specifies the current iteration, η_i specifies the search direction and μ_i specifies the step size. The iteration of the algorithm continues until such time as the

minimisation criteria is satisfied. The principle of the gradient descent method is to adjust the weights of the network in the opposite direction to the gradient, i.e

$$\eta_i = -G\left(\theta_{(i)}\right) \tag{4.36}$$

$$\theta_{(i+1)} = \theta_i - \mu_{(i)} G\left(\theta_{(i)}\right) \tag{4.37}$$

where

$$G\left(\theta_{(i)}\right) = \left.\frac{dV_N\left(\theta, Z^N\right)}{d\theta}\right|_{\theta=\theta_i} \tag{4.38}$$

If the step size μ_i is sufficiently small with this choice of direction, then it is always possible to achieve a reduction of the criterion,

$$V_N\left(\theta_{(i+1)}, Z^N\right) \leq V_N\left(\theta_{(i)}, Z^N\right) \tag{4.39}$$

As alluded to above, this method's convergence is entirely dictated by the step size. Frequently this step size is selected to be a constant. There is no guideline for this selection, but the need to maintain a small step size frequently leads to slow convergence. In Demuth and Beale (2001), an alternative approach uses an adaptive step size to control the convergence. Irrespective of the step size, convergence using this algorithm is linear, and comparatively slow. When applied to neural networks, this method is known as *back-propagation* (Lewis *et al,* 1999), and despite the slow convergence, it has grown in popularity because of its simplicity in implementation and modest storage requirements. The slow convergence property has however led to implementations that are more sophisticated.

The Newton Method

The previous methods rely on a first order approximation to the criterion in order to determine the search direction. The Newton method is a natural extension to the gradient method and uses a second order expansion of the criterion

$$\tilde{V}_N(\theta, Z^N) = V_N(\theta_{(i)}, Z^N) + [\theta - \theta_{(i)}]^T G(\theta_{(i)}) + \frac{1}{2}[\theta - \theta_{(i)}]^T H(\theta_{(i)})[\theta - \theta_{(i)}] \tag{4.40}$$

The differential of the estimate is introduced

$$\psi(t,\theta) = \frac{d\hat{y}(t|\theta)}{d\theta} \tag{4.41}$$

The gradient and Hessian are given as

$$G(\theta) = V_N'(\theta, Z^N) = \frac{1}{N}\sum_{t=1}^{N} \psi(t,\theta)[y(t) - \hat{y}(t|\theta)] \tag{4.42}$$

$$H(\theta) = V_N''(\theta, Z^N) = \frac{1}{N}\sum_{t=1}^{N} \psi(t,\theta)\psi(t,\theta)^T - \frac{1}{N}\sum_{t=1}^{N} \psi'(t,\theta)\varepsilon(t,\theta) \tag{4.43}$$

Define the minimum as

$$0 = G(\theta_{(i)}) + H(\theta_{(i)})[\theta - \theta_{(i)}] \tag{4.44}$$

which gives the update rule

$$\theta_{(i+1)} = \theta_{(i)} - H^{-1}(\theta_{(i)})G(\theta_{(i)}) \tag{4.45}$$

The search direction is determined by solving the system of equations

$$H(\theta_{(i)})\eta_{(i)} = -G(\theta_{(i)}) \tag{4.46}$$

$\eta_{(i)}$ is frequently referred to as the *Newton search direction*. The ideal step size for the Newton method would be one if the underlying criterion were truly quadratic (Sjoberg *et al*, 1995). In practice, the approximation of the criterion (4.40) might only be valid around a certain neighborhood of the current iterate. The full step might therefore bring

the new iterate to a point far from the point predicted by the approximation. To circumvent this problem, a line search of the step size may be incorporated into the Newton method. In such a case, the method is known as the *damped Newton method.* Convergence of the damped Newton method cannot be guaranteed. In addition, calculation of the Hessian is a computationally demanding task. Often approximations to the Hessian matrix are calculated instead. These methods are known as quasi-Newton methods and are discussed further in Dennis and Schnabel (1983). For non-linear least squares problems, use of the quasi-Newton methods for training often leads to poor initial convergence Norgaard *et al* (2000) and Dennis and Schnabel (1983) recommend consideration of the Gauss-Newton methods which are especially suited to the non-linear least squares problem.

Levenberg-Marquardt

A comprehensive description of the Levenberg-Marquardt algorithm may be found in (Norgaard *et al*, 2000), the algorithm is essentially a cross between the gradient descent method already discussed and the Gauss-Newton method (Lewis *et al*, 1999). In this approach, the minimisation is given

$$\hat{\theta} = \arg\min_{\theta} V_N\left(\theta, Z^N\right) \quad \text{subject to} \quad \left|\theta - \theta_{(i-1)}\right| \le \delta_i \tag{4.47}$$

The update rule for the Levenberg-Marquardt algorithm is given as

$$\theta_{(i+1)} = \theta_i + \mu_i \tag{4.48}$$

$$\left[R\left(\theta_{(i)}\right) + \lambda_i I\right]\mu_i = -G\left(\theta_{(i)}\right) \tag{4.49}$$

Where the Hessian is given as

$$R\left(\theta_{(i)}\right)=\left.\frac{d^2V_N\left(\theta,Z^N\right)}{d\theta^2}\right|_{\theta=\theta_i} \tag{4.50}$$

and the small constant λ_i which is used to alleviate ill conditioning problems with calculating the search direction. In practice, the Levenberg-Marquardt uses an approximation to the prediction error as in the case of the Gauss-Newton method. The value of δ_i represents the radius of a trusted region around the current estimate, within which the selection of the search direction for the approximation is assumed to correspond well with the search direction for the criterion $V_N\left(\theta,Z^N\right)$.

The Levenberg-Marquardt algorithm offers significant speed advantages over the basic gradient descent algorithm.

4.5 Neural Network based Identification

Neural networks are a popular tool for pattern recognition and are used increasingly for system identification (Norgaard *et al*, 2001). The neural network used here is a two-layer perceptron network of the form

$$\hat{y}_i(\theta)=F_i\left(\sum_{j=1}^{n_h}W_{ij}f_j\left(\sum_{l=1}^{n_\varphi}w_{jl}\varphi+w_{j0}\right)+W_{i0}\right) \tag{4.51}$$

The network uses '*tansig*' activation functions within the input and hidden layer, the output layer uses a linear activation function in order that the network output is able to take on any value. In the neural network training, the common mean square error of the estimate is used for the criterion of fit:

$$V_N\left(\theta,Z^N\right)=\frac{1}{2N}\sum_{t=1}^{N}\left(y(t)-\hat{y}\left(t|\theta\right)\right)^2 \tag{4.52}$$

W is given as the network weights, F is the activation function, N is the number of data in the training set and w is the network thresholds. The neural network is presented with the ARX structure is given by

$$y(t) = \varphi^T(t)\theta \tag{4.53}$$

where

$$\theta = [a_1 \ldots a_n \quad b_1 \ldots b_m]^T \tag{4.54}$$

$$\varphi(t) = [-y(t-1) \ldots -y(t-n) \quad u(t-1) \ldots u(t-m)] \tag{4.55}$$

θ is the regression vector for tuning, $\varphi(t)$ is the vector of previous inputs (u) and outputs of the system (y). The vector $\varphi(t)$ is presented at the input nodes and the current value of position $(y(t))$ is presented at the output. In the case of the neural network, it was found that the standard identification set did not yield good results. This is discussed in greater detail in Sjoberg,(1995). Instead, a second identification set was introduced which lacked the additional high frequency step-wise excitation signal (Figure 4.4).

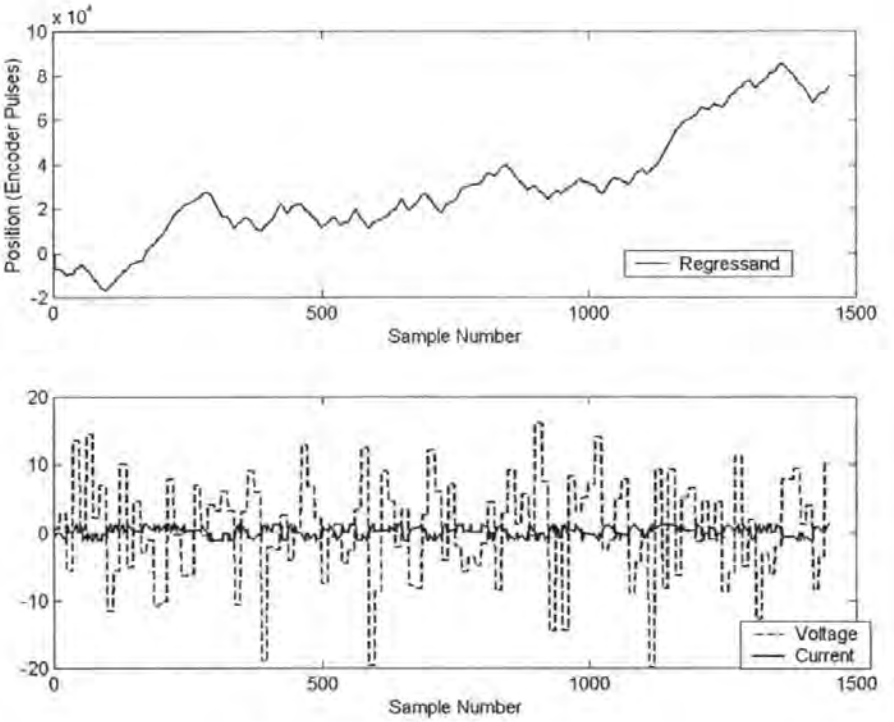

Figure 4.4: *Identification Set 2*

In the previous work, the lag space was selected heuristically through the design of the ARX model. An alternative approach to selecting the lag space was given by He and Asada (1993), this approach relies on the Lipschitz quotients and the assumption that the function that dominates the output is continuous. Under the assumption that the derivative of the output is bounded by some positive value

$$|g_l| = \left|\frac{df_0}{d\varphi_l}\right| \leq B \tag{4.56}$$

given

$$y(t) = f_0\left[\varphi(t), \theta\right] \tag{4.57}$$

introduce the Lipschitz quotient

$$q_{ij} = \left| \frac{y(t_i) - y(t_j)}{\varphi(t_i) - \varphi(t_j)} \right|, \qquad i \neq j \tag{4.58}$$

the Lipschitz condition states that provided the function f_0 is continuous, then the quotient is always bounded. The argument follows that if the differences, $dy = y(t_i) - y(t_j)$, $d\varphi_l = \varphi_l(t_i) - \varphi_l(t_j)$ are small then the approximation may be made

$$dy = \frac{\partial f}{\partial \varphi_1} d\varphi_1 + \frac{\partial f}{\partial \varphi_1} d\varphi_1 + \ldots + \frac{\partial f}{\partial \varphi_r} d\varphi_r \tag{4.59}$$

$$dy = f_1 d\varphi_1 + f_2 d\varphi_2 + \ldots + f_r d\varphi_r \tag{4.60}$$

where r represents the number of regressors. It follows that the Lipschitz quotient may be represented by

$$q_{ij}^{(r)} = \frac{|dy|}{\sqrt{(d\varphi_1)^2 + \ldots + (d\varphi_r)^2}} \tag{4.61}$$

$$q_{ij}^{(r)} = \frac{|f_1 d\varphi_1 + \ldots + f_r d\varphi_r|}{\sqrt{(d\varphi_1)^2 + \ldots + (d\varphi_r)^2}} \tag{4.62}$$

when this equality produced two interesting results in the cases where there are either too many or too few regressors. Consider the case when there is a regressor missing,

$$q_{ij}^{(r-1)} = \frac{|dy|}{\sqrt{(d\varphi_1)^2 + \ldots + (d\varphi_{r-1})^2}} \tag{4.63}$$

$$q_{ij}^{(r-1)} = \frac{\sqrt{(d\varphi_1)^2 + \ldots + (d\varphi_r)^2}}{\sqrt{(d\varphi_1)^2 + \ldots + (d\varphi_{r-1})^2}} \frac{|f_1 d\varphi_1 + \ldots + f_r d\varphi_r|}{\sqrt{(d\varphi_1)^2 + \ldots + (d\varphi_r)^2}} \tag{4.64}$$

In the most extreme example, it will be assumed that the output is dependent entirely on the r^{th} regressor. There will be points where $dy \neq 0$, and disregarding the regressor φ_r

will lead to an infinite Lipschitz quotient. In the case where too many regressors are included

$$q_{ij}^{(r+1)} = \frac{|dy|}{\sqrt{(d\varphi_1)^2 + \ldots + (d\varphi_{r+1})^2}} \tag{4.65}$$

$$q_{ij}^{(r+1)} = \frac{\sqrt{(d\varphi_1)^2 + \ldots + (d\varphi_r)^2}}{\sqrt{(d\varphi_1)^2 + \ldots + (d\varphi_{r+1})^2}} \frac{|f_1 d\varphi_1 + \ldots + f_r d\varphi_r|}{\sqrt{(d\varphi_1)^2 + \ldots + (d\varphi_r)^2}} \tag{4.66}$$

The superfluous regressor in this case will have negligible effect on the Lipschitz coefficient and will lead to an insignificant reduction. The algorithm which is given in He and Asada (1993) has been implemented, the results of which are shown in Figure 4.5. Because of the noise that was present in the current channel, it is difficult to determine anything definite, but the algorithm seems to be suggestive of a lag space of two or four. The lag space of [4 4 1] was selected through comparison of the developed models.

After scaling of the data and training with the Levenberg-Marquardt algorithm, a neural network with '*tansig*' activation functions on the input and hidden layer, and a linear activation function in the output node gave simulation results as shown in Figure 4.6 (NNARX).

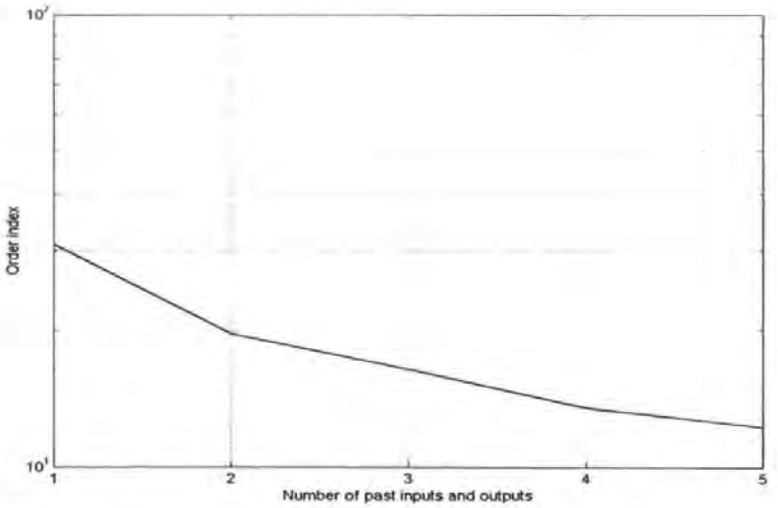

Figure 4.5: *Order Index Versus Lag Space*

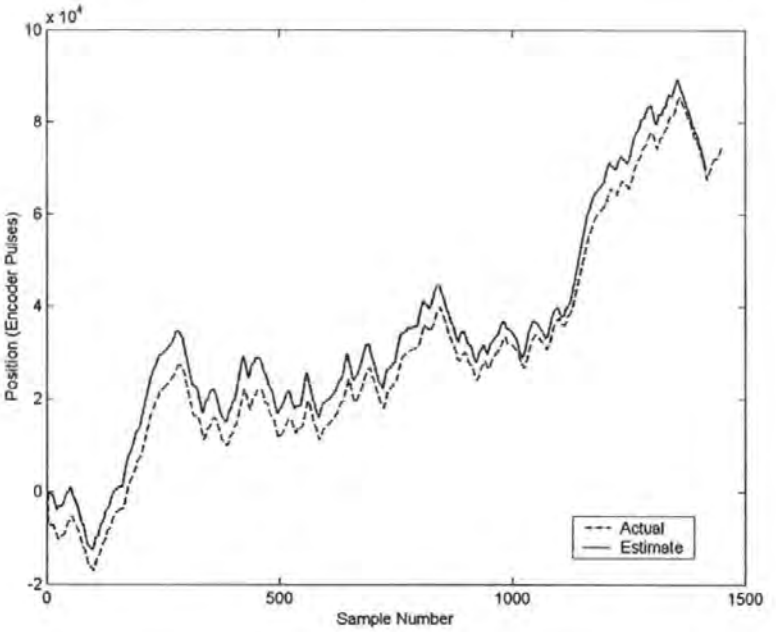

Figure 4.6: *Identification Results for Neural Network*

4.6 Fuzzy Identification

The term *fuzzy identification* has come to represent the use of fuzzy logic in the modelling and representation of a system. Fuzzy models may be viewed as general function approximators and are therefore readily applied to the nonlinear regression problem of the form discussed in the previous sections. The fact that behaviour of a system can be easily represented linguistically e.g.

If *Voltage is High* **and** *Current is High* **then** *Speed is Fast*

naturally provides the user with a useful method by which a systems behaviour can be predicted entirely from empirical observation. Linskog (1996) provides a comprehensive discussion of this approach, which constitutes the first of the two principle methods:

1. A series of **if-then** rules are used to articulate the expert knowledge. The model structure is generated implicitly from the rules supplied by the expert. If fine-tuning is required then Input / Output data may be used with a particular training algorithm. This form of parameter tuning takes advantage of the fact that the fuzzy model may be viewed as a network, analogous to artificial neural networks. From this description, the approach falls under the white or grey-box-modelling paradigm.
2. In the second case, no prior information is assumed about the system, and only numerical data is used to construct the fuzzy rule base. The resulting rules are expected to provide *a posteriori* information about the system. This approach could clearly lead to so-called emergent knowledge acquisition. The expert in this case is more inclined to analyse the model after construction, at which point new rules may be added or old rules modified in order to improve model performance. This approach clearly fits with the black or grey-box modelling approach.

The need for black and grey-box models to be applied in this work has been discussed in previous sections. Clearly, the linguistic interface between the expert and the machine make either of the two basic approaches to fuzzy identification attractive for modelling, since both prior knowledge and collected data may be easily incorporated into the model. In the following sections, the second approach to fuzzy identification is discussed and results from experimental work are given.

4.6.1 Product Space Clustering

The aim of clustering, specifically in this case product space clustering, is to decompose the nonlinear system behaviour into a series of local linear models. According to Verbruggen *et al* (1999), a procedure must be followed in order to arrive at the final model:

1. Data collection
2. Structure Selection
3. Data Clustering
4. Selection of Cluster Number
5. Generation of initial fuzzy model
6. Simplification of the initial model
7. Model validation

It can be seen that the steps 1, 2 and 7 are the same as those proposed earlier within this Chapter, and by Ljung (1998). The remaining steps are peculiar to fuzzy model identification and are therefore discussed in due course.

Data Clustering

The goal of cluster analysis is to partition a given set of data into clusters, which will be subsets of the presented data. The criteria for these clusters is

- Within cluster homogeneity; data within clusters should be as similar as possible.
- Between cluster heterogeneity; data between clusters should be as different as possible.

Of course, similarity is a subjective specification that will be dictated by the data type. Often, since the data is a real valued vector, distance measures can be used as a measure of similarity. In this specific case, consideration is paid to a regression structure for the data clustering. It has already been seen that different regressors may have different levels of relevance to the regressand; therefore, in the design of the experiment proper scaling of the data needs to be carried out in order to achieve reasonable distance measures. Of note is the fact that abstract classes of data can also be assigned integer values. A distance measure can be used once again, however, additional assumptions about the classes must be made, for instance if integer values were assigned classes, the class number 1 must be assumed more similar to class 2 than class 3. Further information and definitions of hard, fuzzy and possibilistic clustering may be found in Appendix C, part 4.

4.6.2 Selecting the Number of Clusters

In the last section, it was seen that partitioning could be achieved for a given data set. In the very simple example, it was also seen that the choice of cluster number was a hindrance to successful partitioning of the data with the first two methods. When clustering is performed on data about which there is no *a priori* knowledge it is usual that

the actual cluster number, c, has to be estimated. The clustering algorithm will then search for c clusters regardless of physical relevance to the system. In this case, the results of analysis with different numbers of clusters need to be compared with one another, based on some measure of quality, to find the optimal number of clusters. The appropriate cluster number can be determined by two principal methods, these are discussed below.

Validity Measures

A standard method for arriving at the correct number of clusters is to use a measure of cluster quality. Validity measures within the context of fuzzy clustering; are used to assess the cluster quality. Criteria such as within cluster distance, entropy and partition density have all been used. It is generally accepted, however that a good cluster may be loosely described as not being particularly fuzzy. This reasoning stems from the fact that if the correct number of clusters has been selected then most of the data should fit neatly into one of the clusters. In the case of misclassification, the clusters cannot be expected to be well separated or compact. Most validity measures therefore concentrate on qualifying the separation and compactness of the clusters.

Cluster validity analysis is performed by clustering the data several times with different values of c. Often it is also performed several times for a given value of c, with different initial fuzzy partitions. Naturally, upon comparison, the number of clusters that minimises the validity measure is deemed the correct number of clusters. The use of validity measures is therefore quite involved because of its heuristic nature.

Compatible Cluster Merging (CCM)

The principle of compatible cluster merging is to begin with c set to a value that is expected to be too high for the data set. The successive merging of compatible clusters is then used to reduce the number of clusters. Clearly, the central element to the success of the CCM method is what qualifies two compatible clusters. The original criteria suggested by Krishnapuram and Freg (1992) are based on the geometrical properties of the cluster covariance matrices. Consider two cluster prototypical points v_i, v_j. Let the eigenvalues and unit eigenvectors of the clusters be denoted $\{\lambda_{i1},\ldots,\lambda_{in}\},\{\lambda_{j1},\ldots,\lambda_{jn}\}$ and $\{\phi_{i1},\ldots,\phi_{in}\},\{\phi_{j1},\ldots,\phi_{jn}\}$ respectively. The criteria are then given

$$\left|\phi_{in}{}^{T}\phi_{jn}\right| \geq k_1, \qquad k_1 \cong 1 \tag{4.67}$$

$$\left|\frac{\phi_{in}{}^{T}\phi_{jn}{}^{T}}{2}\frac{v_i - v_j}{\|v_i - v_j\|}\right| \leq k_2, \qquad k_2 \cong 0 \tag{4.68}$$

$$\frac{\|v_i - v_j\|}{\sqrt{\lambda_i} - \sqrt{\lambda_j}} \leq k_3, \qquad 2 \leq k_3 \leq 4 \tag{4.69}$$

The first of the conditions states that clusters should be merged if they are parallel. The second that the normals of the clusters to the hyperplanes should be orthogonal to the line connecting the cluster centres. The last statement specifies that the clusters should be sufficiently close to one another. The values were derived because this algorithm was originally developed for the clustering of 2D image data. Kaymak and Babuska (1995) introduced the relaxed compatibility criteria for identification and function approximation; in addition, this approach also introduced an automated algorithm to replace the three design constants. They proposed the criteria

$$s_{ij}^1 = \left|\phi_{in}^T \phi_{jn}\right| \geq k_1 \qquad k_1 \cong 1 \tag{4.70}$$

$$s_{ij}^2 = \left\|v_i^* - v_j^*\right\| \leq k_2 \qquad k_2 \cong 0 \tag{4.71}$$

In this case the measure s_{ij}^1 assesses how parallel the clusters are to one another. s_{ij}^2 is used to calculate the distance between clusters. Criteria (4.71) has been relaxed in comparison to (4.68) in order to accommodate cluster merging in noisy data. The two matrices then provide compatibility measures which are used in the algorithm given below

repeat

1. Cluster the data into c clusters
2. Evaluate the compatibility criteria
3. Calculate the compatibility matrix
4. Determine groups of clusters for merging
5. Check the heuristic
6. Compute the new partition metric using

until

4.6.3 Generating the Fuzzy Model from Partitions

It is assumed at this point that the structure of the model has been established this extends to the assumption that the regression data has also been collected and is available. Once the structure is selected, the problem becomes analogous to the non-linear black-box identification problem, in that the regression

$$\hat{y}(t|\theta) = f(\varphi(t), \theta) \tag{4.72}$$

is desired (see equation (4.23)). The difference in methods, however, might loosely be described as the difference between local and global models. Fuzzy modelling in this case is based on the premise that the regression problem can be decomposed into a number of locally linear regression problems. This is the reason why fuzzy models of this type are more readily interpreted and *a priori* knowledge incorporated than the alternative global models, such as neural networks. At this point, a matrix of regression vectors is defined as X, i.e.

$$X = \begin{bmatrix} \varphi_1 \\ \varphi_2 \\ \vdots \\ \varphi_N \end{bmatrix} \tag{4.73}$$

the vector of regressands is denoted Y. The cross product of X and Y is known as the *product space*. The data set Z to be clustered is a subset within this product space, $Z \subset X \times Y$ and is known as the *regression space*. The regression (4.72) defines a surface within this space. If this surface is partitioned into a series of linear surfaces (corresponding to a cluster), an affine Takagi-Sugeno fuzzy rule may be used to represent the local regression, hence an entire rule base may be used to represent the global system. Consideration is now paid to the Takagi-Sugeno model structure before further consideration to system identification is paid.

4.6.4 The Takagi-Sugeno Model

The Takagi-Sugeno model is a rule based fuzzy model suitable for identification of nonlinear systems (Takagi and Sugeno, 1985). The original form was given as per (4.74), where the consequent parameters of the rule are crisp functions of the inputs, i.e.

$$R_i : \text{IF } f(x_1 \text{ is } A_1, \ldots, x_i \text{ is } A_i) \text{ THEN } y_i = g(x_1, \ldots, x_i) \qquad \text{i=1, 2,..., k} \qquad (4.74)$$

where $x \in X \subset \mathbb{R}^P$ is a crisp input vector, A_i is an antecedent multidimensional fuzzy set defined by the membership function $\mu_{Ai}(x) : X \to [0,1]$, $y_i \in \mathbb{R}$ is the scalar output of the i^{th} rule. The index i relates the variable to the i^{th} rule and k is the number of rules in the rule base.

The consequent function, g, is typically chosen as a suitably parameterised function, the functions form will remain constant throughout the rule base, and only the parameters will vary. A useful form of the consequent is the affine linear form of the Takagi-Sugeno model, in which rules are structured according to (4.75)

$$y_i = a_i x + b_i \qquad (4.75)$$

where a_i is the so-called parameter vector and b_i is an offset. Within the product space ($\mathbb{R}^{p+1 \times N}$) the affine Takagi-Sugeno consequents may be viewed geometrically as hyperplanes. The antecedent of the rule defines a fuzzy validity region for the corresponding hyperplane. It is quite clear how a rule base might therefore be used to produce a global, nonlinear function approximation.

The output y of the TS model is computed using the fuzzy mean formula

$$y = \frac{\sum_{i=1}^{K} \beta_i(x) y_i}{\sum_{i=1}^{K} \beta_i(x)} \qquad (4.76)$$

where $\beta_i(x)$ represents the degree of fulfilment of the i^{th} rules antecedent, which is simply a measure of the degree of fulfilment of x in the fuzzy set A_i and is given by

$$\beta_i = \mu_{Ai}(x) \qquad (4.77)$$

Since it may become difficult to interpret multidimensional fuzzy sets, the antecedent proposition is commonly defined in a conjunctive form, given by a series of single dimensional fuzzy sets combined with simple propositions

IF x_{i1} is A_{i1} AND,...,AND x_{ik} is A_{ik} THEN $y_i = a_i x + b_i$ (4.78)

in this case the degrees of fulfilment are calculated as $\beta_i(x) = \mu_{Ai,1}(x_1) \wedge \ldots \wedge \mu_{Ai,P}(x_P)$, where the min operator ($\wedge$) may be replaced by alternative T-norms. In this case, the model output is calculated

$$y = \left(\sum_{i=1}^{K} \gamma_i(x) a_i^T \right) x + \sum_{i=1}^{K} \gamma_i(x) b_i = \tilde{a}^T(x) x + \tilde{b}(x) \tag{4.79}$$

where γ_i is the normalised degree of fulfilment

$$\gamma_i(x) = \frac{\beta_i(x)}{\sum_{j=1}^{K} \beta_j(x)} \tag{4.80}$$

$\tilde{a}(x)$ and $\tilde{b}(x)$ are input dependent parameters, given as convex linear combinations of the constant parameters a_i and b_i through the following relationship

$$\tilde{a}(x) = \sum_{i=1}^{K} \gamma_i(x) a_i \tag{4.81}$$

$$\tilde{b}(x) = \sum_{i=1}^{K} \gamma_i(x) b_i \tag{4.82}$$

The NARX structure discussed previously may be expressed in this pseudo linear form according to the following

$$\hat{y}(k+1) = \sum_{j=1}^{n_y} a_{i,j} y(k-j+1) + \sum_{j=1}^{n_u} b_{i,j} u(k-j+1) + c_i \tag{4.83}$$

4.6.5 Identification in the Product Space

Geometrically the consequents of the TS model discussed above may be represented as hyperplanes in the regression space. The antecedent fuzzy sets serve to divide the regression space in which the regression surface may be locally approximated by the consequent hyperplanes. The task of identification is to find the number, locations and parameters of these hyperplanes such that the regression surface is accurately approximated. This may be achieved through application of a set of fuzzy clustering methods, referred to as *subspace fuzzy clustering algorithms.* Far fuller descriptions of the clustering techniques discussed below may be found in Hoppner *et al* (1999). An implementation of the fuzzy c-means algorithm may be found in the Matlab 'fuzzy logic toolbox' (Roger Jang and Gulley, 2001).

The Fuzzy C-Means Algorithm

The fuzzy c-means algorithm may be used to group the data into probabilistic partitions. In order to achieve this, the optimal cluster centre points must be calculated. The cluster means (or prototypical points) are calculated according to

$$v_i = \frac{\sum_{k=1}^{N} (\mu_{ik})^m z_k}{\sum_{k=1}^{N} (\mu_{ik})^m} \tag{4.84}$$

m denotes the weighting exponent. If m is chosen as one then the fuzzy c means algorithm is a generalisation of the hard c means algorithm. Membership of a data point, z_k is then calculated as a distance from each cluster centre, the distance (4.85) is one such measure that can be used

$$D_{ikA}^2 = (z_k - v_i)^T A (z_k - v_i) \tag{4.85}$$

where A is a norm inducing matrix. Finally, the partition matrix must be updated every iteration according to

$$\mu_{ik} = \frac{1}{\sum_{j=1}^{c} \left(D_{ikA} / D_{jkA} \right)^{2/(m-1)}} \tag{4.86}$$

The fuzzy c-means algorithm is commonly associated with clustering into spherical shells. However, by suitable replacement of the A matrix within the distance measure it is also possible to derive elliptic norms. Despite this additional capability, the fuzzy c-means algorithm is limited in that it cannot detect different cluster shapes and is therefore prefers the fixed cluster form even if it does not exist within the data. In application to fuzzy model identification, this constraint is not ideal. Consideration is now paid to the Gustafson-Kessel algorithm, which is capable of detecting cluster shape.

The Gustafson-Kessel Algorithm

The Gustafson-Kessel (GK) algorithm (Gustafson and Kessel, 1979) is an extension of the FCM algorithm that uses an adaptive distance measure. Each of the clusters has its own norm-inducing matrix, which allows the algorithm to detect shape and orientation of the cluster.

$$D_{ikA}^2 = \left(z_k - v_i \right)^T A_i \left(z_k - v_i \right) \tag{4.87}$$

The shape and size of the clusters is described by the cluster covariance matrices

$$F_i = \frac{\sum_{k=1}^{N} \left(\mu_{i,k} \right)^m \left(z_k - v_i \right) \left(z_k - v_i \right)^T}{\sum_{k=1}^{N} \left(\mu_{i,k} \right)^m} \tag{4.88}$$

The objective function of the GK algorithm now contains the matrix A in its minimisation. Unfortunately, because the objective function is linear in A it cannot be

directly minimised with respect to A. In order to arrive at a solution, the determinant of A is usually constrained. The matrix is then allowed to vary, whilst maintaining a constant determinant. This has the effect of allowing the algorithm to optimise the cluster shape, whilst unfortunately keeping the cluster volume constant.

The algorithm proposed by Gath and Geva (1989), is an extension of the GK algorithm that is also able to take size and density of the cluster into consideration. This property is attractive since there might be regions within the data more suitably approximated by larger or smaller clusters. The algorithm uses an exponential term in the distance measure that can produce very large numbers whilst clustering; this may lead in turn to processor stack overflows in practice.

Antecedent Membership Calculation

The antecedent parameters of the Takagi-Sugeno model may be calculated through application of the distance measure used within the clustering algorithm. In this case only the regressor x, the regressor component of the cluster prototype and the corresponding cluster covariance matrix are used.

The distance measure may be evaluated as

$$D\left(x_k, v_i^x\right) = \left(x_k - v_i\right)^T F_i^x \left(x_k - v_i\right) \tag{4.89}$$

using an inversion, this measure can be converted into the degree of fulfilment. One possible choice of inversion is to use the same equation as for the clustering algorithm Hellendoorn and Driankov (1997).

$$\beta_i\left(x_k\right) = \frac{1}{\sum_{j=1}^{c}\left[d\left(x_k, v_i^x\right) \Big/ d\left(x_k, v_j^x\right)\right]^{2/m-1}} \tag{4.90}$$

which considers all rules and calculates the degree of fulfilment of one rule with respect to the others. As is the case when used within the clustering algorithm, the sum of the membership degrees will equal one.

Consequent Membership Calculation

The fuzzy consequent parameters of the affine Takagi-Sugeno model may be calculated in one of two ways from the data clusters (Babuska, 1997). The first is based around the geometric interpretation of the cluster, using the covariance matrix. The alternative approach is a local least squares optimisation based on the derived fuzzy partition matrix The method based on the covariance matrix is discussed here, since this method has been found to perform better on the data. The eigenstructure of the cluster covariance matrix loosely describes the shape of the cluster. The shortest eigenvector describes the normal vector to the hyperplane spanned by the remaining eigenvectors. The shortest eigenvector is defined as Φ_i. Based on the dataset $Z^N = \left[x^T, y\right]^T$ and the cluster prototype, the consequent may be described implicitly by

$$\Phi_i \cdot \left(Z^N - v_i\right) = 0 \tag{4.91}$$

The statement above means that the inner product of any vector belonging to the hyperplane and the shortest eigenvector is zero. The shortest eigenvector and the cluster prototype may be divided into a vector corresponding to the regressor x and a scalar corresponding to the regressand y. i.e.

$$v_i = \left[\left(v_i^x\right)^T; v_i^y\right]^T \tag{4.92}$$

$$\Phi_i = \left[\left(\Phi_i^x\right)^T; \Phi_i^y\right]^T \tag{4.93}$$

(4.91) may now be rewritten according to

$$\left[\left(\Phi_i^x\right)^T;\Phi_i^y\right]\cdot\left(\left[x^T;y\right]^T-\left[\left(v_i^x\right)^T;v_i^y\right]^T\right)=0 \tag{4.94}$$

After completion of the dot product operation,

$$\left(\Phi_i^x\right)^T\left(x-v_i^x\right)+\Phi_i^y\left(y-v_i^y\right)=0 \tag{4.95}$$

Simplification yields

$$y=\underbrace{-\frac{1}{\Phi_i^y}\left(\Phi_i^x\right)^T}_{a_i^T}x+\underbrace{\frac{1}{\Phi_i^y}\Phi_i^T v_i}_{b_i} \tag{4.96}$$

which is directly equivalent to the Takagi-Sugeno model, (4.75). Figure 4.9 illustrates the result of applying the above theory to the identification set 1, using the familiar [4 4 1] structure. Through the validity measures discussed, 7 clusters was found to be optimum.

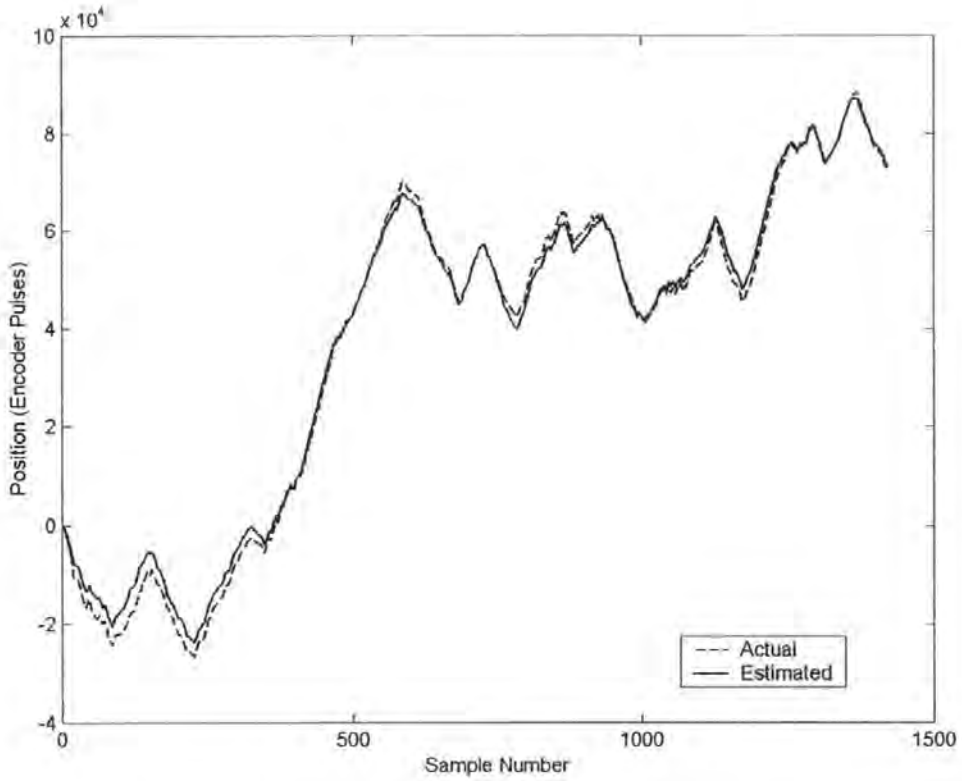

Figure 4.7: *Identification results for fuzzy clustered model*

4.7 Transforms for Regressor Data

In this section, attempts to transform the data to provide greater physical relevance are made. Specifically, the current and voltage data are combined with the power balance equations (PBE's) in order to derive estimates of position directly from the data. The power balance equations give a good model of system performance, their untreated estimation of position is also provided (PBE in Table 4.1). The enhanced information is therefore incorporated with the fuzzy clustering approach in two ways, first the residuals of the PBE estimate are calculated, upon which a clustered model based on the same structure as in the previous section is trained (FRESPBE, Table 4.1), the outputs of both models are then summed together to provide a composite estimate of the position, as

discussed in §4.3.2. In the second approach, the PBE estimate is used in the clustered model as a direct replacement for the voltage regressor (PBEREG, Table 4.1). This approach was adopted after tests demonstrated degraded performance with three regressors (i.e., voltage, current and the PBE estimate).

Using the power balance equations,

$$P_i(t) = V(t) \cdot I(t) \tag{4.97}$$

$$P_o(t) = T_m(t) \cdot \omega(t) \tag{4.98}$$

$$P_l(t) = I(t)^2 \cdot R \tag{4.99}$$

$$P_o(t) = P_i(t) + P_l(t) \tag{4.100}$$

an expression for the motor speed based on quantities assumed constant and the available measurements may be derived,

$$\omega(t) = \frac{V(t) \cdot I(t) - I(t)^2 \cdot R}{I(t) \cdot K \cdot R} \tag{4.101}$$

where P_i is the applied electrical power, P_o is the mechanical output power, and P_l is the power loss. Since $\frac{d\theta(t)}{dt} = \omega(t)$,

$$\theta(t) = \int_0^t \frac{V(t) \cdot I(t) - I(t)^2 \cdot R}{I(t) \cdot K \cdot R} dt \tag{4.102}$$

Figure 4.8 illustrates the estimate of (4.102) based current and voltage data.

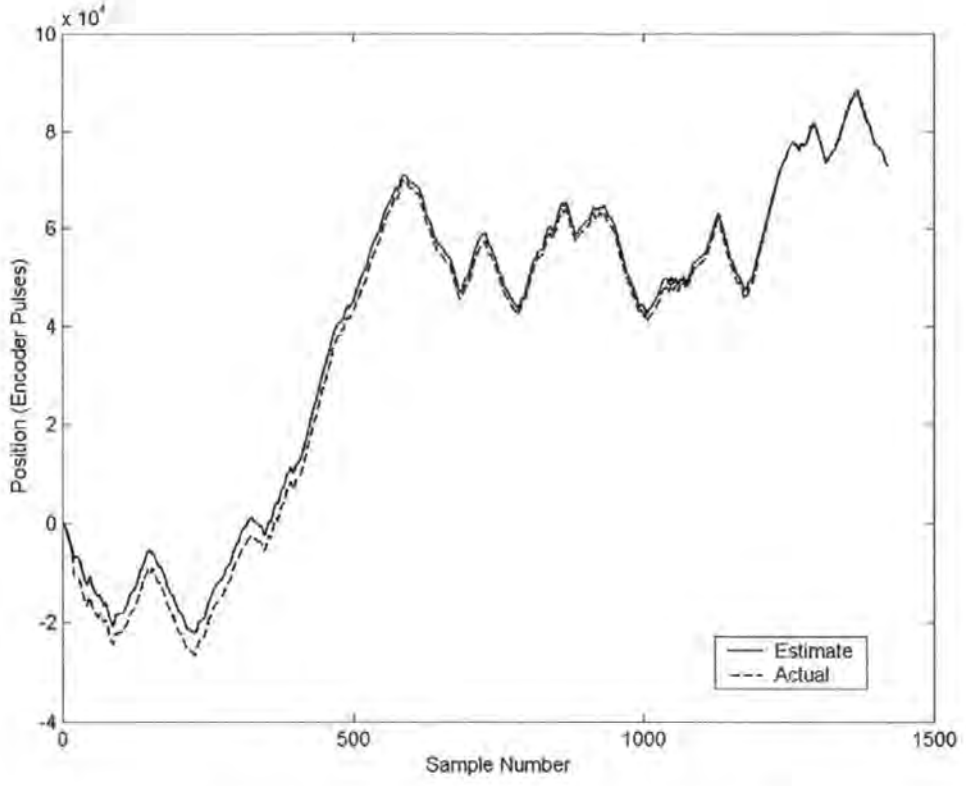

Figure 4.8: *Power Balance Equation Estimate*

Figure 4.9 and Figure 4.10 show the results of applying the FRESPBE and PBEREG model structures respectively. The value of K may be used for tuning of the equation; here a gradient descent method with variable step size is used in order to tune the model. The gradient descent method has been discussed in section 4.5. As mentioned before, use of an adaptive step size can be used in order to obtain the convergence speed of a large step, but the accuracy of a small step. Here an algorithm is proposed based on an initial value for the step size determined by the user. The algorithm (PBEGD) is described below in Algorithm 4.1.

1. Initialise variables $\phi, \tau_{crit}, j = 0$ and $k = 0$
2. Obtain the value for the criterion of fit $V_N\left(\theta_{(i)}, Z^N\right)$
3. Find $\theta_{(i+1)} = \theta_i - \mu_{(i)} G\left(\theta_{(i)}\right)$
4. Obtain the new value for the criterion of fit $V_N\left(\theta_{(i+1)}, Z^N\right)$
5. If $V_N\left(\theta_{(i+1)}, Z^N\right) = V_N\left(\theta_{(i)}, Z^N\right)$ and $j = \phi$ then $k = k + 1$ otherwise $j = j + 1$
6. $\mu_i = \frac{\mu_i}{10^k}$, $V_N\left(\theta_{(i)}, Z^N\right) = V_N\left(\theta_{(i+1)}, Z^N\right)$
7. If $V_N\left(\theta_{(i)}, Z^N\right) > \tau_{crit}$ and $k > \delta$ then repeat the process from step 3

Algorithm 4.1: *Gradient Descent Algorithm for Power Balance Equations*

The value of ϕ determines the number of times the algorithm will search across the minimum, before reducing the step size; τ_{crit} determines the termination criterion in the event that it can be achieved and δ defines the maximum value of k before the algorithm terminates. The initial model performance of this model is shown in Figure 4.8; Figure 4.11 illustrates the estimate after tuning with Algorithm 4.1.

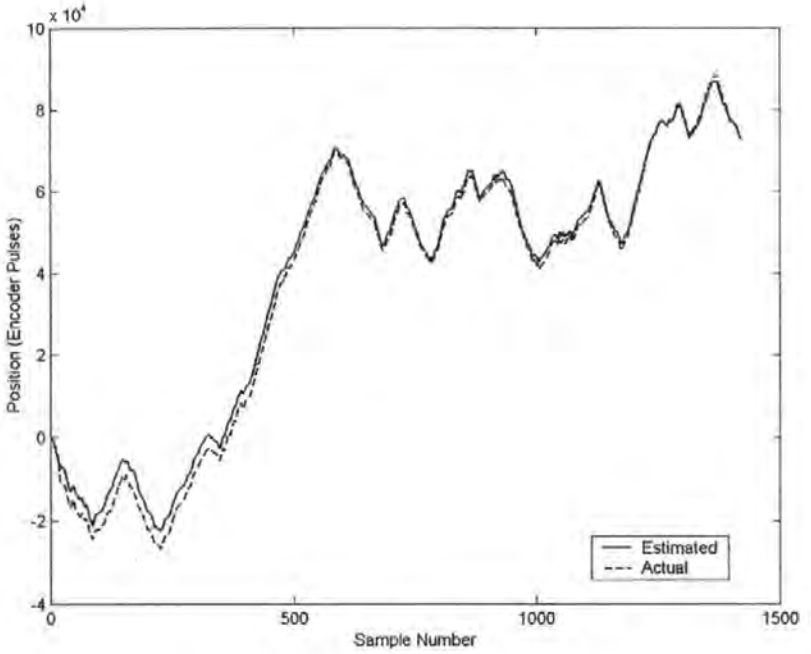

Figure 4.9: *Fuzzy Clustering Based on the Power Balance Equation Residuals*

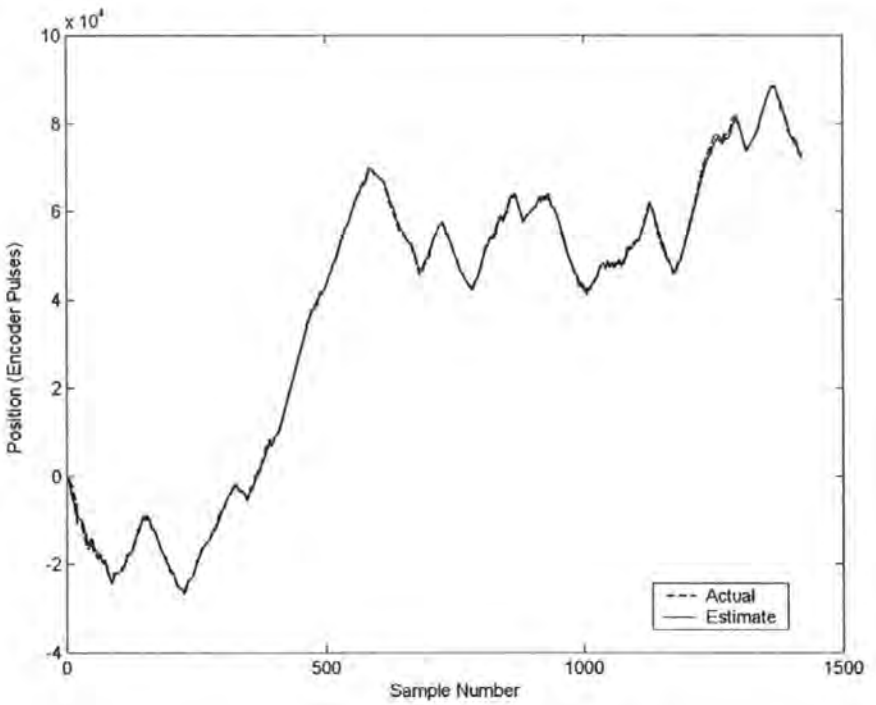

Figure 4.10: *Power Balance Equations as a Regressor for the Fuzzy Clustered Model*

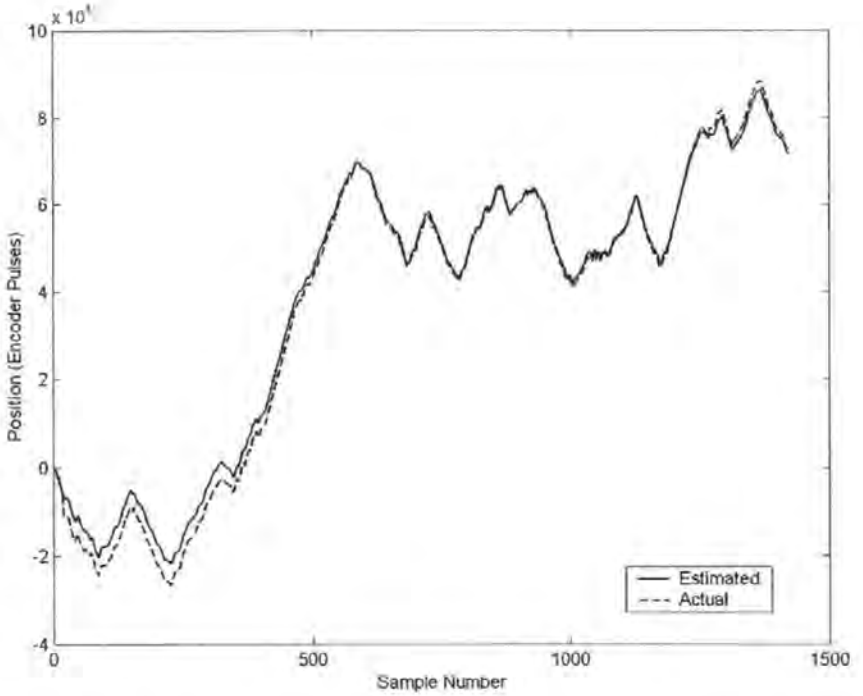

Figure 4.11: *Power Balance Equation Estimate After Tuning with Gradient Descent*

4.8 Summary of Results

Table 4.2 provides a summary of the results obtained within this work. Both the infinity norm and the RMS norm have units of encoder pulses in error. It can be seen how the use of the power balance equations can significantly improve the performance of the identification approaches. It should be noted that the neural network model was both trained and validated on a different data set consequently, comparison in terms of absolute values of error or average error cannot reasonably be compared. However, the VAF measure provides a value for the tracking ability of the model based on the data presented, which provides a reasonable estimate of how the perform. The use of the power balance equations on their own outperform the models trained simply on

input/output data and provides the means to produce accurate models based on the nonlinear identification techniques.

Table 4.1: *Performance of the various approached to identification*

Model	$\|\varepsilon\|_\infty$ (Encoder Pulses)	$\|\varepsilon\|_{rms}$ (Encoder Pulses)	VAF
PC	9961	5574	98.4%
ARX	5370	3046	99.41%
NN ARX	8874	5332	99.55%
FC ARX	5166	1982	99.7%
PBEQU	4352	2326	99.85%
FRESPBE	4938	2351	99.86%
PBEGD	4911	2304	99.68%
PBEREG	2535	594	99.97%

4.9 Discussion

Attention has been paid within this work to the identification of a servomechanism actuated by a brushless DC motor and subjected to large, time variant loads. Specifically the fundamental tenet within system identification has been explored, i.e. to identify only those phenomena that are unknown. It was initially found that a model based purely on empirical observation and a priori knowledge provided a reasonable result, but that significant improvements were ready to be made. The linear ARX structure was found to be of sufficient flexibility to provide a much-improved estimate over the phase coordinate model. Black-box approaches were investigated in terms of a neural network and a fuzzy

clustered rule base, both of which were based on the previously successful ARX structure. The neural network was found to favour strongly purely stepwise varying identification data, which should be considered when comparisons between the models are drawn. It is clear from this exercise in itself that correct selection of the input output data has profound effect on the resulting black-box model. The fuzzy clustered model was found to outperform the linear ARX model. Attention to the incorporation of *a priori* knowledge was paid. In the first attempts, a black-box model was used in a complementary fashion to the white-box model in order to cancel estimation residuals. Incorporation of the white-box model estimate into the black-box model regression structure was found to outperform the previous approach significantly. Finally, the gradient descent training method was adopted from the neural network literature in order to minimise the white-box model error. This model was successful in minimising the root mean squared error of the estimate. The model performs well in comparison to the other models. However, this model has not captured the discontinuities within the data as well as the other models. The VAF measure is testament to this. It should be noted that this model has the advantage of simplicity and minimal computational load once trained over the fuzzy clustered and the neural network models. In a system with diminutive *a priori* understanding, the semi-physical or grey-box approach to modelling has been applied and shown to be a viable approach to obtaining highly accurate results. Subsequent work within the following Chapters will therefore use these grey-box models where possible.

4.10 Notes and References

4.10.1 Notes

A T-Norm operator is a duple function and satisfies the following

$f(0,0)=0, f(A,1)=f(1,A)=A$ (boundary)

$f(A,B)\le f(C,D)$ if A ≤ C and $B \le D$ (monotonicity)

$f(A,B)=f(B,A)$ (commutativity)

$f(A,f(B,C))=f(f(A,B),C)$ (associativity)

The first requirement imposes the correct generalization to crisp sets. The second requirement implies that a decrease in the membership values in A or B cannot produce an increase in the membership value in $A \cap B$. The third requirement implies that the operator is indifferent to the order of the fuzzy sets to be combined. Finally, the fourth requirement allows the intersection of any number of sets to be taken in any order of pair-wise groupings. The most frequently used T-norm operators are

Minimum: $T_{\min}(A,B)=\min(A,B)=A \wedge B$

Algebraic Product: $T_{ap}(A,B)=AB$

Bounded Product: $T_{bp}(A,B)=0 \vee (A+B-1)$

Drastic Product: $T_{dp}(A,B)=\begin{cases} A & \text{if } B=1 \\ B & \text{if } A=1 \\ 0 & \text{if } A,B<1 \end{cases}$

4.10.2 References

Babuska R. 1998. 'Fuzzy Modelling for Control'. Kluwer Academic Publishers.

Demuth H. and Beale M. 2001. 'Neural Network Toolbox Users Guide'. The Mathworks Inc.

Dennis J.E. and Schnabel R.B. 1983. 'Numerical Methods for Unconstrained Optimisation and Nonlinear Equations'. Prentice Hall.

Gath I. and Geva A. 1989. 'Unsupervised Optimal Fuzzy Clustering', IEEE Transactions on Pattern Analysis and Machine Intelligence. 7, 773-781.

Gustafson D and Kessel W. 1979. 'Fuzzy Clustering with a Fuzzy Covariance Matrix', Proc. IEEE CDC, San Diego, 761-766.

He X. and Asada H. 1993. 'A New Method for Identifying Orders of Input Output Models for Nonlinear Dynamical Systems'. Proc. American Control Conference. San Francisco, California. 2520-2523.

Hellendoorn H., and Driankov D. 1997. 'Fuzzy Model Based Identification: Selected Approaches'. Springer Verlag.

Hoppner F., Klawonn F., Kruse R. and Runkler T. 1999, 'Fuzzy Cluster Analysis', John Wiley.

Hunt K.J., Sbarbaro D., Zbikowski R. and Gawthrop P.J. 1992. 'Neural Networks for Control Systems: A Survey'. Automatica. **28**(6). 1083-1112.

Juditsky A., Hjalmarsson H., Beneviste A., Deylon B., Ljung L., Zhang Q. and Sjoberg J., 1995. 'Nonlinear Black-box Modelling in System Identification: Mathematical Foundations', Linkoping University.

Kaymak U. and Babuska R. 1995. 'Compatible Cluster Merging for Fuzzy Modelling', Proc FUZZ-IEEE/IFES. Yokohama. 897-904.

Krishnapuram R and Freg C.-P. 1992. 'Fitting an Unknown Number of Lines and Planes to Image Data Through Compatible Cluster Merging', Pattern Recognition. **25**(4). 385-400.

Krishnapuram R. and Keller J. 1993 'A Possibilistic Approach to Clustering', IEEE Trans. Fuzzy Systems, **1**(2). 98-110

Lewis F.L., Jagannathan S. and Yesildirek A. 1999. 'Neural Network Control of Robot Manipulators and Nonlinear Systems'. Taylor Francis.

Leonartis I.J. and Billings S.A. 1985(a). 'Input-Output Parametric Models for Nonlinear Systems. Part 1: Deterministic Nonlinear Systems'. Automatica. **41**(2). 303-328.

Leonartis I.J. and Billings S.A. 1985(b). 'Input-Output Parametric Models for Nonlinear Systems. Part 2: Stochastic Nonlinear Systems'. Automatica. **41**(2). 329-344.

Lewis F.L., Jagannathan S., Yesildirek A. 1999. 'Neural Network Control of Robot Manipulators and Nonlinear Systems.' Taylor Francis.

Linskog P. 1996. 'Methods, Algorithms and Tools for System Identification Based on Prior Knowledge'. PhD thesis, Linkoping University.

Ljung L. 1998. 'System identification: Theory for the User'. Prentice Hall.

Ljung L. and Glad T. 1994. 'Modelling of Dynamic Systems', Prentice Hall.

Llobet E., Hines E.L. Gardner J.W. and Franco S. 1999., 'Non-destructive Banana Ripeness Determination Using a Neural Network Based Electronic Nose', Measurement Science Technology, **10**, 538-548.

Norgaard M., Ravn O., Poulsen N.K., Hansen L.K. 2000. 'Neural Networks for Modelling and Control of Dynamic Systems.' Springer Verlag.

Norgaard M., Ravn O., Poulsen N.K. 2001. 'NNSYSID and NNCTRL Tools for System Identification and Control with Neural Networks'. IEE Computing and Control engineering, **12**(1), 29-36

Roger Jang J.-S. and Gulley N., 2001. 'Fuzzy Logic Toolbox', The Mathworks Inc. Version 2.

Sjoberg J. 1995. PhD thesis, Linkoping University.

Sjoberg J., Zhang Q., Ljung L., Beneviste A., Deylon B., Glorennec P.-Y., Hjalmarsson H. and Juditsky A. 1995. 'Nonlinear Black-box Modelling in System Identification: A Unified Overview', Automatica. **31**(12). 1691-1724.

Takagi T. and Sugeno M. 1985. 'Fuzzy Identification and its Applications to Modelling and Control'. IEEE Trans. on Systems, Man and Cybernetics, **15**(1), 116-132

Verbruggen H.B., Zimmermann H.-J and Babuska R. 1999. 'Fuzzy Algorithms for Control'. Kluwer Accademic Publishers.

Chapter 5

Sliding Mode Control: Classical Approaches

5.1 Introduction

In the formulation of many control problems there will typically be disparities between the performance of the plant mathematical model and the actual system. These discrepancies may be due to unmodelled system dynamics, parametric variation within the plant or the approximation of a system to a simple model. It is the control engineer's task to produce a controller that will attain prescribed performance despite these discrepancies. This has duly led to an intense research interest in robust control methods, whereby the controller has a low sensitivity to parametric change within the system, but maintains a suitably high disturbance rejection. One particular approach to achieving robust control is through the application of sliding mode.

The term 'sliding mode' first appeared in the context of variable structured systems theory. Now practically all methods for control with variable structured systems are based on the deliberate synthesis of sliding modes. Sliding mode control (SMC) is described as 'deterministic'. One fixed, nonlinear control function is able to provide guaranteed performance over a defined range of parametric variation. This makes SMC attractive since it is simple to implement and reliable. Because it relies on discontinuous switching SMC has found a significant interest within the field of robotics and motor control since there is very little effort in hardware modification required for implementation.

This Chapter is aimed at introducing the reader to SMC and its application to electromechanical devices. The Chapter first provides an introduction to the theory supporting SMC, design examples based on the models derived in the previous Chapter are also given.

Before introducing the theory surrounding sliding mode control, it is necessary to highlight the differences between this class of controller and other types of nonlinear robust controller. It is not within the scope of this work to review each type of controller, however it is possible to group every controller as either belonging to the 'stochastic' or 'deterministic' families. Self-tuning and other adaptive systems fall into the category of stochastic controllers. They constantly monitor parametric change and disturbance and through use of an on-line identification algorithm provide an appropriate globally stable control.

Conversely, the family of deterministic controllers, of which sliding mode is a member, require only fixed nonlinear feedback control functions. They are able to operate over a predetermined space of parameter variation and disturbance without the need for any form of online identification of system parameters. An immediate advantage of this approach is that no statistical information about system parameters is required, robustness is therefore achieved not in the average sense but for all possible values of parameter uncertainty over the design range. Stochastic control systems are naturally more complex and generally more costly due to the additional hardware required for the sensing of these parameters. Within any control system, simplicity and reliability must be principal design targets, this is the primary reason why deterministic control methods are considered here, whilst stochastic control is largely left untreated.

5.2 Mathematical Background

Modern Variable Structure Systems (VSS) are attributed to the work of Barbarashin and Emal'yanov in the early 1960's (Young and Ozugner, 1999). However earlier works from the fifties on discontinuous control actions by Flugge-Lotz and Typskin may be found within the literature. Indeed earlier works illustrating the principles supporting sliding mode control can be found by Kulebakin; and the work of Nickolski makes specific reference to a sliding mode (Zinober, 1994). However it was not until the mid 1970's that works by Itkis (1976) and Utkin (1977) were published in English. Since then Sliding Mode Control (SMC) and VSC in general has been successfully applied to the design of robust regulators, adaptive schemes, tracking systems and fault detection schemes (Hung *et al.* 1993). The purpose of this section is to provide the reader with an introduction to the concepts that will subsequently be applied throughout the remainder of this work.

A variable structure system (VSS) is a class of system whereby the control structure is deliberately varied during the control process. This structure variation is performed according to a predefined set of rules, which will depend on the instantaneous state of the system at time t.

To begin this work the conventional example in terms of the state space method is given. Consider a second-order time invariant relay system given by

$$\begin{aligned} &\ddot{x} + a_2\dot{x} + a_1 x = u + f(t) \\ &u = -M\,\mathrm{sgn}(S) \\ &S = \dot{x} + cx \end{aligned} \tag{5.1}$$

where M, a_1, a_2 and c are constant parameters, $f(t)$ is a bounded disturbance and S is the sliding manifold. The system behavior may be analysed on the phase plane $(x, \dot{x})$.

Figure 5.1 shows the phase plane behaviour for the system in (5.1). It can be seen that the control action (u) is subject to discontinuities at the switching manifold (S=0). Comparison of the state trajectories along the sliding manifold indicates that they belong to two families. The first family correspond to $S>0$ and $u=-M$ and the second corresponds to $S<0$ and $u=M$. Suppose that a representative point (RP) may represent the state of the system at any given instant in time upon the phase plane. Now suppose that the RP is somewhere within the section I at time t_0. The system is bound to follow one of the elliptic phase trajectories toward the sliding manifold. Once the system has reached the manifold it will attempt to penetrate region IV, whereby the phase trajectory switches from elliptic to hyperbolic and is forced back towards region I, where the trajectory once again switches back to elliptic and so the process continues.

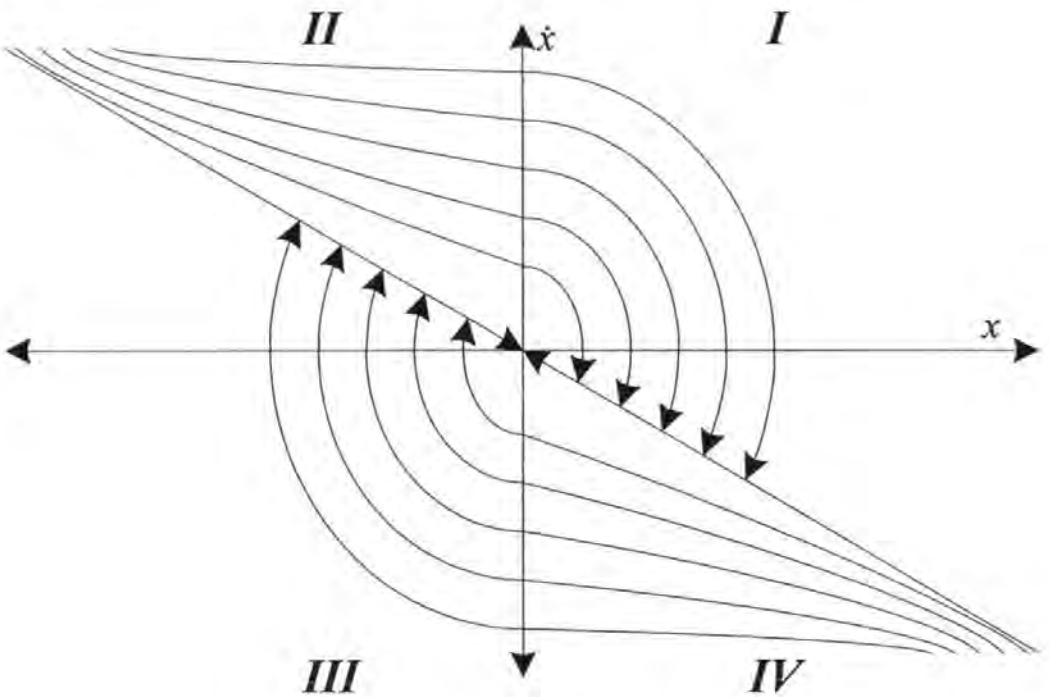

Figure 5.1: The principle of the sliding mode with two unstable phase portraits

Because of the phase trajectory topologies and by the contracting mapping principle the system is globally asymptotically stable. This is the principle behind sliding mode. Perhaps the best analogy to the system behavior whilst in sliding mode was drawn by Itkis (1976) and is quoted here:

> *"The situation recalls the scene in the motion picture "La loi, c'est loi", where the hero, recognised by neither French nor Italian authorities as a citizen and therefore evicted by the customs officials of both countries, is obliged to travel precisely on the international border between them."*

It is a natural conclusion that if in the limit switching across the sliding line is achieved at an infinitely high frequency with infinitesimal amplitude that the system trajectory would coincide with the sliding manifold $S = 0$. Assuming this behavior, the system motion may then be interpreted as

$$\dot{x} + Cx = 0 \tag{5.2}$$

This result is extremely important since it may be seen that the system performance when in sliding mode depends neither on the plant parameters nor the disturbance, $f(t)$ this is the invariance property of sliding mode control (Drazenovic, 1969). Attention is drawn at this point to the fact that if the system parameters are changed i.e. a_1 and a_2 then the RP on the phase plane will be forced to travel along an alternative phase trajectory. Provided that the phase trajectories remain in the opposing sense to one another, it will simply take a different amount of time within the transient before sliding mode is achieved. Whilst a system is in the transient it is referred to as reaching mode for sliding mode control systems.

The concept of sliding mode control has been established, it is now important to provide mathematical proof of the existence of sliding modes, so that control systems may be synthesised.

5.2.1 Problem Statement

This section begins with a formal definition of the concepts described above. A controller will be found to force the controlled system states to reach and thence remain on a predefined surface within the state space, referred to here as the sliding manifold. The system behavior once constrained to move only along this surface is described as the ideal sliding mode. This behavior has the important characteristics of order reduction and invariance to matched uncertainty. Design of a sliding mode controller is a two-stage process. Firstly the design of a surface within the state space such that the specified performance is obtained, and secondly the synthesis of a control law that will be discontinuous around the surface that will maintain an attractiveness to the closed loop motion. It is only at the point when the system reaches the sliding manifold that the system will become invariant to matched uncertainty (Spurgeon, 1991). During the reaching phase the system performance is subject to disturbances, it is therefore an important design goal to minimise the time in the reaching phase.

Consider the time invariant system with m inputs given by the equation

$$\dot{x} = \left[A + \Delta A(t)\right]x(t) + \left[B + \Delta B(t)\right]u(t) + f(x,u,t) \qquad (5.3)$$

Where x = vector of states $\in \mathbb{R}^{n\times 1}$ and u = Vector of controls $\in \mathbb{R}^{m\times 1}$. $A \in \mathbb{R}^{n\times n}$ and $B \in \mathbb{R}^{n\times m}$. Assume that $n > m \geq 1$ and that B is of full rank m, assume also that the tuple(A,B) is controllable. ΔA and ΔB represent uncertainties and variations within the

plant parameters and the control interface respectively. The function f represents uncertain, time-varying additive terms that are assumed unknown but bounded by some function of the state. As stated, it is assumed that all disturbances are matched, i.e. they act only within the input control channels,

$$\Re(B) = \Re([B, \Delta B]) \tag{5.4}$$

Where $\Re$ represents the range space. If it is assumed that the rank of $\left[B + \Delta B(t)\right] = m$ for all $t \geq 0$ then it may be implied that total invariance to parameter variation and uncertainty can be achieved according to a suitable choice of the limiting values of control.

Let $S : \mathbb{R}^n \rightarrow \mathbb{R}^m$ be a linear function defined as

$$S(x) = Sx \tag{5.5}$$

Where $S \in \mathbb{R}^{m \times n}$ is of full rank and is defined as the hyperplane

$$S = \{x \in \mathbb{R}^n : S(x) = 0\} \tag{5.6}.$$

S will be referred to from now on as the *switching function*.

5.2.2 Equivalent Control Method

If the control action in (5.3) is discontinuous with respect to the state vector then traditional methods for analysis of differential equations do not hold, since Lipschitz conditions are normally invoked in order to guarantee the existence of a unique solution (Edwards and Spurgeon, 1998). Since any function that satisfies Lipschitz conditions is necessarily continuous an alternative approach to analysis must be adopted. There are several methods for analysis available within the literature, such as that by Fillipov,

(1988). However, the method of equivalent control proposed by Utkin (1992) is more intuitively appealing and is therefore the subject of this section.

In general, the equivalent control might be described as the control action required to maintain an ideal sliding motion on S. It is assumed initially that the disturbance in (5.3) is zero, such that

$$\dot{x}(t) = Ax(t) + Bu(t) \tag{5.7}$$

Suppose now that at time t_1 the system state reaches the sliding manifold S and an ideal sliding motion takes place. This may be expressed as Sx(t)=0 and $\dot{s}(t) = S\dot{x}(t) = 0$ for all $t \geq t_s$. Substituting S into (5.7) now yields

$$S\dot{x}(t) = SAx(t) + SBu(t) = 0 \qquad \text{for all } t \geq t_s \tag{5.8}$$

Rearranging (5.8) gives

$$SBu(t) = -SAx(t) \tag{5.9}$$

Solving for the control gives

$$U_{eq}(t) = -(SB)^{-1} SAx(t) = -kx(t) \tag{5.10}$$

where

$$k = (SB)^{-1} SA \tag{5.11}$$

$U_{eq}(t)$ is described as the linear open loop control required to force the state trajectory to remain in the null space of S whilst sliding. Through substitution of $U_{eq}(t)$ into the system equation (5.7)

$$\dot{x}(t) = \left(I - B(SB)^{-1} S\right)Ax(t) \qquad \text{for all } t \geq t_s \tag{5.12}$$

$$\dot{x}(t) = (A - Bk)x(t) \tag{5.13}$$

This is the equation for the closed loop dynamics of the system when in the sliding mode. Matched uncertainty occurs within the range space of B ($\Re(B)$). During sliding motion the state trajectory lies entirely within the null space of S ($\aleph(S)$), since these are complementary, i.e.

$$\aleph(S) \cap \Re(B) = \{\emptyset\} \tag{5.14}$$

It may readily be seen that the motion of the system is independent of the nonlinear control and is dependent only upon S, which will serve to determine the matrix k. Suitable choice of k will guarantee convergence of the state vector to the origin.

The equation for equivalent control has now been formulated. It is a reasonable question to ask why the equivalent control could not be applied directly as the control signal, since it is both simple and explicit. The reason becomes clear if one were to employ the following signal as the state feedback control law:

$$u(t) = kx(t) \tag{5.15}$$

At this point some structured uncertainty is introduced to the nominal linear system of (5.7), i.e.

$$\dot{x}(t) = Ax(t) + Bu(t) + D\xi(t, x) \tag{5.16}$$

This is a special case of (5.3) where

$$D\xi(t, x) = f(t, u, x) \tag{5.17}$$

The matrix $D \in \mathbb{R}^{n \times l}$ is known and the function $\xi : \mathbb{R}_+ \times \mathbb{R}^n \to \mathbb{R}^l$ is unknown. This function may be interpreted as the representation of uncertainty within the system matrices A and B, or alternatively as an unknown exogenous perturbation acting on the system. As in the above argument, it is assumed that there exists a controller that is

capable of delivering the state trajectory to the manifold S (after time t_s) and from then onward keeping it on the sliding surface, even in the face of uncertainty and disturbance. It has been seen that this may be taken to represent $\dot{s}(t) = S\dot{x}(t) = 0$ for all $t \geq t_s$. Now following the same argument in the derivation of the equivalent control above yields

$$u_{eq}(t) = -(SB)^{-1}(SAx(t) + SD\xi(t,x)) \text{ for all } t \geq t_s \qquad (5.18)$$

It can be seen that this equivalent control action is now dependent upon the unknown exogenous signal and is thus inutile as a practical feedback control signal. Equivalent control, as stated earlier, is best viewed as a tool for the analysis of the sliding mode since it represents the nominal control effort to maintain the ideal sliding motion.

5.2.3 Existence Conditions

Before moving on to the derivation of specific control structures it is important to first state the sufficient conditions which must be met before an ideal sliding motion may be synthesised. It is clear, and has been stated above that the manifold must be at least locally attractive. In other words, in an unspecified domain around the switching manifold, the state trajectories must be directed toward it. This may be expressed as

$$\lim_{S\to 0^+} \dot{S} < 0 \text{ and } \lim_{S\to 0^-} \dot{S} > 0 \qquad (5.19)$$

The equations must be true for some domain, $\gamma \subset \mathbb{R}^n$. In this case the sliding surface is given

$$\mathrm{D} = S \cap \gamma = \{x \in \gamma, S(x) = 0\} \qquad (5.20)$$

(5.19) is often replaced by the equivalent expression

$$S\dot{S} < 0 \quad (5.21)$$

The expression (5.19) and equivalently (5.21) are termed the *reachability conditions*.

Unfortunately (5.19) and (5.21) do not guarantee the existence of an ideal sliding motion. Rather, these criteria only guarantee that the sliding manifold will be approached asymptotically. A stronger proposition has therefore been made, known as the *η-reachability* condition (Slotine and Li, 1991), given by

$$S\dot{S} \leq -\eta|S| \tag{5.22}$$

This condition can be used in order to guarantee the ideal sliding motion. η is a small positive constant. Rewriting the Lyapunov function, $V(S) = \frac{1}{2}S^2$ as

$$\frac{1}{2}\frac{d}{dt}S^2 \leq -\eta|S| \tag{5.23}$$

and integrating between time 0 and the time at which the manifold is reached (t_s) it follows

$$|S(t_s)| - |S(0)| \leq -\eta t_s \tag{5.24}$$

From this the time t_s must satisfy

$$t_s \leq \frac{|S(0)|}{\eta} \tag{5.25}$$

5.2.4 Design of a Sliding Mode Controller for a BLDC motor

This section considers the development of a sliding mode controller for one of the previous motor models. The motor model from Chapter 3 is considered, the model is given by

$$\begin{bmatrix}\dot{x}_1(t)\\ \dot{x}_2(t)\\ \dot{x}_3(t)\end{bmatrix}=\begin{bmatrix}0 & 1 & 0\\ 0 & 0 & 1\\ 0 & -\dfrac{BR+K_mK_e}{JL} & -\dfrac{BL+R_aJ}{JL}\end{bmatrix}\begin{bmatrix}x_1(t)\\ x_2(t)\\ x_3(t)\end{bmatrix}+\begin{bmatrix}0\\ 0\\ \dfrac{K_m}{JL}\end{bmatrix}u(t) \tag{5.26}$$

Despite the fact that the *η-reachability* condition provides a guarantee of convergence to the manifold in finite time, the normal condition is used here, with the requirement that the system is critically damped.

A suitable sliding manifold is specified by the equation

$$S(x)=C_1x_1+C_2x_2+x_3 \tag{5.27}$$

The control is specified as

$$u=\left[a_1x_1+a_2x_2+d\,\mathrm{sgn}(S)\right]b \tag{5.28}$$

Since for sliding $S\dot{S}<0$ is required,

$$\begin{aligned}S\dot{S}=&\left\{C_2-\frac{BL+R_aJ}{JL}\right\}S^2+\left\{C_1\left(\frac{BL+RJ}{JL}\right)+\frac{K_m}{JL}ba_1-C_1C_2\right\}x_1S\\&+\left\{C_1-C_2^2-\frac{BR+K_mK_e}{JL}+C_2\frac{BL+RJ}{JL}+\frac{K_m}{JL}ba_2\right\}x_2S\\&+\frac{K_m}{JL}bd|S|\end{aligned} \tag{5.29}$$

$$\begin{aligned}S\dot{S}|_{S=0}=&\left\{C_1-C_2^2-\frac{BR+K_mK_e}{JL}+C_2\frac{BL+RJ}{JL}+\frac{K_m}{JL}ba_2\right\}x_2S\\&+\left\{C_1\left(\frac{BL+RJ}{JL}\right)+\frac{K_m}{JL}ba_1-C_1C_2\right\}x_1S\\&+\frac{K_m}{JL}bd|S|\end{aligned} \tag{5.30}$$

Hence if the feedback parameters are chosen to be

$$a_1=\begin{cases}\alpha_1 & if \quad S>0\\ \beta_1 & if \quad S<0\end{cases} \tag{5.31}$$

$$a_2 = \begin{cases} \alpha_2 & if \quad S > 0 \\ \beta_2 & if \quad S < 0 \end{cases} \tag{5.32}$$

then $S\dot{S} < 0$ reduces to

$$\beta_1 < \gamma_1 < \alpha_1 \tag{5.33}$$

$$\beta_2 < \gamma_2 < \alpha_2 \tag{5.34}$$

and

$$d > \frac{JL}{K_m b} \tag{5.35}$$

where

$$\gamma_1 = \frac{1}{b}\frac{JLC_1}{K_m}\left(\frac{BL + R_a J}{JL} - C_2\right) \tag{5.36}$$

$$\gamma_2 = \frac{1}{b}\left\{BR + K_e - \frac{JLC_1}{K_m} - \frac{JLC_2}{K_m}\left(\frac{BL - RJ}{JL} - C_2\right)\right\} \tag{5.37}$$

for stability, according to the definition for the sliding manifold,

$$\lambda_1 = -\frac{C_2}{2} + \frac{1}{2}\sqrt{C_2^2 - 4C_1} \tag{5.38}$$

$$\lambda_2 = -\frac{C_2}{2} - \frac{1}{2}\sqrt{C_2^2 - 4C_1} \tag{5.39}$$

and the condition for zero overshoot is expressed as

$$C_2^2 \geq 4C_1 \tag{5.40}$$

The conditions of reaching are satisfied across the entire state space if

$$C_2 < \frac{BL + RJ}{JL} \tag{5.41}$$

The parameters from Table 5.1 are used

Table 5.1: *Nominal Motor Parameters*

	Parameters		
Symbol	Min.	Max.	Units
J	9e-3	12e-3	Nms^2
B	7e-3	7e-3	Nm/rad/s
T_l	1e-2	50e-2	Nm
L	0.0026	0.0026	H
R_a	0.64	0.64	Ω
K_e	54e-3	54e-3	Vs/rad
K_m	54e-3	54e-3	NmA^{-1}

Insertion of these values into the controller design provides

$C_2 < 25.19$

Therefore, choosing C_2=20 provides $C_1 = 100$. This choice will be justified in simulation later, however, the relationship between transient response and control effort is highlighted here. A lower value of C_2 will result in a lower demand being placed on the controller. From the selection of these two parameters that and the selection of the design gain b=1 the initial controller gains are chosen as per Table 5.2. Figure 5.2 illustrates the time response of the motor to a step input, using the minimum plant parameters from Table 5.1. The corresponding control action is shown in Figure 5.4. The maximum plant parameters are then inserted and the experiment repeated, Figure 5.3 and Figure 5.5 illustrate the time response and control effort respectively. The maximum parameters are then used (Figure 5.3 and Figure 5.5).

Table 5.2: *Controller design parameters*

Parameter	Min	Max	Selected
D	$0.58e^{-3}$	-	0.5
α_1	13.1	-	15
β_1	-	7.5	4
α_2	2.5	-	5
β_2	-	1.9	1.4

Parameters R=0.6 and L=0.5 are then selected to be out of the design bounds placed on them. Figure 5.6 shows the evolution of the position state. Figure 5.8 illustrates the control action, it can be seen that the control action briefly achieves the sliding mode but is unable to maintain it. The controller is now dependent upon the linear control in order to achieve robustness to both matched and unmatched disturbance. As a final point for consideration at this juncture within the work is that the sliding mode controller will always converge to the manifold in finite time, provided that there exists a sufficient control action to achieve this. Control of motor position directly is therefore a poor choice for the control. A test on the nominal system is performed and rather than a unit step input being applied, a signal of ten times is used. The time response and control effort are shown in Figure 5.7 and

Figure 5.9 respectively. The system has achieved a similar rise and settle time, however the control effort is nine times larger. Although within the literature sliding mode position controllers have been reported, because of this very practical limitation, it is far better to adopt sliding mode controllers for speed control, with a major control loop for

position if required. For the purposes of comparison, direct position control will be used within this Chapter, with a view to adjusting the control law later in Chapter 6.

Table 5.3 provides measures of the controller performance. The performance measures used throughout this work are the rise time (T_r), ±2% settling time (T_s), infinity norm of the control effort $\left(\left|u(t)\right|_\infty\right)$ and steady state error (SSE).

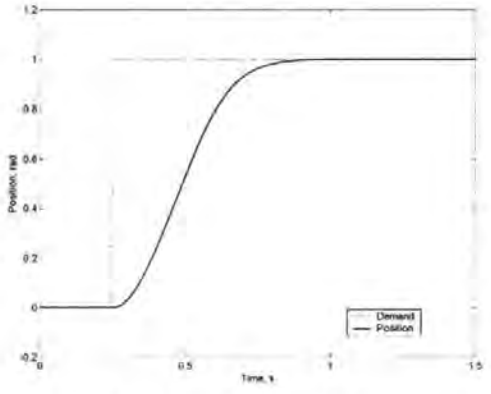

Figure 5.2: *Min. System step response*

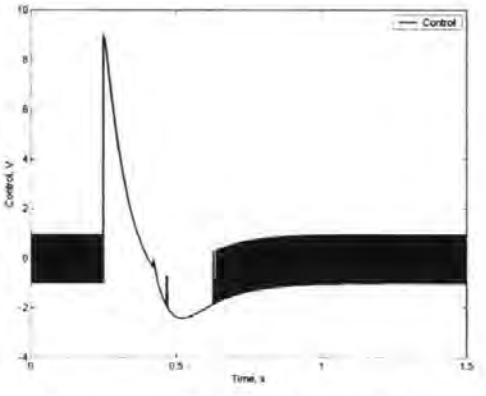

Figure 5.4: *Min System control effort*

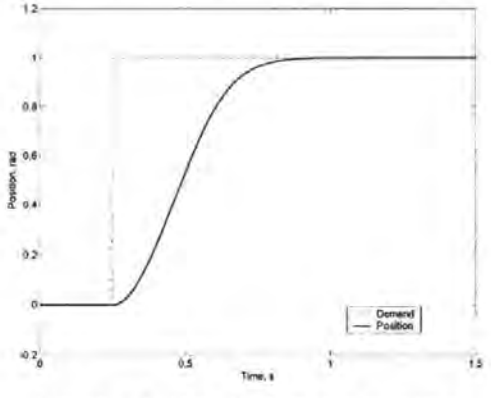

Figure 5.3: *Max. System step response*

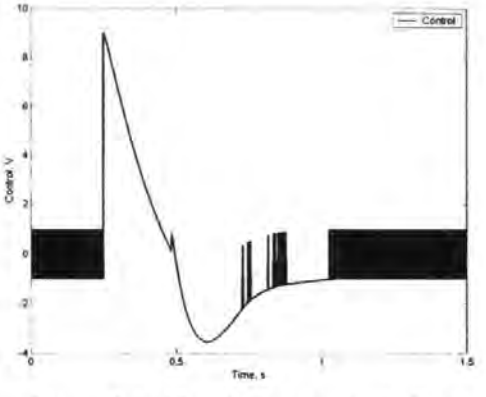

Figure 5.5: *Max. System control effort*

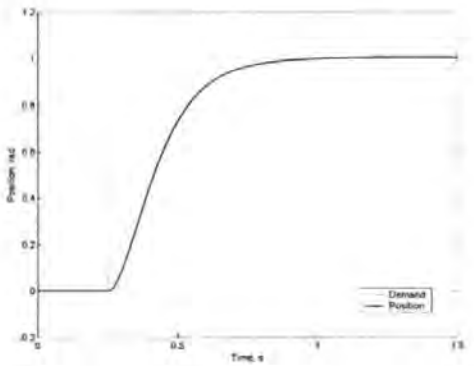

Figure 5.6: *Parameters out of bounds*

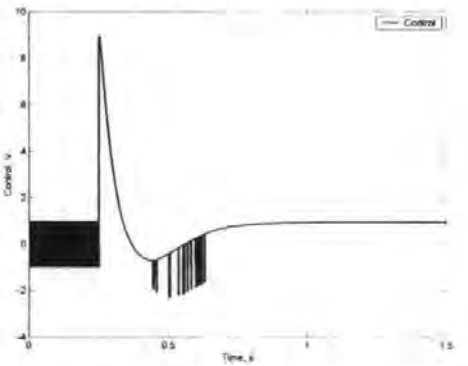

Figure 5.8: *Out of bounds Control effort*

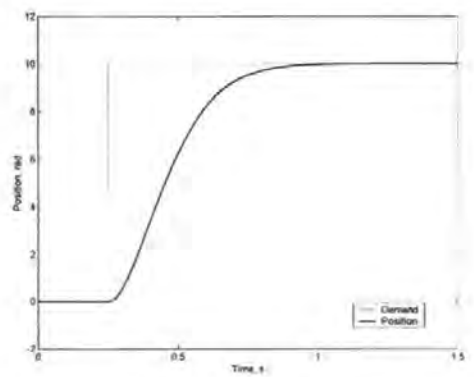

Figure 5.7: *Response to step input=10*

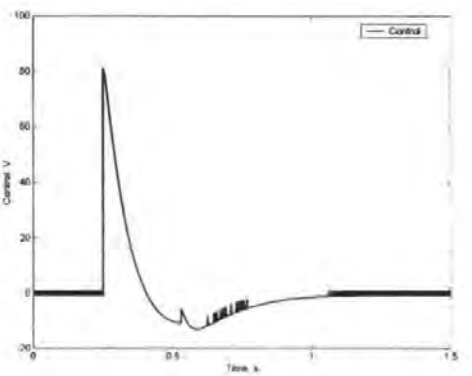

Figure 5.9: *Associated control effort*

Table 5.3: *Controller Performance according to specified measures*

Controller	$\|u(t)\|_\infty$ **(*V*)**	T_r **(*s*)**	T_s **(*s*)**	**SSE (*rad*)**
Min. Param.	9	0.322	0.75	0
Max. Param.	9	0.328	0.76	0
Out. Param.	9	0.34	-	0.022
10x Unit step	81	0.35	0.76	0

5.3 Design Approaches Based on the regular form

It can be seen from (5.7) that the sliding motion is a control independent motion that depends on the choice of sliding surface. The precise effect, however, is not readily apparent. A convenient way to clarify these effects is to first transform the system into a suitable canonical form. In this form the system is decomposed into two connected subsystems, one acting in $\Re(B)$ and the other in $\aleph(S)$. Since by assumption $\text{rank}(B) = n$ there exists an orthogonal matrix $T_r \in \mathbb{R}^{n\times n}$ such that

$$T_r B = \begin{bmatrix} 0 \\ B_2 \end{bmatrix} \tag{5.42}$$

where $B_2 \in \mathbb{R}^{n\times n}$ and is non-singular. Let $z = T_r x$ and partition the new co-ordinates so that

$$z = \begin{bmatrix} z_1 \\ z_2 \end{bmatrix} \tag{5.43}$$

where $z_1 \in \mathbb{R}^{n-m}$ and $z_2 \in \mathbb{R}^m$. The nominal linear system (5.7) can then be written as

$$\dot{z}_1(t) = A_{11}\dot{z}_1(t) + A_{12}z_2(t) \tag{5.44}$$

$$\dot{z}_2(t) = A_{21}z_1(t) + A_{22}z_2(t) + B_2u(t) \tag{5.45}$$

which is referred to as the regular form. Equation (5.44) is referred to as describing the null-space dynamics and equation (5.45) as describing the range-space dynamics. Functions $f_u(t,x)$ and $f_m(t,x,u)$ represent the matched and unmatched uncertainty, projected into the regular form, respectively, For the time being, these uncertainties will not be considered. Suppose the matrix defining the switching function (in the new co-ordinate system) is compatibly partitioned as

$$ST_r^T = [S_1 \quad S_2] \tag{5.46}$$

where $S_1 \in \mathbb{R}^{m\times(n\times m)}$ and $S_2 \in \mathbb{R}^{m\times m}$. Since $SB = S_2B_2$ it follows that a necessary and sufficient condition for the matrix SB to be non-singular is that $\det(S_2) \neq 0$. By design assume this to be the case. During an ideal sliding motion

$$S_1 z_1(t) + S_2 z_2(t) = 0 \qquad \text{for all } t > t_s \tag{5.47}$$

and therefore formally expressing $z_2(t)$ in terms of $z_1(t)$ yields

$$Z_2(t) = -Mz_1(t) \tag{5.48}$$

where $M = S_2^{-1}S_1$. Substituting in (5.44) gives

$$\dot{z}_1(t) = (A_{11} - A_{12}M)z_1(t) \tag{5.49}$$

and thus the problem of hyperplane design may be considered to be a state feedback problem for the system (5.44) where $z_2(t)$ is considered to play the role of the control action. In the context of designing a regulator, the matrix governing the sliding motion ($A_{11} - A_{12}M$) must have stable eigenvalues. The switching surface design problem can therefore be considered to be one of choosing a state feedback matrix M to stabilise the reduced order system (A_{11}, A_{12}). Because of the special structure of the regular form, it follows that the pair (A_{11}, A_{12}) is controllable if and only if (A, B) is controllable. It can be seen from equation (5.46) that S_2 has no direct effect on the dynamics of the sliding motion and acts only as a scaling factor for the switching function. The choice of S_2 is therefore somewhat arbitrary. A common choice however, which stems from the so-called hierarchical design procedure, is to let $S_2 = \Lambda B_2^{-1}$ for some diagonal design matrix $\Lambda \in \mathbb{R}^{m\times m}$ which implies $SB = \Lambda$. By selecting M and S_2 the switching function in equation (5.46) it completely determined.

Several approaches have been proposed for the design of the feedback matrix M including quadratic minimisation, eigenvalue placement and eigenstructure assignment methods. These approaches are discussed in Appendix D, part 1.

5.3.1 State-feedback Control Laws

Of the many different multivariable sliding mode control structures which exist the one that will be considered here is essentially that of Ryan and Corless (1984) and may be described as a unit vector approach. Consider an uncertain system of the form

$$\dot{x}(t) = Ax(t) + Bu(t) + f_m(t,x,u) + f_u(t,x) \tag{5.50}$$

where the function $f_u(t,x): \mathbb{R} \times \mathbb{R}^n \to \aleph(B)$ and $f_m(t,x,u): \mathbb{R} \times \mathbb{R}^n \times \mathbb{R}^m \to \Re(S)$ which represent the unmatched and unmatched uncertainty components of the system, which are unknown but assumed bounded. The function $f_u(t,x)$ is assumed to satisfy

$$\|f_u(t,x)\| \le k_1 \|x\| + k_2 \tag{5.51}$$

The matched uncertainty is assumed to act through the control channels, i.e.

$$f(t, x, u) = B\xi(t, x, u) \tag{5.52}$$

where $\xi(t,x,u): \mathbb{R} \times \mathbb{R}^n \times \mathbb{R}^m \to \mathbb{R}^m$ and is unknown but satisfies

$$\|\xi(t,x,u)\| \le k_1 \|u\| + \alpha(t,x) \tag{5.53}$$

where $1 > k_1 \ge 0$ is a known constant, $\alpha(\cdot)$ is a known function and

$$k_3 < \sqrt{\lambda_{\min} \left\| B_2^{-1} \right\|^{-1}} \tag{5.54}$$

The proposed control law consists of two components; a linear component to stabilise the nominal system; and a discontinuous component. Specifically

$$u(t) = u_l(t) + u_n(t) \tag{5.55}$$

where the linear component is given by

$$u_l(t) = -\Lambda^{-1}(SA - \Phi S)x(t) \tag{5.56}$$

where $\Phi \in \mathbb{R}^{m\times m}$ is any stable design matrix and $\Lambda = SB$ which satisfies

$$k_3\kappa(\Lambda)\left\|B_2^{-1}\right\| < 1 \tag{5.57}$$

The non-linear component is defined to be

$$u_n(t) = -\rho(t,x)\Lambda^{-1}\frac{P_2 s(t)}{\|P_2 s(t)\|} \qquad \text{for all } S \neq 0 \tag{5.58}$$

where $P_2 \in \mathbb{R}^{m\times m}$ is a symmetric positive definite matrix satisfying the Lyapunov equation

$$P_2\Phi + \Phi^T P_2 = -I \tag{5.59}$$

and the scalar function $\rho(t,x)$, which depends only on the magnitude of the uncertainty, is any function satisfying

$$\rho(t,x) \geq \frac{\|S\|\left(\|M\|\left(k_1\|x_1(t)\| + k_2\right) + k_3\|u_l(t)\| + \alpha(t,x)\right) + \gamma_2}{\left(1 - k_3\kappa(\Lambda)\left\|B_2^{-1}\right\|\right)} \tag{5.60}$$

where $\gamma>0$ is a design parameter. In this equation it is assumed that the scaling parameter has been chosen so that $k_1\kappa(\Lambda) < 1$. It can be established that any function satisfying equation (5.60) also satisfies

$$\rho(t,x) \geq \|\xi(t,x,u)\| + \gamma \tag{5.61}$$

and therefore $\rho(t,x)$ is greater in magnitude than the matched uncertainty occurring in equation (5.52). It can be verified that $V(S) = S^T P_2 S$ guarantees quadratic stability for the switching states and in particular

$$\dot{V} \leq -S^T S - 2\gamma \|P_2 S\| \tag{5.62}$$

This control law guarantees that the switching surface is reached in finite time despite the disturbance or uncertainty and once the sliding motion is attained it is completely independent of the uncertainty.

5.3.2 Unit Vector Sliding Mode Control of a Brushless D.C. Motor

This section of the work is devoted to the development of a sliding mode controller for the third order system used previously in Chapter 3, specifically

$$\begin{bmatrix} \dot{x}_1 \\ \dot{x}_2 \\ \dot{x}_3 \end{bmatrix} = \begin{bmatrix} 0 & 1 & 0 \\ 0 & -\frac{B}{J} & \frac{K_m}{J} \\ 0 & -\frac{K_e}{L} & -\frac{R_a}{L} \end{bmatrix} \begin{bmatrix} x_1 \\ x_2 \\ x_3 \end{bmatrix} + \begin{bmatrix} 0 \\ -\frac{u_1}{J} \\ \frac{u_2}{L} \end{bmatrix} \tag{5.63}$$

In this section it is assumed initially that the load torque and the frictional load are negligible, the input control is therefore simply the applied voltage. Additionally it is assumed that the load inertia is not precisely known, such that

$$\frac{K_t}{J} = \frac{K_t}{J_N} + \xi_J \tag{5.64}$$

where J_N is the nominal value of the inertia determined experimentally and

$$|\xi_J| < 0.5 \tag{5.65}$$

The model may be rewritten in the form

$$\begin{bmatrix} \dot{x}_1 \\ \dot{x}_2 \\ \dot{x}_3 \end{bmatrix} = \begin{bmatrix} 0 & 1 & 0 \\ 0 & 0 & \frac{K_m}{J} \\ 0 & -\frac{K_e}{L} & -\frac{R_a}{L} \end{bmatrix} \begin{bmatrix} x_1 \\ x_2 \\ x_3 \end{bmatrix} + \begin{bmatrix} 0 \\ 0 \\ \frac{1}{L} \end{bmatrix} u_2 \tag{5.66}$$

and the model is automatically in the regular form with the matrices given as

$$A_{11} = \begin{bmatrix} 0 & 1 \\ 0 & 0 \end{bmatrix} \tag{5.67}$$

$$A_{12} = \begin{bmatrix} 0 \\ \frac{K_m}{J} \end{bmatrix} \tag{5.68}$$

$$B_2 = \frac{u_2}{L} \tag{5.69}$$

The matrix which defines the switching function is given as

$$M = \begin{bmatrix} M_1 & M_2 \end{bmatrix} \triangleq \begin{bmatrix} \frac{K_m}{J}\omega_n^2 & 2\frac{K_m}{J}\zeta\omega_n \end{bmatrix} \tag{5.70}$$

The characteristic equation of $A_{11} - A_{12}M$ is the quadratic equation

$$\lambda^2 + 2\zeta\omega_n\lambda + \omega_n^2 = 0 \tag{5.71}$$

where the parameters ζ and ω_n represent the damping ratio and the natural frequency respectively. The switching function obtained from the selection of $S_2 = 1$, and the value of M determined previously, is given by

$$S(t) = \begin{bmatrix} \frac{K_m}{J}\omega_n^2 & 2\frac{K_m}{J}\zeta\omega_n & 1 \end{bmatrix} x(t) \tag{5.72}$$

from equation (5.56), the linear component of the control law is given by

$$u_l(t) = -LSAx(t) + L\Phi S(t) \tag{5.73}$$

where Φ represents a negative definite scalar value which will determine the rate of decay of the state onto the switching manifold. Consideration of the range space dynamics in (5.45) reveals that

$$\dot{x}_3 = -\frac{K_e}{L}x_2(t) - \frac{R_a}{L}x_3(t) + \frac{u_2(t)}{L} + f_m(t,x,u) \tag{5.74}$$

The matched uncertainty component is therefore given as

$$f_m(t,x,u) = -\frac{1}{L}\left(K_e x_2(t) + R_a x_3(t) - u_2(t)\right) \tag{5.75}$$

It will be assumed that the motor inductance is not precisely known, but is known to fulfil the bound

$$\delta_L = \frac{L - L_A}{L_A}, |\delta_L| < 0.1 \tag{5.76}$$

where L is the nominal inductance specified by the manufacturer and L_A is the actual phase inductance. It follows from (5.54) that the gain associated with the input uncertainty is

$$k_3 = \frac{1}{10L_A} \tag{5.77}$$

with the bounding function

$$\alpha(t,x) = \frac{1}{10L_A}\left(K_e|x_2(t)| + R|x_3(t)|\right) \tag{5.78}$$

since $\sqrt{\lambda_{\min}\left\|B_2^{-1}\right\|^{-1}} = 1/L_A$ the requirement of (5.54) is satisfied. It can be confirmed that the reduced order sliding motion is given by

$$\dot{x}_1(t) = x_2(t) \tag{5.79}$$

$$\dot{x}_2(t) = -2\zeta\omega_n x_2(t) - \omega_n^2 x_1(t) - \xi_J\left(M_1 x_1(t) + M_2 x_2(t)\right) \tag{5.80}$$

which implies from (5.51) that

$$\left\| f_u(t,u) \right\| \le \frac{1}{2}\|M\|\left\|x(t)\right\| \tag{5.81}$$

Appropriate values of the coefficients are therefore found to be $k_1 = \frac{1}{2}\|M\|$ and $k_2 = 0$. A scalar value for pre-multiplication of the nonlinear control element can now be found. Since $\Lambda = 1/L$ and the parameter $\kappa(\Lambda) = 1$,

$$1 - k_3\kappa(\Lambda)\left\|B_2^{-1}\right\| = 0.9 \tag{5.82}$$

Hence from the scaling function (5.60)

$$\rho(t,x) = \frac{\left(\left|u_1(t)\right| + K_e\left|x_2(t)\right| + R_a\left|x_3(t)\right| + 5L\|M\|^2\left\|x(t)\right\| + 10L\gamma_2\right)}{9L} \tag{5.83}$$

The nominal values of the motor in Table 5.1 are used in addition, the properties of the sliding motion have been assigned as $\zeta = 1$, $\omega_n = 5$ rad/s, $\Phi = -20$ and $\gamma_2 = 0.01$. The simulated time response to a step input of the plant when the nominal parameters are assumed to vary in accordance with Table 5.1 are shown in Figure 5.13 for the plant with minimum parameters and Figure 5.14 for the maximum parameters. Where it was initially assumed that the load friction was nil, its effects have been taken account of within the nonlinear control component.

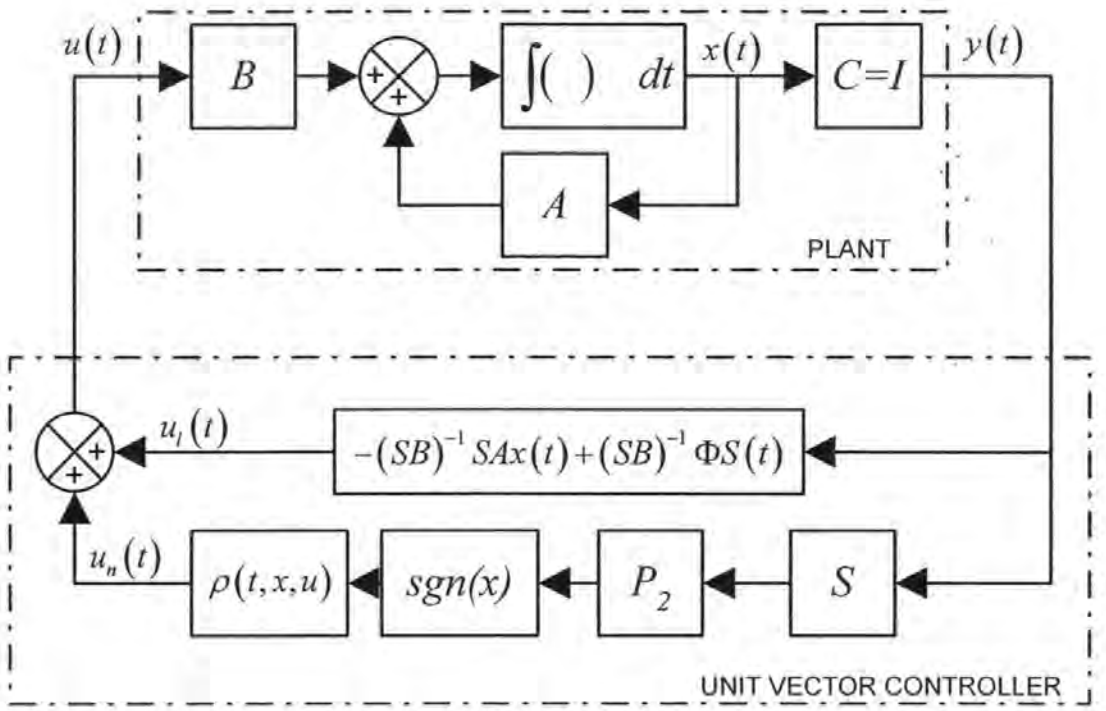

Figure 5.10: *A Unit Vector Sliding Mode Regulator*

A sliding mode regulator (Figure 5.10) has been successfully designed and its performance may be seen in

Figure 5.11 to be satisfactory, requiring 0.75 seconds to converge to the origin given initial conditions of $x_1 = 1, x_2 = 0$ and $x_3 = 0$. Chatter is evident as very high frequency switching within the control channel, the following section will be devoted to methods which will negate this effect. In order to convert the regulator to a controller, it is simply a matter of choosing the correct space in which to control the system.

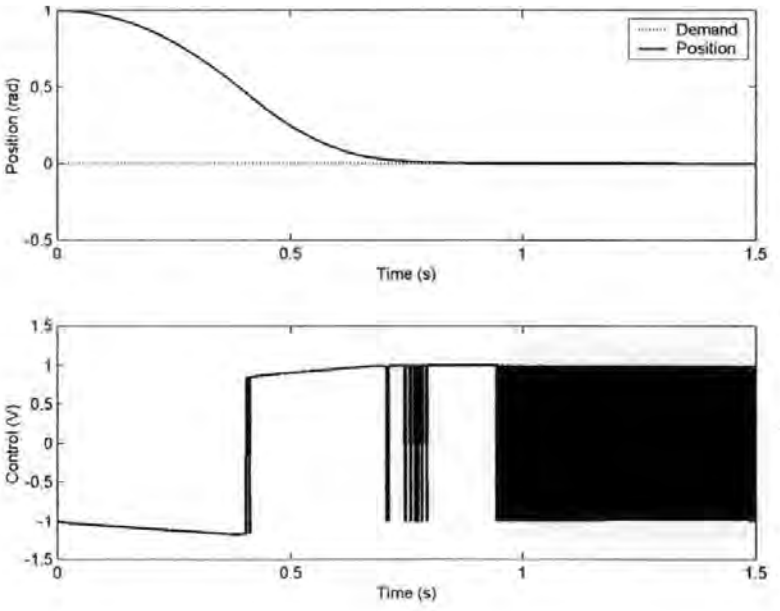

Figure 5.11: *Performance of the Sliding Mode regulator, Top, Position evolution, Bottom, Control effort*

Assuming that there exists an appropriate coordinate transform, the regulator may be used as a controller by introducing a demand, $d(t)$. The regulator will act within the error space in exactly the same manner as before. The principle of the controller acting with the transformation given by (5.84)-(5.86) is shown in Figure 5.12.

$$\varepsilon_1(t) = d(t) - x_1(t) \tag{5.84}$$

$$\varepsilon_2(t) = -x_2(t) \tag{5.85}$$

$$\varepsilon_3(t) = -x_3(t) \tag{5.86}$$

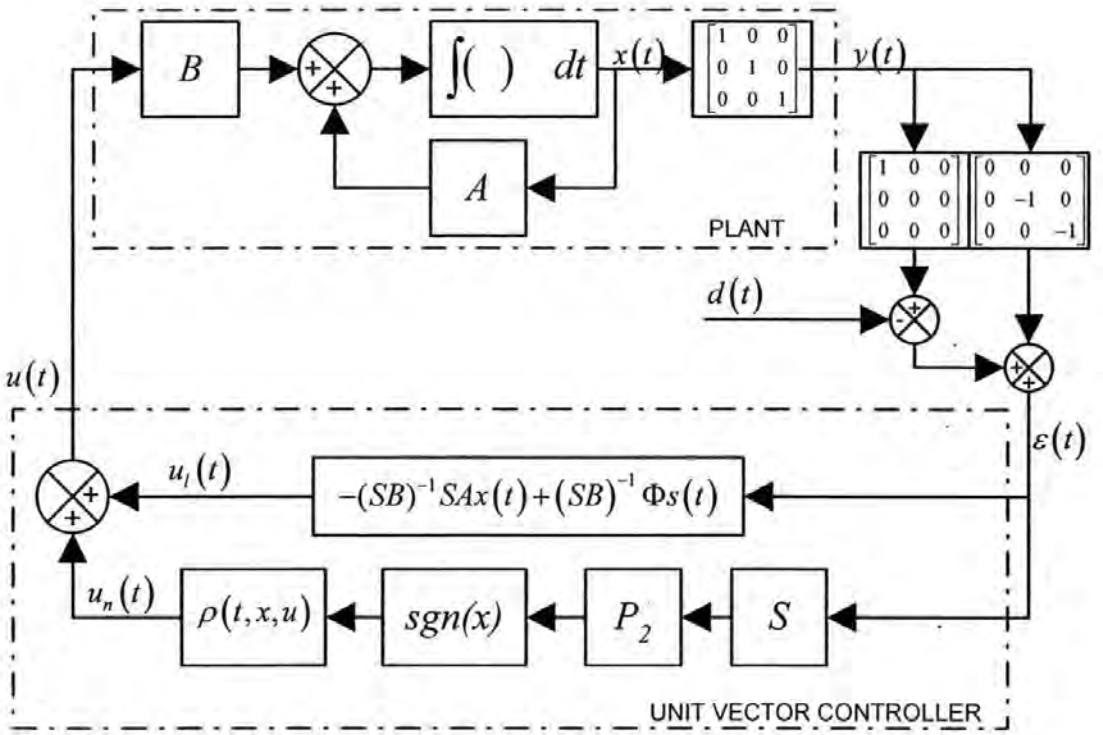

Figure 5.12: *A Unit Vector Sliding Mode Controller*

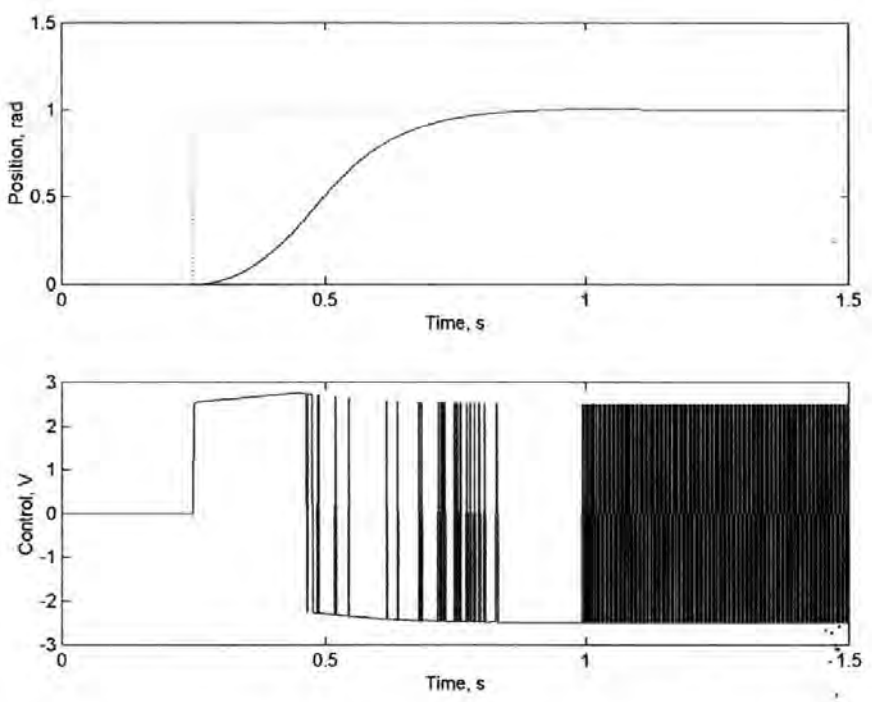

Figure 5.13: *Sliding Mode controller performance with minimum parameters*

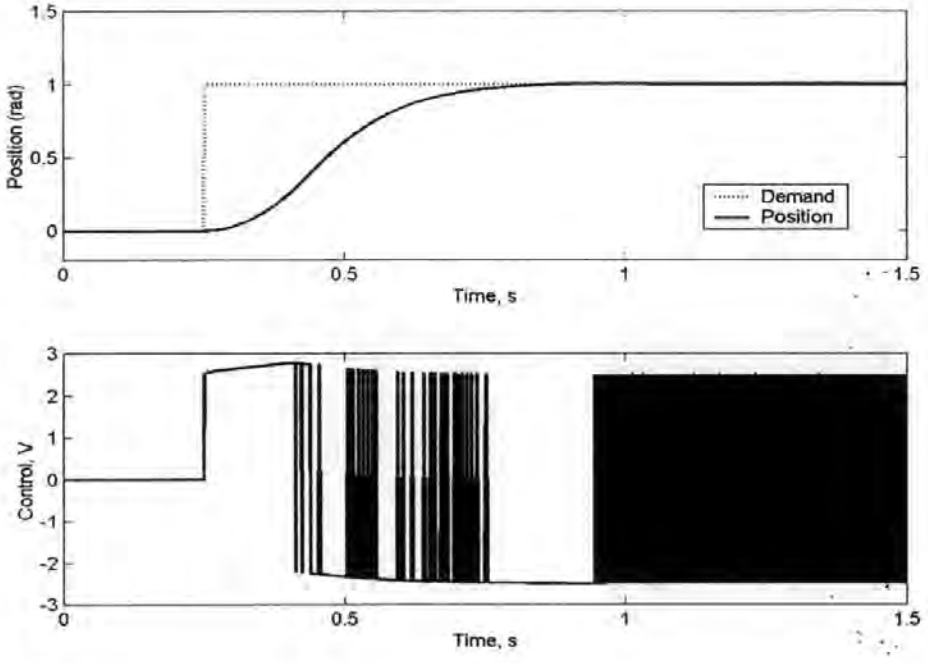

Figure 5.14: *Sliding mode controller performance, plant maximum parameters*

As per the controller developed in the last section, the unit vector controller is able to demonstrate invariance to the bounded parameters, once sliding. It is plain to see that the chatter phenomenon is only just being maintained, illustrating that the controller is only just achieving the sliding mode. It can also be seen that the transient performance, and the rate at which the error state converges onto the manifold is also different. This is the typical performance one would expect to see whilst the controller is in the reaching phase. An important consideration of this work is the controllers robustness to sensor noise. This has not been formally considered within the derivation of the controller and is significant since the circuit used for current measurement from the motor (see Chapter 3) has only a single Resistor-Capacitor filter. Within the simulation, an extraneous noise

signal was introduced, it is assumed that the sensor noise can be modelled by a white noise signal with zero mean. It should be noted that practically, the signal will not match this description (Porat, 1997), but will suffice as an approximation. The signal is assumed to have a 10% signal to noise ratio. The position and control effort are illustrated in Figure 5.15 and Figure 5.16 respectively. The controller maintains the demand, however, since the noise signal is essentially an unmatched disturbance, the system dynamics, even in the sliding mode are effected. Once again, the use of a major-minor feedback loop with the inner sliding mode controller for speed will serve to severely restrict the effect that such signals have on the controlled position (Chapter 6).

The controllers thus far developed have been shown to attain the sliding mode in finite time. The sliding mode theoretically obtained is the ideal sliding mode, which leads to discontinuous control across the manifold S. In the control of electrical machines such control is noted to be naturally discontinuous. However, the implementation of such controllers in a mechanical system will lead to a chatter motion within a boundary of the surface S rather than the ideal, smooth sliding motion. This phenomena is well reported to inflict undue wear and high heat losses within the actuators, the control law would be considered unacceptable. Within the next section, modifications to the control law are described which overcome this difficulty.

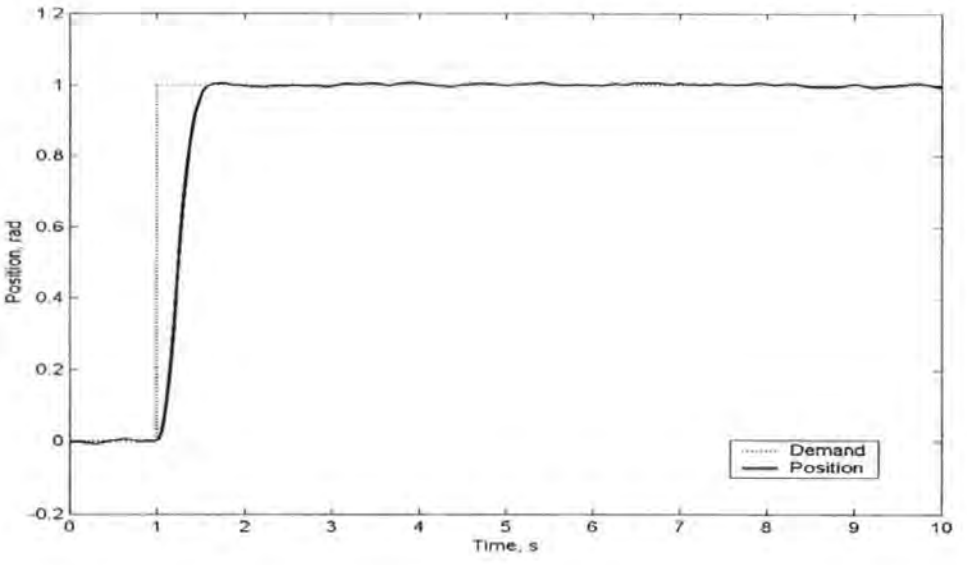

Figure 5.15: *Sliding mode controller position control with current sensor subject to 10% SNR*

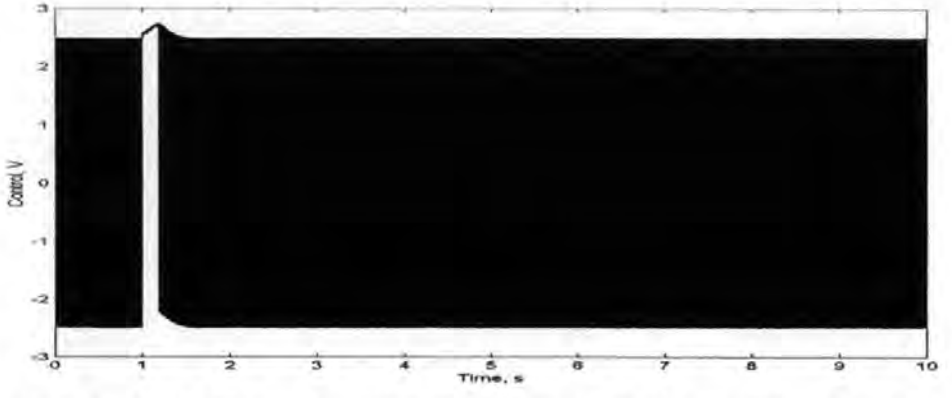

Figure 5.16: *Sliding mode control, with current sensor subject to 10% SNR*

5.4 Anti Chatter Techniques

The many advantages associated with SMC have been extolled within this work. The principle drawback associated with SMC, however, is the phenomenon referred to as

chattering (Young *et al*, 1999). This term is used to describe the finite frequency, finite amplitude oscillation of the controlled state around the sliding manifold.

Chattering has two principle causes; the first is that digital implementations of the SMC with microprocessors of fixed sample rate may cause discretisation chatter (Habibi and Richards, 1992). The second cause is attributed to the fast dynamics in the control loop which are neglected in the system model. These dynamics are excited by the high frequency switching of the controller. In this case, the term 'unmodelled dynamics' refer to inertia associated with actuators and sensors, which in principle is much faster than the system dynamics. However, since a sliding mode controller is in theory infinitely fast, all dynamics of the system should, in principle, be accounted for.

This effect is known to cause undue wear on mechanical components, high heat loss in electrical circuits and low control accuracy (Utkin, 1993). This has naturally served to limit the application of SMC. A very large research effort has therefore been directed at the neutralisation of the chattering effect. This section provides an overview of the techniques applied to date.

To initiate this section, consider a first order plant. The plant is actuated with a second order unmodelled actuator, given by equations (5.87) and (5.88) respectively.

$$\dot{x}(t) = ax(t) + bu(t) + \xi(x,t) \tag{5.87}$$

$$W(p) = \frac{\omega^2}{p^2 + 2\omega p + \omega^2} U(p) = \frac{1}{(\mu p - 1)^2} U(p) \tag{5.88}$$

where a and b are assumed unknown plant parameters with known bounds. $u(t)$ is the control variable and the disturbance $\xi(x,t)$ is also assumed to have known bounds. u(t) is the actual control input, and p represents the Laplace variable (to avoid confusion with

s). ω (ω>0) is used to represent the actuator bandwidth and the relationship ω»a, signifying that the actuator dynamics are significantly faster than the system dynamics, permits the substitution of a small time constant $\mu\left(\mu = 1/\omega > 0\right)$.

5.4.1 Boundary Layer Normalisation

This approach seeks to avoid control discontinuities within the control loop by replacing the discontinuous control law ($\mathrm{sgn}(S)$, Figure 5.17.a) with a continuous saturation function (Figure 5.17.b). This function is an approximation of the manifold $S(t)=0$ with a boundary layer.

The saturation function is given

$$u(t) = \begin{cases} Msign(S(t)) & if\ |S(t)| > \beta \\ \dfrac{M}{\beta} S(t) & if\ |S(t)| \le \beta \end{cases} \qquad (5.89)$$

Where β defines the radius of the boundary layer. Consideration of this function shows that when the representative point is far from the manifold $S(t)$=0, the saturation function behaves precisely as the sign function, and the linear feedback gain is symmetrically saturated with a value of M within this region. Convergence of the state trajectory to the boundary layer is guaranteed through the same arguments for the system employing the sign function. It may be shown (Utkin *et al*, 1999) that provided the unmodelled dynamics are stable and faster than the system dynamics that the controller will be stable. Intuitively it may be seen that higher feedback gains will ultimately cause chatter once again. The stability boundary is given

$$\frac{M}{\beta} < \frac{3\sqrt{2}-4}{b\mu}\left(1-a\mu\right)^2 \tag{5.90}$$

Further it may be shown that for oscillation free trajectories with critically damped eigenvalues the following inequality must hold

$$\frac{M}{\beta} < \frac{3\sqrt{2}-4}{b\mu}\left(1-2a\mu\right)^2 \tag{5.91}$$

One of the clear benefits of the boundary layer approach is that the resulting controller is continuous. The invariance condition is still partially achieved since the state trajectory is now confined to the ε vicinity of the manifold $S(t)=0$. However, since within the ε vicinity of the manifold (i.e. within the boundary layer) the behaviour of the controller is not defined, convergence of the system to the origin of the phase plane is not guaranteed.

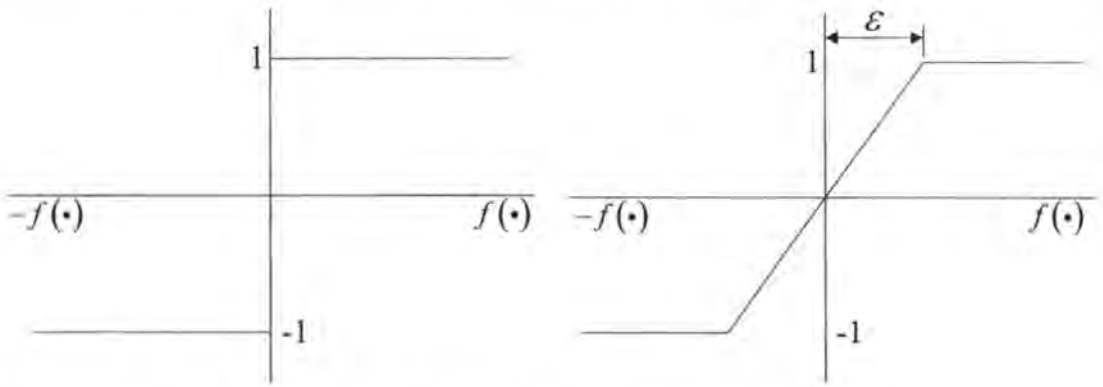

Figure 5.17: *a.(left) the discontinuous sign function b.(right) the continuous saturation function*

The controller developed in § 5.3.5 is now modified in order to incorporate a boundary layer, the discontinuous control action is now given as

$$u_n(t) = -\rho(t,x)\Lambda^{-1}\frac{P_2 S(t)}{\left\|P_2 S(t)\right\|+\varepsilon} \tag{5.92}$$

which provides an approximation to the saturation function where ε is a small positive constant which defines the radius of the boundary layer (Chern and Wong, 1995). The unit vector controller of the previous section has been implemented using a value of 1Nm for the friction, this is in keeping with the initial measurement taken from Chapter 4. Chatter within the control is evident (Figure 5.20). Also evident is the effect of the noise within the current measurement on the steady state (Figure 5.18). This was predicted in §5.3.5. The modified controller response is shown in Figure 5.19 for a boundary layer $\varepsilon = 0.1$. The smoothed control action is shown in Figure 5.21. The introduction of the boundary layer has led to a steady state error within 2% of the demand. The final value of the steady state error will vary depending on the position of the carriage relative to the stage and therefore the perturbation to which it is subjected. As discussed, the boundary layer is only able to provide guarantees of position to within the ε-vicinity. This fact will be of great importance within Chapter 6.

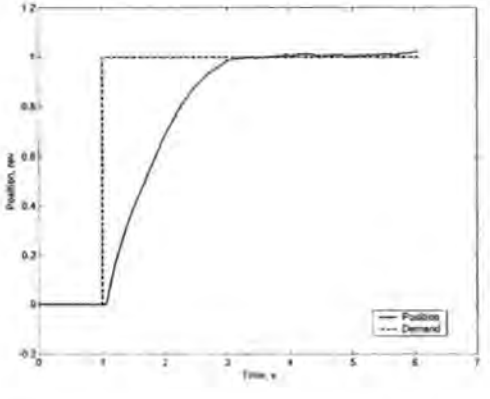

Figure 5.18: *Position control of the linear stage*

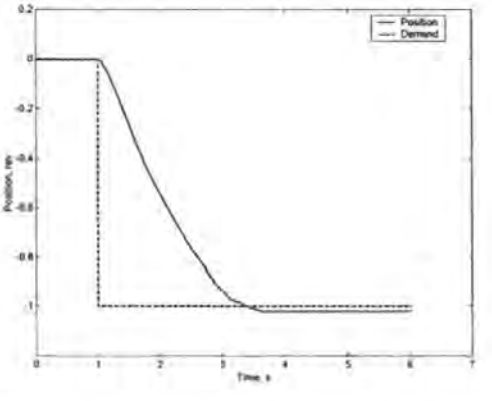

Figure 5.19: *Position Control of the Linear stage with boundary layer*

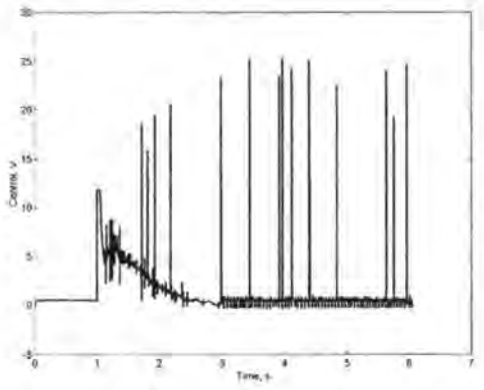

Figure 5.20: *Control effort illustrating chatter*

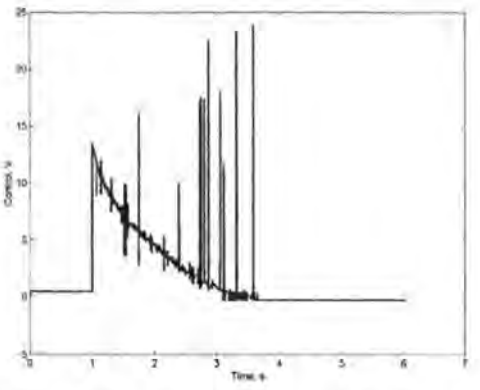

Figure 5.21: *Smoothed control effort*

5.4.2 Observer Based Solution

The boundary layer solution discussed above avoids generating a sliding mode by replacing the discontinuous control action with a continuous one. When employing a continuous controller, it becomes necessary to use some method of converting the discontinuous signal, such as pulse width modulation. Modern motor controllers are discontinuous and are able to switch in the mega hertz region. Whilst the boundary layer approach remains an attractive design option because of its simplicity, for internally high order nonlinear systems, such as the brushless D.C. motor linear control methods become insufficient for control. This has been one of the principle reasons for the interest in SMC. An alternative approach must therefore be conceived that will provide the discontinuous control but alleviate chatter.

The fundamental approach adopted in the observer based solution is to generate the ideal SMC in a secondary, internal observer loop. Ideal sliding mode is possible in the controller since it is entirely generated within the controller software and will not contain

unmodelled dynamics. Despite the discontinuous signal being applied to the plant, no chattering occurs and the system behaves as if the equivalent control were being applied.

Define a first order observer for the system given in (5.7)

$$\dot{\hat{x}}(t) = ax(t) + bu(t) + L_l \bar{x}(t) \tag{5.93}$$

In this case L_l is the linear feedback gain for the observation error $\bar{x}(t) = x(t) - \hat{x}(t)$. The dynamics of the observation error may be described by

$$\dot{\bar{x}}(t) = \xi(x,t) - L_l \bar{x}(t) \tag{5.94}$$

Both the observation error and the disturbance are assumed unknown but bounded. If a manifold is now introduced

$$\hat{S}(t) = x_d(t) - \hat{x}(t) \tag{5.95}$$

then the ideal sliding mode controller for the observer loop may be defined as

$$u(t) = M \operatorname{sgn} \hat{S}(t) \tag{5.96}$$

It is clear that since the observer acts as the controlled system, and since the observer is able to react in the expected manner, that the ideal trajectory of the representative point will be realised. Recalling that in this case the output of the controller may be described as the equivalent control. In order to examine the behaviour of the of the system, the equivalent control method may be employed, solving

$$\dot{\hat{S}}(t) = x_d(t) - ax(t) - bu(t) - L_l \bar{x}(t) \tag{5.97}$$

for the control, yields

$$bu_{eq}(t) = x_d(t) - ax(t) - L_l \bar{x}(t) \equiv 0 \tag{5.98}$$

It is shown in (Utkin *et al*, 1999) that the stability bound in this case is given by

$$L_l + a < \frac{2}{\mu}(1 - a\mu)^2 \qquad (5.99)$$

The observer based solution to chatter prevention requires a greater design effort. However, observers serve to form an integral part of many control applications. It has been shown here that they may easily be included in the controller design. In addition, both full and reduced order observers may be used and the designer is thus afforded a greater flexibility than when designing with the boundary layer solution.

5.4.3 Regular form

Both methods that have been described so far have assumed complete ignorance of the unmodelled actuator and plant dynamics. In reality, however, at least partial information about the unmodelled dynamics can be obtained and additionally actuator outputs may be measured. For instance extremely accurate models are available for the brushless D.C. motor, in terms of the model structure, but parameters of the specific motor are uncertain. It makes sense to include the known dynamics into the controller in order to achieve better system performance.

The principle supporting the regular form approach is that since the actuator and the system are block separated, a cascaded controller may be designed in two steps. The first step is to design the controller for the plant alone, assuming ideal actuator dynamics. Thus the desired actuator outputs w_d are defined. In the second step the actual control effort is used, such that the actuator outputs may be guaranteed to follow the desired output with the relationship $u(t)=u_d(t)$.

Because of the massive number of available models for electric drives and controllers this method is especially attractive. It is important to note, however, that this method is not

applicable systems with unmodelled dynamics principally introduced by sensors, because measurements of both inputs and outputs of the unmodelled dynamics are required. Since sensor inputs are rarely available through measurement, other techniques to avoid chattering such as those discussed above should be employed in systems with unknown sensor dynamics.

Proceeding under the assumption that the main source of unmodelled dynamics is the actuator, and that a reasonable model for the actuator with uncertain parameters is available, for instance

$$W(p)=\frac{\hat{\omega}^2}{p^2+2\hat{\omega}p+\hat{\omega}^2}U(p)=\frac{1}{(\hat{\mu}p+1)^2}U(p) \tag{5.100}$$

where $\hat{w}=1/\hat{\mu}$ serves to provide an estimate of the actuator bandwidth, u(t) is the control input the system and w(t) is the measurable actuator output.

In the first step of the design procedure, a continuous auxiliary control law w_d(t) is developed for the system (5.7) in order to track the desired trajectory x_d(t). It is unimportant which design method is used in order to achieve this, however, due care should be taken in order to ensure that the system will still be able to track the trajectory despite the limited actuator bandwidth.

For the system in equation (5.7), if a first order linear controller of the form

$$w_d(t)=C(x_d(t)-x(t))=Cx_e(t) \tag{5.101}$$

with proportional gain C>0 is used, then the error dynamics will be given

$$\dot{x}_e(t)=b(-Cx_e(t)+h(x,x_d,t)) \tag{5.102}$$

The second step in the design is to drive the error $w_e(t)=w_d(t)-w(t)$ to zero. Since the inner control loop does not contain any unmodelled dynamics, a discontinuous controller may be designed as

$$U(p)=(\hat{\mu}p+1)^2 W_d(p)+M\,\mathrm{sgn}\,S(p) \tag{5.103}$$

with sliding variable

$$S(t)=K\dot{w}_e(t)+w_e(t) \quad (K>0) \tag{5.104}$$

Assuming that the first and second time derivatives of $w_d(t)$ in (5.101) are available, and that the first time derivative of the actuator output dw(t)/dt is also available then the controller (5.103) leads to

$$u(t)=\mu^2\ddot{w}_e(t)+2\mu\dot{w}_e(t)+M\,\mathrm{sgn}\,S(t) \tag{5.105}$$

Using conventional tools for the analysis of sliding mode, it can be shown that $S(t)$ and $dS(t)/dt$ will have opposite signs for bounded $dw(t)/dt$ and $d^2w(t)/dt^2$ if the control gain M is sufficiently high, but bounded.

5.4.4 Disturbance rejection

The previous controller sought to achieve tracking of the desired trajectory with the output of the plant, this approach required the use of a linear control with an estimate of the plant disturbance. However, this disturbance estimate is frequently unobtainable. The final approach discussed here provides a method by which the disturbance may be accurately estimated, whilst still avoiding chattering within the main control loop. This method may be viewed as a special case of integral sliding mode control (Utkin and Shi, 1996).

The principle concept surrounding disturbance rejection via an SMC approach is to split the controller into two components; a continuous controller $u_c(t)$ for overall control of the plant and a discontinuous control $u_d(t)$ for the disturbance rejection and suppression of parametric uncertainty effects. The overall control $u(t)$ takes the form

$$u(t) = u_c(t) + u_d(t) \tag{5.106}$$

Once again, referring to the system described in equation (5.7), assume that the desired trajectory and b are known, but parameter a and disturbance $d(x,t)$ are both unknown. A continuous controller may then be designed as

$$u_c(t) = \frac{1}{b}(Cx_e(t) + \dot{x}_d(t)) \tag{5.107}$$

where C>0 is the proportional feedback gain for the tracking error, $x_e(t)$. If it is assumed at the moment that the system contains no actuator dynamics then the disturbance rejection term of the controller may be set to zero such that $u(t)=u_c(t)$. Substitution of (5.107) into (5.87) then yields

$$\dot{x}_c(t) + Cx_e(t) = -ax(t) - d(x,t) = f(x,t) \tag{5.108}$$

The error dynamics in (5.108) are perturbed by the function $f(x,t) \neq 0$. Since these perturbations are not zero, the tracking error $x_e(t)$ does not go to zero. The discontinuous controller is designed to improve tracking performance by providing an estimate of the disturbance. A manifold is first defined as

$$s(t) = x_e(t) + z(t) \tag{5.109}$$

where z is an auxiliary sliding variable given by

$$\dot{z}(t) = -\dot{x}_d(t) = bu(t) - bM \operatorname{sgn} S(t) \tag{5.110}$$

After differentiation of (5.109), the sliding variable s(t) and the auxiliary variable z(t) may be substituted into the plant model (5.7) to yield

$$\dot{s}(t) = \dot{x}_e(t) + \dot{z}(t) \tag{5.111}$$

$$\dot{s}(t) = -ax(t) - d(x,t) + b\big(u(t) - w(t)\big) - bM \operatorname{sgn} S(t) \tag{5.112}$$

If the actuator output is fully measurable then (5.110) may be rewritten

$$\dot{z}(t) = -\dot{x}_d(t) + bw(t) - bM \operatorname{sgn} S(t) \tag{5.113}$$

Since the actuator time constant is assumed small, sliding mode will exist if M is sufficiently large. The state trajectory will converge to zero after a finite time. If the initial conditions are chosen such that the auxiliary variable $z(0)=-x_e(0)$ then the reaching phase may be completely eliminated by setting $S(0)=0$ in (5.109). Once in sliding mode, equivalent control may be employed in order to analyse the system behaviour. Solving (5.112) with $\dot{S}=0$ and $w(t)=u(t)$ for the discontinuity term yields the continuous equivalent control

$$u_{deq}(t) = \frac{1}{b}\big(-ax(t) - d(x,t)\big) \tag{5.114}$$

$$u_{deq}(t) = \frac{f(x,t)}{b} \tag{5.115}$$

This gives an exact estimate of the disturbance acting on the system under continuous control alone. The second term in (5.106) may then be defined as

$$u_d(t) = u_{deq}(t) \tag{5.116}$$

Now (5.108) may be replaced, so that exact tracking may be achieved with error dynamics given by

$$\dot{x}_e(t) + Cx_e(t) = 0 \tag{5.117}$$

5.5 Discussion

This Chapter has served to introduce fundamental concepts associated with sliding mode control. The motor controller developed around traditional techniques has been applied in simulation and its time domain response shown to correspond well with an equivalent proportional, integral, derivative controller. The important invariance conditions of the controller have been discussed. The control effort of the ideal sliding mode controller is understood to be smooth, however, it is well recognised that the ideal controller cannot be realised and that control chatter is introduced to the system. This phenomena is highly undesirable within a practical system and therefore smoothing techniques have been investigated to achieve smooth control action. Results obtained show how these techniques may be employed at the expense of some other controller property. In the following Chapter, the controllers developed will serve to provide the foundation for more advanced controllers. The design based around the classical approach will serve to form the basis of an integral action controller which takes special advantage of the Bush canonical form. The controller based on the unit vector approach will form the basis of the fuzzy model based controller.

5.6 Notes and References

5.6.1 Notes

The first Markov Parameter, or simply Markov Parameter is given as the matrix product CB. Since this parameter is invariant to the change in state space, this parameter is simply a measure of the system input-output characteristics.

5.6.2 References

Chern T.-L. and Wong J.-S., 1995. 'DSP Based Integral Variable Structure Control for DC Motor Servo Drivers'. IEE Proceedings Part D. **142**(5). 444-451.

Drazenovic B. 1969 "The Invariance Conditions in Variable Structure Systems", Automatica. 5. 287-295.

Edwards C and Spurgeon S.K., 1998. "Sliding Mode Control: Theory and Applications", Taylor Francis.

Filippov A.F., 1988, 'Differential Equations with Discontinuous Right Hand Side', Kluwer Academic Press

Habibi S.R. and Richards R.J. 1992. ' Sliding Mode Control of an Electrically Powered Industrial Robot'. IEE Proceedings Part D. **139**(2). 207-225.

Hung J.Y, Weibing G and Hung J.C. 1993. 'Variable Structure Control: A Survey', IEEE Transactions on Industrial Electronics, **40**(1), 2-21

Itkis U., 1976. 'Control Systems of Variable Structure', John Wiley.

Porat. B. 1997. 'A course in digital signal processing', John Wiley.

Ryan E.P. and Corless M. 1984. 'Ultimate boundedness and asymptotic stability of a class of uncertain dynamical systems via continuous and discontinuous control', IMA journal of mathematical control and information, **1**, 223-242

Slotine J.-J and Li W., 1991. 'Applied Nonlinear Control'. Prentice Hall.

Spurgeon S.K. 1991. 'Choice of Discontinuous Control Components for Robust Sliding Mode Performance', International Journal of Control. **53**. 163-179.

Utkin V.I., 1977. 'Variable Structure Systems with Sliding Modes', IEEE Transactions on Automatic Control. **AC-22**(2), 212-222

Utkin V.I. 1992. 'Sliding Modes in Control Optimisation', Springer Verlag.

Utkin V.I. 1993. 'Sliding Mode Control Design Principles and Applications to Electric Drives', IEEE Industrial Electronics, **40**(1), 23-36

Utkin V.I., Guldner J. and Shi J. 1999. 'Sliding Mode Control in Electromechanical systems', Taylor Francis.

Utkin V.I. and Shi, J. 1996. 'Integral Sliding Mode in Systems Operating under Uncertainty Conditions', Proc. 35th IEEE Conference on Decision and Control. Kobe, Japan. 4591-4596.

Young K.D. and Ozugner U. 1999. 'Variable Structure Systems, Sliding Mode and Nonlinear Control', Springer Verlag.

Young K.D., Utkin V.I. and Ozugner U. 1999. 'A control Engineer's Guide to Sliding Mode Control', IEEE Trans. Control Systems Technology. 7(3). 328-342

Zinober A.S.I. 1994. "Variable Structure and Lyapunov Control". Springer Verlag

Chapter 6

Sliding Mode Control: Advanced Approaches

6.1 Introduction

The previous Chapter served to introduce concepts which form the basis for the remainder of the work reported here. In the course of studying further methods for achieving the sliding mode, two original controllers have been evolved. This Chapter, therefore, aims to achieve two objectives. Firstly, an exposition of the new controllers, which are both based on the concept of introducing an integral action into the control channel, is given, this additional integral action has the effect of increasing system robustness to unmatched disturbances, and reduces steady state error to zero. The first of the two controllers provides a design approach for a standard sliding mode controller in the Bush canonical form and introduces an integral action into the control very simply. The second of the controllers demonstrates improved control performance over previous integral action sliding mode controllers through the introduction of recent theory from the field of computational intelligence.

The second objective of this Chapter is to introduce the remaining concepts, which build on Chapter 5, and will be used later in the development of a sensorless control system, in Chapter 7. Specifically, robust state observers and model following sliding mode control are considered.

6.2 Integral Action Sliding Mode Controllers

The boundary layer has the unique property among chatter reduction techniques of maintaining a guarantee of invariance to parametric uncertainty beyond a certain vicinity of the sliding manifold and robustness within the same vicinity. This leads to a controller with two modalities, and it was first recognised by Ryan and Corless (1984) that the additional freedom afforded by the boundary layer at the manifold could be used to improve the controller robustness to the inclusion of so called unmatched disturbance, i.e. those disturbances which do not act through the system control channels. The Ryan and Corless controller was theoretically elegant, however conservative. Davies and Spurgeon (1993), subsequently made the controller less conservative by considering only a subset of the disturbances considered by Ryan and Corless. The practical applicability of the controller was reported in Davies, Edwards and Spurgeon (1994).

The fundamental extension of these controllers to the traditional sliding mode controllers discussed within the last Chapter is to provide an additional integral action, which seeks to reduce asymptotically steady state error to zero as time tends to infinity. Three extensions to this work are proposed within this Chapter. The first uses the same principle and the properties of the Bush canonical form to provide a controller that radically simplifies the design of an integral action sliding mode controller. The second controller uses the theory as discussed by Spurgeon and Davies (1993) and the observation that controller performance is fundamentally limited by the plant uncertainty. It seems odd that one would argue that the sliding mode, with its guarantees of invariance to parametric uncertainty, is limited in its performance by the said uncertainty. It is indeed the case that transient response is not improved significantly by the use of this

approach, however, the reader will be familiar with the process of selecting the nonlinear gain from the Chapter 5. The magnitude of the nonlinear gain is determined directly from the magnitude of the uncertainty. It follows that reducing plant uncertainty leads to a safe reduction in nonlinear control gain, therefore the boundary layer may be reduced in magnitude and the high initial control response of the controller may also be reduced. Reduction in the boundary layer also leads to an increase in the guaranteed asymptotic tracking accuracy of the controller. The final controller recognises the relative complication of the previous controllers and an approach to reducing this burden is discussed. This final controller succeeds in reducing the computational burden by adopting the same approach as the design of the sliding mode observer; first a proportional-integral controller is developed in compatible coordinates and then a discontinuous control is introduced in order to negate the effects of parametric uncertainty.

The final controller discussed within this section are based on the concept of model following, a model with desired eigenvalues is provided and the uncertain system is constrained to perform in the same manner. This final controller will be of use in Chapter 7, in part as the solution to sensorless precision motion control.

6.2.1 A Canonical Form Integral Action Sliding Mode Controller

The principle motivation for introducing a boundary layer is to negate the effects of control chatter, as discussed in the previous Chapter. The compromise to be made is that the controller is no longer capable of guaranteeing zero steady state error. As described above, it becomes attractive to introduce a feed forward integral action state that will reduce the error to zero asymptotically as time tends to infinity. This section concentrates

on the method for introducing a feed forward integral action state that will be computationally simple to implement. This is achieved through the use of the Bush canonical form and similar arguments from §5.2.4.

Motor Model

As within the last Chapter, the nominal motor parameters are taken as those shown in Table 6.1

Parameters			
Symbol	Min.	Max.	Units
J	0.010687	0.019960	Nms^2
F	7e-3	10.5e-3	Nm/rad/s
T_l	1e-2	50e-2	Nm
L	0.0026	0.0026	H
R_s	0.64	0.64	Ω
K_t	0.54	0.54	$Nm\ A^{-1}$

Table 6.1 : *Motor Parameters*

The objective of the controller will be to control the precise angle of the motor stator. The controller is error actuated and the traditional states are therefore introduced:

$$x_2 = \theta_m - \theta_d \tag{6.1}$$

$$x_3 = \dot{x}_2 = -\omega_m \tag{6.2}$$

$$x_4 = \dot{x}_3 = -\dot{\omega}_m \tag{6.3}$$

where θ_m and θ_d represent actual angular position and desired angular position, respectively. ω_m represents angular velocity of the motor stator. Because the controller does not constrain the system to remain on the sliding manifold, final tracking accuracy of the motor will not be guaranteed. It is therefore attractive to introduce a fourth state, which will be the integral of x_2 over time, i.e. the integral of position error.

$$x_1 = \int_0^t (\theta_m - \theta_d)\, dt \tag{6.4}$$

The motor dynamics may be represented in the controllable canonical form according to

$$\begin{bmatrix} \dot{x}_1(t) \\ \dot{x}_2(t) \\ \dot{x}_3(t) \\ \dot{x}_4(t) \end{bmatrix} = \begin{bmatrix} 0 & 1 & 0 & 0 \\ 0 & 0 & 1 & 0 \\ 0 & 0 & 0 & 1 \\ 0 & 0 & -\dfrac{BR + K_m K_e}{JL_s} & -\dfrac{BL + R_a J}{JL} \end{bmatrix} \begin{bmatrix} x_1(t) \\ x_2(t) \\ x_3(t) \\ x_4(t) \end{bmatrix} + \begin{bmatrix} 0 \\ 0 \\ 0 \\ \dfrac{K_m}{JL_s} \end{bmatrix} u(t) \tag{6.5}$$

The system is now available for the development of the control scheme.

Controller Design

An integral error state has been introduced into the system model. It is not an unreasonable assumption that an accurate measure of this integral could be obtained in practical application. Attention is now drawn to the design of a controller that is able to fully employ this additional state to bring tracking error asymptotically to zero.

Begin by defining a manifold *S(x)* according to

$$S(x) = C_1 x_2 + C_2 x_3 + x_4 \tag{6.6}$$

where C_1 and C_2 are design parameters to be found. Also define the control action to be.

$$V(t) = \left[-e x_1 - a_1 x_2 - a_2 x_3 - d\,\mathrm{sgn}(S) \right] B \tag{6.7}$$

where e, a_1, a_2 and d are design parameters which effect the local components of the control action and B is a control gain which will have a global effect. The well known condition for the existence of the sliding mode (Utkin, 1977) may legitimately be used within the controller design and is given by

$$S\dot{S} < 0 \tag{6.8}$$

from (6.5),(6.6) and (6.7),

$$S\dot{S} = \left\{C_2 - \left(\frac{BL+RJ}{JL}\right)\right\}S^2 + \left\{C_1 - C_2^2 + C_2\left(\frac{BL+RJ}{JL}\right) - \frac{BR+K_mK_e}{JL} - \frac{K_m}{JL}a_2 b\right\}x_3 S + \left\{C_1\left(\frac{BL+RJ}{JL}\right) - C_1C_2 - \frac{K_m}{JL}a_2 b\right\}x_2 S + \left\{\frac{K_m}{JL_s}eb\right\}x_1 - db\frac{K_m}{JL_s}|S| \tag{6.9}$$

Once the system state is close to the sliding surface, (6.9) simplifies to

$$S\dot{S}\Big|_{s\approx 0} = \left\{C_1 - C_2^2 + C_2\left(\frac{BL+RJ}{JL}\right) - \frac{BR+K_mK_e}{JL} - \frac{K_m}{JL}a_2 b\right\}x_3 S + \left\{C_1\left(\frac{BL+RJ}{JL}\right) - C_1C_2 - \frac{K_m}{JL}a_2 b\right\}x_2 S + \left\{\frac{K_m}{JL_s}eb\right\}x_1 - db\frac{K_m}{JL_s}|S| \tag{6.10}$$

Thus in order for (6.8) to hold, the following inequalities must be satisfied.

$$a_1 = \begin{cases} \alpha_1 & \text{if} \quad x_2 S > 0 \\ \beta_1 & \text{if} \quad x_2 S < 0 \end{cases} \tag{6.11}$$

$$a_2 = \begin{cases} \alpha_2 & \text{if} \quad x_3 S > 0 \\ \beta_2 & \text{if} \quad x_3 S < 0 \end{cases} \tag{6.12}$$

which reduces to

$$\beta_1 < \gamma_1 < \alpha_1 \tag{6.13}$$

$$\beta_2 < \gamma_2 < \alpha_2 \tag{6.14}$$

where

$$\gamma_1 = \left[\frac{JLC_1}{bK_m}\left(\frac{BL+RJ}{JL} - C_2\right)\right] \tag{6.15}$$

$$\gamma_2 = \left[\frac{JL}{bK_m}\left(C_1 - C_2^2\right) + C_2\frac{BL+RJ}{K_m} - BR + K_e\right] \tag{6.16}$$

additionally,

$$d > \frac{JL}{bK_m} \tag{6.17}$$

$$e > \frac{JL}{bK_m} \tag{6.18}$$

Once in the sliding mode, *S(x)* defines completely the system dynamic performance, in the absence of unmatched disturbance (Spurgeon, 1991). The eigenvalues of S are given as

$$\lambda_1 = -\frac{C_2}{2} + \frac{1}{2}\sqrt{\left(C_2^2 - 4C_1\right)} \tag{6.19}$$

$$\lambda_1 = -\frac{C_2}{2} - \frac{1}{2}\sqrt{\left(C_2^2 - 4C_1\right)} \tag{6.20}$$

To obtain a damping ratio of 1 or greater the inequality

$$C_2^2 \geq 4C_1 \tag{6.21}$$

must hold, the equality defines the gains for critical damping. In order to ensure that the system is made attractive to the sliding surface, given the inequalities (6.13)-(6.18) and equation (6.9) it is clear that if

$$C_2 < \frac{BL + RJ}{JL} \tag{6.22}$$

then the system will be globally attracted to the sliding manifold. The controller parameters may be formally expressed as

$$\alpha_1 > \frac{1}{b}\max\left(\frac{JLC_1}{K_m}\left(\frac{BL + RJ}{JL} - C_2\right)\right) \tag{6.23}$$

$$\beta_1 < \frac{1}{b}\min\left(\frac{JLC_1}{K_m}\left(\frac{BL + RJ}{JL} - C_2\right)\right) \tag{6.24}$$

$$\alpha_2 > \frac{1}{b}\max\left(\frac{JL}{K_m}\left(C_1 - C_2^2\right) + C_2\frac{BL + RJ}{K_m} - BR + K_e\right) \tag{6.25}$$

$$\beta_2 < \frac{1}{b}\min\left(\frac{JL}{K_m}\left(C_1 - C_2^2\right) + C_2\frac{BL+RJ}{K_m} - BR + K_e\right) \tag{6.26}$$

$$d > \frac{1}{b}\max\left(\frac{JL}{K_m}\right) \tag{6.27}$$

$$e > \frac{1}{b}\max\left(\frac{JL}{K_m}\right) \tag{6.28}$$

$$C_2 < \min\left(\frac{BL+RJ}{JL}\right) \tag{6.29}$$

$$C_1 = \frac{C_2^2}{4} \tag{6.30}$$

Finally, the discontinuous switching function of the control is replaced by a boundary layer. The above derivations are still valid (Utkin *et al*, 1999). Once the motor parameters are inserted into the inequalities (6.23)-(6.30), the following equalities are obtained with the controller gains selected as shown. Most of the controller gains selected show close agreement with the respective minimum or maximum values. The only gain which does not is the dither component *d*. This of course may be chosen to be much smaller with no cost to performance as long as it remains larger than the matched uncertainty component.

$$b\alpha_1 > 17.78 = 20 \tag{6.31}$$

$$b\beta_1 < 8.76 = 5 \tag{6.32}$$

$$b\alpha_2 > 1.46 = 4 \tag{6.33}$$

$$b\beta_2 < 1.23 = 1.1 \tag{6.34}$$

$$bd > 0.58e - 3 = 5 \tag{6.35}$$

$$be > 0.58e - 3 = 0.2 \tag{6.36}$$

$$C_2 = 88 \tag{6.37}$$

$$C_1 = 1936 \tag{6.38}$$

The controller is compared with a sliding mode controller without the integral action, from §5.2.4.

The first test is to demonstrate that the proposed controller can perform equally as well as a typical sliding mode controller in the absence of unmatched disturbance. Figures 6.1 and 6.2 illustrate how the controller can perform well under such conditions; in this case the integral gain is given as 0.2.

In the next test, it is assumed that an additive error is imposed on the speed state of the state output matrix, the two controllers are re-tested under these conditions. The set-point is now reduced in order to make clear the evolution of the position state. Figure 6.3 illustrates the results. It may clearly be seen that the traditional sliding mode controller maintains a steady state error, whereas the proposed controller does indeed reduce the error to zero.

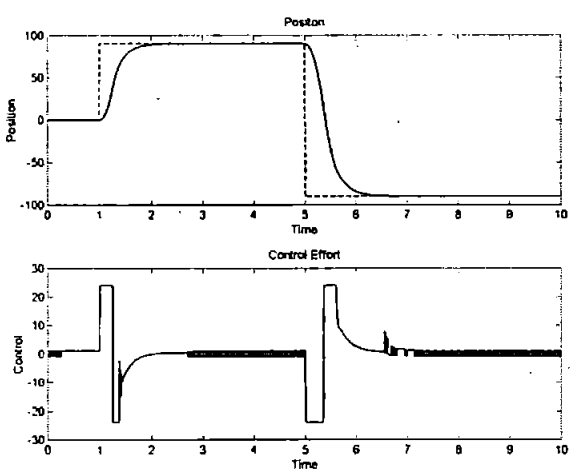

Figure 6.1: *Sliding Mode Controller, Illustrating Control Chatter.*

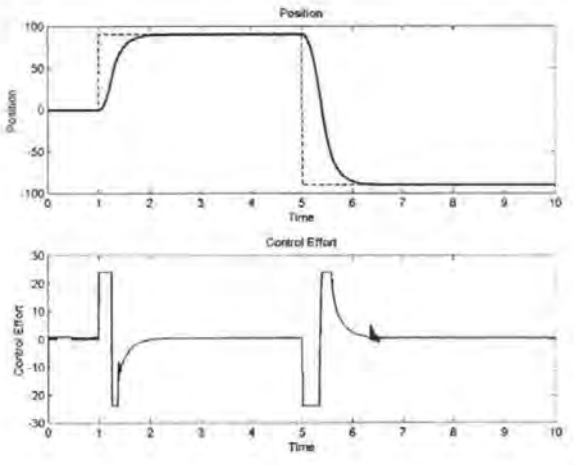

Figure 6.2: *Proposed Controller Performing without Chatter*

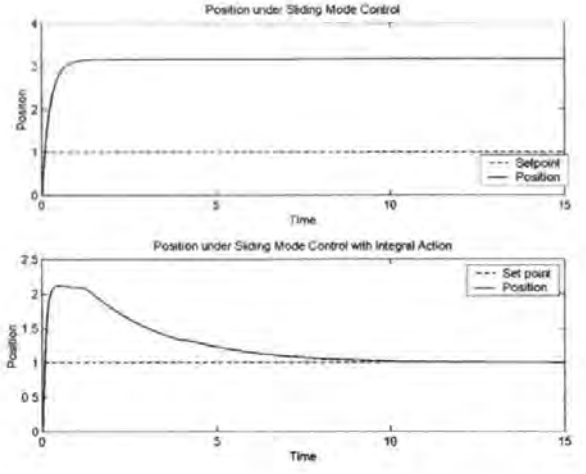

Figure 6.3: *Evolution of Controlled State Under Control by Sliding Mode and Proposed Controller*

6.2.2 Fuzzy Model Based Sliding Mode Control

One drawback in the implementation of sliding mode control is that the guarantees of invariance in general only apply to systems that satisfy the matching condition (Yao, 1993). Disturbance which does not fulfill this condition, i.e. unmatched disturbance is not formally considered within the controller design. A more profound limitation in

practical application is the fundamental requirement that the control law is discontinuous across the sliding manifold, this leads to a phenomenon termed 'control chatter'. It has been seen that a common approach to the negation of chatter is to use the boundary layer approach, in so doing, a compromise must be sought between desired tracking accuracy and controller bandwidth.

Model errors due to parametric uncertainty lead to tracking error in controllers with a continuous approximation to the switching function, within the controller design, the controller feedback gains are increased to reduce these errors. This leads to high gain feedback control and despite the fact that these controllers can in theory use infinite feedback gain to achieve asymptotic tracking, such controllers are physically impractical because of the finite bandwidths associated with real systems.

In Palm (1994) the apparent similarities between the sliding mode and fuzzy controllers were illustrated, which has subsequently motivated considerable research effort in combining the two topologies in a manner that serves to reduce the limitation of the sliding mode. The most common approach to this has been to replace the continuous switching function of the boundary layer with an equivalent fuzzy switching function. However, as pointed out in O'Dell (1997), the fuzzy rule base commonly serves as a mimic of the original switching function and the advantages of such an approach are therefore unclear. Others have used a fuzzy rule base in making the sliding manifold adaptive, e.g. Ha *et al.* (1999), so as to minimise the reaching phase, good results have been reported. Babuška (1998) has demonstrated the ability of the affine Takagi-Sugeno model to model accurately a system through rule extraction from cluster data obtained within the regression space. These models may be used subsequently in order to extract

locally linear state space models of the system and demonstrate model based control of both single input, single output (SISO) and multi input, multi output (MIMO) systems (Roubos *et al.*, 1999).

In this work, a system subjected to parametric uncertainty and disturbance is identified with a fuzzy rule base, the parameters of which are identified through use of the Gustaffson-Kessel subspace clustering algorithm (Chapter 4). Local models of the system under its instantaneous conditions are then extracted and subsequently used to design the sliding mode control gains. In this manner, the resultant controller will be shown qualitatively to improve closed loop transient performance whilst reducing the high gain feedback requirement, as a result of minimising system uncertainty.

Within the following simulation study a third order model of a servomotor is used, the differential equations of which are given according to

$$L\frac{dI_a}{dt} = -I_a R_a - K_e\omega + V_a \tag{6.39}$$

$$J\frac{d\omega}{dt} = -B\omega - T_X + I_a.K_m \tag{6.40}$$

Where L is the motor inductance, I_a the armature current, K_e the back E.M.F constant, ω the angular velocity of the armature, J the moment of inertia, B viscous friction, T_x the external load torque, K_m the motor torque constant and V_a the armature voltage. In addition θ is introduced as the armature angular position. These equations may be rewritten in state space form according to the following,

$$X_1 = \theta, X_2 = \frac{d\theta}{dt} = \omega, X_3 = i \text{ and let } T_X = U_1 \text{ and } V_a = U_2$$

$$\begin{bmatrix} \dot{X}_1 \\ \dot{X}_2 \\ \dot{X}_3 \end{bmatrix} = \begin{bmatrix} 0 & 1 & 0 \\ 0 & -\frac{B}{J} & \frac{K_m}{J} \\ 0 & -\frac{K_e}{L} & -\frac{R_a}{L} \end{bmatrix} \begin{bmatrix} X_1 \\ X_2 \\ X_3 \end{bmatrix} + \begin{bmatrix} 0 \\ -\frac{U_1}{J} \\ \frac{U_2}{L} \end{bmatrix} \qquad Y_1 = \begin{bmatrix} 1 & 0 & 0 \end{bmatrix} \begin{bmatrix} X_1 \\ X_2 \\ X_3 \end{bmatrix} \tag{6.41}$$

The model parameters are taken as shown in Table 6.2:

Parameter	Value (Nominal)	Value (Actual)
R_a	0.64	0.64
L	0.0026	0.0026
K_e	0.54	0.54
K_m	0.54	0.54
J	0.01	0.02
B	7e-3	10.5e-3

Table 6.2: *Motor Parameters*

Next within this work, the mechanism for fuzzy identification of this model is considered. After which, consideration to the sliding mode controller design is given.

Within this work the design approach Spurgeon and Davies (1993) is adopted in order to ensure zero steady state controller error. However, it is also recognised that if the system uncertainty can be reduced, then controller performance may be correspondingly improved. Once local models of the system have been extracted, they may be used in order to provide enhanced information to the sliding mode controller. The principles associated with the design of a sliding mode controller with integral action are considered next.

Integral Action Sliding Mode Controller

As alluded to in the introduction, the ideal sliding motion is control independent and defined only by the choice of sliding surface provided that certain assumptions about the system disturbance hold (Drazenovic, 1969). In terms of controller design it is convenient to convert the system equations into a suitable canonical form. In this form the system is decomposed into two connected subsystems, one acting in within the range space of matrix B and the other within the null space of the manifold *S*. In terms of design, the problem then becomes one of state feedback given desired system eigenvalue locations. Since by assumption the matrix B is of full rank, there exists an orthogonal matrix $T_r \in \mathbb{R}^{n\times n}$ such that

$$T_r B = \begin{bmatrix} 0 \\ B_2 \end{bmatrix} \tag{6.42}$$

where $B_2 \in \mathbb{R}^{m\times m}$ and is non-singular. Let $z = Tx$ and partition the new co-ordinates so that

$$z = \begin{bmatrix} z_1 \\ z_2 \end{bmatrix} \tag{6.43}$$

where $z_1 \in \mathbb{R}^{n-m}$ and $z_2 \in \mathbb{R}^m$. The nominal linear system can then be written as

$$\dot{z}_1(t) = A_{11}z_1(t) + A_{12}z_2(t) \tag{6.44}$$

$$\dot{z}_2(t) = A_{21}z_1(t) + A_{22}z_2(t) + B_2u(t) \tag{6.45}$$

commonly known as the regular form. Equation (6.44) is referred to as describing the null-space dynamics and equation (6.45) as describing the range-space dynamics. From the perspective of the extracted local models, it is convenient to first convert the matrices to the controllability canonical form, thus the system is guaranteed to be in the regular

form for subsequent design. Suppose the matrix defining the switching function (in the new co-ordinate system) is compatibly partitioned with z as

$$ST_r^T = [S_1 \quad S_2] \tag{6.46}$$

where $S_1 \in \mathbb{R}^{m\times(n\times m)}$ and $S_2 \in \mathbb{R}^{m\times m}$. Since $SB = S_2B_2$ it follows that a necessary and sufficient condition for the matrix SB to be non-singular is that the determinant of S_2 is non zero. It is reasonable to assume that this condition will be met by design. During an ideal sliding motion

$$S_1 z_1(t) + S_2 z_2(t) = 0 \qquad \text{for all } t > t_s \tag{6.47}$$

and therefore formally expressing $z_2(t)$ in terms of $z_1(t)$ yields

$$z_2(t) = -Mz_1(t) \tag{6.48}$$

where $M = S_2^{-1}S_1$. Substituting into (6.44) gives

$$\dot{z}_1(t) = (A_{11} - A_{12}M)z_1(t) \tag{6.49}$$

$z_2(t)$ is considered to play the role of the control action. The switching surface design problem can therefore be considered to be one of choosing a state feedback matrix M to stabilise the reduced order system (A_{11}, A_{12}). At this point the unit vector approach is introduced. Consider an uncertain system of the form

$$\dot{x}(t) = Ax(t) + Bu(t) + f(t,x,u) \tag{6.50}$$

where the function $f : \mathbb{R}\times\mathbb{R}^n\times\mathbb{R}^m \to \mathbb{R}^m$ which represents the uncertainties or non-linearities satisfying the so-called matching condition, i.e.

$$f(t,x,u) = B\xi(t,x,u) \tag{6.51}$$

where ξ is unknown but satisfies the following inequality

$$\|\xi(t,x,u)\| \le k_1 \|u\| + \alpha(t,x) \tag{6.52}$$

where $1 > k_l \ge 0$ is a known constant and $\alpha(\bullet)$ is a known function. The proposed control law comprises two components; a linear component to stabilise the nominal linear system; and a discontinuous component. Specifically

$$u(t) = u_l(t) + u_n(t) \tag{6.53}$$

where the linear component is given by

$$u_l(t) = -\Lambda^{-1}(SA - \Phi S)x(t) \tag{6.54}$$

where Φ is any stable design matrix and $\Lambda = SB$. The non-linear component is defined as

$$u_n(t) = -\rho(t,x)\Lambda^{-1}\frac{P_2 s(t)}{\|P_2 s(t)\| + \varepsilon} \quad \text{for all s}\neq 0 \tag{6.55}$$

where P_2 is a symmetric positive definite matrix that satisfies the Lyapunov equation

$$P_2\Phi + \Phi^T P_2 = -I \tag{6.56}$$

and the scalar function $\rho(t,x)$, which depends only on the magnitude of the uncertainty, is any function satisfying

$$\rho(t,x) \ge \frac{(k_1\|u_l\| + \alpha(t,x) + \gamma)}{(1 - k_1\kappa(\Lambda))} \tag{6.57}$$

where $\gamma > 0$ is a design parameter. ε is the radius of the boundary layer may be shown to be dependent on the actuator time constant and inversely proportional to the available control resources. In this equation it is assumed that the scaling parameter has been

chosen so that $k_1\kappa(\Lambda)<1$. It can be established that any function satisfying equation (6.57) also satisfies

$$\rho(t,x)\geq\|\xi(t,x,u)\|+\gamma \tag{6.58}$$

and therefore $\rho(t,x)$ is greater in magnitude than the matched uncertainty occurring in this equation. It can be verified that $V(S)=S^TP_2S$ guarantees quadratic stability for the switching states and in particular

$$\dot{V}\leq -s^Ts-2\gamma\|P_2s\| \tag{6.59}$$

This control law guarantees that the switching surface is reached in finite time despite the disturbance or uncertainty and once the sliding motion is attained it is completely independent of the uncertainty.

Now consider the introduction of additional states $x_r\in\mathbb{R}^p$ satisfying

$$\dot{x}_r=r(t)-y(t) \tag{6.60}$$

where the differentiable signal $r(t)$ satisfies

$$\dot{r}(t)=\Gamma(r(t)-R) \tag{6.61}$$

with Γ a stable design matrix and R a constant demand vector. Augment the states with the integral action states and define

$$\tilde{x}=\begin{bmatrix}x_r\\x\end{bmatrix} \tag{6.62}$$

The associated system and input distribution matrices for the augmented system are

$$\tilde{A}=\begin{bmatrix}0 & -C\\0 & A\end{bmatrix}\text{ and }\tilde{B}=\begin{bmatrix}0\\B\end{bmatrix} \tag{6.63}$$

assuming the pair (A, B) is in regular form, the pair $(\tilde{A}, \tilde{B})$ is also in regular form. The proposed controller seeks to induce a sliding motion on the surface

$$S = \left\{ \tilde{x} \in \mathbb{R}^{n+p} : S\tilde{x} = S_r r \right\} \tag{6.64}$$

where S and S_r are design parameters, which govern the reduced order motion. The hyperplane system matrix and system matrix are partitioned as

$$S = \begin{bmatrix} \overset{n}{\longleftrightarrow} & \overset{m}{\longleftrightarrow} \\ S_1 & S_2 \end{bmatrix} \tag{6.65}$$

$$\tilde{A} = \begin{bmatrix} \overset{n}{\longleftrightarrow} & \overset{m}{\longleftrightarrow} \\ \tilde{A}_{11} & \tilde{A}_{12} \\ \tilde{A}_{21} & \tilde{A}_{22} \end{bmatrix} \begin{matrix} \updownarrow n \\ \updownarrow m \end{matrix} \tag{6.66}$$

and assume $\Lambda = S\tilde{B}$ is non-singular. If a controller exists which induces an ideal sliding motion on S and the augmented states are suitably partitioned, then the ideal sliding motion is given by

$$\dot{x}_1(t) = \left(\tilde{A}_{11} - \tilde{A}_{12}M\right)x_1(t) + \left(\tilde{A}_{12}S_2^{-1}S_r + B_r\right)r(t) \tag{6.67}$$

where $M = S_2^{-1}S_1$ and $B_r = \begin{bmatrix} I^p & 0^{m\times p} \end{bmatrix}^T$. In order for the hyperplane design method to be valid, it is necessary for the matrix pair $\left(\tilde{A}_{11}, \tilde{A}_{12}\right)$ to be completely controllable.

As per the development of the unit vector controller in the previous Chapter, a linear change of coordinates is introduced according to

$$T = \begin{bmatrix} I_n & 0 \\ S_1 & S_2 \end{bmatrix} \tag{6.68}$$

and let

$$\begin{bmatrix} x_1 \\ S \end{bmatrix} \triangleq T \begin{bmatrix} x_1 \\ x_2 \end{bmatrix} \tag{6.69}$$

Then the nominal system may be rewritten in these coordinates as

$$\dot{x}_1 = A_{11}x_1(t) + A_{12}S(t) + B_r r(t) \tag{6.70}$$

$$\dot{S}(t) = S_2 A_{21}x_1(t) + S_2 A_{22}S_2^{-1}S(t) + \Lambda u(t) + S_1 B_r r(t) \tag{6.71}$$

The overall control law is then given by

$$u = u_l(\tilde{x}, r) + u_n(\tilde{x}, r) \tag{6.72}$$

where the discontinuous vector u_n is given by

$$u_n(s, r) = \begin{cases} -\rho_c(u_L, y)\Lambda^{-1} & \text{if } S\tilde{x} \neq S_r r \\ 0 & \text{otherwise} \end{cases} \tag{6.73}$$

It follows that, in terms of the original co-ordinates the control vector u_l is given by

$$u_l(x_1, S, r) = \Lambda^{-1}\left\{-S_2 A_{21}x_1 + \left(\Phi - S_2 A_{22}S_2^{-1}\right)S - \left(\Phi S_r + S_1 B_r\right)r + S_r\dot{r}\right\} \tag{6.74}$$

$$u_l(\tilde{x}, r) = L\tilde{x} + L_r r + L_{\dot{r}}\dot{r} \tag{6.75}$$

with gains defined as

$$L = -\Lambda^{-1}\left(S\tilde{A} - \Phi S\right) \tag{6.76}$$

$$L_r = -\Lambda^{-1}\left(\Phi S_r + S_1 B_r\right) \tag{6.77}$$

$$L_{\dot{r}} = \Lambda^{-1} S_r \tag{6.78}$$

The parameter S_r can take any value and does not affect the stability of the closed loop system.

Model Extraction

The work in Roubos *et al* (1999) presents a method whereby the fuzzy clustered model may be represented as a local linear state space model. The following is an overview of the method adopted. The regression vector, which is represented by ε_l is given by

$$\varepsilon_l(k)=\left[\left\{y_p(k)\right\}_0^{n_{y1}},\ldots,\left\{y_p(k)\right\}_0^{n_{yp}},\left\{u_1(k+1)\right\}_{n_{u11}}^{n_{u1t}},\ldots,\left\{u_m(k+1)\right\}_{n_{u1m}}^{n_{utm}}\right] \tag{6.79}$$

An affine Takagi-Sugeno rule may be represented by

$$y_l(k+1)=\frac{\sum_{i=1}^{K_l}\beta_{li}(\varepsilon_l)\left(\zeta_{li}y(k)+\eta_{li}u(k)+\theta_{li}\right)}{\sum_{i=1}^{K_l}\beta_{li}} \tag{6.80}$$

ζ and η are vectors of polynomials in the previous sample ($y(k-1)$), and θ the offset. K_l is the number of rules of the l^{th} offset. The model output is calculated as the degree of fulfillment $\mu_{il}(\varepsilon_{lh})$ for each antecedent variable and the resulting degrees of fulfillment (β_{li}) for every rule are combined with the linear consequence according to the following

$$\beta_{li}(\varepsilon_l)=\prod_{h=1}^{p}\mu_{ih}(\varepsilon_{lh}) \tag{6.81}$$

Once the Takagi-Sugeno model has been derived, local linear state space models can be calculated according to the following,

$$y_l(k+1)=\frac{\sum_{i=1}^{K_l}\mu_{li}\left(x_l(k)\right)\cdot y_{li}(k+1)}{\sum_{i=1}^{K_l}\mu_{li}\left(x_l(k)\right)} \tag{6.82}$$

$$y_{li}(k+1)=\left(\zeta_{li}y(k)+\eta_{li}u(k)+\theta_{li}\right) \tag{6.83}$$

where

$$\zeta_l^{\bullet}=\frac{\sum_{i=1}^{K_l}\mu_{li}\left(x_l(k)\right)\cdot\zeta_{li}}{\sum_{i=1}^{K_l}\mu_{li}\left(x_l(k)\right)} \tag{6.84}$$

$$\eta_l^{\bullet}=\frac{\sum_{i=1}^{K_l}\mu_{li}\left(x_l(k)\right)\cdot\eta_{li}}{\sum_{i=1}^{K_l}\mu_{li}\left(x_l(k)\right)} \tag{6.85}$$

and

$$\theta_l^{\bullet} = \frac{\sum_{i=1}^{K_l} \mu_{li}\left(x_l(k)\right)\cdot\theta_{li}}{\sum_{i=1}^{K_l} \mu_{li}\left(x_l(k)\right)} \tag{6.86}$$

In the case here, previous inputs are not considered and the A, B and C matrices of the model are thus simplified, the matrices are given

$$A = \begin{bmatrix} \zeta_{1,1}^{\bullet} & \zeta_{1,2}^{\bullet} & \cdots & \zeta_{1,\alpha_1}^{\bullet} \\ 1 & 0 & \cdots & 0 \\ \zeta_{2,1}^{\bullet} & \zeta_{2,2}^{\bullet} & \cdots & \zeta_{2,\alpha_1}^{\bullet} \\ 0 & \vdots & \ddots & \vdots \\ \zeta_{n_0,1}^{\bullet} & \zeta_{n_0,2}^{\bullet} & \cdots & \zeta_{n_0,\alpha_1}^{\bullet} \end{bmatrix} \tag{6.87}$$

$$B = \begin{bmatrix} \eta_{1,1}^{\bullet} & \eta_{1,2}^{\bullet} & \cdots & \eta_{1,n_i}^{\bullet} \\ 0 & \cdots & \cdots & 0 \\ \eta_{2,1}^{\bullet} & \eta_{2,2}^{\bullet} & \cdots & \eta_{2,n_i}^{\bullet} \\ \vdots & \vdots & \ddots & \vdots \\ \eta_{n_0,1}^{\bullet} & \eta_{n_0,2}^{\bullet} & \cdots & \eta_{n_0,n_i}^{\bullet} \end{bmatrix} \tag{6.88}$$

$$C = \begin{bmatrix} 1 & 0 & \cdots & 0 \\ \vdots & & \ddots & \vdots \\ 0 & \cdots & \cdots & 1 \end{bmatrix} \tag{6.89}$$

Controller structure and performance

A benchmark sliding mode controller with integral action (SMCI) of the form previously discussed was designed to control the motor model of equation (6.41), using the nominal parameters of Table 6.2. Simulations were carried out using the actual parameters shown in Table 6.2. The principle of the proposed controller is illustrated in Figure 6.4. The controller uses the design approach outlined in the previous section, thus, stabilising conditions of the controller remain intact. Importantly, the extracted model is used to provide enhanced information to the controller, so that the controller may be made to

adapt to local operating conditions of the system. The controller is therefore referred to as a Fuzzy Adaptive Sliding Mode Controller (FASMC).

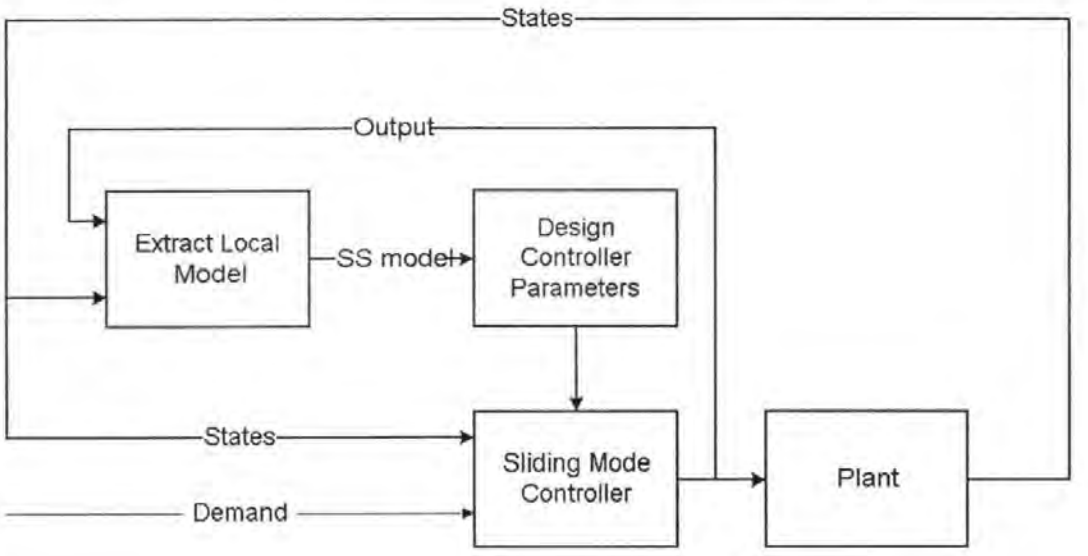

Figure 6.4: *Principle of FASMC*

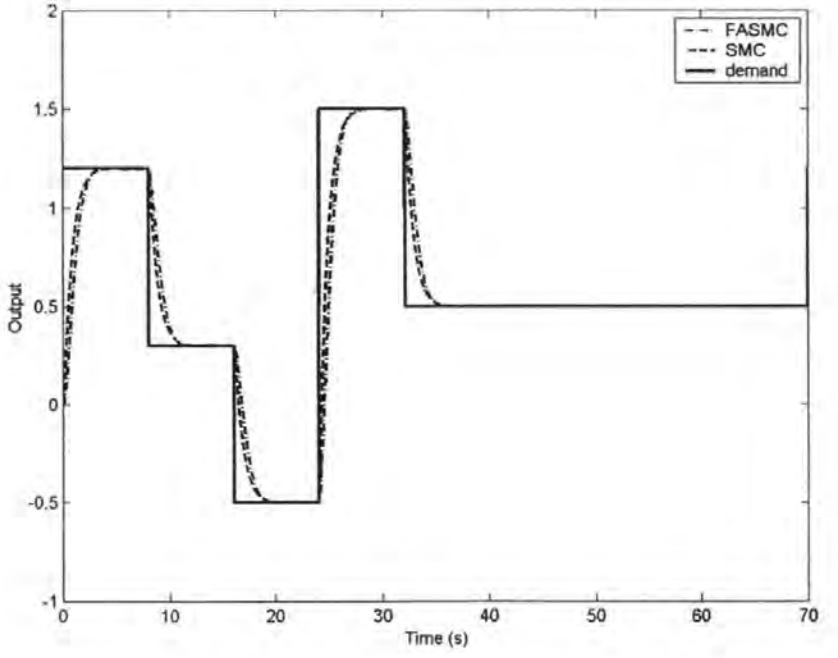

Figure 6.5: *System outputs over 70 seconds*

Both sets of controller eigenvalues were selected to provide unity damping ratio at 22rad/s. The controllers were driven over a simulation sample period of 70 seconds. Results are illustrated in Figure 6.5. It can be seen that in terms of transient response, there is little to differentiate between the two controllers. However, consideration of the corresponding control effort (Figure 6.6) shows that that the high gain requirement of the SMCI has indeed been relaxed by the FASMC. Additionally, the ε-vicinity of the FASMC was manually adjusted to be 6 times smaller than the corresponding SMCI before chatter occurred.

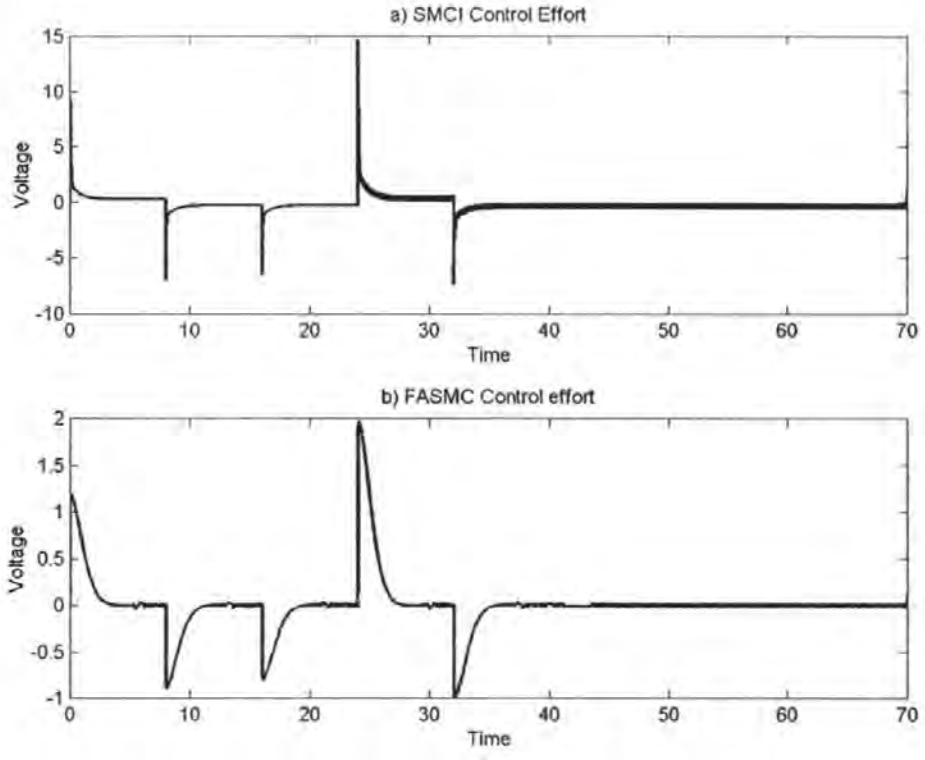

Figure 6.6: *System control efforts*

A second test introduced unmatched disturbance to the system and the fuzzy model retrained to incorporate the uncertainty, the disturbance is analogous to a torque being placed on the motor and forcing rotation in the contrary direction to the demand, which

changes simultaneously with the step increase in load. Figure 6.7 illustrates the effect of the disturbance on the SMCI, it can be seen that the disturbance significantly effects transient performance. Because of the integral action of the SMCI, the system is able to achieve asymptotic tracking as discussed within the literature. The FASMC, on the other hand, recovers the system to the steady state taking only an additional 0.4 seconds when compared to the system without disturbance (Figure 6.8). The obvious error in the initial controlled state trajectory is due to the lack of large controller gain, in the event that the system were subjected to such a stringent test it would be necessary to increase the nonlinear control gain to circumvent this problem.

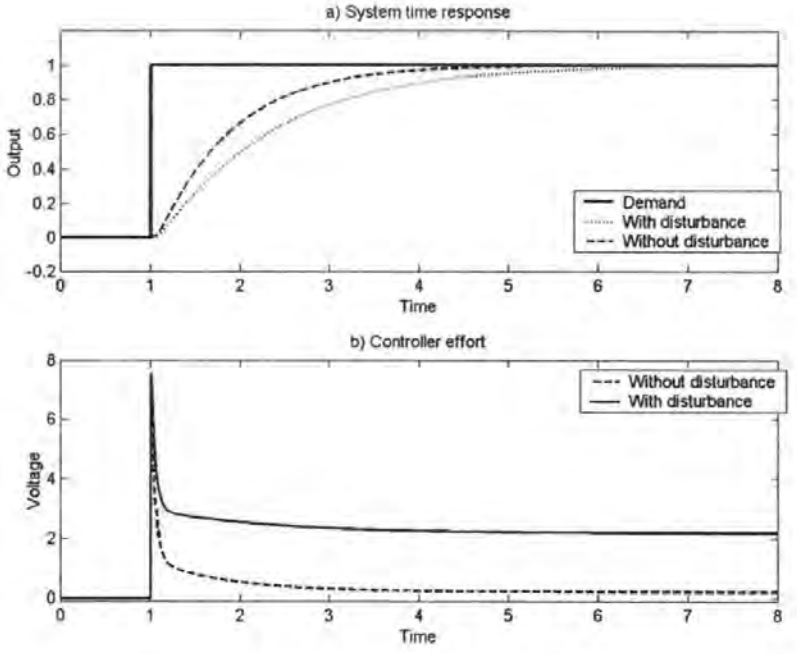

Figure 6.7: *SMCI response to Unmatched Disturbance*

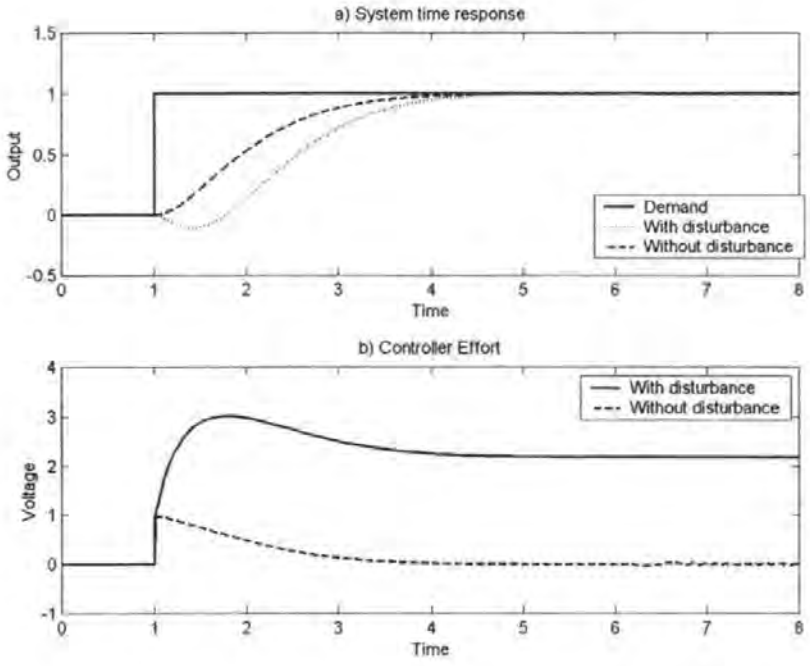

Figure 6.8: *FASMC Response to Unmatched Disturbance*

6.3 Sliding Mode Observers

In the previous sections of this Chapter, the discussion of the control problem was based on the assumption that the system state vector is known. In practice, however, only a few of its components of some of their functions may be measured directly. This gives rise to the *problem of determination or observation* of the state vector through the information available within the measured variables. The field of state estimation has been of interest to researchers since the seminal work of Luenberger (1971), where the observer structure that bears his name (Figure 6.9) was introduced and was shown to be able to recreate the state vector from input-output measurements.

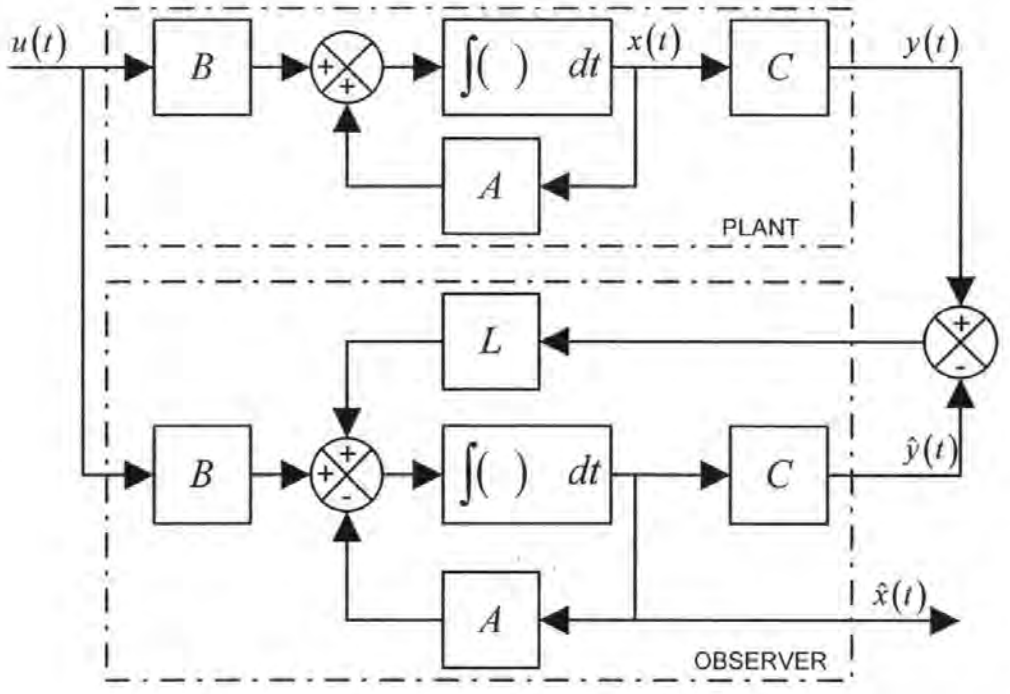

Figure 6.9: *Plant with unobservable states and Luenberger observer*

The Luenberger observer relies on precise knowledge of the plant and it is natural that more recently significant research effort has been dedicated to the development of robust observers, since these have been shown to be convergent in the presence of uncertainty (Misawa and Hedrick, 1989). Walcott and Zak (1987) proposed a variable structure observer which requires the matching condition. Slotine *et al.* (1987) and more recently, Choi *et al.* (1999), have proposed observers that are independent of the matching condition by introducing a Lyapunov design procedure. An early reduced order asymptotic observer was introduced by Utkin (1977) and an observer design based on Utkin's equivalent control method (Utkin, 1992) was developed in Haskara *et al.* (1998). Essentially, a sliding mode observer consists of the standard Luenberger observer to asymptotically reconstruct the original state vector. The deliberate introduction of a

sliding mode into the structure of this observer is then used to guarantee convergence in finite time (Figure 6.10).

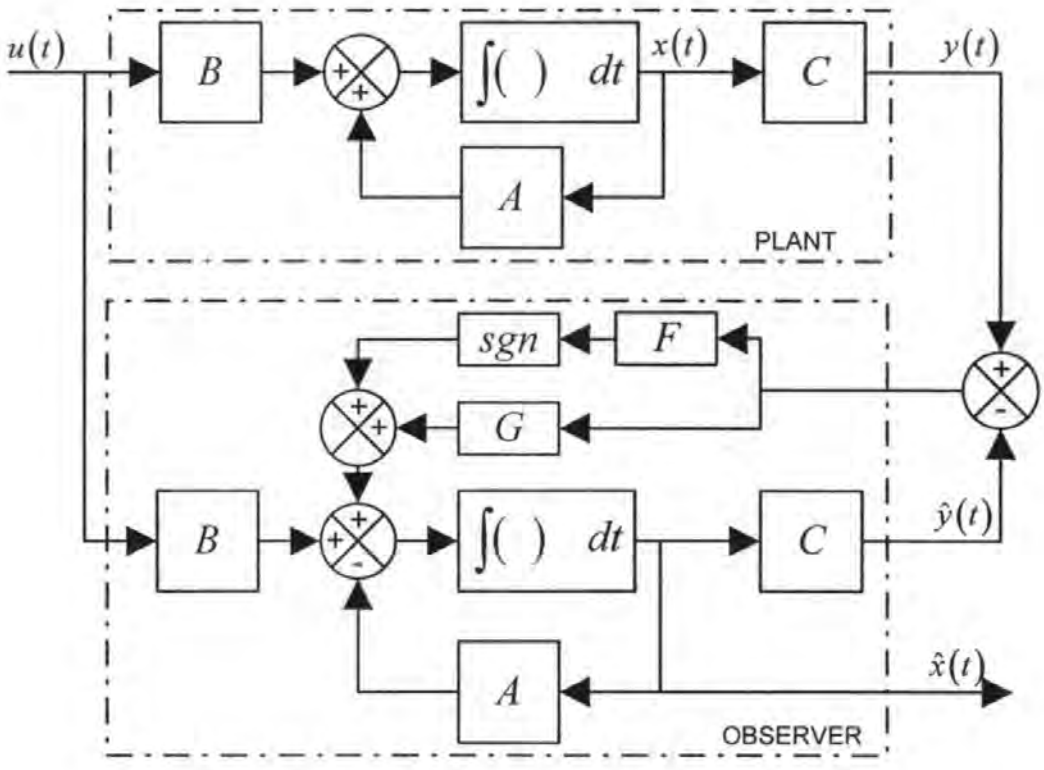

Figure 6.10: *A Sliding Mode Observer with Plant.*

This section is dedicated to the consideration of an observer for the nominal linear system subject to uncertainty described by

$$\dot{x} = Ax(t) + Bu(t) + D\xi(t, y, u) \tag{6.90}$$

$$y(t) = Cx(t) \tag{6.91}$$

where $A \in \mathbb{R}^{n \times n}, B \in \mathbb{R}^{n \times m}, C \in \mathbb{R}^{p \times n}, D \in \mathbb{R}^{n \times q}$ with $q \leq p < n$ and the matrices B,C and D being of full rank. The function $\xi(t, y, u)$ is assumed to be unknown but bounded by a known function. It is further assumed that the states of the system are unknown and only the signals $u(t)$ and $y(t)$ are available.

The objective is to synthesise an observer to generate a state estimate $\hat{x}(t)$ such that the error

$$\varepsilon(t) = \hat{x}(t) - x(t) \tag{6.92}$$

tends to zero despite the presence of uncertainty. Furthermore the intention is to induce a sliding motion on the surface in the error space, according to

$$S_0 = \{\varepsilon \in \mathbb{R}^n : C\varepsilon = 0\} \tag{6.93}$$

The particular observer structure that will be considered may be written in the form

$$\dot{\hat{x}}(t) = A\hat{x}(t) + Bu(t) - G_l C_e(t) + G_n v \tag{6.94}$$

where $G_l, G_n \in \mathbb{R}^{n\times p}$ are appropriate gain matrices and v represents a discontinuous switched component to induce a sliding motion on S_0.

Consider the dynamic system given in (6.90) and (6.91) and assume that

1) rank$(CD) = q$

2) The invariant zeros of (A,D,C) lie in the left half $\mathbb{C}_-$.

It can be shown that under these assumptions there exists a linear change of coordinates $x \to Tx$ such that in the new coordinate system

$$\dot{x}_1(t) = A_{11}x_1(t) + A_{12}x_2(t) + B_1 u(t) \tag{6.95}$$

$$\dot{x}_2(t) = A_{21}x_1(t) + A_{22}x_2(t) + B_2 u(t) + D_2\,\varepsilon(t,y,u) \tag{6.96}$$

$$y(t) = x_2(t) \tag{6.97}$$

where $x_1 \in \mathbb{R}^{n-p}, x_2 \in \mathbb{R}^p$ and the matrix A_{11} has stable eigenvalues. The freedom of choice associated with A_{11} depends on the number of invariant zeros of (A,D,C). The

coordinate system above will be used as a platform for the design of a sliding mode observer. Consider a dynamic system of the form

$$\dot{\hat{x}}_1(t) = A_{11}\hat{x}_1(t) + A_{12}\hat{x}_2(t) + B_1 u(t) - A_{12}\varepsilon_y(t) \tag{6.98}$$

$$\dot{\hat{x}}_2(t) = A_{21}\hat{x}_1(t) + A_{22}\hat{x}_2(t) + B_2 u(t) - \left(A_{22} - A_{22}^s\right)\varepsilon_y(t) + \|D_2\| v \tag{6.99}$$

$$\hat{y}(t) = \hat{x}_2(t) \tag{6.100}$$

where A_{22}^s is a stable design matrix and $\varepsilon_y = \hat{y} - y$. The discontinuous vector v is defined by

$$v = \begin{cases} -\rho(t,y,u)\dfrac{P_2\varepsilon_y}{\|P_2\varepsilon_y\|} & \text{if } \varepsilon_y \neq 0 \\ 0 & \text{otherwise} \end{cases} \tag{6.101}$$

where $P_2 \in \mathbb{R}^{p\times p}$ is a Lyapunov matrix for A_{22}^s satisfying

$$P_2 A_{22}^s + \left(A_{22}^s\right)^T P_2 + I = 0 \tag{6.102}$$

and the scalar function $\rho(t,y,u)$ is chosen so that

$$\|\varepsilon(t,y,u)\| < \rho(t,y,u) \tag{6.103}$$

If the state estimation errors are defined as $\varepsilon_1 = \hat{x}_1 - x_1$ and $\varepsilon_2 = \hat{x}_2 - x_2$ then it is straightforward to show

$$\dot{\varepsilon}_1(t) = A_{11}\varepsilon_1(t) \tag{6.104}$$

$$\dot{\varepsilon}_2(t) = A_{21}\varepsilon_1(t) + A_{22}^s\varepsilon(t) + \|D_2\| v - D_2\varepsilon(t,y,u) \tag{6.105}$$

Furthermore the nonlinear error system in (6.104)-(6.105) is quadratically stable and a sliding motion takes place on the surface defined in (6.93), the dynamic system in (6.98)-

(6.100) may be regarded as an observer for the system in (6.90)-(6.91). It follows that if the linear gain

$$G_l = T^{-1}\begin{bmatrix} A_{12} \\ A_{22} - A_{22}^s \end{bmatrix} \tag{6.106}$$

and the nonlinear gain

$$G_n = \|D_2\| T^{-1}\begin{bmatrix} 0 \\ I_p \end{bmatrix} \tag{6.107}$$

then the observer gain given in (6.98)-(6.100) can be written in terms of the original coordinate system in the form of (6.94).

Another observer, introduced by Walcott and Zak (1987), considers the special case when the uncertainty is matched i.e. when $D = B$. They propose the observer structure given by

$$\dot{z}(t) = Az(t) + Bu(t) - GC\varepsilon(t) + Bv_0 \tag{6.108}$$

where z represents an estimate of the true states x, and $\varepsilon = z - x$ is the state estimation error. The output error feedback gain matrix G is chosen so that the closed loop matrix $A_0 = A - GC$ is stable and has a Lyapunov matrix P satisfying both

$$PA_0 + A_0^T P + Q = 0 \tag{6.109}$$

for some positive definite design matrix Q and the structural constraint

$$PB = C^T F^T \tag{6.110}$$

for some non-singular matrix $F \in \mathbb{R}^{m \times p}$. The discontinuous vector v_0 is given by

$$v_0 = \begin{cases} -\rho_0(t,y,u)\dfrac{FC\varepsilon}{\|FC\varepsilon\|} & \text{if } C\varepsilon \neq 0 \\ 0 & \text{otherwise} \end{cases} \tag{6.111}$$

where $\rho_0(t,y,u)$ is a scalar function which bounds the uncertainty. The observer given in (6.94) may be viewed as a Luenberger observer (Luenberger, 1971) with an additional nonlinear term. It can be shown that assumptions about the triple (A,D,C) are both necessary and sufficient conditions for the existence of such an observer which insensitive to matched uncertainty and induces a sliding motion on

$$Sw = \{\varepsilon \in \mathbb{R}^n : FC\varepsilon = 0\} \tag{6.112}$$

The original formulation of Walcott and Zak required the use of symbolic manipulation to synthesise the matrices G and P that completely define the observer. More recently an analytic solution has been proposed based on the canonical form described in equations (6.95)-(6.97). An appropriate choice of G is that given in (6.106) and an appropriate choice of

$$F = (P_2 B_2)^T \tag{6.113}$$

In the special case of a square system an even more explicit solution can be obtained. This does not require the attainment of the canonical form (6.95)-(6.97) explicitly and in certain circumstances produces an observer with better numerical properties.

6.3.1 Observer Design for a Brushless D.C. Motor

Within this final section, state observers for the brushless DC motor mode are developed. The exposition begins with the development of the traditional Luenberger observer assuming perfect knowledge of the plant (Figure 6.9). The observer is then modified to incorporate a discontinuous term, the new observer may be seen to bear may similarities to the original Luenberger observer (Figure 6.10). Using the parameters in Table 6.3,

plant uncertainty is introduced to the plant and the performance of the observers is once again compared.

Parameter	Nominal Value	Actual Value
R	0.64	0.64
L	21e-3	36e-3
Km	0.32	0.32
Ke	0.32	0.32
J	61.5e-3	91e-3
B	73.8e-3	1e-2

Table 6.3: *Nominal and Actual Motor Parameters*

It is assumed here that the output equation $y(t) = x_1(t)$ may be used. It is also assumed that once again the load torque has negligible effect on the system and may be ignored. The motor model then becomes

$$\begin{bmatrix} \dot{x}_1 \\ \dot{x}_2 \\ \dot{x}_3 \end{bmatrix} = \begin{bmatrix} 0 & 1 & 0 \\ 0 & -\frac{B}{J} & \frac{K_m}{J} \\ 0 & -\frac{K_e}{L} & -\frac{R_a}{L} \end{bmatrix} \begin{bmatrix} x_1 \\ x_2 \\ x_3 \end{bmatrix} + \begin{bmatrix} 0 \\ 0 \\ \frac{1}{L} \end{bmatrix} u_2 \qquad (6.114)$$

$$y = \begin{bmatrix} 1 & 0 & 0 \end{bmatrix} \begin{bmatrix} x_1 \\ x_2 \\ x_3 \end{bmatrix} \qquad (6.115)$$

It is necessary to check the observability of the system. The observability matrix is given by

$$M_0 = \begin{bmatrix} C^T & A^T C^T & \left(A^T\right)^2 C^T \end{bmatrix} = \begin{bmatrix} 1 & 0 & 0 \\ 0 & 1 & -\frac{B}{J} \\ 0 & 0 & \frac{K_m}{J} \end{bmatrix} \tag{6.116}$$

which is of full rank n provided that B,J and K_m are nonzero. The eigenvalues of the observer are determined by the characteristic polynomial

$$\left|\lambda I - (A - LC)\right| = 0 \tag{6.117}$$

$$\left|\lambda I - (A - LC)\right| = \left| \begin{bmatrix} \lambda & 0 & 0 \\ 0 & \lambda & 0 \\ 0 & 0 & \lambda \end{bmatrix} - \begin{bmatrix} 0 & 1 & 0 \\ 0 & -\frac{B}{J} & \frac{K_m}{J} \\ 0 & -\frac{K_e}{L} & -\frac{R_a}{L} \end{bmatrix} + \begin{bmatrix} l_1 \\ l_2 \\ l_3 \end{bmatrix} \begin{bmatrix} 1 & 0 & 0 \end{bmatrix} \right| \tag{6.118}$$

$$\left|\lambda I - (A - LC)\right| = \left\| \begin{bmatrix} \lambda + l_1 & -1 & 0 \\ l_2 & \lambda + \frac{B}{J} & -\frac{K_m}{J} \\ l_3 & \frac{K_e}{L} & \lambda + \frac{R_a}{L} \end{bmatrix} \right\| \tag{6.119}$$

$$\begin{aligned} \left|\lambda I - A + LC\right| = \lambda^3 &+ \left\{\left(\frac{B}{J} + \frac{R_a}{L}\right) + l_1\right\}\lambda^2 + \left\{\left(\frac{BR_a + K_m K_e}{JL}\right) + \left(\frac{B}{J} + \frac{R_a}{L}\right) l_1 + l_2\right\}\lambda \\ &+ \left\{\left(\frac{BR_a + K_m K_e}{JL}\right) l_1 + \frac{R_a}{L} l_2 + \frac{K_m}{J} l_3\right\} \end{aligned} \tag{6.120}$$

Insertion of the nominal motor parameters into the state transition matrix provides an eigenvalue spectrum of

$$\text{eig}(A) = \{0 \quad -4.23 \quad -26.98\} \tag{6.121}$$

The observer eigenvalues are chosen to be far to the left of the plant eigenvalues in order to ensure rapid convergence of the observer onto the plant states, i.e.

$$\mathrm{eig}\left(\lambda I-\left(A-LC\right)\right)=\left\{-10 \quad -15 \quad -35\right\} \tag{6.122}$$

The specification of these eigenvalues leads from (6.120) to the observer gain matrix

$$L=\begin{bmatrix} 28.8 \\ 12.44 \\ 306.46 \end{bmatrix} \tag{6.123}$$

The observer performance is shown for each state in Figure 6.11-Figure 6.16 .

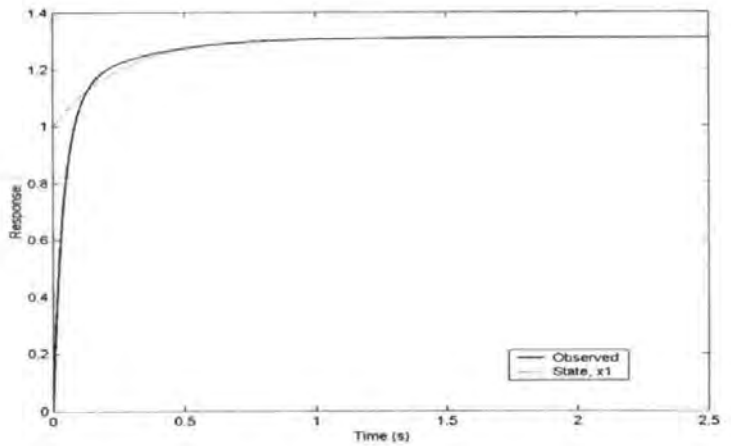

Figure 6.11: *Luenberger Observer Recovering from Initial Position*

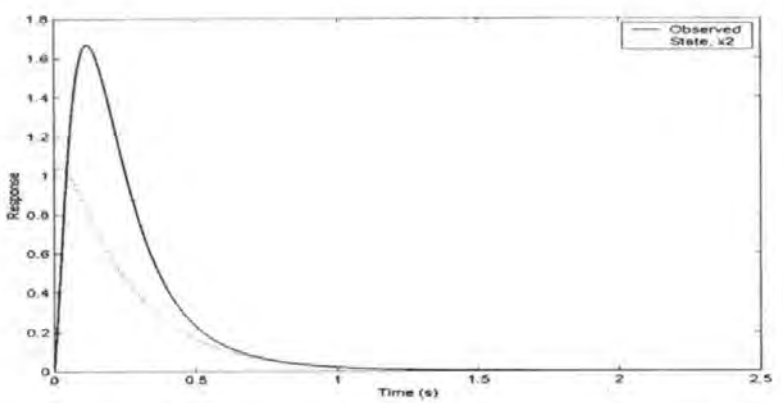

Figure 6.12*: Luenberger Observer Recovering from Initial Speed*

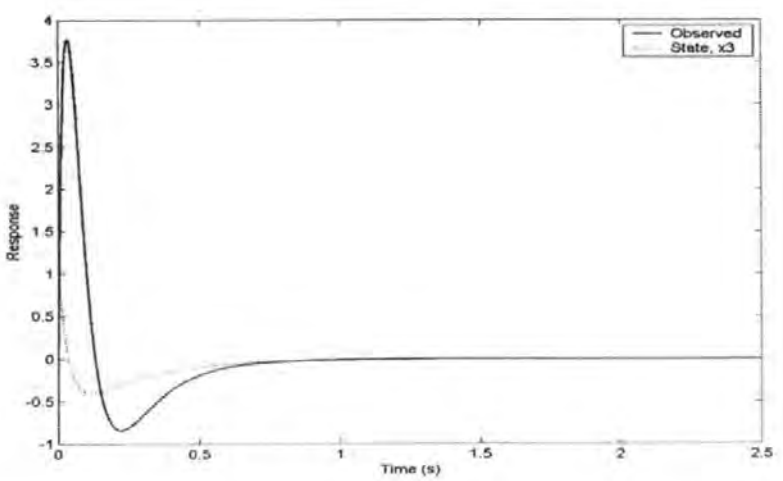

Figure 6.13*: Luenberger Observer Recovering from Initial Current*

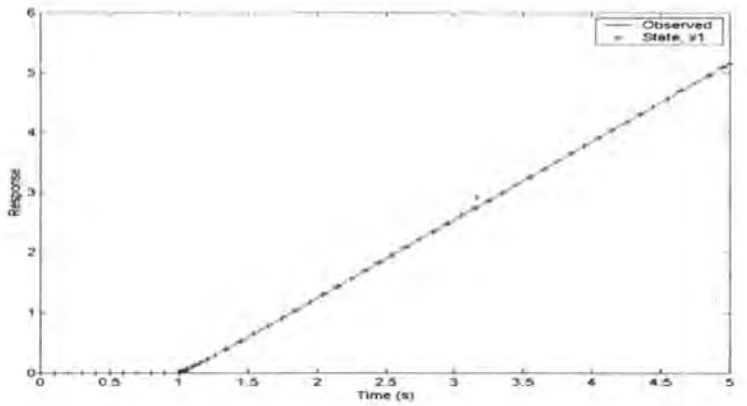

Figure 6.14: *Luenberger Observer Observation of Position in Response to a Step Input*

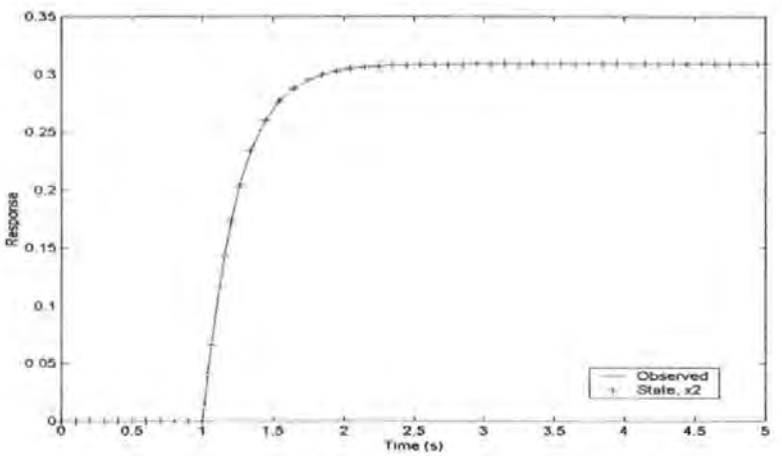

Figure 6.15: *Luenberger Observer Observation of Speed in Response to a Step Input*

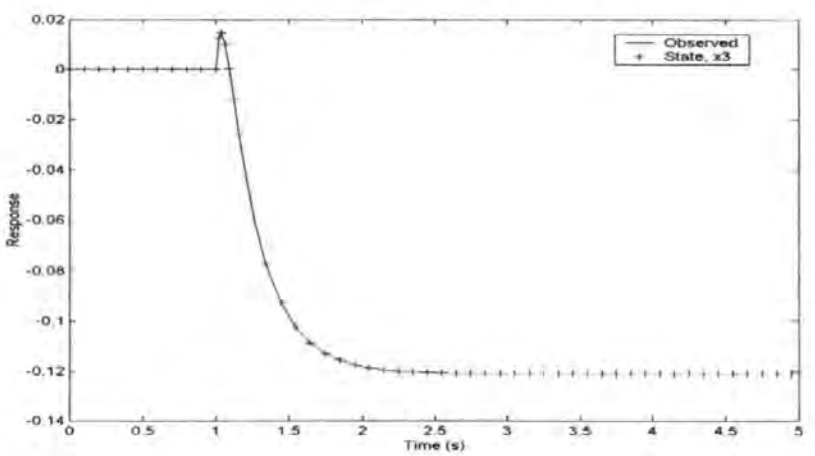

Figure 6.16: *Luenberger Observer Observation of Current in Response to a Step Input*

A sliding mode observer is designed according to the procedures above, using Matlab. The observer is subjected to the same tests as the Luenberger observer and its performance when the perfectly known plant is subject to a step input is illustrated in Figure 6.18-Figure 6.20. Since the plant has two stable invariant zeros, the design was restricted to choosing a single estimation pole, which was selected to be located at -0.5. The uncertainty component, $\rho(t,y,u)$ was selected to be -3. As in the case of the Luenberger observer, perfect state reconstruction was achieved. Uncertainty of the class discussed in equation (6.90) was introduced into the plant states of both the Luenberger observer and the Sliding mode observer (Figure 6.17). This uncertainty takes the form of a random signal of variance 0.02. This choice is sufficient to illustrate the effect without violating (6.103).

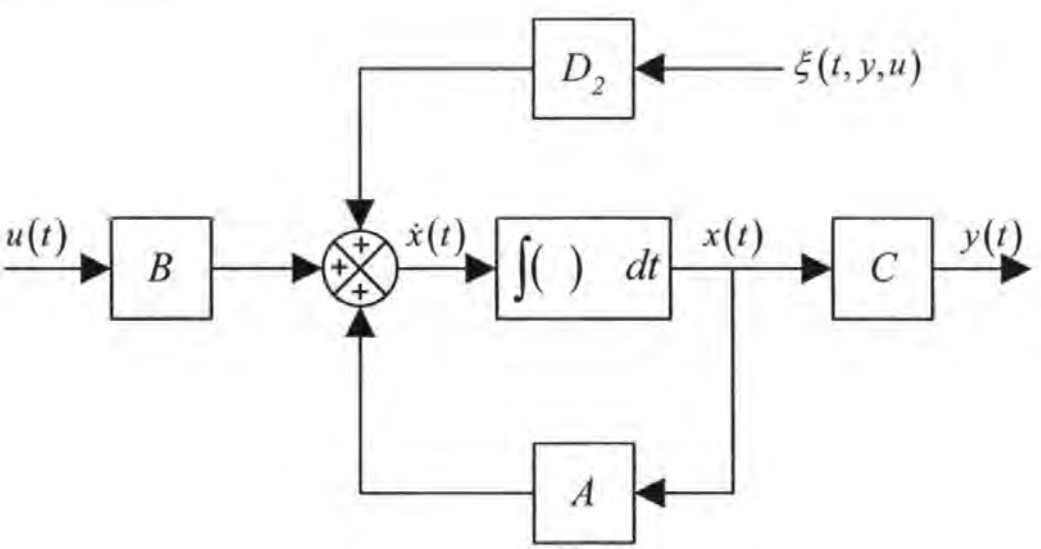

Figure 6.17: *Plant with disturbance*

The matrix D_2 takes the following form

$$D_2 = \begin{bmatrix} 0 \\ 0 \\ 1 \end{bmatrix} \tag{6.124}$$

which leads to a realistic noise component within the current channel. The results are illustrated in Figure 6.21-6.23 for the Luenberger observer and Figure 6.24-6.26 for the sliding mode observer. Provides root mean squared observation errors of the respective observers. The sliding mode observer has been tested under a series of sample periods, k, in order to illustrate that in the limit as $k \to 0$, $\varepsilon \to 0$. It is not however computationally desirable, or indeed feasible to achieve this figure in simulation, therefore as sample period of 0.01 is used as the default for all sliding mode observers and controllers. Finally, parametric uncertainty is introduced according to Table 6.3, this uncertainty is not formally considered within the development above, it is therefore not surprising to see that both observers performance is reduced, although the sliding mode observers performance is on the whole better than that of the Luenberger observer (Figure 6.27 and Figure 6.28), because of the additional robustness to parametric uncertainty.

Table 6.4: *Root Mean Squared State Observation Errors for Luenberger Observer and Sliding Mode Observer at Three Different Sample Periods*

Observer	**Luenberger**	**Sliding Mode k=0.01**	**Sliding Mode k=0.001**	**Sliding Mode k=0.0001**
$\|x_1 - \hat{x}_1\|_{rms}$ (rad)	844e-6	1.3e-3	119.8e-6	9.7e-6
$\|x_2 - \hat{x}_2\|_{rms}$ (rad/s)	24.4e-3	1.5e-3	289.5e-6	64e-6
$\|x_3 - \hat{x}_3\|_{rms}$ (A)	9.6e-3	1.8e-3	544.4e-6	171.7e-6

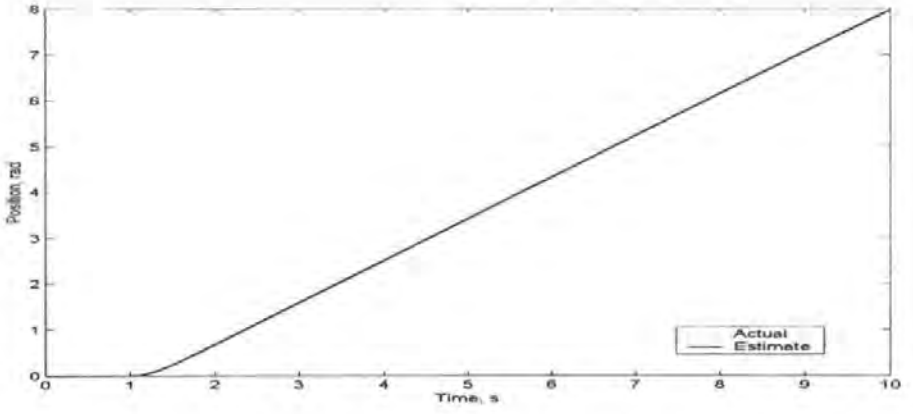

Figure 6.18*: Sliding Mode Observer Position Estimation with Step Input into Ideal System*

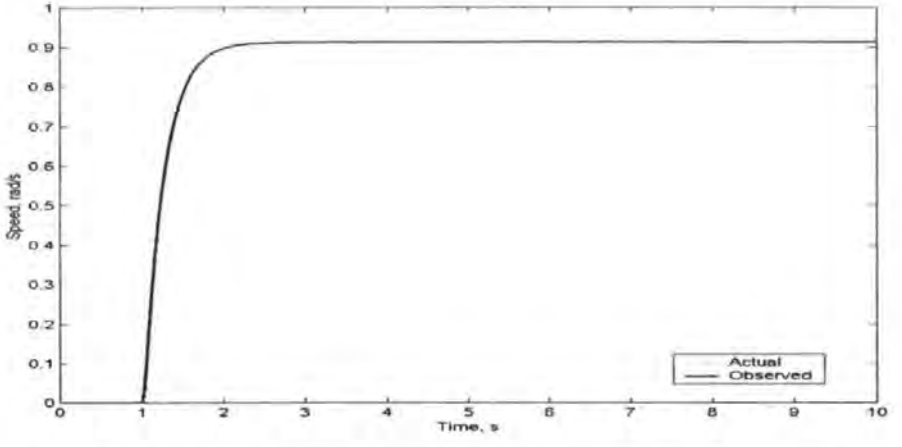

Figure 6.19*: Sliding Mode Observer Speed Estimation with Step Input into Ideal System*

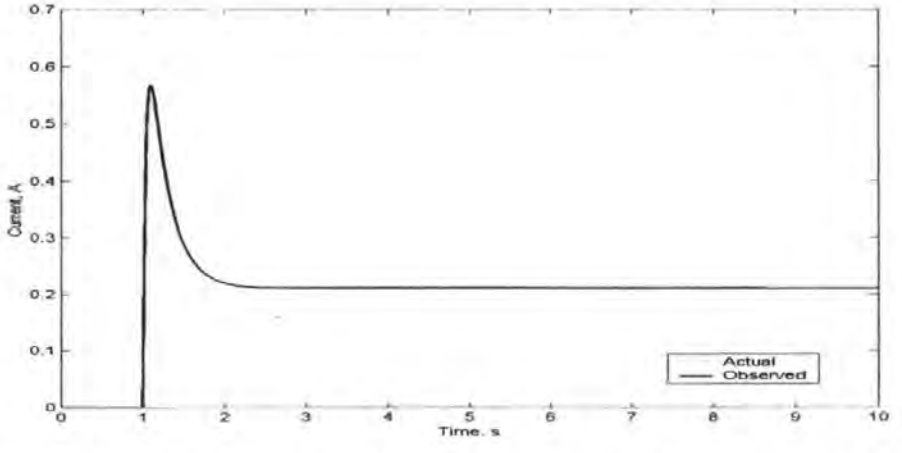

Figure 6.20*: Sliding Mode Observer Current Estimation with Step Input into Ideal System*

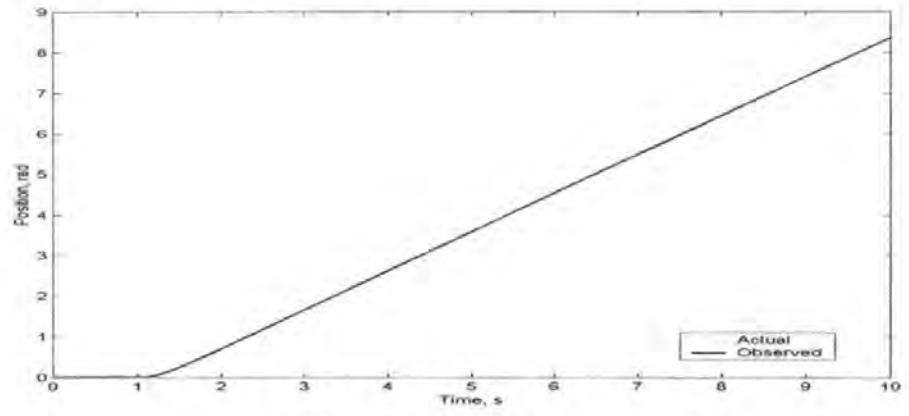

Figure 6.21: *Luenberger Observer State Reconstruction of Position with Plant Subject to Noise*

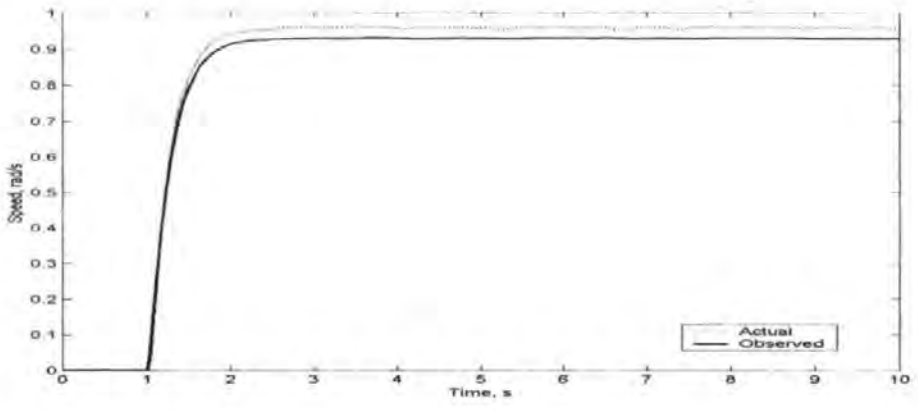

Figure 6.22: *Luenberger Observer State Reconstruction of Speed with Plant Subject to Noise*

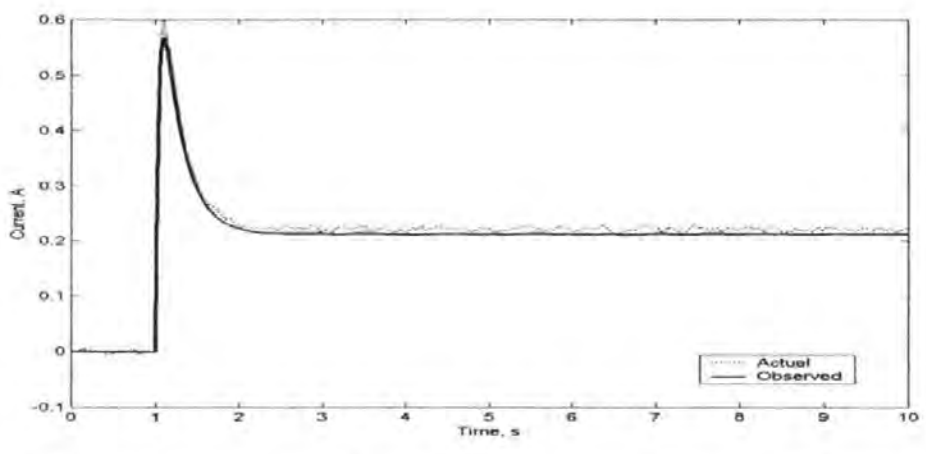

Figure 6.23: *Luenberger Observer State Reconstruction of Current with Plant Subject to Noise*

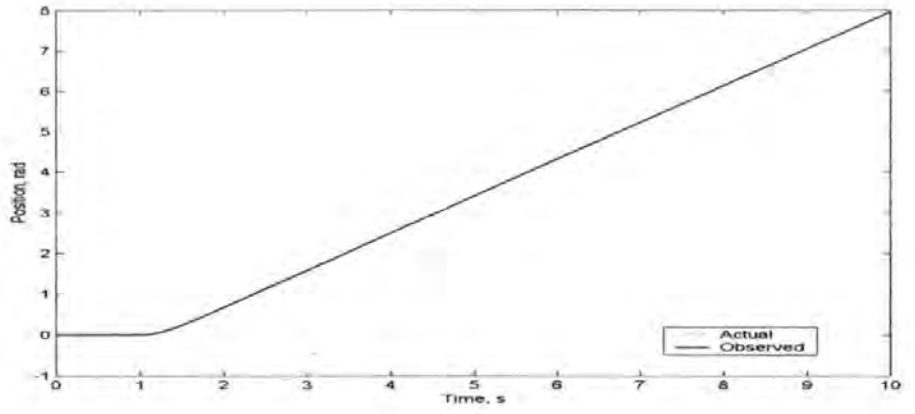

Figure 6.24: *Sliding Mode Observer State Reconstruction of Position with Plant Subject to Noise*

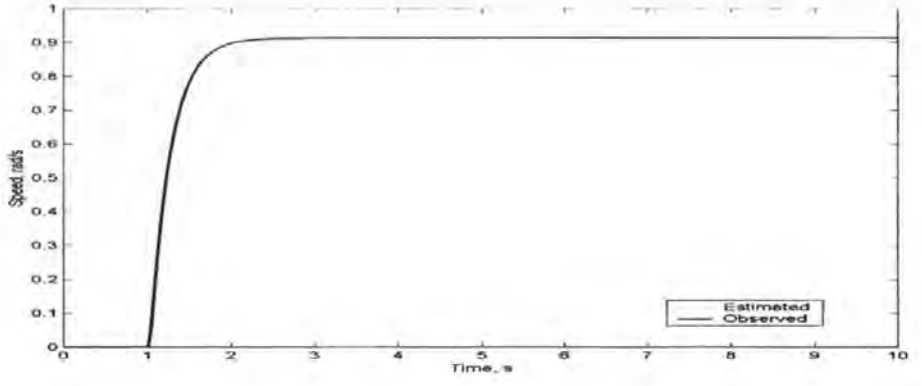

Figure 6.25: *Sliding Mode Observer State Reconstruction of Speed with Plant Subject to Noise*

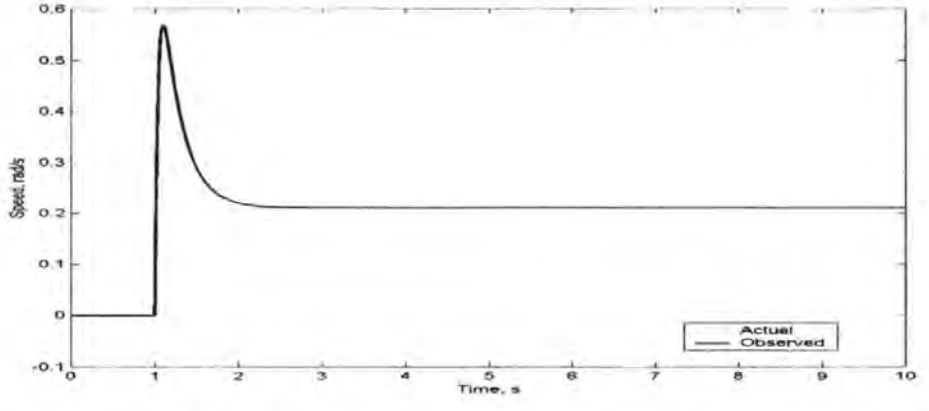

Figure 6.26: *Sliding Mode Observer State Reconstruction of Current with Plant Subject to Noise*

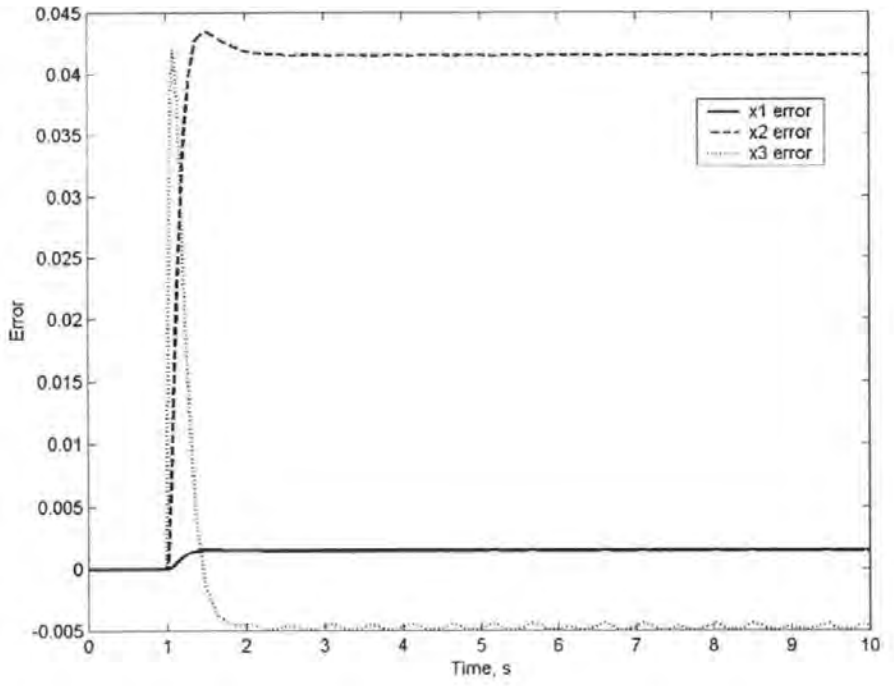

Figure 6.27: *Luenberger Observer State Reconstruction Errors Under Plant Uncertainty*

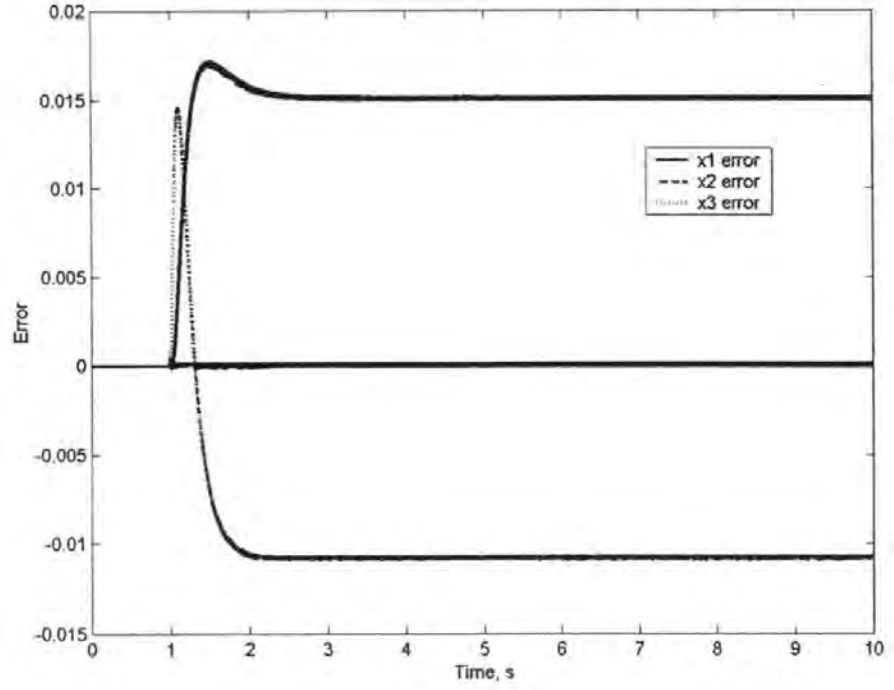

Figure 6.28: *Sliding Mode Observer State Reconstruction Errors Under Plant Uncertainty*

6.4 Model Following Sliding Mode Control

Linear model following control is an efficient control method that avoids the difficulty of specifying a performance index which is usually encountered in the application of optimal control to multivariable control systems. The model that specifies the design objective is part of the system. However, Linear Model Following Control systems are inadequate when the plant is subject to large parameter variations or disturbances. This has led to the development of so called adaptive model following control schemes. There are two approaches to the design of adaptive model following systems using stability conditions. The first is based upon Lyapunov functions e.g. Shackcloth and Butchart (1966), while the second is based upon the hyperstability concept e.g. Landau (1974). Both approaches guarantee that the error tends to zero as $t \to \infty$ but neither offer any direct quantitative design of the error transient.

In model following systems the plant is controlled in such a way that its dynamic behaviour approximates that of a specified plant model. The model plant is part of the system and it specifies the design objectives. The adaptive controller should force the error between the model and the plant to zero as time tends to infinity, i.e. $\lim_{t\to\infty} \varepsilon(t) = 0$.

The plant and the model are described by

$$\dot{x}_p = A_p(t)x_p + B_p(t)u_p \tag{6.125}$$

$$\dot{x}_m = A_m x_m + B_m u_m \tag{6.126}$$

with the error vector given as

$$\varepsilon = x_m - x_p \tag{6.127}$$

It is assumed that the pairs (A_p, B_p) and (A_m, B_m) may be stabilised and that A_m is a stable matrix. Differentiation of (6.127) and insertion of (6.125) and (6.126) provides the following

$$\dot{\varepsilon} = A_m x_m + B_m u_m - A_p x_p - B_p u_p \tag{6.128}$$

Further, subtraction of the term $A_p x_m$ yields

$$\dot{\varepsilon} = A_p \varepsilon + (A_m - A_p) x_p + B_m u_m - B_p u_p \tag{6.129}$$

It follows that perfect model following will result if

$$(A_m - A_p) x_p + B_m u_m - B_p u_p = 0 \tag{6.130}$$

rearranging (6.130) provides the following

$$u_p = B_p^{\dagger}\left((A_m - A_p) x_p + B_m u_m\right) \tag{6.131}$$

insertion of (6.131) into (6.130) yields

$$(A_m - A_p) x_p + B_m u_m - B_p B_p^{\dagger}\left((A_m - A_p) x_p + B_m u_m\right) = 0 \tag{6.132}$$

Clearly, in order to satisfy (6.130) for all x_p and u_m the following equalities must hold

$$\left(I - B_p B_p^{\dagger}\right)(A_m - A_p) = 0 \tag{6.133}$$

$$\left(I - B_p B_p^{\dagger}\right) B_m = 0 \tag{6.134}$$

The equations (6.133) and (6.134) are the conditions for perfect model following as first described by Erzeberger (1968), Equation (6.131) is the equation for implementing the control. This control law leads to a controller response which is determined by the eigenvalues of the model. Since the eigenvalue spectrum of the model may not be determined by the designer the control response might not yield acceptable results. Later,

Chen (1973) proposed a small modification to the controller, by subtracting the term $A_p x_m$ from (6.128), this yields

$$\dot{\varepsilon} = A_m \varepsilon + \left(A_m - A_p\right) x_m + B_m u_m - B_p u_p \tag{6.135}$$

From equation (6.135), it is evident that choosing a control action of the form

$$u_p = u_1 + u_2 \tag{6.136}$$

with

$$u_1 = K\varepsilon \tag{6.137}$$

$$u_2 = B_p^{\dagger}\left(A_m - A_p\right) x_m + B_p^{\dagger} B_m u_m \tag{6.138}$$

will lead to perfect model following if it is possible. Substitution of the control law (6.136)-(6.138) into (6.129) leads to

$$\dot{\varepsilon} = A_m \varepsilon + \left(A_m - A_p\right) x_p + B_m u_m - B_p K\varepsilon - B_p B_p^{\dagger}\left(A_m - A_p\right) x_m - B_p B_p^{\dagger} B_m u_m \tag{6.139}$$

under the assumption that conditions (6.133) and (6.134) hold, then (6.139) simplifies to

$$\dot{\varepsilon} = \left(A_m - B_p K\right)\varepsilon \tag{6.140}$$

In contrast to the controller proposed by Erzeberger, the controller proposed by Chen can have an arbitrary set of eigenvalues determined by the gain matrix K, since the tuple $\left(A_m, B_p\right)$ is controllable. Since (6.140) is identical to the optimal state regulator problem (Anderson and Moore, 1971), then the gain matrix K may be chosen to optimise a quadratic performance index in ε. Hence, the error settling rates may be controlled. Additionally, if only partial state feedback is possible then perfect model following is still possible (Chen, 1973).

Model following control systems were extended to incorporate a discontinuous control component in Young (1978). Following this original design, define an error dependent switching function

$$S(\varepsilon) = S\varepsilon \tag{6.141}$$

which gives rise to a hyperplane in the error space

$$S_\varepsilon = \{\varepsilon \in \mathbb{R}^n : S\varepsilon = 0\} \tag{6.142}$$

As seen in the previous Chapter, during sliding the error state will satisfy the equation

$$S\varepsilon(t) = 0 \tag{6.143}$$

Differentiation and substitution of (6.135) gives

$$S\dot{\varepsilon} = S\left(A_m\varepsilon + \left(A_m - A_p\right)x_m + B_m u_m - B_p u_p\right) = 0 \tag{6.144}$$

If by design the matrix product SB is non-singular, then the equivalent control may be determined as

$$u_{eq} = \left(SB_p\right)^{-1} S\left(A_m\varepsilon + \left(A_m - A_p\right)x_p + B_m u_m\right) \tag{6.145}$$

substitution of the equivalent control into the model following control system of (6.135) gives

$$\dot{\varepsilon} = \left(I - B_p\left(SB_p\right)^{-1} S\right)\left(A_m\varepsilon + \left(A_m - A_p\right)x_p + B_m u_m\right) \tag{6.146}$$

It is assumed that the plant and model dynamic equations satisfy the perfect model matching conditions. Comparison of these equations with the invariance conditions discussed by Drazenovic (1969), it can be seen that the two coincide. Therefore if x_p and u_m are considered disturbances to the error dynamics then the perfect model matching conditions guarantee that the behaviour of the sliding mode controller is

insensitive to these disturbances. If the conditions of (6.133) and (6.134) hold, then equation (6.146) reduces to

$$\dot{\varepsilon} = \left(I - B_p\left(SB_p\right)^{-1} S\right) A_m \varepsilon \tag{6.147}$$

A unit vector type control is now introduced as in the work by Corless *et al* (1985), a discontinuous unit vector control is introduced according to

$$u = u_l + u_n \tag{6.148}$$

with

$$u_l(t) = -\left(SB\right)^{-1}\left(SA_m - \Phi S\right)\varepsilon(t) \tag{6.149}$$

$$u_n = -\rho(t,\varepsilon)\left(SB\right)^{-1}\frac{P_2 S(t)}{\left\|P_2 S(t)\right\|} \tag{6.150}$$

It was pointed out in Chen (1973) and later in Zinober (1981) that the conditions of (6.133) and (6.134) may be met if

$$\text{rank}\left(B_p, B_m\right) = \text{rank}\left(B_p\right) \tag{6.151}$$

$$\text{rank}\left(B_p, A_m - A_p\right) = \text{rank}\left(B_p\right) \tag{6.152}$$

It follows that there exist compatibly dimensioned matrices such that

$$B_p F = A_m - A_p \tag{6.153}$$

$$B_p G = B_m \tag{6.154}$$

This result may be used as an alternative to (6.138), with

$$u_2(t) = Fx_p(t) + Gu_m(t) \tag{6.155}$$

to also achieve perfect model following. The complete model following control scheme is then given according to

$$u(t) = u_l(t) + u_n(t) + u_2(t) \tag{6.156}$$

6.4.1 A Model Following Sliding Mode Controller for a BLDC

Within this section a model following sliding mode controller will be developed using the test rig model used throughout this work so far. Initially, a the plant will assumed to have the state transition matrix

$$A_p = \begin{bmatrix} 0.95 & 1.486 & 0.457 \\ 0.2311 & -0.3087 & 5.2185 \\ 0.6068 & -14.2379 & -29.1786 \end{bmatrix} \tag{6.157}$$

which is stable since it has the eigenvalue spectrum

$$\mathrm{eig}(A_p) = \begin{Bmatrix} 0 \\ -3.28 \\ -21.29 \end{Bmatrix} \tag{6.158}$$

and no poles appear in the right half of the complex plane. The performance of the model used within this work is shown in Figure 6.29. The motor model is given by the equations found in §5.3.5, e.g.

$$\begin{bmatrix} \dot{x}_1 \\ \dot{x}_2 \\ \dot{x}_3 \end{bmatrix} = \begin{bmatrix} 0 & 1 & 0 \\ 0 & -\frac{B}{J} & \frac{K_m}{J} \\ 0 & -\frac{K_e}{L} & -\frac{R_a}{L} \end{bmatrix} \begin{bmatrix} x_1 \\ x_2 \\ x_3 \end{bmatrix} + \begin{bmatrix} 0 \\ -\frac{u_1}{J} \\ -\frac{u_2}{L} \end{bmatrix} \tag{6.159}$$

The controller gains are designed according to the previous section using a Matlab m-file script, these are given as

$$L = \begin{bmatrix} 0.304 & 0.877 & 0.98 \end{bmatrix} \tag{6.160}$$

$$F = \begin{bmatrix} 0 & 0.15 & -0.25 \end{bmatrix} \tag{6.161}$$

$$G = 1 \tag{6.162}$$

$$(SB)^{-1} = 0.05 \tag{6.163}$$

$$P_2 = 5 \tag{6.164}$$

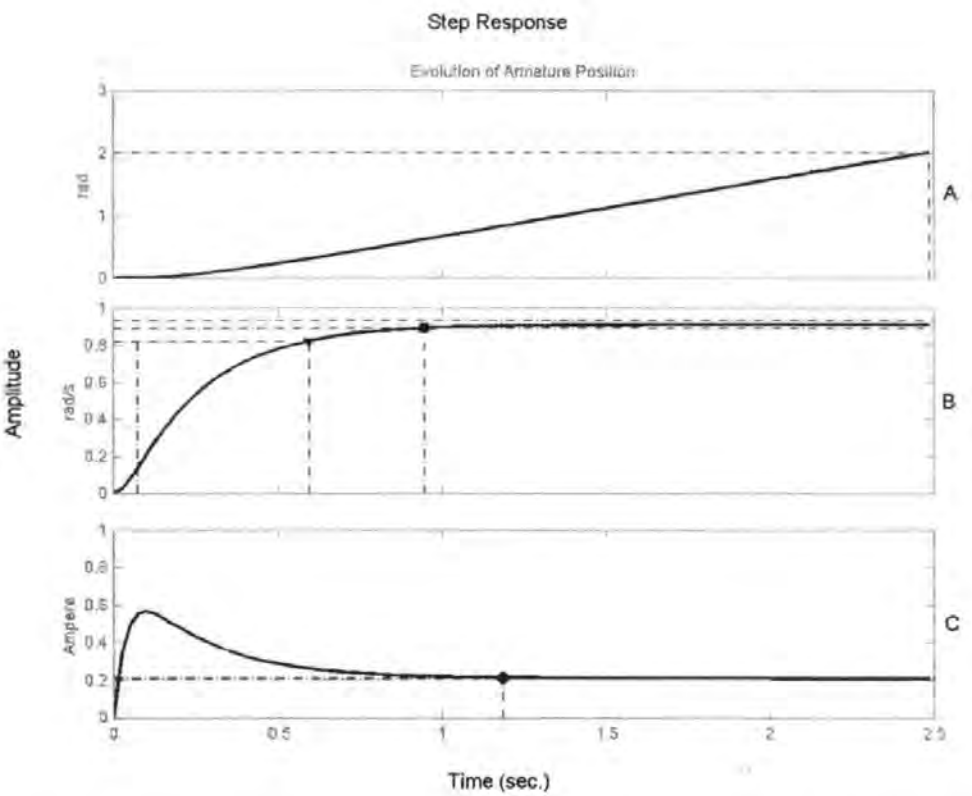

Figure 6.29: *Model response to a step input. A) Evolution of position. B) Evolution of speed. C) Evolution of current.*

The principle of the model following sliding mode controller is illustrated in Figure 6.30. This controller with the controller gains given in (6.160)-(6.164) was implemented in Matlab/Simulink with a value of $\rho = 5$. The results shown in Figure 6.31-Figure 6.37 illustrate how the model following controller is able to force successfully a slower system to follow a system with desired dynamics. The speed of the system shown in Figure 6.33

illustrates an overshoot of plant speed which eventually settles to zero error (Figure 6.34). This is due to the fast eigenvalues selected to ensure convergence of the system states to the model states. It should be noted that in this simulation, the boundary layer was given a radius of zero in order to approximate the ideal performance as closely as possible, as a direct consequence, the controller chatter is plainly visible in the system control effort.

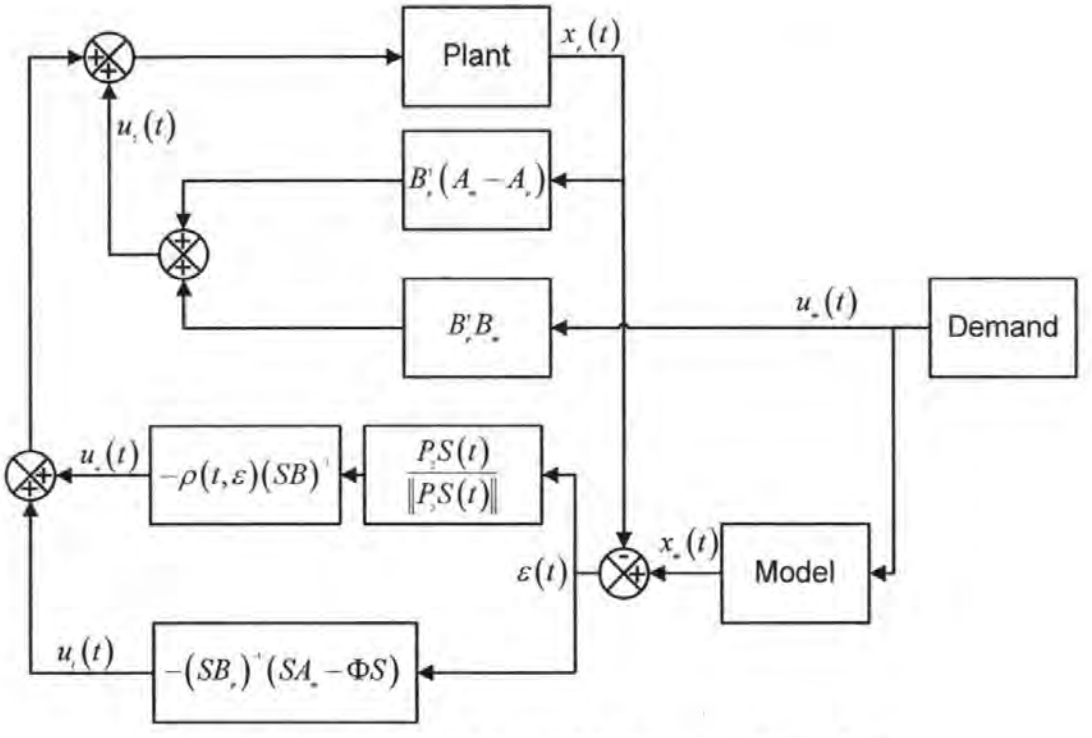

Figure 6.30: *Principle of the Model Following Controller*

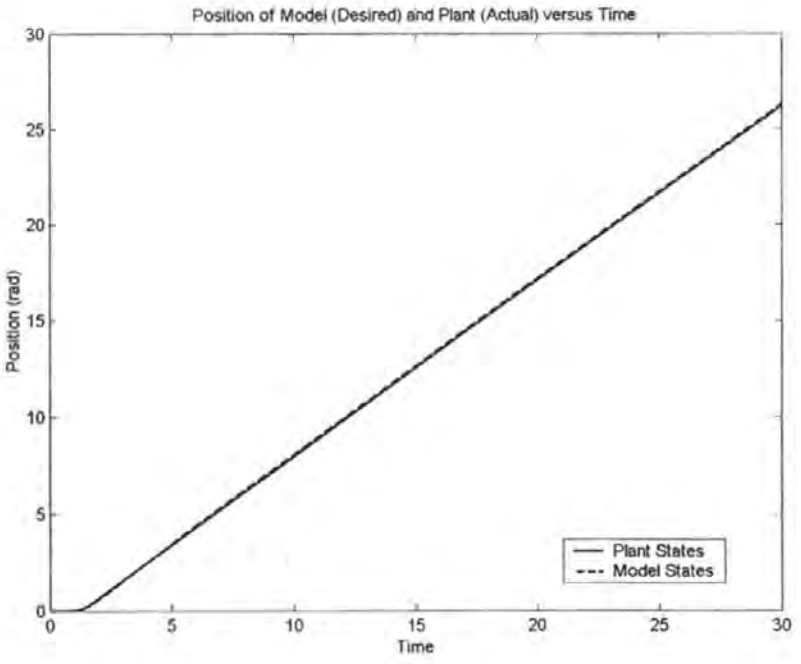

Figure 6.31: *Model and Plant position*

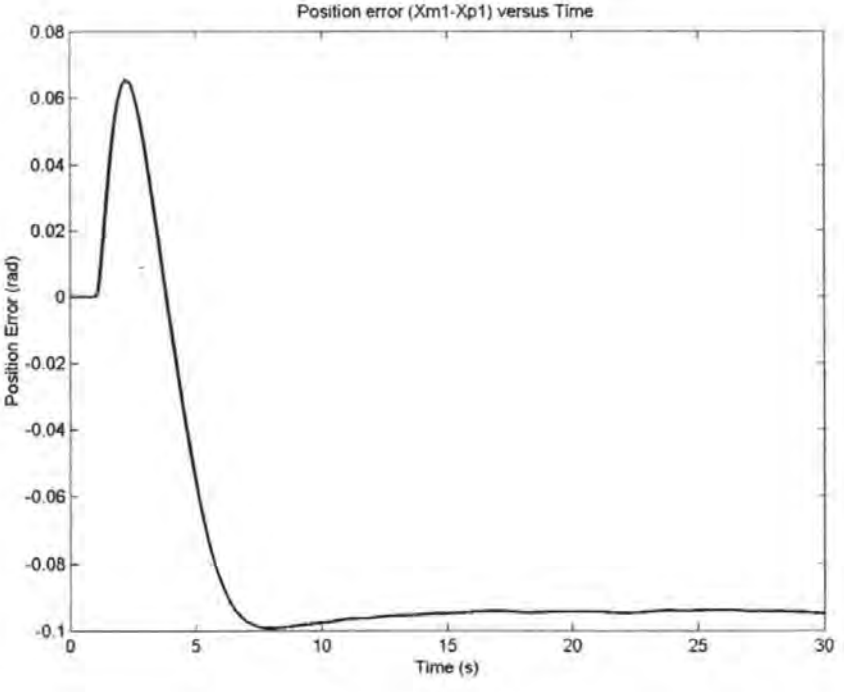

Figure 6.32: *Evolution of Position Error*

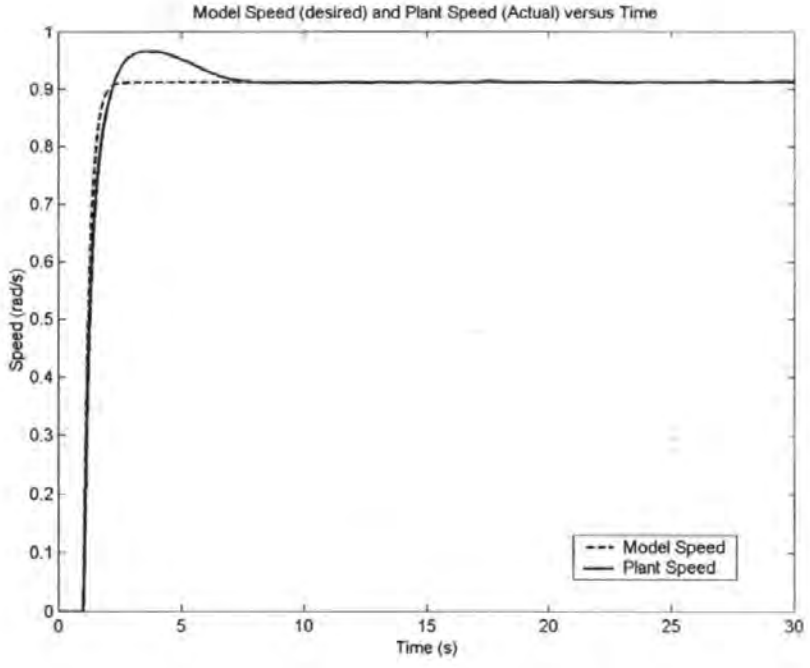

Figure 6.33*: Model and Plant speed*

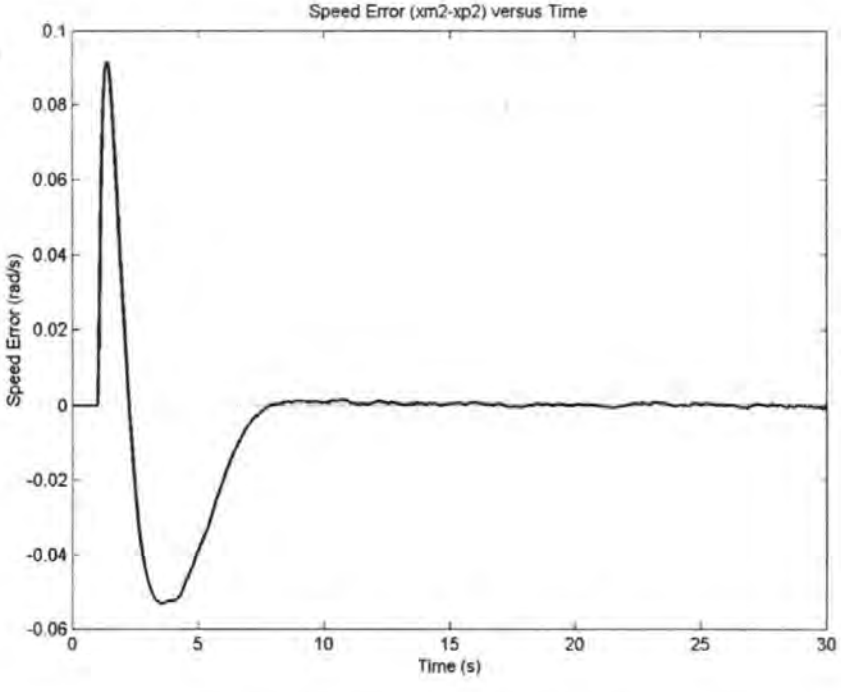

Figure 6.34: Evolution of Speed Error

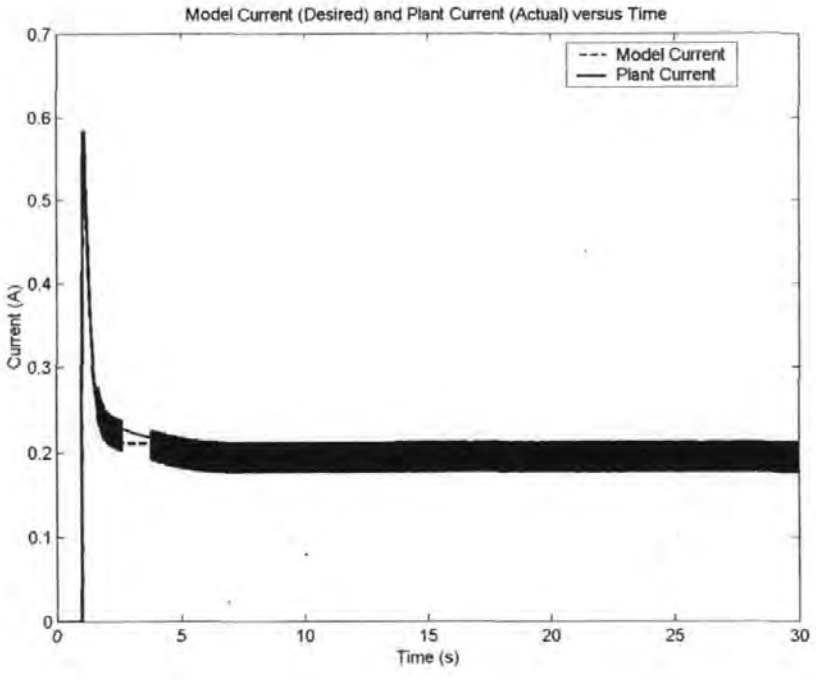

Figure 6.35*: Model and Plant Current*

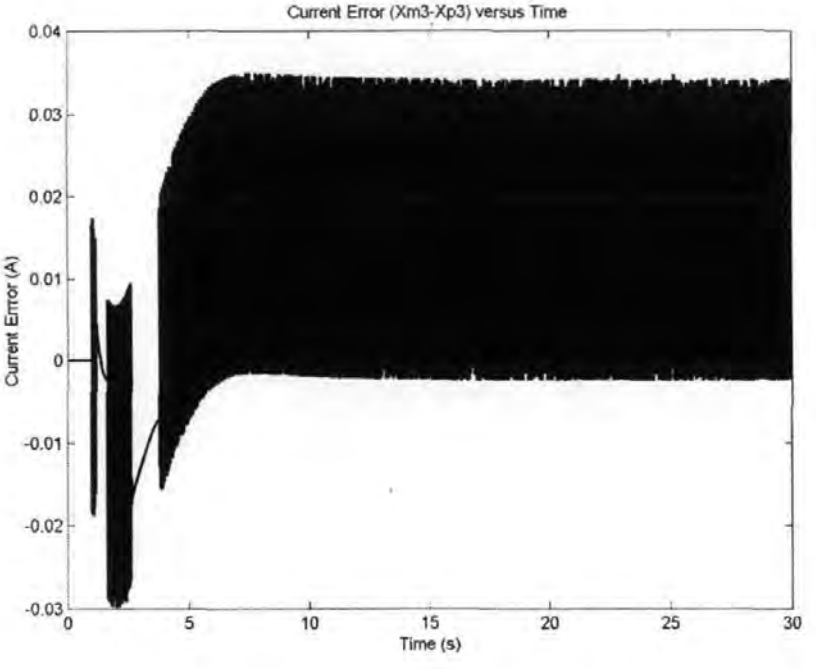

Figure 6.*36: Evolution of Current Error*

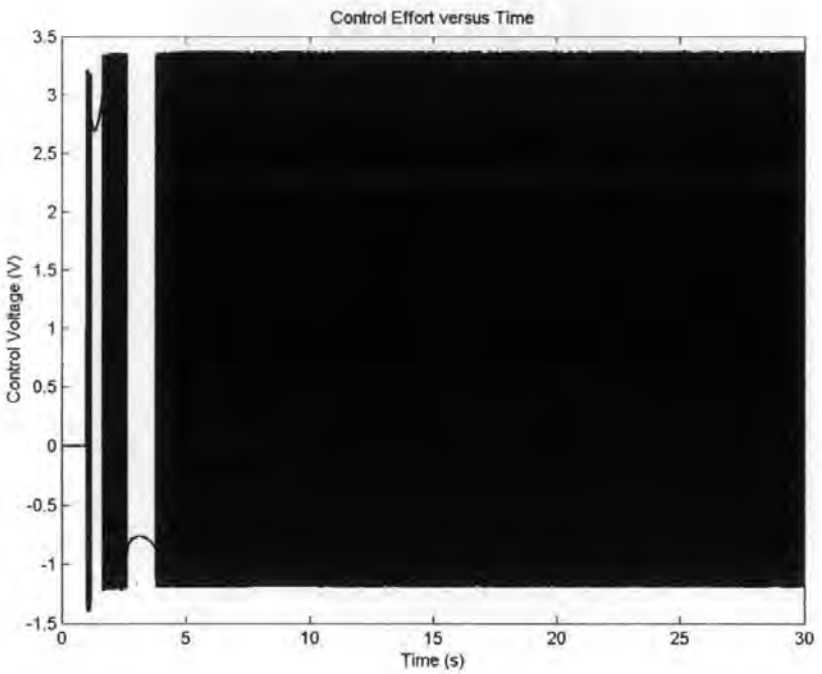

Figure 6.37: *Model Following Control Effort*

6.5 Discussion

The intuitively appealing concept of introducing a feed forward integral control action within a sliding mode controller has been taken from previous work and applied to the design of a controller within the context of a system expressed in the control canonical form. The approach has been shown to provide robustness to unmatched disturbance as the controlled state tends asymptotically towards the demand. The guarantees of sliding, stability and reaching are still ensured through judicious choice of control gains and use of traditional tests. This controller stems from the 'classical' approaches discussed in the early part of the previous Chapter and tends to lend itself readily to implementation since the control can be achieved without the use of matrix manipulation.

The second controller, based on the synergy of sliding mode design approaches and nonlinear black box modelling has been presented. Performance of the controller has

been compared with a benchmark sliding mode controller and the controllers response has been found to be favourable. The controller has demonstrated clear advantages of using fuzzy logic in conjunction with sliding mode. Since the system uncertainties can be significantly reduced through use of fuzzy identification and linearisation techniques, the feedback control gains may be reduced, which in turn leads to a control effort of reduced magnitude. This leads directly to a reduction in the radius of the boundary layer, providing improvements in the final achievable tracking accuracy of the system. Since the fuzzy model does not discriminate between matched and unmatched disturbance, but simply incorporates them into the model, the fuzzy adaptive sliding mode controller also enjoys improvements in the transient control performance when the system is subject to unmatched disturbance. It is finally pointed out that implementation of this algorithm is significantly more complex than the previous integral actions sliding mode controllers.

Robust state observation within the framework of the sliding mode has also been introduced. This approach has been contrasted with the original approach of Luenberger and has been shown to outperform it when subject to certain types of disturbance, providing almost perfect state reconstruction. Finally, model following and the conditions for perfect model following has been explored. It has been seen that since the conditions for perfect model following and the sliding mode invariance conditions (Drazenovic, 1969) coincide, that the sliding mode model following control system is able to force a plant to perform according to a prescribed model, despite the presence of measurement noise.

6.6 References

Anderson B.D.O. and Moore J.B., 1971, 'Linear Optimal Control' Prentice Hall

Babuska R. 1998. Fuzzy Modelling for Control, Kluwer Academic Publishers.

Babuska R. and Verbruggen H.B. 1997. Constructing Fuzzy Models by Product Space Clustering. In: Hellendoorn H. and Driankov D. (eds) Fuzzy Model Identification. Springer-Verlag, 53-90

Chen Y.T., 1973, 'Perfect Model Following with a Real Model', Proc. Joint Automatic Control Conference, 283-293.

Choi J.-H., Misawa E.A. and Young G.E. 1999. A Study on Sliding Mode State Estimation. ASME Journal of Dynamic Systems, Measurement and Control. **121.** 255-260.

Corless M., Goodall D.P., Leitmann G. and Ryan E.P., 1985, 'Model Following Controls For a Class of Uncertain Dynamical System', Proc 7th IFAC/IPOS symp. on Identification and System Parameter Estimation. 1895-1899.

Davies R., Edwards C. and Spurgeon S.K., 1994. 'Robust Tracking with a Sliding Mode' in **Zinober A.S.I.**, 'Variable Structure and Lyapunov Control', Springer Verlag.

Drazenovic B., 1969, 'The Invariance Conditions in Variable Structure Systems', Automatica. **5.** 287-295.

Edwards C and Spurgeon S.K. 1998. Sliding Mode Control: Theory and Applications. Taylor Francis.

Erzeberger H., 1968, 'Analysis and Design of Model Following Control Systems by State Space Techniques', Proc. Joint Automatic Control Conference, 572-581.

Ha Q.P., Rye D.C. and Durrant-Whyte H.F. 1999. Robust Sliding Mode Control with Application, International Journal of Control. 72(12), 1087-1096.

Haskara I., Ozugner U. and Utkin V.I. 1998. On Sliding Mode Observers via Equivalent Control Method. International Journal of Control. **71**(6). 1051-1137

Itkis U. 1976. Control Systems of Variable Structure, John Wiley.

Karunadasa J.P. and Renfrew A.C. 1991, 'Design and implementation of microprocessor based sliding mode controller for brushless servomotor', IEE Proc. Part B, **138**(6), 345-363.

Landau I., 1974, 'Survey of Model Reference Adaptive Techniques', Automatica. **10.** 353-379

Luenberger D.G. 1971. An Introduction to Observers. IEEE Trans. On Automatic Control. **16.** 596-602.

Misawa E.A. and Hedrick J.K. 1989. Nonlinear Observers – A State of the Art Survey. ASME Journal of Dynamic Systems, Measurements and Control. **111**. 342-352.

O'Dell B. 1997 Fuzzy sliding mode control: A critical review, Oklahoma state university, Technical Report ACL-97-001.

Palm R. 1994. Robust Control by Fuzzy Sliding Mode, Automatica, **30**(9), 1429-1438.

Roubos J.A., Mollov S., Babuska R and Verbruggen H.B. 1999 Fuzzy model based predictive control using Takagi-Sugeno models, International journal of Approximate reasoning, **22**, 199-226

Ryan E.P. and Corless M., 1984. 'Ultimate Boundedness and Asymptotic Stability of a Class of Uncertain Dynamical System via Continuous and Discontinuous Feedback Control', IMA Journal of Mathematics and Control Information, **1**, 223-242.

Shackcloth B. and Butchart R.L., 1966, 'Synthesis of Model Reference Adaptive Control Systems by Lyapunov's Second Method', Proc 2nd IFAC Symp. on the Theory of Self Adaptive Control Systems. 145-152.

Slotine J.-J., 1984. 'Sliding Controller Design for Nonlinear Systems', International Journal of Control, **40**, 421-434

Slotine J.-J. and Sastry S.S., 1983 . 'Tracking Control of nonlinear systems using sliding surfaces, with application to robot manipulators', International Journal of Control, **38**, 465-492.

Slotine J.-J., Hedrick J.K. and Misawa E.A. 1987. On Sliding Observers for Nonlinear Systems. ASME Journal of Dynamic Systems, Measurement and Control. **109**.245-252.

Spurgeon S.K., 1991. 'Choice of Discontinuous Control Component for Robust Sliding Mode Performance', International Journal of Control, **53**(1).

Spurgeon S.K. and Davies R., 1993. 'A Nonlinear Control Strategy for Robust Sliding Mode Performance in the Presence of Unmatched Uncertainty', International Journal of Control, **57**(5), 1107-1123

Takagi T. and Sugeno M. 1985 Fuzzy Identification and its applications to Modelling and Control, IEEE Trans. on Systems, Man and Cybernetics, **15**(1), 116-132.

Utkin V.I., 1977. Variable Structure Systems with Sliding Modes. IEEE Transactions on Automatic Control, **AC-22**(2), 212-223

Utkin V.I., 1992. Sliding Modes in Control Optimisation. Springer Verlag.

Utkin V.I., Guldner J. and Shi J., 1999, "Sliding Mode Control in Electromechanical Systems", Taylor Francis.

Utkin V.I. 1977 Variable Structure Systems with Sliding Modes, IEEE Transactions on Automatic Control, AC-**22**(2), 212-222.

Walcott B.L. and Zak S.H. 1987. Combined Observer-Controller Synthesis for Uncertain Dynamical Systems with Applications. IEEE Systems, Man and Cybernetics. **18**. 88-104.

Yao, B. 1992 Adaptive robust control of nonlinear systems with application to control of mechanical systems, PhD Thesis, University of California, 1992

Young K.-K.D., 1977, 'Asymptotic Stability of Model Reference Control Systems with Variable Structure Control', IEEE Trans Automatic Control. **AC-22**(2). 279-281.

Young K.-K.D., 1978, 'Design of Variable Structure Model-Following Control Systems', IEEE Transactions on Automatic Control. **AC-23**(6). 1079-1085.

Zinober A.S.I, 1981, 'Controller Design Using the Theory of Variable Structure Systems', In Harris C.J and Billings S.A., *Self-Tuning and Adaptive Control: Theory and Applications*, Peter Peregrinus.

Zinober A.S.I., 1984, 'Properties of Adaptive Discontinuous Model Following Control Systems', Proc. 4th IMA Int. Conf. on Control Systems. 337-346

Chapter 7

Precision Sensorless Motion Control

7.1 Introduction

Sensorless control was introduced in Chapter 2 as a broad set of techniques which may be applied to the synchronous motor to achieve motion control without the need for a primary feedback sensor. It was seen within that Chapter that the methods considered could each generally be classified in one of three groups. The first of these groups involves the use of instrumentation to measure directly relevant state variables, such as the back EMF component of the signal. The second was based on state observation methods, improved robustness to signal noise and the use of state variables not directly related to armature position was reported. The final group considered was based on artificial intelligence and constitutes the emergent techniques within the sensorless motion control theory. It became abundantly obvious within that Chapter that whilst the approaches apparently worked well for high speed control, at lower and zero speeds very few methods were available. The single approach that does achieve low and zero speed control is based on a heterodyning technique and is achieved at the expense of introducing a good deal of additional electronics. Whether this approach could truly be considered sensorless is something of a moot point.

The Hall effect proximity sensors traditionally used for commutation of the motor can be embedded at manufacture and add little to the size or weight of the system. The lack of pertinent physically measurable states at very low speeds or standstill leads to the early

conclusion within this Chapter, based on the review of Chapter 2, that sensorless precision motion control will only be achievable if the Hall effect sensors are incorporated into the system. It is also concluded that despite the results achieved in sensorless speed control, fundamentally new approaches are required in order to achieve sensorless position control. The objective of this Chapter then becomes one of estimating the armature position using very coarse measurements of position from the Hall effect devices and measurements of available physical state variables. It is noteworthy to mention that there are two methods which are commonly adopted to reconstruct unevenly sampled data, splines or regression analysis. Since within this work, the position data must be extrapolated from previous measurements, the spline approach is not considered since it rapidly leads to instability (Press *et al*, 1997), for a review of spline methods the reader is referred to (Froberg, 1970). The next section of this Chapter moves on to discuss the feedback data available from the Hall effect devices. Following on, a series of approaches to the estimation of the armature position are presented. This chapter concludes with a discussion of the results obtained.

7.1.1 Position Sensing with Hall Effect Proximity Sensors

The Hall effect devices are built into the motor and provide commutation signals once every 120°. Their position is set at manufacture. The power switches used within the amplification unit are then programmed by these sensors to be on or off at each instant during the armature rotation (see Chapter 2). It is conceivable that these Hall effect devices could be used in an alternative modality, whereby the edge of the signal is also of concern. In this case, the Hall effect devices might be used to provide the user with an accurate position update once every 60°. The use of these sensors in this manner does not

provide any special difficulty in the sensing of the signal. Nor indeed does it create a major difficulty in interfacing.

The Hall effect devices switch very accurately at known positions. It may be confirmed on an oscilloscope that this switching action takes place within one encoder increment. The likelihood, however is that despite switching at a finite angle, it will not be precisely 60°. If it is assumed that they do switch precisely once every 60° then a cosine error is likely to result if the sensors are used for position sensing. It will be assumed within this work, that the precise angle at which the Hall effect devices switch can be calibrated before the algorithms are applied. Further, it will be assumed without loss of generality that the sensors within this work switch precisely at 60°.

The state machine discussed in Chapter 3, used in bandwidth reduction of the encoder signal lends itself very well to the measurement of position based on the Hall effect data. This process is briefly reviewed here to illustrate salient differences between the machines. The reader is referred to Chapter 3 for a more thorough treatment of the topic. The Hall effect devices change states according the location of the motor armature. This is illustrated in Figure 7.1.

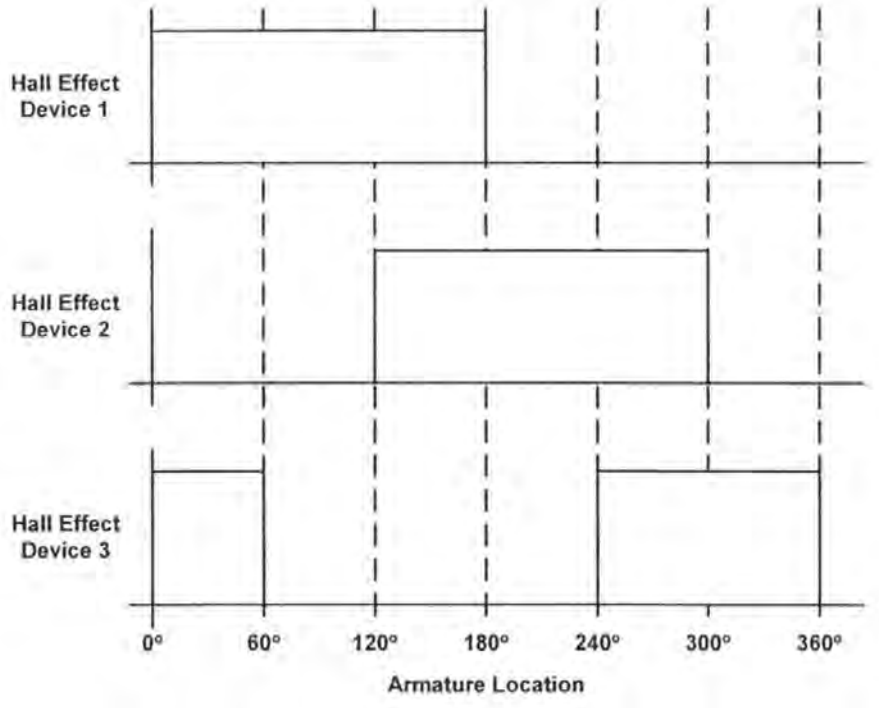

Figure 7.1: *Hall Effect Device Status at Corresponding Armature Position*

If the Hall effect devices are assigned binary values (e.g. HED1=1, HED2=2,HED3=4) then a binary sequence for the Hall effect devices may be derived. Table 7.1 provides the binary representation of the Hall effect device states at each location. Based on the knowledge of the device switching sequence, Figures 3.9 and 3.10 may be extended to accommodate position measurement using the Hall effect devices.

Table 7.1: *Binary Representation of Hall Effect Device States at Various Armature Positions*

Position	30°	90°	150°	210°	270°	330°
Value	5	1	3	2	6	4

The fact that the Hall effect device switching frequency is dependent on the speed of the motor, and not on time elapsed, leads to a case which will be termed within this work as the indeterminate sample frequency. It will be seen over the course of this chapter that this case is ill conditioned, and leads to many problems within the development of

subsequent algorithms. The fictitious example shown in Figure 7.2 illustrates the problem. In the example, the speed of the motor is varying, and it requires varying lengths of time to reach a position whereby the Hall effect device status will change. It should be clear, for example, that $t_1 \neq t_5$ in Figure 7.2. This problem exists within optical encoder feedback, since this device also discretises position. The solution in the case of the encoder is to increase its resolution to ensure the desired accuracy can be obtained. It should therefore also be noted that within this work all of the algorithms are applicable to feedback at higher resolutions than the nominal 60°, and improvements in the accuracy of the algorithms should be expected.

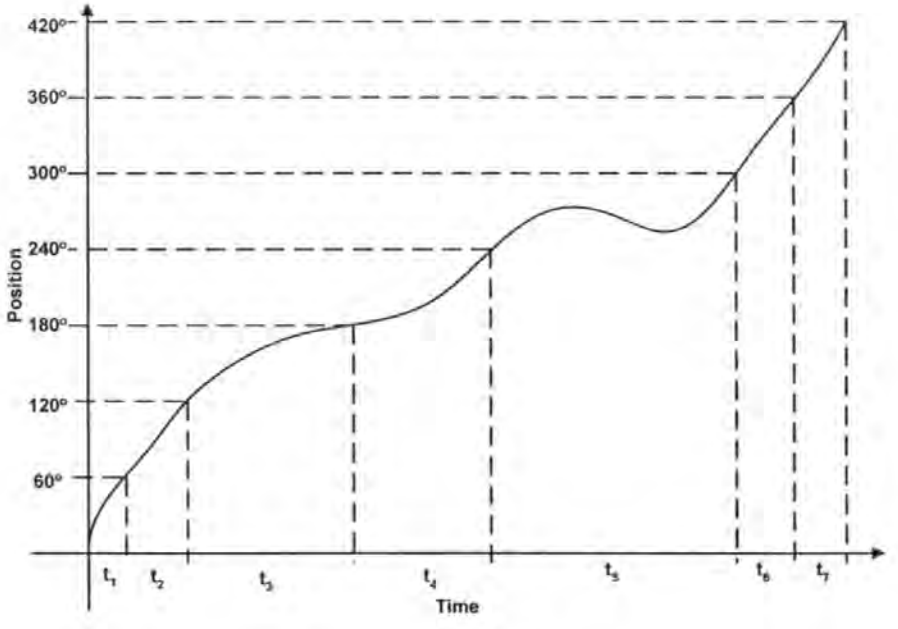

Figure 7.2: *An Illustration of the Indeterminate Sample Frequency Problem*

7.1.2 An Additional Performance Measure

In previous Chapters of this work, several performance measures have been introduced. Most significant to this Chapter are the performance measures of Chapter 4, i.e. the infinity norm, the root mean square of the error and the variance accounted for. Whilst these measures are useful in defining the performance of the system, an additional performance measure is proposed to quantify the smoothness of the estimate with respect to the actual signal. The percentile variance accounted for is once again used but the two signals for comparison are first differentiated. The non-smooth elements of the signals for comparison will be highlighted in their first derivatives, thus the derivative component serves as a high-pass filter. If the model and the plant outputs are not comparable, then the measure is increased. The performance measure is given in (7.1):

$$VAFDT = 100 \cdot \left[1 - \frac{\mathrm{var}\left(\frac{d\hat{y}(t)}{dt} \right)}{\left(\frac{dy(t)}{dt} \right)} \right] \tag{7.1}$$

7.2 Position Control with Stepper Motors

It was discussed in Chapter 2 that the stepper motor is a brushless device that is almost always used without shaft position sensing. The high torque to weight and torque to inertia losses were discussed and the observation that the stepper motor is limited in size, if step accuracy is to be maintained, was made. However, this Chapter considers the use of the synchronous machine without shaft position sensing and the nearest currently available equivalent that exists within current technology is the stepper motor. The objective of this entire work is to formulate a system that is capable of matching currently

available technology. Therefore, consideration to the stepper motor is now paid. The readers attention is drawn immediately to the fact that the synchronous motor maintains advantages over the stepper motor in terms of maximum speed, torque to weight ratio, torque to inertia ratio and torque ripple content. It seems reasonable to suggest that if the equivalent motion control can be achieved with one of the algorithms discussed here, then a system will have been formulated which not only matches, but performs better than currently available equivalent technology.

There are basically three types of stepping motors; variable reluctance, permanent magnet and hybrid. They differ in terms of construction based on the use of permanent magnets and/or iron rotors with laminated steel stators. The common high accuracy stepper motor will provide the user with 200 steps per revolution, or a step angle increment of 1.8°. Stepper motors of higher resolution exist, however, their torque to volume ratio is extremely poor. Lin motors provide a hybrid stepper motor which is capable of a 0.45° step angle, the motor is 44mm in diameter and provides a torque of little over 0.5 Nm. Clearly in small direct drive systems, such as those under discussion here, these motors are unviable design solutions. A further limitation to the stepper motor is its low resonant frequency. When the armature steps from one location to the next it is forced to be held there by magnetic attraction. Since the armature coupled with a load will hold an inertia, the armature frequently overshoots the step position before coming to rest at the equilibrium position. Resonance occurs when the step rate of the armature coincides with the peak overshoot, and in practice leads to a significant reduction in motor torque.

There are options available to improve the step resolution of the motor, however. Half-stepping is a common technique used to improve the motor performance, a technique

referred to as micro-stepping is also available. The micro-stepping technique results in a reduction in motor torque, when the motor is coupled with a frictional load, this technique leads to dead zone within the control. It is therefore essential to minimise all forms of static friction from the load before the micro-stepping technique can be accurately applied. Attempts to apply a micro-stepping technique to a system with lead-screw is considered to be at best optimistic and the technique will not be considered here.

7.2.1 Half-Stepping

Provided that no part of the magnetic circuit is in saturation, exciting two motor windings simultaneously will produce a torque versus position curve that is the sum of the torque versus position curves for the two motor windings taken in isolation. For a two-winding stepper motor, the two curves will be W radians out of phase, and if the currents in the two windings are equal, the peaks and valleys of the sum will be displaced by W/2 radians from the peaks of the original curves, as shown in Figure 7.3. This is the basis of half-stepping. The *two-winding holding torque* is the peak of the composite torque curve when two windings are carrying their maximum rated current (h2). For common two-winding permanent magnet or hybrid stepping motors, the two-winding holding torque will be:

$$h_2 = \sqrt{2} \cdot h_1 \qquad (7.2)$$

where h_1 is the single-winding holding torque This assumes that no part of the magnetic circuit is saturated and that the torque versus position curve for each winding is an ideal sinusoid. If any part of the motor's magnetic circuits is saturated, the two torque curves will not add linearly. As a result, the composite torque will be less than the sum of the

component torques and the equilibrium position of the composite may not be exactly W/2 radians from the equilibrium of the original.

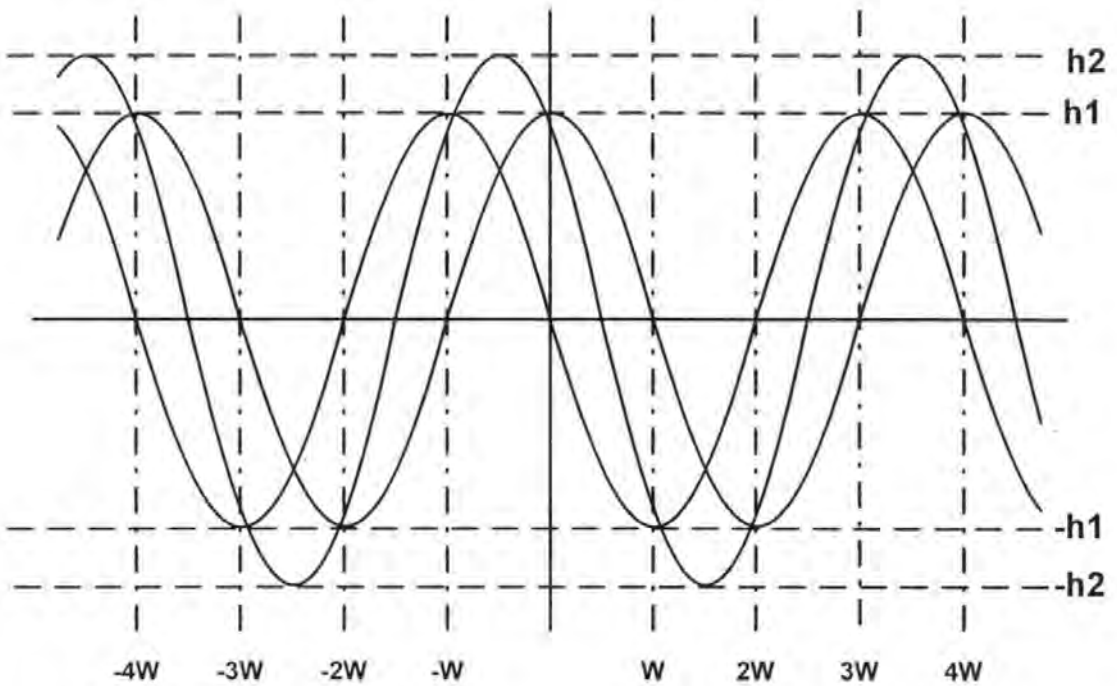

Figure 7.3: *Torque Versus Position Curves for Separately and Simultaneously Exited Windings*

A nominal positioning system will now be described, in which the motor will have selected to provide sufficient torque to actuate the system. The lead screw has a pitch of 1mm. Backlash and hysteretic effects within the system are assumed to be negligible. The stepper motor is assumed to operate at a step increment of 1.8°, which is accurately half-stepped to provide an angle of 0.9° per step increment. This provides an overall resolution for the linear stage of 2.5 microns nominal. This system will be revisited later for comparison with the algorithms derived next within this Chapter.

7.3 The Direct Approach

The first of the approaches, which will be referred to as the direct approach involves the use of the models obtained from Chapter 4. It has already been seen that there exists

disparity between the model and the plant in terms of its performance and is therefore these models are not directly applicable to the accurate estimation of armature position. However, it should be possible, upon a change in the Hall effect device outputs to update the model with a summation of the plant/model residual. It is therefore desirable to find a model with a high VAF measure, since this reflects the tracking accuracy of the system. The infinity norm of the residuals is likely to be high on the first update from the Hall effect devices, however the root mean square of the error should remain low over time. This algorithm uses the fuzzy model based on the power balance equations as the system model and the experimental identification data as the plant. Attention is drawn at this point to the fact that the models developed in Chapter 4 required an identification data set and a separate validation set.

Direct Approach Algorithm

1. Calculate model output, $\theta_{MOD}(k)$
2. Check Hall Effect Devices for change in status
3. If there has been no change go to step 1
4. Calculate new position to get $\mathrm{H}(k)$
5. Calculate residual between model and Hall effect devices,

   $\varepsilon(k) = \mathrm{H}(k) - \theta_{MOD}(k)$
6. Update the model state $\theta_{MOD}(k) = \theta_{MOD}(k) + \varepsilon(k)$

Algorithm 7.1: *The Direct Approach*

The experimental identification data was split into two halves to provide this. In this Chapter the entire identification data set is provided to the algorithms. It should be recognised that the identification data set contains noise and therefore the infinity norm performance measure cannot be fairly compared between the models of Chapter 4 and the algorithms discussed here. The Direct Approach method is given in Algorithm 7.1. Calculation of the Hall effect position is easily achieved, as discussed in §7.1.1. The algorithm was applied to the identification test set, with the additional Hall effect observation stream. Results are illustrated in Figures 7.3-7.5, and tabulated in Table 7.2 at the end of this Chapter. The autocorrelation function of Figure 7.6 indicates that the errors are random and the histogram of Figure 7.5 illustrates a typically Gaussian distribution with zero mean. The direct approach represents the simplest method to be adopted in accurate position estimation and will therefore serve as a benchmark for subsequent methods.

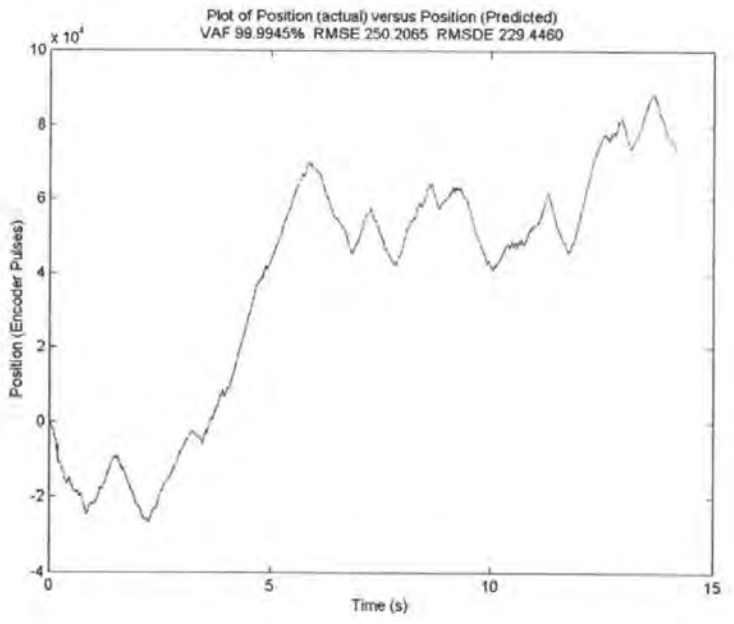

Figure 7.4: *Result of Applying the Direct Approach to the Fuzzy Model*

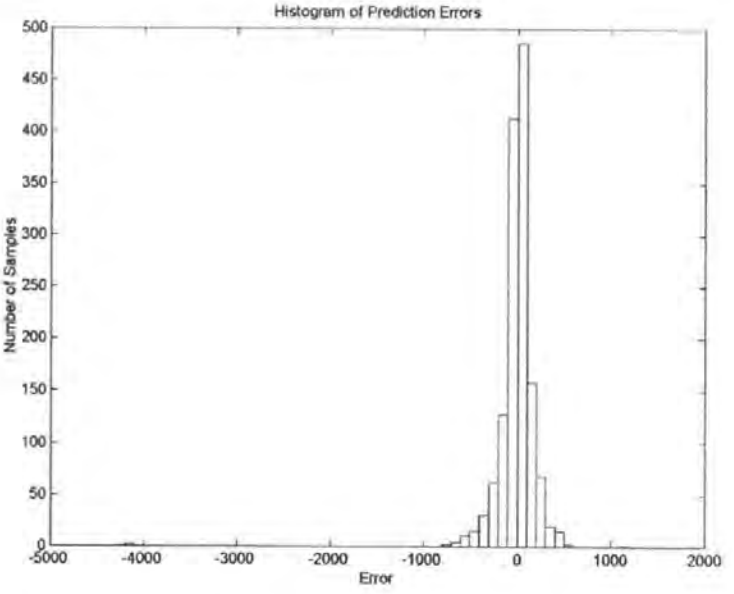

Figure 7.5: *Histogram of Prediction Errors for the Direct Approach*

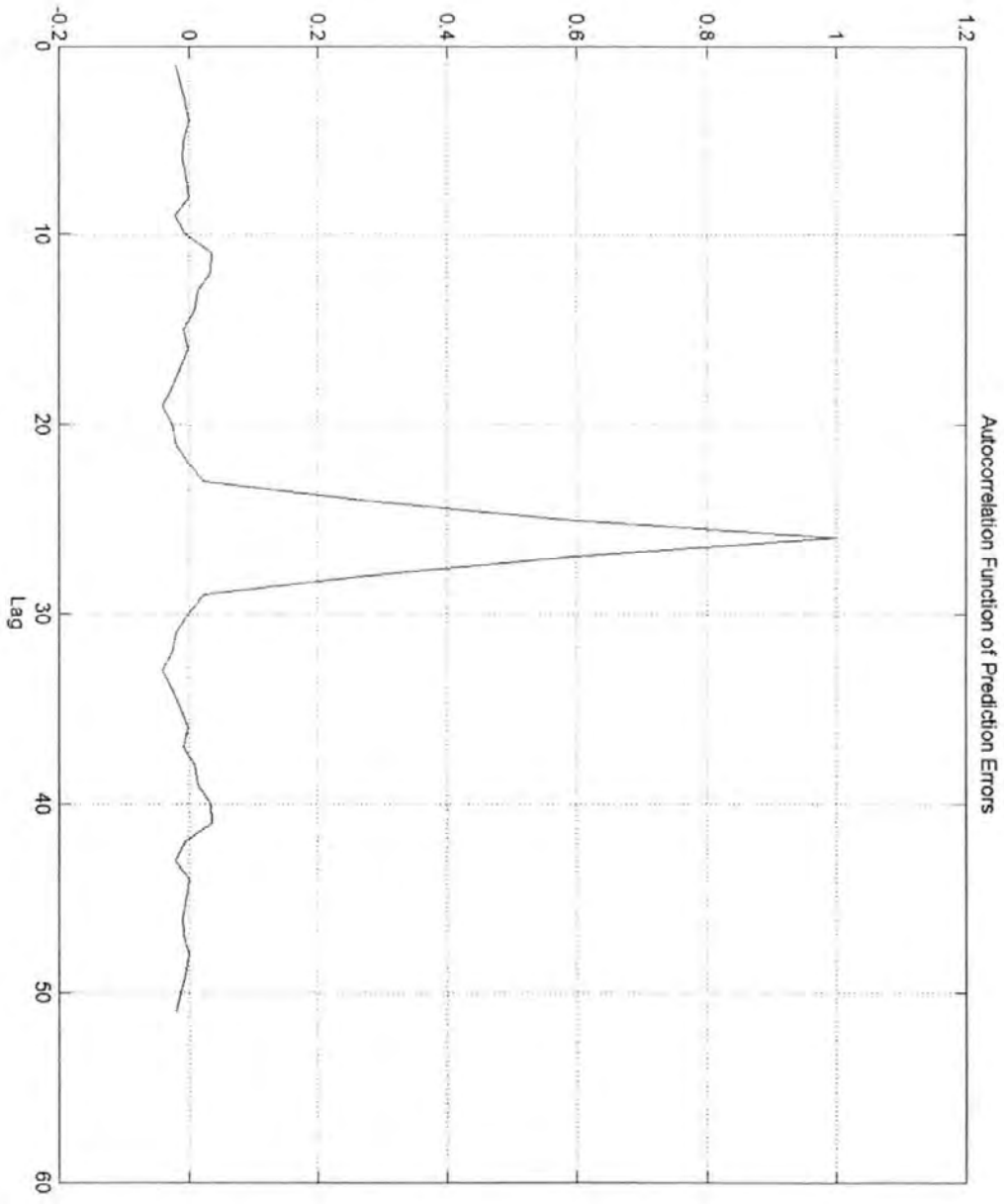

Figure 7.6: *Autocorrelation Function of Prediction Errors*

7.4 Least Squares Estimation

The indeterminate sample frequency problem is a significant hindrance to the implementation of algorithms for which the estimation of position would ordinarily be trivial. Here, the least squares estimation method is discussed, so that an optimal estimate of the time to the next Hall effect device status change can be made. This optimal estimate will be relied upon heavily within the next section to generate an algorithm which will make use of variations in sample frequency.

The basic least squares problem involves the estimation of a quantity $x \in \mathbb{R}^n$ from a vector of linearly related known measurements, $z \in \mathbb{R}^m$.

$$z = Hx + v \tag{7.3}$$

Where the matrix $H \in \mathbb{R}^{m \times n}$, $m \geq n$, and where $v \in \mathbb{R}^m$ is a vector of unknown measurement errors. Using the measurement vector z, an estimate of x, $(\hat{x})$, is desired, such that the sum of the squares of the errors between the actual measurements z and the estimated measurements $H\hat{x}$ is minimised, e.g.

$$J(\hat{x}) = (z - H\hat{x})^{\dagger}(z - H\hat{x}) = v^{\dagger}v = v_1^2 + v_2^2 + v_3^2 + \ldots v_m^2 \tag{7.4}$$

To find the minimum, the partial derivatives of J with respect to each of the elements of $\hat{x}$ are equated to zero

$$\left(\frac{\partial J}{\partial \hat{x}}\right)^{\dagger} = \left[\frac{\partial J}{\partial \hat{x}_1} \quad \frac{\partial J}{\partial \hat{x}_2} \quad \cdots \quad \frac{\partial J}{\partial \hat{x}_n}\right]^T = -H^{\dagger}(z - H\hat{x}) = 0 \tag{7.5}$$

then

$$H^{\dagger}H\hat{x} = H^{\dagger}z \tag{7.6}$$

and therefore

$$\hat{x} = \left(H^{\dagger}H\right)^{-1} H^{\dagger}z \tag{7.7}$$

if H is of full rank, then $H^{\dagger}H$ which is $n \times n$ is of full rank, that is, non-singular. Thus the inverse of $H^{\dagger}H$ exists and the least squares estimate $\hat{x}$ given by equation (7.7) is unique and a minimum. It is a minimum because the matrix of second derivatives of J

$$\frac{\partial^2 J}{d\hat{x}^2} = \frac{\partial}{d\hat{x}}\left(\frac{\partial J}{d\hat{x}}\right) = H^{\dagger}H \tag{7.8}$$

which is symmetric, is positive definite if H is of full rank. Equation (7.7) shows that the least squares estimate $\hat{x}$ is linearly related to the measurements z.

Recursive least squares is an arrangement of the least squares solution in which each new measurement is used to update the previous least squares estimate that was based on previous measurements. Instead of processing all of the measurement data at once, the measurements are processed individually, with each new measurement causing a modification in the current estimate. Least squares estimates are linear transformations of the measurements. The least squares estimate based on the first k+1 measurements can therefore be expressed as a linear transformation of the least squares estimate based on the first k measurements plus a linear correction term based on the $(k+1)^{th}$ measurement alone. The least squares estimate based on k measurements is

$$\hat{x}(k) = \left[H^{\dagger}(k)H(k)\right]^{-1} H^{\dagger}(k)z(k) \tag{7.9}$$

The least squares estimate based on k+1 measurements is

$$\hat{x}(k+1) = \left[H^{\dagger}(k+1)H(k+1)\right]^{-1} H^{\dagger}(k+1)z(k+1) \tag{7.10}$$

Where $H(k+1)$ is $H(k)$ with an additional row $h^{\dagger}(k+1)$

$$H(k+1)=\begin{bmatrix} H(k) \\ h^{\dagger}(k+1) \end{bmatrix} \tag{7.11}$$

and the vector of measurements $z(k+1)$ is the measurement vector $z(k)$ with one additional scalar measurement z_{k+1}.

$$z(k+1)=\begin{bmatrix} z(k) \\ z_{k+1} \end{bmatrix} \tag{7.12}$$

Then

$$\begin{aligned} H^{\dagger}(k+1)H(k+1) &= \begin{bmatrix} H^{\dagger}(k) & h(k+1) \end{bmatrix}\begin{bmatrix} H(k) \\ h^{\dagger}(k+1) \end{bmatrix} \\ &= H^{\dagger}(k)H(k)+h(k+1)h^{\dagger}(k+1) \end{aligned} \tag{7.13}$$

Defining

$$P(k)=\left[H^{\dagger}(k)H(k)\right]^{-1} \tag{7.14}$$

Gives

$$\begin{aligned} P(k+1) &= \left[H^{\dagger}(k+1)H(k+1)\right]^{-1} \\ &= \left[H^{\dagger}(k)H(k)+h(k+1)h^{\dagger}(k+1)\right]^{-1} \\ &= \left[P^{-1}(k)+h(k+1)h^{\dagger}(k+1)\right]^{-1} \end{aligned} \tag{7.15}$$

Relation (7.15) is in a form for which the matrix inversion lemma (see notes) applies. Using the matrix inversion lemma on equation (7.15) gives

$$P(k+1)=P(k)-\frac{P(k)h(k+1)h^{\dagger}(k+1)P(k)}{1+h^{\dagger}(k+1)P(k)h(k+1)} \tag{7.16}$$

which is an update equation for $P(k+1)$ in terms of $P(k)$ and the next measurement equation coefficients, $h(k+1)$. Defining

$$\delta(k+1) = 1 + h^{\dagger}(k+1)P(k)h(k+1) \tag{7.17}$$

$$\kappa(k+1) = P(k)h(k+1)\delta^{-1}(k+1) \tag{7.18}$$

gives an update equation of

$$\begin{aligned} P(k+1) &= P(k) - P(k)h(k+1)\delta^{-1}(k+1)h^{\dagger}(k+1)P(k) \\ &= \left[I - \kappa(k+1)h^{\dagger}(k+1)\right]P(k) \end{aligned} \tag{7.19}$$

The least squares estimate at step k+1 is

$$\hat{x}(k+1) = P(k+1)H^{\dagger}(k+1)z(k+1) \tag{7.20}$$

and after some manipulation, (7.20) becomes

$$\hat{x}(k+1) = \hat{x}(k) + \kappa(k+1)\left[z_{k+1} - h^{\dagger}(k+1)\hat{x}(k)\right] \tag{7.21}$$

The least squares estimate $\hat{x}(k+1)$ based on $k+1$ measurements is the estimate $\hat{x}(k)$ based on k measurements plus a gain

$$\kappa(k+1) = P(k)h(k+1)\delta^{-1}(k+1) \tag{7.22}$$

multiplied by the difference between the new measurement and the predicted measurement

$$h^{\dagger}(k+1)\hat{x}(k) \tag{7.23}$$

based on the previous estimate. These equations for recursive least squares estimation are collected in Algorithm 7.2.

Recursive Least Squares Estimation

Initialisation

$$P(n)=\left[H^{\dagger}(n)H(n)\right]^{-1}, \qquad \hat{x}(n)=P(n)H^{\dagger}(n)z(n)$$

Where

$$H(n)=\left[h^{\dagger}(1) \quad \dots \quad h^{\dagger}(n)\right]^{T}, \qquad z(n)=\left[z_1 \quad \dots \quad z_n\right]^{T}$$

Corrector gain

$$\delta(k+1)=h^{\dagger}(k+1)P(k)h(k+1)+1$$
$$\kappa(k+1)=P(k)h(k+1)\delta^{-1}(k+1)$$
$$P(k+1)=\left[I-\kappa(k+1)h^{\dagger}(k+1)\right]P(k)$$

Predictor-Corrector

$$\hat{x}(k+1)=\hat{x}(k)+\kappa(k+1)\left[z_{k+1}-h^{\dagger}(k+1)\hat{x}(k)\right]$$

Algorithm 7.2: *Recursive Least Squares Approximation*

7.5 The Discrete Approximations Approach

Previous Chapters have dealt with the derivation of relatively complex models of the system. In all cases these models were based on continuous time. The approach proposed here works on the assumption that a state space or fuzzy model can be converted into a discrete equivalent. It will also be assumed, as in the direct approach, that position estimations from the model can be updated upon change in status by the Hall effect devices. Since the conversion to the discrete time has been made, it is possible to take samples from the model at a different sample frequency to the plant. The principal of the approach here is to estimate the length of time it will take to reach the next

transition in the Hall effect devices. In addition, the estimated length of time for the model to reach the equivalent position is calculated. With knowledge of these two values it is possible to vary the apparent model sample frequency, whilst sampling the plant at a constant frequency, so that the model and plant arrive at the Hall effect transition position simultaneously. This should reduce the first derivative component error between the plant and the model. The theory of converting to the discrete time is briefly reviewed before the approach is applied.

Consider the nominal system described by

$$\dot{x}(t) = Ax(t) + Bu(t) \tag{7.24}$$

$$y(t) = Cx(t) + Du(t) \tag{7.25}$$

The discrete time representation of the system is given according to

$$x(k+1) = \Lambda(T)x(k) + \Gamma(T)u(k) \tag{7.26}$$

noting that the discrete time matrices Λ and Γ depend on the sample frequency T. When the sample period is fixed, Λ and Γ are constant. In order to determine the matrices Λ and Γ, the convolution integral given by

$$x(t) = e^{At}x(0) + \int_0^t e^{A(t-\tau)}Bu(\tau)d\tau \tag{7.27}$$

is used as the solution to (7.24). It is assumed that the input $u(t)$ is sampled and fed into a zero order hold, so that it is constant between samples. Since

$$x(k+1) = e^{A(k+1)T}x(0) + e^{A(k+1)T}\int_0^{(k+1)T} e^{-A\tau}Bu(\tau)d\tau \tag{7.28}$$

and

$$x(k) = e^{AkT}x(0) + e^{AkT}\int_0^{kT} e^{-A\tau}Bu(\tau)\,d\tau \tag{7.29}$$

multiplication of (7.29) by e^{AT} and subtraction of the result from (7.28) gives

$$x\big((k+1)T\big) = e^{AT}x(kT) + e^{A(k+1)T}\int_{kT}^{(k+1)T} e^{-A\tau}Bu(\tau)\,d\tau \tag{7.30}$$

Since by assumption

$$u(t) = u(kT) \qquad kT \le t < kT + T \tag{7.31}$$

the constant $u(\tau) = u(kT)$ may be substituted into equation (7.30). If the variable λ is introduced as $\lambda = T - t$, then it may be written that

$$\begin{aligned} x\big((k+1)T\big) &= e^{AT}x(kT) + e^{AT}\int_0^{T} e^{-At}Bu(kT)\,dt \\ &= e^{AT}x(kT) + \int_0^{T} e^{A\lambda}Bu(kT)\,d\lambda \end{aligned} \tag{7.32}$$

By defining

$$\Lambda(T) = e^{AT} \tag{7.33}$$

$$\Gamma(T) = \left(\int_0^{T} e^{A\lambda} \quad d\lambda\right)B \tag{7.34}$$

equation (7.32) may be rewritten as

$$x\big((k+1)T\big) = \Lambda(T)x(kT) + \Gamma(T)u(kT) \tag{7.35}$$

which is of course identical to (7.26). Referring to equation (7.25), the output equation becomes

$$y(kT) = Cx(kT) + Du(kT) \tag{7.36}$$

matrices C and D are constant and do not depend on the sample period T. This approach will now yield the state output at the discrete sampling instant. The output between sample instants is desired and the approach discussed can be easily modified to facilitate this. Using the system given in (7.24) and (7.25), and starting with the initial state $x(t_0)$, the solution to the system is once again given by the convolution integral

$$x(t) = e^{A(t-t_0)}x(t_0) + \int_{t_0}^{t} e^{A(t-\tau)}Bu(\tau)\,d\tau \tag{7.37}$$

The time response of the system is desired at $t = kT + \Delta T$, given $0 < \Delta T < T$. Defining $t = kT + \Delta T$, $t_0 = kT$ and as before $u(\tau) = u(kT)$, the solution of $x(t)$ is then given by

$$\begin{aligned} x(kT+\Delta T) &= e^{A\Delta T}x(kT) + \int_{kT}^{kT+\Delta T} e^{A(kT+\Delta T-\tau)}Bu(kT)\quad d\tau \\ &= e^{A\Delta T}x(kT) + \int_{0}^{\Delta T} e^{A\lambda}Bu(kT)\quad d\lambda \end{aligned} \tag{7.38}$$

given $\lambda = kT + \Delta T - \tau$. Using the definitions (7.33), (7.34) and using (7.26),

$$x(kT+\Delta T) = \Lambda(\Delta T)x(kT) + \Gamma(\Delta T)u(kT) \tag{7.39}$$

the system output can be expressed as

$$\begin{aligned} y(kT+\Delta T) &= Cx(kT+\Delta T) + Du(kT) \\ &= C\Lambda(\Delta T)x(kT) + \left[C\Gamma(\Delta T) + D\right]u(kT) \end{aligned} \tag{7.40}$$

Therefore, the values of the system output, or system states can be computed at any time between sampling instants by calculating the values of $\Lambda(\Delta T)$ and $\Gamma(\Delta T)$ for various values of ΔT. The system is known to maintain a finite sample frequency. Additionally, at an indeterminate time, the Hall effect devices will be able to provide an update on the

system position, as seen in the direct approach. The difficulty associated with the direct approach is the non-smooth response during the update.

The time taken for the model to reach the next Hall effect switching position can be very simply calculated using the speed state ω and the position state θ from the model. Given the current Hall effect position, H, and the magnitude of the Hall effect increment ΔH (constant), the following expression provides an estimate of the time taken to reach the next transition

$$T_{sw} = \frac{\left|\theta - (\mathrm{H} + \Delta\mathrm{H})\right|}{\omega} \tag{7.41}$$

such that

$$\mathrm{H} < \theta < \mathrm{H} + \Delta\mathrm{H} \tag{7.42}$$

Clearly, when ω is at a low speed, T_{sw} will be very large and the sample frequency ΔT_P should be used for the model in such instances. Based on the previous times at which the Hall effect devices have changed state, it is possible to produce a recursive least squares estimate of when the next switch time is likely to occur, T_{HED}. The probability of T_{sw} being equal to T_{HED} is very low since the model is not ideal. In general, the model will reach the position which corresponds to a change in the Hall effect devices, either before or after the plant. Since the discretisation procedure given above does not stipulate a constant value of ΔT, it makes an intuitively appealing proposition to adjust ΔT such that the plant and model reach the next Hall effect switching position simultaneously. Given a fixed sample frequency for the plant, ΔT_P, the equation for the model sample frequency is given simply as

$$\Delta T_M = \Delta T_P + \frac{\Delta T_P \left(T_{SW} - T_{HED} \right)}{T_{HED}} \tag{7.43}$$

Thus ΔT_M will vary around ΔT_P. The results of applying the algorithm are illustrated and tabulated in Figure 7.7 and Table 7.2 respectively. The method is described in Algorithm 7.3. The algorithm uses the recursive least mean squared estimation procedure from §7.4. A simple windowing function is used to obtain the set of most recent samples.

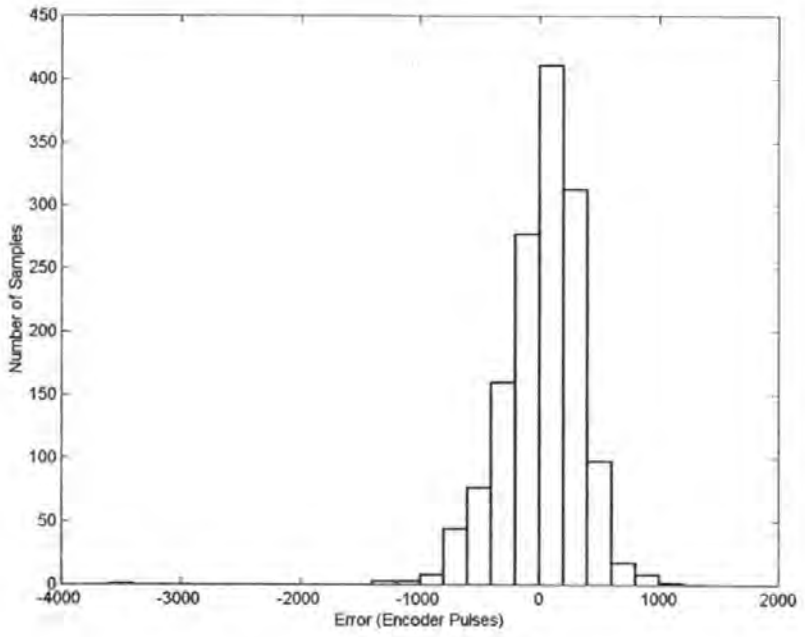

Figure 7.7: *Histogram of Errors produced by Discrete Approximations Approach*

Discrete Approximations Approach Algorithm

1. Calculate model output, $\theta_{MOD}(k)$ and model speed, $\omega_{MOD}(k)$
2. Increase k by ΔT_M
3. If there has been no change keep the current value of T_{HED}, go to 1
4. Calculate new position to get $\theta_{HED}(k)$
5. Calculate residual between model and Hall effect devices,
   $\varepsilon(k) = \mathrm{H}(k) - \theta_{MOD}(k)$
6. Update the model state $\theta_{MOD}(k) = \theta_{MOD}(k) + \varepsilon(k)$
7. Calculate $T_{sw} = \dfrac{|\theta - (\mathrm{H} + \Delta\mathrm{H})|}{\omega}$,
   $T_{HED}(k+1) = T_{HED} + \kappa(k+1)\left[z_{k+1} - h^{\dagger}(k+1)T_{HED}(k)\right]$
8. $\Delta T_M = \Delta T_P + \dfrac{\Delta T_P (T_{SW} - T_{HED})}{T_{HED}}$, Go to Step 1

Algorithm 7.3: *Discrete Approximations Approach Algorithm*

7.6 Kalman Filter with Stirling Interpolation

The celebrated Kalman filter and its several extensions have without doubt been the most used and successful state estimators over the past thirty years. However, their use is contingent on the availability of the required derivatives, and the assumption that they can be obtained with reasonable effort. In the case of this work, as it has already been seen, samples between Hall effect devices are not available, and the derivative does not exist. It makes sense to recast the Kalman filter in a new light and rather than using the

derivative of the covariance matrix, one should attempt to interpolate the covariance matrix using a divided differences scheme. Derivative free Kalman filters and the unscented Kalman filter are recent advances in the field of state estimation. They have been developed because the Kalman filter uses a Taylor series approximation to the derivative, and significant bias or convergence problems have been encountered. It follows that since through use of a polynomial, a certain amount of extrapolation is possible, that observations do not need to be available at each sample. There are many examples of such extensions to the Kalman filter available in the text, for instance Julier and Uhlmann (1994), Ito and Xiong (2000), Norengaard *et al* (2000). The filter realisation proposed by Norengaard *et al* (2000) is particularly attractive since it is also reported to work with observation streams operating at different sample frequencies. The reader is referred to the paper for the derivation of the filter and only those equations which are essential to the algorithm are considered here.

7.6.1 Review of State Estimation for Nonlinear Systems

The complete derivation of the Kalman filter may be found in Appendix D, Part 1. Here, the techniques are reviewed for subsequent development. The nominal system is given as

$$x(k+1) = f(x(k), u(k), v(k)) \tag{7.44}$$

$$y(k) = g(x(k), w(k)) \tag{7.45}$$

$v(k)$ and $w(k)$ are typically assumed to be Gaussian with zero mean and uncorrelated with current and past states. The conditional expectations of the state and covariance matrix are sought, e.g.

$$\bar{x}(k) = \mathrm{E}\left[x(k) \middle| Y^{k-1}\right] \tag{7.46}$$

$$\bar{P}(k) = \mathrm{E}\left[\left(x(k)-\bar{x}(k)\right)\left(x(k)-\bar{x}(k)\right)^T \middle| Y^{K-1}\right] \tag{7.47}$$

where Y^{k-1} is a matrix of previous measurements,

$$Y^{k-1} = \begin{bmatrix} y_0 & y_1 & \cdots & y_{k-1} \end{bmatrix}^T \tag{7.48}$$

It is often the case that the measurement (*a posteriori*) update of the state estimate is restricted to be linear, for the sake of convenience. Selection of the update so that the covariance of the estimation error is minimised, yields the following

$$K_k = P_{xy}(k) P_y^{-1}(k) \tag{7.49}$$

$$\hat{x}_k = \bar{x}_k + K_k\left[y_k - \bar{y}_k\right] \tag{7.50}$$

where

$$\bar{y}_k = \mathrm{E}\left[y_k \middle| Y^{k-1}\right]$$

$$P_{xy}(k) = \mathrm{E}\left[\left(x_k-\bar{x}_k\right)\left(y_k-\bar{y}_k\right)^T \middle| Y^{k-1}\right] \tag{7.51}$$

$$P_y(k) = \mathrm{E}\left[\left(y_k-\bar{y}_k\right)\left(y_k-\bar{y}_k\right)^T \middle| Y^{k-1}\right] \tag{7.52}$$

$$\hat{P}(k) = \mathrm{E}\left[\left(x_k-\hat{x}_k\right)\left(x_k-\hat{x}_k\right)^T \middle| Y^{k}\right] = \bar{P}(k) - K_k P_{yy}(k) K_k^T \tag{7.53}$$

As the various expectations are generally intractable, one form of approximation or another is generally used. For instance, it is well known that the extended Kalman filter is based on Taylor linearisation of the state transition and the output equations.

7.6.2 The Kalman Filter with Sterling's Interpolation

The Kalman filter reported in Norengaard *et al* (2000) makes use of a divided differences scheme to obtain the covariance matrices. The divided difference equations are given here for subsequent reference in the algorithm description

$$S_{x\hat{x}}^{(1)}(k)=\left\{\left(f_i\left(\hat{x}_k+h\hat{s}_{x,j},u_k,\bar{v}_k\right)-f_i\left(\hat{x}_k-h\hat{s}_{x,j},u_k,\bar{v}_k\right)\right)/2h\right\} \tag{7.54}$$

$$S_{xv}^{(1)}(k)=\left\{\left(f_i\left(\hat{x}_k,u_k,\bar{v}_k+h\hat{s}_{v,j}\right)-f_i\left(\hat{x}_k,u_k,\bar{v}_k-h\hat{s}_{x,j}\right)\right)/2h\right\} \tag{7.55}$$

$$S_{y\bar{x}}^{(1)}(k)=\left\{\left(g_i\left(\bar{x}_k+h\bar{s}_{x,j},\bar{w}_k\right)-g_i\left(\bar{x}_k-h\bar{s}_{x,j},\bar{w}_k\right)\right)/2h\right\} \tag{7.56}$$

$$S_{yw}^{(1)}(k)=\left\{\left(g_i\left(\bar{x}_k,\bar{w}_k+hs_{w,j}\right)-g_i\left(\bar{x}_k,\bar{w}_k-h\bar{s}_{w,j}\right)\right)/2h\right\} \tag{7.57}$$

$$S_{x\hat{x}}^{(2)}(k)=\left\{\frac{\sqrt{h^2-1}}{2h^2}\left(f_i\left(\hat{x}_k+h\hat{s}_{x,j},u_k,\bar{v}_k\right)+f_i\left(\hat{x}_k-h\hat{s}_{x,j},u_k,\bar{v}_k\right)-2f_i\left(\hat{x}_k,u_k,\bar{v}_k\right)\right)\right\} \tag{7.58}$$

$$S_{x\hat{x}}^{(2)}(k)=\left\{\frac{\sqrt{h^2-1}}{2h^2}\left(f_i\left(\hat{x}_k,u_k,\bar{v}_k+hs_{v,j}\right)+f_i\left(\hat{x}_k,u_k,\bar{v}_k-hs_{v,j}\right)-2f_i\left(\hat{x}_k,u_k,\bar{v}_k\right)\right)\right\} \tag{7.59}$$

$$S_{y\bar{x}}^{(2)}(k)=\left\{\frac{\sqrt{h^2-1}}{2h^2}\left(g_i\left(\bar{x}_k+h\bar{s}_{x,j},\bar{w}_k\right)+g_i\left(\bar{x}_k-h\bar{s}_{x,j},\bar{w}_k\right)-2g_i\left(\bar{x}_k,\bar{w}_k\right)\right)\right\} \tag{7.60}$$

$$S_{y\bar{x}}^{(2)}(k)=\left\{\frac{\sqrt{h^2-1}}{2h^2}\left(g_i\left(\bar{x}_k,\bar{w}_k+h\bar{s}_{w,j}\right)+g_i\left(\bar{x}_k,\bar{w}_k-h\bar{s}_{w,j}\right)-2g_i\left(\bar{x}_k,\bar{w}_k\right)\right)\right\} \tag{7.61}$$

The a posteriori Filter update

Consider an augmented state vector consisting of state vector and process measurement noise:

$$\breve{x}=\left[\begin{matrix}\bar{\bar{x}}+\Delta\breve{x}\end{matrix}\right]=\begin{bmatrix}\hat{x}+\Delta x\\ \bar{v}+\Delta v\end{bmatrix} \tag{7.62}$$

Since the process noise is assumed to be independent of the state, the conditional covariance of $\Delta\tilde{x}$ is

$$\hat{P}_{\tilde{x}} = \begin{bmatrix} \hat{P} & 0 \\ 0 & Q \end{bmatrix} = \begin{bmatrix} \hat{S}_x & 0 \\ 0 & S_v \end{bmatrix} \begin{bmatrix} \hat{S}_x & 0 \\ 0 & S_v \end{bmatrix}^T = \hat{S}_{\tilde{x}} \hat{S}_{\tilde{x}}^T \tag{7.63}$$

The state estimate can be given by

$$\begin{aligned} \bar{x}_{k+1} = & \frac{h^2 - n_x - n_v}{h^2} f\left(\hat{x}_k, u_k, \bar{v}_k\right) \\ & + \frac{1}{2h^2} \sum_{p=1}^{n_x} f\left(\hat{x}_k + h\hat{s}_{x,p}, u_k, \bar{v}_k\right) + f\left(\hat{x}_k - h\hat{s}_{x,p}, u_k, \bar{v}_k\right) \\ & + \frac{1}{2h^2} \sum_{p=1}^{n_x} f\left(\hat{x}_k, u_k, \bar{v}_k + h\hat{s}_{v,p}\right) + f\left(\hat{x}_k, u_k, \bar{v}_k - h\hat{s}_{v,p}\right) \end{aligned} \tag{7.64}$$

As the basis of the covariance update, the following shall be used

$$\bar{P}(k+1) = \left[S_{x\hat{x}}(k) S_{xv}(k)\right]\left[S_{x\hat{x}}(k) S_{xv}(k)\right]^T \tag{7.65}$$

a factored update of the covariance matrix is introduced using the following compound matrix

$$\bar{S}_x(k+1) = \left[S_{x\hat{x}}^{(1)}(k) \quad S_{xv}^{(1)}(k) \quad S_{x\hat{x}}^{(2)}(k) \quad S_{xv}^{(2)}(k)\right] \tag{7.66}$$

The a-priori Filter update

The a priori estimate of the output is calculated in a similar fashion as for the states

$$\begin{aligned} \bar{y}_k = & \frac{h^2 - n_x - n_w}{h^2} g\left(\bar{x}_k, \bar{w}_k\right) \\ & + \frac{1}{2h^2} \sum_{p=1}^{n_w} g\left(\bar{x}_k + h\bar{s}_{x,p}, \bar{w}_k\right) + g\left(\bar{x}_k - h\bar{s}_{x,p}, \bar{w}_k\right) \\ & + \frac{1}{2h^2} \sum_{p=1}^{n_w} g\left(\bar{x}_k, \bar{w}_k + h\bar{s}_{x,p}\right) + g\left(\bar{x}_k, \bar{w}_k - h\bar{s}_{x,p}\right) \end{aligned} \tag{7.67}$$

and

$$S_y(k) = \left[S_{y\bar{x}}^{(1)}(k) \quad S_{yw}^{(1)}(k) \quad S_{y\bar{x}}^{(2)}(k) \quad S_{yw}^{(2)}(k)\right] \tag{7.68}$$

n_w indicates the dimension of the measurement noise vector. The a priori cross covariance matrix is given by

$$P_{xy}(k) = \bar{S}_x(k) S_{y\bar{x}}(k)^T \tag{7.69}$$

The Kalman gain and the a posteriori update may be carried out according to (7.49) and (7.50), with (7.49) rewritten

$$K_k = P_{xy}(k)\left[S_y(k) S_y(k)^T \right]^{-1} \tag{7.70}$$

The covariance matrix may be written

$$\hat{P} = \left(\bar{S}_x - KS_{yx}^{(1)}\right)\left(\bar{S}_x - KS_{yx}^{(1)}\right)^T + KS_{yw}^{(1)}\left(KS_{yw}^{(1)}\right)^T + KS_{yx}^{(2)}\left(KS_{yx}^{(2)}\right)^T + KS_{yw}^{(2)}\left(KS_{yw}^{(2)}\right)^T \tag{7.71}$$

which has the Cholesky factor

$$\hat{S}_x(k) = \left[\bar{S}_x(k) - K_k S_{yx}^{(1)}(k) \quad K_k S_{yw}^{(1)}(k) \quad K_k S_{yx}^{(2)}(k) \quad K_k S_{yw}^{(2)}(k) \right] \tag{7.72}$$

7.6.3 Results

The filter algorithm discussed above was applied directly to the data. A fuzzy model, who's output is available at every sample was used as the first observation stream with the Hall effect data used as the second. Clearly the Hall effect data is not available at every sample, but is expected to be significantly more accurate than the model. The initial covariance matrices were therefore initialised to reflect this

The results of applying the filter are shown in Figure 7.8, clearly the results do not compare favourably to the direct approach discussed as the benchmark position estimator. The problem occurs because the fuzzy model tends to be trusted more highly between Hall effect device switches, and because the Hall effect devices do not switch often

enough. Despite the apparently poor performance of this filter, it is computationally less expensive than the Kalman or Extended Kalman Filter. It has in addition been shown to outperform either of these approaches. It is poor observation data which causes this performance. The filter is provided with the output of the direct approach algorithm in attempt to provide enhanced information to the filter and the output of the fuzzy model.

Filter Algorithm

1. Initialise $\bar{x}_0$, $\bar{P}(0), k=0$
2. Compute $\bar{y}_k, S_{y\bar{x}}^{(2)}(k), S_{yw}^{(2)}(k)$
3. Compute P_{xy} according to $P_{xy}(k)=\bar{S}_x(k)\left(S_{y\bar{x}}(k)\right)^T$ and perform householder triangularisation on (7.68)
4. Solve $K_k\left[\bar{S}_y(k)S_y(k)\right]^T=P_{xy}$ for the Kalman gain. Since S_y is square and triangular only forward and back substitutions are needed: first solve for $k':k'S_y^T=P_{xy}$ and then solve for $K_k: K_kS_y=k'$.
5. *A posteriori* update of the state estimate $\hat{x}_k=\bar{x}_k+K_k\left(y_k-\bar{y}_k\right)$
6. *A posteriori* update of the covariance matrix factor, $\hat{S}_x(k)$, is performed using Householder triangularisation on (7.72)
7. Determine $\bar{x}_{k+1}, S_{x\bar{x}}(k+1), S_{xw}(k+1)$
8. Use Householder triangularisation on (7.66) to compute $\bar{S}_x(k)$
9. $k=k+1$, go to step 2.

Algorithm 7.4: *Kalman Filter with Sterling Interpolation*

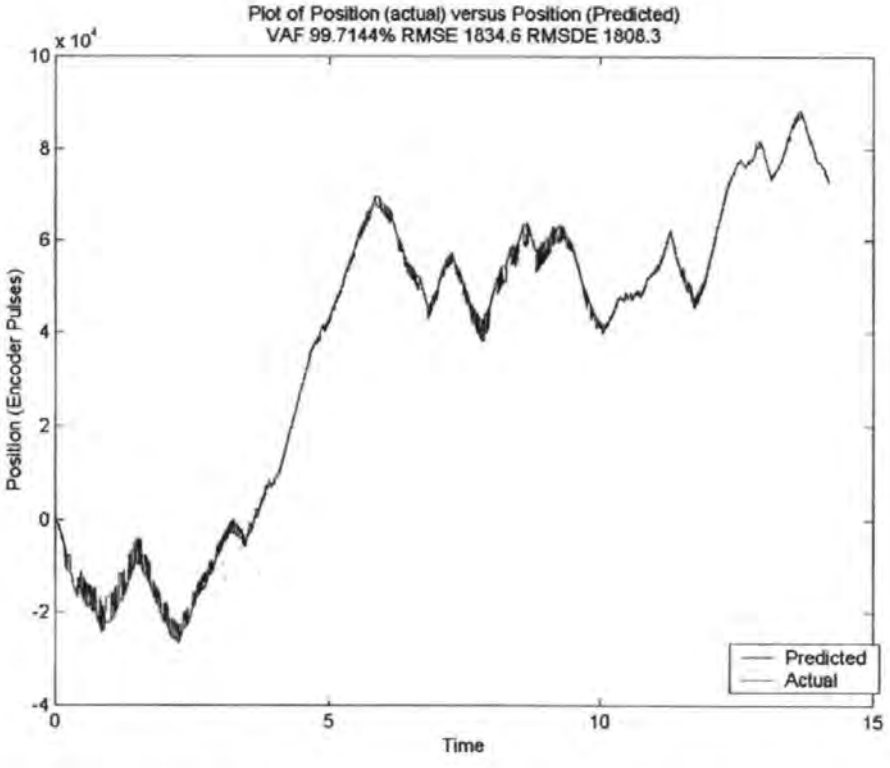

Figure 7.8: *Filter Application to Hall Effect Devices and Fuzzy Model*

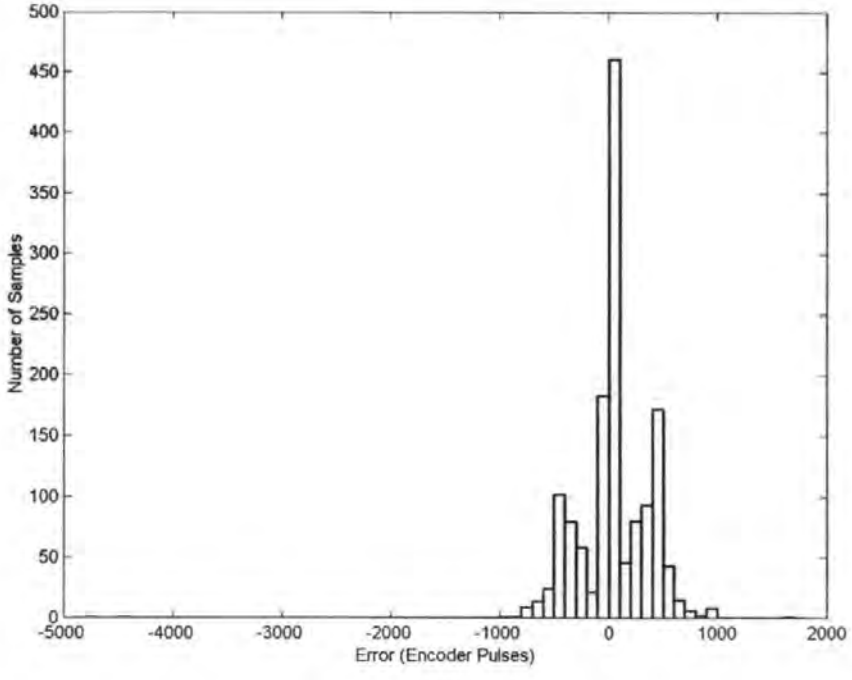

Figure 7.9: *Histogram of Filter Prediction Errors*

It can clearly be observed that the VAF and the RMS measures of the error are worse than the direct approach results. This is due to the state space model which is used within the filter and has a small effect on the accuracy. However, a significant drop in the VAFDE measure, due to the smoothing effect of the filter, has been observed. The implication of this latter result is that the speed estimate of the filter is very close to actual.

7.7 Model Based Fuzzy Sliding Mode Control

Model based sliding mode control was discussed in the previous Chapter. It was demonstrated that the plant could be forced to follow a model perfectly using the theories supporting the sliding mode. A model based on the PBEREG structure of Chapter 4 is used in conjunction with the fuzzy linearisation procedure of Chapter 6, in order to simultaneously provide an estimate of the current location of the armature and provide estimates of the system dynamics, from which controller gains are derived. As in the direct approach discussed above, the Hall effect devices are used to update the model position. Finally, a PID controller is introduced to define the controller performance. The overall system is shown in Figure 7.10

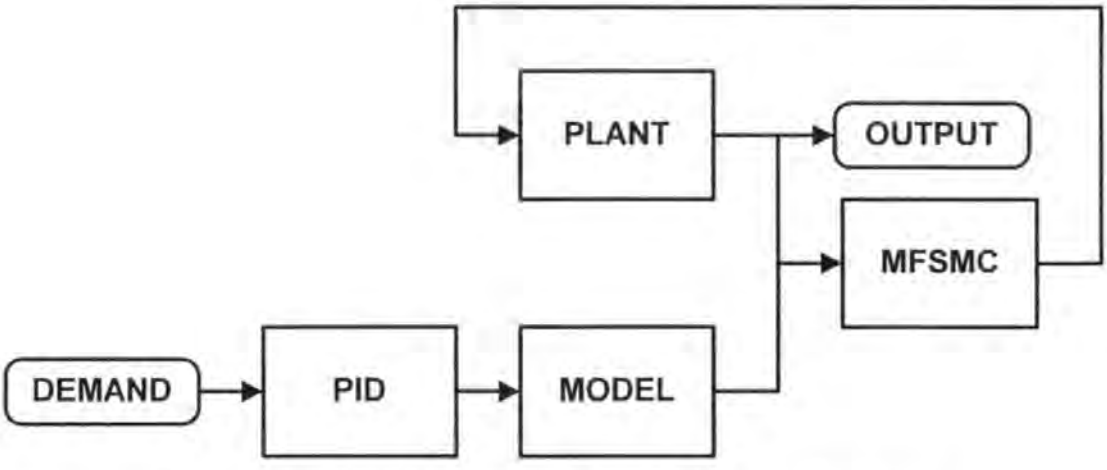

Figure 7.10: *Model Following Sliding Mode Controller System*

Since this algorithm requires that the plant interact with the rest of the system, use of the by now standard identification data set is not possible. For this reason, a purely simulation based study of the following algorithm must be made. Although this is not the ideal case, the use of the PBEREG model has been seen to provide an extremely good approximation to the actual system. Since in addition to this model, a fuzzy model for use within the controller is required, the less accurate fuzzy model based on the voltage and current regressors is also used to provide estimates of the plant dynamics. The nominal state space model is used within the system to provide the states to be followed.

In the last Chapter, the concept of model following was introduced, and the ramifications of the sliding mode model following controller meeting the invariance conditions discussed. To reiterate, the implication of the invariance conditions is that given a plant, it may be forced to follow a model perfectly, rejecting all errors between the model and plant. The assumption, for these conditions to hold, is that the plant is perfectly known. In reality, as has been discussed throughout this work, this is simply not the case. The performance of the model following controller is therefore directly effected by the final

accuracy of the plant model. The first task within the development of this algorithm is therefore to develop a controller which will be capable of adapting to estimated changes in the plant dynamics. A fuzzy model will be used, as in the case of the adaptive sliding mode controller with integral action, to provide these estimates in plant dynamics.

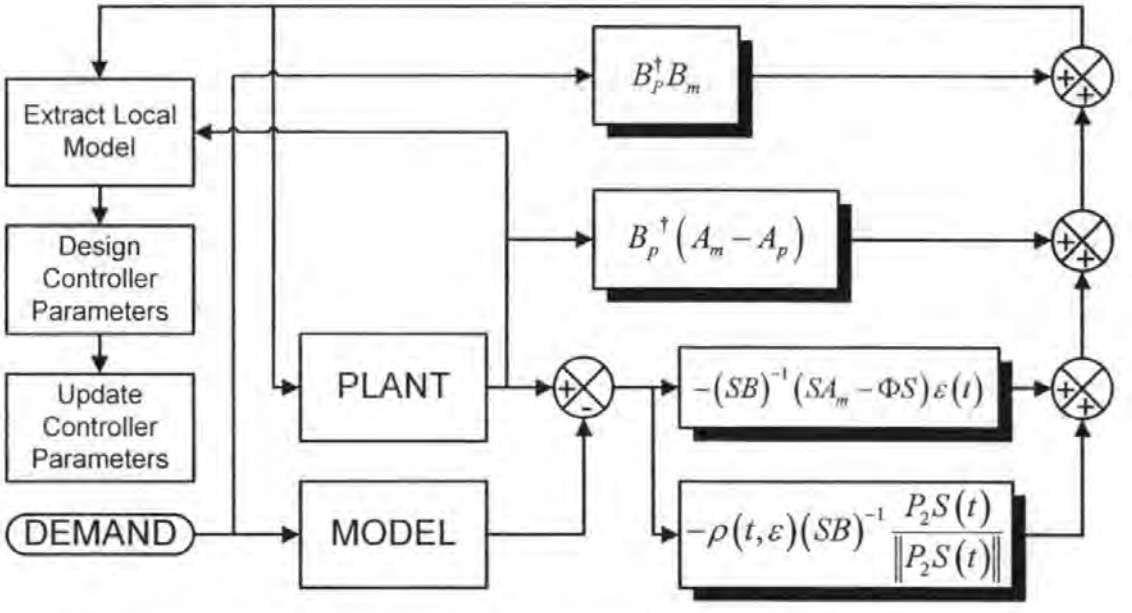

Figure 7.11: *Model Following Sliding Mode Controller Signal Flow Diagram*

Those boxes shown shadowed in Figure 7.11 correspond to the controller gains which are updated by the "update controller parameters" block at each iteration. For a discussion of the controller gains the reader should refer to Chapter 6. In the following, it will be demonstrated that an imperfectly known plant will generate error within the model following control system. After that, it will be demonstrated that use of the controller illustrated in Figure 7.11 will lead to a marked improvement in performance. Initially, it will be assumed that full state feedback is available. The model following controller in both cases is designed with an eigenvalue spectrum of $\{-100 \quad -10+j \quad -10-j\}$, with the null space pole selected as -2.5. The model is treated in the open loop initially, for

reasons of clarity. Unit step changes in speed demand are provided to the model. Figure 7.12 illustrates the result of applying the controller to the imperfectly known plant. The response illustrates a peak overshoot of 66%, with a peak in control effort of 5.2 volts.

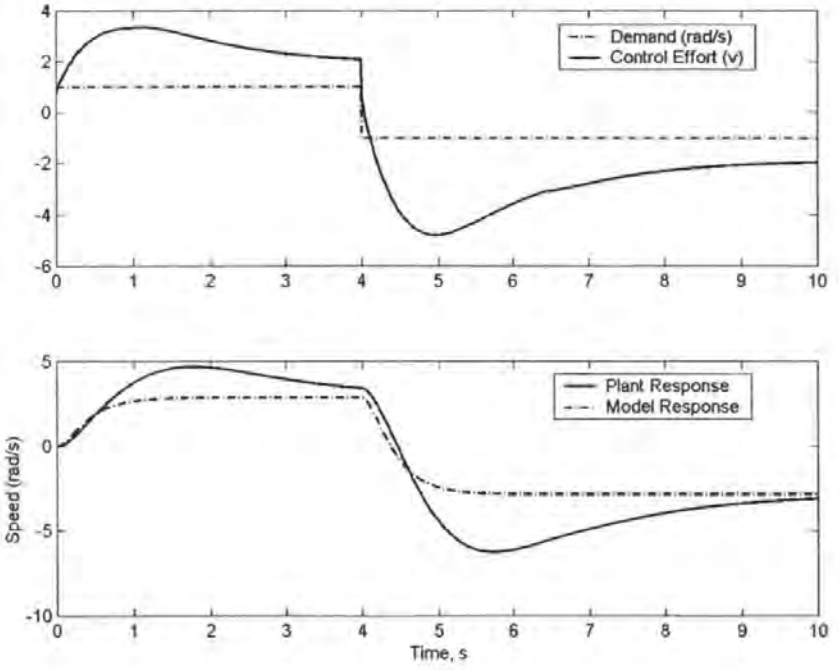

Figure 7.12: *Model Following with an Imperfectly Known Plant*

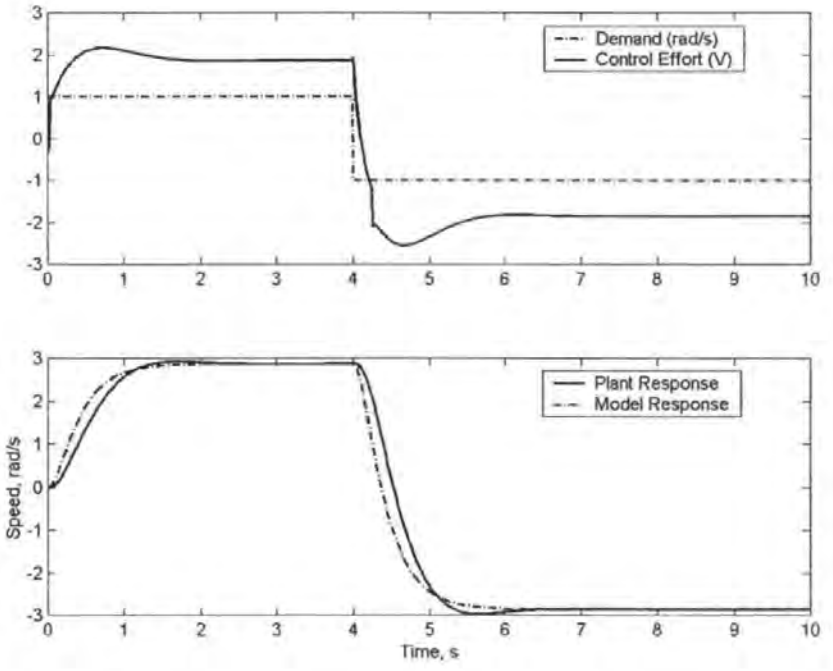

Figure 7.13: *Fuzzy Model Based Model Following with an Imperfectly Known Plant*

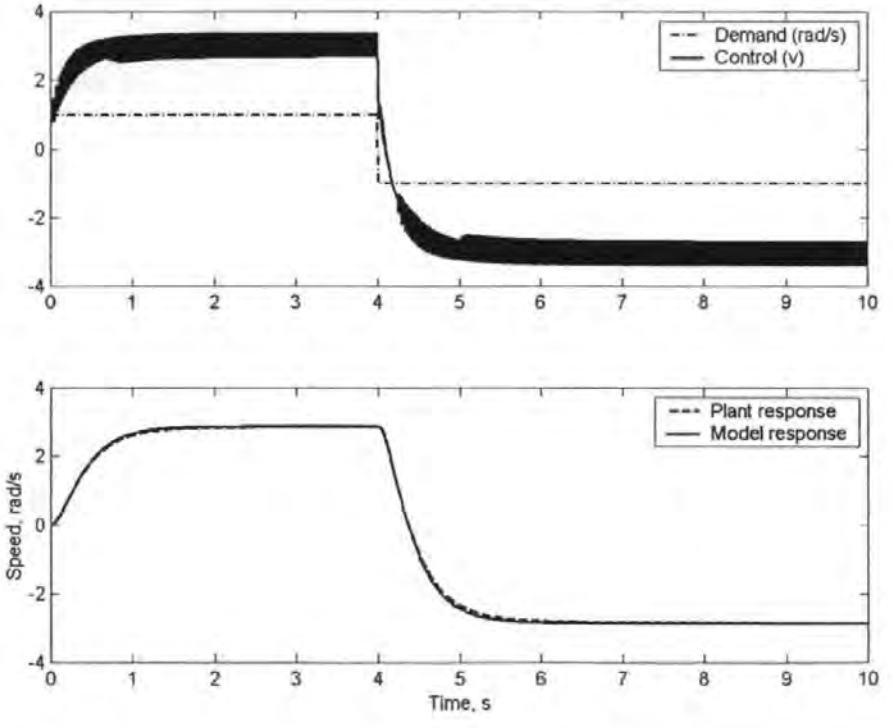

Figure 7.14: *Sliding Mode Model Following Applied to a Perfectly Known Plant*

Figure 7.13 illustrates the result of applying the fuzzy model based controller to the same system. A 4% overshoot exists, the corresponding peak in control effort is reduced to 2.7 volts. The results clearly support the intuitively appealing postulate that minimising error between the nominal plant and actual plant will result in superior control. For completeness, and in order to demonstrate the control effort, the controller was applied to the perfectly known plant. The results are illustrated in Figure 7.14. There is a slight disparity between model and plant in this case. This is due to the selection of the marginally under-damped eigenvalues and the approximation to the ideal switching frequency. It will be noticed that even in the case of the sliding mode controller applied to an imperfectly known plant, the theory suggests asymptotic tracking of the model states, this is clearly visible in Figure 7.12.

In the case of the controller above, full state feedback was assumed. Clearly, this assumption is flawed when attempting to achieve Sensorless control. The direct approach above will be used in conjunction with the fuzzy model of the plant (PBERES). The direct approach is selected because of its computational efficiency and generally good accuracy. The derivative of the algorithm output will be taken to represent system speed. It has been seen that the errors associated with the direct approach are of zero mean, Gaussian distribution and are uncorrelated, i.e. they approximate white noise. It should be noticed that the noise appearing through the encoder measurement channel may be viewed as matched uncertainty, to which of course, the sliding mode is invariant.

Using this approach, it is now demonstrated that speed control may be achieved after an initial transient response. It was discussed in Chapter 2 that applications requiring speed

control are in general more concerned with the steady state response and therefore this transient is not considered to be significant.

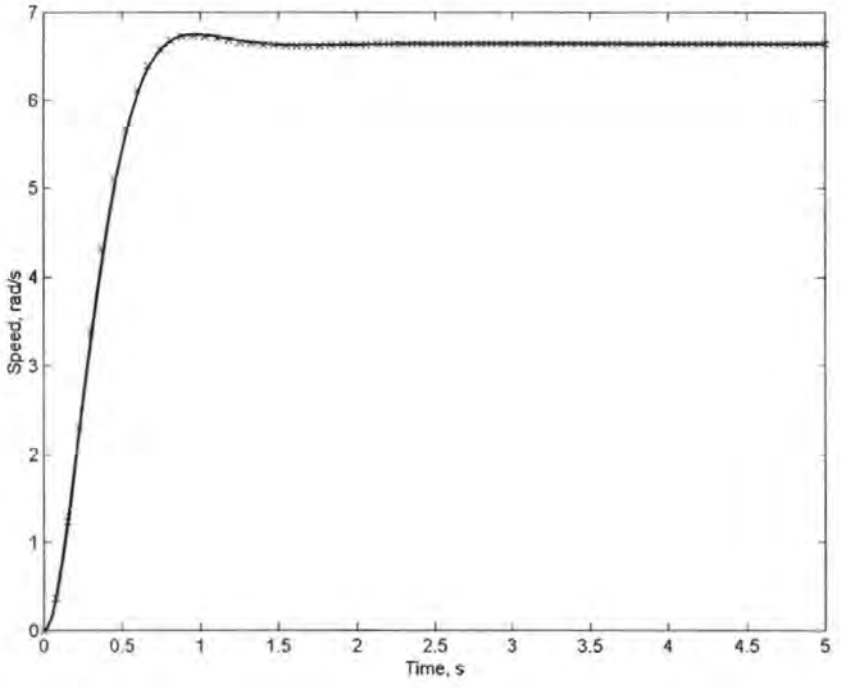

Figure 7.15: Sensorless Model Following Speed Controller, time domain response

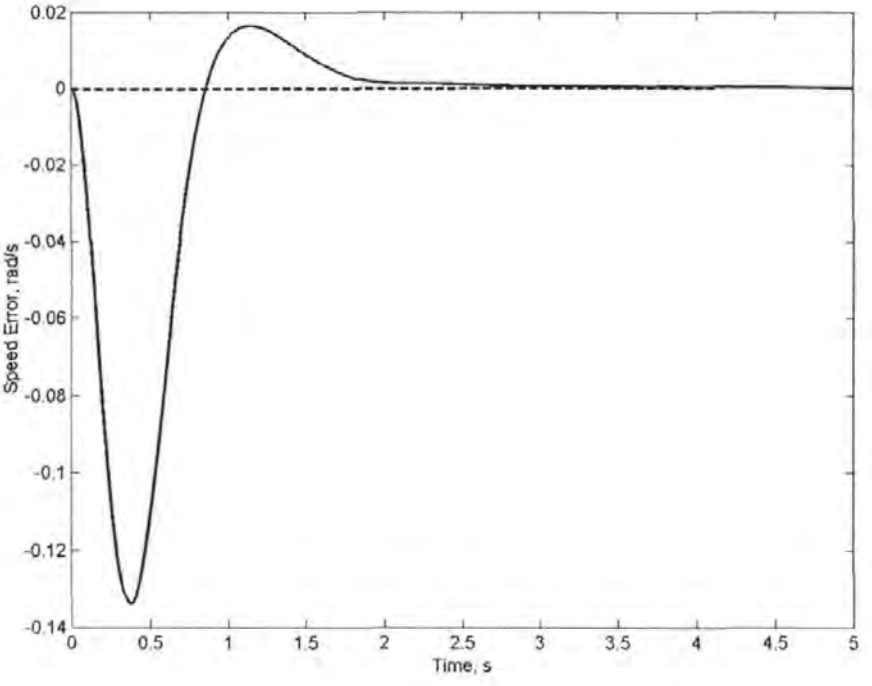

Figure 7.16: *Evolution of Error in Speed*

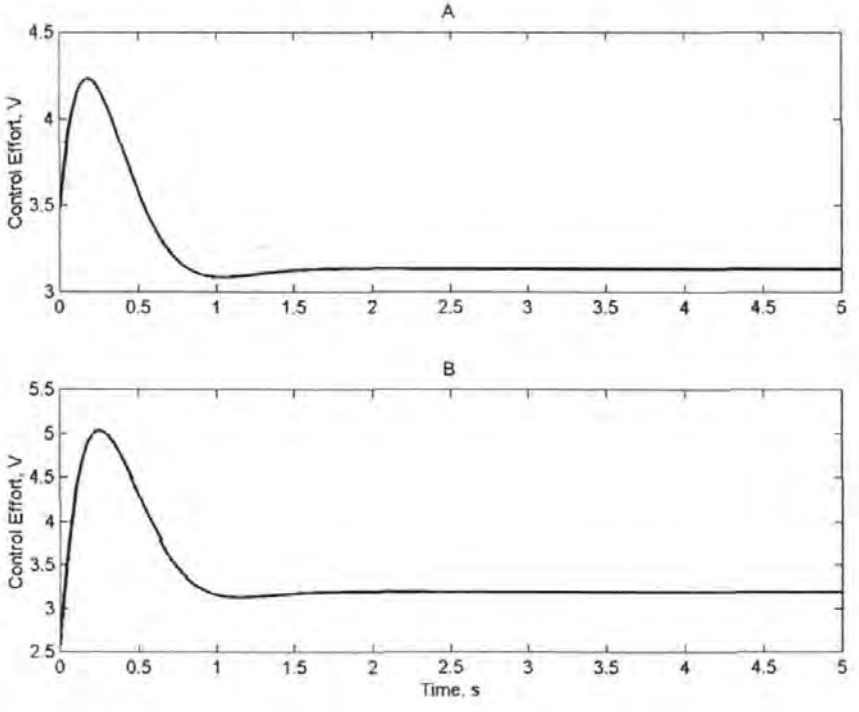

Figure 7.17: *Control Efforts Associated with SMFSC illustrated: A. Model B. Plant*

Because of the high derivative feature of the direct approach, and the associated difficulties in estimating very low system speed, position control is not directly possible through the model following approach. It is however possible to interpret the model following approach in a slightly different manner, and suggest that a model, acting under the control of an external loop could be used to provide position information. The error between plant model and desired model could then be regulated to zero. The fuzzy sliding mode controller with integral action is used to perform this control. However, in this case the feed-forward demand signal used in Chapter 6 is ignored, since there is no demand signal as such, merely the error term which is completely compensated by the nonlinear and integral terms of the controller. This also serves to simplify the design slightly. It stands to reason that the best performance of the algorithm will occur simultaneously with the transition of the Hall effect status. In a similar manner, the worst performance will occur immediately before the transition. It is an attractive prospect that the error between plant model and plant will grow linearly as a function of the distance from the last known Hall effect position. In order to test this corollary, the algorithm will be subjected to three tests. First, the system will be driven to $1.99 \cdot pi = 0.995$ rev (Figure 7.18), $22/12 \cdot pi = 0.9166$ rev (Figure 7.19) and $2 \cdot pi = 1$ rev (Figure 7.20). In order to ensure proper comparison, the model controlling PID is tuned to be overdamped, thus ensuring that spurious Hall effect data, apparent due to plant overshoot, is not included.

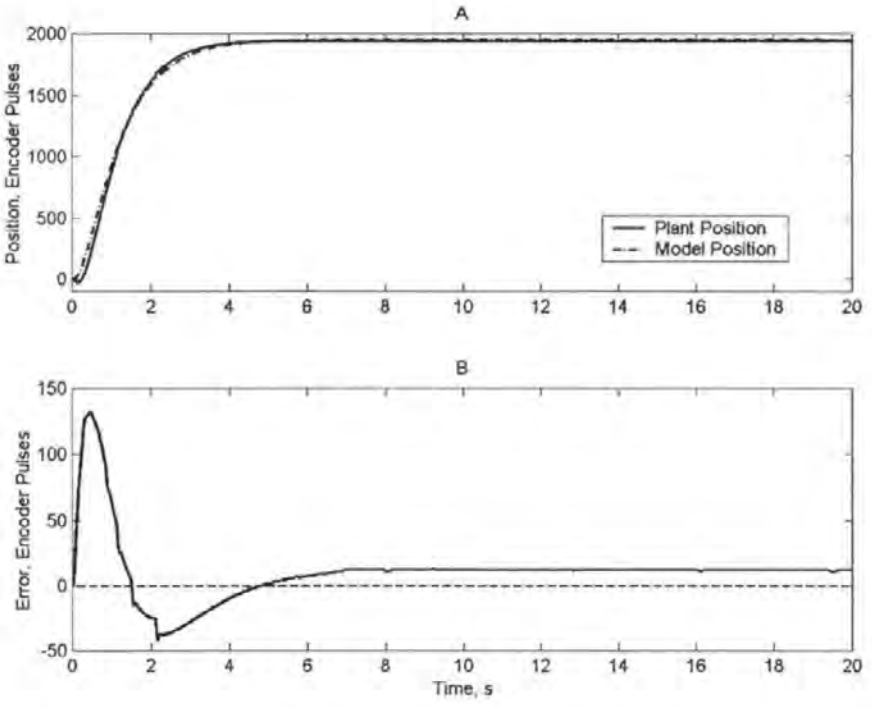

Figure 7.18: *Position estimation at 1.99π radians (12 encoder pulses steady state error)*

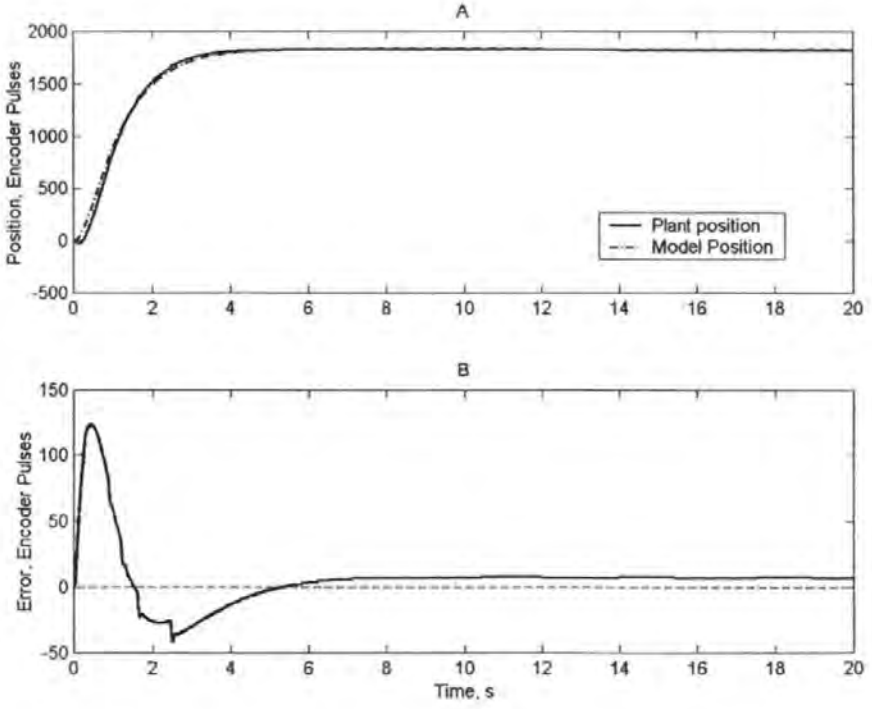

Figure 7.19: *Position estimation at 22/12π radians (6 encoder pulses steady state error)*

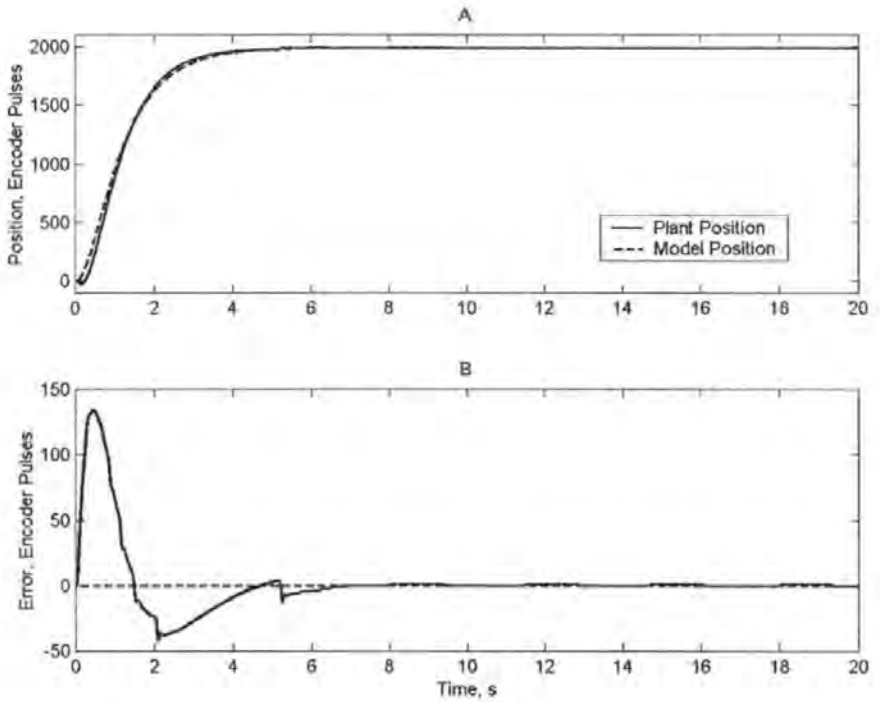

Figure 7.20: *Position estimation at 2π radians (zero steady state error)*

Clearly, the error associated with this algorithm will be strongly dictated by the quality of the plant model. In a final test of the sensorless position controller, the identification data used as the plant data from the other algorithms is used to represent the model. In this manner, quantitative comparisons may be made with the other algorithms. The results are given in Table 7.2.

7.8 Summary of Results

Table 7.2 provides a summary of the results obtained within this Chapter. Both the infinity norm and the RMS norm have units of encoder pulses in error. It can be seen that the direct approach, despite its simplicity performs well in comparison with the more computationally expensive approaches. It should be noted that the algorithms KFSIDA and FMBSSMC both use the direct approach to improve their estimates. This use of the

direct approach in other algorithms represents the same philosophy as in Chapter 4, where an already accurate model was built into other structures to provide enhanced information. The Discrete Approximations approach performs well in terms of all the performance measures used, however, it has already been discussed that this algorithm is computationally intensive and would not represent a viable algorithm unless implemented on a stand alone digital signal processor. The fuzzy model based position controller (FMBSSMC) demonstrates reasonable results. This is made all the more remarkable by the fact that the identification data used never achieves the steady state. Therefore this controller is always kept within the reaching phase and invariance conditions anticipated are not realised.

Table 7.2: *Algorithm Performances as Defined by the Performance Measures*

Algorithm	VAF	VAFDE	$\|\varepsilon\|_{rms}$ (ep)	$\|\varepsilon\|_{\infty}$ (ep)
DIRAPP	99.99	229.45	250.21	4705
DSCAPP	99.99	70.74	312.4	3542
KFSIFM	99.71	1808.3	1834.6	5346
KFSIDA	99.98	29.75	361.13	4705
FMBSSMC	99.91	57.09	974.1	3639.7

7.9 Discussion

This final Chapter has served to draw much of the work from previous Chapters together in order to achieve sensorless precision motion control of a brushless D.C. motor system. The direct approach, which relies purely on an accurate model and Hall effect measurements of position, has been seen to perform well. This algorithm represents the simplest possible approach to position estimation and represents a very small

computational burden. The discrete approximations approach, which relies on least squares estimation of the time taken to the next change in Hall effect status, was seen to reduce the high derivative associated with the direct approach, however, the average error and variance accounted for within the error signals increased. The discrete approximations approach may be viewed as an adaptive method that does not require precise knowledge of the plant. Though this property is extremely attractive, it comes at the cost of high computational burden and does not represent a attractive algorithm for real time implementation. The Kalman filter approach using interpolation reflected the reduction in the high derivative component of the position estimate found in the discrete approximations approach. Once again the reduction in this measure came at the cost of average error and overall tracking accuracy. The algorithm represented a further improvement in estimation over the discrete approximations approach. Although this algorithm is reported within the literature to be able to cope with observation streams at different sample frequencies, this has not been apparent within the experiments. It is not clear whether this is as a result of the unevenly spaced data, or the number of samples attempted between Hall effect status changes. Finally, fuzzy model based sliding mode controllers were investigated as a novel approach to the sensorless control problem. The controllers represent a fundamental shift in the approach to sensorless motion control, whereby the plant is forced to follow a prescribed motion as opposed to forcing the model to estimate the position of the plant.

Through use of these approaches, it has been demonstrated that it is possible to generate a sensorless speed controller which is capable of very low speed operation with zero error after finite time, and a sensorless position controller which will maintain a nominal

integral squared steady state error. Comparisons with the system of §7.2 shows that the position control algorithm will achieve comparable positioning accuracies, with the worst case estimate being of the order 6 microns, and nominal case 3 microns.

7.10 Notes and References

7.10.1 Notes

The matrix inversion lemma makes use of the form

$$\left(\Gamma + uv\right)^{-1} = \Gamma^{-1} - \frac{\Gamma^{-1}uv^{\dagger}\Gamma^{-1}}{1+v^{\dagger}\Gamma^{-1}u} \tag{7.73}$$

The proof of the lemma requires multiplication of (7.73) by $\Gamma + uv^{\dagger}$ to obtain the identity matrix

$$\begin{aligned}\left(\Gamma + uv^{\dagger}\right)^{-1}\left(\Gamma + uv^{\dagger}\right) &= \Gamma^{-1}\left(\Gamma + uv^{\dagger}\right) - \frac{\Gamma^{-1}uv^{\dagger}\Gamma^{-1}\left(\Gamma + uv^{\dagger}\right)}{1+v^{\dagger}\Gamma^{-1}u} \\ &= I + \Gamma^{-1}uv^{\dagger} - \frac{\Gamma^{-1}u\left(v^{\dagger} + v^{\dagger}\Gamma^{-1}uv^{\dagger}\right)}{1+v^{\dagger}\Gamma^{-1}u} \\ &= I + \Gamma^{-1}uv^{\dagger} - \frac{\Gamma^{-1}u\left(1+v^{\dagger}\Gamma^{-1}u\right)v^{\dagger}}{1+v^{\dagger}\Gamma^{-1}u} \\ &= I\end{aligned} \tag{7.74}$$

Choleski's Method of matrix inversion is based on the assumption that the matrix A is symmetric and positive definite. It may be written $A = LL^{T}$, where L is a lower triangular matrix. The inverse may be obtained from

$$A^{-1} = \left(L^{T}\right)^{-1}L^{-1} = \left(L^{-1}\right)^{T}L^{-1} \tag{7.75}$$

and only one inversion of a triangular matrix and one multiplication is required.

Householder's method is presented in Froberg, (1970) pp 130-132.

7.10.2 References

Froberg C.-E. 1970. 'Introduction to Numerical Analysis'. Addison-Wesley

Ito K. and Xiong K. 2000, 'Gaussian Filters for Nonlinear Filtering Problems', IEEE Trans. Automatic Control. 45(**5**). 910-927

Julier S.J. and Uhlmann J.K. 1994. 'A General Method for Approximating Nonlinear Transformations of Probability Distributions'. Technical report. Robotics Research Group, Departments of Engineering Science. University of Oxford.

Norgaard M., Poulsen N.K. and Ravn O. 2000. 'New Developments in State Estimation for Nonlinear Systems', Automatica. 36(**11**). 1627-16-38.

Press W.H., Teukolsky S.A., Vetterling W.T. and Flannery B.P., 1997, 'Numerical Recipes in C', Cambridge University Press.

Chapter 8

Discussion, Conclusions and Suggestions for Future Work

8.1 Discussion and Conclusions

The concept of sensorless motion control was introduced in Chapter 1. Chapter 2 then went on to refine the definition of the theories with respect to motors suitable for small drive systems. It was seen as a result of the further definition of the concept of sensorless motion control that the algorithms discussed loosely fit into one of three categories:

- Direct measurement methods
- Observer based methods
- Artificial intelligence based methods

Of the several methods within each of these sets, only high and medium speed control was generally considered. It was apparent that direct measurement methods were not directly applicable to achieving the goal of this work. In addition, the methods based on artificial intelligence remain an emergent technology, and comparatively nebulous in their definition. Conversely, the observer based methods, specifically those based on the sliding mode, appeared to present realistic scope for extension to low and zero speed motor control.

Chapter 3 described the development of an experimental test rig upon which to test algorithms developed in later Chapters. Models of the system were then developed based on a-priori knowledge of physical properties of the system. A data set was acquired from

the experimental system, based on a series of specifications, which ensured suitability for model validation. Only two of the four models developed provided performances which approximated the real system. It was seen that the variations within the frictional load of the system was a major constraint to the models accuracy. The phase coordinate model, which was one of the two successful models, represented a significant computational overhead, and subsequently, the third order state space model was selected for controller design. The Zeigler-Nichols approach to the selection of PID coefficients was seen within the simulation to provide the characteristic 4:1 decay ratio in the time response. Subsequent implementation of the PID on the actual system led to a hunting response, which was strongly dictated by the variations in frictional perturbation associated with the load. Manipulation of the controller gains led to the demonstration of superior system performance. A full state feedback integral action controller was then developed and applied to the system, experimental results were shown to correlate well with the simulated system response.

Chapter 4 described the identification of the experimental test rig. The commonly used linear difference equation model family was discussed. The auto-regression with exogenous variables model structure was considered, specifically because of its guaranteed stability, and a linear ARX model was developed. Further enhancements to the were made through the introduction of fuzzy clustering, and artificial neural network techniques. The neural network technique was found to strongly favor system excitation signals of a lower frequency, the fuzzy clustered approach was found to perform better than either the neural network or the linear models. Attempts were then made to

aggregate the knowledge of the system obtained from Chapter 3 and the nonlinear identification processes of Chapter4. This was achieved using two different approaches

- The raw data collected from the system was first transformed using *a-priori* knowledge from Chapter 3, to provide the black box structure with data that was of greater physical relevance.
- A prediction error method from Chapter 4 was applied to the model structures from Chapter 3.

The former approach was seen to provide better model estimates, whereas the latter approach served to provide the user with new information about model parameters. The latter approach could therefore have application in data-mining tasks.

The sliding mode was considered in Chapter 5. The invariance property was introduced and the equivalent control method for analysing controller performance was discussed. Several controllers were then developed based on the existing sliding mode control theory and the third order state space model of Chapter 3. The chatter phenomenon was introduced and several methods for preventing its manifestation were considered. Significantly, the boundary layer approach was seen to provide a controller which was globally stable and uniformly bounded. Controllers which employ the boundary layer cannot, however, guarantee final tracking accuracy to any precision beyond the radius of the boundary layer. Practical implementation of the controllers, both with and without the boundary layer illustrated the need for a chatter suppression method. Methods to capitalise on the additional degree of freedom afforded by the boundary layer were discussed in Chapter 6. The first of the two integral action controllers, introduces a simple approach to the design of an integral action controller, which is based on the Bush

companion form. This controller, despite its simplicity was shown to provide asymptotic tracking of the demand. It was shown that this could be achieved even with a boundary layer of sufficient size to suppress chatter. It was shown in Chapter 5 that sliding mode can in theory achieve invariance to parametric uncertainty. In practice, to achieve this, the feedback gains must be increased to accommodate the uncertainty. This leads to theoretical controllers which achieve asymptotic tracking through the selection of infinite feedback gains. However, those controllers do not represent practical solutions because of the impractical specification of system bandwidth. The second of the two controllers evolved in Chapter 6 sought to achieve improved performance over traditional integral action controllers by incorporating enhanced information about the system. This information came from the linearisation of fuzzy models developed in Chapter 4. By virtue of the fact that the controller was then provided with reduced uncertainty within the plant, lower controller gains were selected safely. As a direct result of these reduced controller gains, reductions in the radius of the boundary layer were achieved whilst still suppressing chatter. This reduction in the size of the boundary layer leads directly to improved guarantees of tracking accuracy in finite time, the integral action finally served to ensure asymptotic tracking. Discontinuous Observers were then considered within Chapter 6. Comparisons of performance between the Luenberger observer and the sliding mode observer were made. It was shown that the sliding mode observer was robust to a certain class of disturbance, where errors in state reconstruction were exhibited by the Luenberger observer. Finally in Chapter 6, model following sliding mode control was introduced as a natural extension to observer theory. The conditions for perfect model following were discussed and they were seen to match the conditions of

invariance for sliding mode controllers. A controller without a boundary layer was then developed to provide an illustration of the model following controller performance, near perfect reconstruction of the speed state was illustrated after an initial transient.

Algorithms to achieve sensorless precision motion control were developed in the final section. The problem was identified early within the Chapter as reconstructing a smooth estimate of position from unevenly spaced sample data. Divided difference schemes were reported to be unstable where extrapolation of several samples was required. Reconstruction of the position state then naturally fell to the use of regression models from Chapter 4, coupled with the use of observation streams that would realistically be available from the system. The direct approach was the first method to be considered and successfully integrated nonlinear system models with sensor feedback. The discrete approximations approach was based on the direct approach, but also used a property of discrete time models to ensure better tracking accuracy of the model with the plant. A significant improvement in the smoothness of the estimate was made over the direct approach. A Kalman filter, which used a form of interpolation, was next applied to the problem. The filter had been reported to provide better estimates than the Kalman filter and to be faster than the extended Kalman filter. In addition, the filter was reported to perform well with data of different sample frequencies. Use of the same signals applied within the direct approach led to a significantly worse performance from the filter, because of the instability associated with polynomial extrapolation. However the filter performance was greatly improved by the use of two continuous observation streams. The filter demonstrated extremely good smoothing characteristics. Finally within Chapter 7, the concept of forcing the model to follow the plant was reversed and methods

to force the plant to follow the model were sought. The principle advantage associated with this approach was that control was achieved and the system kinematic parameters are known implicitly. The dynamic performance of the system is dictated by the selection of the model, which may be totally defined by the user. A model following sliding mode controller, which like the second of the integral action controllers developed in Chapter 6, uses a fuzzy model to determine the controller gains, was described. This model has been shown to achieve low speed control, in the order of 60 revolutions per minute, with zero error after an initial transient, which is dictated by the users selection of pole locations. Further, the theory supports much lower speed control to less than 10 revolutions per minute, under the provision that the transient period may be extended. The model following speed controller could not be applied directly to the control of position because of high transients associated with the position correction within the direct approach, and the difficulties associated with estimating zero speed with the hall effect devices. A final controller based loosely on the full state feedback model following controller was described and applied to the problem. The controller was shown to perform position control of an imprecisely known plant to accuracies which approximate those becoming available commercially, typically 3 microns. Because of the numerous advantages the synchronous motor over the alternative forms of actuator, the design solution proposed is considered to be superior to the alternatives. The objective of this work has thus been met.

8.2 Suggestions for Future Research

Future research topics on the theoretical and experimental development of sensorless precision motion control systems should comprise work in three disparate areas. Initial

work would be purely developmental and would first consider the implementation of the sensorless control algorithms in real time. Methods to reduce nonlinearities within the system should be investigated, this would include the use of a ball screw instead of a lead-screw and crossed roller bearings upon which to mount the carriage. The motor amplifier should provide the user with greater control over the torque control loop. The controller should be implemented on a dedicated processor. These improvements will enhance the performance of all the control algorithms discussed within this work. Finally, further work should be carried out to research the incorporation of algorithms which will reduce the effects of backlash, hysteresis and motor torque ripple.

The singular largest constraint on the accuracy of the algorithms discussed within Chapter 7 is the accuracy of the identified models. The second area for further work should therefore be focussed on techniques to improve performance. This work considers the development of system models off-line. It would be distinctly advantageous in a practical system to develop online identification techniques to ensure that the model remains as accurate as possible. Though spline methods are not applicable to the extrapolation of motor position, they can be used for its interpolation. This would provide a neat method for identification of position based on *a-priori* measurements of the Hall effect devices. Within this work, only time domain reconstruction of the Hall effect data is considered. An attractive future proposition would involve the use of frequency domain system identification techniques. Algorithms designed for unevenly spaced data, such as the Lomb-Scargale Periodogram will have to be used to achieve this.

The final area for future research occurs at a more general level. Further applications for the fuzzy model based sliding mode controllers should be found. In addition, an

algorithm capable of neural network linearization should be sought and applied to the design of sliding mode controllers, in the same manner as the fuzzy model based sliding mode controllers. In an alternative scenario, the design of sliding mode controllers could be extended to design based on Diophantine equations, such that polynomial models could be applied directly to the selection of controller gains. Finally, it is acknowledged that significant speed enhancements could be made to the models if a suitable algorithm could be found to map fuzzy clustered models to a neural network structure.

Appendix A

Publications

Contents

Conference Papers

M.J.Knight, R.Sutton, R.S.Burns and D.F.L. Jenkins, 2000, 'Identification of a Brushless D.C. Motor using Grey Box Modelling Techniques', Proc. 14th International Conference on Systems Engineering, ICSE 2000. Coventry UK. 323-328

M.J.Knight, R.Sutton and D.F.L Jenkins, 2001, 'Fuzzy Model Based Sliding Mode Control of a Linear Precision Motion Control System', Proc. International Eusflat Conference. Eusflat 2001. Leicester UK. 164-167.

M.J.Knight, R.Sutton and D.F.L Jenkins, 2001, 'Fuzzy Model Based Sliding Mode Control', International ICSC Congress on Computational Intelligence: Methods and Applications, CIMA 2001. Bangor UK. 788-794

M.J.Knight, R.Sutton, R.S.Burns and D.F.L. Jenkins, 2001, 'A Comparison of Nonlinear Identification Techniques', 7th IEEE Conference on Methods and Models in Automation and Robotics, MMAR 2001. Miedzyzdroje, Poland. 953-958.

Antonio Tiano, Antonio Zirilli, Robert Sutton and Matthew Knight, 2001, 'Nonlinear Identification of a Brushless Motor', 7th IEEE Conference on Methods and Models in Automation and Robotics, MMAR 2001. Miedzyzdroje, Poland. 977-980.

Journal Papers

M.J.Knight, R.Sutton, R.S.Burns and D.F.L. Jenkins, 2001, 'Sensor Bandwidth Reduction for Data Capture', IoP Measurement Science and Technology, **12,** N35-N38

M.J.Knight, R.Sutton and R.S.Burns, *Invited Paper*, 'Fuzzy Model Based Integral Action Sliding Mode Control', Soft Computing. In Press.

M.J.Knight, R.Sutton and R.S.Burns, 'Identification of a Brushless D.C. Servomechanism System', Submitted to the Institute of Measurement and Control.

M.J.Knight and R.Sutton, *Invited Paper*, 'Fuzzy Model Based Sliding Mode Control of a D.C. Servomechanism', submitted to the International Journal of Fuzzy Sets and Systems.

Proc. 14th Int. Conf. on Systems Engineering, ICSE'2000
Coventry University, UK, 12-14 September 2000

IDENTIFICATION OF A BRUSHLESS D.C. MOTOR SYSTEM USING GREY BOX MODELLING

M.J.Knight[1], R.Sutton[1], R.S.Burns[1], D.F.Jenkins[2]

1) *Department of Mechanical and Marine Engineering, University of Plymouth*
2) *Department of Communications and Electronic Engineering, University of Plymouth*
Tel: (01752) 232676 Fax: (01752) 232638 Email: mjknight@plymouth.ac.uk

Keywords: Identification, Servomechanism, Grey box modelling, Brushless DC Motor

Abstract

This paper demonstrates the application of grey box modelling to a servo mechanism actuated by a brushless direct current motor (BLDC) under significant torque perturbation. It is first demonstrated that the application of a third order linear model is insufficient for accurate modelling or simulation of this particular system. A limited test of a common black box model structure is then performed. The effects of poorly understood torque perturbation are illustrated and are identified as the principle cause of modelling error. A grey box model utilising the linear model and input output data is then developed and significant improvement in modelling accuracy is demonstrated.

1 Introduction

On going work at the University of Plymouth is concerned with the development of a linear translation stage for precision motion control. Impetus has been placed on the achievable resolution, repeatability, accuracy and range of the system. With these constraints placed on the design and for reasons discussed below, a brushless direct current (BLDC) motor is envisaged as the device most appropriate for actuation of the stage.

BLDC Motors are used in direct drive applications primarily because of their increased torque/weight ratio. In comparison with their brushed counterpart they eliminate the problems associated with mechanical wear whilst minimising electrical and acoustic noise. In addition the physical construction of the BLDC allows for better heat dissipation and a higher torque/speed ratio is thus achievable [1].

The BLDC does however pose a greater challenge than the brushed equivalent when modelling and control is considered, since it is multi-input by nature and exhibits coupled non-linear dynamics.

For use in precision motion control it is imperative that the effects of torque ripple and frictional effects are identified in order that effective control may be performed [3]. There has been much work within the field of BLDC modelling and identification, in [1], the motor model is treated in detail. In [4] the effects of magnetic saturation and reluctance variation are modelled. [5] builds on the work of [1] and [4] in order to provide a computationally efficient phase variable model of the BLDC.

Whilst there are several studies devoted to modelling the BLDC motor, there are few that deal with modelling the motor once a load is applied. Use of a neural network in specialised learning mode has been shown to cope with the additional unmodelled non-linear effects well [6], however this approach does little to elucidate system parameters for subsequent use in a feedback controller and blackbox control becomes necessary.

2 Modelling

The key problem in system identification is to find a suitable model structure, within which a model that represents a given system to an acceptable degree of accuracy is to be found. Fitting a model once a given structure has been identified (parameter estimation) is in many cases a lesser problem. An axiom within the field of system identification is to estimate only that which is unknown. More specifically, when identifying a system *a priori* knowledge and physical insight about the system should be used where possible. It has become customary to distinguish between the varying levels of prior knowledge, they are described as follows[7]:

- **White Box Models:** These are used to describe the system when it is perfectly known. It has in this case been possible to construct a model entirely

from physical insight and *a priori* knowledge of the system.

- **Black Box Models:** No physical insight is available. In this case the chosen model will have a structure that is known to have sufficient flexibility and has been proven in application.
- **Grey Box Models:** In this case some physical insight is available, but several parameters must be determined from observed data. Under this heading two more explicit sub categories are worthy of consideration:
  - Physical Modelling: A model structure can be built on physical grounds, which has a certain number of parameters to be estimated from observed data.
  - Semi-physical modelling: Physical insight is used to suggest how the observed data comprises certain non-linear elements. These elements are then subjected to identification with black box model structures.

Within the context of this paper, attention is paid primarily a grey box modelling method, since the BLDC motor is well understood and is accessible to mathematical modelling. However, the additional load is poorly understood and modelling of the system directly becomes impossible.

3 Experimental set-up

An experimental test rig has been constructed for model validation. A brushless D.C. motor rated at 250W is used for actuation of a linear stage with 440mm travel. The stage is constructed of a 2mm-pitch lead screw with ground steel slide rails. The stage is subject to large frictional forces, which vary over its entire length. A 500 pulse per revolution quadrature optical encoder is used for position feedback. This provides a linear displacement resolution of 360 microns. Data is captured using a microprocessor unit, within this work τ_s is used to describe sample period.

4 White Box Modelling

There are many excellent texts available that describe the BLDC motor using white box, mathematically derived models. Common models such as the space phasor (d-q) and the phase co-ordinate model are easily found within the literature [2]. However these models are eighth order and non-linear thus posing significant difficulties where simulation is concerned. In addition it becomes exceedingly difficult to design model based controllers around these equations and the motor model is often approximated to a third order state space or transfer function model of the form shown in equation (1).

$$\begin{bmatrix} \dot{X}_1 \\ \dot{X}_2 \\ \dot{X}_3 \end{bmatrix} = \begin{bmatrix} 0 & 1 & 0 \\ 0 & -\frac{B}{J} & \frac{K_m}{J} \\ 0 & -\frac{K_e}{L} & -\frac{R_e}{L} \end{bmatrix} \begin{bmatrix} X_1 \\ X_2 \\ X_3 \end{bmatrix} + \begin{bmatrix} 0 \\ 0 \\ \frac{1}{L} \end{bmatrix} U_1 - \begin{bmatrix} 0 \\ -\frac{1}{J} \\ 0 \end{bmatrix} U_2$$

$$Y = \begin{bmatrix} 1 & 0 & 0 \end{bmatrix} \begin{bmatrix} X_1 \\ X_2 \\ X_3 \end{bmatrix} \qquad (1)$$

Where X_1,X_2 and X_3, are the position, speed and applied current respectively. B is given as the viscous friction, J the moment of inertia, R and L the resistance and inductance of the motor respectively. K_e and K_m are the electrical and mechanical gains of the motor, U_1 is the applied voltage and U_2 is the applied load torque.

For this study the third order model is used and it is accepted that there will be a small disparity between this model and a more accurate model such as one of the two discussed above.

Since this is a white box model, there is assumed no *a priori* knowledge of torsional variance along the stage length, instead a constant measured value of torque is used.

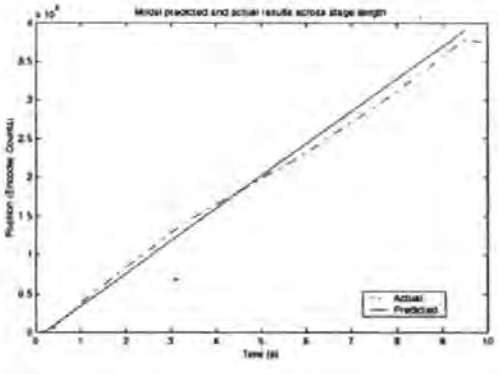

Figure 1. Comparison between model predicted and actual position

Figure (1) illustrates the output of the model in comparison with the results obtained from the actual system. It might be seen that the model is a fair approximation of the system, however the torque perturbation which varies over the length of the stage clearly has a significant effect on the

performance of the system and implicitly effects the performance of the linear model.

5 Black Box Modelling

When a system is poorly understood models are often created using a input output representation. Instead of using a physically relevant state vector, the state of the system is represented by a finite number of past inputs and outputs of the system. A structure commonly used to achieve this is the NARX (Non-linear AutoRegressive with eXogenous input). It has been shown that this structure is able to represent the observable and controllable modes of a large class of discrete-time non-linear systems. It has been shown in [7] that non-linear black box models, specifically the NARX model may be applied more successfully to a brushed D.C. motor than a linear alternative, such as ARX (Auto Regressive with eXogenous input).

The NARX model establishes a relationship between the collection of past input-output data and the predicted output

$$\hat{y}(k+1) = F\begin{pmatrix} y(k),\ldots,y(k-n_y+1), \\ u(k),\ldots,u(k-n_u+1) \end{pmatrix} \quad (2)$$

Where k denotes discrete time samples, n_u and n_y are related to the systems order. There are several other popular structures for input-output modelling, such as the NOE (Non-linear Output Error), which includes past model outputs and the NARMAX (Non-linear Auto Regressive Moving Average with eXogenous inputs) which includes the previous prediction errors in the regression vector. The regression vector of these models cannot be constructed directly from the data, but rather the regression problem must be solved in a recurrent manner. It has been shown that this recurrence may lead to instability, and it becomes very difficult to verify the predictors' stability.

It will be noted at this point that in general piecewise constant or binary signals often employed within identification of linear systems are not suitable for the identification of non-linear systems. Rather sinusoids of varying amplitude and frequency are preferred. At this stage within the work there is no practical way in which input signals of sinusoidal form may be applied. Therefore square wave inputs of varying frequencies and magnitudes are applied, as an approximation. It is noted that this will degrade the performance of the model and the application of sinusoidal inputs will be investigated at a later stage within the work.

Figure 4 shows the performance of the NARX model when trained for a system excited under a 15v, 0.6Hz input signal. This model represents a

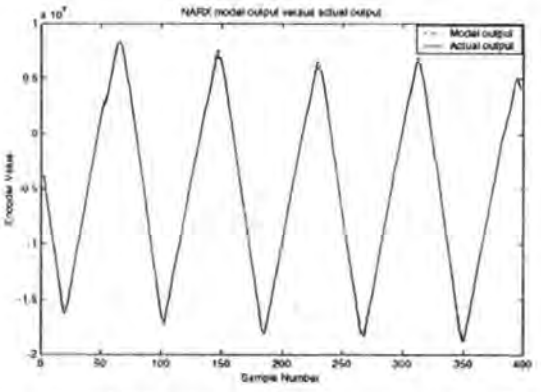

Figure 4: NARX model output compared with actual at 0.6Hz excitation (τ_s = 12.44mS)

significant improvement over the linear model. However, the same NARX model applied to step input-output data performs poorly outside of the trained dataset (Figure 5).

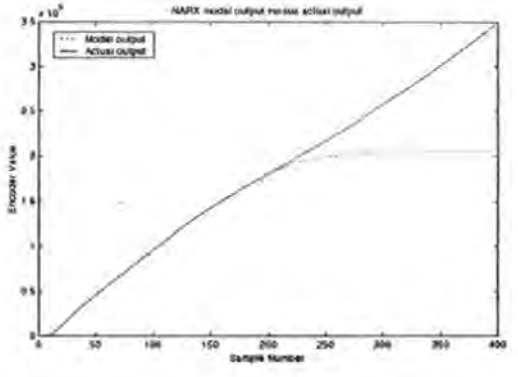

Figure 5: NARX model output in response to a step input (τ_s = 21.15mS)

6 Grey Box Modelling

It may be seen that the accuracy of the linear model is strongly influenced by the unmodelled torque perturbation apparent at the motor shaft (figure 1). This variation may be principally attributed to frictional effects. The solution is clearly to incorporate a model of this torsional variation. Since friction has the property of being time variant, the dynamics of the stage are poorly understood and modelling from first principles becomes impossible. A black box approach

becomes the choice for modelling stage behaviour. At this point the readers attention is drawn to the fact that there are two fundamental categories that distinguish modelling approaches, referred to as Global and Local. The NARX input-output model discussed above is an example of a global model, whereby an attempt to describe the system is made using non-linear functional relationships between system variables. Conversely, local models attempt to cope with complexity and non-linearity of systems by decomposing the modelling problem into a number of simpler, and often linear, sub components. The local modelling technique is conceptually simple and intuitively more appealing since they more closely approximate the methods by which humans learn and solve problems. Fuzzy models may be viewed as local models.

At this point use is made of the input-output data used in training the NARX model. It may be shown that the torque at the motor shaft is given by

$$\tau_l = \frac{\gamma - \frac{d\theta}{dt}}{2100} \qquad (3)$$

Where γ is the no load speed of the motor and 2100 is the torque/speed gradient as specified by the manufacturer.

One of the inputs to the grey box model, which will be discussed in more detail directly is a torque observer which uses the position information that is the subject of estimation. In order to avoid recurrence within the model the following torque observer based upon current might be used.

The equation of motion is given

$$J\frac{d\omega}{dt} = T_m - T_l \qquad (4)$$

where T_m is the electromagnetic torque generated by the motor and T_l is the total perturbing torque at the motor rotor, expressed as

$$T_l = T_i + T_{Lo} + T_f \qquad (5)$$

where T_i, T_{lo} and T_f are the inertial, load and frictional torques respectively. In addition, it may be shown that

$$T_e = K_T \cdot I^* \qquad (6)$$

where I^* is the reference torque current. The parameters within the equations (5) and (6) are J and K_T they deviate from the values rated within the model (J_n and K_{Tn}) by

$$J = J_n + \Delta J \qquad (7)$$

$$K_T = K_{Tn} + \Delta K_T \qquad (8)$$

In terms of torque, the variations of ΔJ and ΔK_T are $\Delta Js\omega_r$ and $\Delta K_T I^*$, respectively. The torque perturbation may therefore be expressed as

$$T_{per} = T_L + \Delta Js\omega_r - \Delta K_T \cdot I^* \qquad (9)$$

Finally, making use of (6),(7) and (8) in (4) the following torque perturbation observer may be derived

$$T_{per} = K_{Tn} \cdot I^* - J_n s\omega_n \qquad (10)$$

The output of this observer might be used as a direct input to the model. However, at this stage this has not been implemented and will be the subject of further work.

The torque data and the output of the linear model subjected to the same excitation signal as the actual system are used as inputs to a multi-input single output fuzzy clustered model. In this respect full knowledge of the system derived mathematically is utilised, but the poorly understood torque perturbation is also incorporated into the model.

Before results are discussed, a description of the fuzzy clustered model is given, the interested reader is referred to [8] for a far more detailed treatment of the concepts outlined here.

6.1 The Affine TS Model

The affine *Takagi-Sugeno* (TS) fuzzy model comprises a set of rules in the following form:

$$If \quad x \quad is \quad A_i \quad then \quad y_i = a_i^T x + b_i$$

$$i = 1,2\ldots,K$$

Where $x \in X \subset \Re^P$ is a crisp input vector, A_I is a multidimensional fuzzy set: $\mu_{Ai}(x): X \to [0,1]$, $y_i \in \Re$ is the scalar output of the I^{th} rule, $a_i \in \Re^P$ is a parameter vector and b_I is a scalar offset. The index I relates the variable to the I^{th} rule and K is the number of rules in the rule base. The output y of the TS model is computed using the fuzzy mean formula

$$y = \frac{\sum_{i=1}^{K} \beta_i(x) y_i}{\sum_{i=1}^{K} \beta_i(x)} \quad (11)$$

Where $\beta_i(x)$ represents the degree of fulfilment of the l^{th} rules antecedent, which is simply a measure of the degree of fulfilment of x in the fuzzy set A_i and is given by

$$\beta_i = \mu_{A_i}(x) \quad (12)$$

Since it may become difficult to interpret multidimensional fuzzy sets, the antecedent proposition is commonly defined in a conjunctive form, given by a series of single dimensional fuzzy sets combined with simple propositions:

If x_1 is $A_{1,1}$ and...and x_P is $A_{1,P}$ then

$$y_i = a_i^T x + b_i$$

in this case the degrees of fulfilment are calculated as

$$\beta_i(x) = \mu_{A_{i,1}}(x_1) \wedge \ldots \wedge \mu_{A_{i,P}}(x_P)$$

where the min operator ($\wedge$) may be replaced by alternative T-norms. In this case the model output is calculated

$$y = \left(\sum_{i=1}^{K} \gamma_i(x) a_i^T \right) x + \sum_{i=1}^{K} \gamma_i(x) b_i = \tilde{a}^T(x) x + \tilde{b}(x) \quad (13)$$

Where γ_i is the normalised degree of fulfilment

$$\gamma_i(x) = \frac{\beta_i(x)}{\sum_{j=1}^{K} \beta_i(x)} \quad (14)$$

$\tilde{a}(x)$ and $\tilde{b}(x)$ are input dependent parameters, given as convex linear combinations of the constant parameters a_i and b_i through the following relationship

$$\tilde{a}(x) = \sum_{i=1}^{K} \gamma_i(x) a_i \quad (15)$$

$$\tilde{b}(x) = \sum_{i=1}^{K} \gamma_i(x) b_i \quad (16)$$

The NARX model discussed above may be expressed in this pseudo linear model according to the following

$$\hat{y}(k+1) = \sum_{j=1}^{n_y} a_{i,j} y(k-j+1) + \sum_{j=1}^{n_u} b_{i,j} u(k-j+1) + c_i \quad (17)$$

6.2 Fuzzy Clustering

Once the structure of the model has been decided, the identification problem becomes a static non-linear regression $y=F(\mathbf{x})$. The regression space is given by

$$Z = (X, Y) \subset \Re^n \quad (18)$$

Where n is the regression space and is given by the dimension of the regressor (p)+1. Within the regression space the equation $y=F(\mathbf{x})$ defines a hypersurface known as a regression surface.

Geometrically the consequents of the TS model discussed above may be represented as hyperplanes in the regression space. The antecedent fuzzy sets serve to divide the regression space in which the regression surface may be locally approximated by the consequent hyperplanes. The task of identification is to find the number, locations and parameters of these hyperplanes such that the regression surface is accurately approximated. This may be achieved through application of a set of fuzzy clustering methods, referred to as *subspace fuzzy clustering algorithms*.

The set of data to be clustered, across the regression space, is constructed by concatenating a matrix containing the regression vectors and the regressand vector. The model under consideration here is a multi input, single output second order system.

The clustering algorithm employed to cluster the data once in the above form is known as the Gustafson-Kessel fuzzy clustering algorithm which may be found discussed in more detail in [8].

Each cluster obtained by the product space clustering of the training data may be regarded as a local linear approximation of the regression hypersurface. The global model may be expressed as a TS model whereby each cluster is used to represent a TS rule through estimation of the consequent parameters and derivation of the antecedent through the fuzzy partition matrix.

7 Results

The identification model described above was applied to the servomechanism data, using 150 of the 450 samples as training data (samples 50-200). The linear model was excited with a step input as

per figure (2). The stage was also fed a step-input signal and the values for torque derived. Results are shown in figure (6) compared against the entire data set. The model may be seen to be extremely accurate with a measured error of zero in simulation.

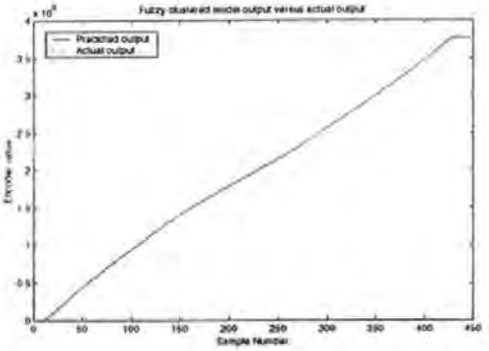

Figure 6: Grey Box model response to a step-input ($\tau_s = 21.15$mS)

Following this test, a 0.8Hz bipolar step input was used to excite both the actual stage and the linear model. Once again the training set used was between the samples 50 and 200. Once again the prediction error is zero figure (7). A data set from a second step input test was used without retraining after the first step input test. In this case there was simulation error. This may be attributed to the fact that since the torque perturbation varies from run to run, the system has actually been trained using a system with fundamentally different dynamics.

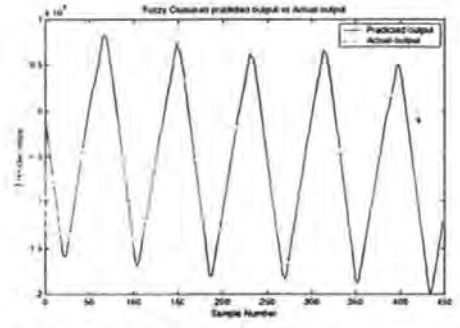

Figure 7. Grey Box model output at 0.8Hz (τ_s = 12.44mS)

8 Conclusions

Within this paper an approach to modelling non-linear, poorly understood systems has been demonstrated. The grey box modelling approach relies on prior data and information, and in the case of the system under consideration, because of the time variant dynamics there cannot be a great deal of certainty concerning the *a priori* input output data. Within this work it has been demonstrated that the grey box approach alleviates the need for an extremely accurate linear model, affording the designer some inaccuracy within the linear model and thus potentially expediting the design process. The black box approach has been shown to perform well with the system under consideration, if a bipolar step input is used for system excitation, however it must be noted that the performance of this model will most likely be improved by the use of sinusoidally excited training data. From point of view of simulation, the system demonstrates extremely high accuracy and if Input-Output data is readily acquired and the system reasonably well understood, then the reader is strongly advised to consider the grey box approach to modelling.

References

[1] P.Pillay and R.Krishnan, "Application Characteristics of Permanent Magnet Synchronous and Brushless D.C. Motors for Servo Drives", IEEE Trans. Ind. App.,Vol. 27, No.5, pp 986-996, September/October 1991

[2] P.Krause, O.Wasynczuk and S.Sudhoff, "Analysis of Electric Machinery", IEEE Press, 1995, ISBN 0-7803-1101-9

[3] L.Dessaint, B.Herbert, H.Huy and G.Cavuoti, "A DSP-Based Adaptive Controller for a Smooth Positioning System", IEEE Trans. Ind. Elec., Vol 37, No.5, pp 372-377, Oct 1990.

[4] N.Hemati and M.Leu, "A Complete Model Characterisation of Brushless DC Motors", IEEE Trans. Ind. App., Vol. 28, No.1, pp 172-180, January/February 1992

[5] G.Phillips, S.Garvey and M.Wright, "Phase Variable Mathematical Modelling of a Brushless DC Motor", Proc. 25th Symposium on incremental motion control systems and devices, pp 287-294, Boston, 1996

[6] G.Otten, T.Vries, J.Amerongen and A.Rankers, "Linear Motor Motion Control Using a Learning Feedforward Controller", IEEE Trans. on Mechatronics, Vol. 2, No. 3, pp 179-187, September 1997.

[7] J.Sjöberg, "Some Examples of Identification with Neural Networks",Technical Report, Dep. of Electrical Engineering, Linköping University, LiTH-ISY-R-1650, 1994

[8] H.Hellendoorn and D.Driankov, "Fuzzy Model Identification – Selected Approaches", Springer Verlag, ISBN 3-540-62721-9, 1997.

Fuzzy Model Based Sliding Mode Control of a Linear Precision Motion Control System

M.J.Knight
DMME, University of Plymouth
Drake Circus, Plymouth. Devon.
mjknight@plymouth.ac.uk

R.Sutton
DMME, University of Plymouth
Drake Circus, Plymouth. Devon.
rsutton@plymouth.ac.uk

D.F.L Jenkins
DCEE, University of Plymouth
Drake Circus, Plymouth. Devon.
dfljenkins@plymouth.ac.uk

Abstract

A method of sliding mode control based on a fuzzy model identified through input output data is presented. In this approach the advantages of the sliding mode control technique are maintained, however parametric uncertainty and unmatched disturbance are acknowledged as limiting factors of controller performance and their effects are sought to be minimised. Controller performance is compared with an equivalent conventional sliding mode controller.

Keywords: Fuzzy model identification, Adaptive sliding mode control, motor control.

Introduction

Precision motion control has relevance in many technological areas, it has found application in medical, electronic manufacture and mechanical disciplines to name but a few. As the requirement for progressively more accurate position control continues to grow, the performance requirements placed on the positioning device become ever more stringent. In systems where friction is present, it is a notoriously difficult phenomenon to measure, in addition to the parametric uncertainties associated with the controller and device load. It is therefore necessary to employ methods of control that will perform in a prescribed manner despite system uncertainty.

One of the earliest approaches to control of uncertain systems was sliding mode control (SMC) or variable structure control (VSC), first introduced to western researchers by the seminal works of Utkin [10] and Itkis [5]. The central feature of SMC is the sliding mode, in which the dynamic motion of the controlled system is constrained to remain within a prescribed subspace of the full state space. The sliding mode is achieved by ensuring that the prescribed manifold within the state space is made attractive to the system [5]. Once the manifold is reached, the system is forced to remain on it thereafter. When on the manifold, i.e. during the sliding motion, the system dynamics are equivalent to a system of lower order, which is insensitive to both parametric uncertainty and unknown disturbances that satisfy the matching condition.

One of the principle drawbacks of sliding mode is that it in general only applies to systems that satisfy the matching condition [11]. Secondly and most significantly, the control law is discontinuous across the sliding manifold, this leads to a phenomenon termed 'control chatter' in practical systems. Chatter involves high frequency control switching and may lead to excitation of previously neglected high frequency system dynamics. Smoothing techniques such as boundary layer normalisation have been employed in order to negate the effects of control chatter, however such an approach leads to a controller that can only guarantee tracking accuracy to within the ε-vicinity of the demand [3], where ε is the radius of the boundary layer. A compromise must therefore be sought between desired tracking accuracy and controller bandwidth.

The apparent similarities between the sliding mode and fuzzy controllers was illustrated in [8], this has subsequently motivated considerable research effort in combining the two topologies in a manner that serves to reduce the mentioned drawbacks of the sliding mode. The most common approach to this has been to replace the continuous switching function of the boundary layer with an equivalent fuzzy switching function. However, as pointed out in [7], the fuzzy rule base commonly serves as a mimic of the original switching function and the advantages of such an approach are therefore unclear. Others, e.g.[4], have used a fuzzy rule base in making the sliding manifold adaptive, so as to minimise the reaching phase, good results have been reported. Babuška [1] has demonstrated the ability of the affine Takagi-Sugeno consequent to locally

model a system through rule extraction from cluster data obtained within the regression space. [9] subsequently uses such fuzzy models in order to extract locally linear state space models of the system and demonstrate model based control of both single input-single output (SISO) and multi input, single output (MISO) systems.

In this work, the parametric uncertainty and disturbances that the system is subject to are recognised as the root cause of the high gain feedback requirement and control chatter. It follows that if these uncertainties can be reduced then enhanced controller performance may be achieved as will be shown.

Fuzzy Modelling

Fuzzy identification is a term used that has come to represent the use of fuzzy logic in the modelling and representation of a system. Since fuzzy models may be viewed as general function approximators, they are readily applied to the nonlinear regression problem. The approach adopted within this work is to decompose the model into a static nonlinear regression. The problem of model identification is then decomposed into two separate problems, the first is selection of the regression structure, the second, the selection of the fuzzy model form, for example, the required number of membership functions and membership crispness.

The desired regression may be expressed in the form

$$\hat{y}(t|\theta) = f(\varphi(t), \theta) \tag{1}$$

It has been shown in [1] that the regression surface within the product space may be represented as a series of local approximations.

Through use of a subspace clustering algorithm such as the Gustafson-Kessel algorithm, it is possible to derive local approximations to this regression surface. Further, through use of the eigenvalues of the cluster covariance matrix given by

$$F_i = \frac{\sum_{k=1}^{N} (\mu_{i,k})^m (z_k - v_i)(z_k - v_i)^T}{\sum_{k=1}^{N} (\mu_{i,k})^m} \tag{2}$$

it is possible to interpret these local models and subsequently derive a fuzzy rule to represent this local approximation. In repeating this process for each data cluster, a global model of the system may be generated.

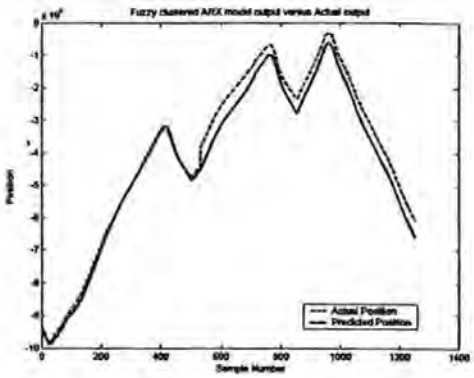

Figure 1: Typical model result compared to system output.

Previous work has considered the accuracy of this approach in comparison to neural networks and 'white box' models, results have demonstrated that this local approach to modelling can provide superior results [6].

Model Extraction

It has been shown in [9] that once the Takagi Sugeno model has been derived, local linear state space models can be calculated according to the following,

$$y_l(k+1) = \frac{\sum_{i=1}^{K_l} \mu_{li}(x_l(k)) \cdot y_{li}(k+1)}{\sum_{i=1}^{K_l} \mu_{li}(x_l(k))} \tag{3}$$

$$y_{li}(k+1) = (\varsigma_{li} y(k) + \eta_{li} u(k) + \theta_{li}) \tag{4}$$

where

$$\zeta_l^* = \frac{\sum_{i=1}^{K_l} \mu_{li}(x_l(k)) \cdot \zeta_{li}}{\sum_{i=1}^{K_l} \mu_{li}(x_l(k))} \tag{5}$$

$$\eta_l^* = \frac{\sum_{i=1}^{K_l} \mu_{li}(x_l(k)) \cdot \eta_{li}}{\sum_{i=1}^{K_l} \mu_{li}(x_l(k))} \tag{6}$$

and

$$\theta_l^* = \frac{\sum_{i=1}^{K_l} \mu_{li}(x_l(k)) \cdot \theta_{li}}{\sum_{i=1}^{K_l} \mu_{li}(x_l(k))} \tag{7}$$

In the case here, previous inputs are not considered and the A, B and C matrices of the model are thus simplified, the matrices are given

$$A = \begin{bmatrix} \zeta_{1,1}^* & \zeta_{1,2}^* & \cdots & \zeta_{1,a_1}^* \\ 1 & 0 & \cdots & 0 \\ \zeta_{2,1}^* & \zeta_{2,2}^* & \cdots & \zeta_{2,a_2}^* \\ 0 & \vdots & \ddots & \vdots \\ \zeta_{n_b,1}^* & \zeta_{n_b,2}^* & \cdots & \zeta_{n_b,a_1}^* \end{bmatrix} \tag{8}$$

$$B = \begin{bmatrix} \eta^*_{1,1} & \eta^*_{1,2} & \cdots & \eta^*_{1,n_i} \\ 0 & \cdots & \cdots & 0 \\ \eta^*_{2,1} & \eta^*_{2,2} & \cdots & \eta^*_{2,n_i} \\ \vdots & \vdots & \ddots & \vdots \\ \eta^*_{n_0,1} & \eta^*_{n_0,2} & \cdots & \eta^*_{n_0,n_i} \end{bmatrix} \quad (9)$$

$$C = \begin{bmatrix} 1 & 0 & \cdots & 0 \\ \vdots & & \ddots & \vdots \\ 0 & \cdots & \cdots & 1 \end{bmatrix} \quad (10)$$

Results

The principle of the proposed controller is illustrated in Figure 2. Essentially, enhanced information about the controlled system may be extracted from the fuzzy model. This information may then be employed in the design of the controller gains in order to achieve optimality of the controller pole locations. In this manner the proposed controller may be described as a Fuzzy Adaptive Sliding Mode Controller (FASMC).

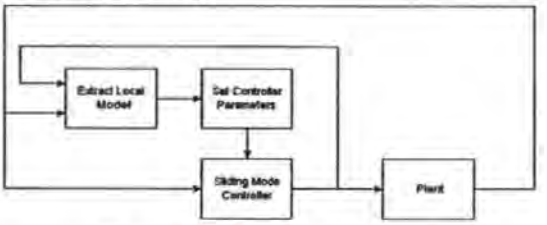

Figure 2: Principle of FASMC

The controller was compared to a benchmark sliding mode controller with integral action [2]. Both controllers were designed to provide critical damping at a natural frequency of 22rad/s. The controllers were tested over a sample period of 70 seconds. Results are illustrated in figure 3.

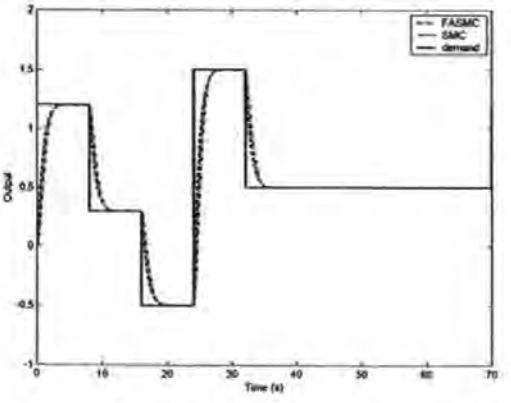

Figure 3: System outputs over 70 seconds

It can be seen that in terms of system response that there is little to differentiate the two.

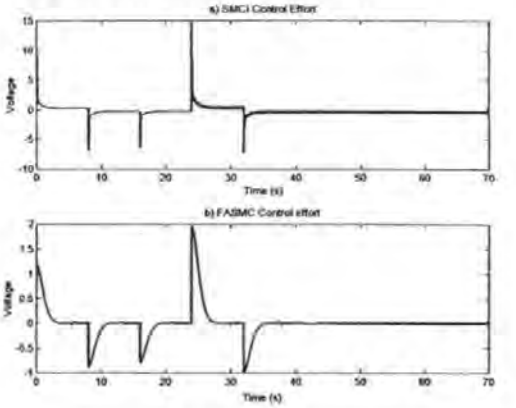

Figure 4: System control efforts

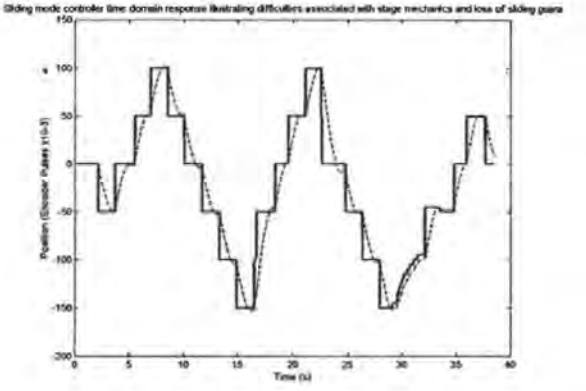

Figure 5: Real time sliding mode controller response

However, consideration of the corresponding control effort (figure 4) shows that that the high gain associated with the SMCI is not apparent with the FASMC. In addition it is worthwhile to note that the ε-vicinity of the FASMC was 6 times smaller than the corresponding SMCI.

Implementation of the SMCI shows good agreement with the simulation results. However, as system load torque varies with position, which is manifested as unmatched disturbance, it can clearly be seen how the controller performance is subject to these effects and how it is left to the integral action states to bring the system back to zero steady state error. This is due entirely to the poor representation of the system by the model.

In a second test, an unmatched disturbance was introduced to the system and the fuzzy model re-trained to incorporate the uncertainty. Figure 6 illustrates the effect of the disturbance on the SMCI, and it can be seen that the disturbance significantly

effects transient performance. Since the disturbance is constant the effects are not as profound as they might be. The FASMC on the other hand appears to recover the system to the steady state in almost the same time as the system without disturbance (figure 6). The initial change in direction is caused by the lack of initial control effort from the controller.

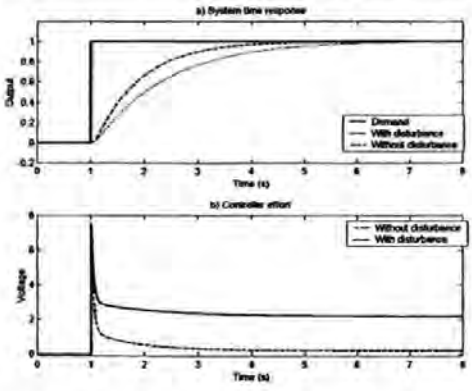

Figure 6: SMCI response to unmatched disturbance

From a practical perspective, it is unlikely that the control system would be subjected to a test of this severity. However, since the load torque has been recognised as unmatched, and since this is known to vary with both position and time [6], similar effects can be observed by simply moving the carriage to a different location and repeating the step change in demand (figure 5).

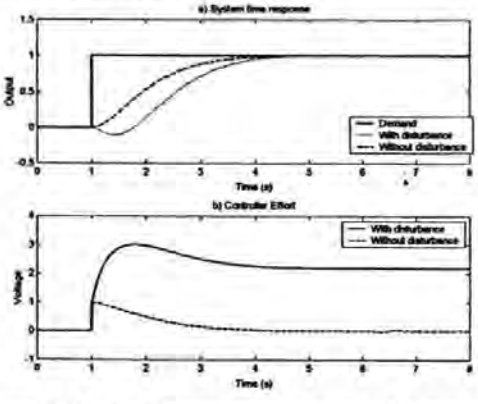

Figure 7: FASMC response to unmatched disturbance

Conclusion

The proposed algorithm has demonstrated how the synergy of traditional control structures and fuzzy logic can be used in order to produce an improved controller. Practical implementation of the sliding mode with integral action controller has demonstrated the ability of this controller to reject unmatched disturbance, as originally discussed in [2], and has also served to validate simulation results obtained. Before the apparent advantages of this controller can be confirmed, further cautious research is required. However, the initial results are suggestive of a controller that demonstrates reduced controller gain, reduced sensitivity to unmatched disturbance and an improved guarantee of final tracking accuracy. Work on the practical implementation of the FASMCI continues.

References

[1] Babuska R, "Fuzzy Modelling for Control", *Kluwer Academic Publishers*, 1998

[2] Davies R., Edwards C and Spurgeon S.K., "Robust tracking with a sliding mode", *in Zinober A.S.I., Variable Structure and Lyapunov Control, Springer-Verlag*, Berlin, pp 51-74. 1994.

[3] Edwards C and Spurgeon S.K. "Sliding Mode Control: Theory and Applications", *Taylor Francis*,1998

[4] Ha Q.P., Rye D.C. and H.F.Durrant-Whyte, "Robust Sliding Mode Control with Application", *International Journal of Control*, 1999. Vol 72, No 12, pp 1087-1096

[5] Itkis U., "Control Systems of Variable Structure", *John Wiley*, 1976.

[6] Knight M.J., Sutton R., Burns R.S, and Jenkins D.F, "A Comparison of Nonlinear Identification Techniques", *Proc. MMAR 2001*, Miedzyzdroje, Poland. pending.

[7] O'Dell B., "Fuzzy sliding mode control: A critical review", *Oklahoma state university*, 1997

[8] Palm R, "Robust Control by Fuzzy Sliding Mode", *Automatica*, 1994. Vol 30, No 9, pp 1429-1438

[9] Roubos J.A., Mollov S., Babuska R and Verbruggen H.B., "Fuzzy model based predictive control using Takagi-Sugeno models", *International journal of Approximate reasoning*, No.22, pp 199-226, 1999

[10] Utkin V.I. "Variable Structure Systems with Sliding Modes", *IEEE Transactions on Automatic Control*, 1977. Vol AC-22 No 2, pp 212-222

[11] Yao, B., "Adaptive robust control of nonlinear systems with application to control of mechanical systems", *PhD Thesis*, University of California, 1992

Fuzzy Model Based Sliding Mode Control

M.J.Knight[1], R.Sutton[1] and D.F.L.Jenkins[2]

1) Department of Mechanical and Marine Engineering, University of Plymouth
2) Department of Communication and Electronic Engineering, University of Plymouth
Tel: (01752)232676 Fax: (01752)232638 Email: *MJKnight@Plymouth.ac.uk*

Keywords: Fuzzy model identification, Adaptive sliding mode control, motor control.

Abstract: A method for combining black box nonlinear models and sliding mode control is presented. In this approach the advantages of the sliding mode control technique are maintained, however parametric uncertainty and unmatched disturbances are acknowledged as limiting factors of controller performance, and their effects are sought to be minimised through the use of local linearisation of the non-linear model. Simulation results demonstrate performance improvements.

1. Introduction

One of the earliest approaches to control of uncertain systems was sliding mode control (SMC) or variable structure control (VSC), first introduced to western researchers in the seminal works of Utkin [1] and Itkis [2]. The central feature of SMC is the sliding mode, in which the dynamic motion of the controlled system is constrained to remain within a prescribed subspace of the full state space. The sliding mode is achieved by ensuring that the prescribed manifold within the state space is made attractive to the system [2]. Once the manifold is reached, the system is forced to remain on it thereafter. When on the manifold, i.e. during the sliding motion, the system dynamics are equivalent to a system of lower order, which is insensitive to both parametric uncertainty and unknown disturbances that satisfy the matching condition.

One of the principle drawbacks in implementation of sliding mode control is that it in general only applies to systems that satisfy the matching condition [3]. Secondly, and more significantly, the control law is discontinuous across the sliding manifold, this leads to a phenomenon termed 'control chatter' in practical systems. Chatter involves high frequency control switching and may lead to excitation of previously neglected high frequency system dynamics. Smoothing techniques such as boundary layer normalisation have been employed in order to negate the effects of control chatter, however such an approach leads to a controller that can only guarantee tacking accuracy to within the ε-vicinity of the demand [4], where ε is the radius of the boundary layer. A compromise must therefore be sought between desired tracking accuracy and controller bandwidth.

In [5] the apparent similarities between the sliding mode and fuzzy controllers was illustrated, which has subsequently motivated considerable research effort in combining the two topologies in a manner that serves to reduce the limitation of the sliding mode. The most common approach to this has been to replace the continuous switching function of the boundary layer with an equivalent fuzzy switching function. However, as pointed out in [6], the fuzzy rule base commonly serves as a mimic of the original switching function and the advantages of such an approach are therefore unclear. Others have used a fuzzy rule base in making the sliding manifold adaptive, e.g. [7], so as to minimise the reaching phase, good results have been reported. Babuška [8] has demonstrated the ability of the affine Takagi-Sugeno model to accurately model a system through rule extraction from cluster data obtained within the regression space. These models may be used subsequently in order to extract locally linear state space models of the system and demonstrate model based control of both single input, single output (SISO) and multi input, multi output (MIMO) systems [9].

In this work, the parametric uncertainty and disturbances that the system is subject to are recognised as the root cause of the high gain feedback requirement and control chatter. It follows that if these uncertainties can be reduced then enhanced controller performance may be expected. The controller improvements are demonstrated through simulation of a D.C. motor with differential equations expressed as

$$L\frac{dI_a}{dt} = -I_a R_a - K_e\omega + V_a \qquad (1)$$

$$J\frac{d\omega}{dt} = -B\omega - T_X + I_a.K_m \qquad (2)$$

Where L is the motor inductance, I_a the armature current, K_e the back E.M.F constant, ω the angular velocity of the armature, J the moment of inertia, B viscous friction, T_x the external load toque, K_m the motor torque constant and V_a the armature voltage. In addition θ is introduced as the armature angular position. These

equations may be rewritten in state space form according to the following,

$X_1 = \theta, X_2 = \frac{d\theta}{dt} = \omega, X_3 = i$ and let

$T_X = U_1$ and $V_a = U_2$

$$\begin{bmatrix} \dot{X}_1 \\ \dot{X}_2 \\ \dot{X}_3 \end{bmatrix} = \begin{bmatrix} 0 & 1 & 0 \\ 0 & -\frac{B}{J} & \frac{K_m}{J} \\ 0 & -\frac{K_e}{L} & -\frac{R_a}{L} \end{bmatrix} \begin{bmatrix} X_1 \\ X_2 \\ X_3 \end{bmatrix} + \begin{bmatrix} 0 \\ -\frac{U_1}{J} \\ \frac{U_2}{L} \end{bmatrix}$$

$$Y_1 = [1 \quad 0 \quad 0] \begin{bmatrix} X_1 \\ X_2 \\ X_3 \end{bmatrix} \tag{3}$$

The model parameters are taken to be

Parameter	Value (Nominal)	Value (Actual)
R_a	1.2Ω	1.5 Ω
L	0.05 H	0.09 H
Ke	0.6	0.6
Km	0.6	0.6
J	0.135	0.15
B	0	0.02

Table 1: Motor parameters

Next within this work, the mechanism for fuzzy identification of this model is considered. After which, consideration to the sliding mode controller design is paid. Results are then presented which demonstrate a significant reduction in controller gain, control chatter and an improvement in controller performance where unmatched disturbance is introduced.

2. Fuzzy Identification

Fuzzy identification is a term used that has come to represent the use of fuzzy logic in the modelling and representation of a system. Since fuzzy models may be viewed as general function approximators, they are readily applied to the nonlinear regression problem. There are two fundamentally different approaches that may be taken in the identification of a system. Firstly the system may be identified through explicit expression of system performance, e.g. '*if* voltage is high *then* velocity is high'. Secondly, and the approach adopted within this work is to decompose the model into a static nonlinear regression. The problem of model identification is then decomposed into two separate problems, the first is selection of the 'regression structure, the second, the selection of the fuzzy model form, for example, the required number of membership functions and membership crispness.

The desired regression may be expressed in the form

$$\hat{y}(t|\theta) = f(\varphi(t), \theta) \tag{4}$$

where y is the regressand, θ the *vector of regressions* which is to be parameterised in the identification process, and the vector $\varphi(t)$ is known as the *regression vector*, its parameters the *regressors*. It has been shown in [8] that the regression surface within the product space may be represented as a series of local approximations.

Through use of a clustering algorithm such as the Gustafson-Kessel algorithm, it is possible to derive local approximations to this regression surface. Further, through the use of the eigenvalues of the cluster covariance matrix given by

$$F_i = \frac{\sum_{k=1}^{N} (\mu_{i,k})^m (z_k - v_i)(z_k - v_i)^T}{\sum_{k=1}^{N} (\mu_{i,k})^m} \tag{5}$$

it is possible to interpret these local models and subsequently derive a fuzzy rule to represent this local approximation. In repeating this process for each data cluster, a global model of the system may be generated. Previous work has considered the accuracy of this approach in comparison to neural networks and 'white box' models, and results have demonstrated that this local approach to modelling can improve results [10].

The rule extraction process is briefly discussed here for completeness, however the reader is directed to [8] for a far more complete discussion.

It has been shown that a useful form of the fuzzy consequent is the affine linear form [11] of the Takagi-Sugeno (TS) model, in which rules are structured according to (6):

$$y_i = a_i^T x + b_i \tag{6}$$

where a_i is the so called parameter vector and b_i is an offset. Within the product space ($\mathbb{R}^{P+1 \times N}$) the affine Takagi-Sugeno consequents may be viewed geometrically as hyperplanes. The antecedent of the rule defines a fuzzy validity region for the corresponding hyperplane. The output y of the TS model is computed using the fuzzy mean formula

$$y = \frac{\sum_{i=1}^{c} \beta_i(x) y_i}{\sum_{i=1}^{c} \beta_i(x)} \tag{7}$$

where $\beta_i(x)$ represents the degree of fulfilment of the i^{th} rules antecedent, which is simply a measure of the degree of fulfilment of x in the fuzzy set A_i and is given by

$$\beta_i = \mu_{Ai}(x) \tag{8}$$

Since it may become difficult to interpret multidimensional fuzzy sets, the antecedent proposition is commonly defined in a conjunctive form, given by a series of single dimensional fuzzy sets combined with simple propositions. In this case the degrees of fulfilment are calculated as $\beta_i(x) = \mu_{Ai,1}(x_1) \wedge \ldots \wedge \mu_{Ai,P}(x_P)$, where the min operator ($\wedge$) may be replaced by alternative T-norms. In this case the model output is calculated

$$y = \left(\sum_{i=1}^{K} \gamma_i(x) a_i^T \right) x + \sum_{i=1}^{K} \gamma_i(x) b_i = \tilde{a}^T(x) x + \tilde{b}(x) \tag{9}$$

where γ_i is the normalised degree of fulfilment, given by

$$\gamma_i(x) = \frac{\beta_i(x)}{\sum_{j=1}^{K} \beta_j(x)} \tag{10}$$

and $\tilde{a}(x)$ and $\tilde{b}(x)$ are input dependent parameters, given as convex linear combinations of the constant parameters a_i and b_i through the following relationship

$$\tilde{a}(x) = \Sigma_{i=1}^{K} \gamma_i(x) a_i \tag{11}$$

$$\tilde{b}(x) = \Sigma_{i=1}^{K} \gamma_i(x) b_i \tag{12}$$

The regression structure discussed previously (4) may be expressed in this pseudo linear form according to the following

$$\hat{y}(k+1) = \sum_{j=1}^{n_y} a_{i,j} y(k-j+1) + \sum_{j=1}^{n_u} b_{i,j} u(k-j+1) + c_i \tag{13}$$

The distance measure of the clustering algorithm, given by

$$D(x_k, v_i^x) = (x_k - v_i)^T F_i^x (x_k - v_i) \tag{14}$$

may be inverted and used to provide the degree of fulfilment of each rule for given data. One possible choice of inversion is to use the same equation as for the clustering algorithm

$$\beta_i(x_k) = \frac{1}{\sum_{j=1}^{c} \left[d(x_k, v_i^x) / d(x_k, v_j^x) \right]^{2/m-1}} \tag{15}$$

which takes all rules into account and calculates the degree of fulfilment of one rule with respect to the others. Once the antecedent parameters have been calculated, the consequent parameters require derivation. There are two ways in which the fuzzy consequent parameters of the affine TS model may be calculated from the data clusters. The first is based around the geometric interpretation of the cluster, using the covariance matrix. The alternative approach is a local least squares optimisation method based on the derived fuzzy partition matrix. The former method is discussed here. The eigenstructure of the cluster covariance matrix loosely describes the shape of the cluster. The shortest eigenvector describes the normal vector to the hyperplane spanned by the remaining eigenvectors. The shortest eigenvector is defined as Φ_i. Based on the dataset $Z^N = [x^T; y]^T$ and the cluster prototype, the consequent may be described implicitly by

$$\Phi_i \bullet \left(Z^N - v_i \right) = 0 \tag{16}$$

The shortest eigenvector and the cluster prototype may be divided into a vector corresponding to the regressor x and a scalar corresponding to the regressand y. i.e.

$$v_i = \left[\left(v_i^x \right)^T ; v_i^y \right]^T \tag{17}$$

$$\Phi_i = \left[\left(\Phi_i^x \right)^T ; \Phi_i^y \right]^T \tag{18}$$

may now be rewritten according to

$$\left[\left(\Phi_i^x \right)^T ; \Phi_i^y \right] \bullet \left(\left[x^T ; y \right]^T - \left[\left(v_i^x \right)^T ; v_i^y \right]^T \right) = 0 \tag{19}$$

After Simplification

$$y = \underbrace{-\frac{1}{\Phi_i^y} \left(\Phi_i^x \right)^T}_{a_i^T} x + \underbrace{\frac{1}{\Phi_i^y} \Phi_i^T v_i}_{b_i} \tag{20}$$

which is directly equivalent to the affine Takagi-Sugeno model consequent.

This approach was employed in the identification of the model given in (3). A regression structure of [3 1] was used with 5 clusters. Of importance to the identification of the model is the selection of the input signal, in this case a stepwise random signal was used. The percentile variance accounted for (VAF) measure, which provides a measure of model tracking accuracy was calculated as 99.2% which indicates good model accuracy.

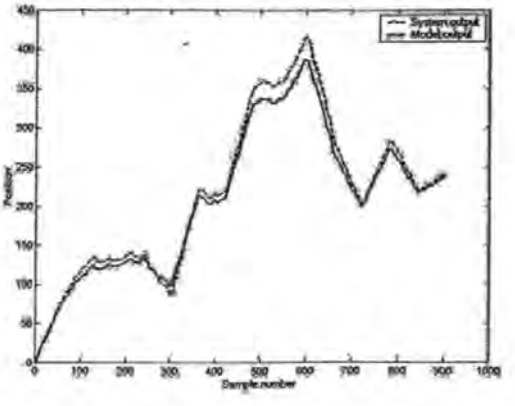

Figure 1: *Model output vs System output*

3. Model Extraction

The work in [9] presents a method whereby the fuzzy clustered model may be represented as a local linear state space model. The following is an overview of the method adopted. The regression vector, which is represented by ε_l is given by

$$\varepsilon_l(k)=\left[\left\{y_p(k)\right\}_0^{n_{a1}},\ldots,\left\{y_p(k)\right\}_0^{n_{ay}} ,\left\{u_1(k+1)\right\}_{n_{a1}}^{n_{a1}},\ldots,\left\{u_m(k+1)\right\}_{n_{dm}}^{n_{dm}}\right] \quad (21)$$

An affine Takagi-Sugeno rule may be represented by

$$y_l(k+1)=\frac{\sum_{i=1}^{K_l}\beta_{li}(\varepsilon_l)\left(\zeta_{li}y(k)+\eta_{li}u(k)+\theta_{li}\right)}{\sum_{i=1}^{K_l}\beta_{li}} \quad (22)$$

ζ and η are vectors of polynomials in the previous sample (y(k-1)), and θ the offset. K_l is the number of rules of the l^{th} offset. The model output is calculated as the degree of fulfilment $\mu_{li}(\varepsilon_{lh})$ for each antecedent variable and the resulting degrees of fulfilment (β_{li}) for every rule are combined with the linear consequence according to the following

$$\beta_{li}(\varepsilon_l)=\prod_{h=1}^{p}\mu_{ih}(\varepsilon_{lh}) \quad (23)$$

Once the Takagi Sugeno model has been derived, local linear state space models can be calculated according to the following,

$$y_l(k+1)=\frac{\sum_{i=1}^{K_l}\mu_{li}(x_l(k))\cdot y_{li}(k+1)}{\sum_{i=1}^{K_l}\mu_{li}(x_l(k))} \quad (24)$$

$$y_{li}(k+1)=\left(\zeta_{li}y(k)+\eta_{li}u(k)+\theta_{li}\right) \quad (25)$$

where

$$\zeta_{li}^{*}=\frac{\sum_{i=1}^{K_l}\mu_{li}(x_l(k))\cdot\zeta_{li}}{\sum_{i=1}^{K_l}\mu_{li}(x_l(k))} \quad (26)$$

$$\eta_{li}^{*}=\frac{\sum_{i=1}^{K_l}\mu_{li}(x_l(k))\cdot\eta_{li}}{\sum_{i=1}^{K_l}\mu_{li}(x_l(k))} \quad (27)$$

and

$$\theta_{li}^{*}=\frac{\sum_{i=1}^{K_l}\mu_{li}(x_l(k))\cdot\theta_{li}}{\sum_{i=1}^{K_l}\mu_{li}(x_l(k))} \quad (28)$$

In the case here, previous inputs are not considered and the A, B and C matrices of the model are thus simplified, the matrices are given

$$A=\begin{bmatrix}\zeta_{1,1}^{*} & \zeta_{1,2}^{*} & \cdots & \zeta_{1,\alpha_1}^{*}\\ 1 & 0 & \cdots & 0\\ \zeta_{2,1}^{*} & \zeta_{2,2}^{*} & \cdots & \zeta_{2,\alpha_1}^{*}\\ 0 & \vdots & \ddots & \vdots\\ \zeta_{n_0,1}^{*} & \zeta_{n_0,2}^{*} & \cdots & \zeta_{n_0,\alpha_1}^{*}\end{bmatrix} \quad (29)$$

$$B=\begin{bmatrix}\eta_{1,1}^{*} & \eta_{1,2}^{*} & \cdots & \eta_{1,n_i}^{*}\\ 0 & \cdots & \cdots & 0\\ \eta_{2,1}^{*} & \eta_{2,2}^{*} & \cdots & \eta_{2,n_i}^{*}\\ \vdots & \vdots & \ddots & \vdots\\ \eta_{n_0,1}^{*} & \eta_{n_0,2}^{*} & \cdots & \eta_{n_0,n_i}^{*}\end{bmatrix} \quad (30)$$

$$C=\begin{bmatrix}1 & 0 & \cdots & 0\\ \vdots & & \ddots & \vdots\\ 0 & \cdots & \cdots & 1\end{bmatrix} \quad (31)$$

4. Sliding Mode

Once local models of the system have been extracted, they may be used in order to provide enhanced information to the sliding mode controller. The theory associated with the design of the sliding mode controller is revised here, and once again the reader is referred to the many excellent texts available on the subject, e.g. [2], [4]. As alluded to in the introduction, the sliding motion is control independent and depends only on the choice of sliding surface. In terms of controller design it is convenient to convert the system equations into a suitable canonical form. In this form the system is decomposed into two connected subsystems, one acting in within the range space of matrix B and the other within the null space of the manifold S. In terms of design, the problem then becomes one of state feedback given desired system eigenvalue locations. Since by assumption the matrix B is of full rank, there exists an orthogonal matrix $T_r \in \mathbb{R}^{nxn}$ such that

$$T_r B=\begin{bmatrix}0\\ B_2\end{bmatrix} \quad (32)$$

where $B_2 \in \mathbb{R}^{mxm}$ and is non-singular. Let $z = Tx$ and partition the new co-ordinates so that

$$z=\begin{bmatrix}z_1\\ z_2\end{bmatrix} \quad (33)$$

where $z_1 \in \mathbb{R}^{n-m}$ and $z_2 \in \mathbb{R}^{m}$. The nominal linear system can then be written as

$$\dot{z}_1(t)=A_{11}z_1(t)+A_{12}z_2(t) \quad (34)$$

$$\dot{z}_2(t)=A_{21}z_1(t)+A_{22}z_2(t)+B_2u(t) \quad (35)$$

commonly known as the regular form. Equation (34) is referred to as describing the null-space dynamics and

equation (35) as describing the range-space dynamics. From the perspective of the extracted local models, it is convenient to first convert the matrices to the controllability canonical form, thus the system is guaranteed to be in the regular form for subsequent design. Suppose the matrix defining the switching function (in the new co-ordinate system) is compatibly partitioned with z as

$$ST_r^T = [S_1 \quad S_2] \tag{36}$$

where $S_1 \in \mathbb{R}^{mx(nxm)}$ and $S_2 \in \mathbb{R}^{mxm}$. Since $SB = S_2B_2$ it follows that a necessary and sufficient condition for the matrix SB to be non-singular is that the determinant of S_2 is non zero. It is reasonable to assume that this condition will be met by design. During an ideal sliding motion

$$S_1 z_1(t) + S_2 z_2(t) = 0 \quad \text{for all } t > t_s \tag{37}$$

and therefore formally expressing $z_2(t)$ in terms of $z_1(t)$ yields

$$z_2(t) = -Mz_1(t) \tag{38}$$

where $M = S_2^{-1}S_1$. Substituting into (34) gives

$$\dot{z}_1(t) = (A_{11} - A_{12}M)z_1(t) \tag{39}$$

$z_2(t)$ is considered to play the role of the control action. The switching surface design problem can therefore be considered to be one of choosing a state feedback matrix M to stabilise the reduced order system (A11, A12).

At this point the unit vector approach is introduced. Consider an uncertain system of the form

$$\dot{x}(t) = Ax(t) + Bu(t) + f(t,x,u) \tag{40}$$

where the function $f : \mathbb{R} \times \mathbb{R}^n \times \mathbb{R}^m \rightarrow \mathbb{R}^m$ which represents the uncertainties or non-linearities satisfying the so-called matching condition, i.e.

$$f(t, x, u) = B\xi(t, x, u) \tag{41}$$

where ξ is unknown but satisfies the following inequality

$$\|\xi(t,x,u)\| \le k_1\|u\| + \alpha(t,x) \tag{42}$$

where $1 > k_1 \ge 0$ is a known constant and $\alpha(\cdot)$ is a known function. The proposed control law comprises two components; a linear component to stabilise the nominal linear system; and a discontinuous component. Specifically

$$u(t) = u_l(t) + u_n(t) \tag{43}$$

where the linear component is given by

$$u_l(t) = -\Lambda^{-1}(SA - \Phi S)x(t) \tag{44}$$

where Φ is any stable design matrix and $\Lambda = SB$. The non-linear component is defined as

$$u_n(t) = -\rho(t,x)\Lambda^{-1}\frac{P_2 s(t)}{\|P_2 s(t)\| + \varepsilon} \quad \text{for all } s \neq 0 \tag{45}$$

where P_2 is a symmetric positive definite matrix that satisfies the Lyapunov equation

$$P_2\Phi + \Phi^T P_2 = -I \tag{46}$$

and the scalar function $\rho(t; x)$, which depends only on the magnitude of the uncertainty, is any function satisfying

$$\rho(t,x) \ge \frac{(k_1\|u_l\| + \alpha(t,x) + \gamma)}{(1 - k_1\kappa(\Lambda))} \tag{47}$$

where $\gamma > 0$ is a design parameter. ε is the radius of the boundary layer may be shown to be dependent on the actuator time constant and inversely proportional to the available control resources. In this equation it is assumed that the scaling parameter has been chosen so that $k_1\kappa(\Lambda) < 1$. It can be established that any function satisfying equation (47) also satisfies

$$\rho(t,x) \ge \|\xi(t,x,u)\| + \gamma \tag{48}$$

and therefore $\rho(t; x)$ is greater in magnitude than the matched uncertainty occurring in this equation. It can be verified that $V(s)=s^TP_2s$ guarantees quadratic stability for the switching states and in particular

$$\dot{V} \le -s^T s - 2\gamma\|P_2 s\| \tag{49}$$

This control law guarantees that the switching surface is reached in finite time despite the disturbance or uncertainty and once the sliding motion is attained it is completely independent of the uncertainty.

Now consider the introduction of additional states $x_r \in \mathbb{R}^p$ satisfying

$$\dot{x}_r = r(t) - y(t) \tag{50}$$

where the differentiable signal r(t) satisfies

$$\dot{r}(t) = \Gamma(r(t) - R) \tag{51}$$

with Γ a stable design matrix and R a constant demand vector. Augment the states with the integral action states and define

$$\tilde{x} = \begin{bmatrix} x_r \\ x \end{bmatrix} \tag{52}$$

The associated system and input distribution matrices for the augmented system are

$$\tilde{A} = \begin{bmatrix} 0 & -C \\ 0 & A \end{bmatrix} \text{ and } \tilde{B} = \begin{bmatrix} 0 \\ B \end{bmatrix} \tag{53}$$

assuming the pair (A, B) is in regular form, the pair $(\tilde{A}, \tilde{B})$ is also in regular form. The proposed controller seeks to induce a sliding motion on the surface

$$S = \{\tilde{x} \in \mathbb{R}^{n+p} : S\tilde{x} = S_r r\} \tag{54}$$

where S and S_r are design parameters, which govern the reduced order motion. The hyperplane system matrix and system matrix are partitioned as

$$S = \left[\overbrace{S_1}^{n} \quad \overbrace{S_2}^{m} \right] \tag{55}$$

$$\tilde{A} = \begin{bmatrix} \overbrace{\tilde{A}_{11}}^{n} & \overbrace{\tilde{A}_{12}}^{m} \\ \tilde{A}_{21} & \tilde{A}_{22} \end{bmatrix} \begin{matrix} \updownarrow n \\ \updownarrow m \end{matrix} \tag{56}$$

and assume $\Lambda = S\tilde{B}$ is non-singular. If a controller exists which induces an ideal sliding motion on S and the augmented states are suitably partitioned, then the ideal sliding motion is given by

$$\dot{x}_1(t) = \left(\tilde{A}_{11} - \tilde{A}_{12}M\right)x_1(t) + \left(\tilde{A}_{12}S_2^{-1}S_r + B_r\right)r(t) \tag{57}$$

where $M = S_2^{-1}S_1$ and $Br = [I_p \; 0_{nxp}]^T$. In order for the hyperplane design method to be valid, it is necessary for the matrix pair $(\tilde{A}_{11}, \tilde{A}_{12})$ to be completely controllable. The overall control law is then given by

$$u = u_l(\tilde{x}, r) + u_n(\tilde{x}, r) \tag{58}$$

where the discontinuous vector u_n is given by

$$u_n(s,r) = \begin{cases} -\rho_\epsilon(u_L, y)\Lambda^{-1} & if\ S\tilde{x} \neq S_r r \\ 0 & otherwise \end{cases} \tag{59}$$

It follows that, in terms of the original co-ordinates the control vector u_l is given by

$$u_l(\tilde{x}, r) = L\tilde{x} + L_r r + L_i \dot{r} \tag{60}$$

with gains defined as

$$L = -\Lambda^{-1}(S\tilde{A} - \Phi S) \tag{61}$$

$$L_r = -\Lambda^{-1}(\Phi S_r + S_1 B_r) \tag{62}$$

$$L_i = \Lambda^{-1} S_r \tag{63}$$

The parameter S_r can take any value and does not affect the stability of the closed loop system.

5. Controller structure and performance

A benchmark sliding mode controller with integral action (SMCI) of the form previously discussed was developed to control the motor model of equation (3), using the nominal parameters of table 1. All simulations were carried out using the actual parameters shown in table 1.

The principle of the proposed controller uses the design procedures discussed above to redesign the controller based on the enhanced information provided by the fuzzy model matrices. The controller is therefore referred to as a fuzzy adaptive sliding mode controller (FASMC) and its principle is illustrated in figure 2,

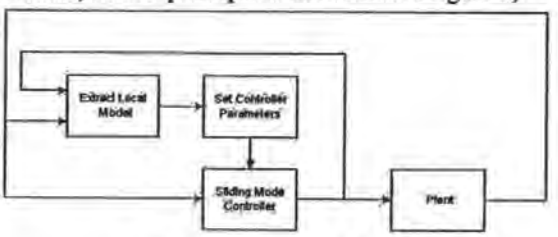

Figure 2: *Principle of FASMC*

both controllers were initially designed to provide damping ratio of 1 at 22rad/s. The controllers were driven over a simulation sample period of 70 seconds. Results are illustrated in figure 3.

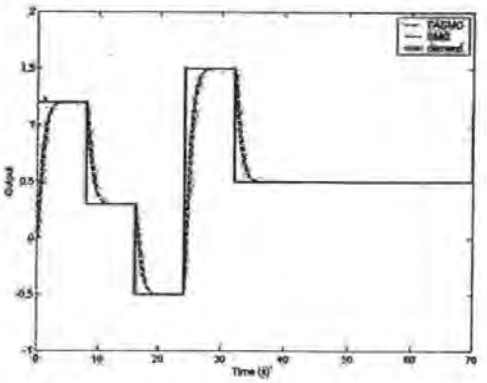

Figure 3: *System outputs over 70 seconds*

It can be seen that in terms of system response that there is little to differentiate between the two. However, consideration of the corresponding control effort (Figure 4) shows that that the high gain requirement of the SMCI is relaxed by the FASMC. In addition it is worthwhile to note that the ε-vicinity of the FASMC was 6 times smaller than the corresponding SMCI.

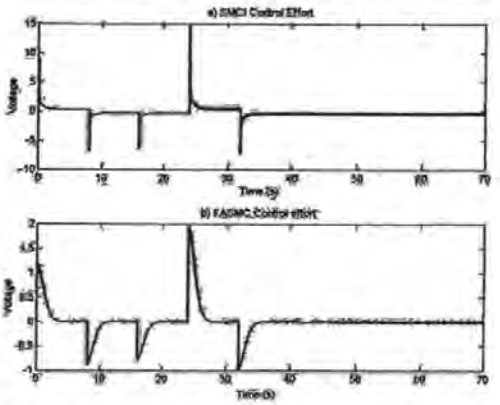

Figure 4: *System control efforts*

A second test introduced unmatched disturbance to the system and the fuzzy model retrained to incorporate the uncertainty. Figure 5 illustrates the effect of the disturbance on the SMCI, it can be seen that the disturbance significantly effects transient performance. Since the disturbance is constant the effects are not as profound as they might be. The FASMC, on the other hand, appears to recover the system to the steady state in almost the same time as the system without disturbance (figure 6). The initial change in direction is caused by the lack of initial control effort from the controller, which in this case is a disadvantage.

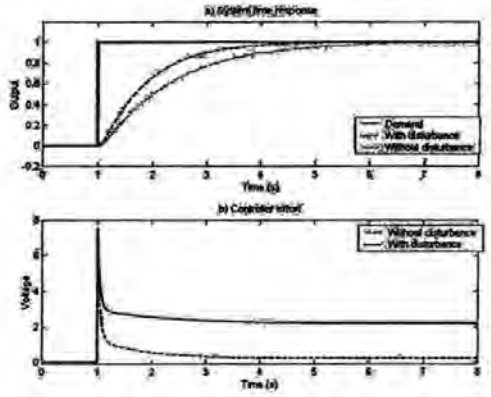

Figure 5: SMCI response to unmatched disturbance

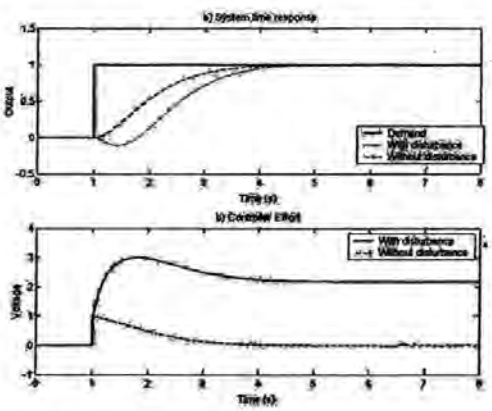

Figure 6: FASMC response to unmatched disturbance

6. Conclusions

A new controller based on sliding mode design approaches and a nonlinear black box model has been presented. Performance of the controller has been compared with a benchmark sliding mode controller and the controllers response has been found to be favourable. This work is currently in its initial stages and further cautious research must be carried out before the apparent advantages of this approach can be confirmed. However, the controller has initially demonstrated clear advantages of using fuzzy logic in conjunction with sliding mode in terms of increased final tracking accuracy, reduced controller gain requirement and reduced sensitivity to unmatched disturbance. FASMC in this work only extends to the SISO case and in addition, it is assumed that input/output data is available for the system it is finally pointed out that implementation of this algorithm is significantly more complex than the SMCI. Further work will concentrate on the implementation of the controller in a practical system and the development of proofs for the apparent controller characteristics. Subsequent work will extend the above work to the MIMO case.

7. References

[1] Utkin V.I. "*Variable Structure Systems with Sliding Modes*", IEEE Transactions on Automatic Control, 1977. Vol AC-22 No 2, pp 212-222

[2] Itkis U., "*Control Systems of Variable Structure*", John Wiley, 1976.

[3] Yao, B., 'Adaptive robust control of nonlinear systems with application to control of mechanical systems", PhD Thesis, University of California, 1992

[4] Edwards C and Spurgeon S.K. "*Sliding Mode Control: Theory and Applications*", Taylor Francis,1998

[5] Palm R, "*Robust Control by Fuzzy Sliding Mode*", Automatica, 1994. Vol 30, No 9, pp 1429-1438

[6] O'Dell B., "*Fuzzy sliding mode control: A critical review*", Oklahoma state university, 1997

[7] Ha Q.P., Rye D.C. and H.F.Durrant-Whyte, "*Robust Sliding Mode Control with Application*", International Journal of Control, 1999. Vol 72, No 12, pp 1087-1096

[8] Babuska R, *Fuzzy Modelling for Control*, Kluwer Academic Publishers,.1998

[9] Roubos J.A., Mollov S., Babuska R and Verbruggen H.B., "*Fuzzy model based predictive control using Takagi-Sugeno models*", International journal of Approximate reasoning, No.22, pp 199-226, 1999

[10] Knight M.J., Sutton R., Burns R.S, and Jenkins D.F, "*Identification of a Brushless D.C. Motor using Grey Box Modelling Techniques*", ICSE 2000, Coventry, UK. pp323-328. 2000

[11] Takagi T and Sugeno M, *Fuzzy Identification and its applications to Modelling and Control*, IEEE Trans. on Systems, Man and Cybernetics, Vol 15, No 1, Jan/Feb 1985

MMAR 2001 28-31 August 2001, Międzyzdroje, Poland
7th IEEE International Conference on Methods and Models in Automation and Robotics

A COMPARISON OF NONLINEAR IDENTIFICATION TECHNIQUES

M.J.KNIGHT †, R.SUTTON †, R.S.BURNS †, D.F.L.JENKINS ‡

†) *Department of Mechanical and Marine Engineering, University of Plymouth*

‡) *Department of Communication and Electronic Engineering, University of Plymouth*

Tel: (01752)232676 Fax: (01752)232638 Email: MJKnight@Plymouth.ac.uk

Abstract. Nonlinear identification techniques are in common use within research domains. This approach to modelling has been shown repeatedly within the literature to provide favourable results when attempting to model poorly understood systems. This paper presents a comparison of fuzzy and neural network identification techniques applied to input/output data collected from an experimental test rig.

Key Words: Identification, fuzzy modelling, neural network modelling.

1. INTRODUCTION

Nonlinear identification techniques are in common use across a broad spectrum of research disciplines. Within the field of system identification, nonlinear models have found application in fields as diverse as chemical process modelling [1] to banana ripeness testing [2].

Within this work nonlinear models based on artificial intelligence are applied to a regression structure for the identification of a custom built linear positioning mechanism. The test system has been specifically designed to exhibit high sensitivity to load nonlinearity. In this case the non-linearity is friction which is well known to be time variant [3], and will be shown to vary with linear displacement. Identification of the system is therefore a nontrivial task and provides the opportunity to compare the modelling approaches adopted.

2. EXPERIMENTAL TEST SYSTEM

The test rig schematic can be found in Figure 1. The incremental encoder (IENC) provides 2000 pulses per revolution of the motor. This is the principle sensor used for position feedback. The gear system in this case is a lead screw with nut, which is coupled between the brushless direct current (BLDC) motor and the mechanism carriage. The amplifier serves to provide the motor with an excitation voltage. All identification data is captured in the open loop, performance of the system is therefore heavily dependent on the frictional perturbation apparent at the motor armature. This friction is due to i) Rubbing and viscous between the nut and the leadscrew ii) Viscous friction between carriage and slide rails iii) manufacturing alignment error and finally, although to a far lesser extent [4] ,iv) friction within the journal bearings.

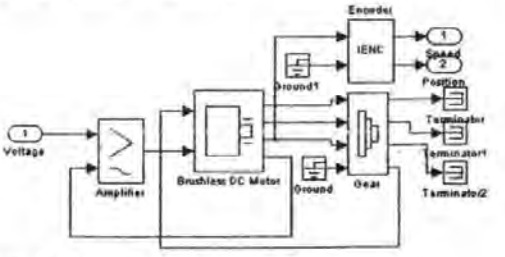

Figure 1: Schematic diagram of test system

Open loop speed of the carriage across the total travel of the stage has been measured in both directions (Fig. 2). The following equation provides the relationship between motor speed and load torque.

$$\omega = \frac{V}{KR} - \frac{T_m}{K^2 R} \qquad (1)$$

Manipulation of (1) yields the ideal angular speed, ω_i (when T_m=0) and the stall torque of the motor, T_{ms} (when ω=0)

The actual torque, assuming a linear relationship between ω and T_L is given as a fraction of the stall torque

$$T_m = T_{ms} \cdot \left(1 - \frac{n}{n_i}\right) - T_F \qquad (2)$$

From Fig. 2 it may now be readily seen that the load torque significantly varies, and is non-symmetrical, across the stage length.

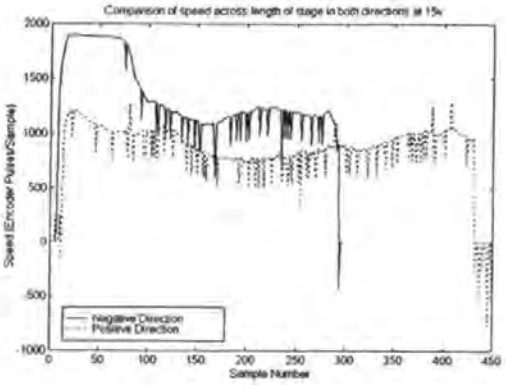

Figure 2: Motor speed across mechanism travel

This fact will be shown to have significant impact on models derived later within this work.
At this point it is timely to introduce the performance measure used to assess the models tested later within this paper. The percentile variance accounted for (VAF) is given as

$$VAF = 100\% \cdot \left[1 - \frac{\mathrm{var}(y - \hat{y})}{\mathrm{var}(y)}\right] \qquad (3)$$

When the model out output ($\hat{y}$) and the system output (y) are identical, the VAF is given as 100%, if the model is in error then the measure is lower. This provides a convenient figure for immediate assessment of model quality.

3. MODELLING

Within the literature there are many models available to describe the BLDC motor. These vary in complexity from comparatively simple third-order state-space models, to extremely elaborate models based on the motor magnetic circuit. Here a compromise between computational load and model accuracy is struck through use of the phase co-ordinate model, a more detailed description of which can be found in [5].

3.1 The phase co-ordinate model

When cylindrical pole permanent magnet rotors are used, all stator inductances are independent of rotor position. Only the motion related inductances between the permanent magnet equivalent circuit and the stator windings depend on rotor position.

$$[L]_{PM} = \begin{bmatrix} L_s & L_{ab} & L_{ab} & L_{af}(\theta_{er}) \\ L_{ab} & L_s & L_{ab} & L_{af}(\theta_{er}) \\ L_{ab} & L_{ab} & L_s & L_{af}(\theta_{er}) \\ L_{af}(\theta_{er}) & L_{af}(\theta_{er}) & L_{af}(\theta_{er}) & 0 \end{bmatrix} \qquad (4)$$

The stator self inductance L_s and the stator/stator mutual inductances L_{ab} are all equal to each other. To a first approximation

$$L_{ab} = -\frac{L_0}{3} \qquad (5)$$

Where L_o is the nominal inductance specified by the manufacturer. The voltage/current equation in phase co-ordinates is:

$$\begin{bmatrix} V_s \\ V_r \end{bmatrix} = \begin{bmatrix} r_s & 0 \\ 0 & r_r \end{bmatrix} \cdot \begin{bmatrix} i_s \\ i_r \end{bmatrix} + \frac{d}{dt}\begin{bmatrix} \lambda_s \\ \lambda_r \end{bmatrix} \qquad (6)$$

with

$$[\lambda] = [L(\theta_{er})] \cdot [i] \qquad (7)$$

$$[i] = [i_a, i_b, i_c, i_{f_0}] \qquad (8)$$

$$[r] = diag[r_s, r_s, r_s, 0] \qquad (9)$$

$$[\lambda] = [\lambda_a, \lambda_b, \lambda_c, 0] \qquad (10)$$

Where i is the applied phase current, r is the nominal stator resistance, λ the magnetic flux and $L(\theta_{er})$ is the time varying inductance, dependent on angular position θ_{er}. The motion equations are given

$$\frac{J}{p}\frac{d\omega_r}{dt} = T_e - T_{Load} \qquad (11)$$

$$\frac{d(\theta_{er})}{dt} = \frac{\omega_r}{p} \qquad (12)$$

Where J is the moment of inertia of the load, p is the number of motor poles, ω_r is the angular velocity of the armature, T_e is the electromagnetic torque and T_{load} is the torque applied by the load. The load torque was taken as 1200mNm nominal, from Fig. 1, i.e. the load torque was considered constant throughout the stage travel. Fig. 3 illustrates the model performance when compared with the actual

performance under step input excitation. All motor parameters were taken

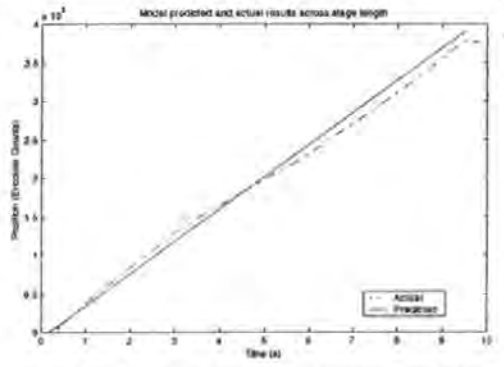

Figure 3. Step input excitation comparison between linear model and actual system response

from the motor manufacturers data sheet. The inertial load of the system was unknown and was used to tune the model. Results can be seen to be quite satisfactory. It is significant that zero speed crossing has not been considered within this simulation. In order to achieve fair comparisons between the models, a validation data set of 30000 samples has been collected, Fig. 4. This data has been subsequently decimated where computational limitations have occurred.

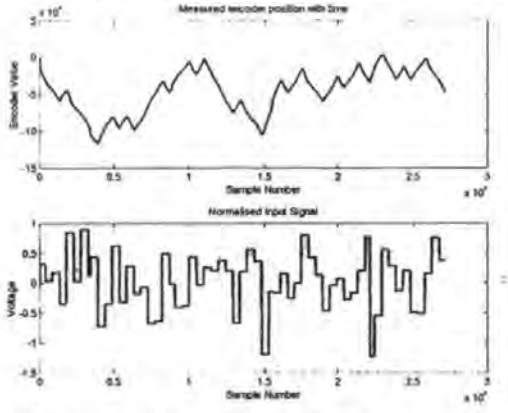

Figure 4. Training and validation data

The fuzzy and neural models require a training set and a validation set. For these models the collected data was divided into halves, and the models were trained on the first set, and tested on the last. Since the motor model does not require training in the same manner as these models, the comparison between the model and system was carried out over the entire test period. The results are shown in Fig. 5. The calculated VAF is given as 38.23%.

It can be seen that the model most likely suffers from incorrect frictional and inertial parameters, in addition the cumulative effects of speed zero crossing, and unmodelled nonlinearities within the system, such as amplifier dead time are attributed to the performance of the model.

4. IDENTIFICATION

In light of the fact that the system parameters are not known precisely, it is preferable to model the system according to the black or grey box modelling paradigms, whereby a structure of known flexibility is chosen and input/output data is used to train the model. The autoregressive with exogenous variable (ARX) structure has been selected for fitting under both neural network and fuzzy methods.

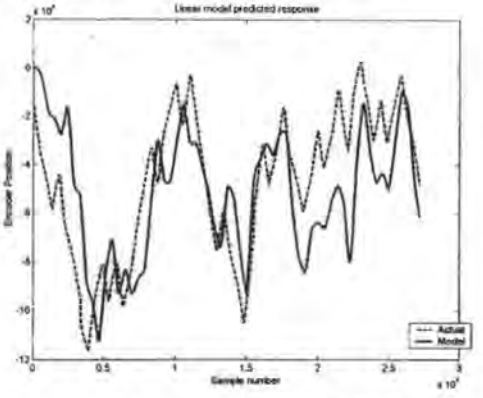

Figure 5. White box model performance with validation data

The ARX structure is introduced as

$$y(t) = \varphi^T(t)\theta \tag{13}$$

where

$$\theta = [a_1 \ldots a_n \quad b_1 \ldots b_m]^T \tag{14}$$

$$\varphi(t) = [-y(t-1) \ldots -y(t-n) \quad u(t-1) \ldots u(t-m)] \tag{15}$$

θ is the regression vector for tuning, $\varphi(t)$ is the vector of previous inputs (u) and outputs of the system (y). When using a neural network or a fuzzy clustering method, the problem neatly divides into

(a) Choosing the regression structure
(b) Choosing the parameters of the tuning method

The difference between the two approaches can be considered as the difference between global modelling (neural network model) and local modelling (fuzzy model). The two are discussed in further detail below. From the perspective of available data, several parameters have been measured directly from the system and are available for use within the regression structure.

(a) Position
(b) Speed
(c) Applied voltage

In addition, with knowledge of the above three parameters, two additional vectors may be calculated

(d) Linear white box model prediction, (4)-(12)
(e) Load torque, (2)

The position vector is used as the regressand in all cases, in addition, because of noise created in numerical differentiation of the position data, the speed vector is only used in the derivation of the load torque vector (e). It has already been seen that the load torque has a significant effect on the system performance and is therefore physically relevant and should be included within the regression structure, possibly after filtration. Whether the applied voltage should be used directly, or first filtered through the motor model is a question under consideration within this paper and is thus deferred for later discussion. The Matlab system Identification toolbox was used for rapid prototyping of the ARX model and a 4,4,1 structure was found to be the most suitable for the available data.

4.1 Neural Network based ARX

Neural networks are a popular tool for pattern recognition and are used increasingly for system identification [6]. The neural network used here is a two-layer perceptron network of the form

$$\hat{y}_i(\theta) = F_i\left(\sum_{j=1}^{n_h} W_{ij} f_j\left(\sum_{l=1}^{n_\varphi} w_{jl}\varphi + w_{j0}\right) + W_{i0}\right) \tag{16}$$

and the mean square error of the estimate is used for the criterion of fit:

$$W_N(\theta, Z^N) = \frac{1}{2N}\sum_{t=1}^{N}\left(y(t) - \hat{y}(t|\theta)\right)^2 + \frac{1}{2N}\theta^T D\theta \tag{17}$$

W is given as the network weights, F is the activation function, N is the number of data in the training set and w is the network thresholds. After scaling of the data and training with the Levenberg-Marquardt algorithm, the model typically gave simulation results as shown in Fig 6. The VAF in this case is 99.98%.

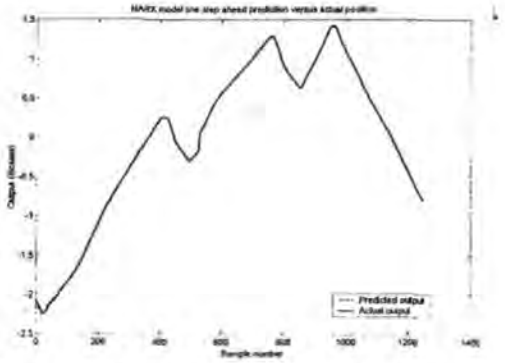

Figure 6. One step ahead neural network model output

These results are based on the step ahead prediction of the system output. In the case where the system output is not immediately known, the step ahead prediction cannot be used and simulation must be based on input signals alone. Fig. 7 illustrates the result of applying the network from Fig. 6 to direct simulation of the system

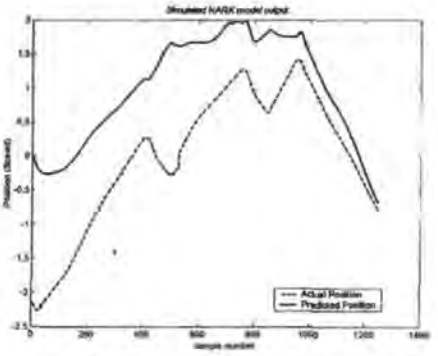

Figure 7. NARX model simulation

The regression structure was based on the load torque and the linear model output, in order to assess the model performance with an alternative regression structure, the model was instead trained with control voltage and load torque, Fig. 8 illustrates a typical result

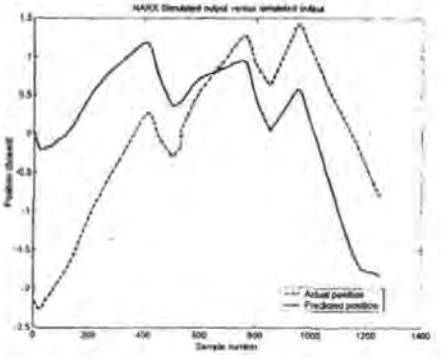

Figure 8. NARX model (Control and Torque regressors)

Whilst this model represents an improvement over the last model (in this case VAF 10%, in the last unmeasurable), there is clearly room for improvement. Further investigation is being carried out.

4.2 Fuzzy based ARX

The term *fuzzy identification* has come to represent the use of fuzzy logic in the modelling and representation of a system. Fuzzy models may be viewed as general function approximators and are therefore readily applied to the nonlinear regression problem of the form discussed in the previous section. The fact that behaviour of a system can be easily represented linguistically e.g.

If *Voltage is High* **and** *Current is High* **then** *Speed is Fast*

naturally provides the user with a useful method by which a systems behaviour can be predicted entirely from empirical observation [7] provides a comprehensive discussion of this approach, which constitutes the first of the two principle methods:

1. The expert knowledge is articulated through a series of if then rules. The model structure is generated implicitly from the rules supplied by the expert.

2. In the second case, no prior information is assumed about the system, and only numerical data is used to construct the fuzzy rule base.

Clearly, the linguistic interface between the expert and the machine make either of the two basic approaches attractive for modelling, since both prior knowledge and collected data may be easily incorporated into the model. The latter of these two approaches is discussed by Babuska [8] and is the foundation for this work.

4.2.1 Data Clustering

The goal of cluster analysis is to partition a given set of data into clusters, which will be subsets of the presented data. The criteria for these clusters is

- Within cluster homogeneity: Data within clusters should be as similar as possible.
- Between cluster heterogeneity: Data between clusters should be as different as possible.

In this case similarity can be measured as a function of distance. Because of the relatively small number of permutations between regression structure and number of clusters, cluster validity was used to select the number of clusters, in this case 7. If the regression surface is partitioned into a series of linear surfaces (corresponding to a cluster), then an affine Takagi-Sugeno fuzzy rule [9] of the form (18) may be used to represent the local regression.

$$R_i : \text{IF } f\left(x_1 \text{ is } A_1, \ldots x_i \text{ is } A_i\right)$$
$$\text{THEN } y_i = a_i^T x + b_i$$

i=1,2,...,k (18)

where $x \in X \subset \mathbb{R}^P$ is a crisp input vector, A_i is an antecedent multidimensional fuzzy set defined by the membership function $\mu_{A_i}(x): X \to [0,1]$, $y_i \in \mathbb{R}$ is the scalar output of the i^{th} rule. The index i relates the variable to the i^{th} rule and k is the number of rules in the rule base.

The consequent function will maintain its form throughout the rule base, only its parameters will vary. The antecedent of the rule defines a fuzzy validity region for the corresponding hyperplane. A rule base might therefore be used to produce a global, nonlinear function approximation.

The NARX structure discussed previously may be expressed in this pseudo linear form according to the following

$$\hat{y}(k+1) = \sum_{j=1}^{n_y} a_{i,j}\, y(k-j+1) +$$
$$\sum_{j=1}^{n_u} b_{i,j}\, u(k-j+1) + c_i \qquad (19)$$

4.2.2 Product Space Identification

The antecedent fuzzy sets serve to divide the regression space in which the regression surface may be locally approximated by the consequent hyperplanes. The task of identification is to find the number, locations and parameters of these hyperplanes such that the regression surface is accurately approximated. This may be achieved through application of a set of fuzzy clustering methods, referred to as *subspace fuzzy clustering algorithms*, specifically the Gustaffson-Kessel (GK) algorithm is used here, discussion of which may be found in [10].

4.2.3 Membership calculation

The antecedent parameters of the Takagi Sugeno model may be calculated through application of the distance measure used within the clustering algorithm. In this case only the regressor x, the regressor component of the cluster prototype and the corresponding cluster covariance matrix are used.

Using the GK algorithm, the distance measure may be evaluated as

$$D\left(x_k, v_i^x\right) = \left(x_k - v_i\right)^T F_i^x \left(x_k - v_i\right) \quad (20)$$

using an inversion, this measure can be converted into the degree of fulfilment. One possible choice of inversion is to use the same equation as for the clustering algorithm [8]

$$\beta_i\left(x_k\right) = \frac{1}{\sum_{j=1}^{c}\left[d\left(x_k, v_i^x\right) \Big/ d\left(x_k, v_j^x\right)\right]^{2/m-1}} \qquad (21)$$

which takes all rules into account and calculates the degree of fulfilment of one rule with respect to the others.

There are two ways in which the fuzzy consequent parameters of the affine Takagi-Sugeno model may be calculated from the data clusters. The first is based around the geometric interpretation of the cluster, using the covariance matrix. The alternative approach is a local least squares optimisation based on the derived fuzzy partition matrix the former method based on the covariance matrix is discussed here. (22) may be derived from the relationship implicit between the shortest eigenvector of the cluster covariance matrix and the regression surface.

$$y = \underbrace{-\frac{1}{\Phi_i^y}\left(\Phi_i^x\right)^T}_{a_i^T} x + \underbrace{\frac{1}{\Phi_i^y}\Phi_i^T v_i}_{b_i} \qquad (22)$$

which can be seen to be directly equivalent to the affine Takagi-Sugeno model,

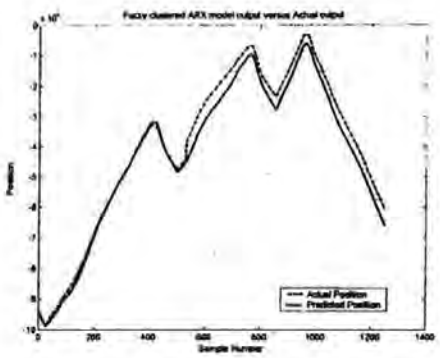

Figure 9. Fuzzy clustered ARX simulation

Fig. 9 illustrates the result of training a fuzzy model according to exactly the same test data for the second neural network model (control voltage and load torque inputs). The VAF in this case is 99.2954%. It should be noted that there is sensor noise present within the validation and training data, and it seems reasonable to assume that both the fuzzy model and the neural network based model could be improved by better training sets. It would also appear that the fuzzy model is to a certain extent robust to these errors (Fig. 9), once again this is a subject under research.

5. DISCUSSION AND CONCLUSIONS

It is generally well accepted that linear models are useful when linearisation around a local operating point is possible. As control system requirements increase in terms of useful operating range, it will become essential that alternative methods for effective system identification become available. Within this work an attempt has been made to compare methods by which this may be achieved. Thus far within the work, the local approach to regression surface approximation has been the most successful, however a far more complete picture will be gleaned once the optimal size for the training set data has been identified and larger validation samples are taken. Further work will also consider the use of alternative regression structures, in the hope that the recurrence introduced by, for instance the auto regressive with moving average model, might serve to further improve performance.

6. REFERENCES

[1] Hellendoorn H., and Driankov D.: Fuzzy model based identification: Selected approaches. Springer Verlag, 1997

[2] Llobet E., Hines E.L., Gardner J.W. and Franco S.: Non-destructive banana ripeness determination using a neural network based electronic nose. Measurement Science Technology, No 10, 1999, pp. 583-548

[3] Armstrong-Helouvry B., Dupont P. and Canudas De Wit C.: A survey of models analysis tools and compensation methods for the control of machines with friction. Automatica, Vol 30, No.7, 1994, pp 1083-1138

[4] Shing T.K.: Dynamics and control of geared servomechanisms with backlash and friction consideration. PhD thesis, University of Maryland, 1994

[5] Krause P., Wasynczuk O, Sudhoff S,: Analysis of Electric Machinery. IEEE Press, 1995

[6] Norgaard M., Ravn O., Poulsen N.K.: NNSYSID and NNCTRL tools for system identification and control with neural networks. IEE Computing and Control engineering, Vol 12, No 1, 2001, pp 29-36

[7] Linskog P.: Methods, Algorithms and Tools for system identification based on prior knowledge, PhD thesis, Linkoping university, 1996

[8] Babuska R.: Fuzzy Modelling for Control. Kluwer Academic Publishers, 1998

[9] Takagi T and Sugeno M: Fuzzy Identification and its applications to Modelling and Control. IEEE Trans. on Systems, Man and Cybernetics, Vol 15, No 1, Jan/Feb 1985

[10] Gustafson D, Kessel W.: Fuzzy clustering with a fuzzy covariance matrix, Proc. IEEE CDC, San Diego, 1979, pp 761-766

IEEE IEEE R&A Soc. MMAR 2001 28-31 August 2001, Międzyzdroje, Poland
7th IEEE International Conference on Methods and Models in Automation and Robotics

NON LINEAR IDENTIFICATION OF A BRUSHLESS MOTOR

ANTONIO TIANO [1,2], ANTONIO ZIRILLI [1],
ROBERT SUTTON [3], MATTHEW KNIGHT [3]

1 DIS, University of Pavia, Via Ferrata 1, 27100 Pavia, Italy, antonio@control1.unipv.it
[2] IAN, National Research Council, Via De Marini 6, 16120 Genova, Italy
[3] Department of Mechanical and Marine Engineering, University of Plymouth, Drakes Circus, Plymouth PL4 8AA, UK, R.Sutton@plymouth.ac.uk

Abstract. This paper is concerned with modelling and identification of a mechanical device consisting of brushless motor and its servomechanism under normal operating conditions. After modelling the system by means of a LUGRE non linear model, a number of experimental tests have been carried out for estimating a set of unknown pertinent parameters. For this purpose a Linear Least Squares Method and a Quasilinearization algorithm, respectively, for a linearized and a non linear model have been used. The results confirm the validity of the non linear LUGRE model as well as the suitability of the Quasilinearization algorithm.

Key Words. Brushless motors, nonlinear systems, identification algorithms

1. INTRODUCTION

Brushless motors have been used during the last years in an increasing number of applications, including industrial process control and robotics, where they are widely used for position and movement control of mechanical devices with multiple degrees of freedom. In order to be able to optimize the performance of such systems in terms of accuracy, robustness and speed it is necessary that adequate and reliable mathematical models of the underlying processes are available. It is worth noting that quite often such models are generally not available at the design stage and they must be determined through a set of identification procedures to be carried out on the real plant, [3], [4].

This paper is concerned with modelling and identification of a mechanical device consisting of a brushless motor and its servomechanism under normal operating conditions. For this purpose a description of the mathematical model used for the motor, the transmission mechanism and the load is given in section 2. This description takes the non linear friction effects into account. In particular the LUGRE model is herewith reviewed, which has been recently developed through a joint co-operation project by the University of Lund (Sweden) and Grenoble (France). This section also includes a complete model including the servomechanism and the experimental set-up used for identification tests.

The identification methods used for determining the dynamical behaviour of the considered mechanical system are described in section 3. Two methods are presented, the former of which is used for identifying the dynamics of a linearized model, while the latter one is used for estimating the parameters of the complete non linear dynamics. Both methods aim at the estimation of pertinent system parameters of continuous-time models with discrete measurements. The former method is essentially based on the Linear Least Squares Method, while the latter one is based on the Quasilinearization algorithm [4].

The results obtained by the identification methods after a number of experimental tests, carried out in different operating conditions, are presented in section 4.

2. MATHEMATICAL MODEL OF MOTOR

The mechanical system, shown in Fig.1, consists of a brushless motor connected through a lead screw (2mm pitch) to hydro-dynamically lubricated slide rails. Motor is a 250W brushless DC motor with 500 ppr quadrature encoder. The motor drive used is a commercially available servo amplifier. Speed control is achieved through a proportional voltage applied at its terminal.

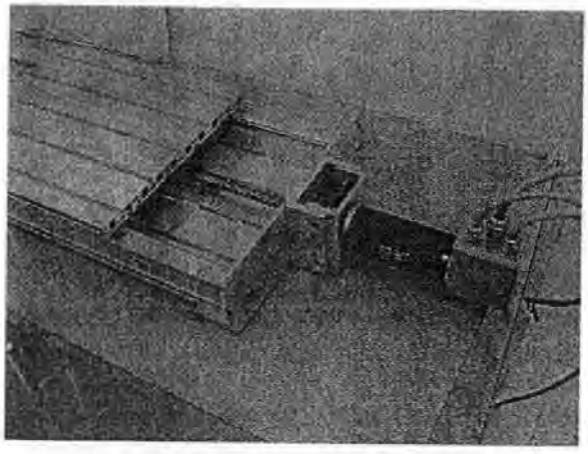

Fig.1 Mechanical system

The mathematical model of the response of the brushless motor rotation angle ϑ_m to the electric driving tension u is assumed to be given by the equation :

$$J_m \ddot{\vartheta}_m = Ku - F \tag{1}$$

where Ku is the active torque, J_m is the total rotational inertia coefficient (motor + load) and F represents the resultant of friction torque. A mathematical model capable to describe the majority of phenomena connected with experimentally observed friction is the LUGRE model [1], [6]. According to this model , it is possible to regard the interaction of two bodies moving with a relative angular velocity v as giving rise to the friction torque:

$$F = \sigma_0 z + \sigma_1 \frac{dz}{dt} + F_v v \tag{2}$$

depending on the internal variable z, which is assumed to evolve according to the equation :

$$\dot{z} = v - \frac{\sigma_0}{g(v)} z|v| \tag{3}$$

$$g(v) = \alpha_0 + \alpha_1 e^{-\left(\frac{v}{v_s}\right)^2} \tag{4}$$

It is convenient to use a state space model, with state vector components $x_1 = \vartheta_m$, $x_2 = \dot{\vartheta}_m$, $x_3 = z$, input variable u and equation:

$$\dot{x} = A_0 x + B_0 u + f(x) \tag{5}$$

where matrices A_0 and B_0 are the linear part and $f(x)$ represents a non linear vector describing the friction nonlinearities. It can be easily verified that such matrices and vector have the form :

$$A_0 = \begin{bmatrix} 0 & 1 & 0 \\ 0 & \vartheta_1 & \vartheta_2 \\ 0 & 1 & 0 \end{bmatrix} \quad B_0 = \begin{bmatrix} 0 \\ \vartheta_3 \\ 0 \end{bmatrix}$$

$$f(x) = \begin{bmatrix} 0 \\ \vartheta_4 \vartheta_5 \dfrac{x_3 |x_2|}{\vartheta_6 + \vartheta_7 e^{-(x_2/\vartheta_8)^2}} \\ \vartheta_5 \dfrac{x_3 |x_2|}{\vartheta_6 + \vartheta_7 e^{-(x_2/\vartheta_8)^2}} \end{bmatrix} \tag{6}$$

If the motor angular variable ϑ_m is assumed to be observed, the output equation is given by:

$$y(t) = [1 \quad 0 \quad 0]x \tag{7}$$

3. IDENTIFICATION ALGORITHM

The identification procedure allows to estimate, on the basis of discrete-time measurements of the input and output variables $\{ u(t_i) \}^{N}_{i=1}$ and e $\{ y(t_i) \}^{N}_{i=1}$ at instants $\{t_i = (i-1)\ h \}^{N}_{i=1}$, the parameter vector :

$$\vartheta = \left[\vartheta_L^T \vartheta_{NL}^T\right]$$

which, according to equation (6), is composed by a linear part and a non linear part given by :

$$\vartheta_L = [\vartheta_1 \vartheta_2 \vartheta_3]^T \quad \vartheta_{NL} = [\vartheta_4 \vartheta_5 \vartheta_6 \vartheta_7 \vartheta_8]^T$$

The identification procedure is composed by a two-step algorithm operating as follows:

- An initial estimate of the linear part is done by means of a Linear Least Squares Method for the continuous time system with discrete measurements;
- An iterative refinement of the complete parameter vector is done by the Quasilinearization method [4].

At the end of the iterative procedure it is possible to obtain both the linearized model and the non linear one. Some particular numerical routines have been used for speeding up the convergence rate, that is normally rather slow for the standard Quasilinearization algorithm.

4. RESULTS

After validating the identification method through as set of artificially generated data files, a number of different identification tests have been carried out on the real palnt and the resulting files have been processed by the above outlined identification procedure. The results obtained are quite satisfactory and confirm the validity of the nonlinear LUGRE model as well as the efficiency of the Quasilinearization algorithm. In fact, it can be noted the quite good agreement between the identified and measured motor responses to the input signals.

Some preliminary results of the non linear identification are shown in Fig. 2 and Fig.3. These results derive from open-loop experiments where the input signal was constituted by a step function and by a sinusoidal function. Other tests, not reported in the paper, conducted by using different types of input signals, confirm the validity of the LUGRE model.

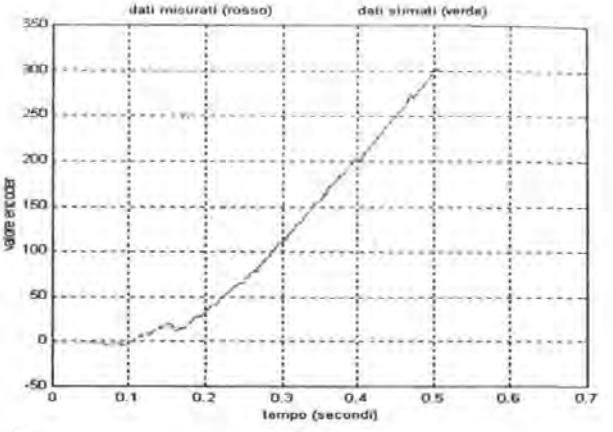

Fig.2 : Comparison of identified and measured after a step input

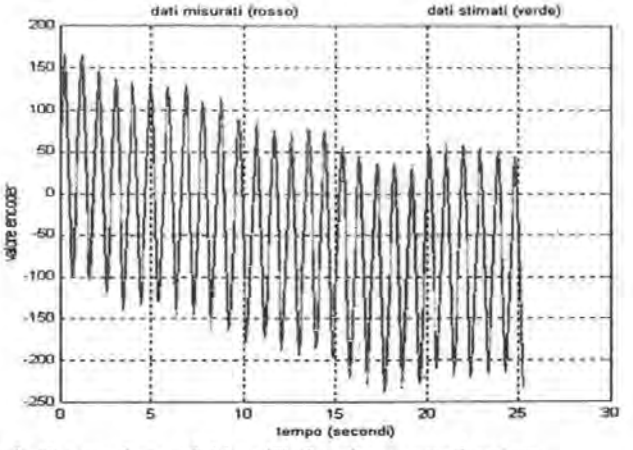

Fig.3: Comparison of identified and measured motor Angles after a sinusoidal input.

5. REFERENCES

1. Canudas de Wit C., Olsson H., Astrom K.J and Lishcinsky P. A new model for coontrol systems with friction. IEEE Trans. On Automatic Control, Vol.4, 1995, pp.419-425
2. Ellis G. Advances in brushless DC motor technology, control and manifacture. 1995. June
3. Friedland B. And Mentzelopoulou S. On estimation of dynamic friction. Proc. IEEE 32th Conference on Decision and Control, S.Antonio, Texas, 1993,pp.1919-1924

4. Kalaba R., Spinger, K. Control, identification and input optimization, Plenum Press, 1982

5. Kenjo T., Nagamori S. Permanent magnet and brushless DC motors, Clarendon Press, 1985

6. Olsson H: Control systems with friction, Doctoral dissertation Dept. Of Automatic Control, Lund Institute of Technology, 1996.

NSTITUTE OF PHYSICS PUBLISHING MEASUREMENT SCIENCE AND TECHNOLOGY
Meas. Sci. Technol. 12 (2001) N35–N38 PII: S0957-0233(01)24684-0

DESIGN NOTE

Sensor bandwidth reduction for data capture

M J Knight[1], R Sutton[1], R S Burns[1] and D F L Jenkins[2]

[1] Department of Mechanical and Marine Engineering, University of Plymouth, Drake Circus, Plymouth PL4 8AA, UK
[2] Department of Communication and Electronic Engineering, University of Plymouth, Drake Circus, Plymouth PL4 8AA, UK

E-mail: MJKnight@Plymouth.ac.uk

Received 10 May 2001, in final form 31 July 2001, accepted for publication 1 August 2001
Published 12 September 2001
Online at stacks.iop.org/MST/12/N35

Abstract

High precision positioning mechanisms with accurate displacement resolutions find employment in many industrial applications. In devices such as incremental encoders, the high resolution comes at the expense of increased sensor bandwidth. This design note describes a low-cost method for implementing effective bandwidth reduction, without reducing the achievable displacement resolution.

Keywords: data capture, sensor bandwidth, incremental encoder, real-time operation

1. Introduction

High precision position control is finding application in many aspects of industry, such as fibre optics, integrated circuit manufacture and machining. Typically, displacement control can be achieved through the use of piezoelectric devices, stepper motors, direct current motors or synchronous machines such as the brushless direct current motor. The latter two actuator categories given above require an additional feedback device for control of armature position. A typical device used for rotary position feedback is the quadrature optical encoder, which provides, in general, three output channels, A, B and I.

Channels A and B are placed 90° out of phase with one another and provide position and direction feedback information [1]. The index (I) channel provides an index pulse once every rotation of the encoder to enable precise 'homing' of the device; this additional channel is not important to this work. A typical encoder might provide 500 pulses per revolution. When used in quadrature (channels A and B together) the effective number of pulses per revolution increases to 2000. If accurate position measurement is required, then all pulses must be registered and counted by the measurement (host) software. The host bandwidth, assuming no additional computational effort, is therefore automatically set to a minimum of

$$\gamma = \frac{2000\,n}{60}\ \text{Hz} \tag{1}$$

where γ is the system bandwidth and n the speed (revolutions per minute) of the motor.

In applications such as data collection it would be attractive to stream data from the system to a host computer. Even in low speed applications it is clear that the bandwidth requirement acts as a constraint on minimum hardware performance.

2. Sensor bandwidth reduction

A solution to this problem has been developed using a PIC microprocessor [2]. The microprocessor accepts the two channel signals from the encoder line driver and acts as a state machine to provide an eight-bit position signal output. In addition, an available ninth output pin is used to provide the host system with information pertaining to the rotational direction of the motor. With the addition of this output, and correct integration with the controller software the bandwidth

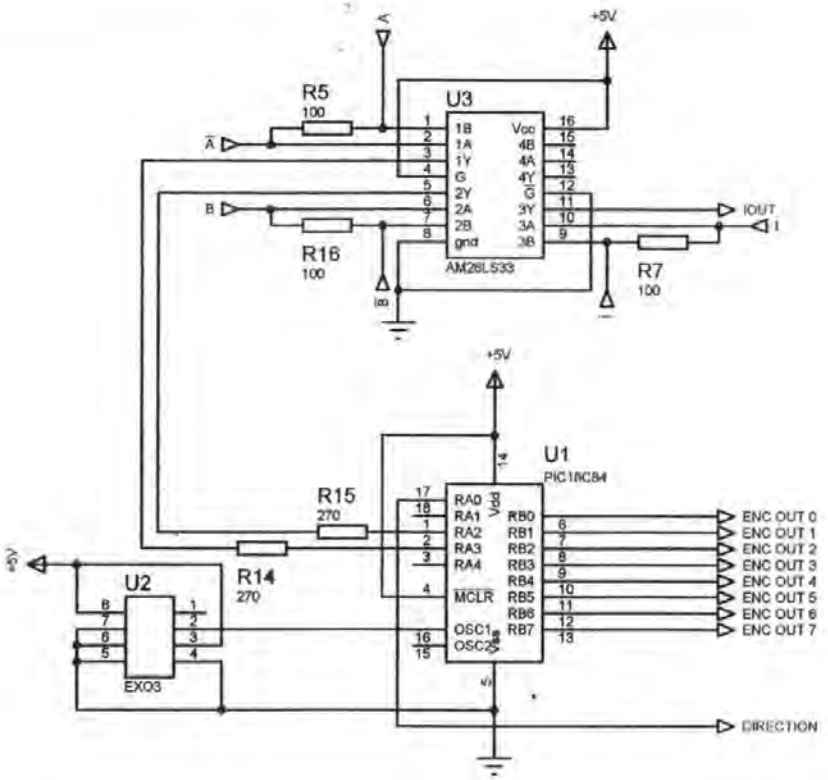

Figure 1. Bandwith reduction circuit.

quirement is effectively reduced from (1) to

$$\gamma = \frac{2000\,n}{15\,300}\ \text{Hz} \tag{2}$$

sing this system it is possible to achieve accurate position edback using a 68 000 microprocessor and a 2000 pulse per volution encoder at motor speeds of up to 1000 revolutions r minute, which would ordinarily far exceed the mechanical pabilities of a typical positioning system.

System design

he bandwidth reduction circuit is shown in figure 1. The line iver (U1) is required to provide the microchip with coherent annel signals. The microprocessor interface consists simply an oscillator circuit (U3) and the microprocessor (U2). The icroprocessor provides TTL compatible signals that may then fed to an appropriate data collection unit. In the example of is work, the data collection unit had an effective bandwidth 8 kHz.

The host C-code and microprocessor embedded code flow agrams are shown in figures 2 and 3 respectively. Figure 2 presents the logical flow through a routine that will be sident within the host process. Its function is to provide solution to the equation

$$T_C = \sum_{i=0}^{i=k} E_i \tag{3}$$

here T_C represents the total encoder count from initialization the current sample k. Of significance are the facts that the otor may travel in both a forward and a reverse sense, and that once having reached 255 pulses in a monotone increasing cycle, or 0 in a monotone decreasing cycle, the firmware will 'wrap' to 0 or 255 respectively. Therefore, knowledge of the previous encoder output, direction and current encoder value are all required in order to calculate the true encoder value and minimize the bandwidth requirement.

Within the diagrams, K and K − 1 are used to represent the current and previous sample respectively. E represents the encoder value, S represents the encoder states. TC indicates the total encoder count and Dir and Direction are used interchangeably to indicate the direction of motor travel.

Figure 3 illustrates the logical flow through the firmware code. There are four possible states (S) in which the output signals might reside. Converting signals A and B to binary representation yields the states

0. Neither A nor B is logical 1
1. A but not B is logical 1
2. B but not A is logical 1
3. A and B are both logical 1

In terms of flow through the states, when travelling in the forward direction the encoder sequence is given by

$$0 \to 2 \to 3 \to 1 \to 0 \to 2 \to 3 \to 1 \ldots$$

Not shown in figure 2 is the code used to reset the total encoder count TC, as indicated in figure 4.

The microprocessor executes, in general, one instruction per cycle and operates at 10 MHz. Once within the software loop, state transition may be checked at up to 1.666 MHz. In the event of a transition, 700 ns is required for processing. The worst case operating scenario is a state change every sample, i.e. once approximately every 0.13 μs; this corresponds to

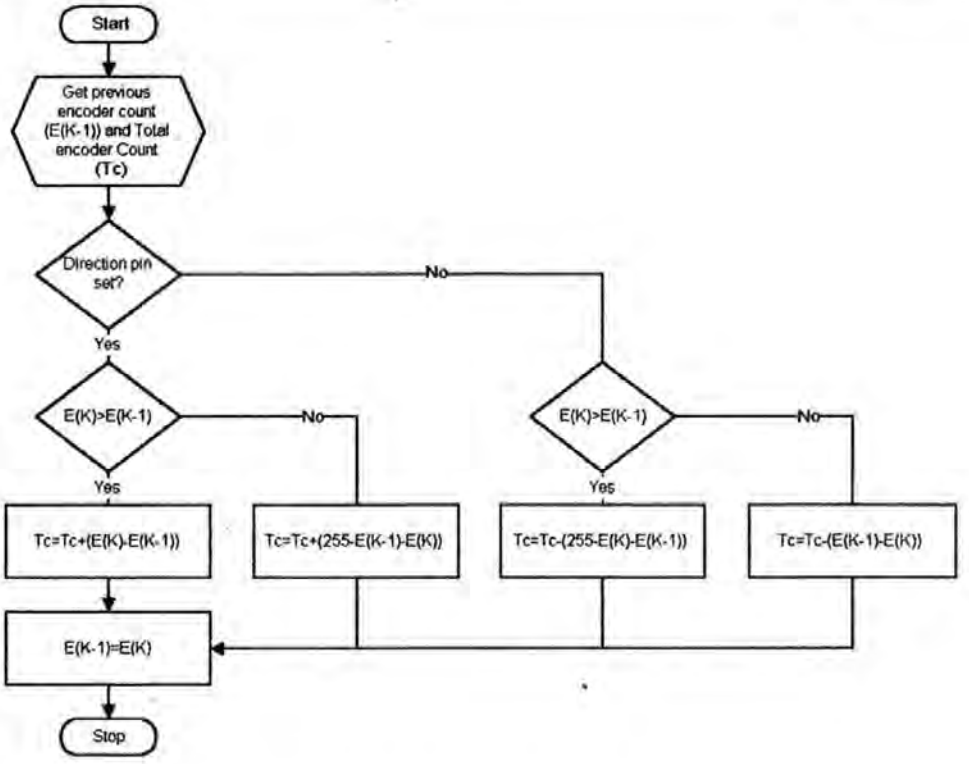

Figure 2. Flow diagram of the host C-code.

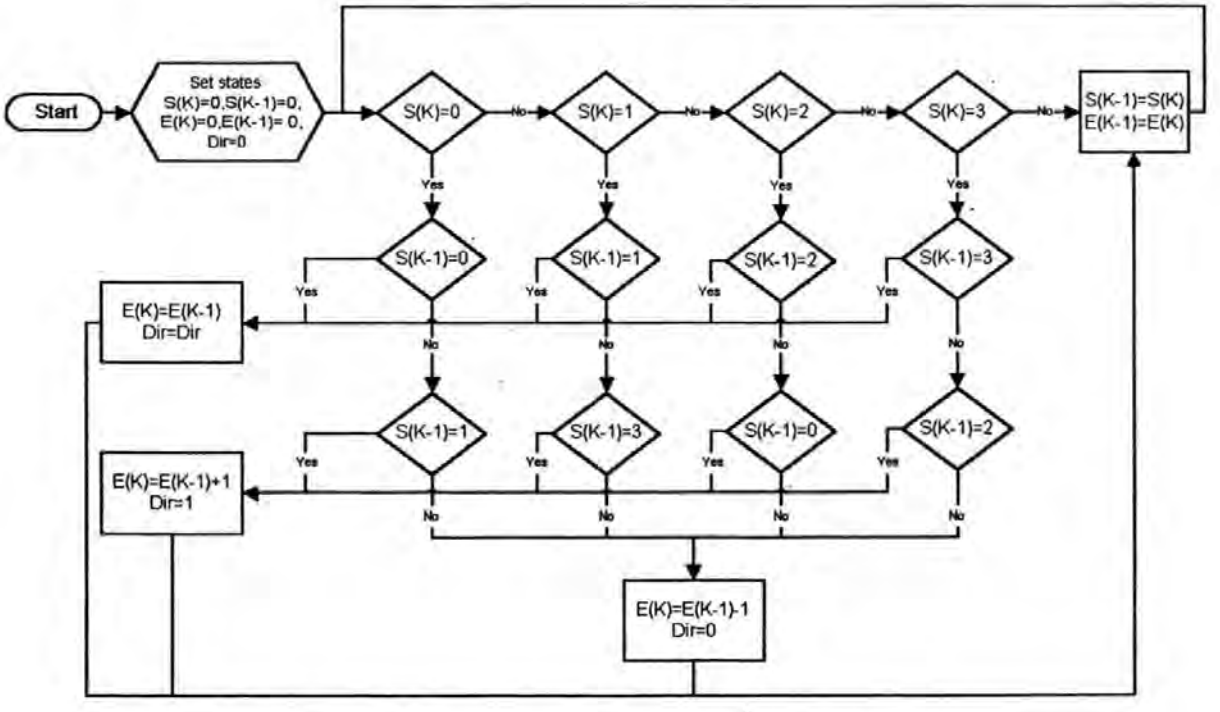

Figure 3. Flow diagram of the microprocessor embedded code.

motor speed of 231 769 revolutions per minute, therefore fectively guaranteeing that every state generated by the ıcoder will be registered.

. Simulink implementation

ımulink is a part of the Mathworks MATLAB™ package ıd provides the user with many attractive features for system identification and control system design. The real-time workshop and windows target provides the user with the capability of data collection through a resident input/output card. Within the example system a PCL-718 data collection card from Advantech was used. This card can operate at up to 10 kHz bandwidth, but limitations of the host personal computer meant that the effective bandwidth was reduced to 8 kHz. The additional seven digital inputs required represented

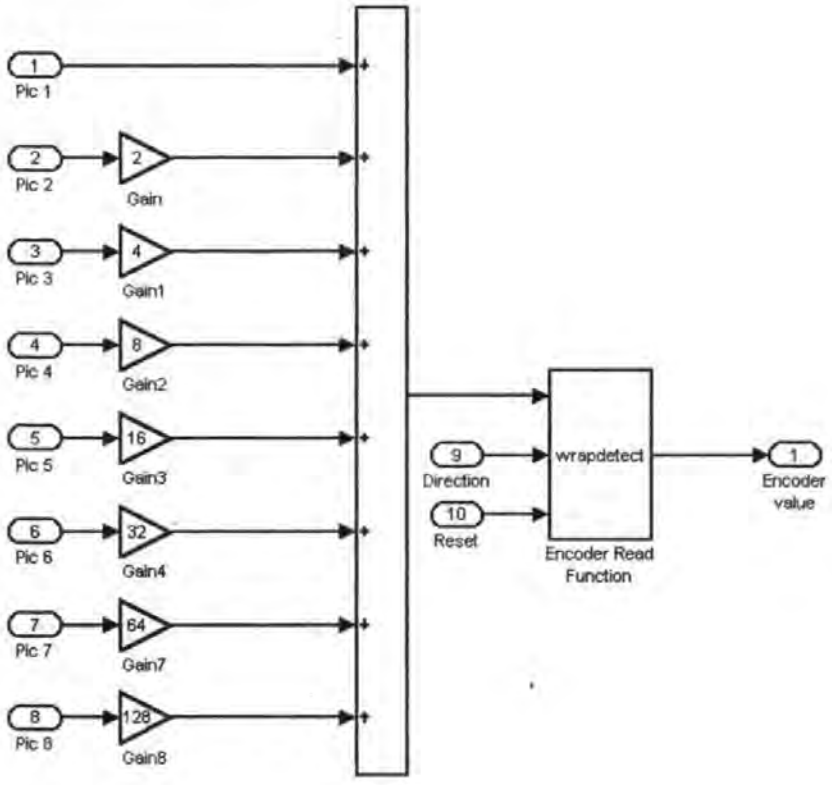

Figure 4. Simulink implementation of the encoder block.

ly a small overhead in sampling in comparison to only o inputs. Through the Simulink environment data can be eamed directly to the personal computer hard disk drive r subsequent analysis. Figure 4 illustrates the Simulink nplementation of the encoder block. The block 'wrap detect' own in figure 4 is represented by figure 2.

Conclusions

method for effective sensor bandwidth reduction has been esented here. Feedback signal fidelity is not compromised in is approach and allows data sampling at significantly reduced equencies. This has clear advantages when computationally tense algorithms are required to execute in real time. Additionally, the system robustness and compatibility with multi-tasking operating systems is tremendously enhanced since the sampling frequency is reduced to an achievable figure.

The overall cost of the hardware to produce the system was less than £5, and in cases where there is only one signal requiring high frequency sampling, this approach offers a cost-effective method to reduce the overall data collection system specification.

References

[1] *Maxon Motor Main Catalogue 2000* (Maxon Motor, 2000)
[2] *PIC 16C8XX Family User's Guide* (Microchip, 1996)

Fuzzy Model Based Integral Action Sliding Mode Control

M.J.KNIGHT, R.SUTTON AND R.S.BURNS

Department of Mechanical and Marine Engineering, University of Plymouth, Drake Circus, Plymouth, PL4 8AA. UK.

mjknight@plymouth.ac.uk fax: (01752)232638 Tel: (01752)232631

Fuzzy model identification *Adaptive sliding mode control* *motor control*

Abstract: A method for combining black box nonlinear models and sliding mode control is presented. In this approach the advantages of the sliding mode control technique are maintained, however parametric uncertainty and unmatched disturbances are acknowledged as limiting factors of controller performance, and their effects are sought to be minimised through the use of local linearisation of the nonlinear model. Simulation results demonstrate performance improvements.

Introduction

One of the earliest approaches to control of uncertain systems was sliding mode control (SMC) or variable structure control (VSC), first introduced to western researchers in the seminal works of Utkin (1977) and Itkis (1976). The central feature of SMC is the sliding mode, in which the dynamic motion of the controlled system is constrained to remain within a prescribed subspace of the full state space. The sliding mode is achieved by ensuring that the prescribed manifold within the state space is made attractive to the system (Itkis, 1976). Once the manifold is reached, the system is forced to remain on it thereafter. When on the manifold, i.e. during the sliding motion, the system is equivalent to an unforced system of lower order, termed the equivalent system, which is insensitive to both parametric uncertainty and unknown disturbances that satisfy the matching condition.

Sliding mode control design is a two stage process, first, sliding manifolds are chosen so that the equivalent system is stable and will yield the desired transient response. Second, the control law is determined based on the specific plant parameters in order to ensure that the sliding mode can be obtained.

One drawback in the implementation of sliding mode control is that the guarantees of invariance in general only apply to systems that satisfy the matching condition (Yao, 1993). Disturbance which does not fulfil this condition, i.e. unmatched disturbance is not formally considered within the controller design. A more profound limitation in practical application is the fundamental requirement that the control law is discontinuous across the sliding manifold, this leads to a phenomenon termed 'control chatter'. Chatter involves high frequency control switching and may lead to excitation of previously neglected high frequency system dynamics. Smoothing techniques such as boundary layer normalisation have been employed in order to negate its effects. Through this approach the transient performance of the closed loop system is maintained, however such an approach leads to a loss of asymptotic stability and a controller that can only guarantee final tracking accuracy to within the ε-vicinity of the demand (Edwards and Spurgeon, 1998), where ε is the radius of the boundary layer. A compromise must therefore be sought between desired tracking accuracy and controller bandwidth.

Model errors due to parametric uncertainty lead to tracking error in controllers with a continuous approximation to the switching function, within the controller design, the controller feedback gains are increased to reduce these errors. This leads to high gain feedback control and despite the fact that these controllers can in theory use infinte feedback gain to achieve asymptotic tracking, such controllers are physically impractical because of the finite bandwidths associated with real systems.

In (Palm, 1994) the apparent similarities between the sliding mode and fuzzy controllers were illustrated, which has subsequently motivated considerable research effort in combining the two topologies in a manner that serves to reduce the limitation of the sliding mode. The most common approach to this has been to replace the continuous switching function of the boundary layer with an equivalent fuzzy switching function. However, as pointed out in (O'Dell, 1997), the fuzzy rule base commonly serves as a mimic of the original switching function and the advantages of such an approach are therefore unclear. Others have used a fuzzy rule base in making the sliding manifold adaptive, e.g. (Ha *et al.*, 1999), so as to minimise the reaching phase, good results have been reported. Babuška (1998) has demonstrated the ability of the affine Takagi-Sugeno model to model accurately a system through rule extraction from cluster data obtained within the regression space. These models may be used subsequently in order to extract locally linear state space models of the system and demonstrate model based control of both single input, single output (SISO) and multi input, multi output (MIMO) systems (Roubos *et al.*, 1999).

In this work, a system subjected to parametric uncertainty and disturbance is identified with a fuzzy rule base, the parameters of which are identified through use of the Gustaffson-Kessel subspace clustering algorithm. Local models of the system under its instantaneous conditions are then extracted and subsequently used to design the sliding mode control gains. In this manner, the resultant controller will be shown qualitatively to improve closed loop transient performance whilst reducing the high gain feedback requirement, as a result of minimising system uncertainty.

Within the following simulation study a third order model of a servomotor is used, the differential equations of which are given according to

$$L\frac{dI_a}{dt} = -I_a R_a - K_e\omega + V_a \qquad (1)$$

$$J\frac{d\omega}{dt} = -B\omega - T_X + I_a.K_m \qquad (2)$$

Where L is the motor inductance, I_a the armature current, K_e the back E.M.F constant, ω the angular velocity of the armature, J the moment of inertia, B viscous friction, T_x the external load toque, K_m the motor torque constant and V_a the armature voltage. In addition θ is introduced as the armature angular position. These equations may be rewritten in state space form according to the following,

$X_1 = \theta, X_2 = \frac{d\theta}{dt} = \omega, X_3 = i$ and let $T_X = U_1$ *and* $V_a = U_2$

$$\begin{bmatrix} \dot{X}_1 \\ \dot{X}_2 \\ \dot{X}_3 \end{bmatrix} = \begin{bmatrix} 0 & 1 & 0 \\ 0 & -\frac{B}{J} & \frac{K_m}{J} \\ 0 & -\frac{K_e}{L} & -\frac{R_a}{L} \end{bmatrix} \begin{bmatrix} X_1 \\ X_2 \\ X_3 \end{bmatrix} + \begin{bmatrix} 0 \\ -\frac{U_1}{J} \\ \frac{U_2}{L} \end{bmatrix} \qquad Y_1 = \begin{bmatrix} 1 & 0 & 0 \end{bmatrix} \begin{bmatrix} X_1 \\ X_2 \\ X_3 \end{bmatrix} \qquad (3)$$

The model parameters are taken as shown in Table 1:

Table 1

Next within this work, the mechanism for fuzzy identification of this model is considered. After which, consideration to the sliding mode controller design is given. Results are then presented which demonstrate a significant reduction in controller gain, control chatter and an improvement in controller performance where an unmatched disturbance is introduced.

Fuzzy Identification

Fuzzy identification is a term used that has come to represent the use of fuzzy logic in the modelling and representation of a system. Since fuzzy models may be viewed as general function approximators, they are readily applied to the nonlinear regression problem. There are two fundamentally different approaches

that may be taken in the identification of a system. Firstly the system may be identified through explicit expression of system performance, e.g. '*if* voltage is high *then* velocity is high'. Secondly, and the approach adopted within this work is to decompose the model into a static nonlinear regression. The problem of model identification is then decomposed into two separate problems, the first is selection of the regression structure, the second, the selection of the fuzzy model form, for example, the required number of membership functions and membership crispness.

The desired regression may be expressed in the form

$$y(t|\theta) = f(\varphi(t), \theta) \quad (4)$$

where y is the regressand, θ the *vector of regressions* which is to be parameterised in the identification process, and the vector $\varphi(t)$ is known as the *regression vector*, its parameters the *regressors*. It has been shown in (Babuska, 1998) that the regression surface within the product space may be represented as a series of local approximations.

Through use of a clustering algorithm, it is possible to derive local approximations to this regression surface. Further, through the use of the eigenvalues of the cluster covariance matrix given by

$$F_i = \frac{\sum_{k=1}^{N} (\mu_{i,k})^m (z_k - v_i)(z_k - v_i)^T}{\sum_{k=1}^{N} (\mu_{i,k})^m} \quad (5)$$

it is possible to interpret these local models and subsequently derive a fuzzy rule to represent this local approximation. In repeating this process for each data cluster, a global model of the system may be generated. Previous work has considered the accuracy of this approach in comparison to neural networks and 'white box' models, and results have demonstrated that this local approach to modelling can improve results (Knight *et al.*, 2001).

The rule extraction process is briefly described here for completeness, however the reader is directed to (Babuska, 1998) for more complete discussion.

It has been shown that a useful form of the fuzzy consequent is the affine linear form (Takagi and Sugeno, 1985) of the Takagi-Sugeno (TS) model, in which rules are structured according to (6):

$$y_i = a_i^T x + b_i \quad (6)$$

where a_i is the so called parameter vector and b_i is an offset. Within the product space ($\mathbb{R}^{p+1\times N}$) the affine Takagi-Sugeno consequents may be viewed geometrically as hyperplanes. The antecedent of the rule defines a fuzzy validity region for the corresponding hyperplane. The output y of the TS model is computed using the fuzzy mean formula

$$y = \frac{\sum_{i=1}^{K} \beta_i(x) y_i}{\sum_{i=1}^{K} \beta_i(x)} \qquad (7)$$

where K is the nmber of rules in the rule base. $\beta_i(x)$ represents the degree of fulfilment of the i^{th} rules antecedent, which is simply a measure of the degree of fulfilment of x in the fuzzy set A_i and is given by

$$\beta_i = \mu_{Ai}(x) \quad (8)$$

Since it may become difficult to interpret multidimensional fuzzy sets, the antecedent proposition is commonly defined in a conjunctive form, given by a series of single dimensional fuzzy sets combined with simple propositions. In this case the degrees of fulfilment are calculated as $\beta_i(x) = \mu_{Ai,1}(x_1) \wedge \ldots \wedge \mu_{Ai,P}(x_P)$, where the min operator ($\wedge$) may be replaced by alternative T-norms. In this case the model output is calculated

$$y = \left(\sum_{i=1}^{K} \gamma_i(x) a_i^T \right) x + \sum_{i=1}^{K} \gamma_i(x) b_i = \tilde{a}^T(x) x + \tilde{b}(x) \qquad (9)$$

where γ_i is the normalised degree of fulfilment, given by

$$\gamma_i(x) = \frac{\beta_i(x)}{\sum_{j=1}^{K} \beta_j(x)} \qquad (10)$$

and $\tilde{a}(x)$ and $\tilde{b}(x)$ are input dependent parameters, given as convex linear combinations of the constant parameters a_i and b_i through the following relationship

$$\tilde{a}(x) = \sum_{i=1}^{K} \gamma_i(x) a_i \qquad (11)$$

$$\tilde{b}(x) = \sum_{i=1}^{K} \gamma_i(x) b_i \qquad (12)$$

The regression structure discussed previously (4) may be expressed in this pseudo linear form according to the following

$$\hat{y}(k+1) = \sum_{j=1}^{n_y} a_{i,j} y(k-j+1) + \sum_{j=1}^{n_u} b_{i,j} u(k-j+1) + c_i \quad (13)$$

The distance measure of the clustering algorithm, given by

$$D(x_k, v_i^x) = (x_k - v_i)^T F_i^x (x_k - v_i) \quad (14)$$

may be inverted and used to provide the degree of fulfilment of each rule for given data. One possible choice of inversion is to use the same equation as for the clustering algorithm

$$\beta_i(x_i) = \frac{1}{\sum_{j=1}^{c} \left[d(x_i, v_i^c) / d(x_i, v_j^c) \right]^{2/(m-1)}} \quad (15)$$

which takes all rules into account and calculates the degree of fulfilment of one rule with respect to the others. Once the antecedent parameters have been calculated, the consequent parameters require derivation. There are two ways in which the fuzzy consequent parameters of the affine TS model may be calculated from the data clusters. The first is based around the geometric interpretation of the cluster, using the covariance matrix (Babuska and Verbruggen, 1997). The alternative approach is a local least squares optimisation method based on the derived fuzzy partition matrix. The former method is discussed here. The eigenstructure of the cluster covariance matrix loosely describes the shape of the cluster. The shortest eigenvector describes the normal vector to the hyperplane spanned by the remaining eigenvectors. The shortest eigenvector is defined as Φ_i. Based on the dataset $Z^N = [x^T, y^T]$ and the cluster prototype, the consequent may be described implicitly by

$$\Phi_i \bullet (Z^N - v_i) = 0 \quad (16)$$

The shortest eigenvector and the cluster prototype may be divided into a vector corresponding to the regressor x and a scalar corresponding to the regressand y. i.e.

$$v_i = \left[\left(v_i^x \right)^T ; v_i^y \right]^T \qquad (17)$$

$$\Phi_i = \left[\left(\Phi_i^x \right)^T ; \Phi_i^y \right]^T \qquad (18)$$

may now be rewritten according to

$$\left[\left(\Phi_i^x \right)^T ; \Phi_i^y \right] \bullet \left(\left[x^T ; y \right]^T - \left[\left(v_i^x \right)^T ; v_i^y \right]^T \right) = 0 \qquad (19)$$

After simplification

$$y = \underbrace{-\frac{1}{\Phi_i^y} \left(\Phi_i^x \right)^T}_{a_i^T} x + \underbrace{\frac{1}{\Phi_i^y} \Phi_i^T v_i}_{b_i} \quad (20)$$

which is directly equivalent to the affine Takagi-Sugeno model consequent. This approach was employed in the identification of the model given in (3). A regression structure of [3 1] was used with 5 clusters. Of importance to the identification of the model is the selection of the input signal, in this case a stepwise random signal was used as shown in figure 1. The percentile variance accounted for (VAF) measure, which provides a measure of model tracking accuracy was calculated as 99.2% which indicates good model accuracy.

Figure 1

The model structure selected uses the applied voltage as the regressor. Performance increases in terms of tracking error and total root mean squared error may be gleaned if the model also uses the motor load current within the regression structure (Knight *et al.*, 2001). However, from the perspective of this work, absolute error of the model is not significant, only the ability of the model to track the regressand. Computational burden is therefore reduced by accepting a marginal degradation in the model performance and only using the single regressor.

Model Extraction

The work in (Roubos *et al.*, 1999) presents a method whereby the fuzzy clustered model may be represented as a local linear state space model. The following is an

overview of the method adopted. The regression vector, which is represented by ε_l is given by

$$\varepsilon_l(k) = \left[\{y_p(k)\}_0^{n_{a1}}, \ldots, \{y_p(k)\}_0^{n_{ap}}, \{u_1(k+1)\}_{n_{d1}}^{n_{b1}}, \ldots, \{u_m(k+1)\}_{n_{dm}}^{n_{bm}} \right] \quad (21)$$

An affine Takagi-Sugeno rule may be represented by

$$y_l(k+1) = \frac{\sum_{i=1}^{K_l} \beta_{li}(\varepsilon_l)\left(\zeta_{li} y(k) + \eta_{li} u(k) + \theta_{li}\right)}{\sum_{i=1}^{K_l} \beta_{li}} \quad (22)$$

ζ and η are vectors of polynomials in the previous sample $y(k-l)$, and θ the offset. K_l is the number of rules of the l^{th} offset. The model output is calculated as the degree of fulfilment $\mu_{il}(\varepsilon_{lh})$ for each antecedent variable and the resulting degrees of fulfilment (β_{li}) for every rule are combined with the linear consequence according to the following

$$\beta_{li}(\varepsilon_l) = \prod_{h=1}^{p} \mu_{ih}(\varepsilon_{lh}) \quad (23)$$

Once the Takagi Sugeno model has been derived, local linear state space models can be calculated according to the following,

$$y_l(k+1) = \frac{\sum_{i=1}^{K_l} \mu_{li}(x_l(k)) \cdot y_{li}(k+1)}{\sum_{i=1}^{K_l} \mu_{li}(x_l(k))} \quad (24)$$

$$y_{li}(k+1) = \left(\varsigma_{li} y(k) + \eta_{li} u(k) + \theta_{li}\right) \quad (25)$$

where

$$\zeta_l^* = \frac{\sum_{i=1}^{K_l} \mu_{li}(x_l(k)) \cdot \zeta_{li}}{\sum_{i=1}^{K_l} \mu_{li}(x_l(k))} \quad (26)$$

$$\eta_l^* = \frac{\sum_{i=1}^{K_l} \mu_{li}(x_l(k)) \cdot \eta_{li}}{\sum_{i=1}^{K_l} \mu_{li}(x_l(k))} \quad (27)$$

and

$$\theta_l^* = \frac{\sum_{i=1}^{K_l} \mu_{li}\left(x_l(k)\right)\cdot\theta_{li}}{\sum_{i=1}^{K_l} \mu_{li}\left(x_l(k)\right)} \qquad (28)$$

In the case here, previous inputs are not considered and the A, B and C matrices of the model are thus simplified, the matrices are given

$$A = \begin{bmatrix} \zeta_{1,1}^* & \zeta_{1,2}^* & \cdots & \zeta_{1,\alpha_1}^* \\ 1 & 0 & \cdots & 0 \\ \zeta_{2,1}^* & \zeta_{2,2}^* & \cdots & \zeta_{2,\alpha_1}^* \\ 0 & \vdots & \ddots & \vdots \\ \zeta_{n_0,1}^* & \zeta_{n_0,2}^* & \cdots & \zeta_{n_0,\alpha_1}^* \end{bmatrix} \qquad (29)$$

$$B = \begin{bmatrix} \eta_{1,1}^* & \eta_{1,2}^* & \cdots & \eta_{1,n_i}^* \\ 0 & \cdots & \cdots & 0 \\ \eta_{2,1}^* & \eta_{2,2}^* & \cdots & \eta_{2,n_i}^* \\ \vdots & \vdots & \ddots & \vdots \\ \eta_{n_0,1}^* & \eta_{n_0,2}^* & \cdots & \eta_{n_0,n_i}^* \end{bmatrix} \qquad (30)$$

$$C = \begin{bmatrix} 1 & 0 & \cdots & 0 \\ \vdots & & \ddots & \vdots \\ 0 & \cdots & \cdots & 1 \end{bmatrix} \qquad (31)$$

Integral Action Sliding Mode

As described in the introduction, the sliding mode is traditionally associated with a switching action which is discontinuous about a prescribed surface within the state space. Practical implementation of a sliding mode controller frequently leads to a phenomenon known as chattering. This is often due to the excitation of previously unmodelled system dynamics. Many solutions have been proposed to prevent chatter. Perhaps the most famous of these is the *boundary layer approach* first proposed by Slotine and Sastry (1983). The approach involves replacing the discontinuous switching function with an equivalent continuous function. The implication of changing the switching function is that the system state is no longer constrained to remain on the prescribed sliding surface, but merely to remain within a certain vicinity of it. It follows directly that the equivalent system dynamics will be to some extent affected by any matched disturbance to which the system is subjected (Spurgeon, 1991).

It was recognised in (Ryan and Corless, 1984) that this additional degree of freedom afforded by the boundary layer at the manifold could be used to improve the controller robustness to so called unmatched disturbance, i.e. those disturbances which do not act within the system control channels. The controller that was subsequently developed was theoretically elegant and intuitively appealing, however it was conservative. By considering a subset of the disturbances originally used in (Ryan and Corless, 1984), the controller was made less conservative in (Spurgeon and Davies, 1993). The fundamental extension of these controllers over the traditional controllers is the introduction of an additional integral action state. This controller state seeks to reduce the steady state error asymptotically to zero. Within this work the design approach is adopted in order to ensure zero steady state controller error. However, it is also recognised that if the system uncertainty can be reduced, then controller performance may be correspondingly improved.

Once local models of the system have been extracted, they may be used in order to provide enhanced information to the sliding mode controller. The principles associated with the design of a sliding mode controller with integral action are considered next. As alluded to in the introduction, the ideal sliding motion is control independent and defined only by the choice of sliding surface provided that certain assumptions about the system disturbance hold (Drazenovic, 1969). In terms of controller design it is convenient to convert the system equations into a suitable canonical form. In this form the system is decomposed into two connected subsystems, one acting in within the range space of matrix B and the other within the null space of the manifold S. In terms of design, the problem then becomes one of state feedback given desired system eigenvalue locations. Since by assumption the matrix B is of full rank, there exists an orthogonal matrix $T_r \in \mathbb{R}^{n \times n}$ such that

$$T_r B = \begin{bmatrix} 0 \\ B_2 \end{bmatrix} \qquad (32)$$

where $B_2 \in \mathbb{R}^{m \times m}$ and is non-singular. Let $z = Tx$ and partition the new co-ordinates so that

$$z = \begin{bmatrix} z_1 \\ z_2 \end{bmatrix} \qquad (33)$$

where $z_1 \in \mathbb{R}^{n-m}$ and $z_2 \in \mathbb{R}^m$. The nominal linear system can then be written as

$$\dot{z}_1(t) = A_{11} z_1(t) + A_{12} z_2(t) \qquad (34)$$

$$\dot{z}_2(t) = A_{21} z_1(t) + A_{22} z_2(t) + B_2 u(t) \quad (35)$$

commonly known as the regular form. Equation (34) is referred to as describing the null-space dynamics and equation (35) as describing the range-space dynamics. From the perspective of the extracted local models, it is convenient to first convert the matrices to the controllability canonical form, thus the system is guaranteed to be in the regular form for subsequent design. Suppose the matrix defining the switching function (in the new co-ordinate system) is compatibly partitioned with z as

$$ST_r^T = [S_1 \quad S_2] \qquad (36)$$

where $S_1 \in \mathbb{R}^{m \times (n \times m)}$ and $S_2 \in \mathbb{R}^{m \times m}$. Since $SB = S_2 B_2$ it follows that a necessary and sufficient condition for the matrix SB to be non-singular is that the determinant of S_2 is non zero. It is reasonable to assume that this condition will be met by design. During an ideal sliding motion

$$S_1 z_1(t) + S_2 z_2(t) = 0 \quad \text{for all } t > t_s \quad (37)$$

and therefore formally expressing $z_2(t)$ in terms of $z_1(t)$ yields

$$z_2(t) = -M z_1(t) \qquad (38)$$

where $M = S_2^{-1} S_1$. Substituting into (34) gives

$$\dot{z}_1(t) = (A_{11} - A_{12} M) z_1(t) \qquad (39)$$

$z_2(t)$ is considered to play the role of the control action. The switching surface design problem can therefore be considered to be one of choosing a state feedback matrix M to stabilise the reduced order system (A_{11}, A_{12}).

At this point the unit vector approach is introduced. Consider an uncertain system of the form

$$\dot{x}(t) = Ax(t) + Bu(t) + f(t,x,u) \qquad (40)$$

where the function $f : \mathbb{R} \times \mathbb{R}^n \times \mathbb{R}^m \rightarrow \mathbb{R}^m$ which represents the uncertainties or non-linearities satisfying the so-called matching condition, i.e.

$$f(t,x,u) = B\xi(t,x,u) \qquad (41)$$

where ξ is unknown but satisfies the following inequality

$$\|\xi(t,x,u)\| \leq k_1 \|u\| + \alpha(t,x) \quad (42)$$

where $1 > k_1 \geq 0$ is a known constant and $\alpha(\bullet)$ is a known function. The proposed control law comprises two components; a linear component to stabilise the nominal linear system; and a discontinuous component. Specifically

$$u(t) = u_l(t) + u_n(t) \quad (43)$$

where the linear component is given by

$$u_l(t) = -\Lambda^{-1}(SA - \Phi S)x(t) \quad (44)$$

where Φ is any stable design matrix and Λ = SB. The non-linear component is defined as

$$u_n(t) = -\rho(t,x)\Lambda^{-1}\frac{P_2 s(t)}{\|P_2 s(t)\| + \varepsilon} \quad \text{for all } S \neq 0 \qquad (45)$$

where P_2 is a symmetric positive definite matrix that satisfies the Lyapunov equation

$$P_2\Phi + \Phi^T P_2 + I = 0 \quad (46)$$

and the scalar function $\rho(t,x)$, which depends only on the magnitude of the uncertainty, is any function satisfying

$$\rho(t,x) \geq \frac{(k_1\|u_l\| + \alpha(t,x) + \gamma)}{(1 - k_1\kappa(\Lambda))} \qquad (47)$$

where γ>0 is a design parameter. The radius of the boundary layer (ε) may be shown to be dependent on the actuator time constant and inversely proportional to the available control resources. In this equation it is assumed that the scaling

parameter has been chosen so that $k_1\kappa(\Lambda)<1$. Where $\kappa(\bullet)$ represents the spectral condition number. It can be established that any function satisfying equation (47) also satisfies

$$\rho(t,x)\geq\|\xi(t,x,u)\|+\gamma \qquad (48)$$

and therefore $\rho(t,x)$ is greater in magnitude than the matched uncertainty occurring in this equation. It can be verified that $V(S)=S^TP_2S$ guarantees quadratic stability for the switching states and in particular

$$\dot{V}\leq -s^Ts-2\gamma\|P_2s\| \qquad (49)$$

This control law guarantees that the switching surface is reached in finite time despite the disturbance or uncertainty and once the sliding motion is attained it is completely independent of the uncertainty.

Now consider the introduction of additional states $x_r\in\mathbb{R}^p$ satisfying

$$\dot{x}_r=r(t)-y(t) \qquad (50)$$

where the differentiable signal $r(t)$ satisfies

$$\dot{r}(t)=\Gamma(r(t)-R) \qquad (51)$$

with Γ a stable design matrix and R a constant demand vector. Augment the states with the integral action states and define

$$\tilde{x}=\begin{bmatrix}x_r\\ x\end{bmatrix} \qquad (52)$$

The associated system and input distribution matrices for the augmented system are

$$\tilde{A}=\begin{bmatrix}0 & -C\\ 0 & A\end{bmatrix} \text{ and } \tilde{B}=\begin{bmatrix}0\\ B\end{bmatrix} \qquad (53)$$

assuming the pair (A,B) is in regular form, the pair $(\tilde{A},\tilde{B})$ is also in regular form. The proposed controller seeks to induce a sliding motion on the surface

$$S=\{\tilde{x}\in\mathbb{R}^{n+p}:S\tilde{x}=S_rr\} \qquad (54)$$

where S and S_r are design parameters, which govern the reduced order motion. The hyperplane system matrix and system matrix are partitioned as

$$S = \begin{bmatrix} \overset{n}{\longleftrightarrow} & \overset{m}{\longleftrightarrow} \\ S_1 & S_2 \end{bmatrix} \qquad (55)$$

$$\tilde{A} = \begin{bmatrix} \overset{n}{\longleftrightarrow} & \overset{m}{\longleftrightarrow} \\ \tilde{A}_{11} & \tilde{A}_{12} \\ \tilde{A}_{21} & \tilde{A}_{22} \end{bmatrix} \begin{matrix} \updownarrow n \\ \updownarrow m \end{matrix} \qquad (56)$$

and assume $\Lambda = S\tilde{B}$ is non-singular. If a controller exists which induces an ideal sliding motion on S and the augmented states are suitably partitioned, then the ideal sliding motion is given by

$$\dot{x}_1(t) = \left(\tilde{A}_{11} - \tilde{A}_{12}M\right)x_1(t) + \left(\tilde{A}_{12}S_2^{-1}S_r + B_r\right)r(t) \qquad (57)$$

where $M = S_2^{-1}S_1$ and $B_r = \begin{bmatrix} I_p & 0_{n\times p} \end{bmatrix}^T$. In order for the hyperplane design method to be valid, it is necessary for the matrix pair $\left(\tilde{A}_{11}, \tilde{A}_{12}\right)$ to be completely controllable. The overall control law is then given by

$$u = u_l\left(\tilde{x}, r\right) + u_n\left(\tilde{x}, r\right) \qquad (58)$$

where the discontinuous vector u_n is given by

$$u_n(s,r) = \begin{cases} -\rho_c\left(u_L, y\right)\Lambda^{-1} & \text{if } S\tilde{x} \neq S_r r \\ 0 & \text{otherwise} \end{cases} \qquad (59)$$

It follows that, in terms of the original co-ordinates the control vector u_l is given by

$$u_l\left(\tilde{x}, r\right) = L\tilde{x} + L_r r + L_{\dot{r}}\dot{r} \qquad (60)$$

with gains defined as

$$L = -\Lambda^{-1}\left(S\tilde{A} - \Phi S\right) \qquad (61)$$

$$L_r = -\Lambda^{-1}\left(\Phi S_r + S_1 B_r\right) \qquad (62)$$

$$L_{\dot{r}} = \Lambda^{-1}S_r \qquad (63)$$

The parameter S_r can take any value and does not affect the stability of the closed loop system.

Controller structure and performance

A benchmark sliding mode controller with integral action (SMCI) of the form previously discussed was developed to control the motor model of equation (3), using the nominal parameters of Table 1. All simulations were carried out using the actual parameters shown in Table 1.

The principle of the proposed controller is illustrated in Figure 2. The controller uses the design approach outlined in the previous section, thus, stabilising conditions of the controller remain intact. Importantly, the extracted model is used to provide enhanced information to the controller, so that the controller may be made to adapt to local operating conditions of the system. The controller is therefore referred to as a Fuzzy Adaptive Sliding Mode Controller (FASMC).

Figure 2

both sets of controller eigenvalues were selected to provide unity damping ratio at 22rad/s. The controllers were driven over a simulation sample period of 70 seconds. Results are illustrated in Figure 3.

Figure 3

It can be seen that in terms of transient response, there is little to differentiate between the two controllers. However, consideration of the corresponding control effort (Figure 4) shows that that the high gain requirement of the SMCI has indeed been relaxed by the FASMC. Additionally, the ε-vicinity of the FASMC was manually adjusted to be 6 times smaller than the corresponding SMCI before chatter occurred.

Figure 4

A second test introduced unmatched disturbance to the system and the fuzzy model retrained to incorporate the uncertainty, the disturbance is analogus to a torque being placed on the motor and forcing rotation in the contrary direction to the demand, which changes simultaneously with the step increase in load. Figure 5 illustrates the effect of the disturbance on the SMCI, it can be seen that the disturbance significantly effects transient performance. Because of the integral action of the SMCI, the system is able to achive asymptotic tracking as discussed within the literature. The FASMC, on the other hand, recovers the system to the steady state taking only an additional 0.4 seconds when compared to the system without disturbance (Figure 6). The obvious error in the initial controlled state trajectory is due to the lack of large controller gains, in the event that the system were subjected to such a stringent test it would be necessary to increase the nonlinear control gain to circumvent this problem.

Figure 5

Figure 6

Conclusions

A new controller based on the synergy of sliding mode design approaches and nonlinear black box modelling has been presented. Performance of the controller has been compared with a benchmark sliding mode controller and the controllers response has been found to be favourable. The controller has demonstrated clear advantages of using fuzzy logic in conjunction with sliding mode. Since the system uncertainties can be significantly reduced through use of fuzzy identification and linearisation techniques, the feedback control gains may be reduced, which in turn leads to a control effort of reduced magnitude. This leads directly to a reduction in the radius of the boundary layer, providing improvements in the final achievable tracking accuracy of the system. Since the fuzzy model does not discriminate between matched and unmatched disturbance, but simply incorporates them into the model, the FASMC also enjoys improvements in the transient control performance when the system is subject to unmached disturbance. The FASMC in this work only extends to the SISO case and in addition, it is assumed that input/output data is available for the system. It

is finally pointed out that implementation of this algorithm is significantly more complex than the SMCI. To date, limited success in the practical implementation of the controller has been enjoyed. Subsequent work will also extend the method to the MIMO case.

References

Babuska R. (1998) Fuzzy Modelling for Control, Kluwer Academic Publishers.

Babuska R. and Verbruggen H.B. (1997) Constructing Fuzzy Models by Product Space Clustering. In: Hellendoorn H. and Driankov D. (eds) Fuzzy Model Identification. Springer-Verlag, 53-90

Drazenovic B. (1969), The Invariance Conditions in Variable Structure Systems, Automatica, 5, 287-295.

Edwards C and Spurgeon S.K. (1998) Sliding Mode Control: Theory and Applications. Taylor Francis.

Ha Q.P., Rye D.C. and Durrant-Whyte H.F. (1999) Robust Sliding Mode Control with Application, International Journal of Control. 72(12), 1087-1096.

Itkis U. (1976) Control Systems of Variable Structure, John Wiley.

Knight M.J., Sutton R., Burns R.S. and Jenkins D.F. (2001). A Comparison of Nonlinear Identification Techniques, Proc IEEE conf. on Methods and Models in Automation and Robotics, Meidzyzdroje, Poland. 953-958.

O'Dell B. (1997) Fuzzy sliding mode control: A critical review, Oklahoma state university, Technical Report ACL-97-001.

Palm R. (1994) Robust Control by Fuzzy Sliding Mode, Automatica, 30(9), 1429-1438.

Roubos J.A., Mollov S., Babuska R and Verbruggen H.B. (1999) Fuzzy model based predictive control using Takagi-Sugeno models, International journal of Approximate reasoning, 22, 199-226

Ryan E.P. and Corless M. (1984) Ultimate Boundedness and Asymptotic Stability of a class of uncertain Dynamical System via Continuous and Discontinuous Feedback Control, IMA Journal of Mathematics and Control Information, 1, 223-242

Slotine J.-J. and Sastry S.S. (1983), Tracking Control of Nonlinear Systems Using Sliding Surfaces, with an application to Robot Manipulators, International Journal of Control, 38, 465-492.

Spurgeon S.K. (1991) Choice of Discontinuous Control Component for Robust Sliding Mode Performance, International Journal of Control, 53(1). 163-179.

Spurgeon S.K. and Davies R (1993), A Nonlinear Control Strategy for Robust Sliding Mode Performance in the presence of Unmatched Uncertainty, International Journal of Control, 57(5), 1107-1123.

Takagi T. and Sugeno M. (1985) Fuzzy Identification and its applications to Modelling and Control, IEEE Trans. on Systems, Man and Cybernetics, 15(1), 116-132.

Utkin V.I. (1977) Variable Structure Systems with Sliding Modes, IEEE Transactions on Automatic Control, AC-22(2), 212-222.

Yao, B. (1992) Adaptive robust control of nonlinear systems with application to control of mechanical systems, PhD Thesis, University of California, 1992

Parameter	Value (Nominal)	Value (Actual)
R_a	1.2Ω	1.5 Ω
L	0.05 H	0.09 H
Ke	0.6	0.6
Km	0.6	0.6
J	0.135	0.15
B	0	0.02

Table 1: Motor parameters

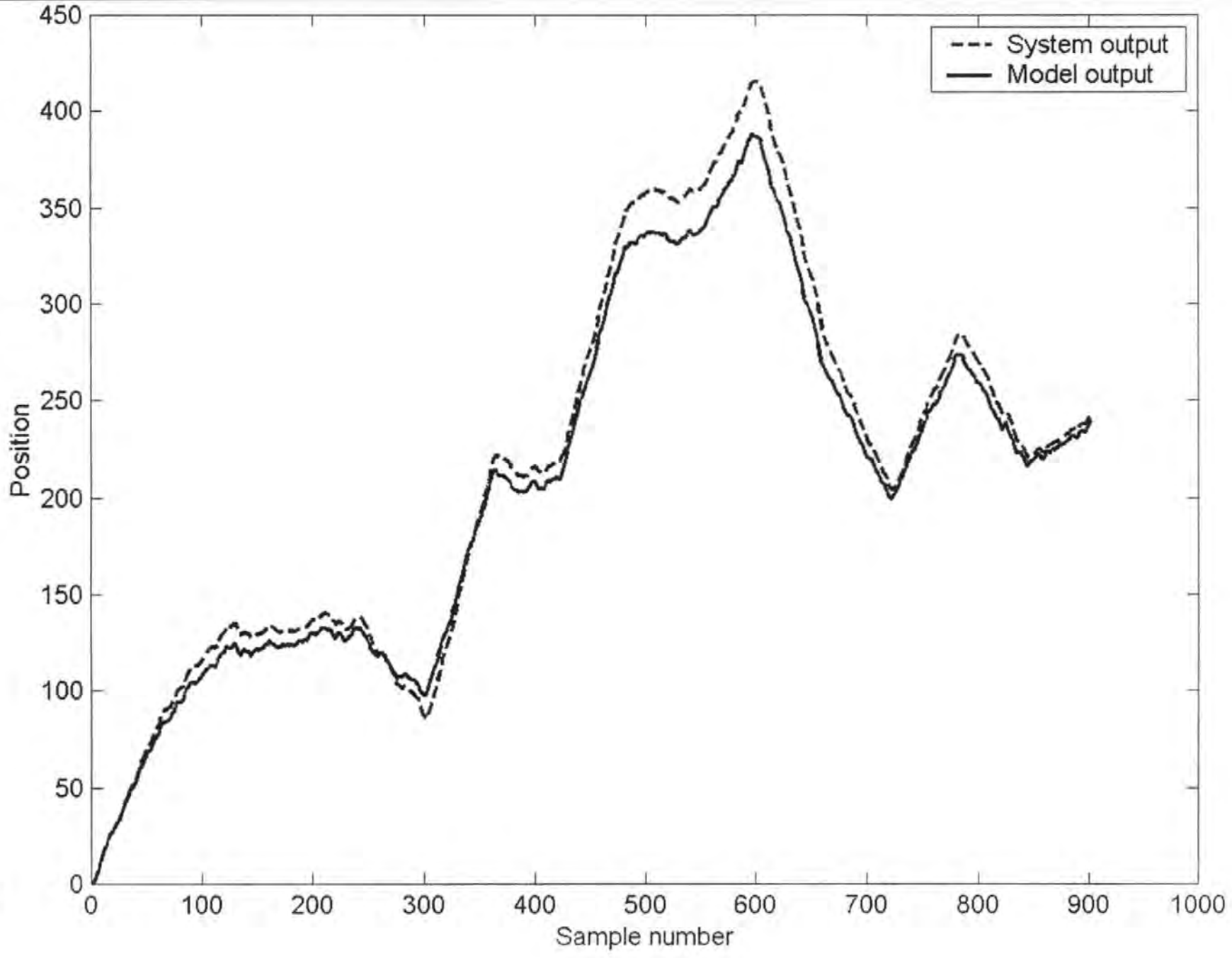
System output
Model output
Position
Sample number
0
50
100
150
200
250
300
350
400
450
0
100
200
300
400
500
600
700
800
900
1000

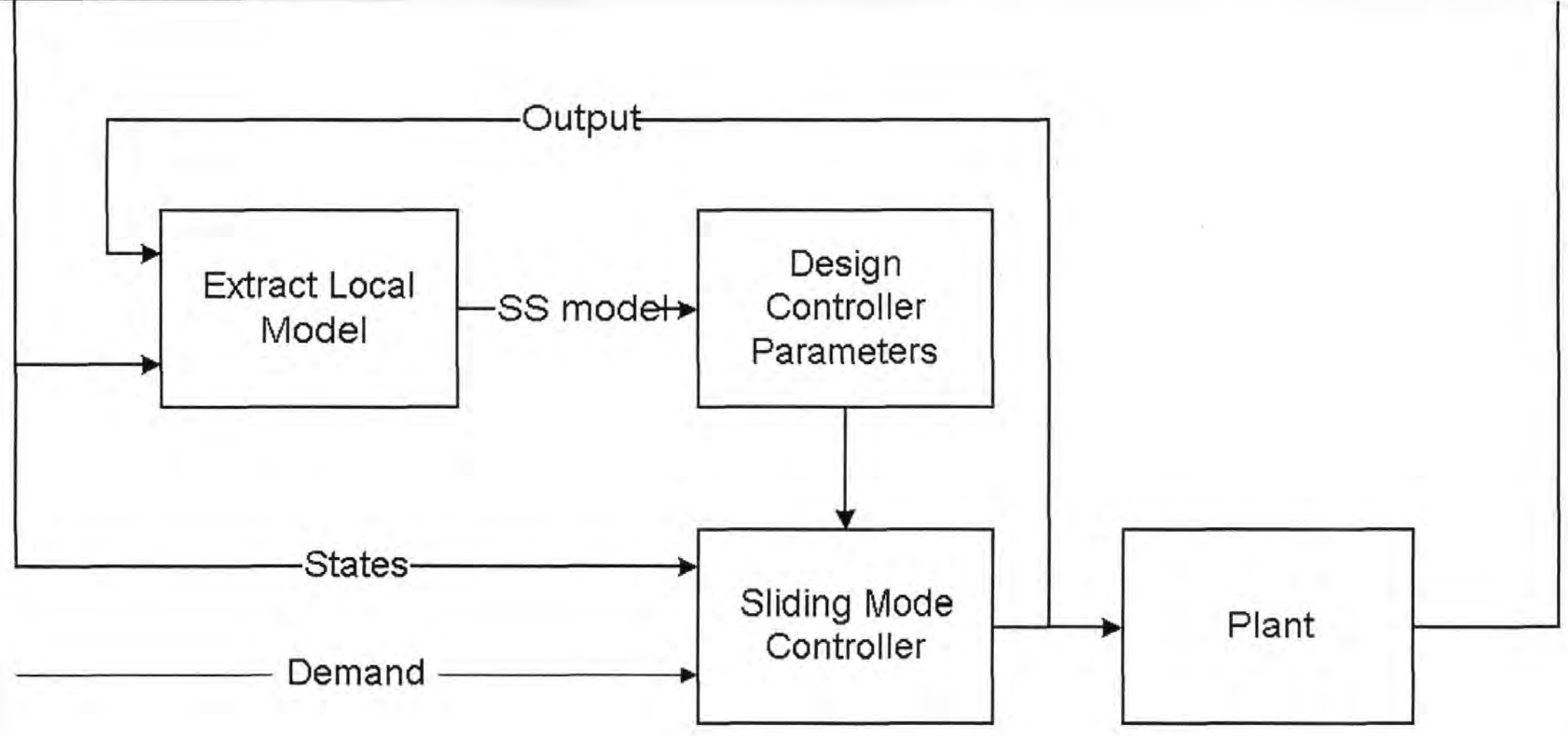
Output
Extract Local Model
SS model
Design Controller Parameters
States
Sliding Mode Controller
Plant
Demand

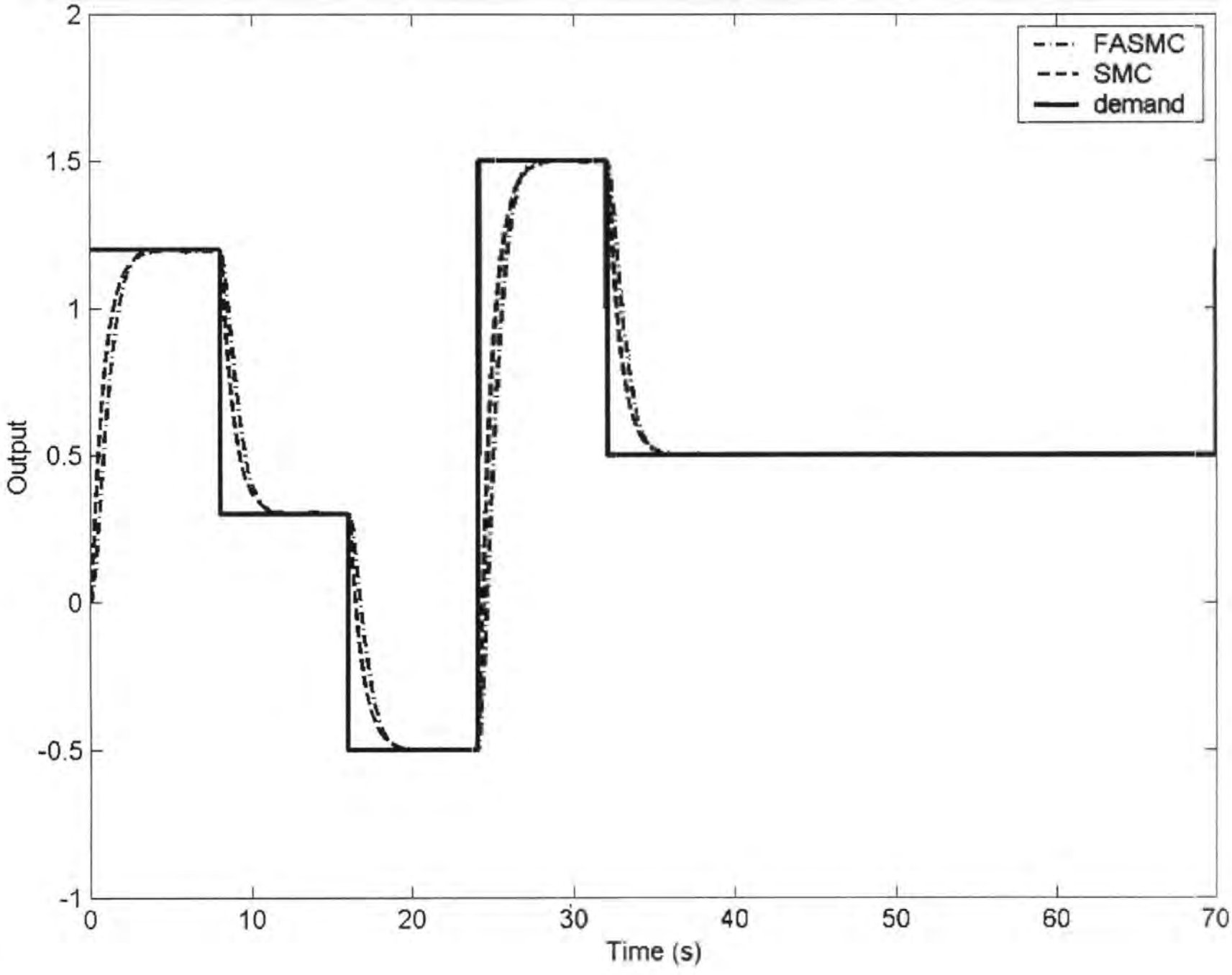
FASMC
SMC
demand
Output
Time (s)
2
1.5
1
0.5
0
-0.5
-1
0
10
20
30
40
50
60
70

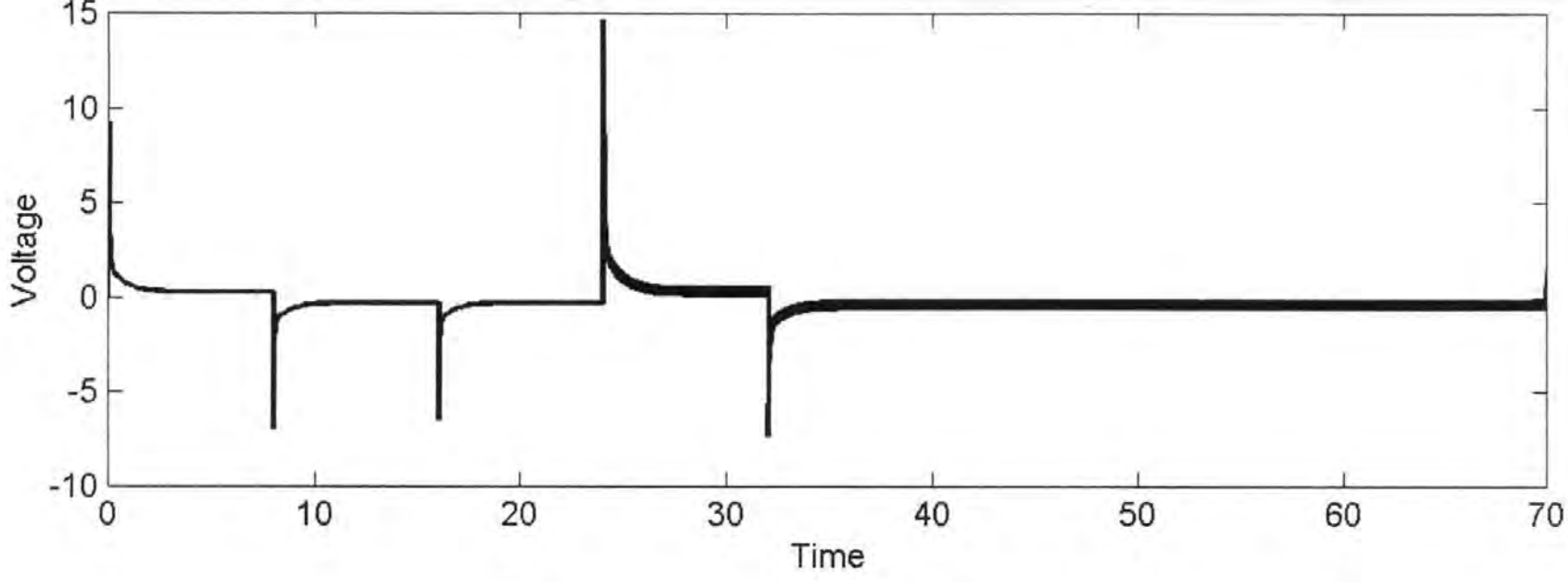

b) FASMC Control effort

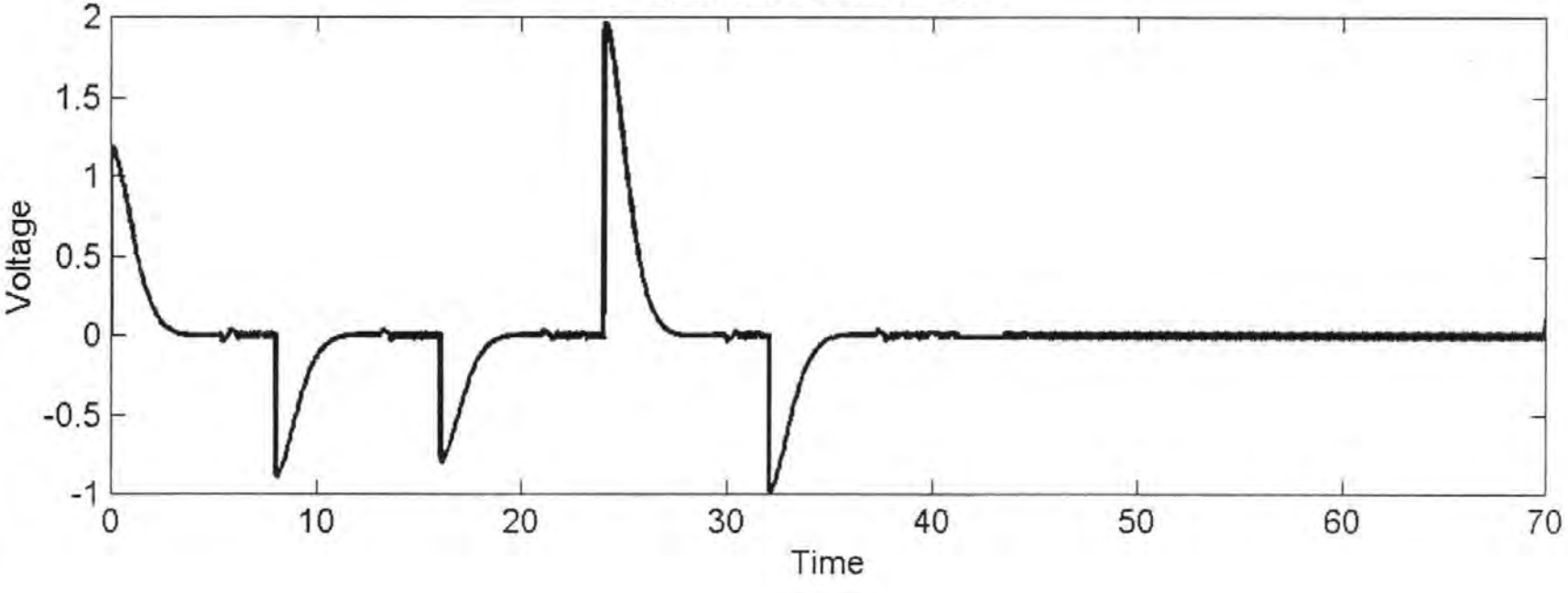

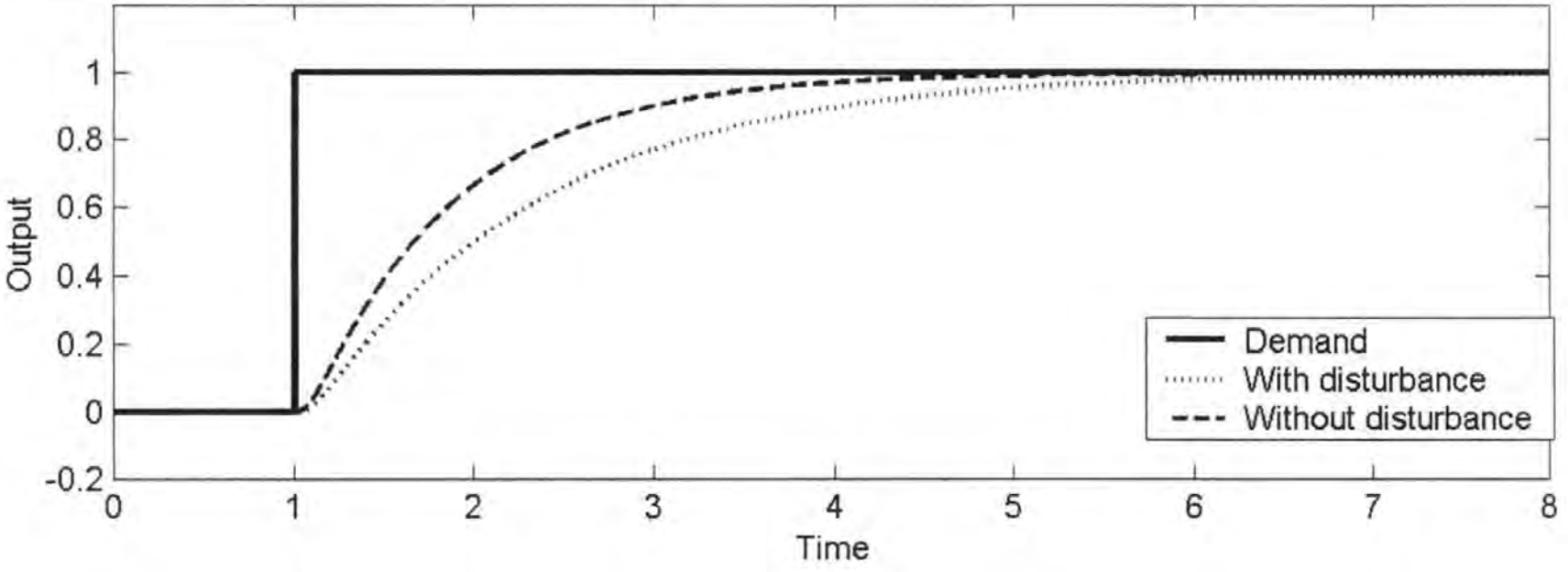

b) Controller effort

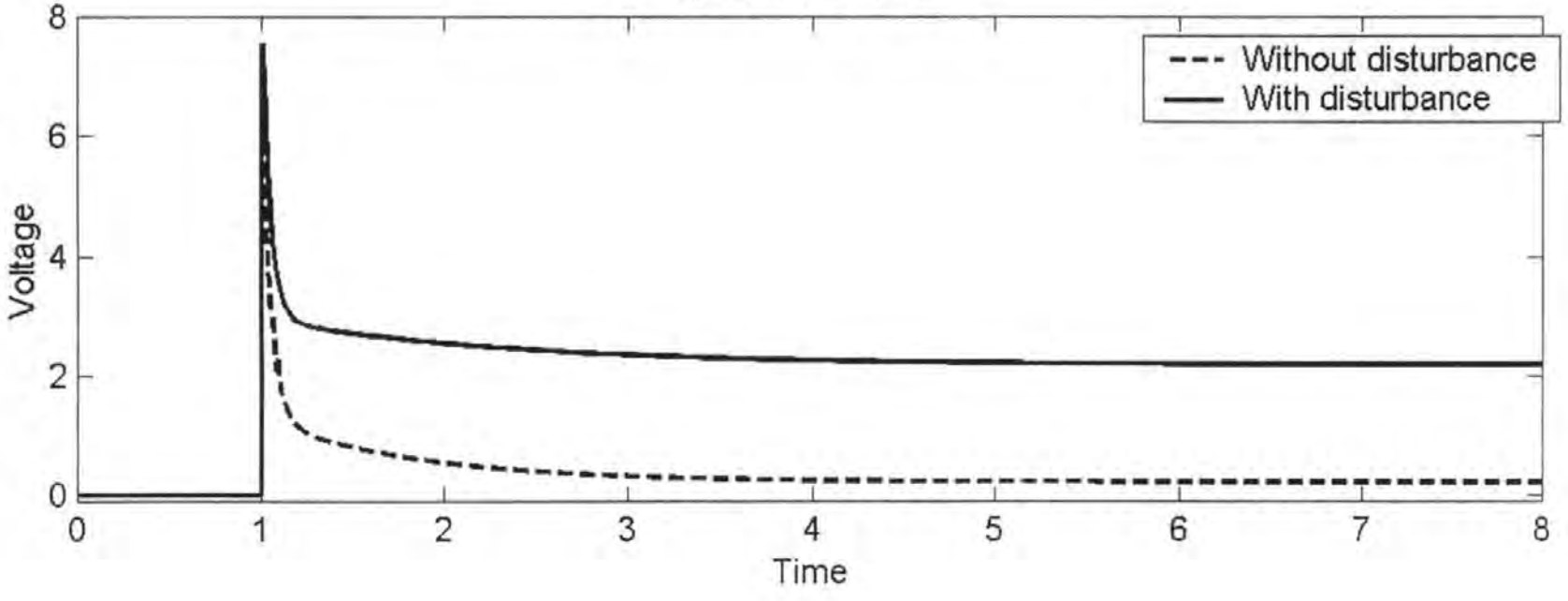

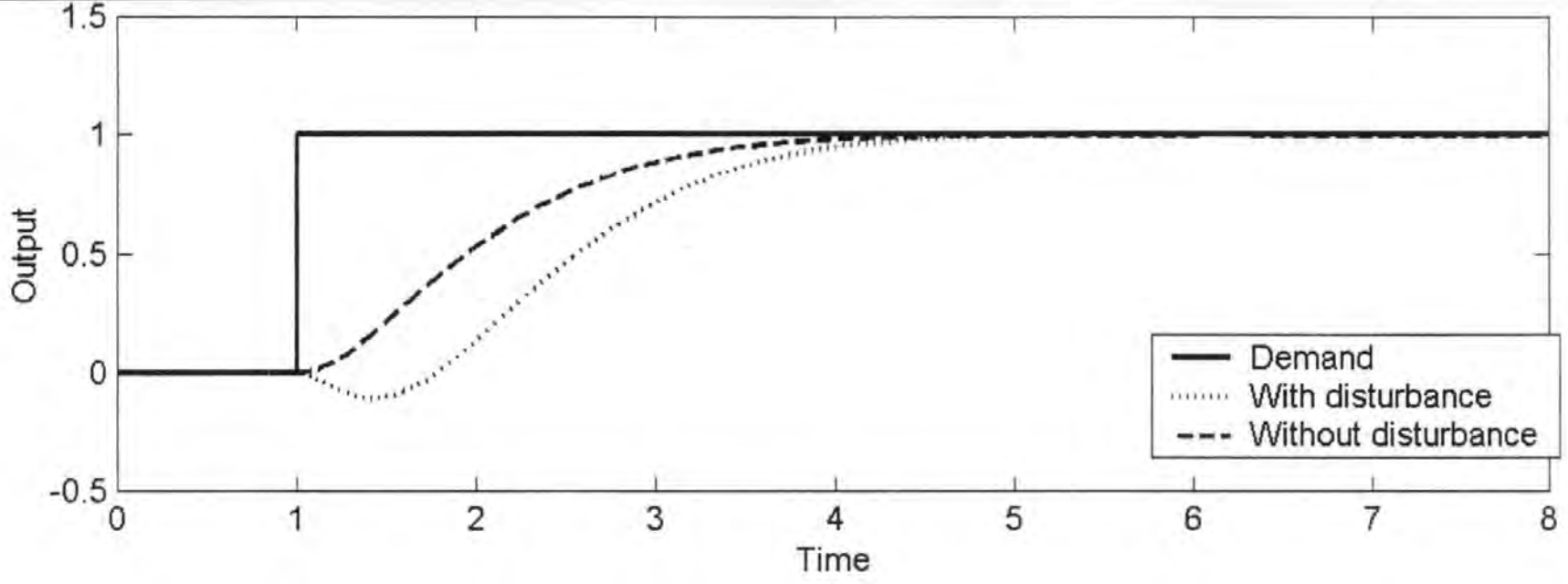

b) Controller Effort

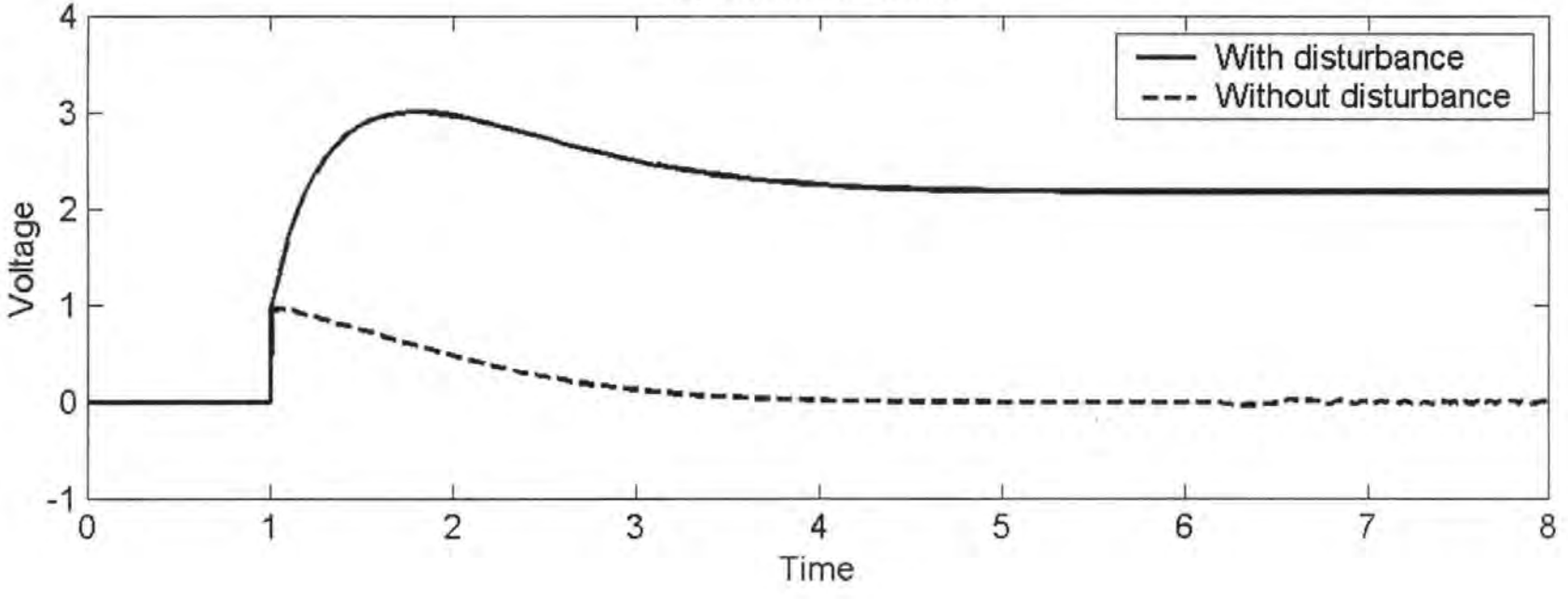

IDENTIFICATION OF A BRUSHLESS D.C. SERVOMECHANISM SYSTEM

M.J.Knight, R.Sutton, R.S.Burns

Marine and Industrial Dynamic Analysis Group,

Department of Mechanical and Marine Engineering,

University of Plymouth

Tel: (01752)232676 Fax: (01752)232638 Email:

MJKnight@Plymouth.ac.uk

Abstract. The paper presents several models derived from both input-output data and *a-priori* knowledge of an experimental test rig. The test rig is based on a brushless dc motor, rigidly coupled to a nonlinear, time-variant frictional load. Models based on the linear difference equation are developed and methods for incorporating *a-priori* knowledge into this structure are then explored. This complementary approach to the use of well founded knowledge and input-output data is found to perform better, according to the performance measures adopted, than the models using input-output data or *a-priori* knowledge alone.

Key Words: Identification, modelling, semi-physical modelling, fuzzy clustering

1. INTRODUCTION

The development of models to describe system behaviour is of interest within many areas of science and engineering. The models, once developed provide the user with a method for describing the behaviour of a system, and the means to develop prediction and control algorithms for the system.

The brushless direct current motor (BLDC) is an attractive option for the actuation of robotic systems primarily because of its low maintenance requirement and its cleanliness, however, it does pose problems to the user in terms of deriving an acceptable model, since it is highly coupled and multi-input. In addition, the load applied to such a system is not typically considered within the modelling literature because of a need to maintain generality within the model derivation. Within this work, a motor coupled to a nonlinear load is explicitly considered and approaches to system identification are explored. A common model derived from physical principles is first described and system fundamentals are outlined. The work then moves on to use nonlinear identification techniques, namely neural networks and fuzzy clustering. The results of the identification are compared in section 7 using common performance measures. Section 6 of this paper, improvements on the identified model performance are made through use of data transformation based on well founded physical relationships. Throughout this work, each of the models are provided with a suitable acronym which is used within the summary of results to identify individual model performance.

2. EXPERIMENTAL TEST SYSTEM

The experimental test system has been designed to provide an analogy with precision motion control systems in common use throughout industry. The system has, however been engineered such that variation in the load torque will have significant effect on the systems dynamic performance. In principle, the motor is linked to a lead screw with a rigid coupling. The nut on the screw is fixed to a central carriage, which is in turn constrained to move in a

single degree of freedom (Fig 1). When the motor is excited, the carriage is forced to move along the lead screw and if motor armature angular position is measured, then the linear displacement of the carriage may also be calculated.

The schematic diagram of the system can be found in Fig 2. The incremental encoder (IENC) provides 2000 pulses per revolution of the motor. This is the principle sensor used for position feedback. The gear system in the diagram corresponds to the lead screw and nut. The amplifier serves to provide the motor with a pulse width modulated excitation voltage and provides correct gating signals to the motor for efficient commutation. Within this work, all identification data is captured from the real system in the open loop, performance of the system is therefore heavily dependent on the frictional perturbation apparent at the motor armature. The frictional load has been shown within the literature to be time variant, e.g. (Armstrong-Helouvry *et al.* 1994), next it will also be shown that the load to which the motor is subjected is also dependent upon carriage position.

The speed of the carriage across the total length of the stage has been measured in both directions (Fig. 3). The following equation, which may be derived from the power balance equations provides the relationship between motor speed and load torque.

$$\omega(t) = \frac{V(t)}{KR} - \frac{T_m(t)}{K^2 R} \tag{1}$$

Where V is the terminal voltage, T_m is the generated torque, ω is the motor angular velocity, K is the motor constant and R is the motor phase resistance. Manipulation of (1) yields the ideal angular speed, ω_i (when T_m=0) and the stall torque of the motor, T_{ms} (when ω=0). The actual torque, assuming a linear relationship between ω and T_L is given as a fraction of the stall torque

$$T_m(t) = T_{ms} \cdot \left(1 - \frac{\omega(t)}{\omega_i}\right) - T_F \tag{2}$$

Where T_f is the motor friction torque. From the relationship given in (2), it may be readily seen from Fig. 2 that the load torque significantly varies, and is non-symmetrical, across the stage length.

It is also important to highlight the fact that the generated torque and the armature current are directly linked according to the equation

$$T_m(t) = K \cdot R \cdot I(t) \tag{3}$$

This relationship and (1) will be fundamental to the selection of input data later in sections five and six.

3. PERFORMANCE MEASURES

Performance measures are extremely important for the validation of derived models. The selection of performance measures is heavily application dependent. Three measures of performance based on common modelling objectives will be used to quantify modelling error $(\varepsilon(t))$. Model error is first described based on the following relationship

$$\varepsilon(t) = y(t) - \hat{y}(t) \tag{4}$$

where $y(t)$ is the system output and $\hat{y}(t)$ is the models estimate of the systems output. The first of the three measures to be used is the infinity norm given by

$$\|\varepsilon\|_\infty \triangleq \sup_{t\geq 0} |\varepsilon(t)| \tag{5}$$

The infinity norm of a signal depends on the extreme values of error. Since extreme values will be sporadic, the infinity norm represents the worst case model estimate.

The root mean square error semi-norm is also used to quantify the performance of the model. As opposed to the infinity norm, where the peak values of error were of concern, here it is the average value of error, the root mean square (RMS) of the error is given by

$$\|\varepsilon\|_{rms} \triangleq \left(\lim_{T\to\infty} \int_0^T \varepsilon(t)^2 \, dt \right)^{1/2} \tag{6}$$

The concept of the RMS error is used commonly within many engineering fields to describe the concept of average value, a low value for this performance measure does not imply that no large peaks in error occur, simply that they are not common and do not contain large values of energy.

The final performance measure is based on the ability of the model output to track the system output. Here, absolute error is only implicitly considered and the impetus is placed on how the signals vary with time. The percentile variance accounted for (VAF) is given as

$$VAF = 100\% \cdot \left[1 - \frac{\mathrm{var}\left(\varepsilon(t)\right)}{\mathrm{var}\left(y(t)\right)} \right] \qquad (7)$$

When the model output ($\hat{y}$) and the system output (y) are identical, the VAF is given as 100%, if the model is in error then the measure is lower. It is interesting to note that from the perspective of developing control algorithms based on the identified model, the VAF is of more significance to the designer, since this describes how well the model has captured the system dynamics.

4. MODELLING

Within the literature there are many models available to describe the BLDC motor. These vary in complexity from comparatively simple third-order state-space models, to extremely elaborate models based on the motor magnetic circuit. Here a compromise between computational load and model accuracy is struck through use of the phase co-ordinate model, a more detailed description of which can be found in (Krause *et al*, 1995).

When cylindrical pole permanent magnet armatures are used, all stator inductances are independent of armature position. Only the motion related inductances between the permanent magnet equivalent circuit and the stator windings depend on the armature angular position. The inductance matrix of the BLDC may therefore be described by

$$[L]_{PM} = \begin{bmatrix} L_s & L_{ab} & L_{ab} & L_{af}(\theta_{er}) \\ L_{ab} & L_s & L_{ab} & L_{af}(\theta_{er}) \\ L_{ab} & L_{ab} & L_s & L_{af}(\theta_{er}) \\ L_{af}(\theta_{er}) & L_{af}(\theta_{er}) & L_{af}(\theta_{er}) & 0 \end{bmatrix} \quad (8)$$

The stator self inductance L_s and the stator/stator mutual inductances L_{ab} are all equal to each other. First approximation yields

$$L_{ab} = -\frac{L_0}{3} \quad (9)$$

Where L_o is the nominal inductance specified by the manufacturer. The voltage/current equation in phase co-ordinates is:

$$\begin{bmatrix} V_s \\ V_r \end{bmatrix} = \begin{bmatrix} r_s & 0 \\ 0 & r_r \end{bmatrix} \cdot \begin{bmatrix} i_s \\ i_r \end{bmatrix} + \frac{d}{dt} \begin{bmatrix} \lambda_s \\ \lambda_r \end{bmatrix} \quad (10)$$

with

$$[\lambda] = [L(\theta_{er})] \cdot [i] \quad (11)$$

$$[i] = [i_a, i_b, i_c, i_{f_0}] \quad (12)$$

$$[r] = diag[r_s, r_s, r_s, 0] \quad (13)$$

$$[\lambda] = [\lambda_a, \lambda_b, \lambda_c, 0] \quad (14)$$

Where i is the applied phase current, r is the nominal stator resistance, λ the magnetic flux and $L(\theta_{er})$ is the time varying inductance, dependent on angular position θ_{er}. The motion equations are given

$$\frac{J}{p}\frac{d\omega_r}{dt} = T_e - T_{Load} \quad (15)$$

$$\frac{d(\theta_{er})}{dt} = \frac{\omega_r}{p} \quad (16)$$

Where J is the moment of inertia of the load, p is the number of motor poles, ω_r is the angular velocity of the armature, T_e is the electromagnetic torque and T_{load} is the load torque apparent at the motor armature. The load torque was taken as 1.2 Nm nominal, from Fig. 2, i.e. the

load torque was considered constant throughout the stage travel. Fig. 4 illustrates the model performance when compared with the actual performance captured from the system. All motor parameters were taken from the motor manufacturers data sheet. The inertial load of the system was unknown and was assumed negligible in comparison to the frictional perturbation. The results of this model are given in section 7, Table 1, PC.

5. IDENTIFICATION

Despite the fact that the motor used for actuation of the system is fairly well understood, it should be clear that there exists only diminutive information about the motor load. The reader is reminded that this load is time variant and that it has been shown to also vary with relative position along the length of the stage. An approach that may be taken in overcoming this latter variation is to use a lookup table within the system to describe relative loads. This leads to high computational storage requirements and is not an appealing solution. Within this section alternative approaches to identification based on input output data collected from the system are explored. Initially the models are provided simply with untreated data from the system. Later within this section attempts will be made to transform the data in such a fashion as to incorporate prior knowledge of the system into the model, and to restrict its overall flexibility.

The process of identification is to choose a model of sufficient flexibility, and one that is known to have performed well in the past. One specific family often employed is based around the linear difference equation. The most simple model from this family is the finite impulse response filter, the next model in the family is the so called auto-regressive with exogenous inputs (ARX) structure. The remaining model structures require recurrence in training and are therefore impossible to implement in the fuzzy clustering approach because the model estimate is not readily available during training. The models discussed here are therefore all based around the ARX structure.

When using a neural network or a fuzzy clustering method, the problem of identification becomes one of choosing the regression structure and choosing the parameters of the tuning method. In essence, the difference between the two approaches can be considered as the difference between global modelling (neural network model) and local modelling (fuzzy model). The two are discussed in further detail below.

The first premise within the process of identification is to assume that input output data of sufficient quality and quantity may be obtained from the system. In addition, it should be noted that signals such as pseudo random binary sequences which are in common use for the identification of linear systems, are not suitable for the identification of nonlinear systems. The input and output nodes from Fig 2. directly correspond to the data available to the model for identification. Position will always be used as the regressand for the model, however an interesting choice, and one that will ultimately effect the accuracy of the model, is which data should be used as regressors. Initially, this work begins with the use of the control voltage where it is assumed that the system is calibrated to faithfully reproduce the signal, and the measured current drawn by the motor. This latter choice is designed to reflect the correlation between load torque apparent at the motor armature and current.

In this work, step wise varying signals of various amplitudes were applied to the system and data was collected over a period of approximately 14 seconds at ten millisecond intervals. This provides a data set (Z^N) that may be neatly divided into two distinct sets, one for validation, the other for training. It was found early on within this work that the fuzzy clustering method and the neural network preferred alternative types of excitation signal. Where the fuzzy clustering algorithm worked better with additional noise placed on the demand signal, the neural network performed better without this noise. Therefore different data was provided to the neural network in order to improve modelling performance. The complete data sets are shown in Fig. 5 and Fig 6.

The method described in (He and Asada, 1993) was used in an attempt to identify the lag space of the chosen regressors. This method relies on the assumption that the system may be represented by a function that is reasonably smooth in the regressors. The regressors used in this work are corrupted by noise and the illustrations of the order index graphs are far from conclusive, however there are knee points at lags of 2 and 4 (Fig. 7). Further use of the Matlab system Identification toolbox, based on these uncertain results did however confirm that the structure [[4 4] [4 4] 1] worked well for the data. Fig. 8 illustrates the result of applying the linear ARX model to the data (ARX).

It is finally worthwhile to note that within this work only model predictive behaviour of the models is considered. If it were possible to use previous values of the system output, i.e., in a step ahead approach to the estimation the tremendously improved results will be observed.

5.1 Neural Network based ARX

Neural networks are a popular tool for pattern recognition and are used increasingly for system identification (Norgaard *et al*, 2001). The neural network used here is a two-layer perceptron network of the form

$$\hat{y}_i(\theta) = F_i\left(\sum_{j=1}^{n_h} W_{ij} f_j\left(\sum_{l=1}^{n_\varphi} w_{jl}\varphi + w_{j0}\right) + W_{i0}\right) \tag{17}$$

The network uses tansig activation functions within the input and hidden layer, the output layer uses a linear transfer function in order that the network output is able to take on any value. In the neural network training, the common mean square error of the estimate is used for the criterion of fit:

$$V_N\left(\theta, Z^N\right) = \frac{1}{2N}\sum_{t=1}^{N}\left(y(t) - \hat{y}\left(t|\theta\right)\right)^2 \tag{18}$$

W is given as the network weights, F is the activation function, N is the number of data in the training set and w is the network thresholds. The neural network is presented with the ARX structure is given by

$$y(t) = \varphi^T(t)\theta \tag{19}$$

where

$$\theta = [a_1 \ldots a_n \quad b_1 \ldots b_m]^T \tag{20}$$

$$\varphi(t) = [-y(t-1) \ldots -y(t-n) \quad u(t-1) \ldots u(t-m)] \tag{21}$$

θ is the regression vector for tuning, φ(t) is the vector of previous inputs (u) and outputs of the system (y). The vector φ(t) is presented at the input nodes and the current value of position ($y(t)$) is presented at the output.

5.1.1 Training Algorithms

In the identification of a system with a neural network, the choice of training algorithm greatly effects the convergence properties of the model. Within this work, two training algorithms are considered explicitly, the Gradient descent method and the Levenberg-Marquardt. These two approaches are discussed next.

Gradient Descent

Gradient descent is a prediction error method. The task of training is to obtain the mapping from the dataset to a set of candidate models,

$$Z^N \rightarrow \hat{\theta} \tag{22}$$

In this case the objective is to minimise the mean square error (18) according to

$$\hat{\theta} = \arg\min_{\theta} V_N(\theta, Z^N) \tag{23}$$

The prediction error method is iterative and generally takes the form

$$\theta_{(i+1)} = \theta_i + \mu_i \eta_i \tag{24}$$

where $\theta_{(i)}$ specifies the current iteration, η_i specifies the search direction and μ_i specifies the step size. The iteration of the algorithm continues until such time as the minimisation criteria is satisfied. The principle of the gradient descent method is at each iteration to adjust the weights of the network in the opposite direction to the gradient, i.e

$$\eta_i = -G\left(\theta_{(i)}\right) \tag{25}$$

$$\theta_{(i+1)} = \theta_i - \mu_{(i)} G\left(\theta_{(i)}\right) \tag{26}$$

where

$$G\left(\theta_{(i)}\right) = \left.\frac{dV_N\left(\theta, Z^N\right)}{d\theta}\right|_{\theta=\theta_i} \tag{27}$$

If the step size μ_i is sufficiently small with this choice of direction, then it is always possible to achieve a reduction of the criterion,

$$V_N\left(\theta_{(i+1)}, Z^N\right) \leq V_N\left(\theta_{(i)}, Z^N\right) \tag{28}$$

Frequently the step size is selected as constant within the training. This can lead to slow convergence of the network due to a need for the step size to remain small. In (Demuth and Beale, 2001), an approach to using an adaptive step size is proposed to control the convergence of the network. This approach will be used later on in section 6.

Levenberg-Marquardt

A comprehensive description of the Levenberg-Marquardt algorithm may be found in (Norgaard *et al*, 2000), the algorithm is essentially a cross between the gradient descent method already discussed and the Gauss-Newton method (Lewis *et al*, 1999). In this approach, the minimisation is given

$$\hat{\theta} = \arg\min_{\theta} V_N\left(\theta, Z^N\right) \quad \text{subject to} \quad \left|\theta - \theta_{(i-1)}\right| \leq \delta_i \tag{29}$$

The update rule for the Levenberg-Marquardt algorithm is given as

$$\theta_{(i+1)} = \theta_i + \mu_i \tag{30}$$

$$\left[R\left(\theta_{(i)}\right) + \lambda_i I\right]\mu_i = -G\left(\theta_{(i)}\right) \tag{31}$$

Where the Hessian is given as

$$R\left(\theta_{(i)}\right) = \left.\frac{d^2 V_N\left(\theta, Z^N\right)}{d\theta^2}\right|_{\theta=\theta_i} \tag{32}$$

and the small constant λ_i which is used to alleviate ill conditioning problems with calculating the search direction. In practice, the Levenberg-Marquardt uses an approximation to the prediction error as in the case of the Gauss-Newton method. The value of δ_i represents the radius of a trusted region around the current estimate, within which the selection of the search direction for the approximation is assumed to correspond well with the search direction for the criterion $V_N\left(\theta, Z^N\right)$.

The Levenberg-Marquardt algorithm offers significant speed advantages over the basic gradient descent algorithm and is therefore used throughout the neural network modelling discussed here.

After scaling of the data and training with the Levenberg-Marquardt algorithm, a neural network with tansig activation functions on the input and hidden layer, and a linear activation function in the output node typically gave simulation results as shown in Fig 9 (NN ARX).

5.2 Fuzzy based ARX

The term *fuzzy identification* has come to represent the use of fuzzy logic in the modelling and representation of a system. Fuzzy models may be viewed as general function approximators and are therefore readily applied to the nonlinear regression problem of the form discussed in the previous section. The fact that behaviour of a system can be easily represented linguistically e.g.

If *Voltage is High* **and** *Current is High* **then** *Speed is Fast*

naturally provides the user with a useful method by which a systems behaviour can be predicted entirely from empirical observation (Linskog, 1996) provides a comprehensive discussion of this approach, which constitutes the first of the two principle methods:

1. The expert knowledge is articulated through a series of **if then** rules. The model structure is generated implicitly from the rules supplied by the expert.

2. In the second case, no prior information is assumed about the system, and only numerical data is used to construct the fuzzy rule base.

The first of these approaches provides the user with a convenient a interface through which prior information may be incorporated into the model via linguistic rules. The latter of these two approaches is data driven and is closely akin to the neural network approach to model derivation. The key advantage, however, is that information about the system may be subsequently extracted from the model once identification is complete. Further discussion on this subject and related topics is given by Babuska (1998) and provides the foundation for this section of the work.

5.2.1 Data Clustering

The goal of cluster analysis is to partition a given set of data into clusters, which will be subsets of the presented data. The criteria for these clusters is

- Within cluster homogeneity: Data within clusters should be as similar as possible.
- Between cluster heterogeneity: Data between clusters should be as different as possible.

In this case similarity can be measured as a function of distance. Cluster validity was used to select the number of clusters because of the relatively small number of permutations between regression structure and number of clusters, in this case 5. If the regression surface is partitioned into a series of linear surfaces (corresponding to a cluster), then an affine Takagi-Sugeno fuzzy rule (Takagi and Sugeno, 1985) of the form (33) may be used to represent the local regression.

$$R_i : \text{IF } f\left(x_1 \text{ is } A_{1,1} \text{ and } x_2 \text{ is } A_{1,2} \text{ and} \ldots \text{and } x_P \text{ is } A_{1,P}\right) \text{THEN } y_i = a_i^T x + b_i \quad \text{i=1,2,...,k} \quad (33)$$

where $x \in X \subset \mathbb{R}^P$ is a crisp input vector, A_i is an antecedent multidimensional fuzzy set defined by the membership function $\mu_{A_i}(x) : X \to [0,1]$, $y_i \in \mathbb{R}$ is the scalar output of the i^{th} rule. The index i relates the variable to the i^{th} rule and k is the number of rules in the rule base.

The consequent function will maintain its form throughout the rule base, only its parameters will vary. The antecedent of the rule defines a fuzzy validity region for the corresponding hyperplane. A rule base might therefore be used to produce a global, nonlinear function approximation.

The ARX structure discussed previously may be expressed in this pseudo linear form according to the following

$$\hat{y}(k+1)=\sum_{j=1}^{n_y} a_{i,j}\, y(k-j+1)+\sum_{j=1}^{n_u} b_{i,j}\, u(k-j+1)+c_i \qquad (34)$$

5.2.2 Product Space Identification

The antecedent fuzzy sets serve to divide the regression space in which the regression surface may be locally approximated by the consequent hyperplanes. The task of identification is to find the number, locations and parameters of these hyperplanes such that the regression surface is accurately approximated. This may be achieved through application of a set of fuzzy clustering methods, referred to as *subspace fuzzy clustering algorithms*, specifically the Gustaffson-Kessel (GK) algorithm is used here, discussion of which may be found in (Gustafson and Kessel, 1979).

5.2.3 Membership calculation

The antecedent parameters of the Takagi Sugeno model may be calculated through application of the distance measure used within the clustering algorithm. In this case only the regressor x, the regressor component of the cluster prototype and the corresponding cluster covariance matrix are used.

Using the GK algorithm, the distance measure may be evaluated as

$$D\left(x_k, v_i^x\right)=\left(x_k-v_i\right)^T F_i^x \left(x_k-v_i\right) \qquad (35)$$

using an inversion, this measure can be converted into the degree of fulfilment. One possible choice of inversion is to use the same equation as for the clustering algorithm (Hellendoorn and Driankov, 1997)

$$\beta_i(x_k) = \frac{1}{\sum_{j=1}^{c}\left[d\left(x_k, v_i^x\right) \Big/ d\left(x_k, v_j^x\right) \right]^{2/m-1}} \tag{36}$$

which takes all rules into account and calculates the degree of fulfilment of one rule with respect to the others.

There are two ways in which the fuzzy consequent parameters of the affine Takagi-Sugeno model may be calculated from the data clusters. The first is based around the geometric interpretation of the cluster, using the covariance matrix. The alternative approach is a local least squares optimisation based on the derived fuzzy partition matrix the former method based on the covariance matrix is discussed here. Equation (37) may be derived from the relationship implicit between the shortest eigenvector of the cluster covariance matrix and the regression surface.

$$y = \underbrace{-\frac{1}{\Phi_i^y}\left(\Phi_i^x\right)^T}_{a_i^T} x + \underbrace{\frac{1}{\Phi_i^y}\Phi_i^T v_i}_{b_i} \tag{37}$$

which can be seen to be directly equivalent to the affine Takagi-Sugeno model, Fig. 10 illustrates the result of training a fuzzy model (FC ARX). It should be noted that there is sensor noise present within the validation and training data, and it seems reasonable to assume that both the fuzzy model and the neural network based model could be improved by better training sets.

6. TRANSFORMS FOR REGRESSOR DATA

In this final section, attempts to transform the data to provide greater physical relevance are made. Specifically, the current and voltage data are combined with the power balance equations (PBE's) in order to derive estimates of position directly from the data. The power

balance equations provide a good model of system performance, their untreated estimation of position is also provided (PBE). The enhanced information is therefore incorporated with the fuzzy clustering approach in two ways, first the residuals of the PBE estimate are calculated, upon which a clustered model based on the same structure as in the previous section is trained (FRESPBE), the outputs of both models are then summed together to provide a composite estimate of the position. In the second approach, the PBE estimate is used in the clustered model as a direct replacement for the voltage regressor (PBEREG). This approach was adopted after tests demonstrated degraded performance with three regressors (i.e., voltage, current and the PBE estimate).

Using the power balance equations,

$$P_i(t) = V(t) \cdot I(t) \tag{38}$$

$$P_o(t) = T_m(t) \cdot \omega(t) \tag{39}$$

$$P_l(t) = I(t)^2 \cdot R \tag{40}$$

$$P_o(t) = P_i(t) + P_l(t) \tag{41}$$

an expression for the motor speed based on quantities assumed constant and the available measurements may be derived,

$$\omega(t) = \frac{V(t) \cdot I(t) - I(t)^2 \cdot R}{I(t) \cdot K \cdot R} \tag{42}$$

where P_i is the applied electrical power, P_o is the mechanical output power, and P_l is the power loss. Since $\frac{d\theta(t)}{dt} = \omega(t)$,

$$\theta(t) = \int_0^t \frac{V(t) \cdot I(t) - I(t)^2 \cdot R}{I(t) \cdot K \cdot R} dt \tag{43}$$

Fig. 11 illustrated the estimate of (43) based on the available current and voltage data. Fig. 12 and Fig. 13 show the results of applying the FRESPBE and PBEREG model structures respectively. The value of K may be used for tuning of the equation, here a gradient descent

method with variable step size is used in order to tune the model. The gradient descent method has been discussed in section 5.1. As mentioned before, use of an adaptive step size can be used in order to obtain the convergence speed of a large step, but the accuracy of a small step. Here an algorithm is proposed based on an initial value for the step size determined by the user. The algorithm (PBEGD) is described below

1. Initialise variables $\phi, \tau_{crit}, j = 0$ and $k = 0$
2. Obtain the value for the criterion of fit $V_N\left(\theta_{(i)}, Z^N\right)$
3. Find $\theta_{(i+1)} = \theta_i - \mu_{(i)} G\left(\theta_{(i)}\right)$
4. Obtain the new value for the criterion of fit $V_N\left(\theta_{(i+1)}, Z^N\right)$
5. If $V_N\left(\theta_{(i+1)}, Z^N\right) = V_N\left(\theta_{(i)}, Z^N\right)$ and $j = \phi$ then $k = k + 1$ otherwise $j = j + 1$
6. $\mu_i = \frac{\mu_i}{10^k}$, $V_N\left(\theta_{(i)}, Z^N\right) = V_N\left(\theta_{(i+1)}, Z^N\right)$
7. If $V_N\left(\theta_{(i)}, Z^N\right) > \tau_{crit}$ and $k > \delta$ then repeat the process from step 3

The value of ϕ determines the number of times the algorithm will search across the minimum, before reducing the step size τ_{crit} determines the termination criterion in the event that it can be achieved and δ defines the maximum value of k before the algorithm terminates. The initial model performance of this model is shown in Fig 11, Fig 14 illustrates the estimate as a result of tuning.

7. SUMMARY OF RESULTS

Table 1 provides a summary of the results obtained within this work. Both the infinity norm and the rms semi-norm have units of encoder pulses in error.

Table 1: *Performance of the various approached to identification*

It can be seen how the use of the power balance equations can significantly improve the performance of the identification approaches. It should be noted that the neural network model was both trained and validated on a different data set and therefore it is only the VAF which provides fair comparison. The use of the power balance equations on their own outperform the models trained simply on input/output data and provides the means to produce accurate models based on the nonlinear identification techniques.

8. DISCUSSION AND CONCLUSIONS

Attention has been paid within this work to the identification of a servo mechanism actuated by a brushless DC motor and subjected to large, time variant loads. Specifically the fundamental tenet within system identification has been explored, i.e. to identify only phenomena which are unknown. It was initially found that a model based purely on empirical observation and a priori knowledge provided a reasonable result, but that significant improvements were ready to be made. The linear ARX structure was found to be of sufficient flexibility so as to provide a much improved estimate over the phase coordinate model. Black box approaches were investigated in terms of a neural network and a fuzzy clustered rule base, both of which were based on the previously successful ARX structure. The neural network was found to strongly favour purely step wise varying identification data, which should be considered when comparisons between the models are drawn. It is clear from this exercise in itself that correct selection of the input output data has profound effect on the resulting black box model. The fuzzy clustered model was found to outperform the linear ARX model. Finally, attention to the incorporation of a priori knowledge was paid. In the first attempts, a black box model was used in a complementary fashion to the white box model in order to cancel estimation residuals. Incorporation of the white box model estimate into the black box model regression structure was found to significantly outperform the previous approach. Finally, the gradient descent training method was adopted from the neural network literature in order to minimise the white box model error. This model was successful

in minimising the root mean squared error of the estimate and performs well in comparison to the other models. However, this model has not captured the discontinuities within the data as well as the other models. The VAF measure is testament to this. It should be noted that this model has the advantage of simplicity and minimal computational load once trained over the fuzzy clustered and the neural network models. In a system with diminutive a priori understanding, the semi-physical or grey box approach to modelling has been applied and shown to be a viable approach to obtaining highly accurate results.

9. REFERENCES

Armstrong-Helouvry B., Dupont P. and Canudas De Wit C. 1994. 'A survey of models analysis tools and compensation methods for the control of machines with friction'. Automatica, **30**(7), 1083-1138

Babuska R. 1998. 'Fuzzy Modelling for Control'. Kluwer Academic Publishers.

Demuth H. and Beale M. 2001. 'Neural Network Toolbox Users Guide'. The Mathworks Inc.

Gustafson D and Kessel W. 1979. 'Fuzzy clustering with a fuzzy covariance matrix', Proc. IEEE CDC, San Diego, 761-766.

He X. and Asada H. 1993. 'A new method for identifying orders of input output models for nonlinear dynamical systems'. Proc. American Control Conference. San Francisco, California. 2520-2523.

Hellendoorn H., and Driankov D. 1997. 'Fuzzy model based identification: Selected approaches'. Springer Verlag.

Krause P., Wasynczuk O, Sudhoff S. 1995. 'Analysis of Electric Machinery'. IEEE Press.

Lewis F.L., Jagannathan S., Yesildirek A. 1999. 'Neural Network Control of Robot Manipulators and Nonlinear Systems.' Taylor Francis.

Linskog P. 1996. 'Methods, Algorithms and Tools for system identification based on prior knowledge'. PhD thesis, Linkoping University.

Norgaard M., Ravn O., Poulsen N.K., Hansen L.K. 2000. 'Neural Networks for Modelling and Control of Dynamic Systems.' Springer Verlag.

Norgaard M., Ravn O., Poulsen N.K. 2001. 'NNSYSID and NNCTRL tools for system identification and control with neural networks'. IEE Computing and Control engineering, **12**(1), 29-36

Takagi T. and Sugeno M. 1985. 'Fuzzy Identification and its applications to Modelling and Control'. IEEE Trans. on Systems, Man and Cybernetics, **15**(1), 116-132

Figure legend

Figure 1: Photograph of system

Figure 2: System Schematic Diagram

Figure 3: Speed of Carriage in Forward and Reverse Direction

Figure 4: Phase Coordinate Model Results

Figure 5: Identification set 1

Figure 6: Identification set 2

Figure 7: Order index versus lag space

Figure 8: Identification results for linear ARX model

Figure 9: Identification results for neural network

Figure 10: Identification results for fuzzy clustered model

Figure 11: Power balance equation estimate

Figure 12: Fuzzy clustering based on the power balance equation residuals

Figure 13: Power balance equations as a regressor for the fuzzy clustered model

Figure 14: Power balance equation estimate after tuning with gradient descent

Model	$\|\varepsilon\|_{\infty}$	$\|\varepsilon\|_{rms}$	VAF
PC	16700	7743	95.73%
ARX	5370	3046	99.41%
NN ARX	8874	5332	99.55%
FC ARX	5166	1982	99.7%
PBEQU	4352	2326	99.85%
FRESPBE	4938	2351	99.86%
PBEGD	4911	2304	99.68%
PBEREG	2535	594	99.97%

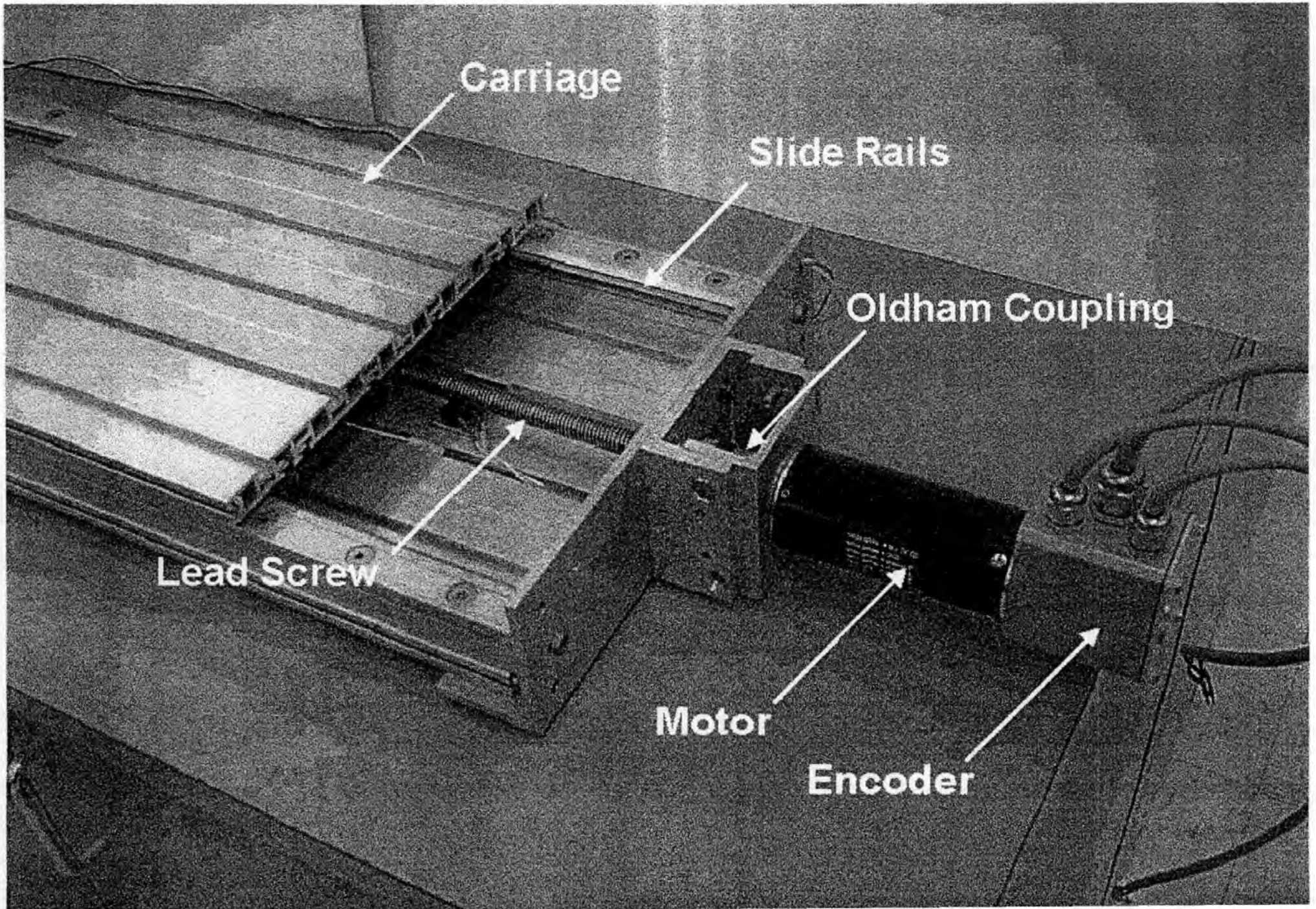
Carriage
Slide Rails
Oldham Coupling
Lead Screw
Motor
Encoder

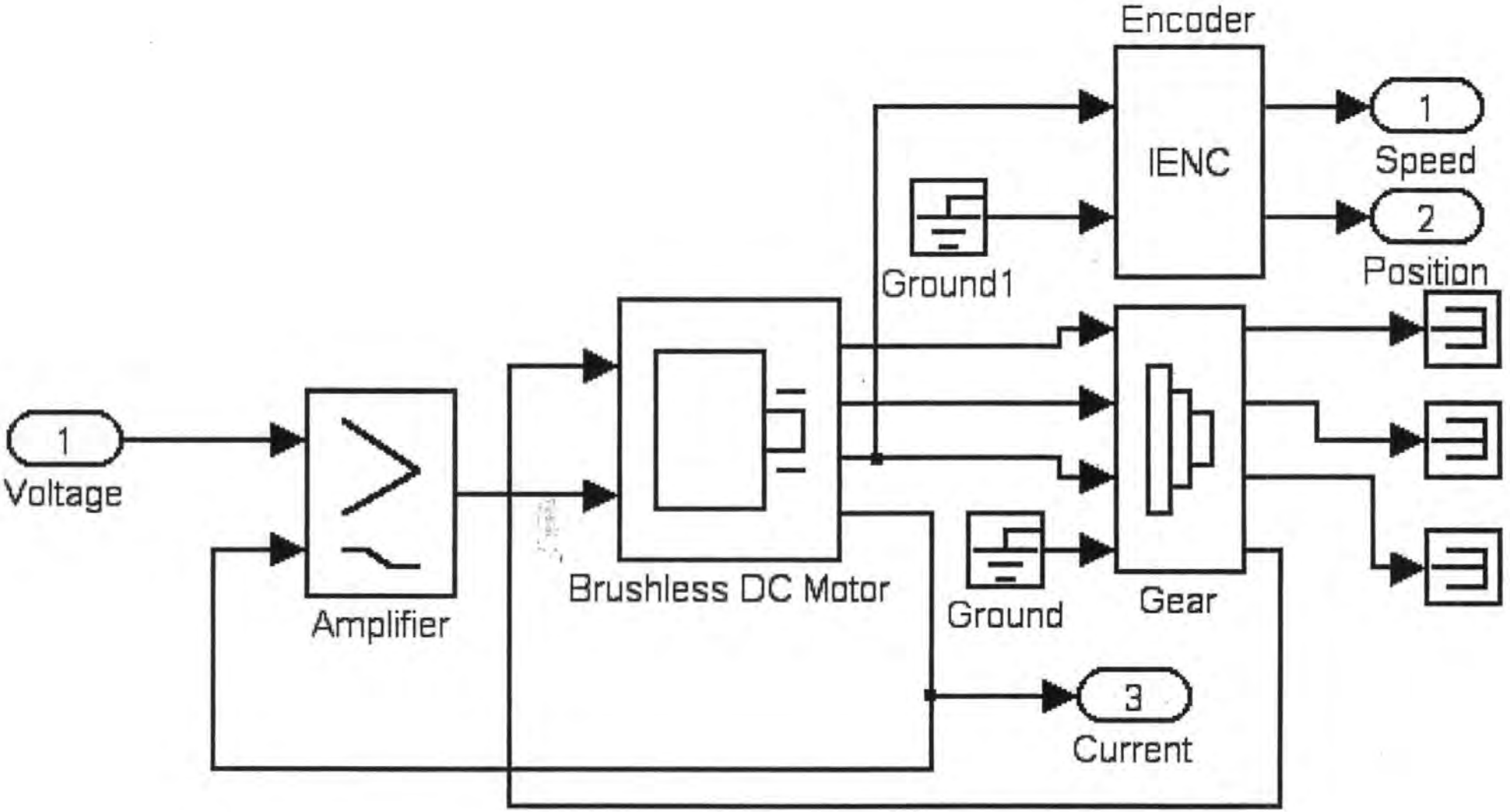
Encoder
IENC
1
Speed
2
Position
Ground1
1
Voltage
Amplifier
Brushless DC Motor
Ground
Gear
3
Current

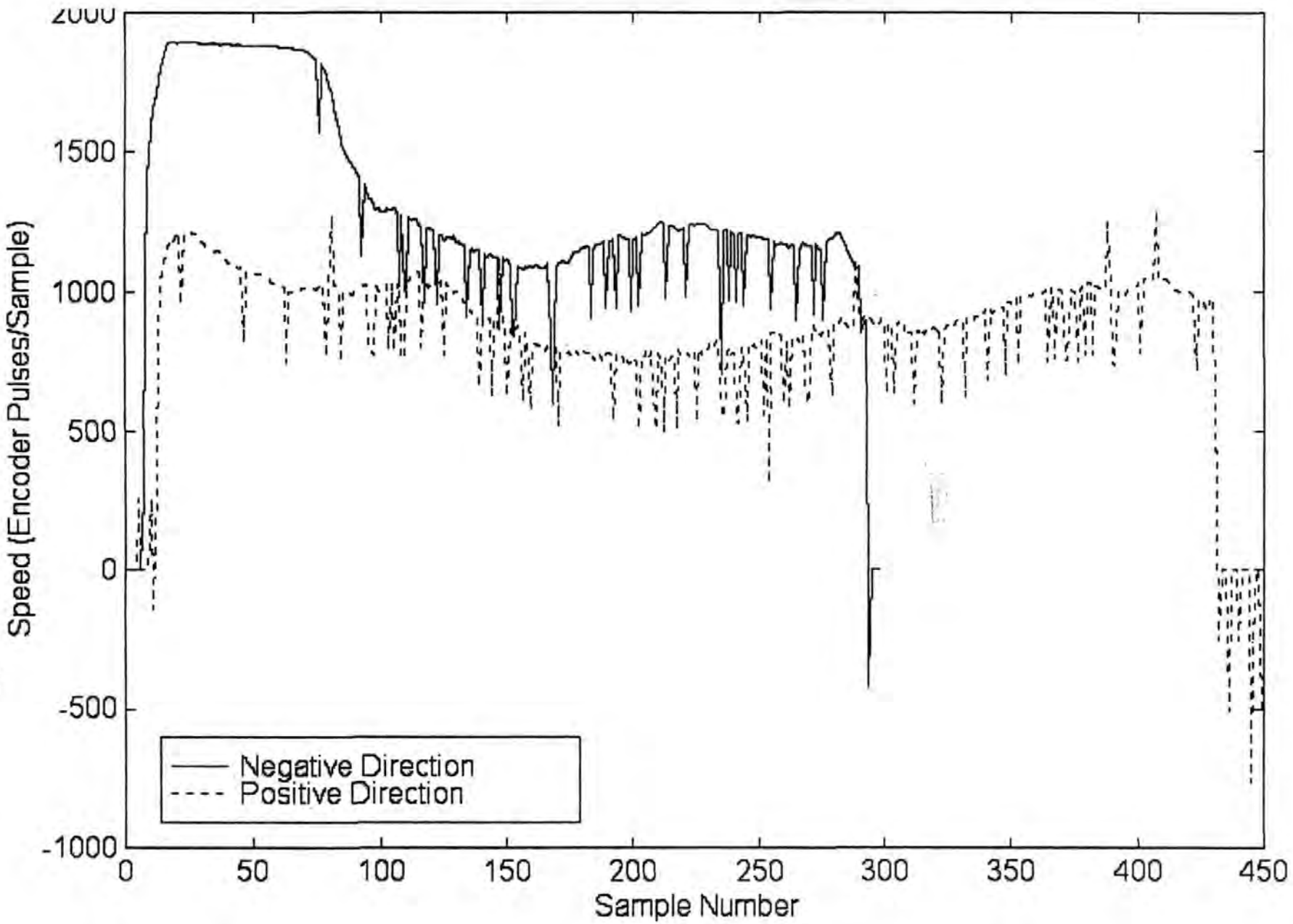
2000
1500
1000
500
0
-500
-1000
Speed (Encoder Pulses/Sample)
0
50
100
150
200
250
300
350
400
450
Sample Number
Negative Direction
Positive Direction

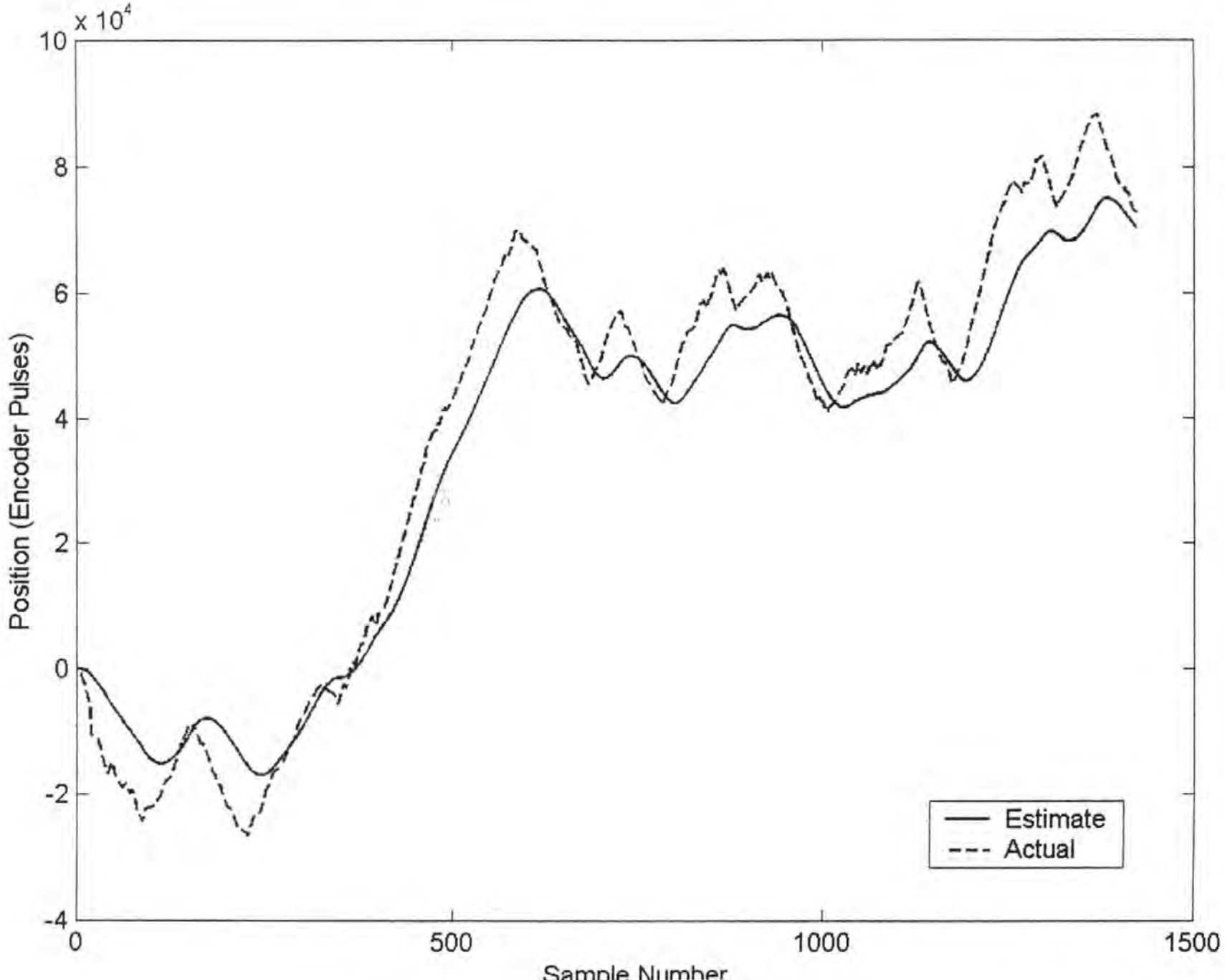
x 10^4
10
8
6
4
2
0
-2
-4
Position (Encoder Pulses)
0
500
1000
1500
Sample Number
Estimate
Actual

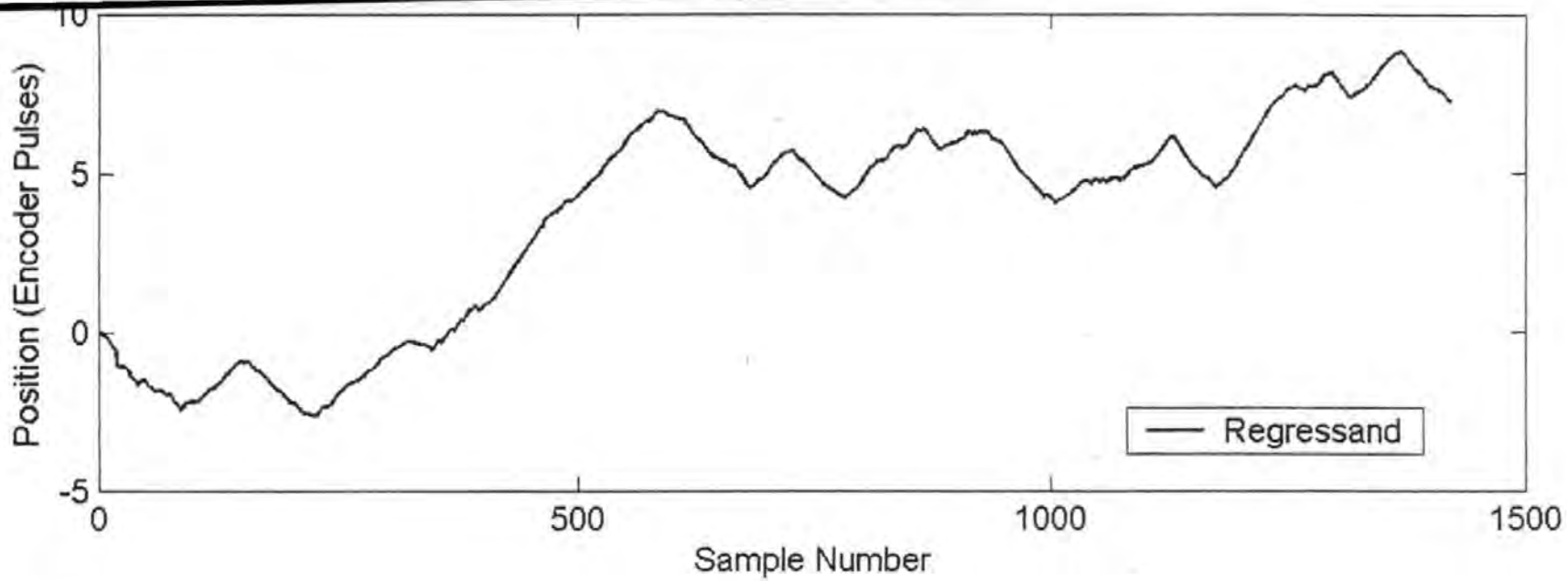
Position (Encoder Pulses)
10
5
0
-5
0
500
1000
1500
Sample Number
Regressand

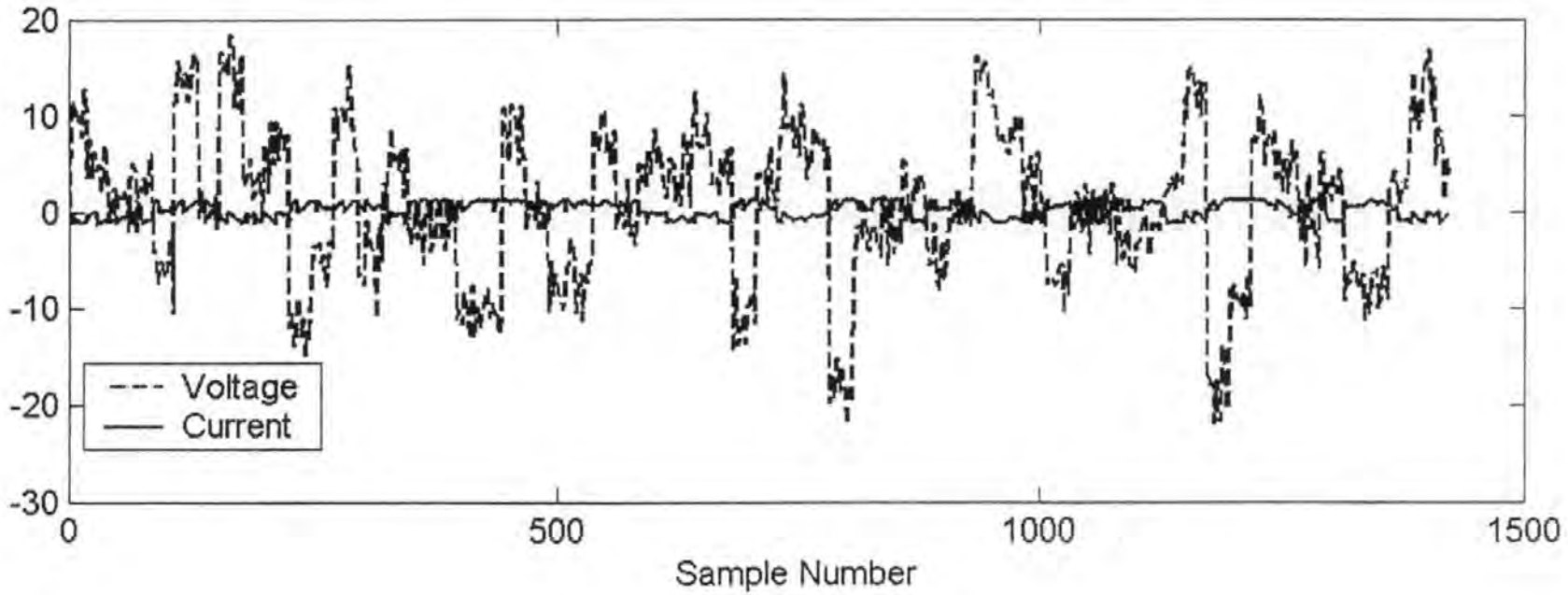
20
10
0
-10
-20
-30
0
500
1000
1500
Sample Number
Voltage
Current

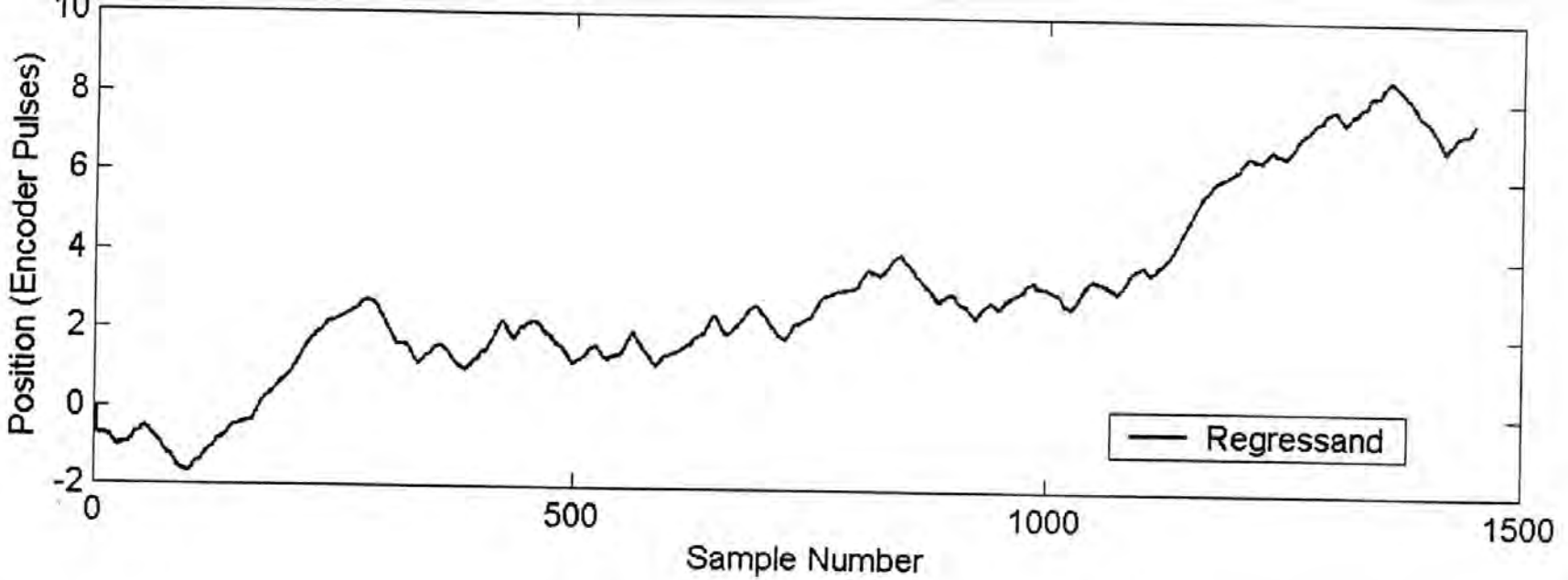
Position (Encoder Pulses)
10
8
6
4
2
0
-2
0
500
1000
1500
Sample Number
Regressand

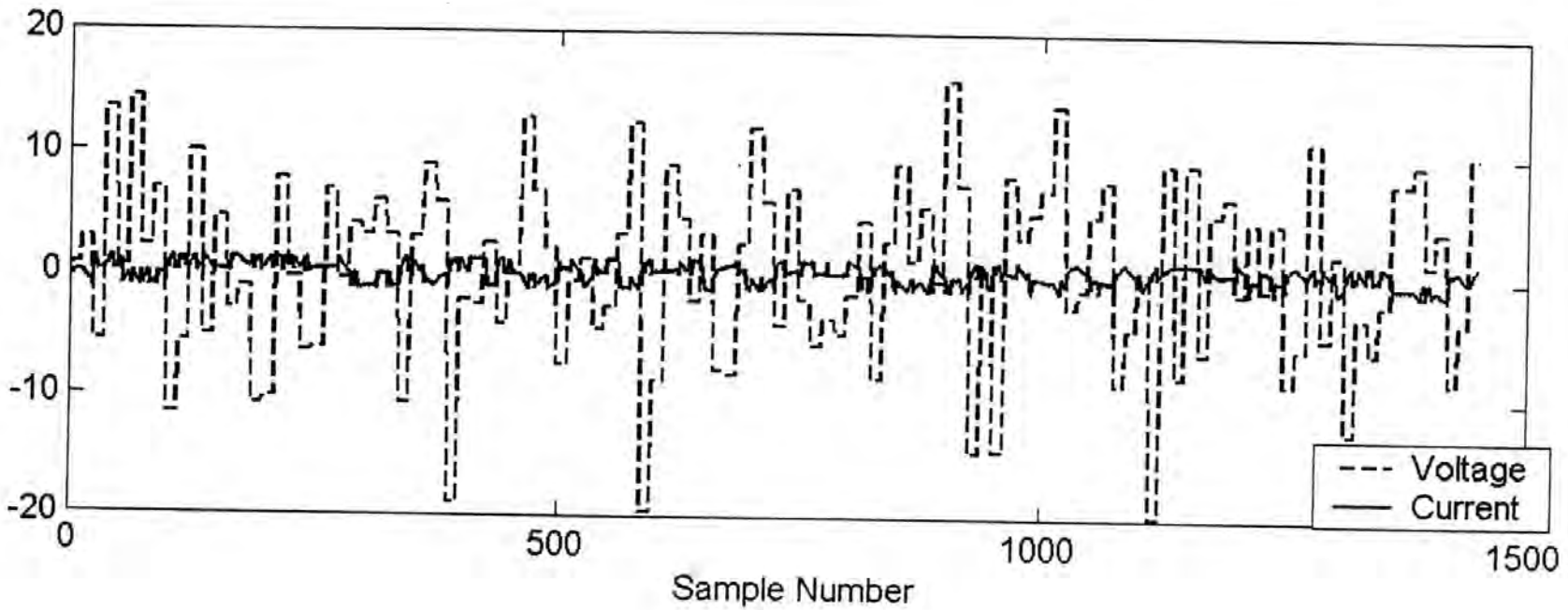
20
10
0
-10
-20
0
500
1000
1500
Sample Number
Voltage
Current

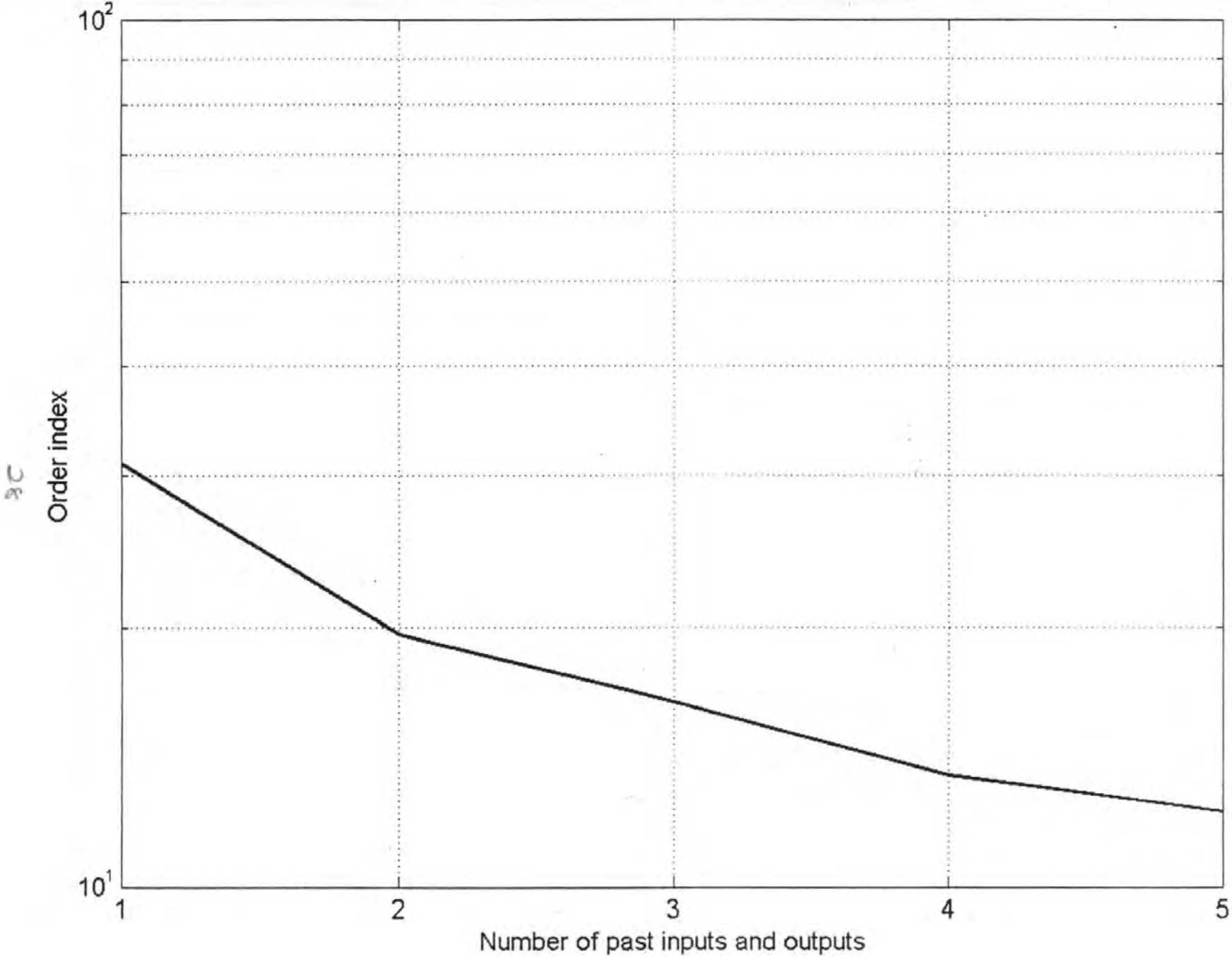
10^2
10^1
Order index
1
2
3
4
5
Number of past inputs and outputs

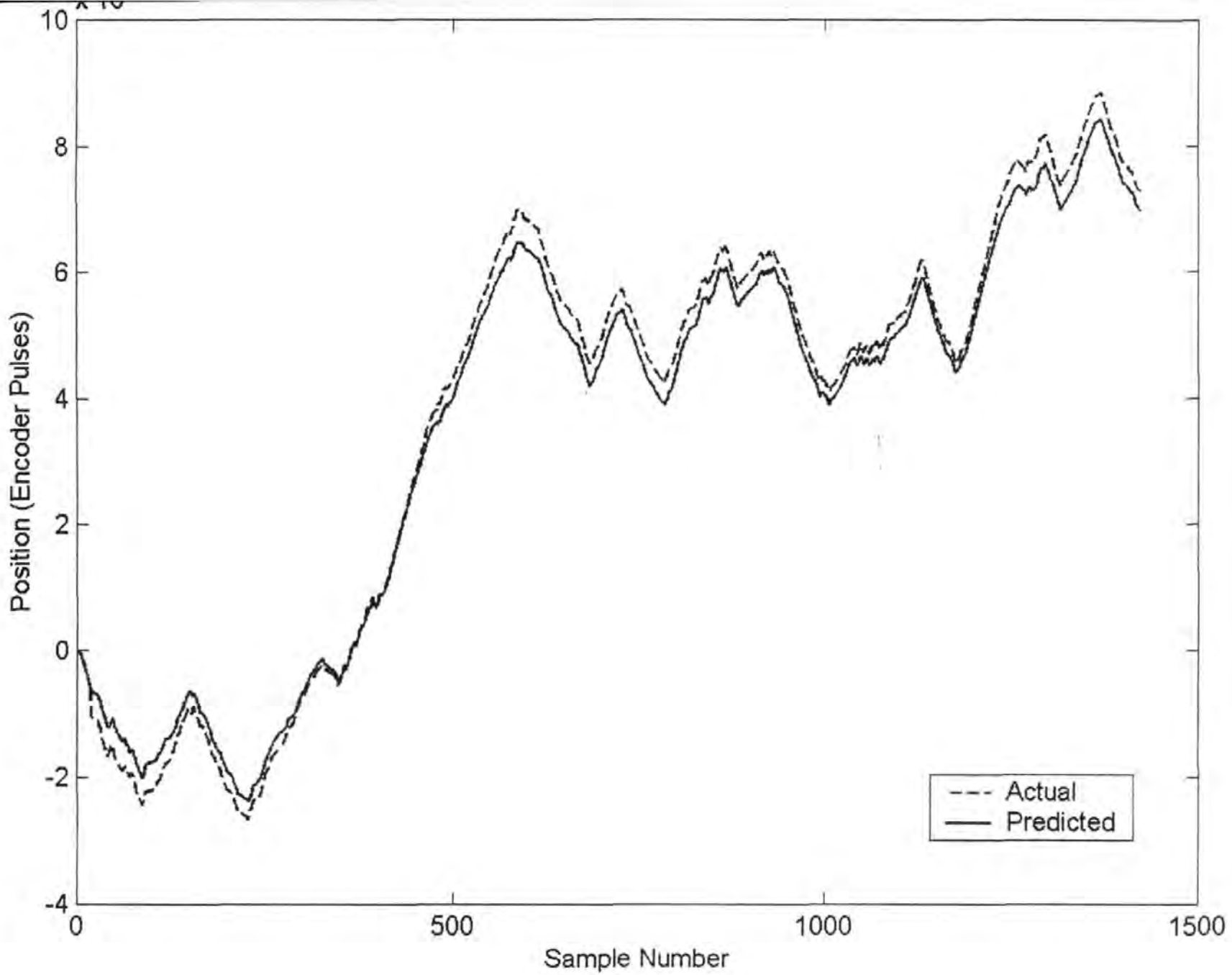
x 10^4
10
8
6
4
2
0
-2
-4
Position (Encoder Pulses)
0
500
1000
1500
Sample Number
Actual
Predicted

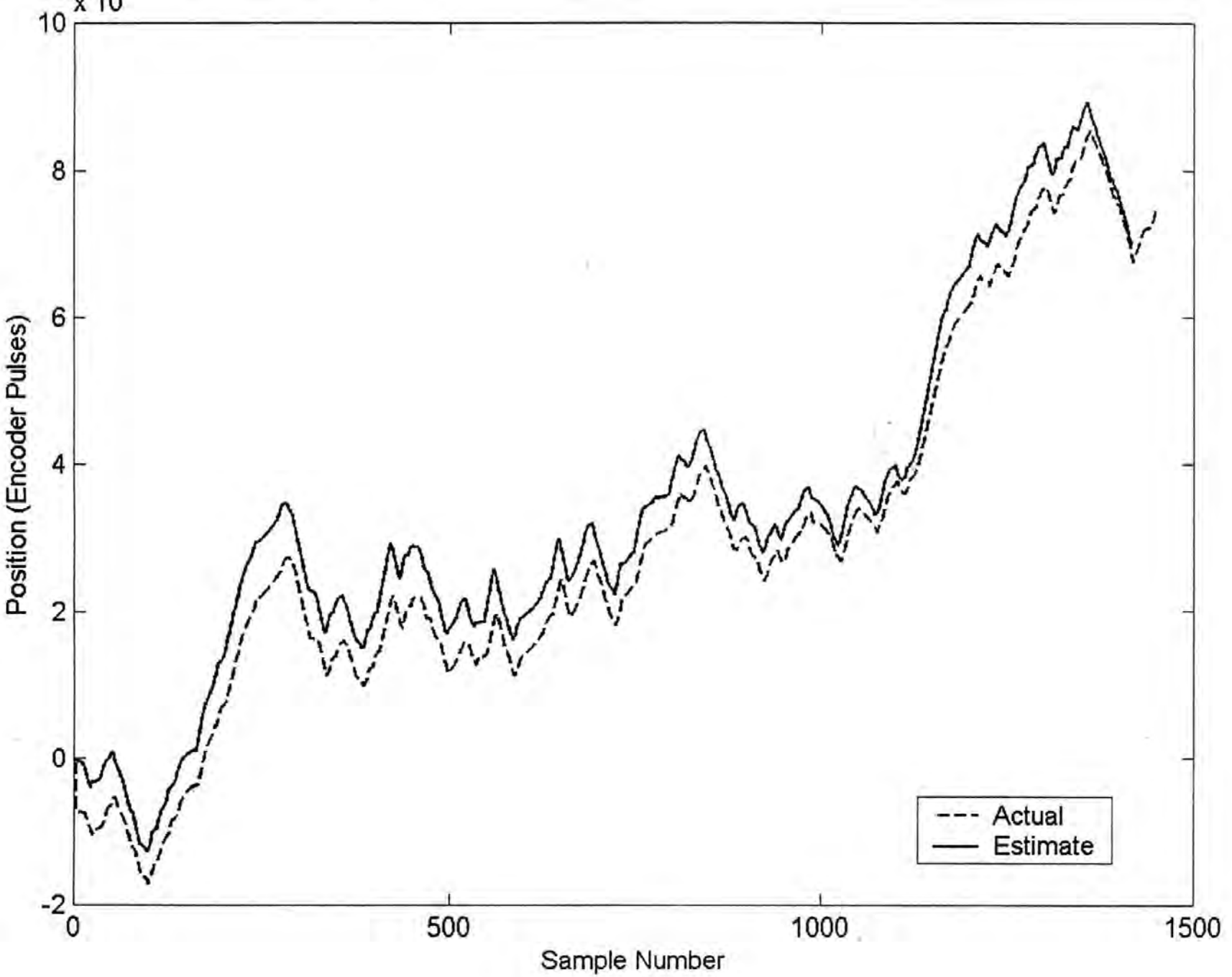
x 10
10
8
6
4
2
0
-2
Position (Encoder Pulses)
0
500
1000
1500
Sample Number
Actual
Estimate

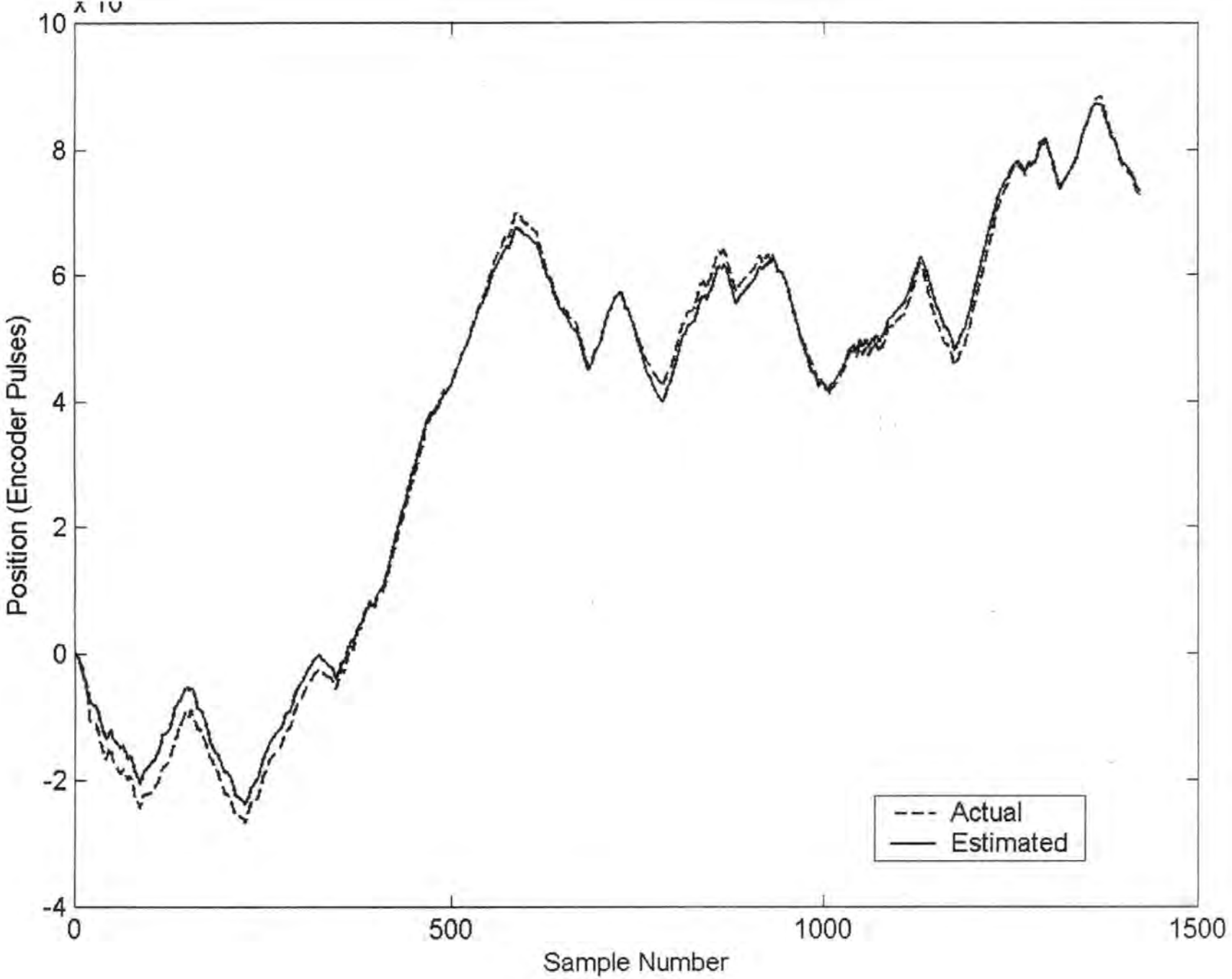
x 10
10
8
6
4
2
0
-2
-4
Position (Encoder Pulses)
0
500
1000
1500
Sample Number
Actual
Estimated

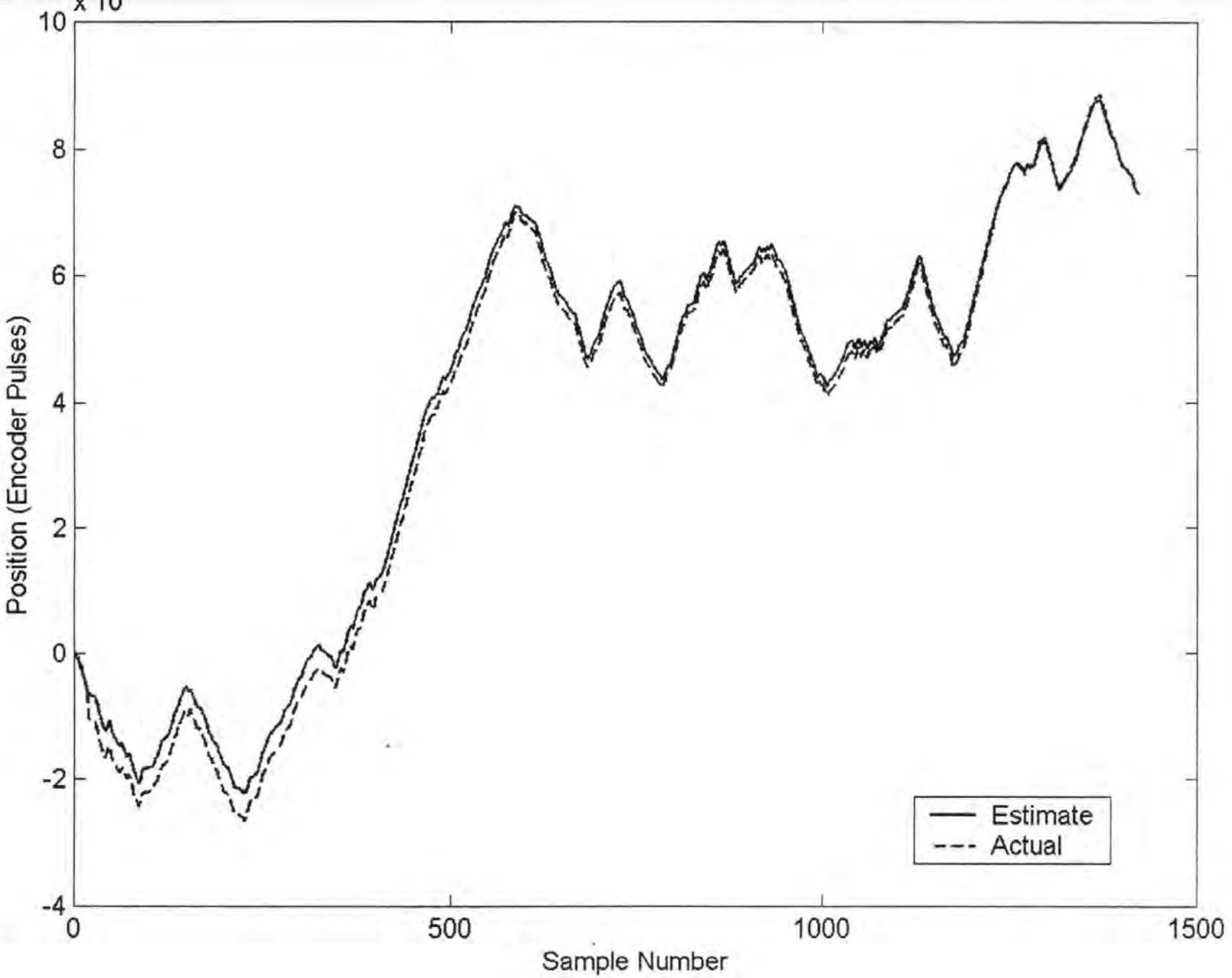
x 10
10
8
6
4
2
0
-2
-4
Position (Encoder Pulses)
0
500
1000
1500
Sample Number
Estimate
Actual

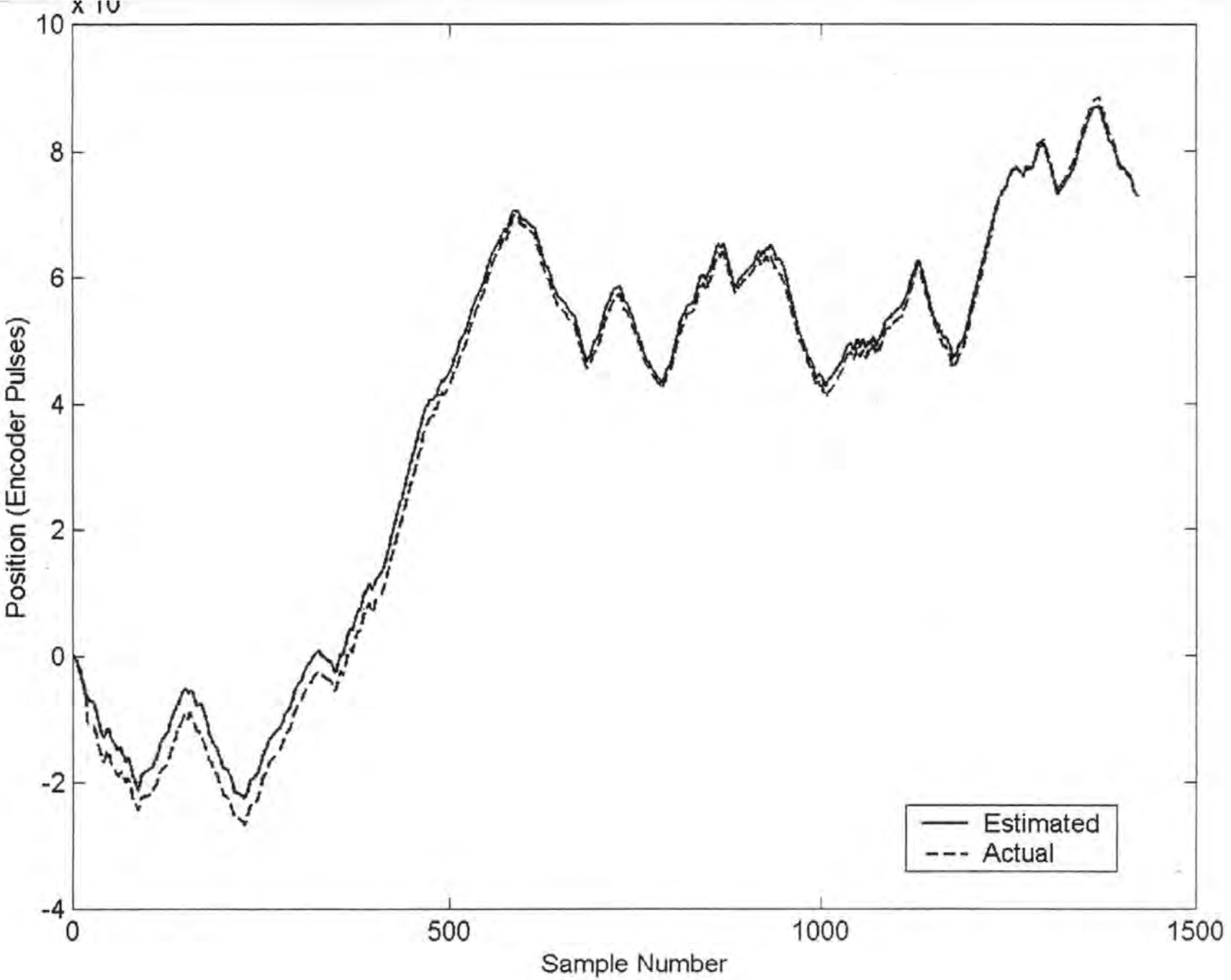
x 10
10
8
6
4
2
0
-2
-4
Position (Encoder Pulses)
0
500
1000
1500
Sample Number
Estimated
Actual

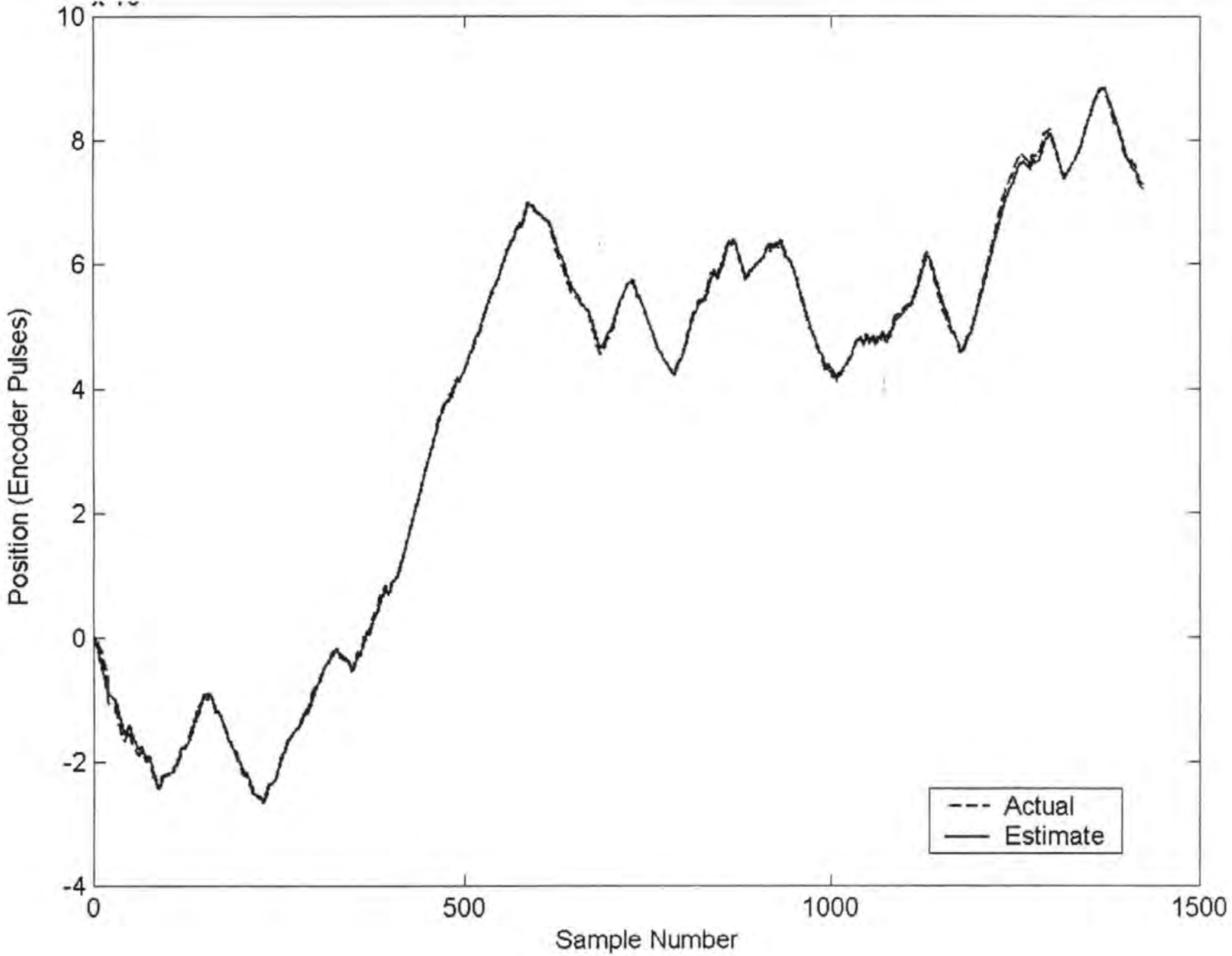
10
8
6
4
2
0
-2
-4
0
500
1000
1500
Position (Encoder Pulses)
Sample Number
Actual
Estimate

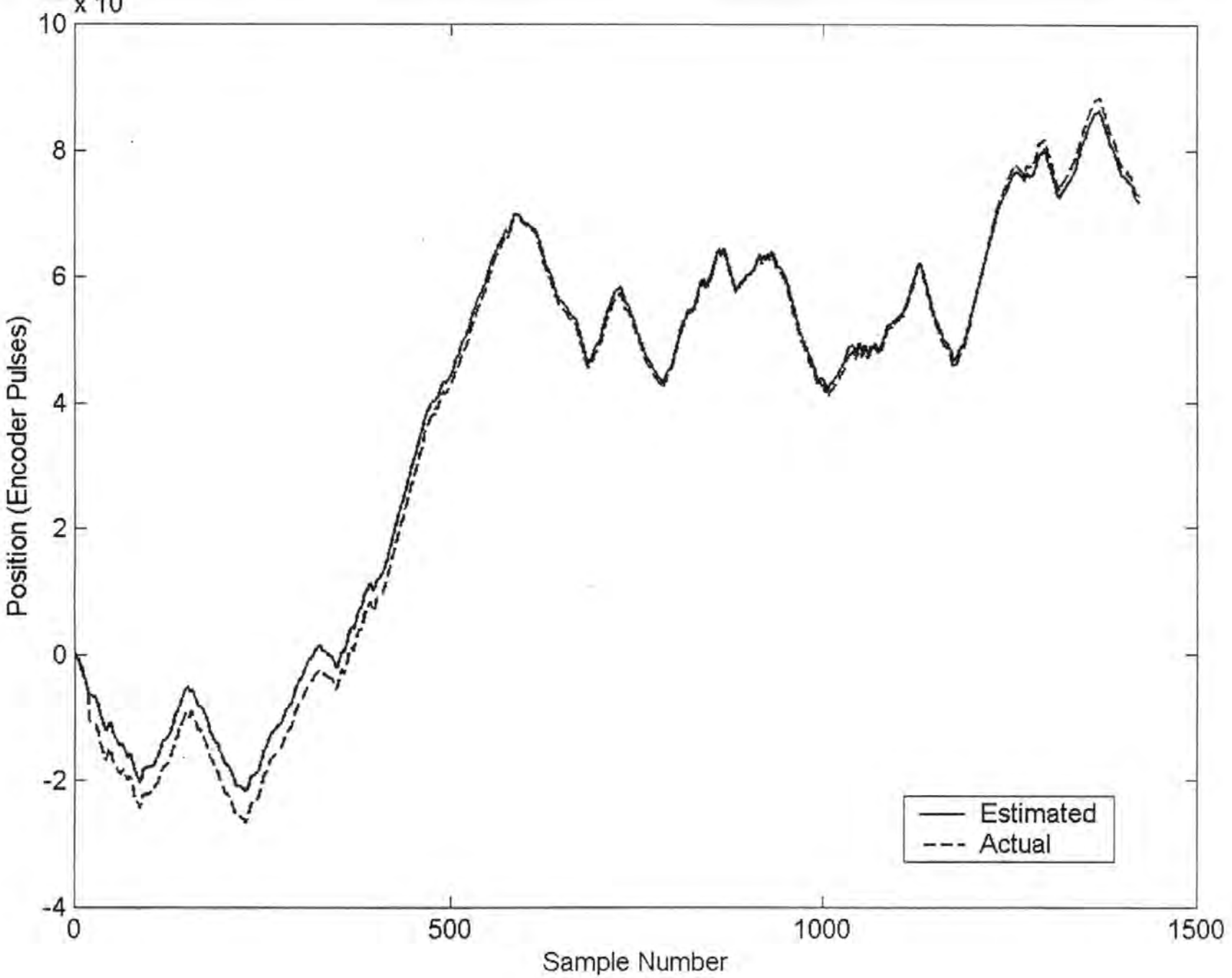
x 10
10
8
6
4
2
0
-2
-4
Position (Encoder Pulses)
0
500
1000
1500
Sample Number
Estimated
Actual

Fuzzy Model Based Sliding Mode Control of a D.C. Servomechanism

M.J.KNIGHT, R.SUTTON

Marine and Industrial Dynamic Analysis Group, Department of Mechanical and Marine Engineering, University of Plymouth, Drake Circus, Plymouth, PL4 8AA. UK.

mjknight@plymouth.ac.uk fax: (01752)232638 Tel: (01752)232631

Adaptive sliding mode control *Motor control* *Fuzzy Clustering*

Abstract: A method for combining black box nonlinear models and sliding mode control schemes is presented. It is demonstrated that the advantages of the sliding mode control technique are maintained. In addition, the effects of parametric uncertainty and unmatched disturbances are minimised through the use of a fuzzy model. Two fuzzy model based sliding mode control topologies are developed from the theory and simulation results demonstrate the usefulness of this approach.

1. Introduction

One of the earliest approaches to control of uncertain systems was sliding mode control (SMC) or variable structure control (VSC), first introduced to western researchers in the seminal works of Utkin [23] and Itkis [10]. The central feature of SMC is the sliding mode, in which the dynamic motion of the controlled system is constrained to remain within a prescribed subspace of the full state space. The sliding mode is achieved by ensuring that the prescribed manifold within the state space is made attractive to the system [10]. Once the manifold is reached, the system is forced to remain on it thereafter. When in the sliding mode, the system is equivalent to an unforced system of lower order, termed the equivalent system, which is insensitive to both parametric uncertainty and unknown disturbances that satisfy the matching condition.

There remain several drawbacks in the implementation of sliding mode controllers. The first is that is that the guarantees of invariance in general only apply to systems that satisfy the matching condition [24]. Disturbance which does not fulfil this condition, i.e. unmatched disturbance is not formally considered within the controller design. A second limitation is the fundamental requirement of a discontinous control law across the sliding manifold, in practical systems this leads to a phenomenon termed 'control chatter'. Chatter involves high frequency control switching and may lead to excitation of previously neglected high frequency system dynamics. In addition it is known to cause high heat losses in electronic systems and undue wear in mechanical systems. Smoothing techniques such as boundary layer normalisation have been employed in order to prevent chatter from manifesting within the control channel. Through this approach the transient performance of the closed loop system is maintained, however, such an approach leads to a loss of asymptotic stability and a controller that can only guarantee final tracking accuracy only to within a certain vicinity of the demand [7]. A compromise must therefore be sought between desired tracking accuracy and controller bandwidth.

Model errors due to parametric uncertainty lead to tracking error in controllers with a continuous approximation to the switching function, within the controller design, the controller feedback gains are increased to reduce these errors. This leads to high gain feedback control and despite the fact that these controllers can

in theory use infinte feedback gain to achieve asymptotic tracking, such controllers are physically impractical because of the finite bandwidths associated with real systems.

In [15] the apparent similarities between the sliding mode and fuzzy controllers were illustrated, which has subsequently motivated considerable research effort in combining the two topologies in a manner that serves to reduce the limitation of the sliding mode, whilst still maintaining the guarantees of global uniform ultimately bounded stability and invariance to matched disturbance. The most common approach to this has been to replace the continuous switching function of the boundary layer with an equivalent fuzzy switching function. However, as pointed out in [14], the fuzzy rule base commonly serves as a mimic of the original switching function and the advantages of such an approach are therefore unclear. Others have used a fuzzy rule base in making the sliding manifold adaptive, e.g. [9], so as to minimise the reaching phase, good results have been reported. Babuška [2] has demonstrated the ability of the affine Takagi-Sugeno model to model accurately a system through rule extraction from cluster data obtained within the regression space. These models may be used subsequently in order to extract locally linear state space models of the system and demonstrate model based control of both single input, single output (SISO) and multi input, multi output (MIMO) systems [16].

In this work, a system is assumed to be subject to parametric uncertainty and disturbance. This system is identified with a fuzzy rule base, the parameters of which are identified through use of the Gustaffson-Kessel subspace clustering algorithm. Local models of the system under its instantaneous conditions are then extracted and subsequently used to design the sliding mode controller gains. It is demostrated that the enhanced knowledge of the system can be applied directly in the synthesis of improved controllers.

Within the following simulation study a third order model of a servomotor is used, the differential equations of which are given according to

$$L\frac{dI_a}{dt} = -I_a R_a - K_e \omega + V_a \qquad (1)$$

$$J\frac{d\omega}{dt} = -B\omega - T_x + I_a . K_m \qquad (2)$$

Where L is the motor inductance, I_a the armature current, K_e the back E.M.F constant, ω the angular velocity of the armature, J the moment of inertia, B viscous friction, T_x the external load toque, K_m the motor torque constant and V_a the armature voltage. In addition θ is introduced as the armature angular position. These equations may be rewritten in state space form according to the following,

$$X_1 = \theta, X_2 = \frac{d\theta}{dt} = \omega, X_3 = i \text{ and let } T_X = U_1 \text{ and } V_a = U_2$$

$$\begin{bmatrix} \dot{X}_1 \\ \dot{X}_2 \\ \dot{X}_3 \end{bmatrix} = \begin{bmatrix} 0 & 1 & 0 \\ 0 & -\frac{B}{J} & \frac{K_m}{J} \\ 0 & -\frac{K_e}{L} & -\frac{R_a}{L} \end{bmatrix} \begin{bmatrix} X_1 \\ X_2 \\ X_3 \end{bmatrix} + \begin{bmatrix} 0 \\ -\frac{U_1}{J} \\ \frac{U_2}{L} \end{bmatrix} \qquad Y_1 = \begin{bmatrix} 1 & 0 & 0 \end{bmatrix} \begin{bmatrix} X_1 \\ X_2 \\ X_3 \end{bmatrix} \qquad (3)$$

The model parameters are taken as shown in Table 1:

Table 1

Next within this work, the mechanism for fuzzy identification of this model is considered. The two controllers based on existing theory are then developed. Finally, two simulation studies are presented the first is based on the integral action controller, the second on the model following controller. Finally the work concludes with a discussion of the results.

2. Fuzzy Identification

Fuzzy identification is a term used that has come to represent the use of fuzzy logic in the modelling and representation of a system. Since fuzzy models may be viewed as general function approximators, they are readily applied to the nonlinear regression problem. There are two fundamentally different approaches that may be taken in the identification of a system. Firstly the system may be identified through explicit expression of system performance, e.g. '**if** voltage is high **then** velocity is high'. Secondly, and the approach adopted within this work is to decompose the model into a static nonlinear regression. The problem of model identification is then decomposed into two separate problems, the first is

selection of the regression structure, and the second is the selection of the fuzzy model form, for example, the required number of membership functions and membership crispness.

The desired regression may be expressed in the form

$$y(t|\theta) = f(\varphi(t), \theta) \tag{4}$$

where y is the regressand, θ the *vector of regressions* which is to be parameterised in the identification process, and the vector $\varphi(t)$ is known as the *regression vector*, its parameters the *regressors*. It has been shown in (Babuska, 1998) that the regression surface within the product space may be represented as a series of local approximations.

Through use of a clustering algorithm, it is possible to derive local approximations to this regression surface. Further, through the use of the eigenvalues of the cluster covariance matrix given by

$$F_i = \frac{\sum_{k=1}^{N} (\mu_{i,k})^m (z_k - v_i)(z_k - v_i)^T}{\sum_{k=1}^{N} (\mu_{i,k})^m} \tag{5}$$

it is possible to interpret these local models and subsequently derive a fuzzy rule to represent this local approximation. In repeating this process for each data cluster, a global model of the system may be generated. Previous work has considered the accuracy of this approach in comparison to neural networks and 'white box' models, and results have demonstrated that this local approach to modelling can improve results [11].

The rule extraction process is briefly described here for completeness, however the reader is directed to [2] for more complete discussion.

It has been shown that a useful form of the fuzzy consequent is the affine linear form [22] of the Takagi-Sugeno (TS) model, in which rules are structured according to (6):

$$y_i = a_i^T x + b_i \tag{6}$$

where a_i is the so called parameter vector and b_i is an offset. Within the product space ($\mathbb{R}^{p+1 \times N}$) the affine Takagi-Sugeno consequents may be viewed geometrically as hyperplanes. The antecedent of the rule defines a fuzzy validity

region for the corresponding hyperplane. The output y of the TS model is computed using the fuzzy mean formula

$$y = \frac{\sum_{i=1}^{K} \beta_i(x) y_i}{\sum_{i=1}^{K} \beta_i(x)} \tag{7}$$

where K is the nmber of rules in the rule base. $\beta_i(x)$ represents the degree of fulfilment of the i^{th} rules antecedent, which is simply a measure of the degree of fulfilment of x in the fuzzy set A_i and is given by

$$\beta_i = \mu_{Ai}(x) \tag{8}$$

Since it may become difficult to interpret multidimensional fuzzy sets, the antecedent proposition is commonly defined in a conjunctive form, given by a series of single dimensional fuzzy sets combined with simple propositions. In this case the degrees of fulfilment are calculated as $\beta_i(x) = \mu_{Ai,1}(x_1) \wedge \ldots \wedge \mu_{Ai,P}(x_P)$, where the min operator ($\wedge$) may be replaced by alternative T-norms. In this case the model output is calculated

$$y = \left(\sum_{i=1}^{K} \gamma_i(x) a_i^T \right) x + \sum_{i=1}^{K} \gamma_i(x) b_i = \tilde{a}^T(x) x + \tilde{b}(x) \tag{9}$$

where γ_i is the normalised degree of fulfilment, given by

$$\gamma_i(x) = \frac{\beta_i(x)}{\sum_{j=1}^{K} \beta_j(x)} \tag{10}$$

and $\tilde{a}(x)$ and $\tilde{b}(x)$ are input dependent parameters, given as convex linear combinations of the constant parameters a_i and b_i through the following relationship

$$\tilde{a}(x) = \Sigma_{i=1}^{K} \gamma_i(x) a_i \tag{11}$$

$$\tilde{b}(x) = \Sigma_{i=1}^{K} \gamma_i(x) b_i \tag{12}$$

The regression structure discussed previously (4) may be expressed in this pseudo linear form according to the following

$$\hat{y}(k+1)=\sum_{j=1}^{n_y} a_{i,j}\,y(k-j+1)+\sum_{j=1}^{n_u} b_{i,j}\,u(k-j+1)+c_i \tag{13}$$

The distance measure of the clustering algorithm, given by

$$D\left(x_k,v_i^x\right)=\left(x_k-v_i\right)^T F_i^x\left(x_k-v_i\right) \tag{14}$$

may be inverted and used to provide the degree of fulfilment of each rule for given data. One possible choice of inversion is to use the same equation as for the clustering algorithm

$$\beta_i(x_k)=\frac{1}{\sum_{j=1}^{c}\left[d\left(x_k,v_i^x\right)/d\left(x_k,v_j^x\right)\right]^{2/m-1}} \tag{15}$$

which takes all rules into account and calculates the degree of fulfilment of one rule with respect to the others. Once the antecedent parameters have been calculated, the consequent parameters require derivation. There are two ways in which the fuzzy consequent parameters of the affine TS model may be calculated from the data clusters. The first is based around the geometric interpretation of the cluster, using the covariance matrix [3]. The alternative approach is a local least squares optimisation method based on the derived fuzzy partition matrix. The former method is discussed here. The eigenstructure of the cluster covariance matrix loosely describes the shape of the cluster. The shortest eigenvector describes the normal vector to the hyperplane spanned by the remaining eigenvectors. The shortest eigenvector is defined as Φ_i. Based on the dataset $Z^N=\left[x^T,y^T\right]$ and the cluster prototype, the consequent may be described implicitly by

$$\Phi_i\bullet\left(Z^N-v_i\right)=0 \tag{16}$$

The shortest eigenvector and the cluster prototype may be divided into a vector corresponding to the regressor x and a scalar corresponding to the regressand y. i.e.

$$v_i=\left[\left(v_i^x\right)^T;v_i^y\right]^T \tag{17}$$

$$\Phi_i = \left[\left(\Phi_i^x \right)^T ; \Phi_i^y \right]^T \tag{18}$$

may now be rewritten according to

$$\left[\left(\Phi_i^x \right)^T ; \Phi_i^y \right] \bullet \left(\left[x^T ; y \right]^T - \left[\left(v_i^x \right)^T ; v_i^y \right]^T \right) = 0 \tag{19}$$

After simplification

$$y = \underbrace{-\frac{1}{\Phi_i^y} \left(\Phi_i^x \right)^T}_{a_i^T} x + \underbrace{\frac{1}{\Phi_i^y} \Phi_i^T v_i}_{b_i} \tag{20}$$

which is directly equivalent to the affine Takagi-Sugeno model consequent.

This approach was employed in the identification of the model given in (3). A regression structure of [3 1] was used with 5 clusters. Of importance to the identification of the model is the selection of the input signal, in this case a stepwise random signal was used as shown in figure 1. The percentile variance accounted for (VAF) measure, which provides a measure of model tracking accuracy was calculated as 99.2% which indicates good model accuracy.

Figure 1

The model structure selected uses the applied voltage as the regressor. Performance increases in terms of tracking error and total root mean squared error may be gleaned if the model also uses the motor load current within the regression structure [11]. However, from the perspective of this work, absolute error of the model is not significant, only the ability of the model to track the regressand. Computational burden is therefore reduced by accepting a marginal degradation in the model performance and only using the single regressor.

3. Model Extraction

The work in [16] presents a method whereby the fuzzy clustered model may be represented as a local linear state space model. The following is an overview of the method adopted. The regression vector, which is represented by ε_i is given by

$$\varepsilon_i(k) = \left[\left\{ y_p(k) \right\}_0^{n_{y1}}, \ldots, \left\{ y_p(k) \right\}_0^{n_{yp}}, \left\{ u_1(k+1) \right\}_{n_{d1}}^{n_{u1}}, \ldots, \left\{ u_m(k+1) \right\}_{n_{dm}}^{n_{um}} \right] \tag{21}$$

An affine Takagi-Sugeno rule may be represented by

$$y_l(k+1)=\frac{\sum_{i=1}^{K_l}\beta_{li}(\varepsilon_l)\left(\zeta_{li}y(k)+\eta_{li}u(k)+\theta_{li}\right)}{\sum_{i=1}^{K_l}\beta_{li}} \tag{22}$$

ζ and η are vectors of polynomials in the previous sample $y(k-l)$, and θ the offset. K_l is the number of rules of the l^{th} offset. The model output is calculated as the degree of fulfilment $\mu_{il}(\varepsilon_{lh})$ for each antecedent variable and the resulting degrees of fulfilment (β_{li}) for every rule are combined with the linear consequence according to the following

$$\beta_{li}(\varepsilon_l)=\prod_{h=1}^{p}\mu_{ih}(\varepsilon_{lh}) \tag{23}$$

Once the Takagi Sugeno model has been derived, local linear state space models can be calculated according to the following,

$$y_l(k+1)=\frac{\sum_{i=1}^{K_l}\mu_{li}(x_l(k))\cdot y_{li}(k+1)}{\sum_{i=1}^{K_l}\mu_{li}(x_l(k))} \tag{24}$$

$$y_{li}(k+1)=\left(\varsigma_{li}y(k)+\eta_{li}u(k)+\theta_{li}\right) \tag{25}$$

where

$$\zeta_l^{\bullet}=\frac{\sum_{i=1}^{K_l}\mu_{li}(x_l(k))\cdot\zeta_{li}}{\sum_{i=1}^{K_l}\mu_{li}(x_l(k))} \tag{26}$$

$$\eta_l^{\bullet}=\frac{\sum_{i=1}^{K_l}\mu_{li}(x_l(k))\cdot\eta_{li}}{\sum_{i=1}^{K_l}\mu_{li}(x_l(k))} \tag{27}$$

and

$$\theta_l^{\bullet}=\frac{\sum_{i=1}^{K_l}\mu_{li}(x_l(k))\cdot\theta_{li}}{\sum_{i=1}^{K_l}\mu_{li}(x_l(k))} \tag{28}$$

In the case here, previous inputs are not considered and the A, B and C matrices of the model are thus simplified, the matrices are given

$$A=\begin{bmatrix} \zeta^*_{1,1} & \zeta^*_{1,2} & \cdots & \zeta^*_{1,\alpha_1} \\ 1 & 0 & \cdots & 0 \\ \zeta^*_{2,1} & \zeta^*_{2,2} & \cdots & \zeta^*_{2,\alpha_1} \\ 0 & \vdots & \ddots & \vdots \\ \zeta^*_{n_0,1} & \zeta^*_{n_0,2} & \cdots & \zeta^*_{n_0,\alpha_1} \end{bmatrix} \tag{29}$$

$$B=\begin{bmatrix} \eta^*_{1,1} & \eta^*_{1,2} & \cdots & \eta^*_{1,n_i} \\ 0 & \cdots & \cdots & 0 \\ \eta^*_{2,1} & \eta^*_{2,2} & \cdots & \eta^*_{2,n_i} \\ \vdots & \vdots & \ddots & \vdots \\ \eta^*_{n_0,1} & \eta^*_{n_0,2} & \cdots & \eta^*_{n_0,n_i} \end{bmatrix} \tag{30}$$

$$C=\begin{bmatrix} 1 & 0 & \cdots & 0 \\ \vdots & & \ddots & \vdots \\ 0 & \cdots & \cdots & 1 \end{bmatrix} \tag{31}$$

4. Integral Action Sliding Mode

As described in the introduction, the sliding mode is traditionally associated with a switching action which is discontinuous about a prescribed surface within the state space. Practical implementation of a sliding mode controller frequently leads to a phenomenon known as chattering. This is often due to the excitation of previously unmodelled system dynamics. Many solutions have been proposed to prevent chatter. Perhaps the most famous of these is the *boundary layer approach* first proposed by [19]. The approach involves replacing the discontinuous switching function with an equivalent continuous function. The implication of changing the switching function is that the system state is no longer constrained to remain on the prescribed sliding surface, but merely to remain within a certain vicinity of it. It follows directly that the equivalent system dynamics will be to some extent affected by any matched disturbance to which the system is subjected [20].

It was recognised by Ryan and Corless [17] that this additional degree of freedom afforded by the boundary layer at the manifold could be used to improve the controller robustness to so called unmatched disturbance, i.e. those disturbances which do not act within the system control channels. The controller that was subsequently developed was theoretically elegant and intuitively appealing,

however it was conservative. By considering a subset of the disturbances originally used in [17], the controller was made less conservative in [21]. The fundamental extension of these controllers over the traditional controllers is the introduction of an additional integral action state. This controller state seeks to reduce the steady state error asymptotically to zero. Within this work the design approach is adopted in order to ensure zero steady state controller error. However, it was also recognised in [12], that if the system uncertainty can be reduced, then controller performance may be correspondingly improved. The principles associated with the design of a sliding mode controller with integral action are considered next. As alluded to in the introduction, the ideal sliding motion is control independent and defined only by the choice of sliding surface provided that certain assumptions about the system disturbance hold [6]. In terms of controller design it is convenient to convert the system equations into a suitable canonical form. In this form the system is decomposed into two connected subsystems, one acting in within the range space of matrix B and the other within the null space of the manifold S. In terms of design, the problem then becomes one of state feedback given desired system eigenvalue locations. Since by assumption the matrix B is of full rank, there exists an orthogonal matrix $T_r \in \mathbb{R}^{n\times n}$ such that

$$T_r B = \begin{bmatrix} 0 \\ B_2 \end{bmatrix} \tag{32}$$

where $B_2 \in \mathbb{R}^{m\times m}$ and is non-singular. Let $z = Tx$ and partition the new co-ordinates so that

$$z = \begin{bmatrix} z_1 \\ z_2 \end{bmatrix} \tag{33}$$

where $z_1 \in \mathbb{R}^{n-m}$ and $z_2 \in \mathbb{R}^m$. The nominal linear system can then be written as

$$\dot{z}_1(t) = A_{11}z_1(t) + A_{12}z_2(t) \tag{34}$$

$$\dot{z}_2(t) = A_{21}z_1(t) + A_{22}z_2(t) + B_2u(t) \tag{35}$$

commonly known as the regular form. Equation (34) is referred to as describing the null-space dynamics and equation (35) as describing the range-space dynamics. From the perspective of the extracted local models, it is convenient to

first convert the matrices to the controllability canonical form, thus the system is guaranteed to be in the regular form for subsequent design. Suppose the matrix defining the switching function (in the new co-ordinate system) is compatibly partitioned with z as

$$ST_r^T = [S_1 \quad S_2] \tag{36}$$

where $S_1 \in \mathbb{R}^{m\times(n\times m)}$ and $S_2 \in \mathbb{R}^{m\times m}$. Since $SB = S_2B_2$ it follows that a necessary and sufficient condition for the matrix SB to be non-singular is that the determinant of S_2 is non zero. It is reasonable to assume that this condition will be met by design. During an ideal sliding motion

$$S_1 z_1(t) + S_2 z_2(t) = 0 \qquad \text{for all } t > t_s \tag{37}$$

and therefore formally expressing $z_2(t)$ in terms of $z_1(t)$ yields

$$z_2(t) = -Mz_1(t) \tag{38}$$

where $M = S_2^{-1}S_1$. Substituting into (34) gives

$$\dot{z}_1(t) = (A_{11} - A_{12}M)z_1(t) \tag{39}$$

$z_2(t)$ is considered to play the role of the control action. The switching surface design problem can therefore be considered to be one of choosing a state feedback matrix M to stabilise the reduced order system (A_{11}, A_{12}).

At this point the unit vector approach is introduced. Consider an uncertain system of the form

$$\dot{x}(t) = Ax(t) + Bu(t) + f(t,x,u) \tag{40}$$

where the function $f : \mathbb{R}\times\mathbb{R}^n\times\mathbb{R}^m \to \mathbb{R}^m$ which represents the uncertainties or non-linearities satisfying the so-called matching condition, i.e.

$$f(t,x,u) = B\xi(t,x,u) \tag{41}$$

where ξ is unknown but satisfies the following inequality

$$\|\xi(t,x,u)\| \le k_1\|u\| + \alpha(t,x) \tag{42}$$

where $1 > k_1 \geq 0$ is a known constant and $\alpha(\bullet)$ is a known function. The proposed control law comprises two components; a linear component to stabilise the nominal linear system; and a discontinuous component. Specifically

$$u(t) = u_l(t) + u_n(t) \tag{43}$$

where the linear component is given by

$$u_l(t) = -\Lambda^{-1}(SA - \Phi S)x(t) \tag{44}$$

where Φ is any stable design matrix and Λ = SB. The non-linear component is defined as

$$u_n(t) = -\rho(t,x)\Lambda^{-1}\frac{P_2 s(t)}{\|P_2 s(t)\| + \varepsilon} \quad \text{for all } S \neq 0 \tag{45}$$

where P_2 is a symmetric positive definite matrix that satisfies the Lyapunov equation

$$P_2\Phi + \Phi^T P_2 + I = 0 \tag{46}$$

and the scalar function $\rho(t,x)$, which depends only on the magnitude of the uncertainty, is any function satisfying

$$\rho(t,x) \geq \frac{(k_1\|u_l\| + \alpha(t,x) + \gamma)}{(1 - k_1\kappa(\Lambda))} \tag{47}$$

where γ>0 is a design parameter. The radius of the boundary layer (ε) may be shown to be dependent on the actuator time constant and inversely proportional to the available control resources. In this equation it is assumed that the scaling parameter has been chosen so that $k_1\kappa(\Lambda) < 1$. Where $\kappa(\bullet)$ represents the spectral condition number. It can be established that any function satisfying equation (47) also satisfies

$$\rho(t,x) \geq \|\xi(t,x,u)\| + \gamma \tag{48}$$

and therefore $\rho(t,x)$ is greater in magnitude than the matched uncertainty occurring in this equation. It can be verified that $V(S) = S^T P_2 S$ guarantees quadratic stability for the switching states and in particular

$$\dot{V} \le -s^T s - 2\gamma \|P_2 s\| \tag{49}$$

This control law guarantees that the switching surface is reached in finite time despite the disturbance or uncertainty and once the sliding motion is attained it is completely independent of the uncertainty.

Now consider the introduction of additional states $x_r \in \mathbb{R}^p$ satisfying

$$\dot{x}_r = r(t) - y(t) \tag{50}$$

where the differentiable signal $r(t)$ satisfies

$$\dot{r}(t) = \Gamma\left(r(t) - R\right) \tag{51}$$

with Γ a stable design matrix and R a constant demand vector. Augment the states with the integral action states and define

$$\tilde{x} = \begin{bmatrix} x_r \\ x \end{bmatrix} \tag{52}$$

The associated system and input distribution matrices for the augmented system are

$$\tilde{A} = \begin{bmatrix} 0 & -C \\ 0 & A \end{bmatrix} \text{ and } \tilde{B} = \begin{bmatrix} 0 \\ B \end{bmatrix} \tag{53}$$

assuming the pair (A, B) is in regular form, the pair $\left(\tilde{A}, \tilde{B}\right)$ is also in regular form. The proposed controller seeks to induce a sliding motion on the surface

$$S = \left\{\tilde{x} \in \mathbb{R}^{n+p} : S\tilde{x} = S_r r\right\} \tag{54}$$

where S and S_r are design parameters, which govern the reduced order motion. The hyperplane system matrix and system matrix are partitioned as

$$S = \begin{bmatrix} \overleftrightarrow{n} & \overleftrightarrow{m} \\ S_1 & S_2 \end{bmatrix} \tag{55}$$

$$\tilde{A} = \begin{bmatrix} \overleftrightarrow{n} & \overleftrightarrow{m} \\ \tilde{A}_{11} & \tilde{A}_{12} \\ \tilde{A}_{21} & \tilde{A}_{22} \end{bmatrix} \begin{matrix} \updownarrow n \\ \updownarrow m \end{matrix} \tag{56}$$

and assume $\Lambda = S\tilde{B}$ is non-singular. If a controller exists which induces an ideal sliding motion on S and the augmented states are suitably partitioned, then the ideal sliding motion is given by

$$\dot{x}_1(t) = \left(\tilde{A}_{11} - \tilde{A}_{12}M\right)x_1(t) + \left(\tilde{A}_{12}S_2^{-1}S_r + B_r\right)r(t) \tag{57}$$

where $M = S_2^{-1}S_1$ and $B_r = \left[I_p \quad 0_{n\times p}\right]^T$. In order for the hyperplane design method to be valid, it is necessary for the matrix pair $\left(\tilde{A}_{11}, \tilde{A}_{12}\right)$ to be completely controllable. The overall control law is then given by

$$u = u_l(\tilde{x}, r) + u_n(\tilde{x}, r) \tag{58}$$

where the discontinuous vector u_n is given by

$$u_n(s, r) = \begin{cases} -\rho_c(u_L, y)\Lambda^{-1} & \text{if } S\tilde{x} \neq S_r r \\ 0 & \text{otherwise} \end{cases} \tag{59}$$

It follows that, in terms of the original co-ordinates the control vector u_l is given by

$$u_l(\tilde{x}, r) = L\tilde{x} + L_r r + L_{\dot{r}}\dot{r} \tag{60}$$

with gains defined as

$$L = -\Lambda^{-1}\left(S\tilde{A} - \Phi S\right) \tag{61}$$

$$L_r = -\Lambda^{-1}\left(\Phi S_r + S_1 B_r\right) \tag{62}$$

$$L_{\dot{r}} = \Lambda^{-1}S_r \tag{63}$$

The parameter S_r can take any value and does not affect the stability of the closed loop system.

5. Model Following Sliding Mode Control

Linear model following control is an efficient control method that avoids the difficulty of specifying a performance index which is usually encountered in the application of optimal control to multivariable control systems. The model that specifies the design objective is part of the system. However, Linear Model

Following Control systems are inadequate when the plant is subject to large parameter variations or disturbances. This has led to the development of so called adaptive model following control schemes. There are two approaches to the design of adaptive model following systems using stability conditions. The first is based upon Lyapunov functions (e.g. Shackcloth and Butchart, [18]), while the second is based upon the hyperstability concept (e.g. Landau, [13]). Both approaches guarantee that the error tends to zero as $t \to \infty$ but neither offer any direct quantitative design of the error transient. The controller to be presented here presents a novel approach to the integration of the fuzzy model to the model following control theory, such that the advantages implicit in using a more accurate model are attained.

In model following systems, the plant is controlled in such a way that its dynamic behaviour approximates that of a specified plant model. The model plant is part of the system and it specifies the design objectives. The adaptive controller should force the error between the model and the plant states to zero as time tends to infinity, i.e. $\lim_{t\to\infty} \varepsilon(t) = 0$. The plant and the model are described by

$$\dot{x}_p(t) = A_p x_p(t) + B_p u_p(t) \tag{64}$$

$$\dot{x}_m(t) = A_m x_m(t) + B_m u_m(t) \tag{65}$$

with the error vector given as

$$\varepsilon(t) = x_m(t) - x_p(t) \tag{66}$$

It is assumed that the pairs (A_p, B_p) and (A_m, B_m) may be stabilised and that A_m is a stable matrix. Differentiation of (66) and insertion of (64) and (65) provides the following

$$\dot{\varepsilon}(t) = A_m x_m(t) + B_m u_m(t) - A_p x_p(t) - B_p u_p(t) \tag{67}$$

Further, subtraction of the term $A_p x_m$ yields

$$\dot{\varepsilon}(t) = A_p \varepsilon(t) + (A_m - A_p) x_p(t) + B_m u_m(t) - B_p u_p(t) \tag{68}$$

It follows that perfect model following will result if

$$(A_m - A_p) x_p(t) + B_m u_m(t) - B_p u_p(t) = 0 \tag{69}$$

rearranging (69) provides the following

$$u_p(t) = B_p^{\dagger}\left(\left(A_m - A_p\right)x_p(t) + B_m u_m(t)\right) \tag{70}$$

insertion of (70) into (69) yields

$$\left(A_m - A_p\right)x_p(t) + B_m u_m(t) - B_p B_p^{\dagger}\left(\left(A_m - A_p\right)x_p(t) + B_m u_m(t)\right) = 0 \tag{71}$$

Clearly, in order to satisfy (69) for all x_p and u_m the following equalities must hold

$$\left(I - B_p B_p^{\dagger}\right)\left(A_m - A_p\right) = 0 \tag{72}$$

$$\left(I - B_p B_p^{\dagger}\right)B_m = 0 \tag{73}$$

The equations (72) and (73) are the conditions for perfect model following as first described by Erzeberger [8], Equation (70) is the equation for implementing the control. This control law leads to a controller response which is determined by the eigenvalues of the model. Since the eigenvalue spectrum of the model may not be determined by the designer the control response might not yield acceptable results. Later, Chen [5] proposed a small modification to the controller, by subtracting the term $A_p x_m$ from (67), this yields

$$\dot{\varepsilon}(t) = A_m \varepsilon(t) + \left(A_m - A_p\right)x_m(t) + B_m u_m(t) - B_p u_p(t) \tag{74}$$

From equation (74), it is evident that choosing a control action of the form

$$u_p(t) = u_1(t) + u_2(t) \tag{75}$$

with

$$u_1(t) = K\varepsilon(t) \tag{76}$$

$$u_2(t) = B_p^{\dagger}\left(A_m - A_p\right)x_m(t) + B_p^{\dagger}B_m u_m(t) \tag{77}$$

will lead to perfect model following if it is possible. Substitution of the control law (75)-(77) into (68) leads to

$$\begin{aligned}\dot{\varepsilon}(t) = A_m\varepsilon(t) + \left(A_m - A_p\right)x_p(t) + B_m u_m(t) - B_p K\varepsilon(t) - \\ B_p B_p^{\dagger}\left(A_m - A_p\right)x_m(t) - B_p B_p^{\dagger}B_m u_m(t)\end{aligned} \tag{78}$$

under the assumption that conditions (72) and (73) hold, then (78) simplifies to

$$\dot{\varepsilon}(t)=\left(A_m-B_pK\right)\varepsilon(t) \tag{79}$$

In contrast to the controller proposed by Erzeberger [8], the controller proposed by Chen [5] can have an arbitrary set of eigenvalues determined by the gain matrix K, since the tuple $\left(A_m,B_p\right)$ is controllable. Since (79) is identical to the optimal state regulator problem [1], then the gain matrix K may be chosen to optimise a quadratic performance index in ε. Hence, the error settling rates may be controlled. Additionally, if only partial state feedback is possible then perfect model following is still possible [5].

Model following control systems were extended to incorporate a discontinuous control component in [25]. Following this original design, define an error dependent switching function

$$S(\varepsilon)=S\varepsilon(t) \tag{80}$$

which gives rise to a hyperplane in the error space

$$S_\varepsilon=\left\{\varepsilon\in\mathbb{R}^n : S\varepsilon(t)=0\right\} \tag{81}$$

As seen in the previous chapter, during sliding the error state will satisfy the equation

$$S\varepsilon(t)=0 \tag{82}$$

Differentiation and substitution of (74) gives

$$S\dot{\varepsilon}(t)=S\left(A_m\varepsilon(t)+\left(A_m-A_p\right)x_m(t)+B_mu_m(t)-B_pu_p(t)\right)=0 \tag{83}$$

If by design the matrix product SB is non-singular, then the equivalent control may be determined as

$$u_{eq}(t)=\left(SB_p\right)^{-1}S\left(A_m\varepsilon(t)+\left(A_m-A_p\right)x_p(t)+B_mu_m(t)\right) \tag{84}$$

substitution of the equivalent control into the model following control system of (74) gives

$$\dot{\varepsilon}(t)=\left(I-B_p\left(SB_p\right)^{-1}S\right)\left(A_m\varepsilon(t)+\left(A_m-A_p\right)x_p(t)+B_mu_m(t)\right) \tag{85}$$

It is assumed that the plant and model dynamic equations satisfy the perfect model matching conditions. Comparison of these equations with the invariance conditions discussed by Drazenovic [6], it can be seen that the two coincide. Therefore if x_p and u_m are considered disturbances to the error dynamics then the perfect model matching conditions guarantee that the behaviour of the sliding mode controller is insensitive to these disturbances. If the conditions of (72) and (73) hold, then equation (85) reduces to

$$\dot{\varepsilon}(t)=\left(I-B_p\left(SB_p\right)^{-1}S\right)A_m\varepsilon(t) \tag{86}$$

A unit vector type control is now introduced as in the work in [4], a discontinuous unit vector control is introduced according to

$$u(t)=u_l(t)+u_n(t) \tag{87}$$

with

$$u_l(t)=-(SB)^{-1}(SA_m-\Phi S)\varepsilon(t) \tag{88}$$

$$u_n=-\rho(t,\varepsilon)(SB)^{-1}\frac{P_2S(t)}{\left\|P_2S(t)\right\|} \tag{89}$$

It was pointed out in [5] and later in [26] that the conditions of (72) and (73) may be met if

$$\operatorname{rank}\left(B_p,B_m\right)=\operatorname{rank}\left(B_p\right) \tag{90}$$

$$\operatorname{rank}\left(B_p,A_m-A_p\right)=\operatorname{rank}\left(B_p\right) \tag{91}$$

It follows that there exist compatibly dimensioned matrices such that

$$B_pF=A_m-A_p \tag{92}$$

$$B_pG=B_m \tag{93}$$

This result may be used as an alternative to (77), with

$$u_2(t)=Fx_p(t)+Gu_m(t) \tag{94}$$

to also achieve perfect model following. The complete model following control scheme is then given according to

$$u(t)=u_l(t)+u_n(t)+u_2(t) \tag{95}$$

6. Simulation studies

Within this work, the derived controllers employ adaptive controller gains. For the sake of clarity, the controller signal flow diagrams illustrate the adaptive gains by means of a shadowed box with an arrow drawn across it. The box entitled "*update controller parameters*" is the part of the algorithm which is responsible for making these changes.

6.1. Integral Action Control

A benchmark sliding mode controller with integral action (SMCI) of the form previously discussed was developed to control the motor model of equation (3), using the nominal parameters of Table 1. All simulations were carried out using the actual parameters shown in Table 1.

The principle of the proposed controller is illustrated in Figure 2. The controller uses the design approach outlined in the previous section, thus, stabilising conditions of the controller remain intact. Importantly, the extracted model is used to provide enhanced information to the controller, so that the controller may be made to adapt to local operating conditions of the system. The controller is therefore referred to as a Fuzzy Adaptive Sliding Mode Controller (FASMC).

Figure 2

both sets of controller eigenvalues were selected to provide unity damping ratio at 22rad/s. The controllers were driven over a simulation sample period of 70 seconds. Results are illustrated in Figure 3.

Figure 3

It can be seen that in terms of transient response, there is little to differentiate between the two controllers. However, consideration of the corresponding control effort (Figure 4) shows that that the high gain requirement of the SMCI has indeed

been relaxed by the FASMC. Additionally, the ε-vicinity of the FASMC was manually adjusted to be 6 times smaller than the corresponding SMCI before chatter occurred.

Figure 4

A second test introduced unmatched disturbance to the system and the fuzzy model retrained to incorporate the uncertainty, the disturbance is analogus to a torque being placed on the motor and forcing rotation in the contrary direction to the demand, which changes simultaneously with the step increase in load. Figure 5 illustrates the effect of the disturbance on the SMCI, it can be seen that the disturbance significantly effects transient performance. Because of the integral action of the SMCI, the system is able to achive asymptotic tracking as discussed within the literature. The FASMC, on the other hand, recovers the system to the steady state taking only an additional 0.4 seconds when compared to the system without disturbance (Figure 6). The obvious error in the initial controlled state trajectory is due to the lack of large controller gains, in the event that the system were subjected to such a stringent test it would be necessary to increase the nonlinear control gain to circumvent this problem.

Figure 5

Figure 6

6.2 Model Following Control

As in the previous case, a benchmark controller based on the traditional theory is developed (Model Following Sliding Mode Controller (MFSMC)). Within this work, three models based on the structure of (3) are assumed. First the model based on the nominal parameters of the motor; this model is assumed to be known, since the parameters will be specified by the manufacturer. Second, the model based on the actual plant; these parameters will be assumed to be unknown, but their variation from the nominal plant parameters are bounded. Finally, the third model is specified based on the desired performance of the system, it is this

model which the plant will be forced to follow. The three sets of parameters are provided in Table 1 as nominal, actual and demand respectively.

In the ideal case, the plant and nominal models will be identical. In this case, the invariance condition leads to a rejection of uncertainty between model and plant and perfect model following will result. Figure 7 illustrates the result of applying the model following sliding mode controller to a system whose parameters are perfectly known. In the simulation study, a demand in speed is applied which for the first four seconds is one, for the remainder of the time the demand is minus one. For the purposes of simplicity, the demand system is treated in the open loop, therefore the model armature speed which is not equal to the demand is a result of the motor steady state gain. Nearly perfect model following is achieved using the range space eigenvalue assignment $\{-100 \quad -10+j \quad -10-j\}$, with the null space pole set to {-2.5}.

Figure 7

In the case of model following the invariance conditions are used to reject errors between the demand model and the nominal model. In the practical case, there will also be disparity between the nominal and plant models and an error in the model following will result (Figure 8). The magnitude of this error will be entirely dependent upon how much in error of one another the models are.

Figure 8

It follows that provided a fuzzy model can be found which reduces the uncertainty of the plant, errors due to model disparity will be reduced when model following. The structure of the fuzzy model based model following sliding mode controller (FMMF) is shown in Figure 8.

Figure 9

Figure 10

Uncertainty in the plant is introduced and the two controllers are resimulated. The results are illustrated in Figure 9 (MFSMC) and Figure 10 (FMMF). It is immediately obvious that the two controllers now lack the control chatter of the ideal case. This is because the controllers are not achieving the sliding mode, merely attempting to converge to it. As anticipated, perfect model following is not achieved. The control effort of the FMMF controller is significantly reduced in amplitude over the MFSMC, and approximates the amplitudes associated with the ideal case. It follows that the task of the fuzzy model and the model following controller is identical in that the root mean square (RMS) error between the model and the plant should be minimised, whist the percentile variance accounted for should be maximised. In the ideal case the RMS error will be zero and the VAF will be 100%. Constraints in simulation do not permit the ideal case since the switching frequency of the discontinuous control component is theoretically infinite. However, an approximation to this ideal case, at a sample frequency of 1kHz in simulation provides the results of model following shown in Table 2.

Table 2

7. Conclusions

Two new controllers based on the synergy of sliding mode design approaches and nonlinear black box modelling have been presented. Performance of the controllers has been compared with that of benchmark sliding mode controllers and the controllers response have been found to be favourable. The controllers have demonstrated obvious advantages in using fuzzy logic in conjunction with sliding mode. In the case of the first controller it is seen that since the system uncertainties can be significantly reduced through use of fuzzy identification and linearisation techniques, the feedback control gains may be reduced, which in turn leads to a control effort of reduced magnitude. This leads directly to a reduction in the radius of the boundary layer, providing improvements in the final achievable tracking accuracy of the system. Since the fuzzy model does not discriminate between matched and unmatched disturbance, but simply incorporates them into the model, the FASMC also enjoys improvements in the transient control performance when the system is subject to unmached disturbance. The model following controller is based on the premise that there

will be disparity between the nominal and actual systems. This will be true in all practical cases. Since the sliding mode offers the invariance property to the rejection of errors between the nominal system and demand system, any errors which occur between nominal system and plant will not be formally considered within the controller. It is therefore necessary to introduce the fuzzy model in place of the nominal model in order to minimise uncertainty within the plant. This approach is shown to significantly reduce the errors between the plant and demand transient performance. The controller presented here is shown to significantly outperform the traditional model following sliding mode controller when plant uncertainty exists.

8. References

[1] **Anderson B.D.O. and Moore J.B.**, (1971), 'Linear Optimal Control' Prentice Hall

[2] **Babuska R.** (1998). 'Fuzzy Modelling for Control', Kluwer Academic Publishers.

[3] **Babuska R. and Verbruggen H.B.** (1997). 'Constructing Fuzzy Models by Product Space Clustering'. In: Hellendoorn H. and Driankov D. (eds) *Fuzzy Model Identification*. Springer-Verlag, 53-90

[4] **Corless M., Goodall D.P., Leitmann G. and Ryan E.P.** (1985), 'Model Following Controls For a Class of Uncertain Dynamical System', Proc 7th IFAC/IPOS symp. on Identification and System Parameter Estimation. 1895-1899.

[5] **Chen Y.T.**, (1973). 'Perfect Model Following with a Real Model', Proc. Joint Automatic Control Conference, 283-293.

[6] **Drazenovic B.**, (1969). 'The Invariance Conditions in Variable Structure Systems', Automatica. 5. 287-295.

[7] **Edwards C and Spurgeon S.K.** (1998) 'Sliding Mode Control: Theory and Applications'. Taylor Francis.

[8] **Erzeberger H.**, (1968), 'Analysis and Design of Model Following Control Systems by State Space Techniques', Proc. Joint Automatic Control Conference, 572-581.

[9] **Ha Q.P., Rye D.C. and Durrant-Whyte H.F.** (1999). 'Robust Sliding Mode Control with Application', International Journal of Control. 72(12), 1087-1096.

[10] **Itkis U.** (1976). 'Control Systems of Variable Structure', John Wiley.

[11] **Knight M.J., Sutton R., Burns R.S, and Jenkins D.F.** (2001). 'A Comparison of Nonlinear Identification Techniques', Proc IEEE conf. on Methods and Models in Automation and Robotics, Meidzyzdroje, Poland. 953-958.

[12] **Knight M.J., Sutton R., Burns R.S.**, (2002). 'Fuzzy Model Based Integral Action Sliding Mode Control', Soft Computing, In Press.

[13] **Landau I.**, (1974), 'Survey of Model Reference Adaptive Techniques', Automatica. **10**. 353-379

[14] **O'Dell B.** (1997). 'Fuzzy Sliding Mode Control: A Critical Review', Oklahoma state university, Technical Report ACL-97-001.

[15] **Palm R.** (1994). 'Robust Control by Fuzzy Sliding Mode', Automatica, **30**(9), 1429-1438.

[16] **Roubos J.A., Mollov S., Babuska R and Verbruggen H.B.** (1999). 'Fuzzy Model Based Predictive Control using Takagi-Sugeno Models', International journal of Approximate reasoning, **22**, 199-226

[17] **Ryan E.P. and Corless M.** (1984). 'Ultimate Boundedness and Asymptotic Stability of a Class of Uncertain Dynamical System via Continuous and Discontinuous Feedback Control', IMA Journal of Mathematics and Control Information, **1**, 223-242

[18] **Shackcloth B. and Butchart R.L.**, (1966). 'Synthesis of Model Reference Adaptive Control Systems by Lyapunov's Second Method', Proc 2nd IFAC Symp. on the Theory of Self Adaptive Control Systems. 145-152.

[19] **Slotine J.-J. and Sastry S.S.** (1983). 'Tracking Control of Nonlinear Systems Using Sliding Surfaces, with an application to Robot Manipulators', International Journal of Control, **38**, 465-492.

[20] **Spurgeon S.K.** (1991). 'Choice of Discontinuous Control Component for Robust Sliding Mode Performance', International Journal of Control, **53**(1). 163-179.

[21] **Spurgeon S.K. and Davies R.** (1993). 'A Nonlinear Control Strategy for Robust Sliding Mode Performance in the presence of Unmatched Uncertainty', International Journal of Control, **57**(5), 1107-1123.

[22] **Takagi T. and Sugeno M.** (1985) 'Fuzzy Identification and its Applications to Modelling and Control', IEEE Trans. on Systems, Man and Cybernetics, **15**(1), 116-132.

[23] **Utkin V.I.** (1977) 'Variable Structure Systems with Sliding Modes', IEEE Transactions on Automatic Control, **AC-22**(2), 212-222.

[24] **Yao, B.** (1992) 'Adaptive Robust Control of Nonlinear Systems with Application to Control of Mechanical Systems', PhD Thesis, University of California, 1992

[25] **Young K.-K.D.**, (1977), 'Asymptotic Stability of Model Reference Control Systems with Variable Structure Control', IEEE Trans Automatic Control. **AC-22**(2). 279-281.

[26] **Zinober A.S.I**, (1981), 'Controller Design Using the Theory of Variable Structure Systems', In Harris C.J and Billings S.A., *Self-Tuning and Adaptive Control: Theory and Applications*, Peter Peregrinus.

Figure 1: Model output vs System output

Figure 2: Principle of FASMC

Figure 3: System outputs over 70 seconds

Figure 4: System control efforts

Figure 5: SMCI response to unmatched disturbance

Figure 6: FASMC response to unmatched disturbance

Figure 7: Near Perfect Model Following

Figure 8: Principle of FMMF

Figure 9: Model Following with an Imperfectly Known Plant

Figure 10: Fuzzy Model Following with an Imperfectly Known Plant

Parameter	Value (Nominal)	Value (Actual)	Value (Desired)
R_a (Ω)	1.2	1.5	0.66
L (H)	0.05	0.09	0.066
Ke (Vs/rad)	0.6	0.6	0.1
Km (Nm A^{-1})	0.6	0.6	0.84
J (Nms^2)	0.135	0.15	0.2
B (Nm/rad/s)	0	0.02	0.02

Table 1: Motor parameters

Measure	Ideal Case	Unknown Plant (MFSMC)	Unknown Plant (FMMF)
VAF	99.98%	84.83%	98.84%
RMS	0.039	1.63	0.29

Table 2: Performance Measures for the Model Following Controllers

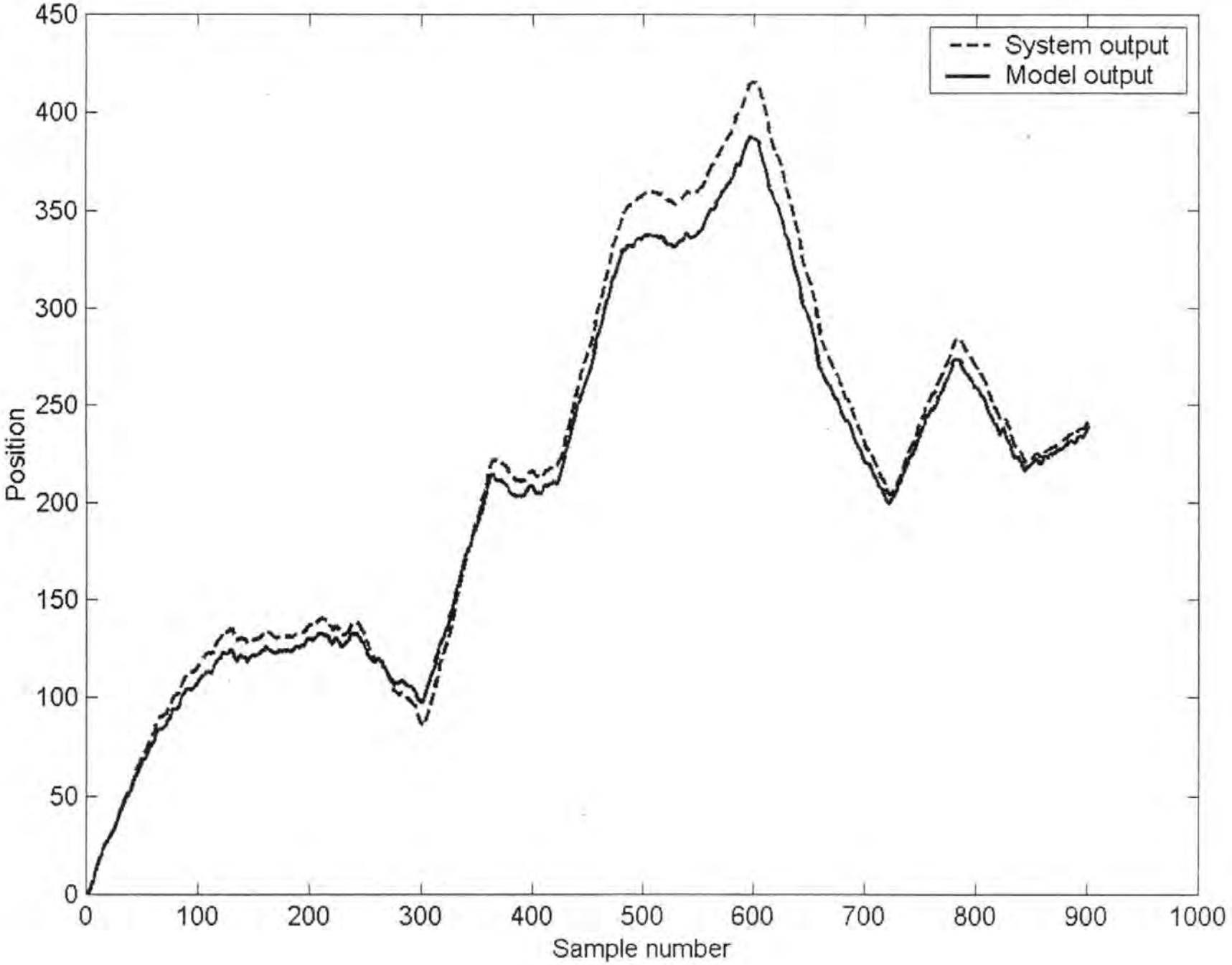
System output
Model output
Position
Sample number
0
50
100
150
200
250
300
350
400
450
0
100
200
300
400
500
600
700
800
900
1000

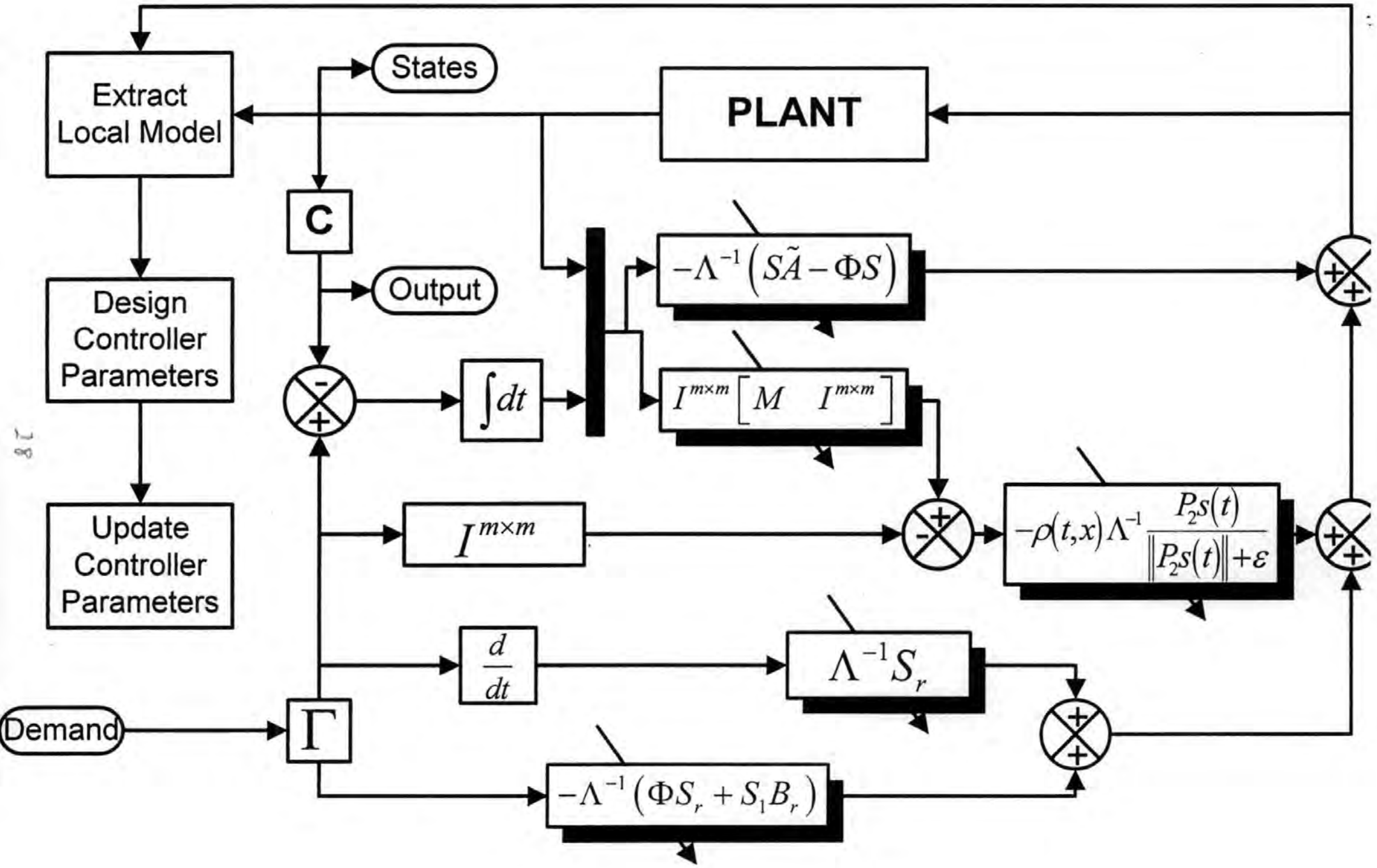
Extract Local Model
States
PLANT
C
Output
Design Controller Parameters
$\int dt$
$-\Lambda^{-1}\left(S\tilde{A}-\Phi S\right)$
$I^{m\times m}\begin{bmatrix} M & I^{m\times m}\end{bmatrix}$
Update Controller Parameters
$I^{m\times m}$
$-\rho(t,x)\Lambda^{-1}\frac{P_2 s(t)}{\|P_2 s(t)\|+\varepsilon}$
$\frac{d}{dt}$
$\Lambda^{-1}S_r$
Demand
Γ
$-\Lambda^{-1}\left(\Phi S_r + S_1 B_r\right)$

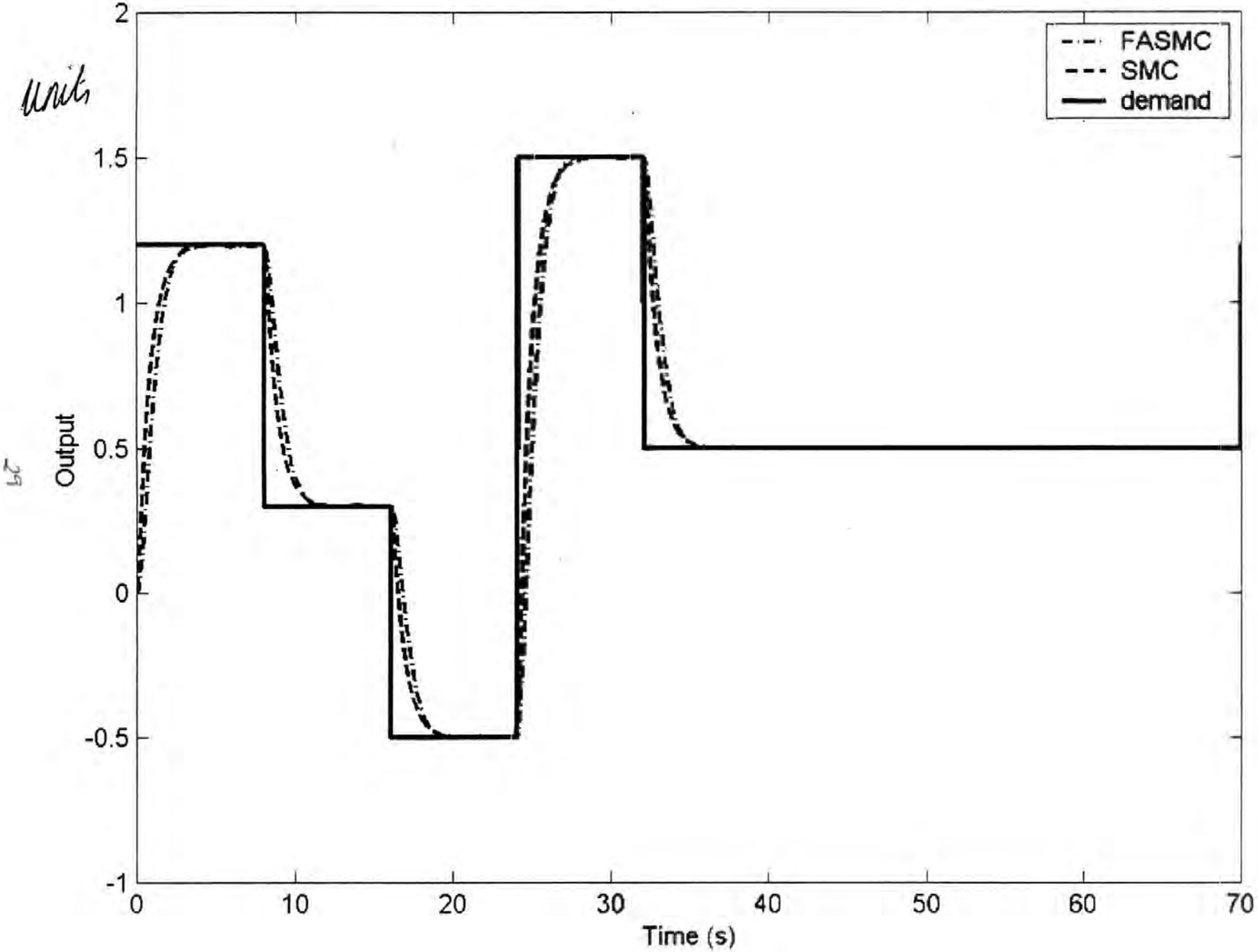
FASMC
SMC
demand
Output
Time (s)
2
1.5
1
0.5
0
-0.5
-1
0
10
20
30
40
50
60
70

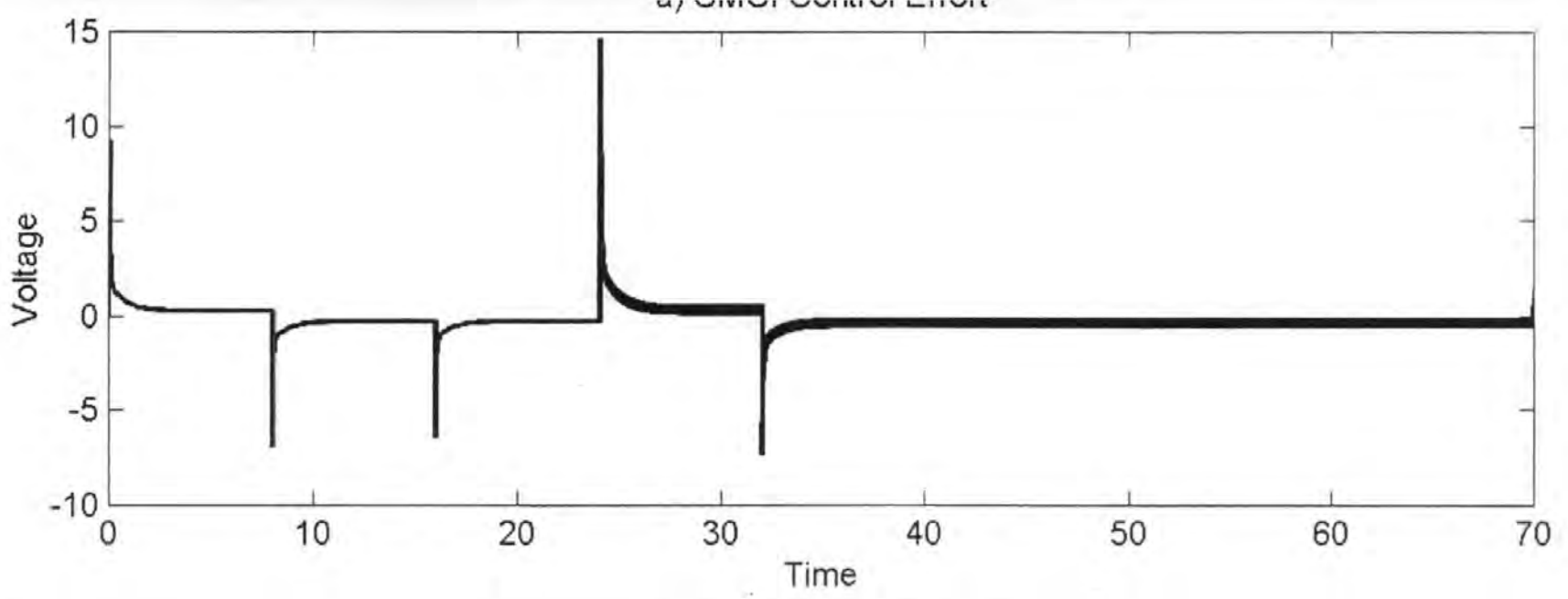

b) FASMC Control effort

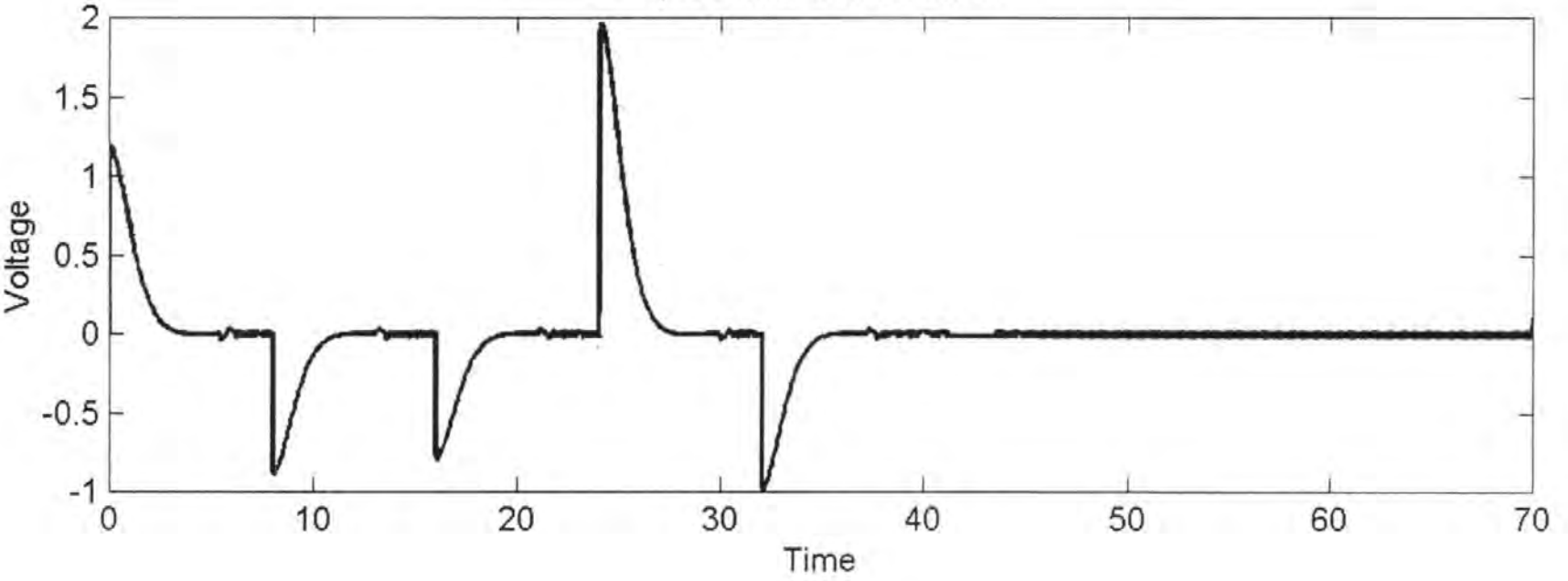

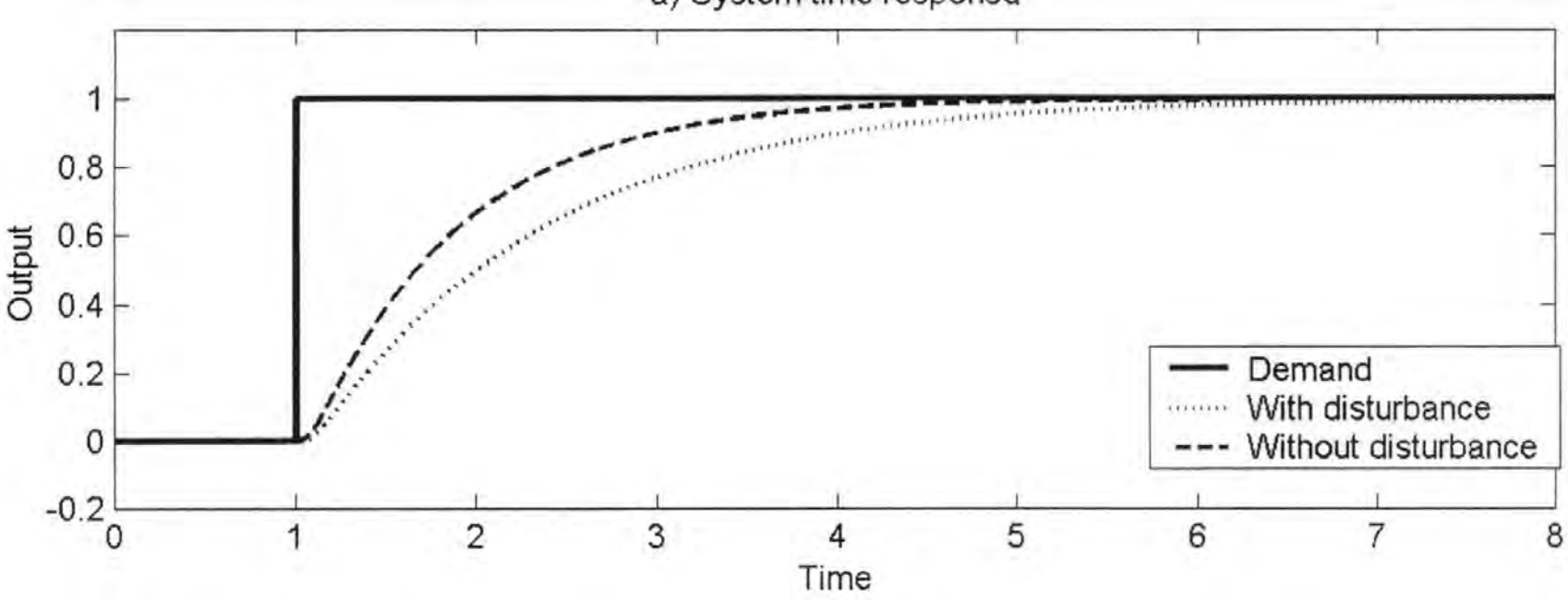

b) Controller effort

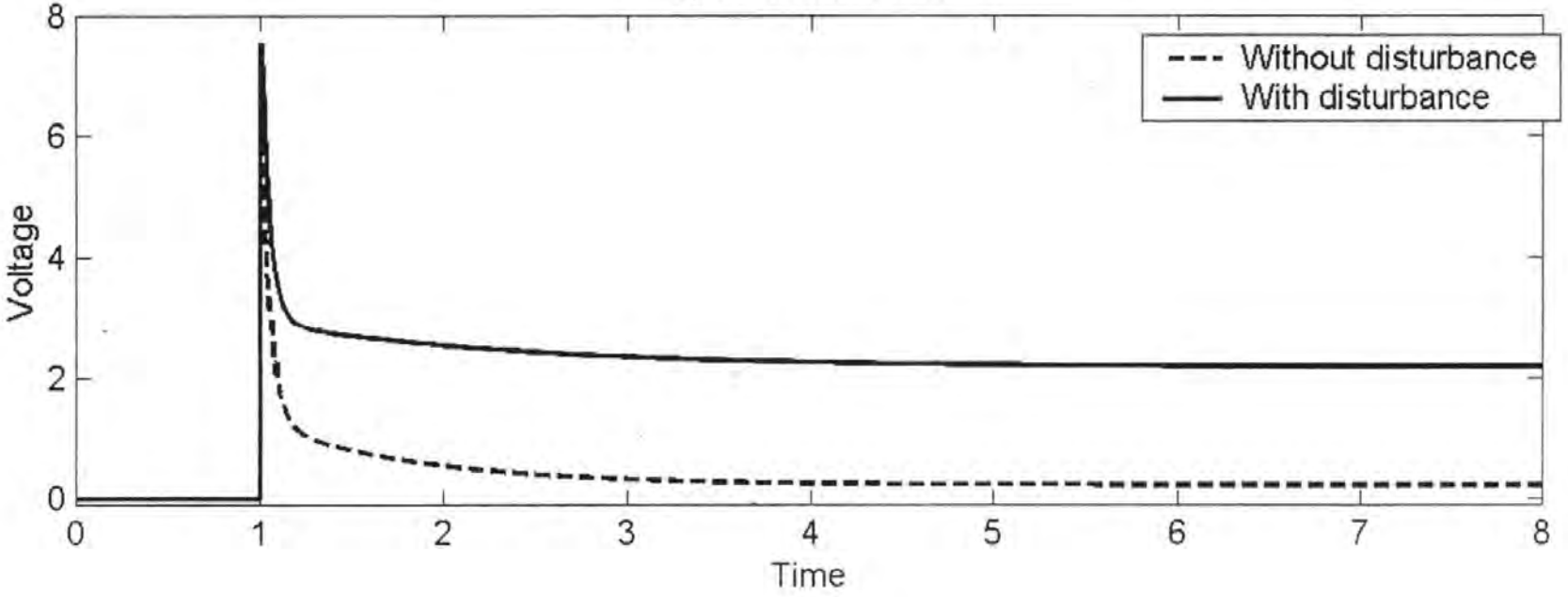

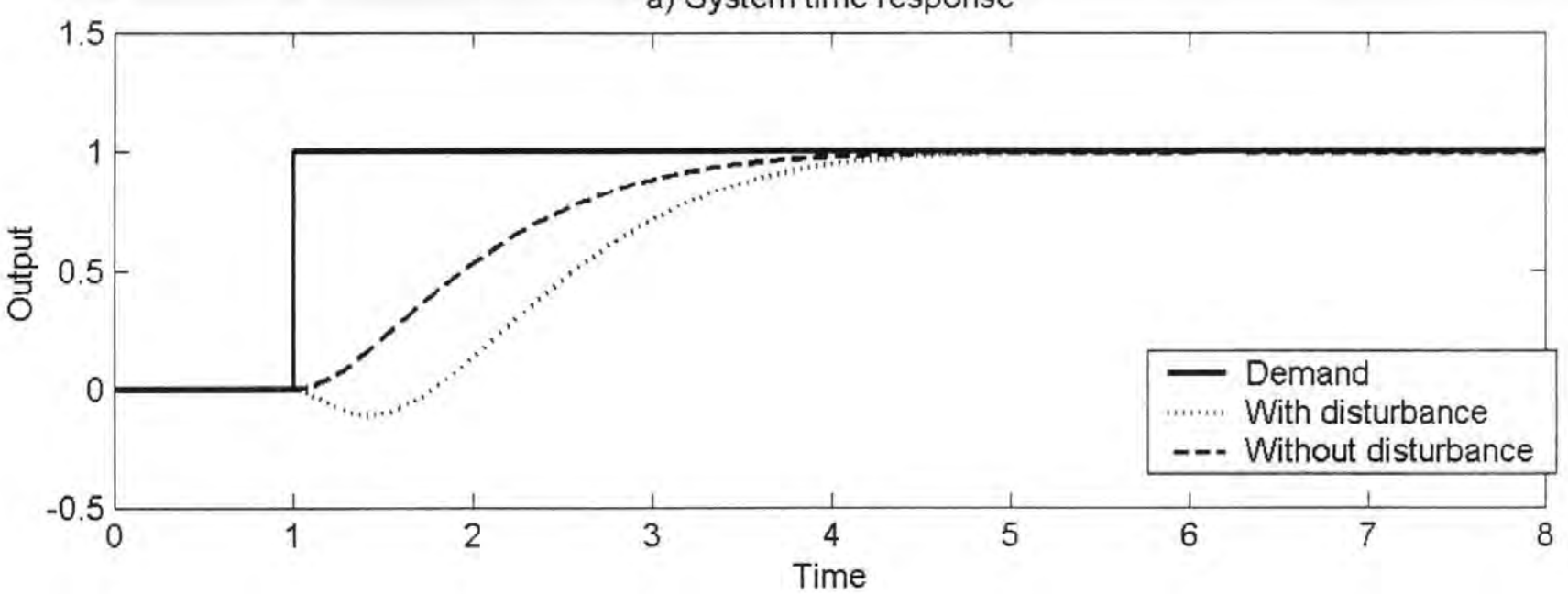
a) System time response
Output
Time
Demand
With disturbance
Without disturbance

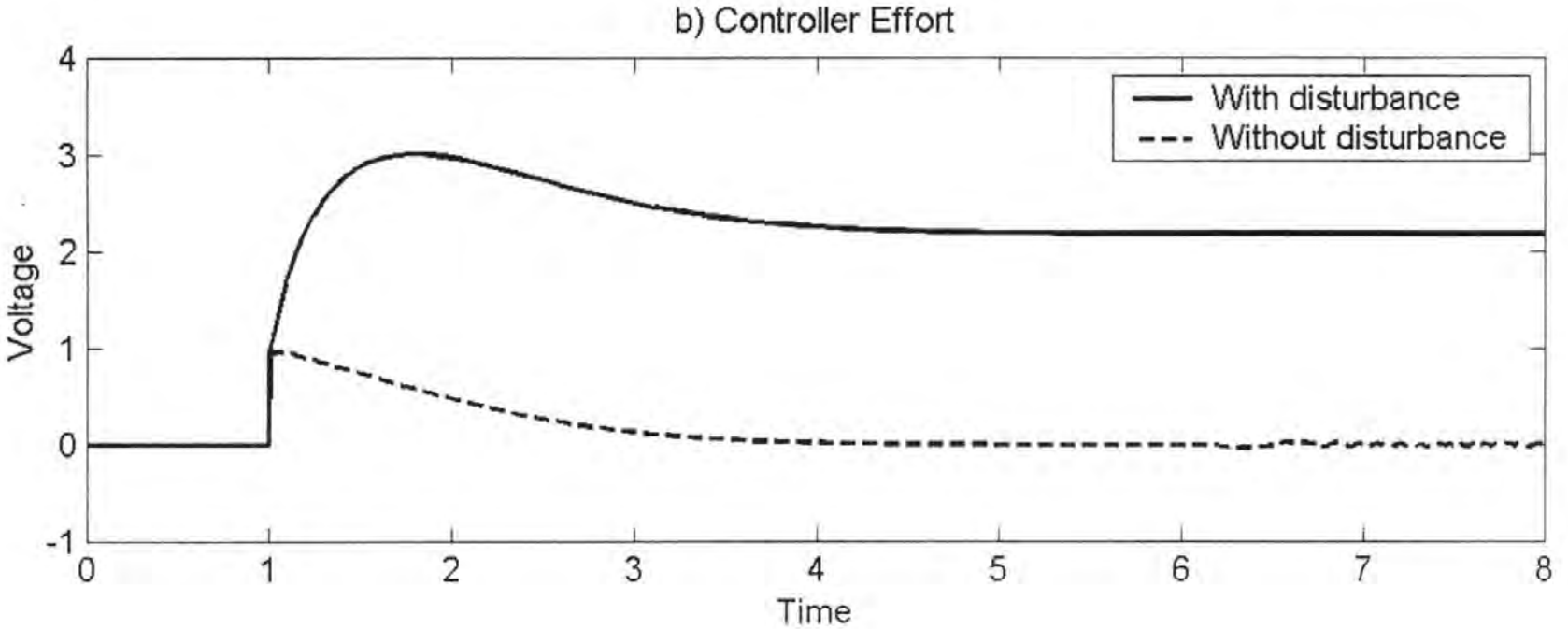
b) Controller Effort
Voltage
Time
With disturbance
Without disturbance

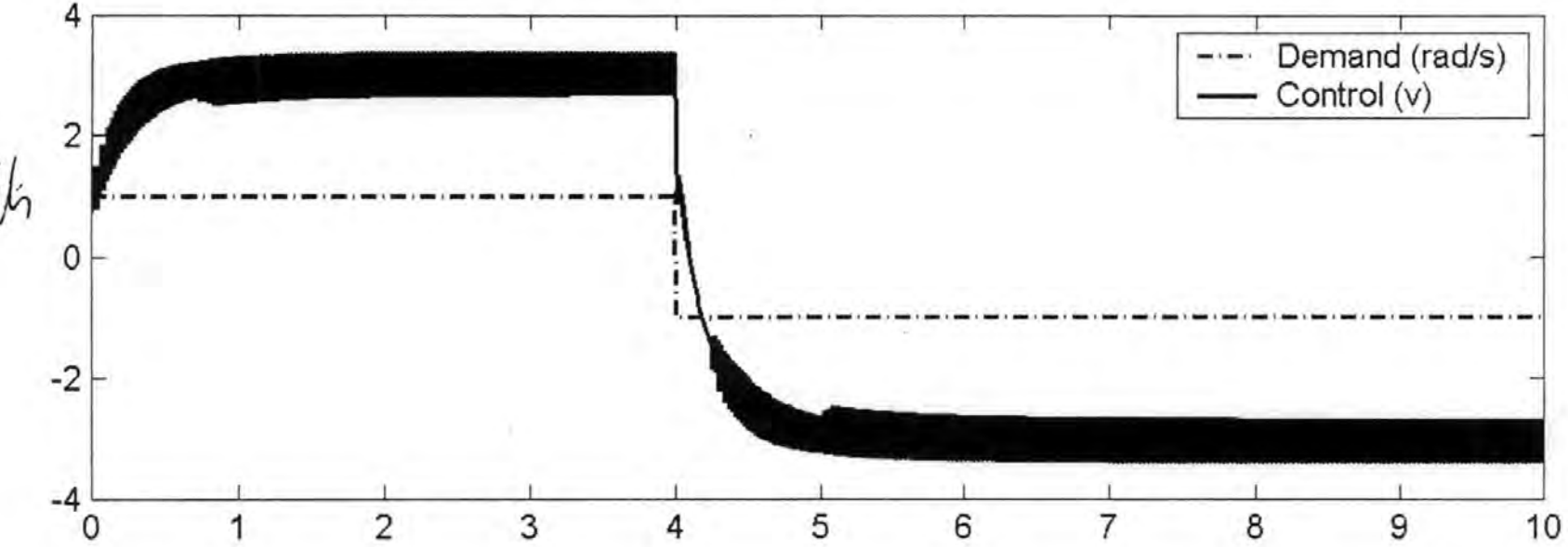
Demand (rad/s)
Control (v)
4
2
0
-2
-4
0
1
2
3
4
5
6
7
8
9
10

units

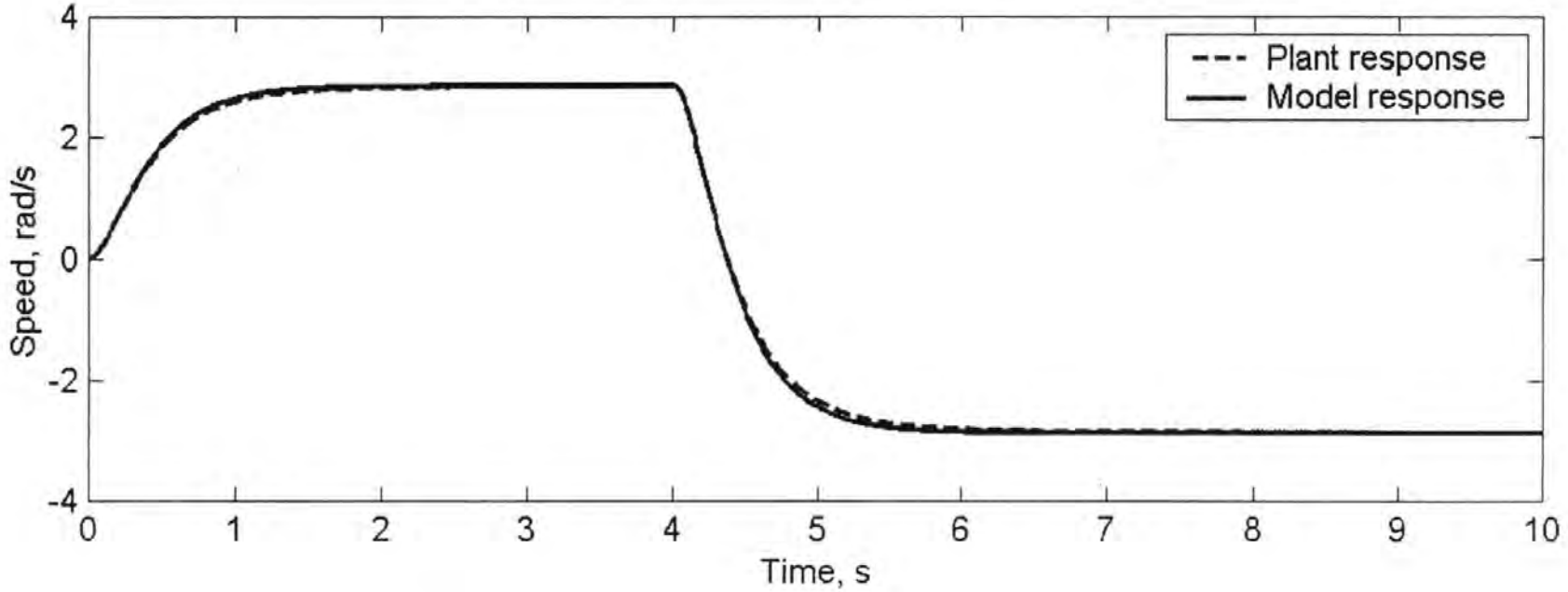
Plant response
Model response
Speed, rad/s
Time, s
4
2
0
-2
-4
0
1
2
3
4
5
6
7
8
9
10

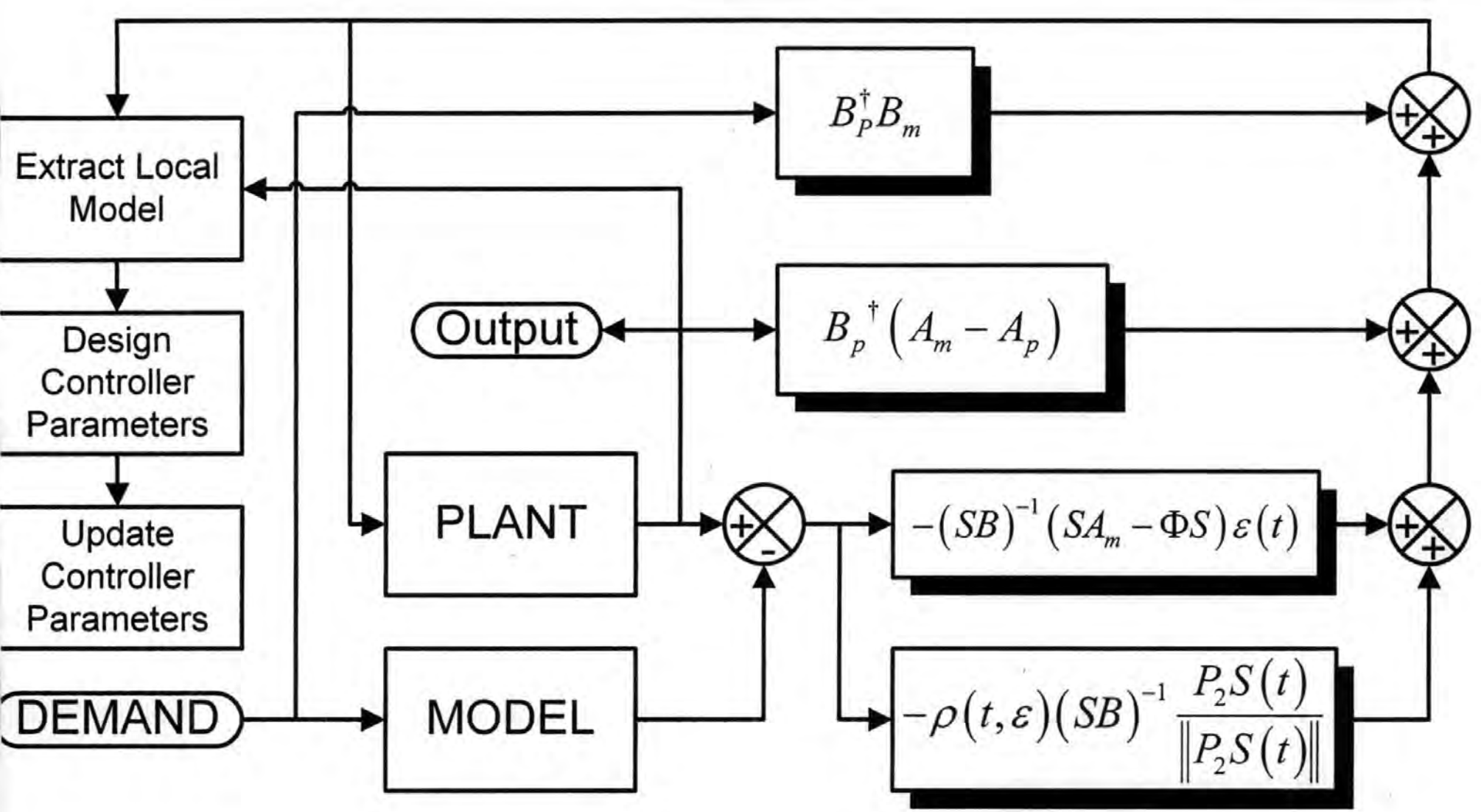
Extract Local Model
Design Controller Parameters
Update Controller Parameters
DEMAND
Output
PLANT
MODEL
$B_P^{\dagger} B_m$
$B_p^{\dagger}\left(A_m - A_p\right)$
$-(SB)^{-1}\left(SA_m - \Phi S\right)\varepsilon(t)$
$-\rho(t,\varepsilon)(SB)^{-1}\dfrac{P_2 S(t)}{\left\|P_2 S(t)\right\|}$

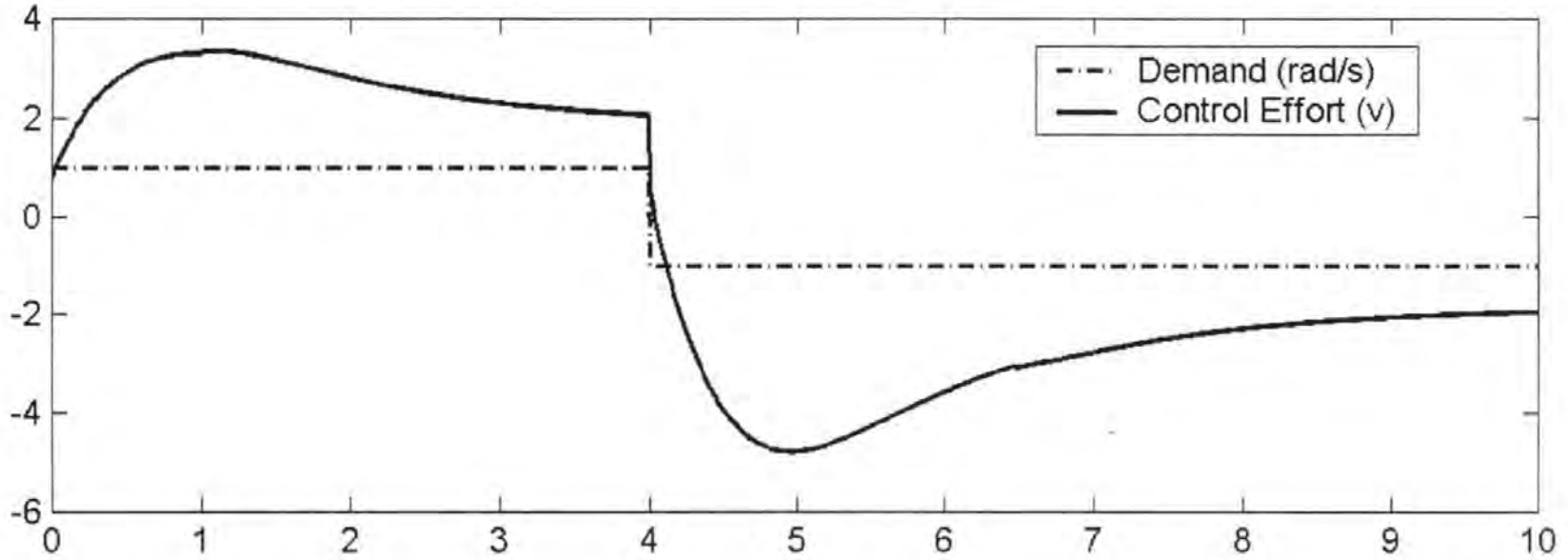
Demand (rad/s)
Control Effort (v)
4
2
0
-2
-4
-6
0
1
2
3
4
5
6
7
8
9
10

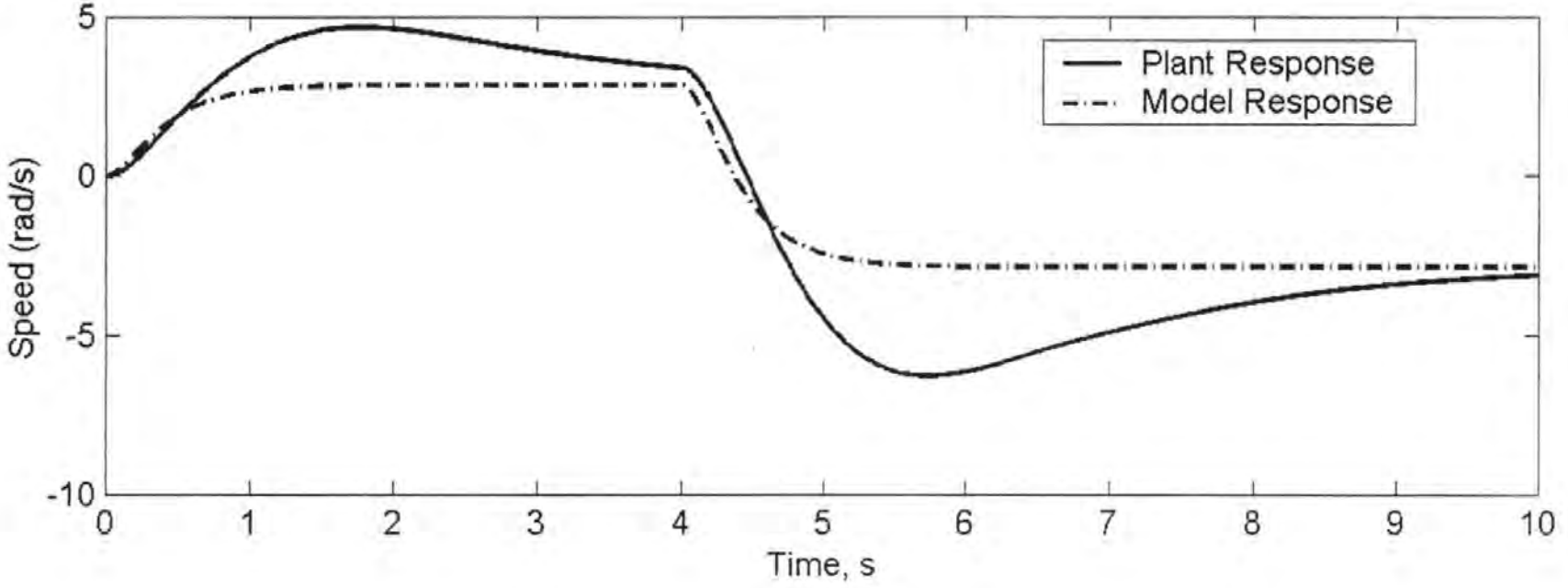
Plant Response
Model Response
Speed (rad/s)
5
0
-5
-10
0
1
2
3
4
5
6
7
8
9
10
Time, s

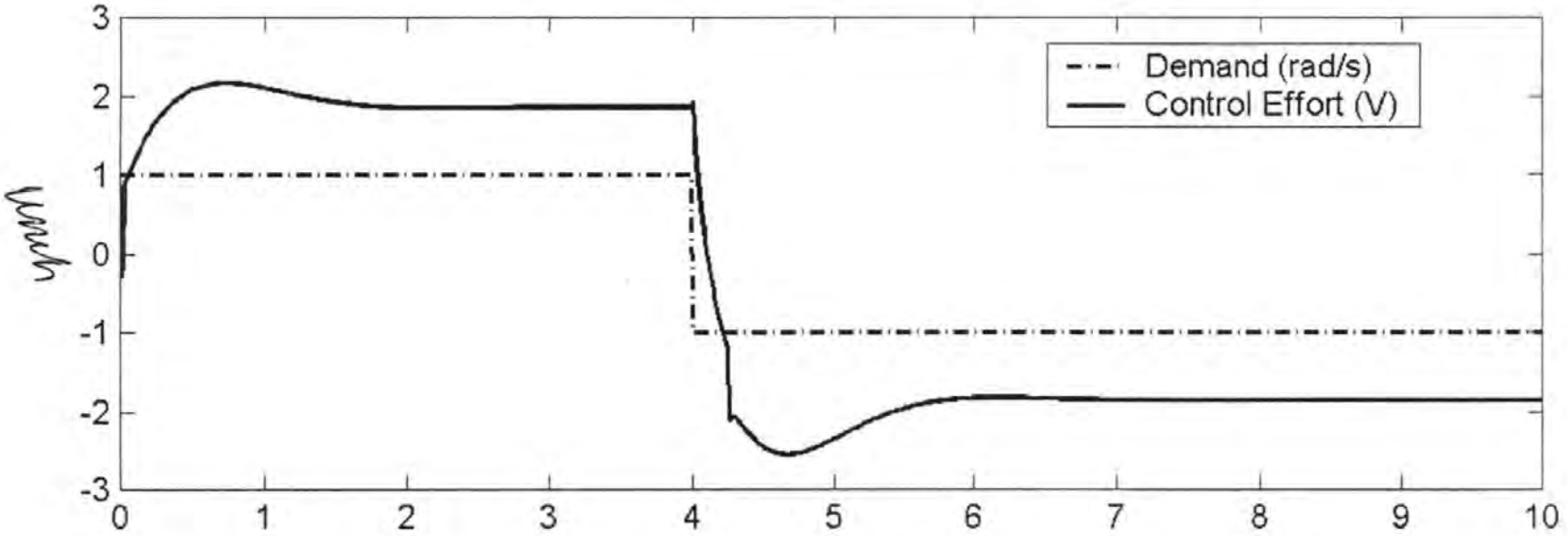
Demand (rad/s)
Control Effort (V)

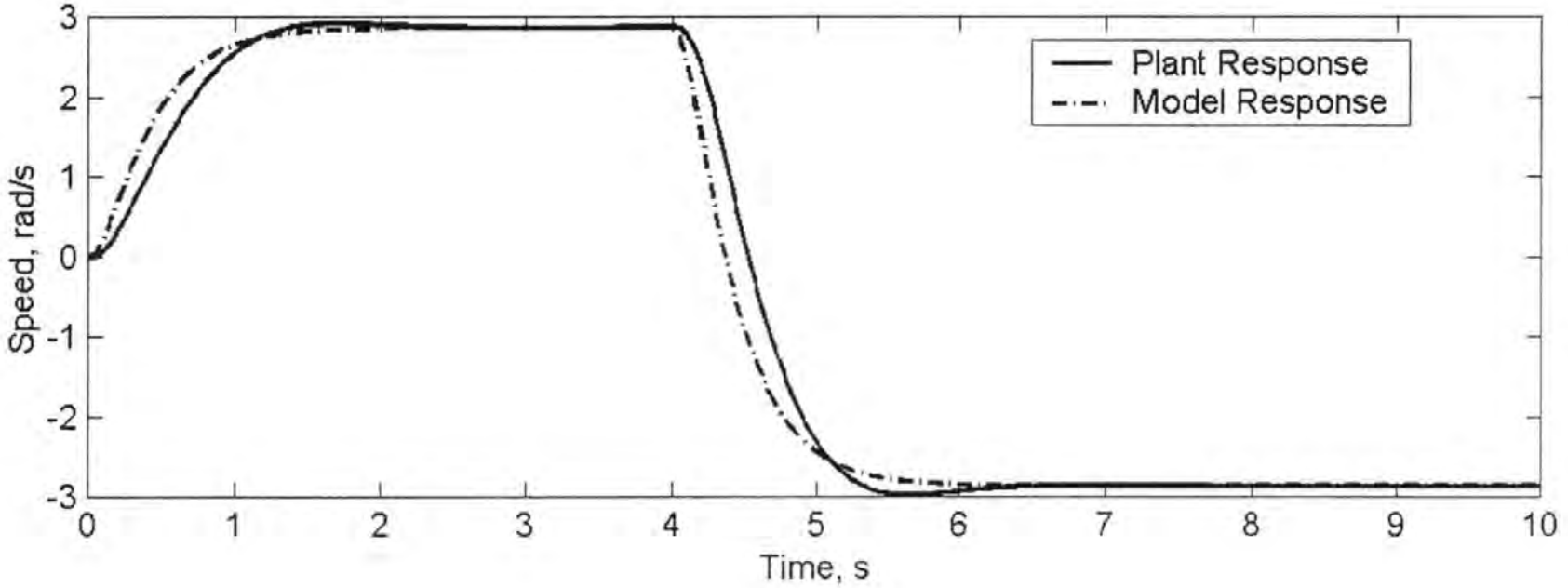
Plant Response
Model Response
Speed, rad/s
Time, s

APPENDIX B

DATA SHEETS AND CIRCUIT DIAGRAMS

Part A: Data Sheets

Digital Encoder HP HEDL 9140

500 Counts per turn, 3 Channels, with Line Driver

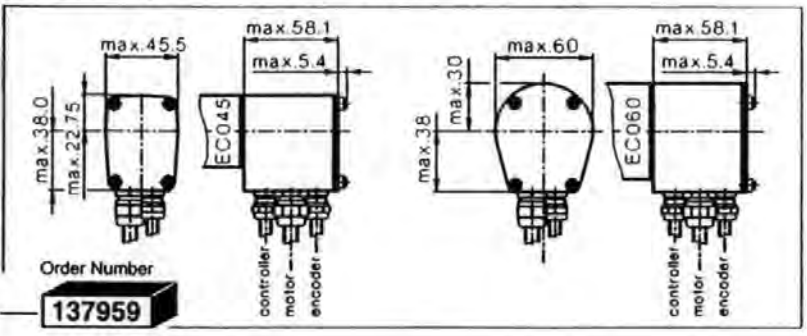

Order Number

137959

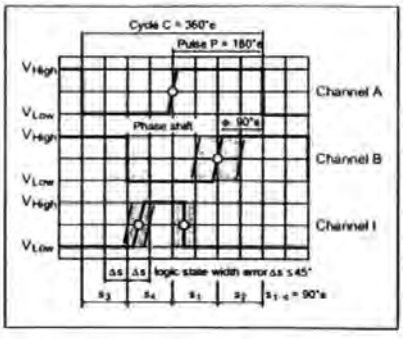

+ Motor Order Number

— **maxon EC motor Ø45 mm**
brushless, 150 Watt, "Y- or Δ-circuit"*
Details see page 107

— **maxon EC motor Ø45 mm**
brushless, 150 Watt, "Y- or Δ-circuit"*
Details see page 107

— **maxon EC motor Ø45 mm**
brushless, 150 Watt, "Y- or Δ-circuit"*
Details see page 107

— **maxon EC motor Ø45 mm**
brushless, 150 Watt, "Y- or Δ-circuit"*
Details see page 107

— **maxon EC motor Ø45 mm**
brushless, 250 Watt, "Y- or Δ-circuit"*
Details see page 108

— **maxon EC motor Ø45 mm**
brushless, 250 Watt, "Y- or Δ-circuit"*
Details see page 108

— **maxon EC motor Ø45 mm**
brushless, 250 Watt, "Y- or Δ-circuit"*
Details see page 108

— **maxon EC motor Ø45 mm**
brushless, 250 Watt, "Y- or Δ-circuit"*
Details see page 108

— **maxon EC motor Ø45 mm**
brushless, 250 Watt, "Y- or Δ-circuit"*
Details see page 108

— **maxon EC motor Ø60 mm**
brushless, 400 Watt, "Y- or Δ-circuit"*
Details see page 109

— **maxon EC motor Ø60 mm**
brushless, 400 Watt, "Y- or Δ-circuit"*
Details see page 109

+ Gearhead

max.127.4

Planetary Gearhead
Ø42 mm, 2.94-14.7 Nm
Details see page 157

Planetary Gearhead
Ø42 mm, 2.94-14.7 Nm
Details see page 157

max.159.6

Planetary Gearhead
Ø42 mm, 2.94-14.7 Nm
Details see page 157

Planetary Gearhead
Ø62 mm, 8-50 Nm
Details see page 158

Planetary Gearhead
Ø42 mm, 2.94-14.7 Nm
Details see page 157

Planetary Gearhead
Ø62 mm, 8-50 Nm
Details see page 158

max.187.3

Planetary Gearhead
Ø81 mm, 20-120 Nm
Details see page 159

+ Brake

Brake Ø28 mm
24 VDC. 0.4 Nm
Detail page 188

Brake Ø28 mm
24 VDC. 0.4 Nm
Detail page 188

Brake Ø28 mm
24 VDC. 0.4 Nm
Detail page 188

Brake Ø28 mm
24 VDC. 0.4 Nm
Detail page 188

Brake Ø28 mm
24 VDC. 0.4 Nm
Detail page 188

*please specify on your order

Technical Data			
Supply voltage	5 V ± 10%	Index pulse width (typical)	90°e
Output signal	TTL compatible	Operating temperature range	0/+70°C
Number of channels	2 + 1 Index Channel	Moment of inertia of code wheel	≤ 0.6 gcm²
Counts per turn	500	Max. acceleration	250'000 rad s⁻²
Phase shift Φ (nominal)	90°e	Output current per channel	min. -1 mA, max. 5 mA
Logic state width s	min. 45°e	Max. operating frequency	min. 100 kHz
Rise time* *(typical at C_L = 25 pF, R_L = 11 kΩ, 25°C)	180 ns	■ Stock program	
Fall time* *(typical at C_L = 25 pF, R_L = 11 kΩ, 25°C)	40 ns	□ Standard program	
		Special program (on request!)	

Pin Allocation		
Cable white	=	V_{CC} 5V DC
Cable brown	=	GND
Cable green	=	Channel $\overline{A}$
Cable yellow	=	Channel A
Cable grey	=	Channel $\overline{B}$
Cable pink	=	Channel B
Cable blue	=	Channel $\overline{I}$ (index)
Cable red	=	Channel I (index)
Cablesize 8 x 0.25 mm²		

maxon EC motor

Ø45 mm, brushless, 250 Watt

CE approved

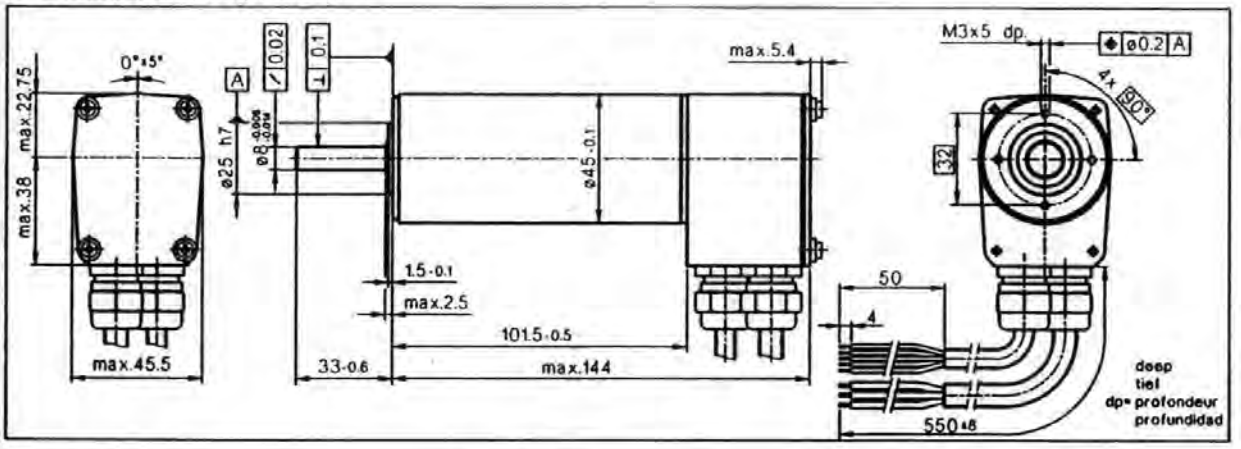

Motor Type:
maxon EC motor Ø45 mm, brushless . . .

Order Number
Motor Data

. . . "Y-circuit", 250 Watt, ball bearings		136207	136208	136209						
. . . "Δ-circuit", 250 Watt, ball bearings					136210	136211	136212			
1 Assigned power rating	W	250	250	250	250	250	250			
2 Nominal voltage	Volt	24.00	36.00	48.00	24.00	36.00	48.00			
3 No load speed	rpm	5300	6300	6500	9100	11000	11100			
4 Stall torque	mNm	2250	3000	3250	3910	5260	5670			
5 Speed/torque gradient	rpm/mNm	2.40	2.10	2.00	2.34	2.10	1.97			
6 No load current	mA	435	370	290	1139	1062	816			
7 Terminal resistance phase to phase	Ohm	0.46	0.64	1.04	0.15	0.21	0.35			
8 Max. permissible speed	rpm	12000	12000	12000	12000	12000	12000			
9 Max. continuous current at 5'000 rpm	A	7.10	6.00	4.70	12.5	10.6	8.20			
10 Max. continuous torque at 5'000 rpm	mNm	283	300	306	286	303	304			
11 Max. efficiency	%	83.0	85.0	85.0	84.2	85.2	85.6			
12 Torque constant	mNm/A	43.3	54.0	71.0	25.0	31.2	41.0			
13 Speed constant	rpm/V	220	175	135	382	306	233			
14 Mechanical time constant	ms	5.00	5.00	5.00	5.00	5.00	5.00			
15 Rotor inertia	gcm²	209	209	209	209	209	209			
16 Terminal inductance (phase to phase)	mH	0.17	0.26	0.44	0.06	0.09	0.15			
17 Thermal resistance housing-ambient	K/W	1.70	1.70	1.70	1.70	1.70	1.70			
18 Thermal resistance winding-housing	K/W	1.10	1.10	1.10	1.10	1.10	1.10			
19 Thermal time constant winding	s	16	16	16	16	16	16			
20 Thermal time constant stator	s	850	850	850	850	850	850			

Operating Range

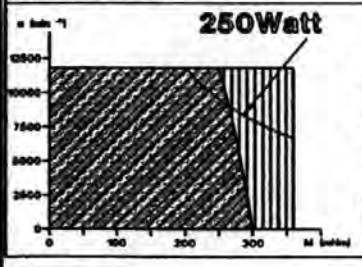

Comments

(Details on page 102)

Continuous operation
In observation of above listed thermal resistances (lines 17 and 18) the maximum permissible winding temperature will be reached during continuous operation at 25°C ambient.
= Thermal limit.

Short term operation
The motor may be briefly overloaded (recurring).

maxon Modular System

Planetary Gearhead
Ø42 mm
2.94-14.7 Nm
Details page 157

Planetary Gearhead
Ø62 mm
8-50 Nm
Details page 158

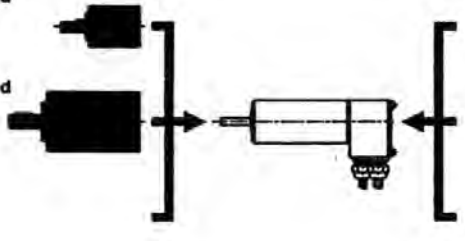

Resolver
Ø26 mm, 10 V
Details page 185

Digital-Encoder
HP HEDL 9140
500 CTP, 3 chan.
Details page 178

Brake
Ø28 mm, 24 VDC
0.4 Nm
Details page 188

Stock program
Standard program
Special program (on request!)

- Motor connector Screwed cable gland PG7
- Axial play at axial load < 20 N 0 mm
  > 20 N max. 0.14 mm
- Preloaded ball bearings
- Max. ball bearing loads
  axial (dynamic) 20 N
  radial (5 mm from flange) 180 N
  Press-fit force (static) 170 N
  same as above, shaft supported 5000 N
- Radial play/ball bearings 0.02 mm
- Ambient temperature range -20/+125°C
- Max. permissible winding temperature +125°C
- Weight of motor 1150 g
- Protection to IP54
- Values listed in the table are nominal.

Cable	Connection
Cable 1	motor winding 1
Cable 2	motor winding 2
Cable 3	motor winding 3
Cable white	Hall sensor 3
Cable brown	Hall sensor 2
Cable green	Hall sensor 1
Cable yellow	GND
Cable gray	V_{Hall} 4.5÷24V DC

- Options: Temperature monitoring (PTC), motor connector with plug

Part B: Circuit Diagrams

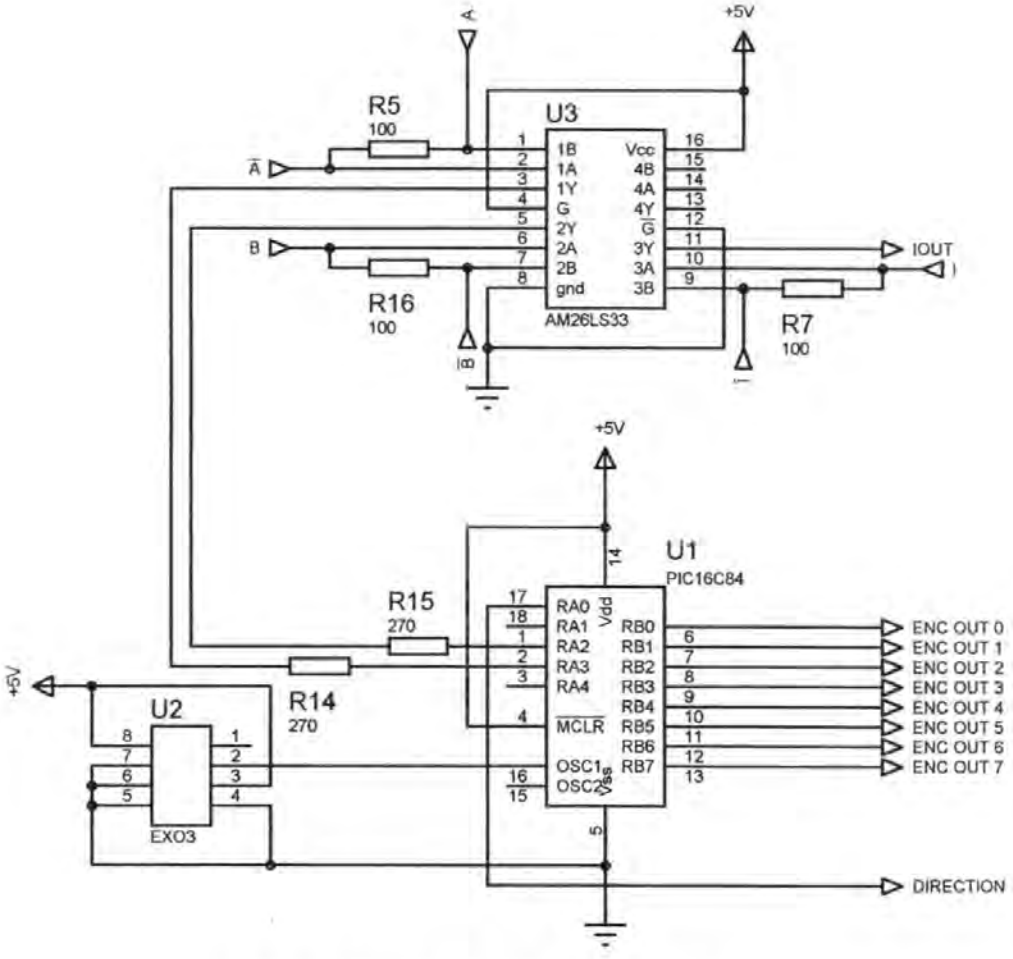

Figure B.1: *Bandwidth Reduction Circuit*

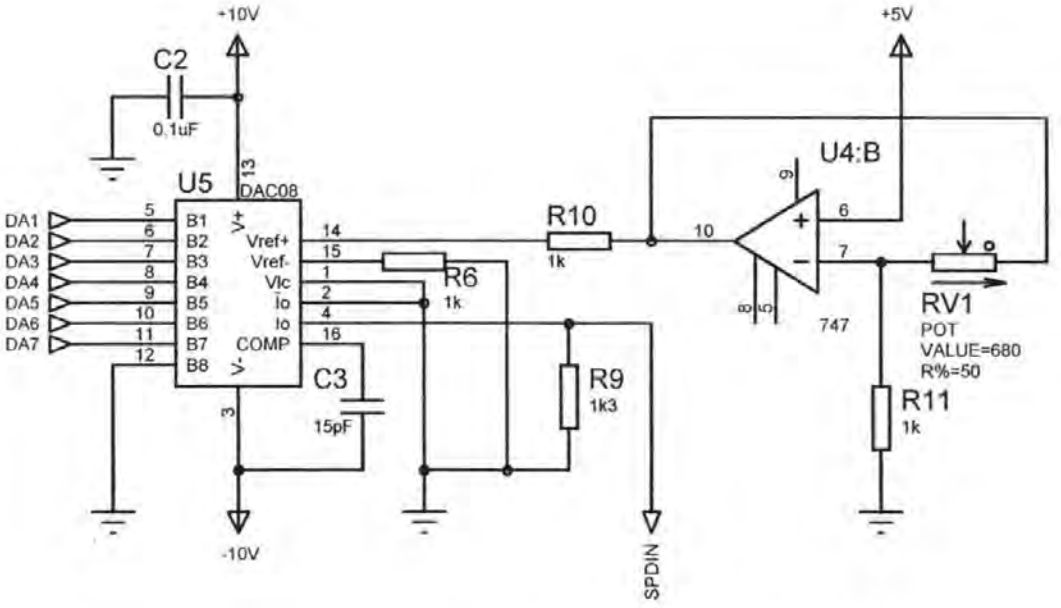

Figure B.2: *Interface to provide analogue speed signal from 7 bit input*

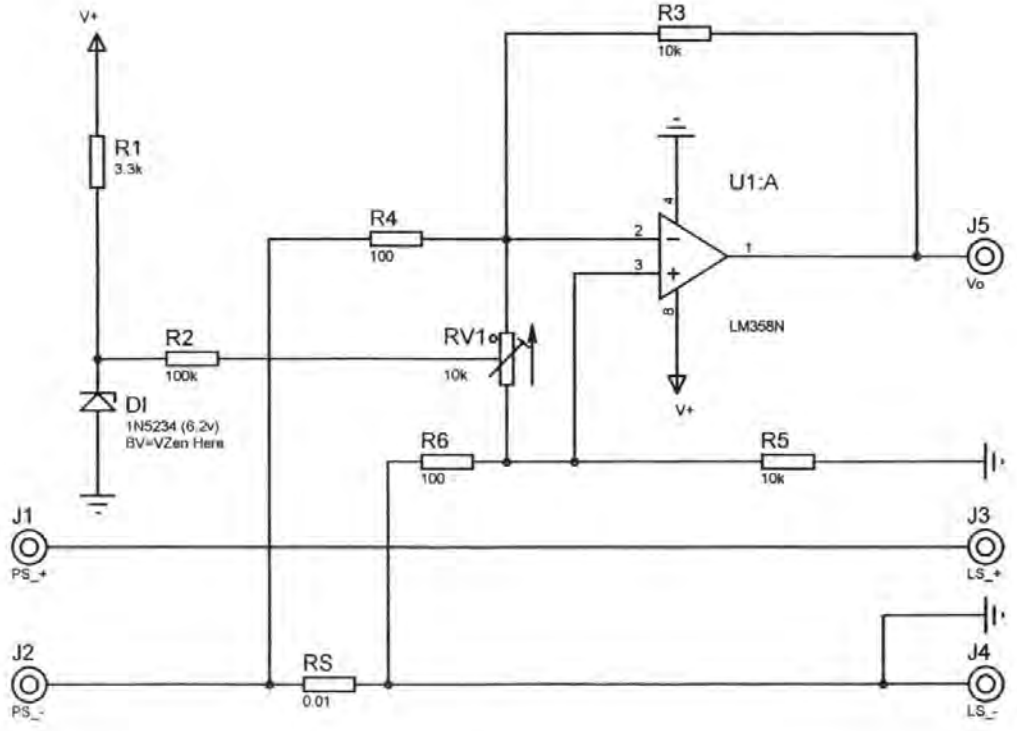

Figure B.3: *Load Current Sensing Circuit*

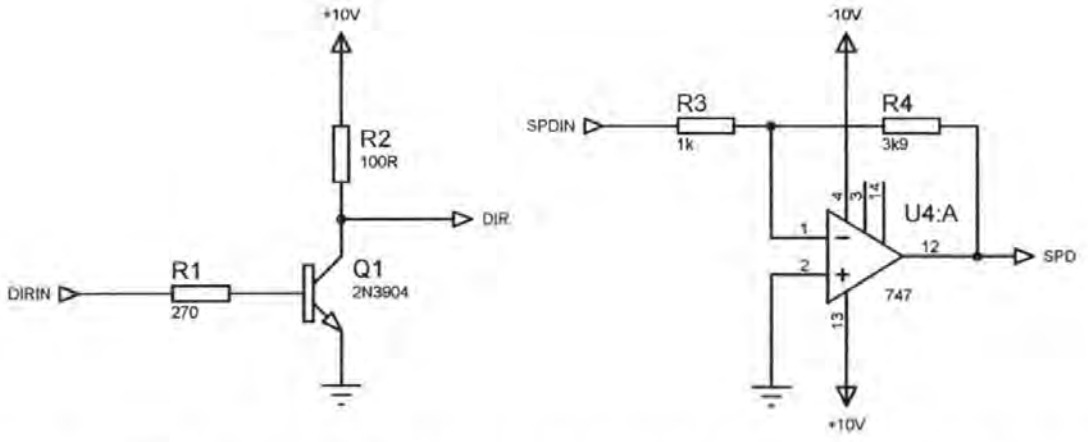

Figure B.4: *Interface providing amplification of speed signal and direction information*

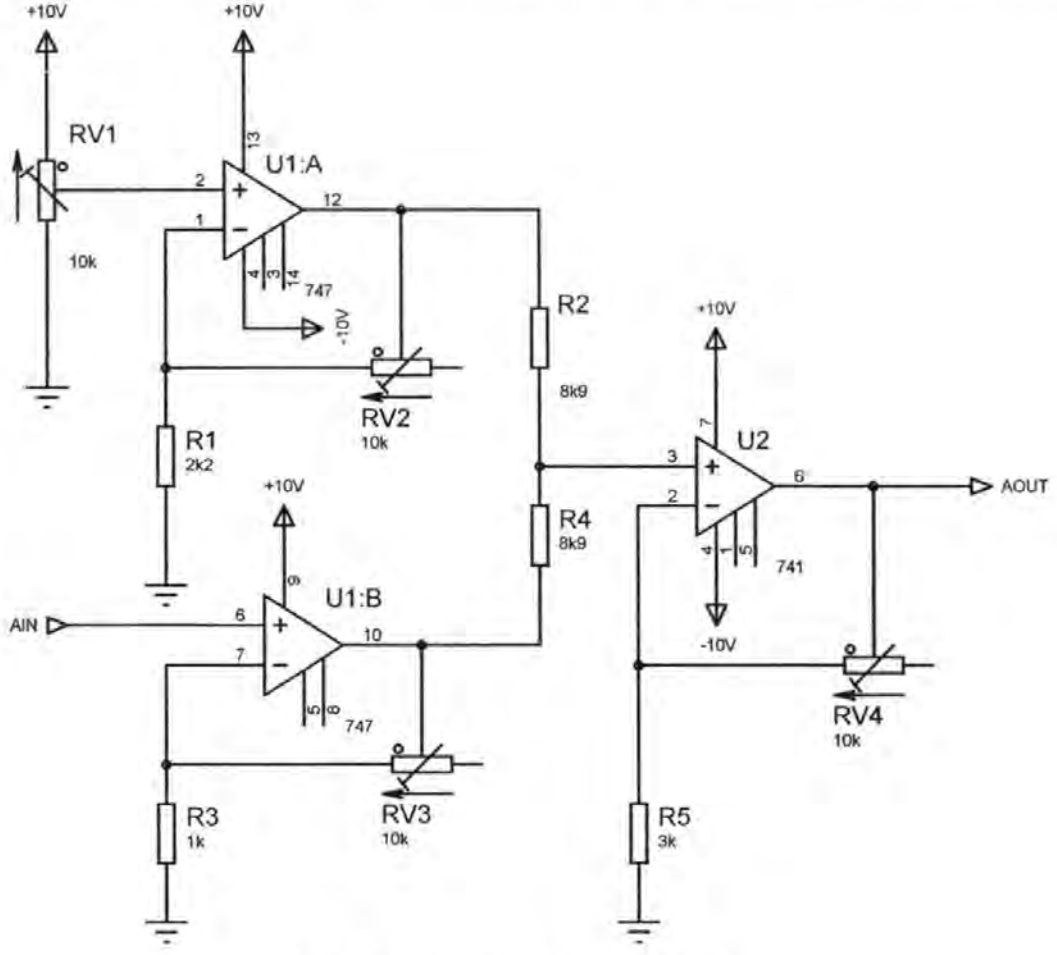

Figure B.5: *Calibration Amplifiers*

Motor Models and Supporting System Identification Theory

Part 1: The Space Phasor Model

According to Chapter 3, (Vas, 1993), the stator current space phasor, $\bar{i}_s$ in stator co-ordinates may be defined as

$$\bar{i}_s^s = \frac{2}{3}\cdot\left(i_a + a\cdot i_b + a^2\cdot i_c\right) \tag{C.1}$$

The superscript s is used to denote stationary *dq* variables. From (3.89) and (3.84) the phase a flux linkage λ_a is given

$$\lambda_a = L_{aa}i_a + L_{ab}i_b + L_{ac}i_c + L_{af}i_f + L_{ad_r}i_{d_r} + L_{aq_r}i_{qr} \tag{C.2}$$

The inductance definition given in (3.85) yields

$$\lambda_a = L_{sl}\mathbb{R}\left(\bar{i}_s\right) + \frac{3}{2}L_o\mathbb{R}\left(\bar{i}_s\right) + \frac{3}{2}L_2\mathbb{R}\left(\bar{i}_s^{\bullet}e^{2j\theta_{er}}\right) + L_{af}\mathbb{R}\left(i_f^r e^{j\theta_{er}}\right) + L_{sd_r}\mathbb{R}\left(i_{d_r}{}^r e^{j\theta_{er}}\right) - \mathbb{R}\left(jL_{sq_r}{}^r i_{q_r} e^{j\theta_{er}}\right) \tag{C.3}$$

The stator flux space phasor $\bar{\lambda}_s$ is:

$$\bar{\lambda}_s^s = \frac{2}{3}\left(\lambda_a + a\lambda_b + a^2\lambda_c\right) \tag{C.4}$$

Applying the structure of (C.2) to λ_b and λ_c allows the re-expression of (C.4)

$$\bar{\lambda}_s^s = L_{sl}\bar{i}_s^{\,s} + \frac{3}{2}L_o\bar{i}_s^{\,s} + \frac{3}{2}L_2\bar{i}_s^{s^{\bullet}}e^{2j\theta_{er}} + L_{sf}i_f{}^r e^{j\theta_{er}} + L_{sd_r}i_{d_r}{}^r e^{j\theta_{er}} - L_{sq_r}ji_{q_r}{}^r e^{j\theta_{er}} \tag{C.5}$$

Multiplying (C.5) by $e^{-j\theta_{er}}$ to obtain:

$$\bar{\lambda}_s^s e^{-j\theta_{er}} = \left(L_{sl} + \frac{3}{2}L_0\right)\bar{i}_s^s e^{-j\theta_{er}} + \frac{3}{2}L_2\left(\bar{i}_s^s e^{-j\theta_{er}}\right)^{\bullet} + L_{sf}i_f{}^r + L_{sd_r}i_{d_r}{}^r + jL_{sq_r}i_{q_r}{}^r \tag{C.6}$$

The relationships

$$\bar{\lambda}_s = \bar{\lambda}_s^{\,s} e^{-j\theta_{er}} \tag{C.7}$$

$$\bar{i}_s = \bar{i}_s^{\,s} e^{-j\theta_{er}} \tag{C.8}$$

are space phasors in rotor co-ordinates (aligned with rotor d axis). With (C.7) and (C.8), (C.6) becomes:

$$\bar{\lambda}_s = \left(L_{sl} + \frac{3}{2} L_0 \right) \bar{i}_s + \frac{3}{2} L_2 \bar{i}_s^{\,*} + L_{sf} i_f^{\,r} + L_{sd_r} i_{d_r}^{\,r} + j L_{sq_r} i_{q_r}^{\,r} \tag{C.9}$$

Next, the stator phase equations in stator co-ordinates are:

$$r_s i_a - V_a = -\frac{d\lambda_a}{dt} \tag{C.10}$$

$$r_s i_b - V_b = -\frac{d\lambda_b}{dt} \tag{C.11}$$

$$r_s i_c - V_c = -\frac{d\lambda_c}{dt} \tag{C.12}$$

These may be translated to space phasors as

$$r_s \bar{i}_s^{\,s} - \bar{V}_s^{\,s} = -\frac{d\bar{\lambda}_s^{\,s}}{dt} = -\frac{d}{dt}\left(\bar{\lambda}_s e^{j\theta_{er}} \right) = -e^{j\theta_{er}} \frac{d\bar{\lambda}_s}{dt} - j\omega_r \bar{\lambda}_s e^{j\theta_{er}} \tag{C.13}$$

The final form of (C.13) is:

$$r_s \bar{i}_s - \bar{V}_s = -\frac{d\bar{\lambda}_s}{dt} - j\omega_r \bar{\lambda}_s \tag{C.14}$$

$$\omega_r = \frac{d\theta_{er}}{dt} \tag{C.15}$$

and

$$V_0 = r_s i_0 + L_{sl} \frac{di_0}{dt} \tag{C.16}$$

$$i_0 = \frac{\left(i_a + i_b + i_c \right)}{3} \tag{C.17}$$

Coincidentally, these expressions are identical to those for the induction machine. Only the flux definition (C.13) is different.

$$\overline{\lambda}_s = \lambda_d + j\lambda_d \tag{C.18}$$

$$\lambda_d = L_{sl} i_d + \lambda_{dm} \tag{C.19}$$

$$\lambda_{dm} = L_{dm} i_d{}^r + L_{sf} i_f{}^r + L_{sd} i_{d_r}{}^r \tag{C.20}$$

with

$$L_{dm} = \frac{3}{2}(L_0 + L_2) \tag{C.21}$$

$$L_{qm} = \frac{3}{2}(L_0 - L_2) \tag{C.22}$$

L_{dm} and L_{qm} are called the d - q magnetising inductances. The rotor to stator currents may be reduced to .

$$\frac{i_f}{i_f{}^r} = \frac{L_{sf}}{L_{dm}} = K_f \tag{C.23}$$

$$\frac{i_{d_r}}{i_{d_r}{}^r} = \frac{L_{sd}}{L_{dm}} = K_d \tag{C.24}$$

$$\frac{i_{q_r}{}^r}{i_{d_r}{}^r} = \frac{L_{sq}}{L_{dm}} = K_q \tag{C.25}$$

$$\lambda_{dm} = L_{dm} i_{dm} \tag{C.26}$$

$$i_{dm} = i_d + i_f + i_{d_r} \tag{C.27}$$

$$\lambda_{qm} = L_{qm} i_{qm} \tag{C.28}$$

$$i_{qm} = i_q + i_{qr} \tag{C.29}$$

$$i_m = \sqrt{i_{dm}{}^2 + i_{qm}{}^2} \tag{C.30}$$

Magnetic saturation may be accounted by unique $\lambda_{dm}(i_m)$ and $\lambda_{qm}(i_m)$ functions to be either calculated or measured. The stator equations (C.14) and (C.15) in dq co-ordinates become

$$V_d = r_s i_d + \frac{d\lambda_d}{dt} - \omega_r \lambda_q \tag{C.31}$$

$$V_q = r_s i_q + \frac{d\lambda_q}{dt} + \omega_r \lambda_d \tag{C.32}$$

Adding the rotor equations in rotor dq co-ordinates

$$V_f = r_f i_f + \frac{d\lambda_f}{dt} \tag{C.33}$$

$$r_{d_r} i_{d_r} + \frac{d\lambda_{d_r}}{dt} = 0 \tag{C.34}$$

$$r_{q_r} i_{q_r} + \frac{d\lambda_{q_r}}{dt} = 0 \tag{C.35}$$

$$\lambda_f = L_{fl} i_f + \lambda_{dm} \tag{C.36}$$

$$\lambda_{d_r} = L_{d_r l} i_{d_r} + \lambda_{dm} \tag{C.37}$$

$$\lambda_{q_r} = L_{q_r l} i_{q_r} + \lambda_{qm} \tag{C.38}$$

The torque, T_e, is:

$$T_e = \frac{3}{2} p \mathbb{R}\left(j \bar{\lambda}_s \bar{i}_s^* \right) = \frac{3}{2} p \left(\lambda_d i_q - \lambda_q i_d \right) \tag{C.39}$$

Finally, the d-q variables are related to the abc variables by the Park transformation:

$$\bar{V}_s = V_d + j V_q = \frac{2}{3}\left(V_a + a V_b + a^2 V_c \right) e^{-j\theta_{er}} \tag{C.40}$$

$$a = e^{-j\frac{2\pi}{3}} \tag{C.41}$$

Notice also that all rotor variables are reduced to the stator:

$$V_f = \frac{V_f^{\,r}}{K_f} \tag{C.42}$$

$$r_f = \frac{r_f^{\,r}}{K_f^{\,2}} \tag{C.43}$$

$$L_{fl} = \frac{L_{fl}^{\,r}}{K_f^{\,2}} \tag{C.44}$$

$$r_{d_r} = \frac{r_{d_r}^{\,r}}{K_d^{\,2}} \tag{C.45}$$

$$L_{d,l} = \frac{L_{d,l}^{\,r}}{K_d^{\,2}} \tag{C.46}$$

$$r_{q_r} = \frac{r_{q_r}^{\,r}}{K_q^{\,2}} \tag{C.47}$$

$$L_{q,l} = \frac{L_{q,l}^{\,r}}{K_q^{\,2}} \tag{C.48}$$

The motion equation (3.96) is to be added. Like the phase co-ordinate model, the *dq* model is also of 8^{th} order and non-linear but contrary to the phase co-ordinate model, the coefficients are position independent.

Part 2: Additional Model Structures

Finite Impulse Response (FIR)

The simplest model is the finite impulse response structure, which corresponds to the choice of all monic polynomials within (4.17) equal to one. The model is thus described

$$y(t) = B(q^{-1})u(t) + e(t) \tag{C.49}$$

The corresponding predictor is given

$$\hat{y}(t|\theta) = B(q^{-1})u(t) \tag{C.50}$$

Or, expressed in regressor form

$$\hat{y}(t|\theta) = \varphi^T(t)\theta \tag{C.51}$$

where the regression vector is given

$$\varphi(t) = [u(t-1), u(t-2), \ldots, u(t-m)] \tag{C.52}$$

the corresponding parameter vector is

$$\theta = [b_0, b_1, \ldots, b_m] \tag{C.53}$$

AutoRegression with Moving Average (ARMA)

The Auto Regression with Moving Average process introduces the noise component to the model. In this case, the polynomials set equal to one are D, B and F. The regression model is therefore

The regression model is described by

$$\hat{y}(t|\theta) = \varphi^T(t,\theta)\theta \tag{C.54}$$

with

$$\varphi(t,\theta) = [y(t-1), \ldots, y(t-n) \quad \varepsilon(t,\theta), \ldots, \varepsilon(t-k,\theta)] \tag{C.55}$$

the corresponding parameter vector is

$$\theta = [a_1, \ldots, a_n \quad c_1, \ldots, c_k] \tag{C.56}$$

AutoRegressive, Moving Average with eXogenous inputs (ARMAX)

A more general form of the ARX model is the ARMAX model that has a structure corresponding to polynomials F and D equal to 1. In this case, the residuals of the estimation are introduced to the regression vector. The regression model is described by

$$\hat{y}(t|\theta) = \varphi^T(t,\theta)\theta \tag{C.57}$$

with

$$\varphi(t,\theta) = [y(t-1),\ldots,y(t-n) \quad u(t-1),\ldots,u(t-m) \quad \varepsilon(t,\theta),\ldots,\varepsilon(t-k,\theta)] \tag{C.58}$$

the corresponding parameter vector is

$$\theta = [a_1,\ldots,a_n \quad b_0,\ldots,b_m \quad c_1,\ldots,c_k] \tag{C.59}$$

The inclusion of the C polynomial implies a relationship between the regression vector and model parameters, this structure can be described as recurrent, and estimation of model parameters becomes more complex.

Output Error (OE)

The Output Error model corresponds to the polynomials A, C and D in (4.17) equal to one, i.e.

$$\hat{y}(t|\theta) = \varphi^T(t,\theta)\theta \tag{C.60}$$

with

$$\varphi(t,\theta) = [\hat{y}(t-1|\theta),\ldots,\hat{y}(t-n|\theta) \quad u(t-1),\ldots,u(t-m)] \tag{C.61}$$

$$\theta = [-f_r,\ldots,-f_r \quad b_0,\ldots,b_m] \tag{C.62}$$

Other forms

Table 4.1 provides details of some linear black-box model structures not discussed above.

Table 4.1: *Black-box model structures*

Structure Name	Polynomials set equal to 1
ARARX	F,C
ARARMAX	F
BJ (Box Jenkins)	A

Part 3: A Discussion of the Bias-Variance Tradeoff

Bias and Variance

Revisiting (4.11), the model of highest quality may be described by

$$\theta_*(m) = \arg \min_{\theta} \bar{V}(\theta) \tag{C.63}$$

in this case m is used to describe the dimension of the parameter vector. The vector $\theta_*(m)$ will depend on the properties of φ. A quality measure will be introduced for a given $\hat{\theta}_N$ as

$$E\bar{V}(\hat{\theta}_N) = V_*(m) \tag{C.64}$$

The model may be interpreted as describing the models' expected input output data fit to the system, given a new data set with the same regressor properties. $\hat{\theta}_N$ is the estimate of θ based on the dataset Z^N (4.7).

Now assume that the minimisation (C.63) has been achieved and a set of parameters for the estimate $\hat{\theta}_N$ has been obtained. It is also assumed that the model $\theta_*(m)$ is acceptable, at least in the sense that the model residuals are white noise. (C.64) may be expressed as

$$V_*(m) = E\bar{V}(\hat{\theta}_N) = \lambda + E\left\| f(\varphi(t)) - f(\varphi(t), \hat{\theta}_N) \right\|^2 \tag{C.65}$$

(C.65) approximates to

$$V_*(m) = E\bar{V}(\hat{\theta}_N) \approx \underbrace{\lambda}_{Noise} + \underbrace{E\|f(\varphi) - f(\varphi,\theta_*(m))\|^2}_{Bias} + \underbrace{E\|f(\varphi,\theta_*(m)) - f(\varphi,\hat{\theta}_N)\|^2}_{Variance} \quad \text{(C.66)}$$

From (C.66) it can be seen that if the noise component is negligible, then $V_*(m)$ can be decomposed into two parts, namely one due to bias and the other due to variance of the estimation.

Clearly,

$$\lim_{N\to\infty} \hat{\theta}_N \to \theta_*(m) \quad \text{(C.67)}$$

In this case, only the bias component will be contained in $V_*(m)$. The estimate will converge to the best case system approximation, for a given structure and size. Consider the parameter vector $\hat{\theta}_N$; it will have a covariance matrix describing its deviation from the ideal, $\theta_*(m)$. Applying this error to the resultant variation in prediction performance

$$E\|f(\varphi(t),\hat{\theta}_N) - f(\varphi(t),\theta_*(m))\|^2 \approx \lambda\frac{m}{N} \quad \text{(C.68)}$$

Combining (C.66) and (C.68)

$$V_*(m) = E\bar{V}(\hat{\theta}_N) = \lambda + \lambda\frac{m}{N} + E\|f(\varphi) - f(\varphi,\theta_*(m))\|^2 = \bar{V}(\theta_*(m)) + \lambda\frac{m}{N} \quad \text{(C.69)}$$

The expected loss of estimation accuracy when the model is applied to a new data set is given in (C.69). With a loss function defined as per (4.11) and (4.12), the equivalent equation for the expected approximation performance when the model is applied to the training data is given

$$EV_N(\hat{\theta}_N) \approx \bar{V}(\theta_*(m)) - \lambda\frac{m}{N} \quad \text{(C.70)}$$

Clearly, the potential approximation ability of a given model structure increases with *m*. However, an increase in the number of parameters used leads to a direct penalty within

the variance contribution. Increasing the number of parameters by one (m+1) is attractive since it decreases $V_*(\theta(m))$, however if the decrease is less than λ/N then the addition of this parameter will degrade the overall model performance $V_*(m)$. Parameters such as these are termed *spurious*. Often the term *"overfit"* is used to describe what happens to the model when spurious parameters are used. The bias component in (C.66) is minimised for a given parameter dimension by minimising the number of functions used to parameterise the regression vector (i.e. the number of basis functions in f). A good deal of research interest currently focuses upon finding high quality basis functions that are capable of function approximation.

Part 4: Hard, Fuzzy and Probabilistic Partitions

Hard Partitioning

Imagine that the data in Figure C.1 needs partitioning into two clusters. Clearly, from the diagram there are two distinct sets of data {1-5} and {8-12}. There remain two data points that do not readily fit either of the clusters satisfactorily.

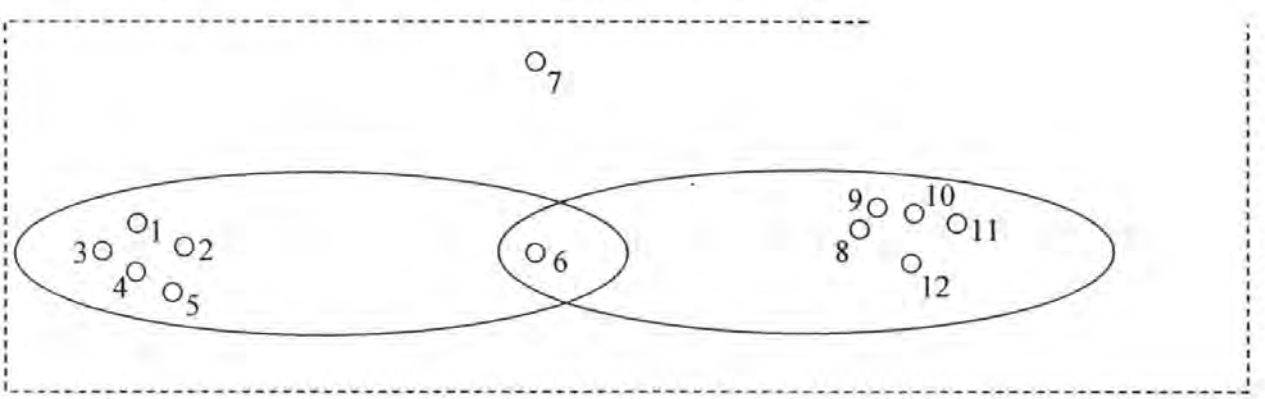

Figure C.1: *A data set in* $\mathbb{R}^2$

A hard partition may be expressed by the following properties

$$\bigcup_{i=1}^{c} A_i = Z \tag{C.71}$$

$$A_i \cap A_j = \varnothing, \qquad 1 \le i \ne j \le c \tag{C.72}$$

$$\varnothing \subset A_i \subset Z, \qquad 1 \le i \le c \tag{C.73}$$

(C.71) stipulates that all data supplied in Z be collectively contained in the subsets A_i. (C.72), on the other hand, stipulates that none of the subsets may be empty, or completely contain Z. Finally (C.72) ensures that the subsets are disjoint. These conditions may instead be expressed in terms of the equivalent logical relationships

$$\bigvee_{i=1}^{c} \mu A_i = 1 \tag{C.74}$$

$$\mu A_i \wedge \mu A_j = 0, \qquad 1 \le i \ne j \le c \tag{C.75}$$

$$0 < \mu A_i < 1, \qquad 1 \le i \le c \tag{C.76}$$

The degrees of membership of data to a given cluster can be represented in a matrix format, denoted U. This matrix will represent hard partitioning, if and only if the following criteria, which are follow directly from equations (C.74)-(C.76), are met

$$\mu_{ik} \in \{0,1\}, \qquad 1 \le i \le c,\ 1 \le k \le N \tag{C.77}$$

$$\sum_{i=1}^{c} \mu_{ik} = 1, \qquad 1 \le k \le N \tag{C.78}$$

$$0 < \sum_{k=1}^{n} \mu_{ik} < N \tag{C.79}$$

Consider the twelve data points in Figure C.1, the data might be partitioned into two subsets by

$$U = \begin{array}{c|cccccccccccc} & 1 & 2 & 3 & 4 & 5 & 6 & 7 & 8 & 9 & 10 & 11 & 12 \\ \hline 1 & 1 & 1 & 1 & 1 & 1 & 1 & 0 & 0 & 0 & 0 & 0 & 0 \\ 0 & 0 & 0 & 0 & 0 & 0 & 0 & 1 & 1 & 1 & 1 & 1 & 1 \end{array} \qquad \text{(C.80)}$$

Clearly, the resulting partition matrix is not entirely satisfactory. The problem stems from the fact that each data point must be assigned exclusively to a cluster. This may lead to misrepresentation of the data, in the case of the example above, neither point 6 or 7 fit closely with the remaining points. Arguably, they would constitute another class of the data, however, it will be shown later that each cluster is represented by a membership function and unnecessary introduction of additional clusters is unattractive. Fuzzy and probabilistic cluster partitioning may instead be employed to overcome the problems associated with hard partitioning.

Fuzzy Partitioning

In the case of fuzzy partitioning the requirement

$$\mu_{ik} \in \{0,1\}, \qquad 1 \le i \le c,\ 1 \le k \le N \qquad \text{(C.81)}$$

is relaxed, such that any given data may have a real valued membership of between zero and one to any cluster, i.e.

$$\mu_{ik} \in [0,1], \qquad 1 \le i \le c,\ 1 \le k \le N \qquad \text{(C.82)}$$

provided that its total degree of membership to all clusters is one, i.e. (C.78) remains true. The partition matrix could possibly be rewritten

$$U = \begin{array}{c|cccccccccccc} & 1 & 2 & 3 & 4 & 5 & 6 & 7 & 8 & 9 & 10 & 11 & 12 \\ \hline 1 & 1 & 1 & 1 & 1 & 1 & 0.5 & 0.3 & 0 & 0 & 0 & 0 & 0 \\ 0 & 0 & 0 & 0 & 0 & 0 & 0.5 & 0.7 & 1 & 1 & 1 & 1 & 1 \end{array} \qquad \text{(C.83)}$$

In this case, it can be seen that the data point 6 is accurately represented, since it is between the distinct sets of data. However, arguably point 7 is still misrepresented, since

it is further away from the two clusters than point 6, yet still has an equal effect on the clusters.

Probabilistic partitioning

The final partitioning method relaxes (C.78), such that the membership of a data point does not have to sum to one across the clusters. Instead the less restrictive constraint that for all k there exists a value of i such that the membership of data i,k is greater than zero, formally

$$\exists i, \mu_{ik} > 0, \forall k \tag{C.84}$$

The matrix U may now be expressed as

$$U = \begin{array}{cccccccccccc} 1 & 2 & 3 & 4 & 5 & 6 & 7 & 8 & 9 & 10 & 11 & 12 \\ \hline 1 & 1 & 1 & 1 & 1 & 0.5 & 0.15 & 0 & 0 & 0 & 0 & 0 \\ 0 & 0 & 0 & 0 & 0 & 0.5 & 0.2 & 1 & 1 & 1 & 1 & 1 \end{array} \tag{C.85}$$

The lower degree of representation of either of the clusters is now represented by the lower assigned membership. This form of partitioning is also referred to as possibilistic partitioning e.g. Chapter 4,(Krishnapuram and Keller 1993 and Hoppner *et al.*, 1999); here the term probabilistic is adopted as per Chapter 4, (Krishnapuram and Freg, 1992).

APPENDIX D

Additional Control Theory

Part 1: State Feedback Matrix Design Methods

Robust Eigenstructure Assignment

For the case of a scalar controlled problem, specification of the (n - 1) eigenvalues associated with the sliding mode will uniquely determine the matrix M of equation (5.48) For multi-input systems this is not the case. In such a situation the available degrees of freedom may be used to modally shape the system response by a judicious choice of eigenvector form and/or ensure that the resulting closed-loop system is maximally robust to system parameter variations. However the eigenvector corresponding to a given eigenvalue must lie in an allowable sub-space which is determined by the system matrix, the input matrix and the eigenvalue itself. To evaluate robustness, a bound upon the individual eigenvalue sensitivity c_i is given by

$$Max\{c_i\} \le \kappa(V) = \|V\|\|V^{-1}\| \qquad \text{(D.1)}$$

Here $\kappa(V)$ denotes the condition number of the matrix V of right eigenvectors and is a measure of the orthogonality of the eigenvectors v_i. The closer the eigenvectors of a matrix are to being orthogonal, the smaller is the associated condition number and the greater the robustness of the eigenvalue locations to changes in the elements of the matrix. In robust eigenstructure assignment the feedback matrix is obtained by assigning a set of linearly independent right eigenvectors corresponding to the state feedback

required eigenvalues such that the matrix of eigenvectors is as well-conditioned as possible.

Direct Eigenstructure Assignment

In the previous subsection, the additional degrees of freedom in the pole placement problem for multi-input systems were used to minimise the condition number of the associated eigenvalues. If information is known about a desirable weighting of the system states for each mode, it is possible to choose a desired eigenvector specification. Again this will not necessarily be achievable because it may not lie within the prescribed allowable sub-space.

Quadratic Minimisation

Consider the problem of minimising the quadratic performance index

$$J = \frac{1}{2}\int_{t_s}^{\infty} x(t)^T Q x(t)\ dt \tag{D.2}$$

where Q is both symmetric and positive definite and t_s is the time at which sliding motion commences. The aim is to minimise equation (D.2) subject to the system equation (5.7) under the assumption that sliding takes place. It is assumed that the state of the system at time t_s, $x(t_s)$, is a known initial condition and is such that $x(t) \rightarrow 0$ as $t \rightarrow 1$. The matrix Q from equation (D.2) is transformed and partitioned compatibly with z so that

$$T_r Q T_r^T = \begin{bmatrix} Q_{11} & Q_{12} \\ Q_{12}^T & Q_{22} \end{bmatrix} \tag{D.3}$$

and subsequently define

$$\hat{Q} = Q_{11} - Q_{12} Q_{22}^{-1} Q_{21} \tag{D.4}$$

and

$$v = z_2 + Q_{22}^{-1}Q_{21}z_1 \tag{D.5}$$

After some algebraic manipulation equation (D.2) may then be written in the new Co-ordinate system as

$$J = \frac{1}{2}\int_{t_s}^{\infty} z_1^T \hat{Q} z_1 + v^T Q_{22} v \; dt \tag{D.6}$$

Recall the constraint equation may be written as

$$\dot{z}_1(t) = A_{11}z_1(t) + A_{12}z_2(t) \tag{D.7}$$

Eliminating the z_2 contribution from equation (D.7) using equation (D.5) the modified constraint equation becomes

$$\dot{z}_1(t) = \hat{A}z_1(t) + A_{12}v(t) \tag{D.8}$$

where

$$\hat{A} = A_{11} - A_{12}Q_{22}^{-1}Q_{21} \tag{D.9}$$

The positive definiteness of Q ensures that $Q_{22} > 0$, so that Q_{22}^{-1} exists, and also that $\hat{Q} > 0$. Furthermore, the controllability of the original (A, B) pair ensures that the pair ($\hat{A}$, A_{12}) is controllable. The problem thus becomes that of minimising the functional (D.6) subject to the system (D.7) and thus can be interpreted as a standard linear-quadratic optimal state-regulator problem.

PART 2: DERIVATION OF THE DISCRETE TIME KALMAN FILTER

Some Results for Linear Mean Square Estimation

There are four results for LMMS estimation which are key to the development of the Kalman filter. Because of their importance their derivations are included as notes at the end of this appendix.

Minimum Mean Square Estimate

For the random vectors x and z, the LMMS estimate of x given z is

$$\hat{x} = \mathrm{E}\left[(x-m_x)(z-m_z)^T\right]\left\{E\left[(z-m_z)(z-m_z)^T\right]\right\}^{-1}(z-m_z)+m_x \qquad \text{(D.10)}$$

Where m_x is the mean of x and m_z is the mean of z. Specifically, if x and z are zero-mean random vectors, then the LMMS estimate of x based on z is

$$\hat{x} = \mathrm{E}\left[xz^T\right]\left\{\mathrm{E}\left[zz^T\right]\right\}^{-1} z \qquad \text{(D.11)}$$

Orthogonality of the Measurements and Estimation Error

This result, known as the orthogonality principle, states that if x, z and $\hat{x}$ satisfy equation (D.10), then the measurement vector $z-m_z$ is orthogonal to the estimation error $x-\hat{x}$, that is

$$\mathrm{E}\left[(z-m_z)(x-\hat{x})^T\right]=0 \qquad \text{(D.12)}$$

Estimation of Linear Composition

For the random vectors x, y, w and z if

$$x = Ay + Bw \qquad \text{(D.13)}$$

Then the LMMS estimate of x based on z is given by

$$\hat{x} = A\hat{y} + B\hat{w} \tag{D.14}$$

Where $\hat{y}$ is the LMMS estimate of y based on z and $\hat{w}$ is the LMMS estimate of w based on z.

Incorporation of Orthogonal Data

For the random vectors x, z_1 and z_2, if $z_1 - m_{z1}$ and $z_2 - m_{z2}$ are orthogonal,

$$\mathrm{E}\left[\left(z_1 - m_{z1}\right)\left(z_2 - m_{z2}\right)^T\right] = 0 \tag{D.15}$$

The LMMS estimate of x based on z_1 and z_2 is

$$\hat{x} = \hat{x}_1 + \hat{x}_2 + m_x \tag{D.16}$$

Where $\hat{x}_1$ is the estimate of x based on $z_1 - m_{z1}$ and $\hat{x}_2$ is the estimate of x based on $z_2 - m_{z2}$.

THE DISCRETE TIME KALMAN FILTER

The derivation of the Kalman filter in its simplest form is now presented. Some nomenclature to be used is first introduced:

$\hat{x}(k+1|k)$ is the LMMS estimate of $x(k+1)$ based on $z(1), z(2), \ldots, z(k)$

$\hat{x}(k+1|k+1)$ is the LMMS estimate of $x(k+1)$ based on $z(1), z(2), \ldots, z(k+1)$

$\hat{z}(k+1|k)$ is the LMMS estimate of $z(k+1)$ based on $z(1), z(2), \ldots, z(k)$

Similar definitions are used for estimates and so forth. Some other useful definitions follow

$\Delta x(k+1|k) = x(k+1) - \hat{x}(k+1|k)$ is the state prediction error.

$\Delta x(k+1|k+1) = x(k+1) - \hat{x}(k+1|k+1)$ is the state estimation error

$\Delta z(k+1|k) = z(k+1) - \hat{z}(k+1|k)$ is the measurement prediction error

$P(k+1|k) = \mathrm{E}\left[\Delta x(k+1|k)\Delta x^T(k+1|k)\right]$ is the state prediction error covariance

$P(k+1|k+1) = \mathrm{E}\left[\Delta x(k+1|k+1)\Delta x^T(k+1|k+1)\right]$ is the state estimation error covariance

Prediction and Correction

Prediction

For the system

$$x(k+1) = F(k)x(k) + w(k) \tag{D.17}$$

$$z(k+1) = H(k+1)x(k+1) + v(k+1) \tag{D.18}$$

Using the linear composition result shown in equation (D.14) results in the optimal estimate of $x(k+1)$ given data through the k^{th} step.

$$\hat{x}(k+1|k) = F(k)\hat{x}(k|k) + \hat{w}(k|k) \tag{D.19}$$

If equation (D.10) is used the estimate is

$$\hat{w}(k|k) = \mathrm{E}\left[w(k)z^T(k)\right]\left\{E\left[z(k)z^T(k)\right]\right\}^{-1} z(k) \tag{D.20}$$

Because $w(k)$ and $z(i)$, $i = 1,2,\ldots,k$ are uncorrelated, then

$$\mathrm{E}\left[w(k)z^T(k)\right] = 0 \tag{D.21}$$

Therefore, equation (D.20) gives

$$\hat{w}(k|k) = 0 \tag{D.22}$$

And equation (D.19) reduces to

$$\hat{x}(k+1|k) = F(k)\hat{x}(k|k) \tag{D.23}$$

Where $\hat{x}(0|0) = \mathrm{E}[x(0)] = 0$. This is to say that the best prediction of the state at the next step is to pass the estimate from the previous step through the system state coupling matrix F. In a similar fashion, applying the linear composition result in equation (D.14) to the stochastic system output

$$z(k+1) = H(k+1)x(k+1) + v(k+1) \tag{D.24}$$

Gives

$$\hat{z}(k+1|k) = H(k+1)\hat{x}(k+1|k) + \hat{v}(k+1|k) \tag{D.25}$$

Because $v(k)$ and $z(i)$ are uncorrelated for $k \neq i$

$$\hat{v}(k+1|k) = 0 \tag{D.26}$$

And therefore

$$\hat{z}(k+1|k) = H(k+1)\hat{x}(k+1|k) \tag{D.27}$$

Indicating that the best prediction of the next measurement is to pass the predicted state through the measurement coupling matrix H.

Correction

Proceeding to the corrector equations. The measurement prediction errors

$$\Delta z(k+1|k) = z(k+1) - \hat{z}(k+1|k) \tag{D.28}$$

Are also termed the measurement residuals, or innovations. Rather than using the original measurements $z(1), z(2), \ldots, z(k), \ldots$, it is expedient to use the measurement

residuals $\Delta z(1|0), \Delta z(2|1), \ldots, \Delta z(k|k-1), \ldots,$ as the measurements. The two are equivalent because either may be found deterministically from the other. Collecting the residuals through step k into a single vector of measurements

$$\Delta z_k = \begin{bmatrix} \Delta z(1|0) & \Delta z(2|1) & \ldots & \Delta z(k|k-1) \end{bmatrix}^T \tag{D.29}$$

The quantity $\hat{x}(k+1|k)$ then denotes the LMMS estimate of $x(k+1)$ based on Δz_k. Using the orthogonality principle in equation , the measurement residuals and the estimation error are orthogonal, that is

$$\mathrm{E}\left\{\Delta z_k \left[x(k+1) - \hat{x}(k+1|k)\right]^T\right\} = 0 \tag{D.30}$$

Postmultiplying both sides of equation X by $H^T(k+1)$ gives

$$\mathrm{E}\left\{\Delta z_k \left[x(k+1) - \hat{x}(k+1|k)\right]^T\right\} H^T(k+1) = 0 \tag{D.31}$$

Because Δz_k and $v(k+1)$ are uncorrelated

$$\mathrm{E}\left\{\Delta z_k \left[z(k+1) - \hat{z}(k+1|k)\right]^T\right\} = \mathrm{E}\left[\Delta z_k \Delta z^T(k+1|k)\right] = 0 \tag{D.32}$$

Because the collection of measurements Δz_k through step k and the measurements $\Delta z(k+1|k)$ at step $k+1$ are orthogonal, any LMMS estimates based on Δz_k and $\Delta z(k+1|k)$ are, according to the equation (D.16), the sum of the two individual estimates

$$\hat{x}(k+1|k+1) = \hat{x}(k+1|k) + \mathrm{E}\left[x(k+1)\middle|\Delta z(k+1|k)\right] \tag{D.33}$$

Which is an expression of result 4, the incorporation of orthogonal data where $\mathrm{E}\left[x(k+1)|\Delta z(k+1|k)\right]$ is defined as the best estimate of $x(k+1)$ based on $\Delta z(k+1|k)$.

The incorporation of new data in the form of the residuals only involves making additive corrections to the previous predictions, not complete recalculations.

Using result 1, for the minimum mean square estimate, then

$$\begin{aligned} \mathrm{E}\left[x(k+1)\middle|\Delta z(k+1|k)\right] &= \mathrm{E}\left[x(k+1)\Delta z^T(k+1|k)\right]\times \\ &\left\{\mathrm{E}\left[\Delta z(k+1|k)\Delta z^T(k+1|k)\right]\right\}^{-1}\Delta z(k+1|k) \end{aligned} \tag{D.34}$$

If the Kalman gain is defined as

$$K(k+1) = \mathrm{E}\left[x(k+1)\Delta z^T(k+1|k)\right]\left\{\mathrm{E}\left[\Delta z(k+1|k)\Delta z^T(k+1|k)\right]\right\}^{-1} \tag{D.35}$$

Then equation (D.33) becomes

$$\hat{x}(k+1|k+1) = \hat{x}(k+1|k) + K(k+1)\Delta z(k+1|k) \tag{D.36}$$

Kalman Gain and Error Covariances

Kalman Gain

Finding an expression for the recursive calculations of the Kalman gain sequence $K(1), K(2), K(3), \ldots,$ is the most involved part of Kalman filtering. As it shall soon be discovered, the solution consists of a set of three recursive equations with coupled matrices, from which the Kalman gains can be computed.

Substituting equation (D.18) into the measurement residual in equation (D.28) gives

$$\begin{aligned} \Delta z(k+1|k) &= z(k+1) - \hat{z}(k+1|k) \\ &= H(k+1)x(k+1) + v(k+1) - H(k+1)\hat{x}(k+1|k) \\ &= H(k+1)\Delta x(k+1|k) + v(k+1) \end{aligned} \tag{D.37}$$

From equation (D.37)

$$\begin{aligned}\mathrm{E}\left[\Delta z(k+1|k)\Delta z^T(k+1|k)\right] &= H(k+1)\mathrm{E}\left[\Delta x(k+1|k)\Delta x^T(k+1|k)\right] \\ &\times H^T(k+1)+H(k+1)\mathrm{E}\left[\Delta x(k+1|k)v^T(k+1)\right] \\ &+\mathrm{E}\left[v(k+1)\Delta x^T(k+1|k)H^T(k+1)\right] \\ &+\mathrm{E}\left[v(k+1)v^T(k+1)\right]\end{aligned} \tag{D.38}$$

Because $v(k+1)$ and $\Delta x(k+1|k)$ are uncorrelated

$$\mathrm{E}\left[\Delta x(k+1|k)v^T(k+1)\right]=\mathrm{E}\left[v(k+1)\Delta x^T(k+1|k)\right]^T=0 \tag{D.39}$$

Using the definition of the state prediction error covariance gives

$$P(k+1|k)=\mathrm{E}\left[\Delta x(k+1|k)\Delta x^T(k+1|k)\right]^T=0 \tag{D.40}$$

And equation becomes

$$\mathrm{E}\left[\Delta z(k+1|k)\Delta z^T(k+1|k)\right]\doteq H(k+1)P(k+1|k)H^T(k+1)+R(k+1)$$

Similarly, using the definition of the state prediction error results in

$$\begin{aligned}\mathrm{E}\left[x(k+1)\Delta z^T(k+1|k)\right] &= \mathrm{E}\left\{\left[\Delta x(k+1|k)+\hat{x}(k+1|k)\right]\left[\Delta z^T(k+1|k)\right]\right\} \\ &= \mathrm{E}\left[\Delta x(k+1|k)\Delta z^T(k+1|k)\right]+\mathrm{E}\left[\hat{x}(k+1|k)\Delta z^T(k+1|k)\right]\end{aligned} \tag{D.41}$$

Because $v(k+1)$ is uncorrelated with $\hat{x}(k+1|k)$ and because the estimate $\hat{x}(k+1|k)$ and the estimation error $\Delta x(k+1|k)$ are orthogonal,

$$\mathrm{E}\left[\hat{x}(k+1|k)\Delta z^T(k+1|k)\right]=0 \tag{D.42}$$

Therefore

$$\mathrm{E}\left[x(k+1)\Delta z^T(k+1|k)\right]=\mathrm{E}\left[\Delta x(k+1|k)\Delta z^T(k+1|k)\right] \tag{D.43}$$

Using equation (D.37) results in

$$\Delta z(k+1|k) = H(k+1)\Delta x(k+1|k) + v(k+1) \tag{D.44}$$

And

$$\begin{aligned} \mathrm{E}\left[x(k+1)\Delta z^T(k+1|k)\right] &= \mathrm{E}\left\{\Delta x(k+1|k)\left[H(k+1)\Delta x(k+1|k) + v(k+1)\right]^T\right\} \\ &= \mathrm{E}\left\{\begin{bmatrix}\left[\Delta x(k+1|k)\Delta x^T(k+1|k)H^T(k+1)\right] \\ +\left[\Delta x(k+1|k)v^T(k+1)\right]\end{bmatrix}\right\} \end{aligned} \tag{D.45}$$

But $v(k+1)$ and $\Delta x(k+1|k)$ are uncorrelated, and therefore

$$\mathrm{E}\left[\Delta x(k+1|k)v^T(k+1)\right] = 0 \tag{D.46}$$

Thus

$$\begin{aligned} \mathrm{E}\left[x(k+1)\Delta z^T(k+1|k)\right] &= \mathrm{E}\left[\Delta x(k+1|k)\Delta x^T(k+1|k)H^T(k+1)\right] \\ &= P(k+1|k)H^T(k+1) \end{aligned} \tag{D.47}$$

And therefore the Kalman gain is

$$\begin{aligned} K(k+1) &= \mathrm{E}\left[x(k+1)\Delta z^T(k+1)\right]\left\{\mathrm{E}\left[\Delta z(k+1)\Delta z^T(k+1)\right]\right\}^{-1} \\ &= P(k+1|k)H^T(k+1)\left[H(k+1)P(k+1|k)H^T(k+1) + R(k+1)\right]^{-1} \end{aligned} \tag{D.48}$$

Error Covariances

If the system equation is used

$$x(k+1) = F(k)x(k) + w(k) \tag{D.49}$$

And

$$\hat{x}(k+1|k) = F(k)\hat{x}(k|k) \tag{D.50}$$

Then the state prediction error is

$$\begin{aligned} \Delta x(k+1|k) &= x(k+1) - \hat{x}(k+1|k) \\ &= F(k)\Delta x(k|k) + w(k) \end{aligned} \tag{D.51}$$

And the state prediction error covariance is

$$\begin{aligned} P(k+1|k) &= \mathrm{E}\left[\Delta x(k+1|k)\Delta x^T(k+1|k)\right] \\ &= \mathrm{E}\left\{\left[F(k)\Delta x(k|k)+w(k)\right]\left[F(k)\Delta x(k|k)+w(k)\right]^T\right\} \\ &= F(k)\mathrm{E}\left[\Delta x(k|k)\Delta x^T(k|k)\right]F^T(k)+F(k)\mathrm{E}\left[\Delta x(k|k)w^T(k)\right] \\ &+\mathrm{E}\left[w(k)\Delta x^T(k|k)\right]F^T(k)+\mathrm{E}\left[w(k)w^T(k)\right] \end{aligned} \tag{D.52}$$

Because $x(k|k)$ and $w(k)$ are uncorrelated,

$$\mathrm{E}\left[\Delta x(k|k)w^T(k)\right]=\mathrm{E}\left[w(k)\Delta x^T(k|k)\right]=0 \tag{D.53}$$

Giving

$$P(k+1|k)=F(k)P(k|k)F^T(k)+Q(k)+P(0|0)=P(0) \tag{D.54}$$

Where $P(k|k)$ is the estimation error covariance. Finally, for the equations to be recursive, an equation for the covariance of the state estimate error $P(k+1|k+1)$ is required. If equation (D.36) is used

$$\hat{x}(k+1|k+1)=\hat{x}(k+1|k)+K(k+1)\Delta z(k+1|k) \tag{D.55}$$

The state estimation error becomes

$$\Delta z(k+1|k)=H(k+1)\Delta x(k+1|k)+v(k+1) \tag{D.56}$$

Substituting the measurement prediction error in equation (D.37)

$$\Delta z(k+1|k)=H(k+1)\Delta x(k+1|k)+v(k+1) \tag{D.57}$$

Into equation (D.57) gives

$$\begin{aligned} \Delta x(k+1|k+1) &= \Delta x(k+1|k)-K(k+1)H(k+1)\Delta x(k+1|k)-K(k+1)v(k+1) \\ &= \left[I-K(k+1)H(k+1)\right]\Delta x(k+1|k)-K(k+1)v(k+1) \end{aligned} \tag{D.58}$$

Hence,

$$\begin{aligned}P(k+1|k+1) &= \mathrm{E}\left[\Delta x(k+1|k+1)\Delta x^T(k+1|k+1)\right] \\ &= \left[I - K(k+1)H(k+1)\right]\mathrm{E}\left[\Delta x(k+1|k)\Delta x^T(k+1|k)\right] \\ &\times\left[I - K(k+1)H(k+1)\right]^T - \left[I - K(k+1)H(k+1)\right] \\ &\times\mathrm{E}\left[\Delta x(k+1|k)v^T(k+1)\right]K^T(k+1) - K(k+1) \\ &\times\mathrm{E}\left[v(k+1)\Delta x^T(k+1|k)\right]\left[I - K(k+1)H(k+1)\right]^T \\ &+K(k+1)\mathrm{E}\left[v(k+1)v^T(k+1)\right]K^T(k+1)\end{aligned} \tag{D.59}$$

Because $\Delta x(k+1|k)$ and $v(k+1)$ are uncorrelated

$$E\left[v(k+1)\Delta x^T(k+1|k)\right] = \mathrm{E}\left[\Delta x(k+1|k)v^T(k+1)\right]^T = 0 \tag{D.60}$$

Giving

$$\begin{aligned}P(k+1|k+1) &= \left[I - K(k+1)H(k+1)\right]P(k+1|k) \\ &\times\left[I - K(k+1)H(k+1)\right]^T + K(k+1)R(k+1)K^T(k+1)\end{aligned} \tag{D.61}$$

Equation (D.61) may be put into a simpler form as follows

$$\begin{aligned}P(k+1|k+1) &= \left[I - K(k+1)H(k+1)\right]P(k+1|k) - P(k+1|k)H^T(k+1)\times K^T(k+1) \\ &+K(k+1)\left[H(k+1)\times P(k+1|k)H^T(k+1) + R(k+1)\right]K^T(k+1)\end{aligned} \tag{D.62}$$

But from equation (D.48),

$$K(k+1)\left[H(k+1)P(k+1|k)H^T(k+1) + R(k+1)\right] = P(k+1|k)H^T(k+1) \tag{D.63}$$

Therefore, equation (D.61) simplifies to

$$P(k+1|k+1) = \left[I - K(k+1)H(k+1)\right]P(k+1|k) \tag{D.64}$$

And the Kalman filter is completely derived.

Summary of Equations

Plant Model: $$x_{K+1} = \Phi_k x_k + \Gamma_k u_k + G_k \omega_k \quad \text{(D.65)}$$

Observation Model: $$z_k = H_k x_k + v_k \quad \text{(D.66)}$$

Predictive Estimate: $$\hat{x}_{k+1|k} = \Phi_k \hat{x}_{k|k} + \Gamma_k u_k + G_k \bar{\omega}_k \quad \text{(D.67)}$$

Current Estimate: $$\hat{x}_{k|k} = \hat{x}_{k|k-1} + K_k \left(z_k - H_k \hat{x}_{k|k-1} \right) - \bar{v}_k \quad \text{(D.68)}$$

Gain: $$K_k = P_{k|k-1} H_K^T \left\{ H_k P_{k|k-1} H_k^T + R_k \right\}^{-1} \quad \text{(D.69)}$$

***A priori* covariance:** $$P_{K+1|k} = \Phi_k P_{k|k} \Phi_k^T + G_k Q_k G_k^T \quad \text{(D.70)}$$

***A Posteriori* covariance:** $$P_{k|k} = P_{k|k-1} - K_k H_k P_{k|k-1} \quad \text{(D.71)}$$

Plant Noise Model: $$cov\{\omega_i, \omega_k\} = Q_k \delta_{i,k}, E\{\omega_k\} = 0 \quad \text{(D.72)}$$

Measurement Noise Model: $$cov\{v_i, v_k\} = R_k \delta_{i,k}, E\{v_k\} = 0 \quad \text{(D.73)}$$

Kronecker delta function: $$\delta_{i,j} = \begin{cases} 1 & i = j \\ 0 & i \neq j \end{cases} \quad \text{(D.74)}$$